Universidade do Minho
Escola de Engenharia

Ana Catarina Cardoso Lima

Development of natural-based hydrogel particles using a biomimetic methodology

outubro de 2014

Universidade do Minho
Escola de Engenharia

Ana Catarina Cardoso Lima

Development of natural-based hydrogel particles using a biomimetic methodology

Tese de Doutoramento em Bioengenharia

Trabalho realizado sob a orientação do
Professor Doutor João Filipe Colardelle da Luz Mano

outubro de 2014

STATEMENT OF INTEGRITY

I hereby declare having conducted my thesis with integrity. I confirm that I have not used plagiarism or any form of falsification of results in the process of the thesis elaboration. I further declare that I have fully acknowledged the Code of Ethical Conduct of the University of Minho.

University of Minho, _____

Full name:_____

Signature:_____

In Memory of My Lovely Grandfather

Acknowledgements

After 4 years of arduous work it is the moment to express my gratitude to the people who supported me throughout this PhD.

Em primeiro lugar, e porque são os mais importantes, quero agradecer à minha família em especial aos meus pais *Aurora* e *Manuel* e aos meus irmãos *Miguel Ângelo* e *Nuno.* Sem as vossas palavras de motivação e apoio incondicional esta dura jornada não teria sido possível. Não há palavras que possam descrever o meu sentimento de gratidão para convosco.

To my supervisor, *Professor João F. Mano*, for all the discussions, for all the suggestions to improve my work, and for encourage me to participate in wide range of activities which allowed me to grow significantly at professional and personal level, thank you very much.

Quiero también expresar mi mayor gratitud a la *Profesora Carmen Álvarez-Lorenzo* y al *Profesor Ángel Concheiro*, por acogerme en su laboratorio (Departamento de Farmacia y Tecnología Farmaceútica, Universidad de Santiago de Compostela) durante 1 año y medio, por sus consejos, su paciencia, por toda la ayuda prestada, por su apoyo en momentos de desanimo y también por su esfuerzo para intentar que yo hablase castellano. A todos mis compañeros del departamento: *Bárbara Blanco, Isa Rial, Susana Simões, Luis Días Gomes, Manuela Curcio, Clara, Mariajo, Elena, Alejandro, Maria de Matos, Rosalía, Sonia y Marga,* muchas gracias por vuestro cariño. Una mención especial merecen mis compañeras de mesa *Lidia Pereiro, Patricia Días Rodríguez* y *Ana Puga*, por su amistad, consejos, ayuda, palabras de optimismo en los momentos difíciles y por las alegrías y el buen ambiente compartido a lo largo de mi estancia. Gracias a todos también por el esfuerzo en intentar que yo hablase castellano. Este pequeño texto es la prueba de que sus esfuerzos por entrenarme en el español tuvieron algunos resultados!

I am grateful to *Professor Rui L. Reis* for the possibility of working in such a renowned group as well as for the using of the facilities at AvePark.

I should also acknowledge to *MIT Portugal Program* for accepting me in Bioengineering Systems doctoral program, and the *Portuguese Foundation for Science and Technology* (FCT) for my PhD grant SFRH/BD/71395/2010.

During the modules of the *Bioengineering Systems Doctoral Program* I had the opportunity to meet fantastic people both colleagues and professors. Professionally, I acquired a broad knowledge about a wide range of areas; personally, I learned a lot from all of you! A very special thank to *Joana Rodrigues* and *Rui Pereira* for all the great moments in Lisbon, Braga and Coimbra! It is good to see that after 4 years we are good friends, always ready to support each other's.

I want to deliver a word of appreciation and admiration to *Professor João Pedro Conde* and *Dr. Virginia Chu* for hosting me in INESC MN for 2 months where I had the opportunity to learn, in a practical way, about microfabrication techniques and more important to show me how it is useful working in a group where the knowledge is constantly shared in order to improve the work of all team members. Moreover, I would like to acknowledge to the other elements of the INESC MN group for always helping me, and finally a very special thank you to my old friend *Pedro Novo* for the patience and all the support in the lab work. No doubts that was a great pleasure to work with the smarter guy of 2005/2006 UBI´s Biomedical Sciences group.

I would like to express my gratitude to *Professor Ilídio J. Correia* for receiving me in CICS (University of Beira Interior), as well as for the great contribution for a chapter of this thesis and for the efforts to provide me all the necessary conditions to do my work. No doubt that was and is a great pleasure for me being received in my first home (UBI) and work with a small but promising team. A very special thank you to *Ana Sofia Silva, Tiago Valente,* and *Patricia Batista* for the help in the lab and for the good moments spent in Covilhã.

In 3B´s I have been very privileged to meet and to collaborate with many other great people who became friends over the last several years. I would like to acknowledge all the 3B's Research Group team. To *Catarina Custódio, Mariana Oliveira* and *Clara Correia*, thank you very much for the contribution for a few work presented in this thesis. I am also particularly thankful to *Nuno Oliveira, Álvaro Leite, Rui Costa, Pedro Costa, Silvia Mihaila* and *Diana Pereira,* who have been constantly present in my life during the last years. No much words to say, you are all very special for me not only for the support, nice words, encouragement in the difficulties but also for being there in special moments as well as in many experiences and adventures lived outside 3B´s, which became these years much happier. To *Isabel Neto, Sara Gil, Sofia Caridade, Silvia Oliveira, Pedro Carvalho, Alesandra Zonari, Praveen Sher, Sara Oliveira,*

Diana Ribeiro, Albino Martins, Dennis Link and Joana Marques Silva for the help in any moment and mainly for the smiles and shared good moments inside or outside the 3B´s building!

De uma forma mais pessoal, queria deixar uma palavra de agradecimento também àqueles que demonstraram ter uma presença importante ao longo destes últimos 4 anos. Uma palavra de enorme admiração e agradecimento ao *João Requicha* que esteja onde estiver, está sempre disponível quer para me ajudar, quer para me ouvir pacientemente! *Ana Dias* e *Ester Ferreira*, muito obrigada pelos bons momentos que passamos desde que cheguei aos 3B's e que se têm revelado constantes apesar das distâncias que nos separam. *Alberta Domingues*, uma palavra de agradecimento por todo o apoio nos momentos de maior desmotivação, pelas longas conversas, pela tua paciência, pelos conselhos e também pela partilha de muitas coisas e momentos bons ao longo de tantos anos. *Tânia Martins* e *Diana Gaspar*, as calorinhas que não praxei na Covilhã mas que por coincidências da vida se cruzaram comigo em Braga e em Santiago de Compostela, respectivamente. Muito obrigada pela preocupação constante, pela boa disposição que vos caracteriza e acima de tudo pela amizade crescente ao longo dos últimos anos. Um muito obrigado também ao *Tiago Marques*, pela ajuda, pelas palavras de incentivo, pelas repreensões, e acima de tudo pela paciência para comigo em todos os momentos ao longo deste último ano e meio.

Abstract

Superhydrophobic (SH) surfaces have been greatly explored in the biomedical field. Such surfaces are inspired by the repellent properties of natural structures. The most well known example is the lotus leaf, which has the capacity to repeal the water droplets due to the presence of micro/nano topographical features and the low surface energy. One particular application of artificial SH surfaces is their employment as supports where liquid droplets of aqueous-based polymeric solutions are dispensed, acquiring an almost spherical shape. Through application of one or multiple hardening steps solid particles are obtained in a fast way. Using this methodology, a variety of functional natural-based hydrogel spherical systems encapsulating cells and/or drugs are proposed in this thesis. The strategy of the first proposed system is the incorporation of cyclodextrins (CDs) in the dextran-methacrylate (Dex-MA) microgels networks in order to improve their loading efficiency for hydrophobic drugs. The formation of inclusion complexes between CDs and dexamethasone, when the CDs were copolymerized, increased significantly the amount of drug in the Dex-MA particles, when compared with formulations without or with freely dispersed CDs. Chitosan (Chi), unless it has been modified, is soluble in acidic media, which turn it incompatible with encapsulation of cells or pH sensitive molecules. The second system proposed envisaged a mild Chi-based system with two sequential hardening steps, where dexamethasone or fibroblast-like cells were successfully entrapped. SH surfaces methodology was also used to co-encapsulate cells and proteins into hydrogel particles without compromise the cell viability and protein activity. Collagen combined with platelet lysates were used to obtain easy-to-handle spherical formulations being capable to act as *in situ* growth factors release system as well as reservoirs of human adipose derived stem cells, for applications in skin regeneration. Mesenchymal stem cells derived from bone marrow and fibronectin were also encapsulated inside alginate spheres and the system was studied for bone regeneration. The control of the release of bioactive agents may be achieved by adjusting the chemistry and physical parameters such as particles architecture. Multicompartmentalized systems have emerged and are envisioned to be the next area of development due to the possibility to confines various bioactive agents exhibiting a variety of release kinetics. Taking advantage of the simplicity of the SH surfaces methodology, core/shell and multilayered particles composed by Dex-MA and alginate were efficiently prepared, with cells or drugs encapsulated into individual compartments. The developed work shows that a wide variety of particles useful for biomedical application, ranging from homogeneous spherical matrices to compartmentalized systems, could be obtained under mild conditions and in a fast way, using SH surfaces.

Resumo

Superfícies superhidrofóbicas (SH) têm vindo a ser exploradas no campo biomédico. Estas superfícies são inspiradas nas propriedades repelentes de estruturas naturais. O exemplo mais conhecido é a folha de lotus, com a sua capacidade de repelir gotas de água devido à presença de micro/nano estruturas e baixa energia de superfície. Uma aplicação particular das superfícies SH artificiais é a sua utilização como suportes onde gotas de soluções poliméricas de base aquosa são dispensadas, adquirindo uma forma quase esférica. Através da aplicação de um ou múltiplos passos de solidificação, partículas sólidas são obtidas de uma forma rápida. Usando esta metodologia, uma variedade de hidrogéis funcionais de base natural, encapsulando células e/ou fármacos, são propostos nesta tese. A estratégia do primeiro sistema proposto é a incorporação de ciclodextrinas (CDs) em microgéis de dextrano-metacrilatado (Dex-MA), com o intuito de melhorar a sua capacidade de carga para fármacos hidrofóbicos. A formação de complexos de inclusão entre CDs e dexametasona, quando as CDS estavam co-polimerizadas, aumentou significativamente a quantidade de fármaco no interior das partículas, quando comparadas com formulações sem, ou com CDs livres. O quitosano, a não ser que esteja modificado, é solúvel em meios ácidos, o que o torna incompatível com o encapsulamento de células ou moléculas sensíveis ao pH. O segundo sistema proposto teve como objectivo a produção de sistemas não agressivos, através de dois passos sequenciais de gelificação do quitosano, onde dexametasona e/ou fibroblastos foram encapsuladas com sucesso. A metodologia das superfícies SH foi também usada para o co-encapsulamento de células e proteínas em hidrogéis sem comprometer a viabilidade das células nem a atividade das proteínas. Colagénio combinado com lisados de plaquetas foram usados para obter formulações fáceis de manusear, sendo estas capazes de atuar como sistema de libertação de factores de crescimento *in situ* e também como reservatório de células estaminais derivadas do tecido adiposo, para a regeneração de pele. Em outro sistema apresentado, células estaminais mesenquimais e fibronectina foram encapsulados em esferas de alginato e o sistema foi estudado para regeneração óssea. O controlo da libertação de agentes bioativos pode ser conseguido através do ajuste da química e de parâmetros físicos tal como a arquitetura das partículas. O potencial dos sistemas multi-compartimentalizados tem emergido devido à possibilidade de encapsulamento de vários agentes bioativos exibindo diferentes cinéticas de libertação. Aproveitando a simplicidade da metodologia das superfícies SH, partículas com uma ou mais camadas, compostas por Dex-MA e alginato foram eficientemente preparadas, encapsulando células e fármacos em compartimentos individuais. Os trabalhos desenvolvidos mostram que uma grande variedade de partículas úteis para aplicações biomédicas, desde matrizes esféricas homogéneas até sistemas compartimentalizados, podem ser obtidos em condições não agressivas e de uma forma rápida, usando superfícies SH.

Table of Contents

List of Abbreviations and Acronymes

A

AA	Acrylic acid
aAPCs	Artificial antigen presenting cells
Al	Aluminium
ALP	Alkaline phosphatase
ATDC5	Mouse chondrogenic cell line

B

BCA	Bicinchoninic acid
BCH	Bovine articular chondrocytes
bFGF	Basic fibroblaste growth factor
BG-NPs	Bioglass nanoparticles
BSA	Bovine serum albumine

C

CA	Contact angle
CAH	Contact angle hysteresis
CAM	Chorioallantoic membrane
Calcein-AM	Calcein acetomethoxy
CCK-8	Cell counting kit
CD	Cyclodextrin
CHI	Chitosan
Coll	Collagen
CT	Computed tomography
Cu	Copper

D

Da	Dalton
DAPI	4′,6-diamidino-2-phenylindole dihydrochloride
DEX or dex	Dextran
Dex-HEMA	dextran-hydroxyethyl methacrylate
DEX-MA or Dex-MA	Dextran-metacrylate
DMA	Dynamic mechanical analysis
DMAEMA	Dimethyl aminoethyl methacrylate
DMAP	4-(N,N-dimethylamido)pyridine
DMEM	Dulbecco's modified Eagle's medium
DMSO	Dimethyl sulfoxide
DS	Degree of Substitution
dsDNA	Double stranded DNA

E

ECM	Extracelular matrix
EDS	Energy-dispersive X-ray spectroscopy
EDTA	Ethylenediamine tetraacetic acid
ELISA	Enzyme-linked immunosorbant assay
ELR	Elastin-like recombinamer
ePTFE	Expanded polytetrafluoroethylene
EQ.	Equation

F

FBS	Fetal bovine serum
FITC	Fluorescein-5(6)-isothiocyanate
FN	Fibronectin
FTIR	Fourier transform infrared

G

GLY	Glycine
GMA	Glycidyl methacrylate

H

hASC	Human adipose-derived stem cells
HEA	2-Hydroxyethyl acrylate
HeLa	Cervical cancer cells
HEMA	Hydroxyethyl methacrylate
HEMAPC	Hydroxuethyl methacrylate phosphatidylcholine
HepG2	Hepatocellular carcinoma cells
HPLC	High-performance liquid chromatography
HSA	Human serum albumine
HUVECS	Human umbilical vein endothelial cells

I

ICP	Inductive coupled plasma

L

L929	Mouse lung fibroblasts cell line
LbL	Layer-by-Layer
LDH	Lactate dehydrogenase

M

M3T3-E1	Murine osteoblastic cell line
MG63	Human fibroblasts from osteosarcoma
MRI	Magnetic resonance imaging
MSCs	Mesenchimal stem cells
MTS	(3-(4,5-dimethylthiazol-2-yl)-5-(3-carboxymethoxyphenyl)-2-(4-sulfophenyl)-2H- tetrazolium)
MTT	(3-[4,5-dimethylthiazol-2-yl]-2,5-diphenyltetrazolium bromid)
MW	Molecular weight
MWCO	Molecular weight cut-off

N

NIH-3T3	Mouse fibroblasts cell line
NMA	(Hydroxymethyl)acrylamide
NMR	Nuclear magnetic resonance

O

OD	Optical density

N

PAA	Poly (acrylic acid)
PBS	Phosphate buffered saline
PBut	Poly(butadiene)
PCL	Poly(ε-caprolactone)
PCUs	Poly(carbonate urethane)s
PDGF-BB	Platelet derived growth factor
PDMS	Polydimethylsiloxane
PEDT	Poly(3,4-ethylene dioxythiolphene)
PEE	Poly(ethyl ethylene)
PEG	Poly (ethylene glycol)
PEGDA	Poly (ethylene glycol) diacrylate
PEO	Poly(ethylene oxide)
PFDTS	Perfluorodecyltriethoxysilanes
PFPO	Perfluoropropylene oxide
PGA	Poly(L-glutamic acid)
PGC-C18	Poly(glycerol monoestereare- ε-caprolactone)
PHB	Poly(hydroxybutyrate)
pHEMA	Poly(2-hydroxyethyl methacrylate)
PI	Propidium iodide
PL	Platet lysates
PLA	Poly(lactic acid)
PLGA	Poly(lactic-co-glycolic acid)
PLL	Poly(L-lysine)
PLLA	Poly(L-lactic acid)
PMAA	Poly(methacrylic acid)
PNIPAAM	Poly(N-isopropylacrylamide)
PP	Polypropylene
PPEEA	Poly(2-aminoethyl ethylene phosphate)
PRINT	Particle replication in non-wetting templates
Pro	Proline
PS	Polystyrene
PU	Polyurethane

Q

QD	Quantum dot

R

RGD	Arginine-glycine-aspartate
RhoB	Rhodamine B
rMSCs	Rat mesenchymal stem cells
RT	Room temperature

S

SaOs-2	Human osteoblast cell line
SD or S.D. or s.d.	Standard Deviation
SEM	Scanning electron microscopy
SH	Superhydrophobic
SLIPS	Slippery liquid-infused porous surfaces
SK-MEL-28	Human melanoma cells

T

TEM	Transmission electron microscopy
THF	Tetrahydrofuran
TMP	2,2,4-trimethylpentane
TPP	Tripolyphosphate

U

US	Ultrasound imaging
UV	Ultraviolet

V

VEGF	Vascular endothelial growth factor
VIS	Visible

Others

β -GP	β-glycerophosphate
γ-CD	Gamma-cyclodextrin
γ-CD-NMA	Acrylamidomethyl-gamma-cyclodextrin
μCT	MicroComputed Tomography

List of Figures

Chapter 2. Micro/Nano Structured Superhydrophobic Surfaces in the Biomedical Field. Part II: Applications Overview

SECTION III. Natural-Based Spherical Systems, Prepared on Superhydrophobic Surfaces, for Applications in the Biomedical Field

Chapter 5. Free and Copolymerized γ-Cyclodextrins Regulate the Performance of Dexamethasone-Loaded Dextran Microspheres for Bone Regeneration

Chapter 6. Sequential Ionic Thermogelation of Chitosan Spherical Hydrogels Prepared Using Superhydrophobic Surfaces to Immobilize Cells and Drugs.

Chapter 7. Fast and Mild Strategy, Using Superhydrophobic Surfaces, to Produce Collagen/Platelet Lysate Gel Beads for Skin Regeneration

vessels at 3 days post- implantation. *p<0.05, significantly different from the Coll. #p<0.05, significantly different from Coll+PL1×. $p<0.05, significantly different from PL1×.

Chapter 8. Novel Methodology Based on Biomimetic Superhydrophobic Substrates to Immobilize Cells and Proteins in Hydrogel Spheres for Applications in Bone Regeneration

Chapter 9. Biomimetic Methodology to Produce Polymeric Multilayered Particles for Biotechnological and Biomedical Applications

List of Tables

Chapter 6. Sequential Ionic Thermogelation of Chitosan Spherical Hydrogels Prepared Using Superhydrophobic Surfaces to Immobilize Cells and Drugs.

Chapter 7. Fast and Mild Strategy, Using Superhydrophobic Surfaces, to Produce Collagen/Platelet Lysate Gel Beads for Skin Regeneration

Chapter 8. Novel Methodology Based on Biomimetic Superhydrophobic Substrates to Immobilize Cells and Proteins in Hydrogel Spheres for Applications in Bone Regeneration

Short *Curriculum Vitae*

Ana Catarina Lima graduated in Biomedical Sciences at University of Beira Interior (Portugal) in 2008. In 2010 she completed the Master degree in Biomedical Engineering at the University of Minho (Portugal). She started working in the field of biomaterials in 2009, when she joined the 3B's Research Group for preparing her master dissertation. During this period, she became familiar with the techniques for preparation of particles as drug release systems. During the master, she was accepted to integrate in MIT Portugal Doctoral Program in Bioengineering Systems. In September 2010, Ana Catarina started the intensive curricular courses in four Portuguese Universities (Universidade do Minho, Universidade de Coimbra, Instituto Superior Técnico, and Universidade Nova de Lisboa) expanding her knowledge in technological innovation, entrepreneurship, bioprocess engineering, cell and tissue engineering, computational biosystems science and engineering, nanobiotechnology and biomaterials, and principles and practices of drug development. In February 2011, Ana Catarina had the opportunity to visit the INESC Microsistemas e Nanotecnologias, a private and non-profit institute focused in micro and nano fabrication using optical and e-beam lithography. During 2 months, under supervision of Professor João Pedro Conde, she became familiar with procedures to design and produce surfaces with predefined patterns. After this experience, Ana Catarina started her laboratorial PhD work developing spherical natural-based systems where cells and/or drugs were entrapped, for applications in the biomedical field. During 3 months, from April to July 2011, she was received in Healthcare Science Research Center of University of Beira Interior (Portugal) where she had the opportunity to perform *in vivo* experiments. Returning to 3B's she continued to develop other systems and in October 2012 she moved to Santiago de Compostela, where for one year and a half worked with Professor Carmen Alvarez-Lorenzo, at Faculty of Pharmacy at University of Santiago de Compostela (Spain), in development of controlled drug release systems for tissue engineering applications. Ana Catarina was involved in the preparation of national (Portuguese Foundation for Science and Technology and Luso-Spanish Integrated Actions 2012) grant proposals. In 2013 she was selected to attend to an international summer course in BASF (a world leading chemical company) where she had the opportunity to gain insight into the chemical industry and to learn about R&D, engineering, technology, marketing and production. In August 2014, Ana Catarina was also selected to represent Portugal in a leadership course (Biocamp 2014) in a multinational pharmaceutical company: Novartis. Finally, Ana Catarina is author in 7 papers and co-author in 1 paper, all published in international refereed journals. Furthermore, she has participated in some conferences in her research field in the form of 9 poster communications.

List of Publications

The work developed under the scope of this PhD thesis resulted in the publications listed below:

Papers in international scientific journals with referees

1. **Lima A. C.**, Alvarez-Lorenzo C. and Mano J. F., Advances in particulate systems for biomedical applications: non-spherical and compartmentalized approaches, submitted.
2. **Lima A. C.** and Mano J. F., Micro/nano structured superhydrophobic surfaces in the biomedical field. Part I: basic concepts and biomimetic qpproaches, Nanomedicine *(Lond.)* 10(1), DOI: 10.2217/NNM.14.174 (In press).
3. **Lima A. C.** and Mano J.F., Micro/nano structured superhydrophobic surfaces in the biomedical field. Part II: applications overview, Nanomedicine *(Lond.)* 10(2), DOI: 10.2217/NNM.14.175 (In press).
4. **Lima A. C.**, Mano J. F., Concheiro A. and Alvarez-Lorenzo C., Fast and mild strategy, using superhydrophobic surfaces, to produce collagen/platelet lysate gel beads for skin regeneration, Stem Cells Reviews and Reports 2014, DOI 10.1007/s12015-014-9548-6 (In press).
5. **Lima A. C.**, Puga A. M., Mano J. F., Concheiro A. and Alvarez-Lorenzo C., Free and copolymerized γ-cyclodextrins regulate performance of dexamethasone-loaded dextran microspheres for bone regeneration, Journal of Materials Chemistry B 2014, 2: 4943-4956.
6. **Lima A. C.**, Correia C. R., Oliveira M. B. and Mano J.F., Sequential ionic and thermogelation of chitosan spherical hydrogels prepared using superhydrophobic surfaces to immobilize cells and drugs, Journal of Bioactive and Compatible Polymers 2013, 28: 50-65.
7. **Lima A. C.**, Custódio C. A., Alvarez-Lorenzo C. and Mano J.F., Biomimetic methodology to produce polymeric multilayered particles for biotechnological and biomedical applications, Small 2013, 9: 2487-2492.
8. **Lima A. C.**, Batista P., Valente T. A. M., Silva A. S., Correia I. J. and Mano J. F., Novel methodology based on biomimetic superhydrophobic substrates to immobilize cells and proteins in hydrogel spheres for biomedical applications, Tissue Engineering Part A 2012, 19: 1175-1187.

Publications resulting from collaborative work

1. Puga A. M., **Lima A. C.**, Mano J. F., Concheiro A. and Alvarez-Lorenzo C., Pectin-coated chitosan microgels crosslinked on superhydrophobic surfaces for 5-fluorouracil encapsulation, Carbohydrate Polymers 2013, 98: 331-340.

Conference abstracts published in international scientific journals

1. **Lima A. C.**, Custódio C. A., Alvarez-Lorenzo C. and Mano J.F., Multilayered polymeric particles production using superhydrophobic surfaces methodology for drug delivery and tissue engineering applications, Journal Tissue Engineering and Regenerative Medicine 2012, 6 (Suppl.2): 17.
2. **Lima A. C.**, Batista P., Valente T. A. M., Silva A. S., Correia I. J. and Mano J. F., Novel methodology based on biomimetic superhydrophobic substrates to immobilize cells and proteins in hydrogel spheres for tissue engineering applications, Journal Tissue Engineering and Regenerative Medicine 2012, 6 (Suppl. 1): 196.

Invited lectures

1. **Lima A. C.,** and Mano J. F., Processing of particles using natural-based polymers, *2nd 3B's Symposium on Biomaterials and Stem Cells in Regenerative Medicine*, January 2012, Guimarães (Portugal).

Conference posters

1. **Lima A. C.** and Mano J. F., Superhydrophobic Surfaces as Platforms for Cells and Drugs Encapsulation for Tisse Engineering Purposes, 4th MIT Portugal Program Conference, Coimbra, Portugal, June 2014.
2. **Lima A. C.**, Puga A. M., Alvarez-Lorenzo C., Concheiro A. and Mano J. F. Dexamethasone-loaded γ-cyclodextrin-dextran microspheres for bone regeneration, 17th International Cyclodextrin Symposium, Saarbrücken, Germany, May 2014.
3. **Lima A. C.,** Puga A. M., Alvarez-Lorenzo C., Concheiro A. and Mano J. F., Dextran-γ-cyclodextrin microspheres for dexamethasone controlled release in bone regeneration, *9th World Meeting on Pharmaceutics, Biopharmaceutics and Pharmaceutical Technology*, Lisbon, Portugal, April 2014.
4. **Lima A. C.**, Custódio C. A., Alvarez-Lorenzo C. and Mano J. F., Multilayered particles production using superhydrophobic surfaces methodology for biomedical applications, *25th European Conference on Biomaterials*, Madrid, Spain, September 2013.
5. **Lima A. C.**, Correia C. R., Oliveira M. B. and Mano J. F. Smart chitosan particles for cells and drugs encapsulation obtained using the superhydrophobic surfaces technology, *TERMIS-EU*, Istanbul, Turkey, June 2013.

6. **Lima A. C.**, Custódio C. A., Alvarez-Lorenzo C. and Mano J. F., Multilayered polymeric particles production using superhydrophobic surfaces methodology for drug delivery and tissue engineering applications, *TERM STEM 2012*, Guimarães, Portugal, October 2012.

7. **Lima A. C.**, Batista P., Valente T. A. M., Silva A. S., Correia I. J. and Mano J.F., Novel methodology based on biomimetic superhydrophobic substrates to immobilize cells in hydrogel spheres for tissue engineering applications, *3rd TERMIS World Congress*, Vienna, Austria, September 2012.

8. **Lima A. C.**, Alvarez-Lorenzo C., and Mano J. F., Novel methodology based on biomimetic superhydrophobic substrates to immobilize cells and bioactive agents in hydrogel spheres for biomedical applications, *2nd ICVS/3B´s Associate Laboratory Meeting*, Braga, Portugal, May 2012.

9. **Lima A. C.**, Alvarez-Lorenzo C., and Mano J. F., Novel methodology based on biomimetic superhydrophobic substrates to immobilize cells and bioactive agents in hydrogel spheres for biomedical applications, *3rd Conference MIT Portugal*, Guimarães, Portugal, May 2012.

Introduction to the Thesis Format

This thesis is divided into 4 main sections containing a total of 10 chapters. Section I correspond to the general introduction to the thesis. The second section provides a detailed overview of the experimental methods and materials used. The experimental results obtained and their discussion are showed in the section III. The last section compiles the final remarks and the future perspectives in the context of this work. The chapters of this thesis are all based on peer-reviewed papers published or submitted for publication and contain: abstract, introduction, experimental section, results and discussion, conclusions and acknowledgements. A list of references is also provided in each chapter. The follow paragraphs summarize the content of each chapter.

Section I. General Introduction

Chapter 1. Micro/Nano Structured Superhydrophobic Surfaces in the Biomedical Field. Part I: Basic Concepts and Biomimetic Approaches

This chapter is focused on the description of the characteristics of extreme wettable surfaces, as well as the main examples found in Nature, which inspired the production of artificial superhydrophobic surfaces. This chapter also describes the interactions of substrates with extreme wettabilities with proteins and cells.

Chapter 2. Micro/Nano Structured Superhydrophobic Surfaces in the Biomedical Field. Part II: Applications Overview.

In the sequence of the previous chapter, the second one intends to demonstrate that biomimetic superhydrophobic surfaces may be used in a wide range of applications in the biomedical field. In this chapter are compiled the applications of superhydrophobic surfaces explored until the current date. In addition, it is analyzed and discussed the main fragilities as well as hypothesis about the potential and the future directions that superhydrophobic surfaces should taken to improve the results in this area.

Chapter 3. Advances in Particulate Systems for Biomedical Applications: Non-spherical and Compartmentalized Approaches

This chapter reports the importance of the physical characteristics of the particles, namely shape and compartmentalization, in their performance when used in therapeutic strategies (*e.g.* drug release/delivery, cell carriers), or as diagnosis tools. Special attention is given to non-spherical systems

and multicompartmented particles. Representative examples demonstrate the importance of physical design parameters when the particles are used in biomedical applications.

Section II. Materials and Methods

Chapter 4. Detailed Description of Experimental Testing and Materials

Detailed description of the materials properties and explanation of the techniques used to obtain the results described in this thesis.

Section III. Natural-Based Spherical Systems, Prepared on Superhydrophic Surfaces, for Applications in the Biomedical Field

Chapter 5. Free and copolymerized γ-cyclodextrins regulate the performance of dexamethasone-loaded dextran microspheres for bone regeneration

This chapter aims to demonstrate that hydrogel-based particles may be efficiently loaded with hydrophobic drugs and be capable to control the release of such molecules. Dextran-MA particles incorporating CDs in a free form or copolymerized may be obtained using the superhydrophobic surfaces methodology and may be loaded with dexamethasone. The presence of the CDs as structural monomers is crucial to control the fixation and the release of this molecule.

Chapter 6. Sequential Ionic and Thermogelation of Chitosan Spherical Hydrogels Prepared Using Superhydrophobic Surfaces to Immobilize Cells and Drugs

In this chapter, a strategy was proposed to harden chitosan particles for cells or drugs encapsulation in mild conditions, starting from an acidic chitosan solution. The neutralization of the solution with β-glycerophosphate and the subsequent ionic crosslinking were effective in the production of easy-to-handle gel particles without jeopardize the cell viability. In addition, the β-glycerophosphate allowed the improvement of the mechanical properties of the system under physiological conditions. The system was also studied as a drug container.

Chapter 7. Fast and Mild Strategy, Using Superhydrophobic Surfaces, to Produce Collagen/Platelet Lysate Gel Beads for Skin Regeneration

This chapter presents a system capable to harden in 10-15 min when submitted to physiological temperatures, co-encapsulating cells and a cocktail of bioactive agents. Particles composed by collageb and platelet lysates were studied as potential systems to supply skin damaged regions with cells (adipose-derived stem cells) and growth factors.

Chapter 8. Novel Methodology Based on Biomimetic Superhydrophobic Substrates to Immobilize Cells and Proteins in Hydrogel Spheres for Applications in Bone Regeneration

Similarly to chapter 7, this chapter presents another system encapsulating a protein and cells. Fibronectin and autologous mesenchymal stem cells were encapsulated in calcium crosslinked alginate particles. The obtained system was firstly studied in vitro, and then applied in the regeneration of a cranial bone lesion in a rat model.

Chapter 9. Biomimetic Methodology to Produce Polymeric Multilayered Particles for Biotechnological and Biomedical Applications

This chapter demonstrates that the superhydrophobic surfaces methodology is a versatile technique where multicompartmented (core/shell and multilayered particles) may be produced in fast way and under dry conditions. Two different approaches were proposed: cells encapsulated in the external layer of core/shell particles composed by Dex-MA/alginate, respectively; and model drugs encapsulated in Dex-MA core/shell and multilayered particles. The characteristics of both complex structured spherical systems were studied in order to evaluate their potential for biomedical and biotechnological applications.

Section IV. Concluding Remarks

Chapter 10. Conclusions and Future Perspectives

The last chapter of this thesis describes the main conclusions of the work developed. To complement this information, a reflection about the current limitations and the future perspectives are also reported.

Section I

General Introduction

Chapter 1

Micro/Nano Structured Superhydrophobic Surfaces in the Biomedical Field. Part I: Basic Concepts and Biomimetic Approaches

1.1. Abstract

Inspired by natural structures, great attention has been devoted on the study and development of surfaces with extreme wettable properties. The meticulous study of such natural systems revealed that the micro/nano topography of the surface is critical to obtain unique wettability features, including superhydrophobicity. However, the surface chemistry also has an important role in such surface characteristics. As the interaction of biomaterials with the biological *milieu* occurs at the surface of the materials it is expected that synthetic substrates with extreme and controllable wettability ranging from the superhydrophilic to the superhydrophobic regimes could bring new possibilities of new investigations of cell-materials interactions on non-conventional surfaces and development of alternative devices with biomedical utility. This chapter will describe in detail how proteins and cells interact with micro/nano structured surfaces exhibiting extreme wettabilities.

This chapter is based on the following publication:
Lima A. C. and Mano J. F., Micro/Nano Structured Superhydrophobic Surfaces in the Biomedical Field. Part I: Basic Concepts and Biomimetic Approaches, Nanomedicine (Lond.), 10(1), DOI: 10.2217/NNM.14.174 (*In press*).

1.2. Introduction

The surface of the biomaterials plays a relevant role in determining the outcome of the interactions between the materials and the biological environment. The properties of the surfaces manage the deposition of biomolecules and microorganisms, as well as adhesion, spreading, growth, migration and position of cells [1]. Significant properties of the surfaces of biomaterials include chemistry, elasticity, morphology and wettability. The manipulation of these characteristics has been emerged as an important point of research in materials science in order to achieve the set of the properties more appropriate for specific biological functions. In this chapter we will focus our attention on the pertinence of surfaces wettability in the biomedical field, specifically at the level of the interactions of cells and proteins with superhydrophobic/superhydrophilic platforms.

Surfaces with extreme wettabilities combined with low/high adhesive properties have been biomimetized after an intensive investigation to understand how Nature has developed surfaces with such characteristics. The ability to produce synthetically such kind of structures has attracted huge interest due to their potential for applications in microfluidic, controlled drug delivery and self-cleaning surfaces [2].

Wettability is currently evaluated by the static and dynamic behavior of a liquid droplet over the surface [3]. The apparent contact angle (CA, θ), which is the angle formed by a liquid droplet on the three phase contact line – Figure 1.1, A – characterizes the static behavior. The dynamic comportment is evaluated by the sliding angle (α, the inclination angle of the surface that cause the droplet roll off) and contact angle hysteresis (CAH, the difference between advancing and receding CA) (Figure 1.1, B). Based on these definitions, the surface is classified as wetting, if the CA is lower than 90° and as nonwetting, if the CA is higher than 90°. When the liquid droplet is water the surfaces are called “hydrophilic” and “hydrophobic”, respectively (Figure 1.1, C and D) [2]. In terms of energy, wettable surfaces exhibit high values which may vary between 500 and 5000 mNm^{-1}. Conversely, nonwettable surfaces are characterized by low surface energy with values ranging from 10 to 50 mNm^{-1} [2].

One type of nonwettable surfaces very well explored in the last years are the superhydrophobic ones, characterized by exhibiting water CAs greater than 150° (Figure 1.1, E). There are two types of superhydrophobic surfaces differing in the adhesive properties. If the CAH is lower than 5° the surface is non-adhesive and at minimum inclination, the droplets of water roll off. Otherwise, if the CAH is higher, the water droplet stay preferentially adhered onto the surface.

The cooperation of the topographic design of the roughness with the intrinsic chemistry of the materials defines the wettability of the surfaces. In terms of topography, the existence of micro/nano roughness affects significantly the wettability properties of the materials since it increases the CA in low energy

surfaces and decreases it in high energy surfaces [4]. The most relevant traditional parameters to characterize the roughness of the surfaces (root-mean-square, correlation length, fractal dimension) were reviewed elsewhere [5], where it was also detailed the influence of such parameters in the wetting state of hierarchical natural structures.

In the case of low adhesive superhydrophobic surfaces the existence of a hierarchical roughness from the nano to the micro scale, lead to a minimal contact between the liquid and the surface. The water dispensed onto this type of platforms acquires almost a spherical shape, in order to minimize the energy, being suspended on the top of the micro/nano structures that compose the surface and at minimal inclinations the droplets roll off [6]. In high adhesive surfaces the droplets also acquire a near-spherical shape due the presence of micro/nano structures but do not roll off easily. The different design of the surface features, when compared with low adhesive surfaces, explains the different behavior. In general the high adhesive superhydrophobic surfaces present a larger pitch which allows the liquid impregnation into the microstructures but only partially within the nanostructures [7].

Physical models have been proposed to rationalize the effect of roughness and surface energy. The Young model (Figure 1.1, F) describes the contact between a sessile drop onto rigid, homogeneous, flat and inert surfaces - ideal smooth surfaces. Wenzel´s (Figure 1.1, H) proposed an equation to predict the influence of the surface roughness or morphology on the CA [3,4]. In this model it is assumed that water penetrates into the grooves of the surface structures. Otherwise, the Cassie-Baxter model (Figure 1.1, G) depicts the case in which the air bubbles entrapped inside the grooves of the topographic features prevent the water penetration, meaning that the liquid is only in contact with the top of the exposed protrusions. Transitions from the Cassie-Baxter to Wenzel state may occur and an intermediate state may be achieved (Figure 1.1, I). This shift is usually caused by the non-homogeneous distribution of structural and chemical features or even droplets press and impact [4].

Currently, it is well know that the chemistry and the presence of micro/nano structures constitute key parameters influencing directly the performance of implantable materials due to the interaction with blood or extracellular matrix proteins as well as with the different cell types - such cross-talk between biomaterials surfaces and all biological components will strongly dictate the integration or rejection of the devices [8]. The surface of the materials constitutes the first line of contact with the biological parts not only in implanted materials but also in devices for diagnosis, treatment and diseases prevention.

In the last 5-10 years, much work has been performed in the development and application of superhydrophobic surfaces but, until now, to the best of our knowledge a compilation of the most recent applications in the biomedical field was never presented.

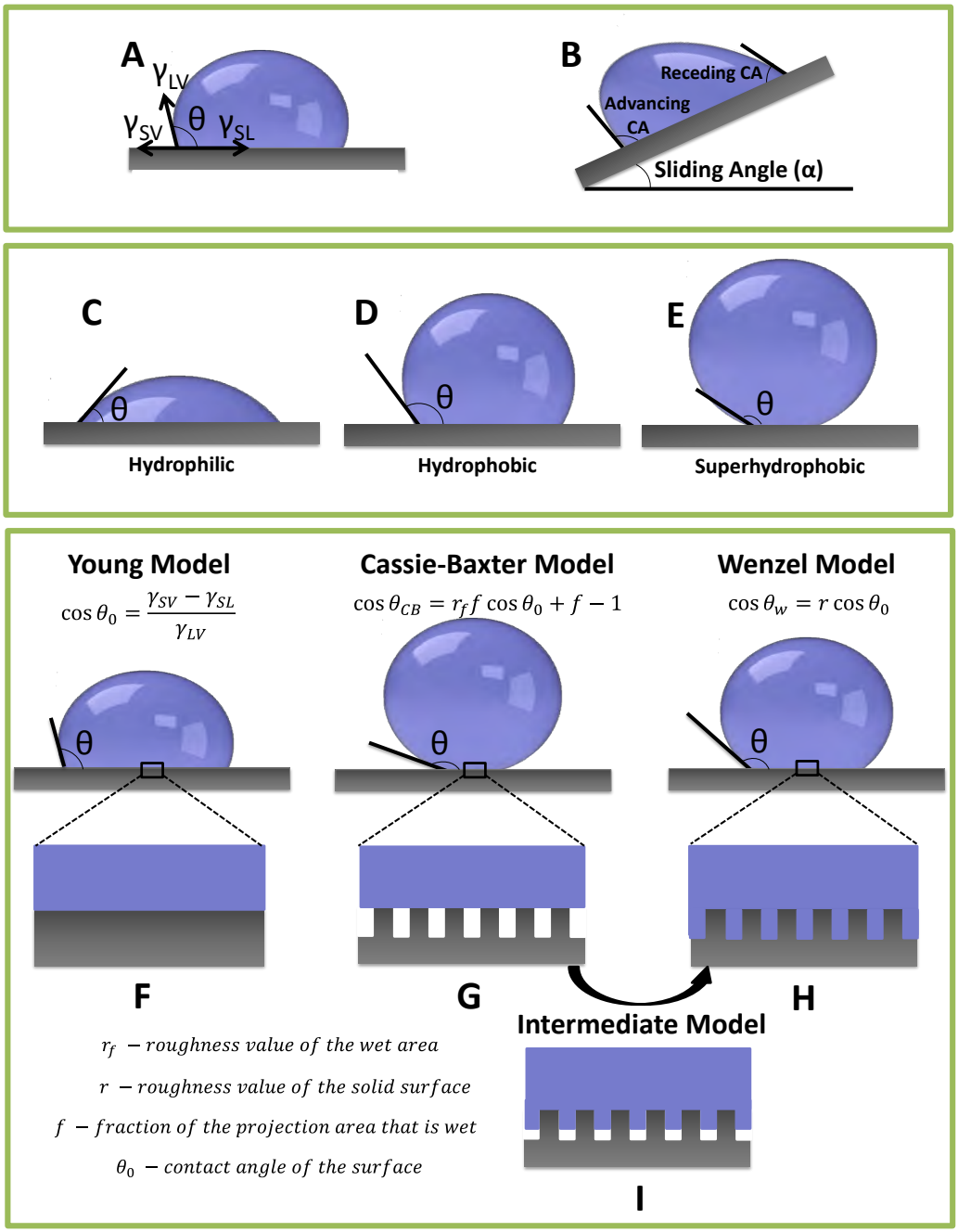

Figure 1.1. Liquid droplets contacting solid surfaces form a contact angle θ where 3 different interfaces are involved: solid/liquid (SL), liquid/vapor (LV) and solid/vapor (SV). The wettability of the surfaces is evaluated regarding the static and dynamic behavior of the droplets. The static conditions comprise the apparent contact angle (CA, θ) which is the angle formed by a liquid droplet on the three phase contact lines (A). The dynamic behavior is related to the sliding angle (α), this means the inclination angle of the surface which cause the droplet roll off; and the contact angle hysteresis (CAH) determined by the difference between advancing CA and receding CA (B). Depending on the CA formed by a water droplet, the surfaces can be hydrophilic (θ<90°, C), hydrophobic (θ>90°, D), superhydrophobic (θ>150°, E) and superhydrophilic (non represented). Developed mathematical models could explain the droplet-surface interaction: the Young's (F) model relates the CA to interfacial tensions (energies, γ) in an ideal smooth surface; Cassie-Baxter (G), Wenzel´s (H), and the intermediate (I) models have in consideration the effect of surface roughness.

We will first overview the different repellent surfaces found in Nature, detailing the relationship between micro and nano structures and wettability. Such section will be followed by a brief description of the recreation, at the lab scale, of the most relevant micro/nano structured natural surfaces. This first part will also highlight the interactions of the proteins and cells with micro and nano structured surfaces, whereas the most important medical applications of the superhydrophobic surfaces will be compiled in the chapter 2 of this thesis.

1.3. Surface Micro/Nano Structures and Special Wettability of Natural Systems

Natural systems offer us a huge number of examples of surfaces with very peculiar properties in terms of structures and functions. The perfect combination of both allows the achievement of maximal performance for a certain role. Exploring plants and animals enables to find a huge diversity of complex surfaces – see Figure 1.2.

The most well-known and studied natural superhydrophobic structure is the isotropic surface of the lotus leaf (Figure 1.2, E). The extreme water-repellent properties of such biosurfaces results from the dual-scale hierarchical roughness, which is composed by papillose epidermal cells (Figure 1.2, E.1), with sizes comprised between 5 and 10 μm, covered by epicular waxes with approximately 150 nm (Figure 1.2, E.2) [9]. When water droplets falls on the lotus leaf, they are just in contact with the hydrophobic wax crystals on the top of the papillae, meaning that the contact between droplets and the surface is minimal. The hierarchical structure of the leaf surface is one of the promoters of CAs higher than 150° and CAH lower than 5°. Such characteristics are crucial for the self-cleaning effect; the droplets easily roll off the leaf carrying out contaminating particles (Figure 1.2, A) [10]. Lotus leaves are then classified as non-adhesive superhydrophobic surfaces.

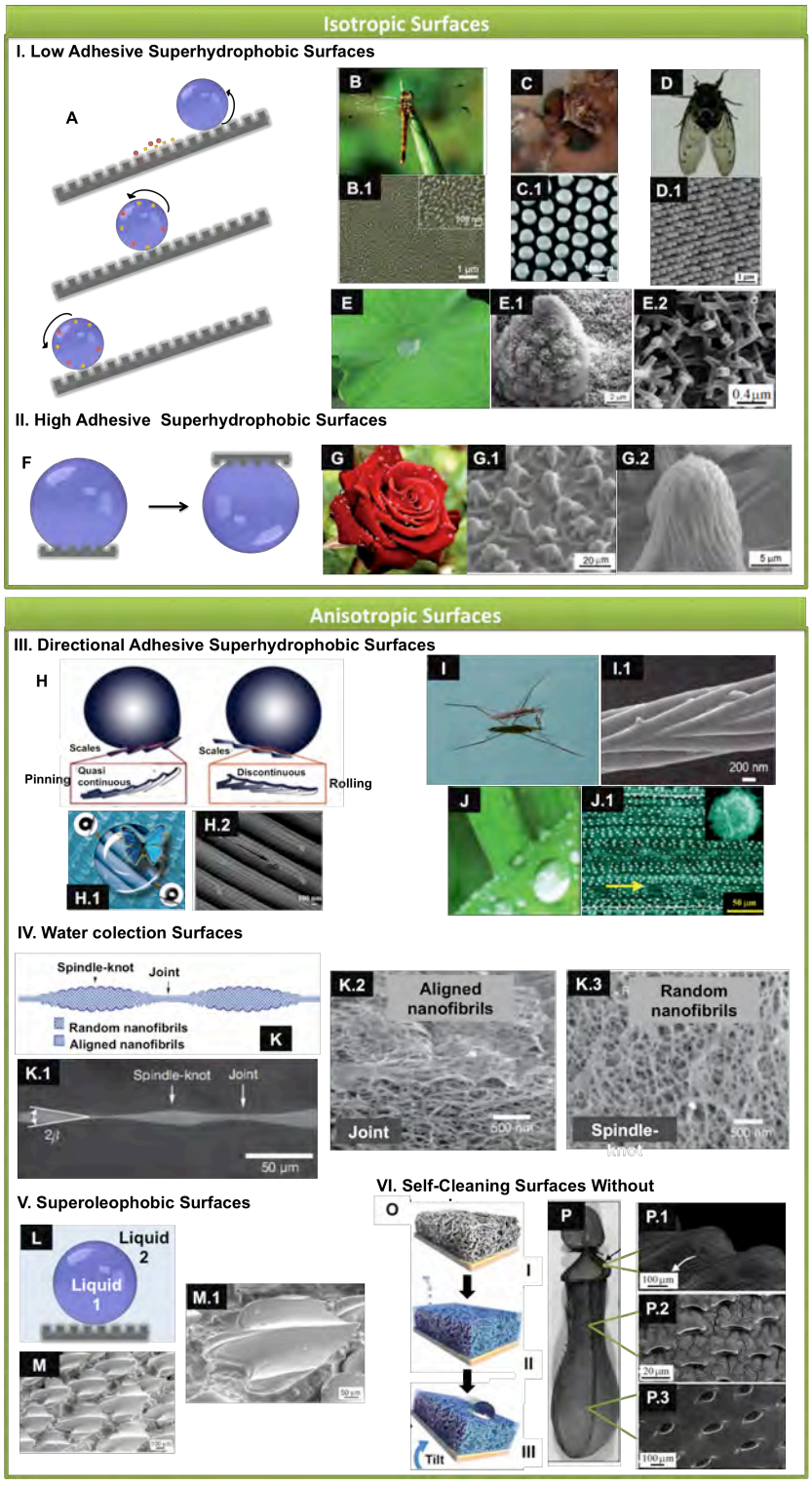

Figure 1.2. Examples of isotropic and anisotopic micro/nano structured surfaces found in Nature. Superhydrophobic isotropic surfaces are the most well studied structures and include low adhesive (I) and high adhesive (II) structures. Low adhesive superhydrophobic surfaces exhibiting self-cleaning effect (A) comprise insect wings (B, B.1), mosquito eyes (C, C.1), cicada wings (D, D.1) and lotus leaf (E, E.1-2), where the water droplets roll off easily when the surface is slightly inclined. High adhesive surfaces (F) as the case of some rose petals (G, G.1-2) have the capacity to retain the water droplets without roll off. Anisotropic natural structures exhibit directional adhesion (III). Representative examples are butterfly wings (H, H.1-2), water stride legs (I, I.1) and rice leaves (J, J.1). Other substrates could be used to collect water (IV), such as spider silk (K, K.1-3);

repel oil products (V) when surrounded by liquids (L) as it is the case of shark skin (M, M.1); or even have self-cleaning properties where the droplets slip without rolling off (VI; O) being the most well-known case the *Nepenthes pitcher* plant (P, P.1-3). The scanning electron microscopy images of each natural system show that independently of the general behavior of the surfaces, they are composed by a hierarchical arrangement of micro and nano topographic structures.

B, B.1, G and I, adapted from [77] with permission of RSC; C and C.1, adapted from [78] with permission of Wiley; D, D.1 and H.1, adapted from [26] with permission of Wiley; E, E.1-2, adapted from [79] with permission of the authors; G.1-2, adapted from [7] with permission of ACS Publications; H and H.2, adapted from [80] with permission of RSC; I.1, adapted from [81] with permission of NPG; J and J.1, adapted from [82] with permission of Wiley; K and K.1-3, adapted from [14] with permission of NPG; M and M.1, adapted from [83] with permission of IOP Publishing; O, adapted from [25] with permission of NPG; P, P.1-3, adapted from [84] with permission of Springer.

An opposite effect is displayed by the rose petals which are also superhydrophobic but have the ability to retain small water droplets without rolling off when the surface is inclined or even tilted down (Figure 1.2, F and G) [7]. The adhesive effect derives from their array of micropapillae, comprising diameters of *ca.* 16 μm and heights of *ca.* 7 μm (Figure 1.2, G.1), with nanoscaled cuticular folds, *ca.* 730 nm in width, on their top (Figure 1.3, G.2) [11]. When compared with the lotus leaf surface, rose petals have higher distances between the microstructures. The liquid droplets deposited onto such structures penetrate into the microscale grooves and just partially between nanostructures due to the formation of air gaps (Wenzel model) [7,12], resulting in a strong adhesion between the liquid and the rose petal surface.

Nature also developed anisotropic surfaces in which the droplets of water can roll off following a preferential direction dictated by the structural features. Remarkable examples are butterfly wings (Figure 2, H), water stride legs (Figure 1.2, I) and rice leaves (Figure 1.2, J). In the case of butterfly wings, they have multiscale structures composed by aligned shingle-like scales (Figure 1.2, H.1). Flexible nanotips are on the top of the ridging nanostrips both rearranged in a certain direction (Figure 1.2, H.2). Such oriented structured surface allows the adhesion and directional moving of the liquid on the solid surface. Similar behavior could be seen in rice leaves [13].

Another type of natural surfaces allows the collection of water from the atmosphere in order to ensure the survival of the biological system under extreme drought environments. The most well-known cases are the desert beetles, cactus spines and spider silk (Figure 1.2, K and K.1). For example, in the case of the spider silk two main driving forces act simultaneously allowing the propelling of water droplets through the fibers: (I) the differences of surface free energy along the fibers and (II) the pressure differences between the inner and exterior of the water droplets. The differences in free energy and droplet pressure are caused by the intercalary spindle knots composed by random nano fibrils (Figure 1.2, K.3) and joints composed by aligned nano fibrils (Figure 1.2, K.2). The droplets are condensed and targeted to surround the spindle knots [14].

The previous described examples are air/liquid/solid systems, meaning interaction of liquids with solid-air surfaces. However, there are liquid/liquid/solid natural systems that have recently attracted researchers' attention. Such solid surfaces (*e.g.* sharkskin (Figure 1.2, M), fish scales and clam shells) present liquid repellency when involved by a liquid environment (Figure 1.2, L). The surfaces are maintained clean when surrounded by oil polluted water and exhibit anti-bioadhesion properties. A detailed study of shark skin revealed the presence of a kind of tooth-like scale arrays (dermal denticles) with longitudinal grooves aligned according to the water flow direction (Figure 1.2, M.1). Due to the movement of the water through the surface structures, shark skin has low drag and prevents the adhesion and growth of marine organisms as well as the contamination by oily substances [15]. The understanding of the underlying phenomenology of such natural surfaces could have relevance in the biomedical area as it could help in the design of new antifouling substrates, channels and tubes with low dragging in fluid transport, or surfaces with particular biological effects upon in contact with cells and tissues.

Although differently to the lotus leaves, Nepenthes pitcher plants (Figure 1.2, P and P.1-3) present a very peculiar self-cleaning effect. The liquid droplets slip instead of rolling along the surface (Figure 1.2, O). This type of plants is well known due to their capability to capture and digest arthropods, absorbing nutrients from them, after their slipping through the walls of the plants cavities [16]. Depending on the nutritional requirements of the plant, the inner surface of the pitcher switch from a wet state, during which the insects slip, to a dry state, where anchorage points are provided to prevent the insects sliding. The wettability is then a key factor in the survival of these plants. In this natural system, the micro roughness does not increase the hydrophobicity as it occurs in lotus leaves. The organized ridges that composed the roughness of the pitcher act as capillary forces inducing the rapid spreading of the water droplets along the wet surface, even against gravity forces [17].

1.4. Biomimetic Surfaces

During the course of evolution, biological systems have achieved distinct intelligent processes and properties relevant for their survival. The capacity of adaptation of the natural systems, in order to circumvent adverse conditions has inspired engineers to develop new functional materials [18]. Detailed analysis of the previous described natural structures revealed that the intrinsic materials properties and the micro/nano topographic structures play a crucial role in the wettability nature of the surfaces. These unique and versatile properties have led to the design and creation of novel superantiwetting surfaces: (I) Superhydrophobic (Figure 1.3, I) [19]; (II) Superoleophobic (Figure 1.3, II) [20,21]; (III) Superamphiphobic (or Superomniophobic) (Figure 1.3, III) [22]; (IV) Smart switchable (Figure 1.3, IV) [23]

(V) Anisotropic surfaces/water collecting surfaces [24] and (VI) Slippery liquid-infused porous surfaces (SLIPS) [25].

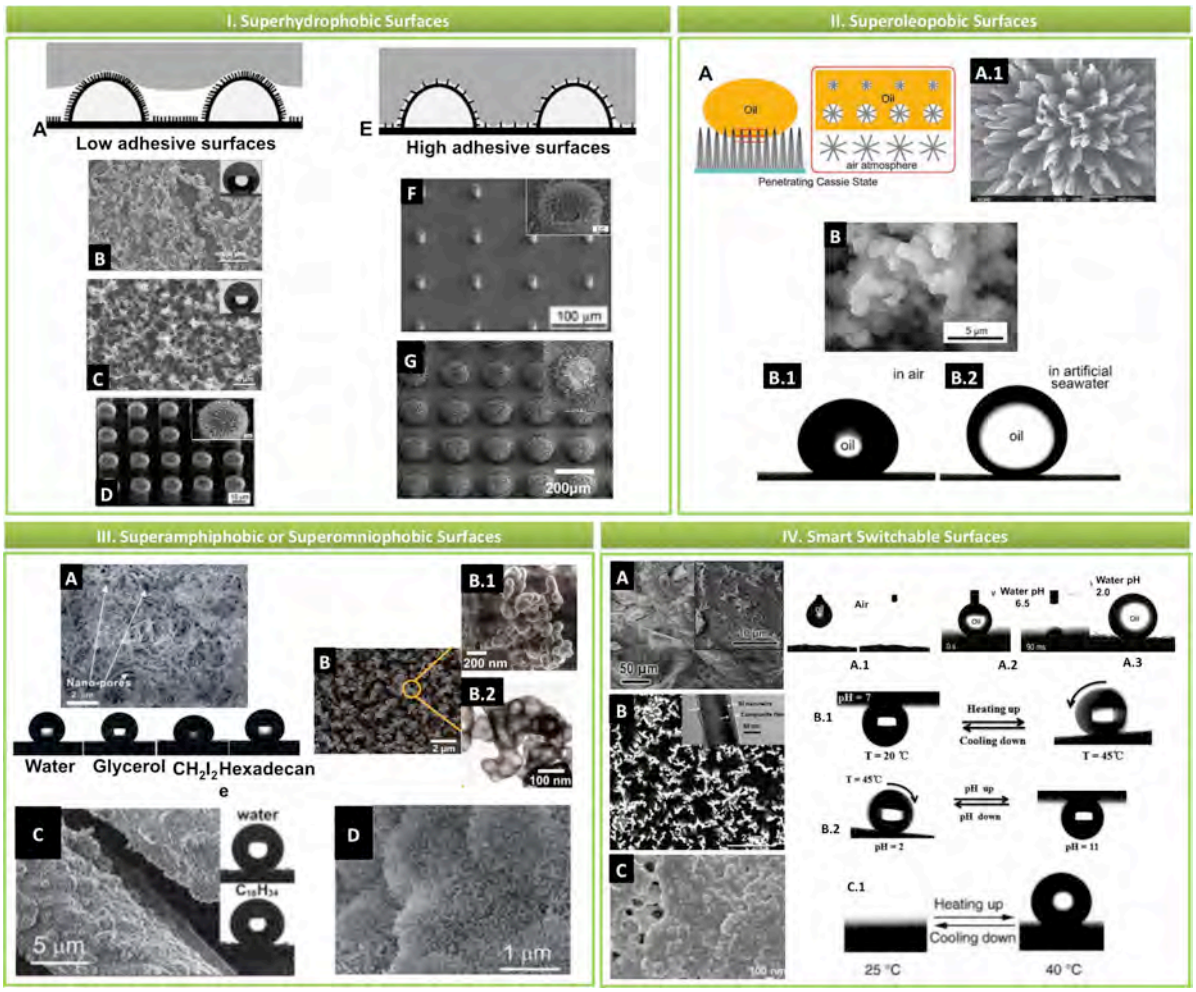

Figure 1.3. Examples of micro/nano structured artificial surfaces produced by inspiration from natural systems. I) Examples of superhydrophobic surfaces with low adhesion where the liquid droplets are suspended on the top of the nano structures (A): polystyrene (B), copper (C) and a micropatterned Si replica (D). Examples of high adhesive superhydrophobic surfaces, where the water enters through the micro exposed elements but air pockets prevent the penetration into the nano roughness (E), are: micro patterned epoxy resin coated with nanostructures of n-hexatriacontane (F) and hierarchical hairy carbonaceous fibers deposited on micro patterned Si (G). II) Superoleophobic surfaces of $Cu(OH)_2$ nanoneedle arrays capable to control the oil adhesion depending on the nanostructures at the surface and the preloads on the oil droplet (A, A.1) and aluminum coated with a polyelectrolyte multilayer treated with perfluorooctanoate which repels oil in dry and wet environments (B, B.1-2). III) Surfaces capable to repel both water and organic liquids are named superamphiphobic or superomniophobic. Examples are coralline-like structured surfaces obtained by spraying nanocomposites of fluorinated multi-walled carbon nanotubes and fluorinated polyurethane (A); surfaces obtained by carbon nanospheres deposition, coated with a silica shell (B), in which the carbon core was removed by calcination (B.1), revealing a structured silica coating with holes (B.2); cotton textiles coated with micro and nano silica particles (C); and etched and fluorinated aluminum (D). IV) Smart surfaces capable to change their behavior when subjected to a certain stimulus have also been developed: textile surfaces capable to switch from superoleophilic to

superoleophobic when immersed in a certain aqueous medium (A, A.1-3); hierarchical structured surfaces coated with poly(*N*-isopropylacrylamide-*co*-acrylic acid) (PNIPAAm-*co*-AAc) (B) which are adhesive or non-adhesive depending on the temperature (B.1) and on the pH of the droplet (B.2); and silicon coated with PNIPAAm (C), surfaces that depending on the temperature are superhydrophilic or superhydrophobic (C.1).

I) A, E and F adapted from the reference [7] with permission of ACS Publications; B and C adapted from the reference [30] with permission of Springer; D, adapted from the reference [85] with permission of RSC; G, adapted from the reference [86] with permission of Wiley. II) A and A.1, adapted from the reference [87] with permission of Wiley; B and B.1-2, adapted from the reference [88] with permission of ACS Publications. III) A, adapted from the reference [89] with permission of RSC; B and B.1-2, images were adapted from reference [90] with permission of AAAS; C, adapted from the reference [91] with permission of ACS Publications; D, adapted from the reference [92] with permission of RSC. IV) A and A.1-3, adapted from the reference [93] with permission of NPG; B and B.1-2 the images were adapted from the reference [94] with permission of RSC; C and C.1 images were adapted from the reference [95] with permission of Wiley.

The design of artificial bio-inspired surfaces involves up to five steps: (I) the search and subsequent detailed study of the unique wetting phenomena of the natural structure; (II) study of the correlation between multiscale structures and the wettability properties; (III) design and synthesis of adequate molecules; (IV) design of the multiscale structures; and (V) surface fabrication [18,26].

Lotus leaf has been the main inspiring natural source to develop artificial non-adhesive superhydrophobic surfaces. Two strategies have been traditionally used: (I) creation of micro/nano roughness onto low surface energy materials or (II) modification of micro/nano rough surfaces with materials owning low surface energy [27]. Combining physical and chemical methods, namely lithography, vapor deposition, plasma technique, sol-gel processing, layer-by-layer, among others, as reviewed elsewhere [28], two general designs may be obtained: surfaces with micro/nano random structures [29–33], and surfaces with controlled topographic features [34–37]. A recent review reported the latest advances in the general design of artificial superhydrophobic surfaces [19]. When the obtained micro/nano structured surfaces do not achieve the desired CA or sufficiently low surface energy to perform a certain function, other strategies were developed to circumvent this issue. In general, post-fabricated surfaces could be treated with self-assembled monolayers of alkanothiols, organic silanes, fatty acids, aromatic azide or spin-coated with perfluorononane [28].

Usually, the organic solvents are polar and present lower surface tensions than water (for example, n-hexadecane 27.5mNm^{-1}, n-decane 23.8mNm^{-1} versus water 72.8mNm^{-1}) [38], which makes more difficult the production of surfaces that repeal organic liquids than superhydrophobic ones. Nevertheless, superoleophobic surfaces may also be obtained combining micro/nano roughness and coatings using materials with very low surface energy [39–42].

Most of the developed artificial superoleophobic surfaces are oil repellent when surrounded by liquids (liquid/liquid/solid systems). However, the evolution in surfaces preparation allowed the production of

solid/air/liquid superoleophobic systems. High adhesive properties (equivalent to water adhesion onto rose petals) of artificial superoleophobic platforms turn difficult the organic droplets rolling off and consequently prevent the self-cleaning effect [39,43–45]. Artificial self-cleaning surfaces with capability to repel organic substances were created using fish scales [15,46] and Nepenthes pitcher [25] as sources of inspiration. The amazing slippery properties of Nepenthes pitcher lead to the development of four-phase systems, namely air/liquid/liquid/solid surfaces, denominated by SLIPS [25]. SLIPS-based systems are composed by micro/nano structures embedded with a lubricant fluid. Differently from lotus leaves, these natural structures demonstrated slipperiness, without hysteresis, of pure or even complex liquids: blood and oil, ice, dust, insects and even bacteria [47,48]. The lubricant forms a continuous film, meaning that the friction onto the micro/nano structures of the solid surface is very low. The film has the same function as the air pockets on lotus leaves [25]. In addition, after a physical damage, SLIPS have the capability of self-healing [25]. Just selecting a lubricant immiscible with water and oils [49], SLIPS may exhibit omniphobic properties [22].

Functionalized surfaces capable to switch their wettability in a reversible way, as a response to an external stimuli (temperature, pH, photon energy, electric field, humidity, electrochemical and chemical treatments) [2] have been proposed due to increasing interest for a wide variety of applications. An overview of this kind of surfaces is reported elsewhere [10]. However, irreversible modifications of the physicochemical properties of super-repellent surfaces could also be important for their application or integration in other devices. Accurate, controllable, cost-effective and fast techniques to perform surface modifications/patterning are challenging [50]. The possibility to tailor optical, mechanical, chemical, wettable, among others characteristics, in confined and pre-selected areas has allowed the production of arrays which could be used as microfluidic devices and as screening chips. A detailed description of the applications of patterned superhydrophobic surfaces in biomedical field will be reported in the chapter 2 of this thesis. In general, there are two possibilities to control the wettability of the surfaces: (I) playing with the organization and spatial distribution of the micro/nano roughness and (II) modifying the chemical properties of the micro/nano structured surfaces by exposing hydrophilic or hydrophobic groups or even bonding/adsorbing biochemical cues [51]. For example, the increment of oxygen-rich groups is a pathway to increase the wettability of the surfaces. The treatment of poly(L-lactic acid) (PLLA) and polystyrene (PS) superhydrophobic surfaces by plasma and UV/Ozone exposure have been demonstrated useful to control the surface wettability [31, 52, 53]. Such treatments induced the formation of oxygen-containing species (C-O, C=O, O-C=O) responsible to increase the surface free energy and consequently turn the surface more wettable independently of the micro/nano roughness. In both PLLA and PS cases, depending on the

exposure time, the wettability of the surfaces was controlled within extreme ranges of CAs, in an accurate manner. The use of masks (generally platforms with predefined holes of controlled geometries) is a straightforward approach to confine the desired modifications into pre-selected areas, allowing the production of patterned superhydrophobic surfaces with the most favorable design for the proposed application.

Having in consideration that smart and bioinstructive substrates have been widely used in the biomedical field [54, 55] we hypothesized that the combination of such features with extreme wettability could bring new possibilities of developing devices with unique features for both *in vivo* and *ex vivo* applications.

1.5. Interaction of Cells and Proteins with Superhydrophobic Surfaces

The interaction between cells and materials at the chemical or even physical level is extremely important for the success of therapeutic/diagnosis strategies involving implantable biomaterials [56]. Conceptually, four stages are involved in cell-material interactions: (I) adsorption of proteins from the biological milieu; (II) cells perception and sensing of the adsorbed cues; (III) cell attachment and finally (IV) the spreading or other biological consequence of the cells.

Studies on cell-material interactions on surfaces varying their wettable properties, have been greatly focused within the hydrophilic-hydrophobic range (20°<CAs<110°). However, the curiosity about the biological response beyond such contact angles interval have been encouraging the development of new works in order to get further insights on such complex phenomena.

The unique properties of the superhydrophobic surfaces triggered an increasing interest in their application in the biomedical field. However, the biological performance of such type of surfaces needs to be previously understood with maximum detail. Just a very few works have been published reporting the interaction of proteins or cells with such micro/nano structured highly repellent surfaces. As explained in the previous sections of this chapter, the properties of the superhydrophobic surfaces are related with their micro/nano structured surface and surface chemistry, being both properties directly correlated with the wettability. Then, it is critical to understand the effect of these characteristics, in an individual manner, on protein and cells behavior. The current status of this field will be described in detail in the follow sub sections.

1.5.1. Proteins Adsorption

The first happening, when any material is implanted in the human body, is the coating of the surface by proteins present in the blood or interstitial fluids (ECM proteins). Hydrophobic interactions, electrostatic attraction, van der Waals forces and hydrogen bonding are involved in protein adsorption [57–58]. In a general way, proteins tend preferentially to adsorb strongly on non-polar than on polar, on high surface tension than on low surface tension and on charged than on non-charged surfaces [59]. The destabilization of the proteins caused by non-polar surfaces facilitates the protein structural reorganization and reorientation leading to strong inter protein and protein-surface interactions [60]. In addition, it was also demonstrated that topography has a great influence on protein adsorption [57]. The adsorption can be more pronounced onto the nanostructured surfaces due to the existence of higher number of active sites as a consequence of higher surface area. However, the existence of roughness at the micro or nano scale is closely related to the surface wettability that could have an independent effect of the change in the exposed surface area. Several works have been developed focusing the interaction of proteins and cells with micro/nano structured surfaces with extreme repellent properties, as it was recently reviewed elsewhere [61,62]. Table 1.1 compiles the studies reported in literature focusing the interaction of proteins and cells with superhydrophobic surfaces.

Table 1.1. Overview of the literature reports involving the study of proteins adsorption and cells adhesion/proliferation onto materials with superhydrophobic properties.

Natural Inspiration	Artificial Material	Modification Performed	Contact Angle (CA)	Biological Entity	Observations	Ref.
Lotus leaves	ePTFE	Biaxial stretching	CA >150˚	HSA	No adsorption was detected under environmental conditions; The degassing of protein solutions and surfaces improved the protein adsorption due to the air pockets removal, which increased the contact between the protein solution and the surface.	[63]
Lotus leaves and bird feathers	TiO_2 nanotubes film onto a titanium substrate	Electrochemical anodization Patterning: photocatalytic lithography	0<CA<154˚	BSA FBS Human fetal osteoblast (hFOB 1.19) Human fibroblasts from osteosarcoma (MG63) HeLa cells	Low amount of BSA bound to the superhydrophobic domains in the presence of trapped air; Significant amount of BSA was bound to the superhydrophilic domains with trapped air; After air removal, the protein adsorbed was similar in superhydrophobic and superhydrophilic areas; The protein composition of the cell suspension affected the adhesion of the cells. The effect of entrapped air was not visible; Cell adhesion did not correlate with bound protein in a one-for-one way.	[64]
Lotus leaves	PS	Phase separation	CA ≈160˚	FN Murine osteoblastic cell line (MC3T3-E1)	FN adsorbed in lower density and in a different conformation onto superhydrophobic PS when compared with normal PS; Uneven distribution of FN in superhydrophobic PS with micro-regions not covered by the protein; In superhydrophobic surfaces the vinculin was randomly distributed inside the cells; the actin cytoskeleton is not completely matured; The low FN density adsorbed onto superhydrophobic surfaces led to lack of focal adhesion formation and actin organization; Cells were able to proliferate and maintain a stable population up to 21 days on the superhydrophobic PS but in a low density than normal PS.	[65]
Lotus leaves	PS	Phase separation Post-fabrication treatment: Argon plasma	0<CA<151.4˚ Gradient of wettabilities	FN Myoblast cell line	Amount of FN adsorbed onto the surfaces was found to decrease monotonically with increasing wettability; The optimal FN conformation was observed on hydrophilic surfaces due to their surface nanotopography and surface energy; Non-monotonic dependence of the degree of differentiation on surface wettability: the maximal enhancement of differentiation was obtained on the hydrophylic surfaces; The alteration on FN conformation onto superhydrophobic areas delayed the cell adhesion; The cell density increased substantially with increasing wettability and it was observed stabilization between hydrophilic and superhydrophilic platforms.	[66]
Lotus leaves	PS and PLLA	Phase separation	CA≈150˚	BSA Murine osteoblastic cell line (MC3T3-E1) Bovine articular chondrocytes (BCH)	Protein adsorption was lower in superhydrophobic surfaces (rough substrates), when compared to more wettable substrates (smooth substrates); No differences were found on protein adsorption between superhydrophobic PS and PLLA, despite the differences in the roughness morphology; Cell viability was lower onto rough than at smooth counterparts, which could be correlated by the amount and conformation of adsorbed protein; The proliferation of both cell types was inhibited onto rough surfaces;	[67]

					MC3T3-E1 cells seemed to be less affected than BCH.	
-	Titanium	Etching and oxidation	CA≈92-157˚	Human fibroblasts from osteosarcoma (MG63)	Surfaces just exhibiting nanostructures seemed to regulate osteoblast proliferation; The differentiation of osteoblast was not significantly affected by the absence of micro roughness; The combination of micro/submicro/nano structures resulted in a synergistic effect on cell differentiation and local factors secretion (osteoprotegerin and VEGF).	[72]
Lotus leaves	PLLA	Phase separation	CA≈154˚	Rat bone marrow derived stem cells	Superhydrophobic (rough) surfaces inhibited cell adhesion and proliferation when compared with non-superhydrophobic (smooth) substrates; The repellence of the surfaces prevented their contact with the cell culture medium, and consequently the protein adsorption and cell adhesion.	[74]
Lotus leaves	PLLA	Phase separation Post-fabrication treatment: Argon plasma	0<CA<154˚ Gradient of wetabilities	Mouse lung fibroblast cell line (L929)	In comparison with smooth PLLA, almost no cells adhered onto rough PLLA (superhydrophobic surbstrates); The superhydrophobic surfaces treated with plasma lost the water repellence properties in a controlled way until reach a superhydrophilic behavior; The cell attachment onto rough substrates was dependent on wettability; Optimal cell attachment in surfaces with CA ca. 90˚.	[31]
Lotus leaves	PS	Phase separation Post-fabrication treatment: UV/O_3 exposure	0<CA<155˚ Different wettabilities	Human osteoblast cell line (SaOs-2) Mouse lung fibroblast cell line L929 Mouse chondrogenic cell line (ATDC5)	SaOs-2 and ATDC5 cells did not proliferate on superhydrophobic PS but L929 cell line exhibited a good proliferation; The attachment of SaOs-2 was higher for the PS surfaces (rough and smooth) treated for more time; and the high proliferation was observed in rough surfaces treated for intermediate times.	[52]
-	Silicon and a negative tone resist (AZ5214)	Optical lithography (Deep Reactive Ion Etching Process)	160˚<CA<170˚	Neurons and astrocytes	Neuronal-glial co-cultures were successfully supported in the micro/nano roughness surface; 3D neural networks were obtained being closer to the brain structure than 2D cultures.	[75]

The adsorption of human serum albumin (HSA) was studied in expanded polytetrafluororethylene (ePTFE), a commonly used hydrophobic material in biomedical applications. ePTFE may become superhydrophobic upon stretching due to the formation of a fibrillar surface structure [63]. Under ambient conditions no protein adsorption was measured onto the superhydrophobic material. However, when the ePTFE surfaces were degassed, a significant protein adsorption was detected. The air entrapped in the features of the ePTFE surperhydrophobic surface prevented intimate contact with HAS solutions and consequently low protein adsorption. Huang *et al.* [64] confirmed the effect of air trapped on protein adsorption using surfaces coated with TiO_2 nanotubes. The surfaces were patterned with superhydrophobic/superhydrophilic areas. The air trapped in TiO_2 nanotubes prevented the contact of the protein solution with superhydrophobic domains. The protein adsorption was inhibited onto such regions when compared with superhydrophilic ones. However, this was reversed when the surfaces were sonicated and the air trapped in the nanostructures was displaced: more protein was detected in superhydrophobic than in superhydrophilic areas. Once again the extraction of the gas induces the transition from the Cassie-Baxter to a Wenzel regime where the protein solution could contact with a major surface area. Cassie-Baxter-based superhydrophobic surfaces are then considered resistant to protein adsorption due to the trapped air between the micro/nano stuctures, which acts as a "virtual layer" and impedes the subsequent platelet and cell adhesion.

Fibronectin (FN) adsorption was analyzed onto PS superhydrophobic surfaces, a standard material used in cell cultures [65]. The physical modification of the PS platforms did not affect the chemical properties of the surface. Again, lower density of FN with a changed conformation was found onto micro/nano structured surfaces when compared with smooth platforms. As a consequence, the cell behavior was significantly affected [65]. Micro/nano structured PS superhydrophobic surfaces were then chemically modified by plasma treatment in order to investigate the influence of wettability in FN adsorption and conformation [66]. As expected, the amount of FN adsorbed decreased monotonically with increasing wettability, since this protein tend to adsorb in greater amounts onto hydrophobic surfaces. However, the conformation did not follow the same tendency. In micro/nano rough surfaces with hydrophilic properties, the protein adopted a more favorable conformation than in hydrophobic or superhydrophilic areas. This observation highlights a very important point that we consider worth to be studied in more detail, besides the total protein content, surfaces with extreme wettabilities could direct distinct conformational changes in the adsorbed proteins. Protein adsorption onto two different superhydrophobic materials obtained by the same methodology was compared [67]. Superhydrophobic PS and PLLA were prepared using a phase separation method. The different physical properties of the polymers induced the appearance of

completely different topographical structures. Once again, the non-wettable properties of the rough surfaces prevented the contact between the bovine serum albumin (BSA) solution and the surfaces, decreasing the amount of protein adsorbed. No differences were observed between the both materials in examination. Such kind of results suggests that the general wettability characteristics of a surface have a stronger influence on protein adsorption than its specific chemical and topographical properties.

As demonstrated by all of the above described reports, the composition, orientation and the conformation of the adsorbed proteins could be determinant in cell attachment. The adsorbed proteins should exhibit appropriate conformations in order to maintain their biological functions, in particular the capacity to be recognized by the cells. In order to improve the performance of micro/nano structured superhydrophobic surfaces, surface modifications may be advantageous, namely the covalent grafting of key cell adhesive groups or the modification of surface chemistry by increment of the number of oxygen-rich species.

In the opposite case of superhydrophilic surfaces, the higher adsorption of water produces repulsive forces on the proteins preventing their deposition and consequently the adhesion of the cells.

1.5.2. Cells Interactions

Cells sense the surrounded environment through membrane ion channels and a series of receptors. Integrins are the main responsibles for the establishment of connections between the cells and the surface [68] as well as to control cell shape changes, proliferation and cell migration. Integrins are composed by two non-covalently associated subunits (α and β) integrated in the cell membrane. There are several types of α and β subunits and their combination determines the ligand specifity of the integrin. Although it is known that the complex process of cell-biomaterial interactions occurs after protein adhesion, the mechanism itself is not completely understood. It is known, however, that it is dependent on the surface properties (wettability, flexibility, topography, surface charge, chemistry and mechanical), on the type of cells and on the presence of proteins or other biochemical cues [53,56,61,69].

Since topography have a great influence on cell behavior, data have been reported on cell interaction with micro/nano surface structures such as grooves, ridges, steps, pores, wells and nodes at micro or nano scales [70]. Micro and nano patterned surfaces have been studied to understand the effect of the topography in cell behavior. An overview of the potential of chemical and topographical effect on cell-material crosstalk was reported elsewhere [56]. It is very well-known that materials surface chemistry, topography and consequently wettability influence cell stages, namely differentiation, proliferation, matrix production, cell morphology and orientation [71]. One particular example is the influence of surface characteristics in the osteointegration of implanted materials. For example, Gittens *et al.* [72] showed that

combined micro/submicro roughness and a high density of nanostuctures enhanced osteoblast differentiation, new bone formation *in vitro*, a better bone-to-implant contact *in vivo* and improved clinical rates in wound healing [72,73]. Such kind of hierarchical structure mimics the structure of the bone during the remodeling process. The resorption lacunae performed by osteoclasts consist in microscale pits (*ca.* 100 μm in diameter and 50 μm in depth) composed by submicro-scale structures and nano scale features created by fibers of the collagen [72]. Due to the synergistic effect of the combination of structures with different sizes in osteointegration, efforts have been done to obtain tailored hierarchical structured surfaces with appropriated chemical and surface energy properties [72]. Regarding the general properties of the superhydrophobic surfaces we hypothesize interesting possibilities of using such substrates in bone tissue engineering purposes.

Similarly to that described for protein adsorption, the elevated repellency of superhydrophobic surfaces could prevent the contact of the cells with the entire surface area. Consequently the cells just have the chance to adhere onto the peaks of the micro/nano structures exposed onto the materials, limiting the adhesion and proliferation of the cells. On the other hand, the super-repellent surfaces exhibiting a Wenzel state should permit the penetration of the liquids in the micro-roughness, providing more points for proteins and cells adhesion [69]. Therefore any interpretation of the performance of cells adhering to superhydrophobic surfaces should require a careful characterization of how liquids and proteins interact with the micro/nano features of the substrates.

The study of the interactions between bone marrow derived stem cells and PLLA biodegradable superhydrophobic membranes exhibiting random micro/nano surface structures showed an inhibitory effect in cell adhesion and proliferation when compared with smooth PLLA [74]. Veiga *et al.* [31] demonstrated that fibroblast-like cells exhibited a similar behavior when cultured onto the same PLLA surfaces. However, when the surfaces were treated with argon plasma, the hydrophilicity increased due to the formation of oxygen-rich groups on the surface, and the cell attachment was improved. Controlling the plasma treatment, gradients of wettabilities were produced allowing the control of cell adhesion in the space [31]. Based on that, and considering that PS is the standard material used in cell culture, Oliveira *et al.* [52] studied the cell adhesion/proliferation onto superhydrophobic PS, also obtained by a phase separation method. A vast range of wettabilities was obtained by treating the surfaces with UV/Ozone exposure for different times. The treatment did not modify significantly the nano/micro surface structures, but introduced oxygen-containing groups onto the surface, in a similar way of PLLA treated with argon plasma described above. The interaction of different cell types with smooth and rough PS surfaces was extensively investigated [52]. For short culturing time periods (4h and 2 days) the studied cell types

presented a rounder shape in superhydrophobic PS than after 6 days, where a few SaOs-2 (osteoblast-like cells) and ATDC-5 (chondrocyte-like cells) were spread. In smooth PS, all the cell types presented a normal morphology. The cell number over time was significantly high for L929 (fibroblasts) cells than the other cell types, probably due to their intrinsic higher proliferation rate. In addition it was observed that SaOs-2 and ATDC-5 did not proliferate onto rough or smooth PS when compared with normal PS used in cell culture plates. SaOs-2 adherence and proliferation was also studied onto UV/Ozone PS surfaces [52]; such cells showed a preference to hydrophilic environments independently of the roughness of the surface. Such results were also confirmed in another study [67]. In that work, the response of a cell line (murine osteoblastic cell line MC3T3-E1) and a primary cell culture (bovine articular chondrocytes isolated from cartilage of calf legs) seeded onto two different superhydrophobic surfaces (PS and PLLA) was studied in detail. The different roughness of both surfaces reduced the affinity of both types of cells, being the proliferation inhibited, and both cell types exhibited similar behavior. It was concluded that the overall wettability was the main factor affecting the cell behavior and not only the polymer chemistry or surface topography [67].

The above mentioned examples confirmed the huge effect of wettability on cell behavior. The biological behavior could vary according to the cell type. The interaction of primary neurons with superhydrophobic surfaces, composed by nanopatterned pillars obtained by lithography, was studied in order to evaluate the ability for 3D network formation [75]. Neurons presented an enhanced survival rate when compared with 2D standard cultures, which are flat surfaces. They adhered to the pillar sidewalls and pulled between the structures in a suspending position, developing a mature network. In this particular case, the superhydrophobic surface acts as a 3D scaffold. Such substrates could be interesting to perform *in vitro* toxicity assays, as they could constitute a good model to study cancer cells differentiation and migration in a more realistic way.

The previously described works demonstrate that the control of the adsorbed biomolecules and the spatial distribution of adhered cells are highly dependent on the combination of chemical and structural properties of the surface. Taking advantages of the performance of the micro/nano structures superhydrophobic surfaces implantable materials and other kind of devices were develop. An overview of the most relevant applications in biomedical field is compiled in chapter 2 of this thesis [76].

1.6. Conclusions

This review addressed a very concise compilation of the main characteristics of natural structures with extreme repellent properties. Surface topography and chemistry are the key factors to achieve such

behavior. Inspired by the properties of natural surfaces, artificial superhydrophobic platforms have been developed through different processes, combining micro/nano features and low surface energy materials. The unique properties of the superhydrophobic surfaces have been explored regarding their influence in protein adsorption and cell adhesion and proliferation. Though being in a quite early stage, such studies were designed to understand the performance of such platforms in a biological context. Superhydrophobic surfaces have shown to be resistant to protein adsorption; but such effect could be dependent on how liquid interacts with the micro/nano texture (*e.g.* Cassie-Baxter versus Wenzel cases, or self-cleaning versus adhesive surfaces). Comparing with smooth substrates, the adhesion and proliferation of the cells were also affected when they were seeded onto such micro/nano rough surfaces and also when such surfaces were subjected to further chemical modifications. The possibility to manipulate the wettability of the micro/nano structured surfaces both in all extended surface area and in confined sites by using appropriate masks, has been extending the employment of superhydrophobic surfaces in the biomedical field. The most relevant examples will be compiled in the chapter 2 of this thesis.

1.7. Future Perspectives

The behavior of natural repellent systems has inspired the development of artificial superhydrophobic surfaces, however, their application have been greatly focused on materials for industrial applications or improvement of simple tasks in the daily life. Just in the last few years appeared the first reports associated with biomedical applications, but the studies related with biological integration of superhydrophobic surfaces are still in an early stage. More investigation about superhydrophobic surfaces interaction with biological entities and detailed explanations for the phenomena occurred at such kind of interfaces may constitute a driving force to extend future research. Since the protein adsorption is a dynamic process, involving attachment, detachment and conformation changes, the performance of superhydrophobic surfaces when studied in dynamic conditions (flowing environments) could give a more realistic view of those types of interactions. Until now, just static conditions are reported in literature.

A deep understanding of the protein-superhydropobic surfaces interactions is important for the development of biomaterials, since protein adsorption is related with bacteria adhesion and formation of thrombus. In particular more investigation would be required on the conformational organization of adsorbed proteins in surfaces exhibiting wettabilities ranging from the superhydrophilic to the superhydrophobic range.

Many methodologies have been used to modify the surfaces of the materials. However, most of the materials changed to achieve a superhydrophobic behavior are not able to be used in applications inside

human body due to the non-biocompatible properties or even the instability of the surfaces which may cause adverse responses when applied for long time periods. Advances in materials science research have been improved parameters such as stability, robustness and durability of surfaces, but more work is still to be done to obtain high performance and biocompatible superhydrophobic platforms.

We also expect major advances in industrial production of superhydrophobic surfaces, including large areas with homogeneous properties and patterned platforms with areas of contrasting wettabilities. Once again, the stability of the surfaces in order to prevent or avoid the intermediate wettable state, resultant of the transition from a Cassie-Baxter to a Wenzel stage, constitutes a challenge. For example, the design of topographical structures with greater or optimized geometries could be a strategy to achieve more stable surfaces. Such progresses should be accompanied by the latest development micro/nano fabrication technologies.

Moreover, having into account that superomniophobic surfaces are composed by materials and roughness that induce even lower surface energy when compared with superhydrophobic surfaces, the behavior and these surfaces should also be explored in biological context in order to obtain a preliminary overview of body acceptance when the surface of biomaterials show capacity to repeal water and organic (*e.g.* lipidic) molecules.

1.8. Acknowledgements

Ana Catarina Lima is grateful for financial support from Portuguese Foundation for Science and Technology (FCT) through the grant SFRH/BD/71395/2010. The authors also acknowledge the national funds through FCT in the scope of project PTDC/CTM-BIO/1814/2012

1.9. References

[1] Skorb E. V. and Andreeva D.V., Surface nanoarchitecture for bio-applications: self-regulating intelligent interfaces, Advanced Functional Materials 2013, 23: 4483–4506.

[2] Verplanck N., Coffinier Y., Thomy V. and Boukherroub R., Wettability switching techniques on superhydrophobic surfaces, Nanoscale Research Letters 2007, 2: 577–596.

[3] Bellanger H., Darmanin T., Taffin de Givenchy E. and Guittard F., Chemical and physical pathways for the preparation of superoleophobic surfaces and related wetting theories, Chemical Reviews 2014, 114: 2694–716.

[4] Yan Y. Y., Gao N. and Barthlott W., Mimicking natural superhydrophobic surfaces and grasping the wetting process: a review on recent progress in preparing superhydrophobic surfaces, Advanced Colloid Interface Science 2011, 169: 80–105.

[5] Nosonovsky M. and Bhushan B., Biologically inspired surfaces: broadening the scope of roughness, Advanced Functional Materials 2008, 18: 843–55.

[6] Gao L. and McCarthy T. J., The "lotus effect" explained: two reasons why two length scales of topography are importante, Langmuir 2006, 22: 2966–7.

[7] Bhushan B. and Her E. K. Fabrication of superhydrophobic surfaces with high and low adhesion inspired from rose petal, Langmuir 2010, 26: 8207–17.

[8] Yao X., Song Y. and Jiang L., Applications of bio-inspired special wettable surfaces, Advanced Materials 2011, 23: 719–34.

[9] Wang J., Chen H., Sui T., Li A. and Chen D., Investigation on hydrophobicity of lotus leaf: Experiment and theory, Plant Science 2009, 176: 687–95.

[10] Anastasiadis S. H., Development of functional polymer surfaces with controlled wettability, Langmuir 2013, 29: 9277–90.

[11] Feng L., Zhang Y., Xi J., Zhu Y., Wang N., Xia F. and Jiang L., Petal effect: a superhydrophobic state with high adhesive force, Langmuir 2008, 24: 4114–9.

[12] Bhushan B. and Nosonovsky M., The rose petal effect and the modes of superhydrophobicity. Philosophical Transactions of the Royal Society A 2010, 368:4713–28.

[13] Bixler G. D., Theiss A., Bhushan B. and Lee S. C., Anti-fouling properties of microstructured surfaces bio-inspired by rice leaves and butterfly wings, Journal of Colloid Interface Science 2014, 419: 114–33.

[14] Zheng Y., Bai H., Huang Z., Tian X., Nie F. -Q., Zhao Y. and Jiang L., Directional water collection on wetted spider silk, Nature 2010, 463: 640–3.

[15] Bhushan B., Biomimetics inspired surfaces for drag reduction and oleophobicity/philicity, Beilstein Journal of Nanotechnology 2011, 2: 66–84.

[16] Bohn H. F. and Federle W., Insect aquaplaning: Nepenthes pitcher plants capture prey with the peristome, a fully wettable water-lubricated anisotropic surface, Proceedings of the National Academy Science U.S.A. 2004, 101: 14138–43.

[17] Bauer U., and Federle W., The insect-trapping rim of Nepenthes pitchers: surface structure and function, Plant Signal & Behavior 2009, 4: 1019-23.

[18] Liu M., Wang S. and Jiang L., Bioinspired multiscale surfaces with special wettability, MRS Bulletin 2013, 38: 375–82.

[19] Celia E., Darmanin T., Taffin de Givenchy E., Amigoni S. and Guittard F., Recent advances in designing superhydrophobic surfaces, Journal of Colloid Interface Science 2013, 402: 1–18.

[20] Xue Z., Liu M. and Jiang L., Recent developments in polymeric superoleophobic surfaces, Journal of Polymer Science Part B Polymer Physics 2012, 50: 1209–24.

[21] Tuteja A., Choi W., Ma M., Mabry J. M., Mazzella S. A., Rutledge G. C., Mckinley G. H. and Cohen R. E., Designing superoleophobic surfaces, Science 2007, 318: 1618–22.

[22] Kota A. K., Choi W. and Tuteja A., Superomniphobic surfaces: Design and durability, MRS Bulletin 2013, 38: 383–90.

[23] Xin B. and Hao J., Reversibly switchable wettability, Chemical Society Reviews 2010, 39: 769–82.

[24] Hancock M. J. and Demirel M. C., Anisotropic wetting on structured surfaces, MRS Bulletin 2013, 38: 391–6.

[25] Wong T. –S., Kang S. H., Tang S. K. Y., Smythe E. J., Hatton B. D., Grinthal A. and Aizenberg J., Bioinspired self-repairing slippery surfaces with pressure-stable omniphobicity, Nature 2011, 477: 443–7.

[26] Xia F. and Jiang L., Bio-Inspired, smart, multiscale interfacial materials, Advanced Materials 2008, 20: 2842–2858.

[27] Ma M. and Hill R. M., Superhydrophobic surfaces, Current Opinion Colloid Interface Science 2006, 11: 193–202.

[28] Zhang X., Shi F., Niu J., Jiang Y. and Wang Z., Superhydrophobic surfaces: from structural control to functional application, Journal of Materials Chemistry 2008, 18: 621.

[29] Qian B. and Shen Z., Fabrication of superhydrophobic surfaces by dislocation-selective chemical etching on aluminum, copper, and zinc substrates, Langmuir 2005, 21: 9007–9.

[30] Lima A. C., Song W., Blanco-Fernandez B., Alvarez-Lorenzo C. and Mano J. F., Synthesis of temperature-responsive dextran-MA/PNIPAAm particles for controlled drug delivery using superhydrophobic surfaces, Pharmaceutical Research 2011, 28: 1294–305.

[31] Song W., Veiga D. D., Custódio C. A. and Mano J. F., Bioinspired degradable substrates with extreme wettability properties, Advanced Materials 2009, 21: 1830–1834.

[32] Huang L., Lau S. P., Yang H. Y., Leong E. S. P., Yu S. F. and Prawer S., Stable superhydrophobic surface via carbon nanotubes coated with a ZnO thin film, Journal of Physical Chemistry B 2005, 109: 7746–8.

[33] Li Y., Huang X. J., Heo S. H., Li C. C., Choi Y. K., Cai W. P. and Cho S. O., Superhydrophobic bionic surfaces with hierarchical microsphere/SWCNT composite arrays, Langmuir 2007, 23; 2169–74.

[34] Dorrer C. and Rühe J., Some thoughts on superhydrophobic wetting, Soft Matter 2009, 5: 51-61.

[35] Herbertson D. L., Evans C. R., Shirtcliffe N. J., McHale G. and Newton M. I., Electrowetting on superhydrophobic SU-8 patterned surfaces, Sensors Actuators A: Physical 2006, 130-131: 189–193.

[36] Zhu L., Feng Y., Ye X. and Zhou Z., Tuning wettability and getting superhydrophobic surface by controlling surface roughness with well-designed microstructures, Sensors Actuators A: Physical 2006, 130-131: 595–600.

[37] Fürstner R., Barthlott W., Neinhuis C. and Walzel P., Wetting and self-cleaning properties of artificial superhydrophobic surfaces, Langmuir 2005, 21: 956–61.

[38] Zhang J., Wang A. and Seeger S., Nepenthes pitcher inspired anti-wetting silicone nanofilaments coatings: preparation, unique anti-wetting and self-cleaning behaviors, Advanced Functional Materials 2014, 24: 1074–1080.

[39] Xie Q., Xu J., Feng L., Jiang L., Tang W., Luo X. and Han C. C., Facile creation of a super-amphiphobic coating surface with bionic microstructure, Advanced Materials 2004, 16: 302–305.

[40] Kiuru M. and Alakoski E., Low sliding angles in hydrophobic and oleophobic coatings prepared with plasma discharge method, Materials Letters 2004, 58: 2213–2216.

[41] Nicolas M., Guittard F. and Géribaldi S., Synthesis of stable super water- and oil-repellent polythiophene films, Angewandt Chemie International Edition 2006, 45: 2251–4.

[42] Hoefnagels H. F., Wu D., de With G. and Ming W. Biomimetic superhydrophobic and highly oleophobic cotton textiles, Langmuir 2007, 23; 13158–63.

[43] Feng X. J. and Jiang L., Design and creation of superwetting/antiwetting surfaces, Advanced Materials 2006, 18: 3063–78.

[44] Darmanin T. and Guittard F., Molecular design of conductive polymers to modulate superoleophobic properties, Journal of the American Chemical Society 2009, 131: 7928–33.

[45] Zimmermann J., Rabe M., Artus G. R. J. and Seeger S., Patterned superfunctional surfaces based on a silicone nanofilament coating, Soft Matter 2008, 4: 450-52.

[46] Liu M., Wang S., Wei Z., Song Y. and Jiang L., Bioinspired design of a superoleophobic and low adhesive water/solid interface, Advanced Materials 2009, 21: 665–69.

[47] Epstein A. K., Wong T. –S., Belisle R. A., Boggs E. M. and Aizenberg J., Liquid-infused structured surfaces with exceptional anti-biofouling performance, Proceedings of the National Academy of Science of the U.S.A. 2012, 109: 13182–7.

[48] Stone H. A., Ice-phobic surfaces that are wet, ACS Nano 2012, 6: 6536–40.

[49] Ma W., Higaki Y., Otsuka H. and Takahara A. Perfluoropolyether-infused nano-texture: a versatile approach to omniphobic coatings with low hysteresis and high transparency, Chemical Communications 2013, 49: 597–9.

[50] Manna U., Broderick A. H. and Lynn D. M., Chemical patterning and physical refinement of reactive superhydrophobic surfaces, Advanced Materials 2012, 24: 4291–5.

[51] Arima Y, and Iwata H., Effect of wettability and surface functional groups on protein adsorption and cell adhesion using well-defined mixed self-assembled monolayers, Biomaterials 2007, 28: 3074-82.

[52] Oliveira S. M., Song W., Alves M. and Mano J. F., Chemical modification of bioinspired superhydrophobic polystyrene surfaces to control cell attachment/proliferation, Soft Matter 2011, 7: 8932–41.

[53] Neto A. I., Custódio C. A., Song W. and Mano J. F., High-throughput evaluation of interactions between biomaterials, proteins and cells using patterned superhydrophobic substrate, Soft Matter 2011, 7: 4147.

[54] Mano J. F., Stimuli-Responsive Polymeric Systems for Biomedical Applications, Advanced Engineering Materials 2008, 10: 515–27.

[55] Custódio C. A., Reis R. L. and Mano J. F., Engineering biomolecular microenvironments for cell instructive biomaterials, Advanced Healthcare Materials 2014, 3: 797-810.

[56] Alves N. M., Pashkuleva I., Reis R. L. and Mano J. F., Controlling cell behavior through the design of polymer surfaces, Small 2010, 6: 2208-20.

[57] Akkas T., Citak C., Sirkecioglu A. and Güner F. S., Which is more effective for protein adsorption: surface roughness, surface wettability or swelling? Case study of polyurethane films prepared from castor oil and poly(ethylene glycol), Polymer International 2012, 62: 1202-9.

[58] Roach P., Farrar D., Perry C. C., Interpretation of protein adsorption: surface-induced conformational changes, Journal of the Americal Chemical Society 2005, 127: 8168–73.

[59] Rabe M., Verdes D. and Seeger S., Understanding protein adsorption phenomena at solid surfaces, Advanced Colloids & Interface Science 2011, 162: 87-106.

[60] Anand G., Sharma S., Dutta A. K., Kumar S. K. and Belfort G, Conformational transitions of adsorbed proteins on surfaces of varying polarity, Langmuir 2010, 26: 10803-11.

[61] Oliveira S. M., Alves N. M. and Mano J. F., Cell interactions with superhydrophilic and superhydrophobic surfaces, Journal of Adhesion Science and Technology 2014, 28: 843–63.

[62] Song W. and Mano J. F., Interactions between cells or proteins and surfaces exhibiting extreme wettabilities, Soft Matter 2013, 9: 2985.

[63] Leibner E. S., Barnthip N., Chen W., *et al.* Superhydrophobic effect on the adsorption of human serum albumin, Acta Biomaterialia 2009, 5: 1389–98.

[64] Huang Q., Lin L., Yang Y., Hu R., Vogler E. A. and Lin C., Role of trapped air in the formation of cell-and-protein micropatterns on superhydrophobic/superhydrophilic microtemplated surfaces, Biomaterials 2012, 33: 8213–20.

[65] Ballester-Beltrán J., Rico P., Moratal D., Song W., Mano J. F. and Salmerón-Sánchez M., Role of superhydrophobicity in the biological activity of fibronectin at the cell–material interface, Soft Matter 2011, 7: 10803.

[66] Cantini M., Sousa M., Moratal D., Mano J. F. and Salmerón-Sánchez M., Non-monotonic cell differentiation pattern on extreme wettability gradients, Biomaterials Science 2013, 1: 202-12.

[67] Lourenço B. N., Marchioli G., Song W., *et al.* Wettability influences cell behavior on superhydrophobic surfaces with different topographies, Biointerphases 2012, 7: 46.

[68] Hersel U., Dahmen C. and Kessler H., RGD modified polymers: biomaterials for stimulated cell adhesion and beyond, Biomaterials 2003, 24: 4385–415.

[69] Stevens M. M. and George J. H., Exploring and engineering the cell surface interface, Science 2005, 310: 1135–8.

[70] Bettinger C. J., Langer R. and Borenstein J. T., Engineering substrate topography at the micro- and nanoscale to control cell function, Angewandt Chemie International Edition 2009, 48: 5406–15.

[71] Jayaraman M., Meyer U., Bühner M., Joos U. and Wiesmann H. -P., Influence of titanium surfaces on attachment of osteoblast-like cells in vitro, Biomaterials 2004, 25: 625–31.

[72] Gittens R. A., McLachlan T., Olivares-Navarrete R., *et al.* The effects of combined micron-/submicron-scale surface roughness and nanoscale features on cell proliferation and differentiation, Biomaterials 2011, 32: 3395–403.

[73] Luz G. M. and Mano J. F., Mineralized structures in nature: examples and inspirations for the design of new composite materials and biomaterials, Composites Science and Tecnology 2010, 70: 1777-88.

[74] Alves N. M., Shi J., Oramas E., Santos J. L., Tomás H. and Mano J. F., Bioinspired superhydrophobic poly(L-lactic acid) surfaces control bone marrow derived cells adhesion and proliferation, Journal of Biomedical Materials Research A 2009, 91: 480–8.

[75] Limongi T., Cesca F., Gentile F., *et al.* Nanostructured superhydrophobic substrates trigger the development of 3D neuronal networks, Small 2013, 9: 402–12.

[76] Lima A. C. and Mano J. F., Micro/Nano Structured Superhydrophobic Surfaces in the Biomedical Field. Part 2: Applications Overview, Nanomedicine (Lond.), 10(1), DOI: 10.2217/NNM.14.175 (In press).

[77] Zhang Y. –L., Xia H., Kim E. and Sun H. -B., Recent developments in superhydrophobic surfaces with unique structural and functional properties, Soft Matter 2012, 8: 11217.

[78] Gao X., Yan X., Yao X., Xu L., Zhang K., Zhang J., Yang B. and Jiang L., The dry-style antifogging properties of mosquito compound eyes and artificial analogues prepared by soft lithography, Advanced Materials 2007, 19: 2213–2217.

[79] Ensikat H. J., Ditsche-Kuru P., Neinhuis C. and Barthlott W., Superhydrophobicity in perfection: the outstanding properties of the lotus leaf, Beilstein Journal of Nanotechnology 2011, 2: 152–161.

[80] Zheng Y., Gao X., and Jiang L., Directional adhesion of superhydrophobic butterfly wings, Soft Matter 2007, 3: 178.

[81] Gao X. and Jiang L., Biophysics: Water-repellent legs of water striders, Nature 2004, 432: 36.

[82] Feng L., Li S., Li Y., Li H., Zhai J., Song Y., Liu B., Jiang L. And Zhu D., Super-Hydrophobic Surfaces: From Natural to Artificial, Advanced Materials 2002, 14: 1857–1860.

[83] Jung Y. C. and Bhushan B., Biomimetic structures for fluid drag reduction in laminar and turbulent flows, Journal of Physics: Condensed Matter 2010, 22: 035104.

[84] Koch K., Bhushan B. and Barthlott W., Multifunctional plant surfaces and smart materials. In: Springer handbook of nanotechnology, Bhushan B (Ed.), Springer 2010, Heidelberg, Germany, 1399-1436.

[85] Koch K., Bushan B., Jung Y. C. and Barthlott W., Fabrication of artificial Lotus leaves and significance of hierarchical structure for superhydrophobicity and low adhesion, Soft Matter 2009, 5: 1386-93.

[86] Zhao Y., Qin M., Wang A. and Kim D., Bioinspired superhydrophobic carbonaceous hairy microstructures with strong water adhesion and high gas retaining capability, Advanced Materials 2013, 25: 4561–5.

[87] Yao X., Gao J., Song Y. and Jiang L., Superoleophobic surfaces with controllable oil adhesion and their application in oil transportation, Advanced Functional Materials 2011, 21: 4270–6.

[88] Zhang G., Zhang X., Huang Y. And Su Z., A surface exhibiting superoleophobicity both in air and in seawater, ACS Applied Materials Interfaces 2013, 5: 6400–3.

[89] Wang X., Hu H., Ye Q., Gao T., Zhou F. and Xue Q., Superamphiphobic coatings with coralline-like structure enabled by one-step spray of polyurethane/carbon nanotube composites, Journal of Materials Chemistry 2012, 22: 9624.

[90] Deng X., Mammen L., Butt H. –J. and Vollmer D., Candle soot as a template for a transparent robust superamphiphobic coating, Science 2012, 335: 67–70.

[91] Leng B., Shao Z., de With G. and Ming W., Superoleophobic cotton textiles, Langmuir 2009, 25: 2456–60.

[92] Yang J., Zhang Z., Xu X., Men X., Zhu X. and Zhou X., Superoleophobic textured aluminum surfaces. New Journal of Chemistry 2011, 35: 2422.

[93] Zhang L., Zhang Z. and Wang P., Smart surfaces with switchable superoleophilicity and superoleophobicity in aqueous media: toward controllable oil/water separation, NPG Asia Materials 2012, 4: e8.

[94] Cheng Z., Lai H., Du M., Zhu S., Zhang N. and Sun K., Super-hydrophobic surface with switchable adhesion responsive to both temperature and pH, Soft Matter 2012, 8: 9635.

[95] Sun T., Wang G., Feng L., Biqian L., Yongmai M., Lei J. and Zhu D., Reversible switching between superhydrophilicity and superhydrophobicity, Angewandte Chemie International Edition 2004, 43: 357–60.

Chapter 2

Micro/Nano Structured Superhydrophobic Surfaces in the Biomedical Field. Part II: Applications Overview

2.1. Abstract

The properties of the surfaces define the acceptance and integration of biomaterials *in vivo* as well as materials efficiency when used at research or manufacturing level. The presence of micro/nano topographical structures and low surface energy could bring several advantages when highly repellent surfaces are employed in the biomedical field. Biomimetic superhydrophobic surfaces have been explored for diverse applications: (I) as an intrinsic characteristic of biomaterials to be implanted; (II) as materials to exhibit special interaction with biological entities; or (III) to be used in *ex vivo* applications. This chapter aims to focus the main motivations and requirements in the biomedical field that pushed the utilization of superhydrophobic surfaces as suitable alternatives, as well as the great evolution of applications emerged in the last few years.

This chapter is based on the following publication:
Lima A. C. and Mano J. F., Micro/Nano Structured Superhydrophobic Surfaces in the Biomedical Field. Part II: Applications Overview, Nanomedicine (Lond.), 10(1), DOI: 10.2217/NNM.14.175 (In press).

2.2. Introduction

The design of innovative materials aimed to improve the quality of life of the patients is a continuous concern of clinicians, engineers and scientist. Materials for the regeneration of tissues or to replace damaged organs are examples of applications. The first contact between the material and the biological *milieu* occurs at the surface of the material, where is triggered a cascade of complex interactions [1]. The characteristics of the surfaces determine the biointegration of the material. The non-specific adsorption of proteins is the first instantaneously event, where surface properties such as chemistry, charge, topography and wettability play a crucial role [2]. The acceptance/integration of the biomaterials is defined by the control of the type, amount and conformation of the adsorbed proteins accompanied by cell response from the surrounded environment [3]. In the last few years, the study of the protein adsorption and cells attachment/proliferation onto the surfaces was extended from intermediary wettability states (hydrophilic-hydrophobic) to extreme wettabilities, namely superhydrophilic and superhydrophobic [4-6]. This was motivated by the unique characteristics of surfaces obtained by inspiration in natural features, where the surface topography and chemistry play a crucial role [7]. Surfaces with extreme wettability have been shown capable to modulate the interfacial reactions of the biological entities and the surfaces of the materials. Besides influencing protein adsorption and eukaryotic cells attachment and proliferation, wettability effects platelet adhesion/activation, blood coagulation, and adhesion of bacteria [4]. The ideal sequence of interactions between the biological moieties and the biomaterials surfaces could be easily disturbed by adverse responses such as bacterial adhesion and infection [8], inflammation, and formation of a fibrotic capsule [9,10], being, once again, the intrinsic properties of surfaces important in controlling the performance of the implant.

Materials could also be used in other biomedical applications which do not involve the direct contact with the inner of human body. Beyond scaffolds, cell carriers, drug delivery systems, prosthesis, among others, the wettability and the design of the micro/nano topographical structures at the interfaces also have an important role in the performance of a vast range or medical devices, namely diagnostic tools, biosensors, medical textiles, devices to produce the biomaterials and supports for fundamental research in biomedicine and biology. The employment of micro/nano structured surfaces, as it is the case of superhydrophobic substrates, could provide advantages that should be explored in such contexts. For example, beyond playing an important role in biocompatibility of the materials, micro/nano structured superhydrophobic surfaces are also known for contamination prevention and durability of materials [11]. The special behavior of the superhydrophobic surfaces encouraged the development of several materials and devices for biomedical applications with new or improved performance. The most representative

examples are summarized in Table 2.1. In the next sections representative examples will be overviewed on the use of the superhydrophobic surfaces in the biomedical field.

Table 2.1. Representative examples of the applications of bioinspired superhydrophobic surfaces in the biomedical field.

Applications	Examples		Superhydrophobic platform/material	Observations
Drug Release Systems	Fiber mesh		PCL/PGC-C18 [12]	• Membranes with >25% PGC-C18 were in metastable-Cassie state; • The membranes composed by 30% and 50% PGC-C18 showed only *ca.* 10% SN-38 release over 9 weeks whereas 10% PGC-C18 released *ca.* 60%; • Degassed fiber mesh (10% PGC-C18) released 80% on the content in less than 20 days.
Production of biomaterials with spherical-shape	Simple matrices	Dextran-MA/PNIPAAm: insulin and BSA encapsulation [21]	PS, Cu, Al	• Temperature responsive particles obtained by UV light exposure; • Particles with more PNIPAAm had higher swelling variations according to the temperature; • The release of insulin and BSA was followed during 2 days and less amount of proteins was detected at physiological temperatures when compared with room temperature; • Particle size: millimetric range.
		Chitosan: fibroblasts and drug encapsulation [26]	PS	• Particles for cell encapsulation obtained by a sequential process of crosslinking; • Upon in physiological simulated conditions the stiffness of the gels was improved due to attractive chitosan-chitosan forces: *ca.* 26 kPa at 20˚C and *ca.* 70 kPa at 37˚C. • Viable fibroblasts for 7 days; • Dexamethasone fast release: *ca.* 60% released after 2h; • Particle size: *ca.* 2.7 mm.
		Collagen/Platelet Lysate gels: co-encapsulation of growth factors and human adipose-derived stem cells [22]	PS	• Fast crosslinking of the gels: 10-15 min at 37˚C; • Platelet lysates caused higher cell proliferation; • The cells migrate from the particles and established cell-cell communications, forming a tissue membrane; • Formulation without cells were also effective in accelerating the recovery of a simulated scratching and demonstrated angiogenic potential forming a strong blood vessel network in CAM model. • Very fast release of VEGF and PDGF-BB: 100% released after 8 h. • Particle size: 1.5-2.5 mm
		Alginate: co-encapsulation of mesenchymal stem cells and FN [23]	PS	• Particles ionically crosslinked; • Mesenchymal stem cells and FN were successfully co-encapsulated in mild conditions; • The cells remained viable for more than 20 days; • The combination of cells and proteins improved the regeneration of bone, visualize *in vivo;* • Particle size: *ca.* 2 mm
		Dextran and γ-Cyclodextrins (post-preparation loading with dexamethasone) [24]	PS	• Dextran combined with structural monomers of γ-cyclodextrins was *ca.* 7 times more efficient in dexamethasone loading than particles without or with free cyclodextrins in the structure. • Sustained release of dexamethasone for at least 10 days. • The particles showed good cytocompatibility and good performance in inducing osteogenic differentiation of human adipose-derived stem cells, after 7 days in culture.
		Elastin-like recombinamers with RGD domains (scaffolds) [29]	PS	• SaOs-2 cells adhered onto the scaffolds surface due to the RGD domains in the elastin structure; • Particles with a crosslinking degree of 22% and 60% were compared; • The cells demonstrated preference for surfaces with higher stiffness corresponding to the more crosslinked structures; • Particle size: 800-900 μm

Production of biomaterials with spherical-shape		Methacrylamide chitosan microgels [37]	Glass-based	• Chitosan crosslinked by UV exposure after dispensing onto the surface using a spray system; • Size of the obtained microgels: <320 μm.
	Hierarchical systems	Chitosan beads/magnetic microparticles [28]	PS	• Chitosan/genipin beads containing magnetic microparticles (Fe_3O_4, diameter ranging from 5–50 μm); • L929 cells were capable to adhere onto the surface of the beads; • The pathway of the particles inside a reactor was controlled by applying a magnetic field.
		SiO_2-CaO nanoparticles organized in a milli-sized structure [32]		• The evaporation of the droplet containing nanoparticles led to a spontaneous assembly into polycrystalline aggregates: mesocrystals with sizes *ca.* 5 μm were formed; • After immersion into simulated body fluid for 7 days an apatite film grew on the surface of the samples.
		PNIPAAm/Au or Ag nanoparticles [35]	PFTE superhydrophobic surface covered by 2,2,4-trimethylpentane	• Au nanoparticles *ca.* 10 nm; Ag nanoparticles *ca.* 15 nm; • Nanoparticles embedded in NIPAAm + crosslinkers solution were sprayed onto the surface; • Obtained magnetic particles with sizes comprising 200-500 μm.
	Core-shell and multilayered systems	Dextra-MA/Alginate [31]	Cu	• Core/shell particles: Core: dextran-MA photocrosslinked encapsulatin $CaCl_2$; Shell: Alginate with L929 cells crosslinked by the Ca^{2+} diffused from the core; • Each particle may be multifunctional: some compartments may be reservoirs for drugs and others for cells.
		Dextran-MA [31]		• Hydrogels with a core/shell and multiple layered structure were obtained by sequentially dispensing and crosslinking dextran-MA onto the previously crosslinked structures. UV light exposure was used to induce the hardening of the particles; • The thickness of the layers was controlled by the volume dispensed, for example 2 μL led to a thickness of *ca.* 140 μm and 6 μL *ca.* 500 μm; • Depending on the relative location of the encapsulated drugs, they were sequentially released: the drug model entrapped in the shell was released immediately and the drug model encapsulated in the core had a delay of *ca.* 30 min.
		Chitosan/Pectin [30]	PS	• Core/shell microgels: Core: chitosan crosslinked under glutaraldehyde atmosphere; Shell: pectin ionically crosslinked; • Particles capable to control the release of an anti-tumor drug (5-fluorouracil); • The pectin shell just dissolved in basic conditions, being the system resistant to acidic environments; • The chitosan core improved the effect of the drug against cancer cells (HeLa and SK-MEL-28 cells).
Screening systems	Analytical sensor for blood typing [40]		Substrate coated with Teflon powder embedded in a UV curable varnish	• CA_{blood}>150˚; • Blood sample: 3 droplets with 10 μL each; • Anti-A, B and D solution was injected into the blood droplets dispensed onto the superhydrophobic surfaces; • The droplets were monitored during 180s, taking photos at 30s intervals and then processed by image analysis; • Squares of 5 x 5 mm on the top part of the droplets were the selected areas to be analyzed.
	Materials properties: bioactivity of two different types of bioglass nanoparticles [42]		PLLA (superhydrophobic platforms patterned with superhydrophilic squares by UV/O_3 treatment)	• Binary (SiO_2–CaO) and ternary (SiO_2–CaO–P_2O_5) nanoparticles were confined into the wettable squares; • Ca/P ratios obtained for both types of nanoparticles were close to hydroxyapatite stoichiometric theoretical value, after immersed in simulated body fluid for 3 and 7 days; • Binary nanoparticles exhibited lower peaks of P and Ca than the ternary: ternary BG-NPs were more bioactive than the binary.
	Proteins-cells-interactions	Adsorption of proteins followed by cells adhesion [44]	PS (superhydrophobic platforms patterned with superhydrophilic spots)	• Albumin and fibronectin were adsorbed onto the 1x1 mm wettable squares varying their concentration and the proportion between both proteins • 4 μL of protein solution/spot; • The adsorption was dependent on the concentration of protein in

Screening systems	Proteins-cells-interactions	Adsorption of proteins followed by cells adhesion [44]	PS (superhydrophobic platforms patterned with superhydrophilic spots)	the solution; • The cells were seeded onto the spots, after protein adsorption (10 µL of cells suspension): For the same total protein: more cells adhered in the spots with higher content of fibronectin; For the same proportion albumin:fibronectin the cells adhered more onto the spots with higher total protein.
		Hydrogels (cell encapsulation) [45]		• Hydrogel liquid solutions containing L929 and MC3T3-EI cells (4 µL) were confined into the wettable areas (4 mm^2) and allowed to solidify via ionic crosslinking; • Combinations of materials were analyzed: alginate, chitosan, gelatin, collagen and hyaluronic acid; • Direct image analysis of the gels (calcein-AM and DAPI staining) was compared with destructive conventional methods (MTS and DNA quantification): the results of both methods had coincident tendencies.
		Scaffolds (cell adhesion and proliferation) [46]		• Solutions of biomaterials (9 chitosan/alginate combinations per chip) were dispensed onto the hydrophilic regions; • The scaffolds were obtained by a complexation reaction and *in situ* neutralization followed by freeze-drying; • The µCT allowed the rapid access *in situ* to the porosity of the scaffolds. • The properties of the scaffolds on the superhydrophobic chip were compared with scaffolds with the same composition but produced in a 96 cell culture plate (controls): the E' followed the same tendency and had similar values; • The relative position in the chip did not affect any result; • Cell metabolic activity and number accessed by conventional methods was in agreement with results obtained by image analysis of the scaffolds onto the chip; • The volume of solution used to prepare the scaffolds in the chips was 1/50 of the volume used in 96 well plates; • It was verified a time saving of 9x in the µCT analysis.
		Nanocomposite hydrogels (interaction with pre-osteoblasts) [47]		• 30 formulations of chitosan/bioglass nanoparticles gels crosslinked with distinct amounts of genipin were analyzed into a single chip; • *In situ* evaluation of both mechanical/viscoeleastic properties under physiological-like conditions; • Cell-materials interactions: After 1 day: selective cell adhesion; After 3 days: different cell proliferation and morphology in the different formulations; • Neither cell adhesion nor cell proliferation depended directly of materials mechanical/viscoelastic properties; • The optimal condition was soft hydrogels composed by 2% (w/v) chitosan with 12.5% (w/w) nanoparticles and crosslinked with 2.5% (w/w) genipin.
		Scaffolds inflammatory response *in vivo* [48]		• Each chip had 36 spots with 4mm^2; • Scaffolds composed by two polymers were prepared in each spot: chitosan + alginate or carrageenan; • The chips were implanted subcutaneously in Wistar rats and compared with scaffolds implanted one-by-one (conventional procedures); • The inflammatory response evaluated through lymphocyte analysis and histology of conventional scaffolds was consistent with the results obtained in the chip; • The relative position onto the chip did not affect the results; • Empty chips demonstrated cells adhered onto the wettable regions and no cells adhered onto superhydrophobic areas: very mild signals of inflammation were found 24h post implanting.
	Cell-cell communications and signaling		Silicon and glass patterned with superhydrophilic areas [51]	• NIH 3T3 fibroblast cells adhered selectively onto superhydrophilic areas of the patterned surfaces; • Cell-cell communications: Distances <150 µm: capacity to extend and communicate with neighboring cells; Distances >400 µm: no extension of the cells was observed; Distances between 200-400 µm: the cells partially extended to

Screening systems				neighboring.
	Cell-cell communications and signaling		HEMA-EMA or PFPMA patterned with superhydrophilic areas [49]	• Wnt (signaling protein of the brain) propagated without cell-cell contact: Wnt ligand expressing cells were cultured adjacently without direct contact with cells expressing aWnt reporter system. • Surfaces used for co-cultures of cells confined into different compartments showed 0.6% of MLTy mCherry and less than 0.1% of HeLa-GFP cells were capable to migrate and cross the superhydrophobic border after 48h of culture.
	Others	Drug release profiles [54]	PS	• The release of BSA-FITC from alginate beads was followed by fluorescence microscopy and the release profiles were similar than those obtained by conventional *in vitro* studies; • Each particle was analyzed individually.
		Drug cytoxicity in microtissues [52, 53]		• Superhydrophobic arrays with micro-indentations to induce rose petals effect (adhesion) or with wettable small areas (1 mm^2); • Droplets of fibroblast-like cells suspension were deposited onto the micro-indentations or wettable areas and the surfaces were inverted allowing the formation of cells-spheroids by gravitational sedimentation (diameter 400-600 μm); • Different concentrations of doxorubicin were introduced into the droplets and cell viability monitored by image analysis (Live/dead staining): the cell viability decreased with the increase of drug concentration.
Fabrics	Anti-microbial textiles		Cotton/Ag nanoparticles [78]	• Non-modified cotton did not show any antibacterial activity whereas the modified cotton killed all the bacteria around the sample; • The reduction of bacterial growth was *ca.* 99% for superhydrophobic cotton; • No significant differences were observed between cotton coated with Ag nanoparticles superhydrophobic and not superhydrophobic; • Effective against Gram-positive and Gram-negative bacteria; • The antibacterial effect was a result of the leaching of bioactive Ag^+ ions.
			Cotton [80]	• Stable antibacterial effect and washing resistant coating with low surface energy materials (PDMASU and PFOTES); • Free of any antibacterial agent (*e.g.* Ag nanoparticles); • Cotton almost superhydrophobic ($CA_{water} \approx 147^\circ$) and oleophobic ($CA_{n\text{-}hexadecane} \approx 120^\circ$); • Non washed modified cotton showed a reduction of *Escherichia coli* bacteria of nearly 100% whereas washed cotton (10cycles) a reduction of *ca.* 60%.
Blood contact materials	Blood contact medical devices		PDMS [82,83]	• The treatment of PDMS with CO_2-pulse laser (superhydrophobic) and grafted with HEMAPC (superhydrophilic) demonstrated less adhered platelets than non-treated PDMS and glass, demonstrating that extreme wettabilities affect the platelet adhesion and activation; • A relationship between the surface micro/nano roughness and platelet adhesion was verified onto PDMS patterned surfaces: the higher the hydrophobicity caused by the roughness, the lower was the platelet adhesion.
			PCUs/carbon nanotubes [84]	• $CA > 163^\circ$ derived from the low surface energy caused by fluorinated alkyl side chains in the PCU and the roughness caused by the coating with carbon nanotubes; • Smooth surfaces (with the same chemistry) were more susceptible to platelet adhesion than nanostructured surfaces. • The early and further activation of the platelets (detected by the PAC-1 (gpIIb/IIIa) and CD62p (P-selectin) markers) was reduced in nanostructured superhydrophobic surfaces.
			PP [85]	• Microstructured surfaces composed by a porous network; • $CA \approx 158^\circ$; • The anti-fouling properties could be related by the air entrapped in the structures that prevented the contact of the platelets with the surface.

Blood contact materials	Vascular grafts	ePTFE [91,92]	• Superhydrophobic ePTFE vascular grafts (obtained by ion beam etching, CA 140-150°) with 1.5 mm of internal diameter were not occluded after being implanted in rabbits for 1 week. The non-modified counterparts were obstructed; • Later, the same grafts were tested in rabbits (1.5 mm internal diameter) and pigs (3.5 mm internal diameter) failing 15 min-1 h post-implanting in the right carotid artery; • No explanations were found for such opposite results.

2.3. Drug Release Systems

Drug release systems have been developed to protect and optimize the release of bioactive agents in order to improve their efficiency and decrease possible systemic side effects. One type of release systems is based on micro/nano sized carriers (micro/nano particles and capsules, vesicles, micelles and dendrimers) which are normally designed to be injected systemically until reach the target site. The other type is based on implantable systems for the local release of bioactive agents. These formulations include gels, rods, wafers and films, in which targeting or migration through bloodstream is not required. In any case the release of the therapeutic agent relies on the interfacial properties between the system and the biological *milieu*, through which the mass transport must occur. Any changes in the surface properties of such devices could have huge effects in their performance.

Based on the repellent properties of superhydrophobic surfaces, Yohe *et al.* hypothesized that 3D superhydrophobic materials could be advantageous when acting as matrices for prolonged and local drug delivery [12]. Materials with appropriate micro/nano roughness, where air is entrapped and acts as a removable barrier, may delay/difficult the mass transport of a drug from the bulk of the material to the liquid environment. Those systems have to be used for local release because the air is removed in the same rate that the surrounded liquid diffuse and wet the structure, which mean that after a certain time period the entire system is involved by the liquid being the release no more controlled by the superhydrophobic properties of the system. Prolonged therapies for pain management, chronic diseases requiring permanent drugs administration or prevention of tumor recurrence after surgical resections, are possible applications for this type of systems.

A superhydrophobic micro-sized fiber mesh composed by poly(ε-caprolactone) (PCL) and poly(glycerol monostearate-co-ε-caprolactone) (PGC-C18) was obtained by electrospinning (Figure 2.1, A and B) [12,13]. The high repellency of the mesh slowed the water penetration and the air entrapped acted as a removable barrier causing a delay in the release of the drug (Figure 2.1, D). The amount of PGC-C18 dictated the wettability properties of the mesh: below 25% predominated the Wenzel state; above this value the mesh transited to a Cassie regime (Figure 2.1, C), decreasing the release rate of an anticancer drug (SN-38) – Figure 2.1, E. This innovative concept was extended and a similar system was studied for

anticancers dual release to prevent locoregional recurrence in colorectal cancer [13]. Herein, it was demonstrated that the 3D fiber-meshes had appropriated mechanical properties for surgical buttressing and released both chemotherapeutic agents for more than 90 days, resulting in significant cytotoxicity of human colorectal cancer cells.

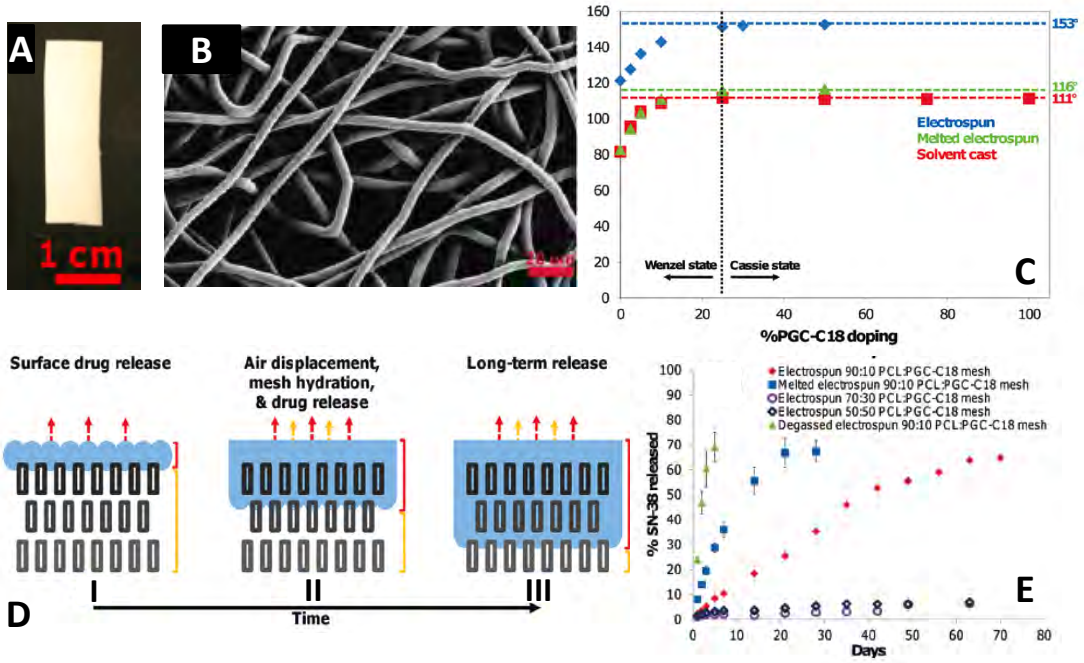

Figure 2.1. Superhydrophobic electrospun strip (A) and the microstructure of the meshes composed by PCL complemented with 10% PGC-C18 (B). The CA of the electrospun meshes varies in function of the amount of PGC-C18 used (C) and a transition between the Wenzel and Cassie state occurred for higher content of PGC-C18. (D) Schematic representation of the release mechanism from the superhydrophobic meshes. (E) Release profiles of SN-38 from PCL solely and PCL+PGC-C18 meshes. The images were adapted from the reference [12,13] with permission of ASC Publications and Elsevier, respectively.

We believe that the underlying concept used by these authors could be extended to drug release systems with other geometries (*e.g.* particles or other solid implantable devices) and sizes, by using adequate materials and technologies to texturize non-flat elements. For instance, particles with a superhydrophobic surface have already been produced by coating silica microparticles with polydopamine, which acted as reactive template to generate silver nanoparticles [14]. A lotus-leaf like surface structure was obtained. This concept should be possible to be applied in other kind of core materials. Superhydrophobic release systems could be especially important to control and to sustain the release of drugs that are released in a very fast way when encapsulated in conventional carriers. For example, the burst release of highly aqueous soluble drugs may be retarded turning the surface of the system superhydrophobic.

2.2. Superhydrophobic Platforms for the Production of Spherical-Shaped Particles

The spherical shape has been a widely employed geometry in particulate objects for biomedicine applications. In general, spherical particles or capsules from nano to milli sizes are explored as reservoirs for the release of bioactive agents [15], namely synthetic or natural small molecules, proteins, antigens, DNA, or even as cell containers [16,17] or scaffolds for cell growth [18].

The capacity of water droplets to acquire an almost spherical shape on the top of lotus leaves inspired the development of an innovative methodology aiming for a more efficient and cost-effective process to produce spherical particles. Our group suggested the use of biomimetic superhydrophobic surfaces as possible platforms to produce spherical hydrogel beads [19]. Aqueous solutions (containing a polymeric precursor, bioactive agents or even cells) were dispensed onto superhydrophobic surfaces using a micropipette (Figure 2.2, A). Microppipeting allowed the control of the volume dispensed, within a certain range, and consequently the size of the obtained particles (Figure 2.2, B). Depending on the polymers used, an adequate crosslinking process or solvent evaporation protocol must be applied to induce the hardening of the liquid droplets (Figure 2.2, C).

In general, such method is highly cost-effective: no waste residues are produced, organic solvents are usually not required and is not necessary to use complex apparatus. In comparison with the conventional technologies to produce particles, the superhydrophobic methodology exhibits some important advantages [20]: (I) high encapsulation efficiency, due to the air-liquid interface where the particles harden and consequently the absence of a surrounded liquid medium from where the encapsulated molecules may diffuse and be lost (encapsulation efficiency of ≈100%); (II) a negligible contact area between the droplet and the surface due to the droplet suspension onto the micro/nano roughness of the platform; (III) absence of organic solvents, high temperatures or even mechanical forces that may be aggressive for labile molecules, living cells or even microorganisms; (IV) narrow particle size distribution due to the control of the volume dispensed to produce the particles; (V) the particles harden individually, preventing particle aggregation; (VI) possibility to produce complex spherical systems such as multilayered or hierarchical particles, in an easy way.

Non-adhesive superhydrophobic surfaces should be selected in order to facilitate particles collection. Polystyrene (PS), metallic copper and aluminum surfaces exhibiting “lotus effect” were tested and demonstrated to be effective in the production of dextran-methacrylate/poly(*N*-isopropylacrylamide) (PNIPAAm) spherical-shaped gels [21]. The smart milli-sized particles obtained were crosslinked by UV light exposure and showed distinct release profiles when subjected to temperatures above or below the

lower critical solution temperature of PNIPAAm (≈32°C) (Figure 2.2, E.2). More complex systems regarding the structure, composition and content have been reported taking advantage of this methodology as producing technique. The most relevant and representative examples in biomedical field will be described in this section.

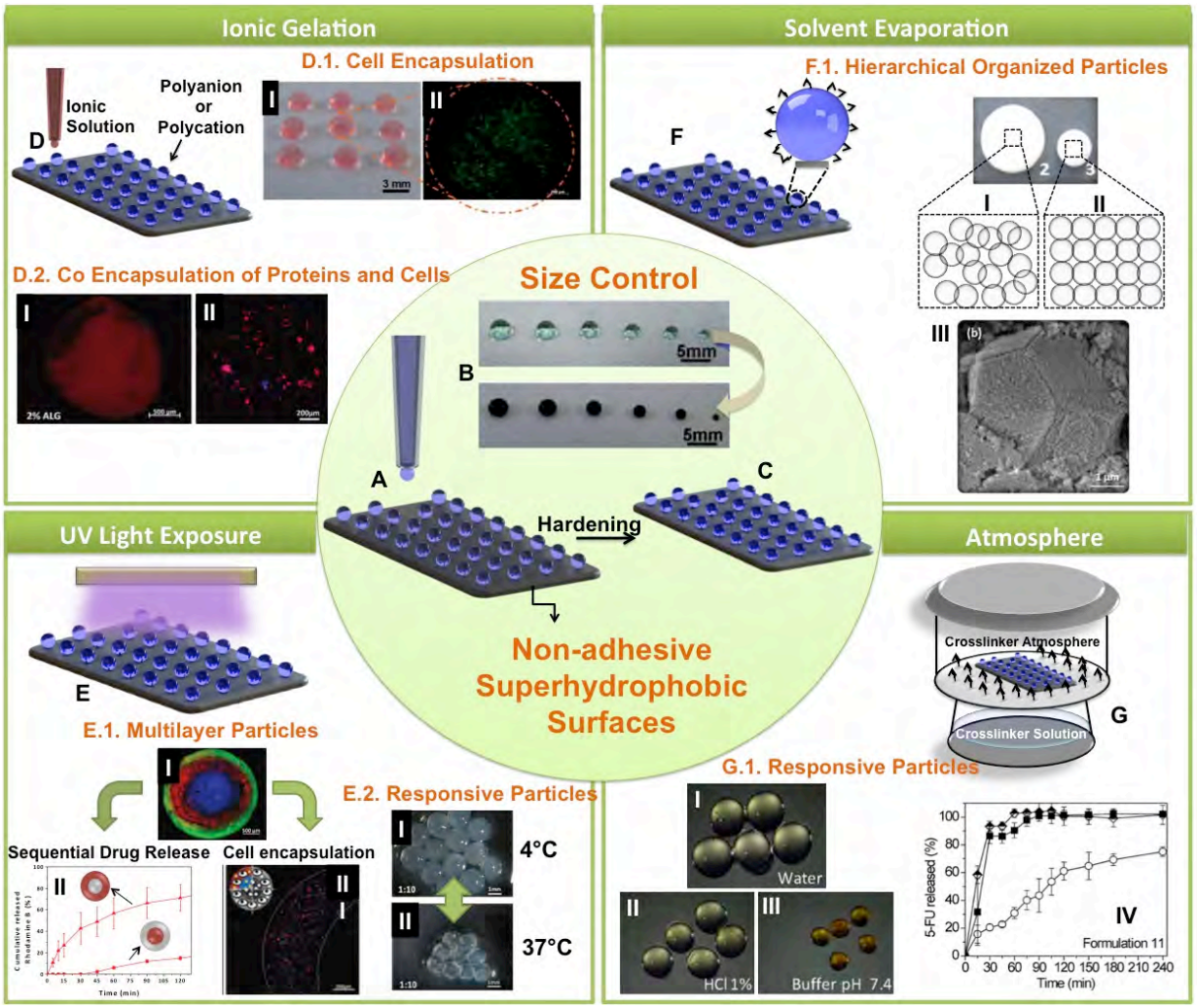

Figure 2.2. Aqueous dispersions containing polymers, cells or bioactive agents may be dispensed onto the non-adhesive superhydrophobic surfaces (A) with controlled sizes (B) and hardened (C) through different processes depending on the polymers used. Alginate particles ionically crosslinked by dispensing $CaCl_2$ (D) were used to encapsulate cells (D.1) and co-encapsulate fibronectin and mesenchymal stem cells (D.2, I and II, respectively). Using photocrosslinkable polymers, such as dextran-methacrylate, spherical hydrogels may be obtained by UV light exposure (E). Multilayer particles were produced (E.1, I) for sequential drug release (E.1, II) and cell encapsulation (E.3, III). Responsive particles (E.2, I and II) composed by dextran-methacrylate and poly(*N*-isopropylacrylamide) controlled the release profile of insulin and BSA according to the temperature. Simply by solvent evaporation (F) hierarchical particles composed by bioactive glass nanoparticles (F.1) were obtained. Initially the nanoparticles are randomly dispersed (I) in the aqueous medium and when the solvent evaporates they become organized (II) in a spherical-shape (III). Responsive chitosan microgels crosslinked under glutaraldehyde atmospheric environment (G, G.1) and coated with pectin layers were produced to release an anti-tumor agent, preferentially in sites with specific pH, such as

gastro-intestinal tract. B and D.1, adapted from the reference [19] with permission of RSC; D.2, adapted from the reference [23] with permission of Mary Ann Liebert, Inc.; E.1 (I), adapted from the reference [31] with permission of Wiley; E.2 (I and II), adapted from the reference [21] with permission of Springer; F.1, adapted from the reference [32] with permission of RSC; G and G.1, adapted from the reference [30] with permission of Elsevier.

For many tissue and cell engineering strategies, hydrogels should be designed to be able to encapsulate living cells and maintain their viability upon implantation. For example, particles of collagen in combination with platelet lysates and human adipose-derived stem cells were produced in a very fast way, incubating liquid droplets onto superhydrophobic surfaces at 37 °C for 10-15 minutes [22]. Those particles induced a rapid cell proliferation and migration. Consequently the establishment of cell-cell communications led to a spontaneously formation of a tissue layer where the particles were interconnected by the cells. Due to the cocktail of growth factors provided by the platelet lysates such particles also showed angiogenic potential. The advantage of those particles as cells and growth factors suppliers were hypothesized to be useful for skin regeneration. The co-encapsulation of cells and a protein into alginate beads, as implantable systems for bone regeneration were also obtained using superhydrophobic surfaces [23]. The mild conditions provided by the superhydrophobic surfaces methodology resulted in the high viability of the incorporated cells evaluated over 3 days post-encapsulation, as well as through the release of viable cells, for more than 20 days. The absence of coagulation baths prevented the loss of fibronectin through migration from the particle to the surrounded medium (Figure 2.2, D.2). The combination of cells and fibronectin in the final system improved the regeneration of a cranial bone defect in Wistar rats within 4 weeks, when compared with particles without cells. Particles with improved capacity to be loaded with hydrophobic drugs were produced by photopolymerization of dextran and γ-cyclodextrins onto the superhydrophobic surfaces [24]. Besides not being loaded with cells, such particles demonstrated potential to be used in bone tissue engineering strategies due to their efficient capacity to induce osteogenic differentiation of human adipose-derived stem cells.

In the last examples particles were prepared using a unique crosslinking step. Multiple crosslinking stages are useful to produce systems with improved mechanical properties [25] or in the design of injectable/smart systems. Superhydrophobic surfaces showed to be suitable to implement such kind of sequential procedures. In a first stage, chitosan beads were ionically crosslinked in order to turn the beads manageable. In a second step, a rising in temperature above 37 °C led to a reinforcement of the mechanical properties of the final 3D structure due to the establishment of other attractive forces caused by the presence of β-glycerophosphate [26]. Dexamethasone and fibroblast-like cells were encapsulated independently in these beads to validate the applicability of this system in the biomedical field. Those

chitosan-based gels are interesting implantable systems because the beads are handleable and flexible at room temperature, increasing stiffness just after implantation.

Besides systems able to encapsulate cells, some strategies are based on particulate systems able to sustain cell adhesion and proliferation over the surface that could be used as injectable scaffolds [27] or in biomaterials for cell expansion [28]. In a previous work it was shown that spherical scaffolds of elastin-like recombinamers with RGD domains could harden onto superhydrophobic surfaces by liophilization [29]. The spherical porous scaffolds were then collected and crosslinked by immersion in hexamethylene diisocyanate. The particles were found to act as excellent supports for cell adhesion and growth. In order to avoid crosslinking liquid baths, the crosslinking of such scaffolds could take place in adequate atmospheric environment, similarly with reported chitosan particles hardened under a glutaraldehyde atmosphere (Figure 2.2 G) [30]. Controlling the time of exposure to the vapor, different crosslinking degrees could be obtained.

Superhydrophobic surfaces were also efficient in producing more complex spherical structures. Compartmental systems are relevant when multiple drug release is required or when different cell types need to be encapsulated. Lima *et al.* [31] demonstrated that through a bottom-up approach, the successive deposition of layers of hydrogel precursor solutions onto superhydrophobic surfaces alternated with crosslinking steps allowed the production of concentric multilayer particles (Figure 2.2, E.1). Depending on the volume dispensed, the thickness of the hydrogel layers could be controlled. The release kinetics of a drug-model was controlled depending on its relative location in two-compartmentalized particles. Cells were also immobilized successfully in the outer layer of the particles, in order to facilitate the access to nutrients and O_2.

Using the principle of multilayer systems, pectin coated chitosan microgels, suitable for oral administration of an anti-tumor drug, were produced using superhydrophobic surfaces (Figure 2.2, G and G.1) [30]. The coating with pectin improved the control of the drug release in acidic conditions, preventing the release in the stomach and allowing the release in the intestine where it should be absorbed. In comparison with solubilized form, the effectiveness of 5-fluorouracil was improved when encapsulated inside those microgels.

Another explored spherical design was the production of multiscale systems composed by elements organized at the micro/macro levels. Magnetic microparticles were encapsulated in chitosan beads. The magnetic beads were tested to be applied in tubular bioreactors for cell culture due to the capability of cells to adhere and proliferate onto the surface of the particles, as well as their retention in a specific site where a magnetic field was applied [28]. Luz *et al.* [32] demonstrated that superhydrophobic surfaces

were suitable platforms to form hierarchical systems composed by SiO_2–CaO based bioactive nanoparticles (BG-NPs). A colloidal suspension of BG-NPs was dispensed onto the superhydrophobic platforms and organized particles were obtained after self-assembly induced by evaporation (Figure 2.2, F and F.1). Due to the bioactive properties of the BG-NPs [33], the spherical aggregates demonstrated to have potential to promote apatite deposition in physiological-like conditions. Application of these particles as bone bonding material was hypothesized. Following this principle of self-assembly induced by evaporation Shao *et al.* [34] used superhydrophobic surfaces as platforms to concentrate molecules. This approach could be particularly useful in processing of samples for biochemical life sciences analysis. Spheres were obtained through the evaporation of the droplet, where analytes such as DNA or proteins were included. The loss of material was minimal when compared with non superhydrophobic substrates. The extreme repellency of the used surfaces prevented the typical "coffee staining effect".

Based on the idea of Song *et al.* [19] in using biomimetic superhydrophobic surfaces to produce hydrogel particles, Hu *et al.* [35] proposed a different strategy also to produce hydrogel spheres. While in the first methodology the particles were in contact with the superhydrophobic surface and surrounded by air (Figure 2.2), in this work, a hydrophobic commercial PTFE surface was covered by an organic solvent (2,2,4-trimethylpentane (TMP)) and aqueous spherical droplets were formed on the interface, after being dispensed using a micropipette or a spray (Figure 2.3 B, B.1-3). Similarly with the superhydrophobic surfaces technique, the particle size was controlled by the volume dispensed; however the evaporation of the droplets during crosslinking was prevented by the presence of the organic solvent surrounded the produced particles. Hierarchical particles composed by poly(2-hydroxyethyl methacrylate) (pHEMA) and PNIPAAm encapsulating Au or Ag nanoparticles were obtained. A specific application was not demonstrated but we envisage an antibacterial and bactericidal potential of this particles due to the presence of Au and Ag nanoparticles, known to have antimicrobial properties.

In most of the works described above micropipettes were used to dispense the precursor solutions onto the superhydrophobic surfaces. The main disadvantage is the impossibility to dispense smaller volumes than *ca.* 2 μL [31]. In addition, part of the liquid could remain adhered in the micropipette tip which in the case of very small volumes leads to an inaccuracy of the volume dispensed or even the impossibility to dispense the droplet onto the superhydrophobic surfaces due to the high repellent forces. The search for more accurate and automated dispensing systems is still a challenge to scale up this technology toward the production of smaller particles.

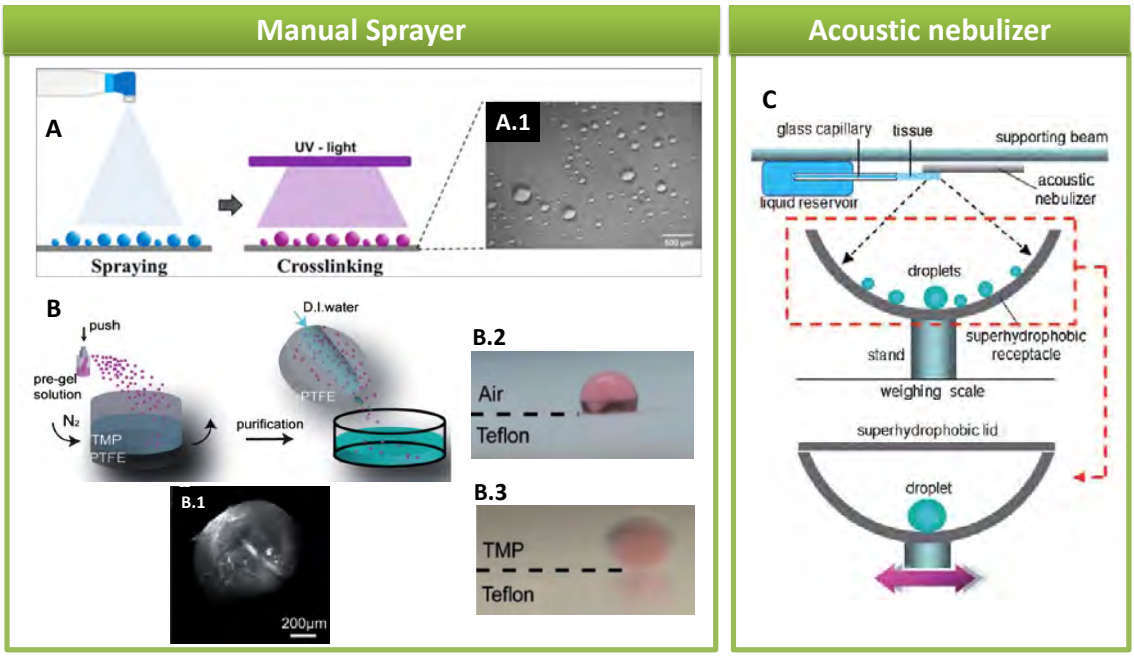

Figure 2.3. Spraying systems proposed to dispense droplets onto superhydrophobic surfaces. A generic spraying device was proposed to decrease the size of the particles produced using the solid-air interface between the superhydrophobic surfaces and the atmosphere (A). Photocrosslinkable chitosan (methacrylamide chitosan) was used and particles with diameters lower than 320 μm, in a hydrated state, were obtained. A similar spraying system was also used to produce hydrogel particles in a solid-liquid interface (B). Superhydrophobic surfaces (from PTFE) were immersed into an organic liquid (TMP); then the polymeric solution containing the monomer, co-monomer, crosslinker and initiator was sprayed onto the organic liquid. Micro scale particles were obtained (B.1). The typical shape of the precursor solution at air-PTFE and TPM-PTFE interfaces are shown in B.3 and B.3, respectively. A precise dispensing system based on an acoustic wave nebulizer which delivers a spray aerosol droplets onto a superhydrophobic surface (C) was also proposed. By an accurate measurement of the weight of the dispensed droplets, the exact volume is determined. The gentle shaking of the superhydrohobic surface joint the small droplets into a single one. A, adapted from the reference [37] with permission of ACS Publications; B, B.1-4 adapted from the reference [35] and C from [36] with permission of RSC.

Having this in consideration, Vuong *et al.* [36] proposed an innovative, stable and precise microliter dispensing system. The technology principle was based on spraying the solution onto the superhydrophobic surface using an acoustic nebulizer (Figure 2.3, C). To control the volume of the droplet a weighing scale was used and the volume dispensed varied linearly with the operation time of the nebulizer. Another strategy to decrease the size of the obtained was proposed recently [37]. Methacrylamide chitosan aqueous solutions were dispensed onto superhydrophobic surfaces using a generic spraying device (Figure 2.3, A). After crosslinked by UV light exposure particles were obtained with diameters below 320 μm. The Cassie-Baxter regime of the surfaces allowed the preservation of the spherical droplets shape since their diameters were significantly larger than the pitch between the structures that composed the superhydrophobic platform. The average pitch of the surface was at least 1

order of magnitude shorter than the diameter of the smallest prepared droplets. In fact having an accurate dispensing system through which the particle size could be controlled, the only limitation to obtain particles in the nano scale is the distance between the top of the features that composed the superhydrophobic surface in use. More efforts should be made to improve such technology to permit high-throughput generation of sub-millimetric particles, including the use of mobile substrates and optimized methodologies to retrieve the obtained particles from the platforms. The examples exposed are based on the use of superhydrophobic surfaces, where water-based spherical droplets are generated. In the future, we expect that other kind of surfaces will be employed to support organic-based systems that will allow producing particles based on polymers soluble in such solvents [38]. This could extend tremendously the impact of the technology in the pharmaceutical industry.

2.5. Screening Systems based on Superhydrophobic Surfaces

2.5.1. Analytical Sensors

Miniaturized analytical devices using methods and strategies based on biochemistry, immunology and molecular biology have been developed as very important tools in monitoring health status worldwide. There are several advantages in scaling down biological analysis [39]. In general, the molecules that are desired to detect or to quantify could be present in very small amounts being micrometer-sized systems better suited than conventional laboratory tests tubes. In addition, small amounts of biological samples are required as well as smaller volumes of expensive reagents enable saving costs. Waste is reduced and parallel detections could be performed easily. The fabrication of chips has made a great progress. However, the high costs in manufacturing and, sometimes, the requirement of sophisticated instrumentations prevent their extensive application in the clinic. The demand for low-cost, disposable, as well as simple devices for massive, rapid or even multi-analyte detections for both clinical diagnosis and the study of chemical or biological entities was the driven force to investigate the application of alternative cheap platforms for sensor applications.

The use of superhydrophobic substrates has shown to be applied in innovative analytical solutions. A lab-on-chip analytical sensor was proposed based on the concept of spherical-shaped liquid droplets supported on superhydrophobic surfaces [38]. In this idea, droplets containing specific analytes may be dispensed onto the repellent surfaces, where a certain reaction occurs inside. The detection could be achieved by measuring the color intensity of recorded images [40] like in the case of liquid marbles [41]. Superhydrophobic surfaces are advantageous since as more repellent they are, more elevated is the center of gravity of the droplets, which facilitate the visualization and recording of the micro-scale physical

transformations or biochemical reactions occurring inside. Moreover, the use of non-adhesive superhydrophobic surfaces may prevent contaminations and allow their reuse. Such simple and fast technique may permit the development of chemical and biological reactions and biochemical assays in a high-throughput manner with reduced costs.

The demand for more accurate and rapid typing tests in blood transfusion/transplantation medicine as well as in blood banking for screening or cross-checking donors was the driving force to explore superhydrophobic surfaces as suitable platforms for blood typing assays. Li *et al.* used polymeric superhydrophobic platforms to observe the haemagglutination reaction of human red cells [40]. The reaction occurring inside the blood droplet can be followed/recorded using a digital camera. Then, the collected images are processed by specific software for blood typing determination (Figure 2.4, A). The successful results in ABO and RhD blood assays and the low production cost of superhydrophobic surfaces proof that such platforms are interesting to be used as laboratory consumables to support micro reactors for biochemical assays. We envisage that the versatility of the technology could permit the extension of such tests towards the detection of other biochemical markers and the use of other physiological fluids.

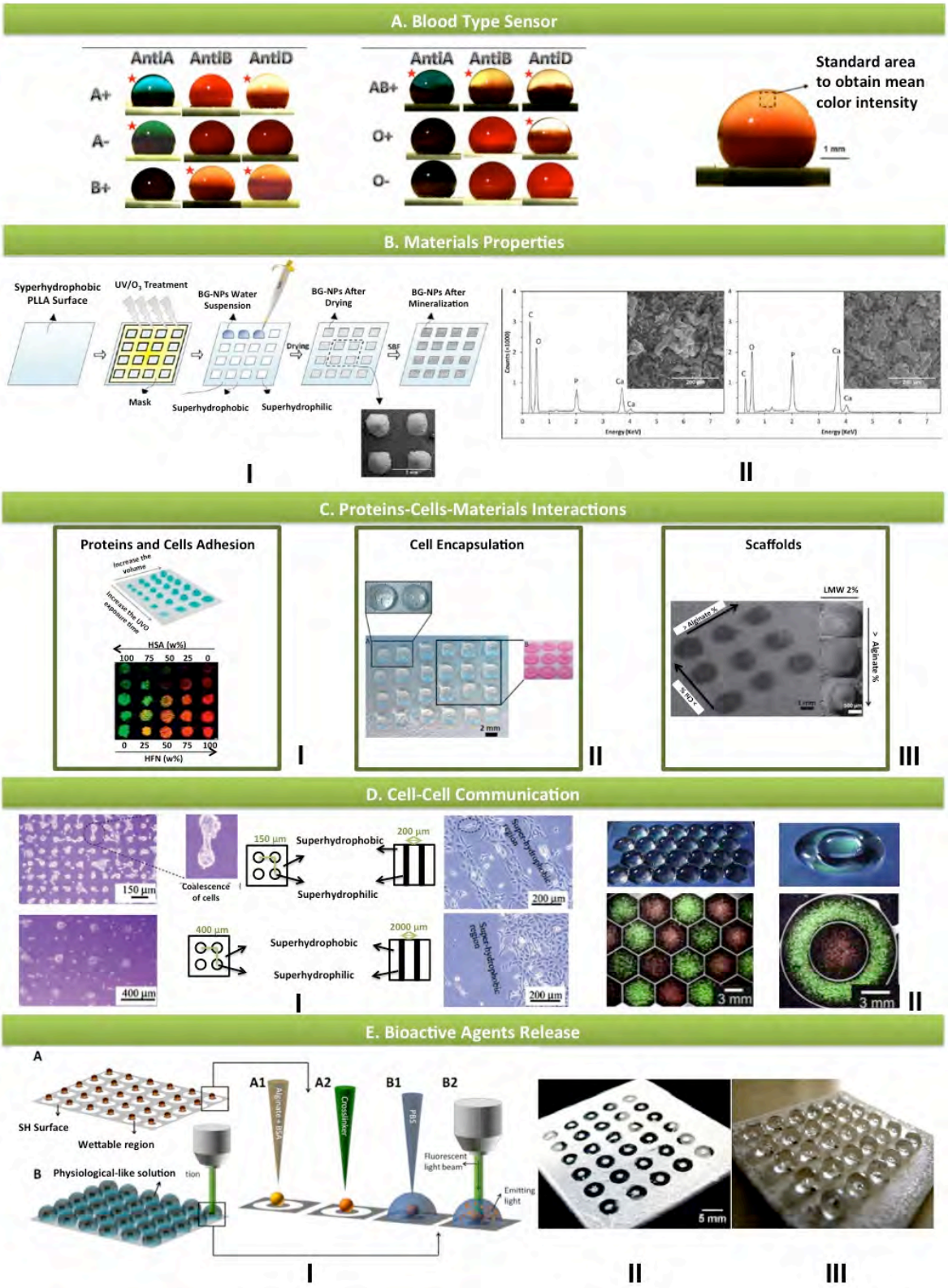

Figure 2.4. Examples of screening systems using superhydrophobic surfaces. (A) Blood type screening test obtained by colorimetric analysis of the droplets dispensed on the superhydrophobic surfaces, and where blood agglutination occurred after a mixture with antibodies (Anti-A, Anti-B and Anti-D). The red stars indicate where blood aggregation was triggered. (B) Square patterned superhydrophobic surfaces to analyze the bioactivity of different inorganic nanoparticles dispensed onto the hydrophilic areas (I). The nanoparticles were confined in such areas after solvent evaporation. The apatite deposition in each

spot was analyzed by EDS after immersion the chip in simulated body fluid medium (II). (C) Patterned chips for the study of proteins-cell-materials interactions: (I) proteins and subsequent cell adhesion; (II) viability of cells encapsulated in hydrogels with different compositions and (III) cell proliferation and viability on scaffolds also with different compositions. (D) Micro patterned superhydrophobic surfaces used to study cell-cell communications. Cells adhered on the superhydrophilic areas, however depending on the distance (I), cells could establish cell-cell direct contact. Different designs of the patterned areas may be produced and used to study more than one type of cells (II). (E) Ring-shaped patterned chip (II) to follow the release of fluorescent molecules from each spherical shaped particle fixed on the center of each ring (III). The quantification was obtained by imaging analysis of captured fluorescent microscopy images over time. A, adapted from the reference [40] and B from [42] with permission of Elsevier; C, adapted from the follow references: [44] (I), [45] (II) and [46] (III) with permission of RSC and Wiley; D, adapted from the references [51] (I) and [49] (II) with permission of ACS Publications and Elsevier; E, adapted from the reference [54] with permission of ACS Publications.

2.5.2. Screening of Materials Properties

The possibility to screen the properties or effectiveness of multiple materials in a unique assay, decreasing the variability of the conditions, reducing costs and obtaining results in a fast way, lead to an increase interest in chips development for materials analysis. The principle is the printing of homogenous platforms with areas with certain properties or designs capable to retain the deposited materials. The entire chip is subjected to the same treatment with the aim to evaluate the desired effect/properties and compare *in situ* the different formulations tested in the different places of the chip. Different materials, concentrations or even combinations may be tested easily onto such platforms.

Considering these statements and the possibility to pattern superhydrophobic platforms using a simple and cost-effective procedure, biodegradable superhydrophobic PLLA surfaces were patterned with small superhydrophilic squares to be employed as devices for *in situ* tests. As a first example of application, the obtained chips were used as disposable arrays to characterize, *in vitro,* the bioactivity of inorganic materials [42], a major important aspect of biomaterials to be used in orthopedic applications [43]. The proof-of-concept was performed by dispensing in the superhydrophilic areas suspensions of binary (SiO_2-CaO) and ternary (SiO_2-CaO-P_2O_5) nanoparticles, let them dry and then immersing the entire chip in simulated body fluid (Figure 2.4, B I). The particles were confined into the wettable areas due to the strong contrast in surface tension with the surrounding superhydrophobic regions. The results demonstrated that ternary system promoted and enhanced apatite deposition, and such flat chips may be used in combinatory assays to easily evaluate certain properties of materials using very small amounts of samples (Figure 2.4, B II) [42]. Since the entire array is subjected to exactly the same conditions, more reliable results may be achieved. In principle such chips could be used to test other properties and also other classes of materials. Some more examples will be given in the next sections.

2.5.3. Screening of Proteins-Cells-Materials Interactions

The study of the interactions between superhydrophobic surfaces and proteins or cells in conjoint to the possibility to modify its wettability have pushed the development of chips for high-throughput screening where materials characteristics, and different biological responses may be evaluated in a single experiment. An array obtained by patterning PS superhydrophobic surfaces was explored as a multiplexing tool for the evaluation of the biological performance of independent combinations of biomaterials, cells and culture media [44]. Albumin and fibronectin, two proteins with important role in a variety of biomedical and biological aspects, were first adsorbed in the wettable zones of superhydrophobic-based chips. The interaction of cells with different concentrations and combinations of the two proteins was studied (Figure 2.4, C I). The results demonstrated that for the same total protein concentration, the cells preferred the spots with major proportion of fibronectin. For the same proportion between fibronectin and albumin, the cells adhered better in the spots with higher total protein amount. Such results were expected since fibronectin present RGD and PHSRN sequences which are integrin binding domains. In this case cell behavior was probed in essentially 2D environments. It would be interesting to extend this technology towards three-dimensional architectures, much more interesting for testing biomaterials and devices for tissue engineering. The same arrays were then used as combinatorial platforms for screening of cell interactions with different combinations of 3D materials with relevance in tissue engineering [45]. Two cell types were encapsulated in a vast range of natural-based miniaturized hydrogels (Figure 2.4, C II). The viability of encapsulated cells was determined via image analysis and compared with traditional materials/cell destructive testing methods. The results from the two characterization sources were similar, proving that image analysis of the array constitute a reliable and fast method for cell viability evaluation when encapsulated into different types of materials. The main limitation of this strategy is the difficulty to be used to analyze opaque materials, as the on-chip tests are based on image analysis. However, the hydrogels are highly hydrated and are most of the time transparent.

Besides hydrogels, porous structures are important for tissue engineering applications. The production of 3D millimetric scaffolds was performed *in situ* over the PS superhydrophobic substrates (Figure 2.4, C III) [46]. The structures were characterized regarding mechanical properties, porosity and pore size. The proportion between materials (sodium alginate and chitosan) was varied and cell-materials interactions were also evaluated by looking at the metabolic activity and cell number using both destructive methods and direct image-based analysis. This work demonstrated that these small chips could be considered reliable platforms for *in vitro* screening of the main properties currently assessed in scaffolds

characterization as well as for preliminary biological studies. The mechanical/viscoelastic properties of chitosan/bioglass nanoparticles composites and the respective interaction with pre-osteoblast cells was studied in detail using the same PS chips [47].

In vitro experiments are very important in the first assessment of the biological behavior of biomaterials. The next step always involves the testing of the best formulations using appropriate *in vivo* models. Conventional *in vivo* screening of materials involves their implanting one by one, requiring often an highly number of animals, which in turn trigger ethical questions and elevated experimental costs. Patterned devices with areas of contrast wettablities, produced onto flat and flexible films, were hypothesized to be powerful tools for detection of hit spots with promising properties and exclude materials with uninteresting characteristics [48]. A group of scaffolds, fabricated from the combination of different amounts of chitosan, alginate and carrageenans, were dispensed as arrays over flexible patterned superhydrophobic PS chips. The chips were analyzed upon being implanted subcutaneously in rats [48]. The results obtained on-chip were compared with conventional individual implantation of the scaffolds and showed that these platforms could be used for high-content evaluation of *in vivo* biomaterials response. The employment of cheap superhydrophobic platforms as high-throughput devices for *in vivo* screening clearly mark an important step in biomaterials development. Time and costs could be saved and more realistic results could be obtained due to the consideration of the complex *in vivo* environment. In the referred work [48], just the inflammatory response caused by the biomaterials was explored. In the future, hybrid structures combining cells and materials should be tested in order to extend this methodology towards cell therapies for regenerative medicine.

2.5.4. Screening of Cell-Cell Communications

Tissue´s development involves the organization of multiple cell types undergoing processes such as intercellular communication and cell signaling. These complex phenomena are crucial for the whole organism development. The culture of multiple cell types in separated but adjacent compartments is a recurrent strategy to mimic these events. However, the existent techniques for cell patterning are complicated and have some limitations, which include the restricted geometry of the patterns and the number of the cell types used [49,50].

The easy manufacturing processes to produce and pattern superhydrophobic surfaces, as well as the possibility to confine in certain areas different types of cells, have encouraged the use of such platforms for cell-cell interactions studies. For example, silicon and glass micropatterned surfaces were used to study the effect of the distance between adjacent cells. Cells adhered selectively onto the well-defined

wettable areas. Cell-cell interactions were affected by the distance between the superhydrophilic neighbor areas. For distances below 250 μm, cells were able to form filopodia projections and establish direct communication [51] – Figure 2.4, D I. In order to study the interactions between different cell types, surfaces of poly(2-hydroxyethyl methacrylate)-co-(ethylene dimethacrylate) (HEMA-EMA) or 2,2,3,3,3-pentafluoropropyl methacrylate (PFPMA) grafted onto glass slides were patterned with distinct geometrical features [49] – Figure 2.4, D II. Suspensions containing different cell types were confined in the hydrophilic areas, creating multiple culture reservoirs in the same substrate. Once again, the cells adhered onto the more hydrophilic areas forming a monolayer. The entire platform was cultivated in conjoint standard culture medium to collect data related with cell-cell interactions and signaling processes. This strategy could be a valuable tool for creating complex cell patterns, just using the resources existent in conventional cell culture labs. No special apparatus are required to perform such cell cultures.

Until now just cell-cell interaction studies at 2D level were performed, however, we envisage that patterned superhydrophobic surfaces could be interesting platforms to study the interactions of the cells when seeded onto 3D structures. The motivation is related to the fact that 3D rearrangements will be closer to the *in vivo* conditions, and would constitute better models for fundamental studies as well as in the development of screening and fabrication platforms in drugs development, models of diseases and tissue engineering. A first insight related with 3D cell structures, though not applied to cell-cell communications studies, was presented using superhydrophobic platforms to obtain cell spheroids. Based on a rose petals effect, which enables the fixation of the aqueous droplets, flat PS superhydrophobic surfaces were patterned with micro-indentations where liquid droplets containing cells were immobilized. Facing down the platforms with the droplets, 3D agglomerates of cells were obtained by gravity effect [52]. Such device was hypothesized to be applied in biomedical field as micro-bioreactors where chemical and biological combinatorial tests may be performed, for example, the screening of the cytotoxicity of drugs on micro-tissues. Instead of suspending aqueous spherical droplets containing cells, semi-spherical droplets were dispensed over transparent wettable spots distributed in superhydrophobic PS surfaces [52]. By inverting the system, spheroids could be also generated for drug screening tests. In this case the transparent windows existing in each spot facilitate the visualization of the individual spheroid and the independent liquid exchange in each droplet.

2.5.5. Screening of the Release of Bioactive Agents

In vitro release studies of bioactive agents are rather important since they constitute the first prediction of the performance of drug delivery systems when applied *in vivo*. Such preliminary studies are recurrent

tests used in lab research since they allow re-designing the systems in order to obtain the desired profiles/characteristics. Standard *in vitro* procedures are laboring and consume significant amounts of resources and lab space. The automation and miniaturization of conventional methodologies require complex, large and expensive mechanical systems. Patterned superhydrophobic surfaces were proposed as cheap platforms able to be used in high-throughput quantification of biomolecules released from biomaterials matrices [54]. Superhydrophobic surfaces were patterned to obtain a hydrophilic transparent disc containing a superhydrophobic opaque spot in the center (Figure 2.4, E II). Such donnut-shape was patterned in the surface of a superhydrophobic chip. A polymeric solution (sodium alginate - based) incorporating a bioactive agent model (bovine serum albumin labelled with a fluorescent marker) was dispensed on the superhydrophobic spots remaining with an almost spherical shape (Figure 2.4, E I A1 and III). Such matrices were crosslinked with calcium ions (Figure 2.4, E I A2), in a similar process used in the preparation of alginate particles for theophylline release [19]. Each transparent ring was then filled with a physiological-like fluid acting as individual release media (Figure 2.4, E I B1). Over time the release of the molecules in each spot was followed by acquisition of fluorescent microscopy images (Figure 2.4, E I B2). The comparison between the image analysis results and *in vitro* conventional studies demonstrated that this technique was quite reliable, and minimal amounts of reagents and space were used [54].

In principle all the systems described in the section 2.2 for drug release applications are suitable to be tested in this chip, provided that the bioactive agent to be studied was previously labelled with a fluorescent molecule. Furthermore, this technology may also be generalized to other types of matrices as well as other crosslink pathways. The use of confocal microscopy (or other advanced 3D imaging technologies) to monitor the distribution of the drug in the entire volume of each particle as a function of time could permit a true 4D monitoring of the release of entrapped molecules inside the matrices.

2.6. Microfluidic Devices Based on Superhydrophobic Surfaces

Nano/microfluidic devices have been used in several biomedical applications [55]. Devices for cell culture [56], medical diagnosis (*e.g.* biosensors) [57], and microparticles production [58] are just a few examples. Nano/microfluidic systems are emerging as powerful tools bring advantages such as minimal use of reagents/samples, quality control and miniaturization when compared with conventional procedures. Such devices exploit small size and the characteristics of the fluids flow inside the channels, offering as well new capabilities in the control of concentrations of molecules in space and time [59].

In microfluidics, the wettability of the channels is important to manipulate the flow of the liquids. Water super-repellent surfaces were hypothesized to bring advantages due to the possibility to reduce the drag in microchannels (low-friction) [60] and to produce microvalves [61].

In another approach, the surface-tension driven force using selective hydrophobic/hydrophilic contrast is an interesting strategy to control the liquid flow and it is the principle for the development of superhydrophobic-based open microfluidic devices [62]. In this case the liquid can flow in pre-defined paths [63] without the need of physical walls in the channels. The micro/nano roughness in combination with the chemistry inside the channels will dictate the behavior of the liquid flow [64].

The demand for more affordable, accurate, simple and low cost technologies for diagnosis (*e.g.* infectious diseases) or even to measure the health status have inspired the application of paper in microfluidic devices [65]. The introduction of paper with contrast wettabilities in biomedical area started with patterned paper where hydrophilic millimetric-sized channels surrounded by hydrophobic regions was proposed as suitable low-cost platforms for multiplex bioassays [66]. Hydrophilic channels were created and a sample of liquid could migrate from one edge through the channels by capillary action to achieve 3 distinct detection areas (control and two detection chambers). The device was used to quantify glucose and BSA from 5 μL of urine [66]. Based on this system, a more complex device was proposed for the detection of biomarkers of the liver: alkaline phosphatase, aspartate aminotransferase and total serum protein. The reliable results obtained using blood from a finger stick showed that such device could be used in routine clinical screening [67].

The importance of paper as a simple and cheap substrate for many biomedical and biological applications has pushed the development of methodologies to enhance its water repellency. For example, superhydrophobic paper was obtained by a phase separation technique through the precipitation of poly(hydroxybutyrate) (PHB) onto the surface of paper [68, 69]. Such paper was easily patterned using argon plasma treatment and hypothesized to be used in applications such as microfluidic or lab-on-paper devices [70]. Recently, the same superhydrophobic paper was patterned by printing and writing processes [68]. The inject printing of hydrophilic ink with distinct grey intensities allowed to control the wettability of the surface and the liquids flow. Aqueous-based liquids were driven through the patterned channels just by tilting the surface.

Patterned PS superhydrophobic surfaces were proposed by Oliveira *et al.* [62] as possible open-microfluidic devices (Figure 2.5, A). Such surfaces exhibited higher wetting contrast when compared with hydrophobic ones, turning the liquid flow through the superhydrophilic paths in horizontal position more efficient than in hydrophilic channels patterned on smooth surfaces. Since PS is the material used in cell

culture dishes, we envisage that such microfluidic devices patterned with appropriated designs could be used for screening of cell cultures under dynamic conditions.

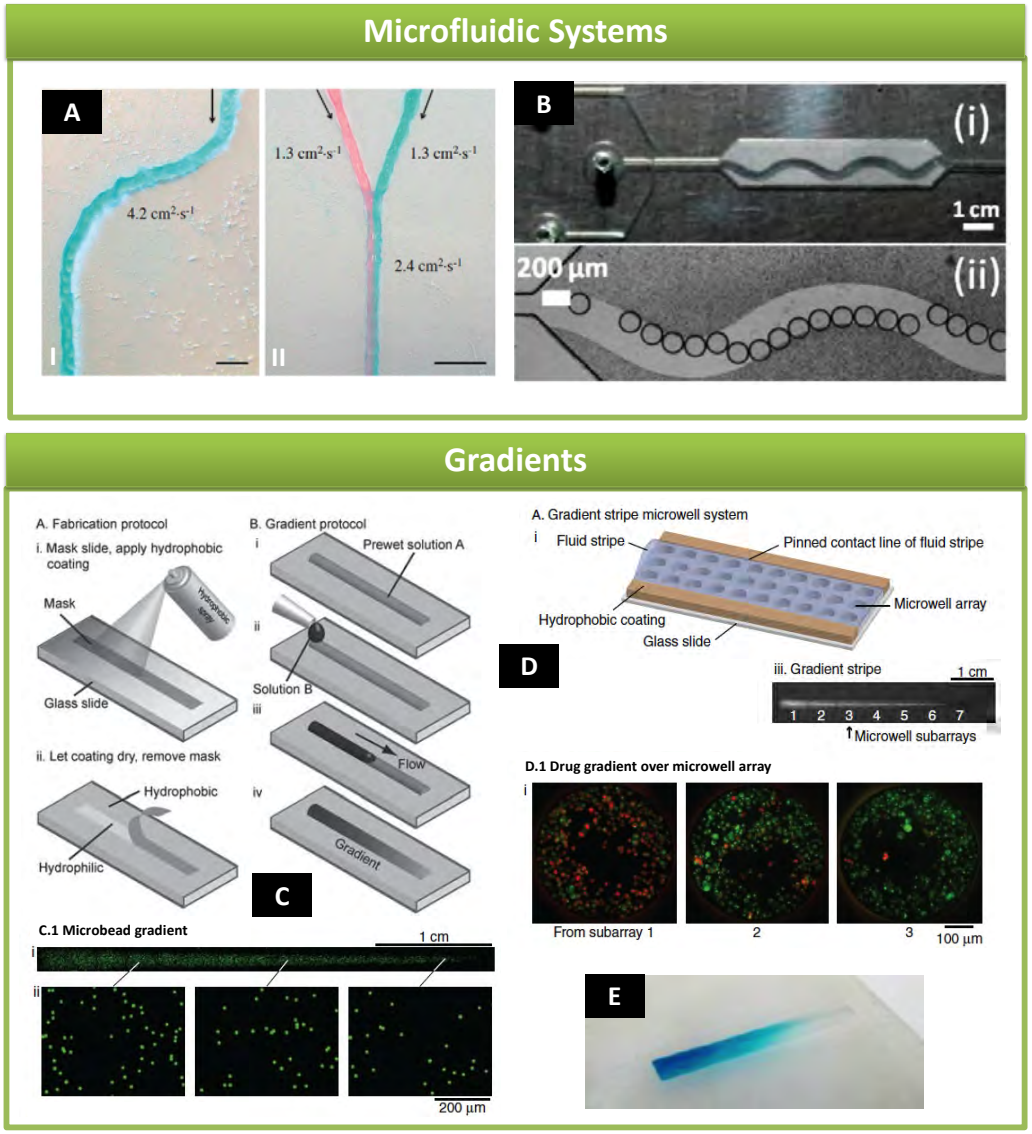

Figure 2.5. General microfluidic systems proposed using different superhydrophobic and highly water repellent surfaces: (A) polystyrene superhydrophobic platform patterned by argon plasma treatment or UV/Ozone exposure was proposed as a microfluidic platform for continuous liquids flowing and; (B) PDMS microfluidic platform where the flow of the droplets was controlled along the desired path. (C) Process to fabricate a glass-based hydrophobic platform to produce microbead gradients (C.1) by dispensing a suspension of green fluorescein microparticles. The same surface modification strategy was implemented in a microwell system (D). Cells were seeded inside the microweels and a gradient of doxorubicin concentration was created. The viability of the cells in contact with different amounts of drug was accessed by Live/Dead assay (live cells were green and dead cells were red) (D.1). (E) Superhydrophobic glass coated with diatomaceous earth, where a channel-like pattern was obtained by argon plasma treatment, showed to be a suitable device to produce gradients of concentrations of materials/molecules. A, adapted from the reference [62] with permission of The Japan Society of Applied Physics; B, adapted from the reference [71]

with permission of ACS Publishing; C and D, adapted from the reference [74] with permission of Wiley; E, adapted from the reference [73] with permission of ACS Publishing.

Draper *et al.* fabricated patterned polydimethylsiloxane (PDMS) superhydrophobic surfaces to be integrated in microfluidic devices for passive manipulation of droplets flow at the micro scale level (Figure 2.5, B) [71]. The innovation is that no pillars or electrodes were required to control the movement of the droplets inside the channels which turn the system simpler to operate. Acceleration, deceleration, merging, and path control could be controlled just by playing with surface design and repulsion properties of the channels. This strategy could be useful for analytical and detection devices.

The existence of a gradient of properties, concentration of molecules, content of particles or other relevant ingredients, turn such type of anisotropic biomaterials interesting for biomolecules delivery, drug screening and cell biology studies [72]. The extreme contrast of surface tensions obtained in patterned superhydrophobic surfaces encouraged the development of a bench top methodology powered by capillary flow and molecular diffusion of precursor liquids into a defined path to obtain gradients in hydrogels [73]. An easy and rapid microfluidic device to formulate gradients in-house was recently proposed [74]. Wettable channels were defined onto a glass coated with a hydrophobic spray (Figure 2.5, C A). The precursor solution was pipetted in the pre-wetted hydrophilic channels (Figure 2.5, C B). The liquid flowed through and created a gradient by convection, in a short time period. This concept was applied in simple straight channels where a gradient (Figure 2.5, C.1) and a cross gradient of microparticles content was generated and in a microwell system, that permitted to study the effect of a drug gradient on cell viability (Figure 2.5, D). Other kind of substrates, such as superhydrophobic glass or PS coated with siliceous exoskeleton of diatoms patterned by argon plasma treatment, were also proposed to produce these kind of materials (Figure 2.5, E) [73].

Due to the relevant role of the gradients of cues in biomedicine, it is expected in the next few years a significant increase of the employment of materials with these characteristics mainly for cell-based experiments and high throughput screening under dynamic conditions or through gradients of distinct properties.

2.7. Superhydrophobic Textiles in Biomedicine

When in contact with human body, textiles have appropriate temperature and humidity conditions to promote the growth of micro-organisms. The rapid and uncontrolled colonization by microbes could lead to serious healthcare problems. Having into account the increasing concern related with public hygiene, the research to fight against micro-organisms growth have been gained attention. The modification of

textiles is an interesting strategy to achieve this purpose. One specific case in biomedicine is the battle to eliminate bacterial strains. Such micro-organisms develop resistance to antibiotics easily and in a very fast way. The development of innovative strategies is continuously required in order to obtain novel antibacterial or bactericide products [75].

It is well known that inorganic nano-structured materials, namely Ag, Au, ZnO, TiO_2, Cu nanoparticles, have anti-microbial properties [76]. For example, silver is known to be 'oligo-dynamic', having anti-microbial and bactericidal effects but low toxicity to human cells. Silver effect has been demonstrated against more than 650 diseases-causing organisms as well as in prevention of biofilms formation [75,76]. Regarding this, the coating of textiles with silver nanoparticles merged as a way to promote the antibacterial properties of fabrics [77]. Superhydrophobic cotton was obtained after being coated with silver nano particles with 100-500 nm and treated with octyltrithoxysilanes (Figure 2.6, A) [78]. The incorporation of silver nanoparticles demonstrated to be efficient against both Gram-positive (*Staphylococcus aureus)* (Figure 2.6, B) and Gram-negative bacteria (*Escherichia coli*) (Figure 2.6, C).

An interrelationship between low surface energy of cotton fibers and bacteria growth inhibition was established [79]. In this way, the coating of cotton fabrics with materials having low energy, such as fluoropolymers and silicon-based polymers, were reported as an alternative strategy to obtain anti-microbial hydrophobic and oleophobic surfaces [80]; without the need of incorporating anti-microbial substances.

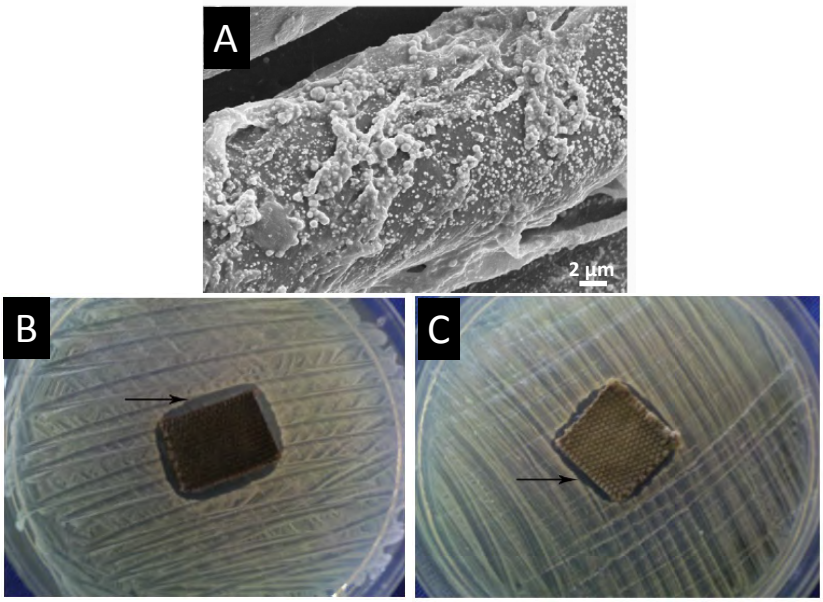

Figure 2.6. (A) Structure of the fibers of superhydrophobic cotton. The structure of the fibers became rough, due to the presence of the nanoparticles. The antibacterial activity of the superhydrophobic cotton was verified against *Staphylococcus aureus* (B) and *Escherichia coli* (C). Images adapted from the reference [78] with permission of Elsevier.

Biomedical applications of superhydrophobic anti-microbial textiles were not explored until now. We envisage that the combination of anti-microbial properties with an extreme water/oil repellency behavior may be advantageous in the biomedical field. For example, pressure ulcers affect millions of hospitalized patients each year. The normal healing process is frequently impaired due to the development of biofilms in the ulcer site [81]. The employment of highly repellent textiles that do not absorb undesirable fluids, being easily cleaned, and combined with the capability to inhibit the bacteria contamination of the ulcers, could prevent their evolution until reach critical states or even avoid some interference in the normal healing process.

2.8. Biomaterials in Contact with Blood

2.8.1. Biomaterials for Medical Devices

Direct blood contact materials, which include implantable systems and devices for catheterization, drainage and blood circulation, may trigger undesirable interactions between blood and the device. Blood proteins adsorb rapidly onto materials surface, followed by the adhesion and activation of the platelets. During the activation of the platelets, coagulation factors are released and may promote the formation of thrombus, causing the functional failure of the devices. The fabrication of blood-compatible materials is still a challenge. Tailoring the surface chemical composition, surface roughness and consequently the wettability, constitutes a possible strategy to achieve adequate properties for this purpose. Therefore, also in this case superhydrophobic surfaces could be used.

Khorasini *et al*. [82] developed a strategy to improve the antithrombogenic properties of PDMS. Despite owning good general physical and chemical properties under biological environment, PDMS lacks in the long-term stability being required an improvement of its antithrombogenic properties. PDMS with extreme wettabilities were studied to prevent the platelet adhesion. Applying a CO_2 pulsed laser treatment the hydrophobicity of PDMS was incremented. The water CA raised from 105° to 170° (superhydrophobic PDMS). In order to achieve proper comparisons, superhydrophilic PDMS was obtained by grafting hydroxyethylmethacrylate phosphatidylcholine (HEMAPC), where the water CA decreased to values around 10°. The laser treatment leads to the appearance of roughness onto the PDMS surface that was then attenuated by HEMAPC grafting. Platelet adhesion was found to be very limited onto both superhydrophobic and superhydrophilic PDMS, when compared with the untreated material. These results allowed concluding that chemical cues, such as grafting of negative-charge groups, and extreme wettability properties of PDMS inhibit platelet activation.

To better investigate the influence of the topography on platelets adhesion, a study was developed comparing the effect of the micro with nano structures onto PDMS surfaces [83]. PDMS with micro-pillars demonstrated low platelet adhesion when compared with smooth PDMS (Figure 2.7, A.1-6). Since the wettability is directly related to surface topography, a correlation between the wettability of the PDMS and the adhesion of the platelets was established. The lower the spacing between the micro-pillars, the more hydrophobic was the PDMS surface and less platelets adhered (Figure 2.7, A.2-4). In addition, PDMS with nano-grooves was also studied (Figure 2.7, A.5). These patterned surfaces were not superhydrophobic but inhibited platelet adhesion, probably due to the small spacing between the grooves which prevented the pseudopodium formation. In order to generalize the tendencies above described, these kinds of studies should be extended to other materials and on textured surfaces decorated with different geometrical features.

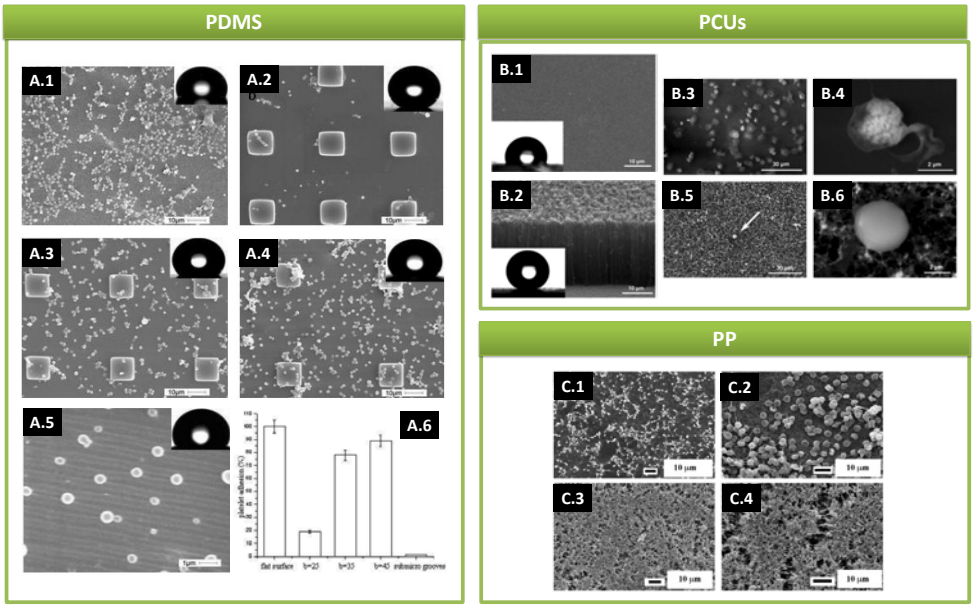

Figure 2.7. Platelets adhesion onto PDMS smooth (A.1), micro patterned with different distances between the pillars (A.2-A.4) and sub micro grooved (A.5) surfaces. The quantification of platelets demonstrates that submicra structures and lower pitches in micropatterned PDMS inhibited platelet adhesion (A.6). Poly(carbonate urethane) (PCU) was also studied to averiguate the effect of superhydrophobicity. Smooth surfaces (B.1, CA ≈109.1°±1.58) were coated with aligned carbon nanotubes (B.2, CA ≈163.6°±1.18). Higher number of platelets with a spread morphology was observed on smooth PCUs (B.3 and B.4) when compared with superhydrophobic ones (B.5). The superhydrophobic PCU surface was clean and just a very few round shape platelets (B.6) were found. The blood compatibility of polypropylene (PP) was studied when films were in contact with platelet rich plasma and fresh human blood. The original PP films exhibited higher platelet adhesion (C.1) as well as blood cells (C.2). In contrast, the superhydrophobic surfaces exhibited an opposite effect, where almost no platelets (C.3) or blood cells (C.4) were visualized. A.1-6, adapted from the reference [83] with permission of Trans Tech Publications; B.1-6, adapted from the reference [84] with permission of Wiley; C.1-4, adapted from the reference [85] with permission of Elsevier.

Poly(carbonate urethane)s (PCUs) (Figure 2.7, B.1) are used in biomedical applications due to their acceptable blood compatibility and long term-stability. The increment on PCU hydrophobicity was achieved by coating their surface with vertically aligned carbon nanotubes with diameters of *ca.* 40 nm and length of 20 μm (Figure 2.7, B.2) [84]. The adhesion of activated platelets was much higher on smooth than on superhydrophobic nanostructured PCUs (Figure 2.7, B.3 and B.5). The nanostructured surfaces remained without adhered platelets after the experiments. As seen before with patterned PDMS, PCUs coated with nanotubes surfaces may be as well a good strategy to improve the hemocompatibility of biomaterials. Once again, the methodology used to perform the coating with carbon nanotubes should be tested in other materials used in blood-contact applications and long term cytotoxicity studies should also be done.

The effect of surface micro/nano structures and superhydrophobicity was also tested in polypropylene (PP) materials [85]. Both platelets and blood cells did not adhered onto modified PP surfaces (Figure 2.7, C.1-2 versus C.3-4); the main reason could be related to the presence of an air layer on the superhydrophobic surface that acts as a "virtual wall" (Cassie-Baxter regime), preventing the contact between platelets and the material.

All the previously reported studies analyzed the materials in static conditions, meaning that the material was placed in contact with plasma rich platelets and the number of platelets adhered was determined. However, dynamic studies are required to investigate the effect of continuous flow of blood or even *in vivo* implantation, in order to obtain more reliable information on the hemocompatibility of the materials.

2.8.2. Vascular Grafts

A more specific case of blood-contact materials are grafts or patches used in the treatment of vascular diseases. Different strategies have been proposed to prevent coagulation and platelet adhesion in these devices. For example, enzymes or cells with antithrombogenic properties have been attached onto the surface of materials aimed at being in contact with blood. However, some problems results from those strategies. Enzymes can lose their activity, compromising the antithrombogenic effect. In addition, some studies reporting the coating of materials with endothelial cells demonstrate controversial results, being inconclusive about the benefits of this coating [86–88]. Expanded polytetrafluoroethylene (ePTFE) has been reported as one of the most inert polymers being interesting for biomedical applications due to its non-thrombogenic properties [89]. One of the strategies proposed to improve the performance of ePTFE was the modification of the wettability of the luminal side of the vascular graft. Using ion beam etching, the CAs raise from 109° to 140°-150°. An independent study revealed an inhibition of the spreading of

skin fibroblasts onto superhydrophobic ePTFE when compared with the same material exhibiting a hydrophilic surface [90]. In order to verify the effectiveness of the superhydrophobic properties in vascular grafts applications, *in vivo* studies were performed in rabbits' carotid arteries using the same ePTFE grafts [91]. The results revealed that after 1 week post implantation the treated hydrophobic grafts remained clear and untreated grafts were occluded. No anticoagulants were administered and the surface remained superhydrophobic for at least 6 months [91].

A very similar study was reported by Toes *et al.* [92], using the same ePFTE grafts and patches (also treated with ion beam etching). Blood interactions with the implants as well as their in vivo performance were both evaluated. The results demonstrated that the superhydrophobic treatment did not improve the performance of the grafts. After 15 min - 1 h they were completely occluded in the two tested animal models utilized: rabbits and pigs. Such controversial results were not expected and no reasons were found to explain the failure of the superhydrophobic ePFTE *in vivo*. This means that more studies are required using different materials, grafts with different inner diameters as well as different *in vivo* models to conclude the real influence of superhydrophobicity in this kind of applications.

2.9. Conclusions

The unique properties of superhydrophobic surfaces have been explored in a variety of applications in the biomedical field. Superhydrophobic materials aimed to be used in direct contact with human body, such as drug release systems, showed benefits in sustain the release for long time periods. Superhydrophobic vascular grafts were hypothesized to improve the antithrombogenic properties of the grafts, but the controversial results obtained *in vivo* did not allow concluding about the effective benefits of superhydrophobicity. However, for blood contact materials, such as catheterization and blood passing, the majority of the modified materials proposed demonstrated that the presence of micro/nano roughness and extreme wettabilities prevented platelet adhesion and activation. Independently of the wettability, the presence of nano features was critical to impede the adhesion of platelets. Fabrics were also modified to obtain other properties such as anti-microbial capacity. The most used process was the coating with inorganic-based nanoparticles with anti-microbial characteristics, which in turn increased the roughness of the cotton fibers until reach a superhydrophobic behavior. A correlation between low energy surfaces and anti-microbial properties was established in absence of added anti-microbial agents.

Superhydrophobic surfaces demonstrated appropriated properties to execute *in vitro* tests. Patterned platforms exhibiting areas of wettability contrasts were proposed as devices for high-throughput screening. Superhydrophobic-based chips could be produced using simple and cost-effective methodologies. Until

now the effectiveness in the screening of properties of materials, materials-proteins-cells interactions, cell spheroids response to drugs, cell-cell communications and drug release systems was successfully demonstrated. Patterned surfaces as open microfluidic devices have been proposed, but applications should be better explored in the future.

For more industrial applications, superhydrophobic surfaces were proposed to suppress some disadvantages of the conventional methodologies employed to produce particles. It was demonstrated that highly repellent platforms were successful in producing drug release systems or cell-laden spherical biomaterials in mild conditions and with high encapsulation efficiency. The nano roughness inherent to superhydrophobic surfaces as well as efficient dispensing systems of small droplets have been conditioned the production of nanoparticles using this approach.

2.10. Future Perspectives

Very interesting applications of micro/nano structured superhydrophobic surfaces in the biomedical field have emerged in the last few years. The understanding of the biological interactions with this kind of surfaces still in immature stage, being required deeper explanations for their performance *in vivo*. Focusing in the particular case of vascular grafts, the examples reported using superhydrophobic grafts in animal models are quite inconclusive. We strongly believe that new investigations combining the most advanced materials used in those applications combined with cutting-edge technology could bring detailed explanation for the real influences of the materials characteristics on hemocompatibility. So far, membranes for controlled drug release were the only superhydrophobic systems proposed for implanting. The effect of superhydrophobicity should be extend to systems (including 3D devices) such as particles, scaffolds, patches, prosthesis with convoluted shapes, among others, and the integration in different human body tissues or organs studied in detail.

We also expect major advances in industrial production of superhydrophobic surfaces, including large areas with homogeneous properties and patterned platforms with areas of contrasting wettabilities, which in turn could be used as consumable devices in biotechnological and biomedical research and industry. Superhydrophobic chips are being well explored for a wide range of screening tests: materials characterization, drug screening, *in vitro* biological testes and *in vivo* materials testing. Such miniaturized systems are cheap alternatives for selection of the most appropriate materials to be applied in the biomedical field.

Regarding the immature stage of the superhydrophobic-based microfluidic devices it is estimated that in the next few years such substrates will be greatly explored for medical diagnosis, biomaterials testing or even in cell studies.

The use of superhydrophobic surfaces as platforms for producing particles has also demonstrated great advances in the last 4 years. Despite all the advantages of the technique and the different systems developed to encapsulate cells and drugs, efforts have also been done to decrease the size of the particles to amplify their possible applications. The size of the particles is limited by the dispensing system used as well as by the peak-to-peak distance of the surfaces roughness. In order to scale up this 2D particles production technology the development of an accurate automatic dispensing system is required.

One of the most obvious application of superhydrophobic films is the coating of textiles to avoid the water impregnation. However, the full potential of these special textiles in biomedical applications have not been explored, in particular the combination of such properties with others (*e.g.* stimuli responsiveness, advanced mechanical properties, anti-microbial).

The fast growing in the application of the superhydrophobic surfaces in the biomedical field verified in the last 5 years was an impulse for the pursuance in exploration for more applications that will require the effort of multidisciplinary and creative teams.

2.11. Acknowledgements

The authors are grateful for the Portuguese Foundation for Science and Technology (FCT) financial support in the scope of project PTDC/CTM-BIO/1814/2012. Ana Catarina Lima thanks FCT for the PhD grant (SFRH/BD/71395/2010).

2.12. References

[1] Wilson C. J., Clegg R. E., Leavesley D. I. and Pearcy M. J., Mediation of Biomaterial–Cell Interactions by Adsorbed Proteins: A Review, Tissue Engineering Part A 2005, 11: 1-18.

[2] Alves N. M., Pashkuleva I., Reis R. L. and Mano J. F., Controlling cell behavior through the design of polymer surfaces, Small 2010, 6: 2208-20.

[3] Koegler P., Clayton A., Thissen H., Santos G. N. C. and Kingshott P., The influence of nanostructured materials on biointerfacial interactions, Advanced Drug Delivery Reviews 2012, 64: 1820–39.

[4] Oliveira S. M., Alves N. M. and Mano J. F., Cell interactions with superhydrophilic and superhydrophobic surfaces, Journal of Adhesion Science and Technology 2014, 28: 843–63.

[5] Song W. and Mano J. F. Interactions between cells or proteins and surfaces exhibiting extreme wettabilities, Soft Matter 2013, 9: 2985.

[6] Lima A. C. and Mano J. F., Micro/Nano Structured Superhydrophobic Surfaces in the Biomedical Field. Part I: Basic Concepts and Biomimetic Approaches, Nanomedicine (Lond.), 10(1), DOI: 10.2217/NNM.14.174 (*In press*).

[7] Liu K., Yao X. and Jiang L., Recent developments in bio-inspired special wettability, Chemocal Society Reviews 2010, 39: 3240-55.

[8] Katsikogianni M. and Missirlis Y.F., Concise review of mechanics of bacterial adhesion to biomaterials of techniques used in estimating bacteria-material interactions, European Cells Materials 2004, 8: 37-57.

[9] Paul N. E., Skazik C., Hardwardt M., Bartnecka M., Deneckea B., Kleec D., Salber J. and Zwadlo-Klarwasser G., Topographical control of human macrophages by a regularly microstructured polyvinylidene fluoride surface, Biomaterials 2008, 29, 4056-64.

[10] Cao H., Mchugh K., Chew S. Y. and Anderson J. M., The topographical effect of electrospun nanofibrous scaffolds on the *in vivo* and *in vitro* foreign body reaction, Journal of Biomededical Materials Research Part A 2010, 93A: 1151–9.

[11] Shang H. M., Wang Y., Takahashi K., Cao G. Z., Li D. and Xia Y. N., Nanostructured superhydrophobic surfaces, Journal of Materials Science 2005, 40, 3587–91.

[12] Yohe S. T., Colson Y. L. and Grinstaff M. W., Superhydrophobic materials for tunable drug release: using displacement of air to control delivery rates, Jounal of the American Chemical Society 2012, 134: 2016–9.

[13] Yohe S. T., Herrera V. L. M., Colson Y. L. and Grinstaff M. W., 3D superhydrophobic electrospun meshes as reinforcement materials for sustained local drug delivery against colorectal cancer cells, Journal of Controlled Release 2012, 162: 92–101.

[14] Zhang L., Wu J., Wang Y., Long Y., Zhao N. and Xu J., Combination of Bioinspiration: A general route to superhydrophobic particles, Journal of the American Chemical Society 2012, 134: 9879-81.

[15] Oliveira M. B. and Mano J. F., Polymer-based microparticles in tissue engineering and regenerative medicine, Biotechnology Progress 2011, 27: 897-812.

[16] Correia C. R., Reis R. L. and Mano J. F., Multilayered Hierarchical Capsules Providing Cell Adhesion Sites, Biomacromolecules 2013, 14:, 743-51.

[17] Orive G., Hernández R. M., Gascón A. R., Calafiore R., Chang T. M. S., De Vos P., Hortelano G., Hunkeler D., Lacík I., Shapiro A. M. and Pedraz J. L., Cell encapsulation: promise and progress, Nature Medicine 2003, 9: 104–7.

[18] Custódio C. A., Santo V. E., Oliveira M. B., Gomes M. E., Reis R. L. and Mano J. F., Functionalized Microparticles Producing Scaffolds in Combination with Cells, *Advanced Functional Materials 2014,* 24: 1391–400.

[19] Song W., Lima A. C. and Mano J. F., Bioinspired methodology to fabricate hydrogel spheres for multi-applications using superhydrophobic substrates, Soft Matter 2010, 6: 5868.

[20] Lima A. C., Sher P. and Mano J. F., Production methodologies of polymeric and hydrogel particles for drug delivery applications, Expert Opinion on Drug Delivery 2012, 9: 231–48.

[21] Lima A. C., Batista P., Valente T. A. M., Silva A. S., Correia I. J. and Mano J. F., Novel methodology based on biomimetic superhydrophobic substrates to immobilize cells and proteins in hydrogel spheres for applications in bone regeneration, *Tissue Engineering Part A 2013,* 19: 1175-87.

[22] Lima A. C., Mano J. F., Concheiro A. and Alvarez-Lorenzo C., Fast and mild strategy, using superhydrophobic surfaces, to produce collagen/platelet lysates gel beads for skin regeneration, Stem Cell Reviews and Reports 2014, (in press).

[23] Lima A. C., Song W., Blanco-Fernandez B., Alvarez-Lorenzo C. and Mano J. F., Synthesis of temperature-responsive dextran-MA/PNIPAAm particles for controlled drug delivery using superhydrophobic surfaces, Pharmaceutical Research 2011, 28: 1294–305.

[24] Lima A. C., Puga A. M., Mano J. F., Concheiro A. and Alvarez-Lorenzo C., Free and copolymerized g-cyclodextrins regulate the performance of dexamethasone-loaded dextran microspheres for bone regeneration, Journal of Materials Chemistry B 2014, 2: 4943-56.

[25] Gong J. P., Why are double network hydrogels so tough?, Soft Matter 2010, 6: 2583.

[26] Lima A. C., Correia C. R., Oliveira M. B. and Mano J. F., Sequential ionic and thermogelation of chitosan spherical hydrogels prepared using superhydrophobic surfaces to immobilize cells and drugs, Journal of Bioactive and Compatible Polymers 2013, 29: 50–65.

[27] Cruz D. M., Ivirico J. L., Gomes M. M., Ribelles J. L., Sánchez M. S., Reis R. L. and Mano J. F., Chitosan microparticles as injectable scaffolds for tissue engineering, Journal of Tissue Engineering and Regenerative Medicine 2008, 2: 378–80.

[28] Song W., Oliveira M. B., Sher P., Gil S., Nóbrega J. M. and Mano J. F., Bioinspired methodology for preparing magnetic responsive chitosan beads to be integrated in a tubular bioreactor for biomedical applications, Biomedical Materials 2013, 8: 045008.

[29] Oliveira M. B., Song W., Martín L., Oliveira S. M., Caridade S. G., Alonso M. Rodriguez-Cabello J. C. and Mano J. F., Development of an injectable system based on elastin-like recombinamer particles for tissue engineering applications, Soft Matter 2011, 7: 6426.

[30] Puga A. M., Lima A. C., Mano J. F., Concheiro A. and Alvarez-Lorenzo C., Pectin-coated chitosan microgels crosslinked on superhydrophobic surfaces for 5-fluorouracil encapsulation, Carbohydrate Polymers 2013, 98: 331–40.

[31] Lima A. C., Custódio C. A., Alvarez-Lorenzo C. and Mano J. F., Biomimetic methodology to produce polymeric multilayered particles for biotechnological and biomedical applications, Small 2013, 9: 2487-92.

[32] Luz G. M. and Mano J. F., A nanotectonics approach to produce hierarchically organized bioactive glass nanoparticles-based macrospheres, Nanoscale 2012, 4: 6293–7.

[33] Luz G. M. and Mano J. F., Preparation and characterization of bioactive glass nanoparticles prepared by sol-gel for biomedical applications, Nanotechnology 2011, 22: 494014.

[34] Shao F., Ng T. W., Liew O. W., Fu J. and Sridhar T., Evaporative preconcentration and cryopreservation of fluorescent analytes using superhydrophobic surfaces, Soft Matter 2012, 8: 3563.

[35] Hu L., Chen Z. and Serpe M. J., Interface assisted synthesis of complex hydrogel particles, Soft Matter 2012, 8: 10095.

[36] Vuong T., Qi A., Muradoglu M., Cheong B. H. –P., Liew O. W., Ang C. X., Fu J., Yeo L., Friend J. and Ng T. W., Precise drop dispensation on superhydrophobic surfaces using acoustic nebulization, *Soft Matter* 2013, 9: 3631.

[37] Costa A. M. S., Alatorre-Meda M., Oliveira N. M. and Mano J. F., Biocompatible polymeric microparticles produced by a simple biomimetic approach, Langmuir 2014, 30: 4535–9.

[38] Rial-Hermida M. I., Oliveira N. M., Concheiro A., Alvarez-Lorenzo C. and Mano J. F., Bioinspired superamphiphobic surfaces as a tool for polymer- and solvent-independent preparation of drug-loaded spherical particles, Acta Biomaterialia 2014, DOI: 10.1016/j.actbio.2014.06.009.

[39] Lindström S. and Andersson-Svahn H., Miniaturization of biological assays-overview on microwell devices for single-cell analyses, Biochimica et Biophysica Acta 2011, 1810: 308–16.

[40] Li L., Tian J., Li M. and Shen W., Superhydrophobic surface supported bioassay – An application in blood typing, Colloids and Surfaces B Biointerfaces 2013, 106: 176–180.

[41] Oliveira N. M., Correia C. R., Reis R. L. and Mano J. F., Liquid marbles for high-throuput biological screening of anchorage-dependent cells, Advanced Healthecare Materials 2014, DOI: 10.1002/adhm.201400310.

[42] Luz G. M., Leite A. J., Neto A. I., Song W. and Mano J. F., Wettable arrays onto superhydrophobic surfaces for bioactivity testing of inorganic nanoparticles, Materials Letters 2011, 65: 296–9.

[43] Alves N. M., Leonor I. B., Azevedo H. S., Reis R. L. And Mano J. F., Designing biomaterials based on biomineralization of bone, Journal of Materials Chemistry 2010, 20:, 2911.

[44] Neto A. I., Custódio C. A., Song W. and Mano J. F., High-throughput evaluation of interactions between biomaterials, proteins and cells using patterned superhydrophobic substrates, Soft Matter 2011, 7: 4147.

[45] Salgado C. L., Oliveira M. B. and Mano J. F., Combinatorial cell – 3D biomaterials cytocompatibility screening for tissue engineering using bioinspired superhydrophobic substrates, Integrative Biology 2012, 4: 318–27.

[46] Oliveira M. B., Salgado C. L., Song W. and Mano J. F., Combinatorial on-chip study of miniaturized 3D porous scaffolds using a patterned superhydrophobic platform, Small 2013, 9: 768–78.

[47] Oliveira M. B., Luz G. M. and Mano J. F., A combinatorial study of nanocomposite hydrogels: on-chip mechanical/viscoelastic and pre-osteoblast interaction characterization, Journal of Materials Chemistry B 2014, 2: 5627.

[48] Oliveira M. B., Ribeiro M. P., Miguel S. P., Neto A. I., Coutinho P., Correia I. J. and Mano J. F., In vivo high-content evaluation of three-dimensional scaffolds biocompatibility, Tissue Engineering Part C Methods 2014, doi:10.1089/ten.tec.2013.0738.

[49] Efremov A. N., Stanganello E., Welle A., Scholpp S. and Levkin P. A., Micropatterned superhydrophobic structures for the simultaneous culture of multiple cell types and the study of cell-cell communication, Biomaterials 2013, 34: 1757–63.

[50] Wright D., Rajalingam B., Selvarasah S., Dokmeci M. R. and Khademhosseini A., Generation of static and dynamic patterned co-cultures using microfabricated parylene-C stencils, Lab Chip 2007, 7: 1272–9.

[51] Ishizaki T., Saito N. and Takai O., Correlation of cell adhesive behaviors on superhydrophobic, superhydrophilic, and micropatterned superhydrophobic/superhydrophilic surfaces to their surface chemistry, Langmuir 2010, 26: 8147–54.

[52] Neto A. I., Correia C. R., Custódio C. A. and Mano J. F., Biommetic miniaturized platform able to sustain arrays of liquid droplets for high-throughput combinatorial tests, Advanced Functional Materials 2014, DOI: 10.1002/adfm.201400503.

[53] Oliveira M. B., Neto A. I., Correia C. R., Rial-Hermida M. I., Alvarez-Lorenzo C. and Mano J. F. Superhydrophobic chips for cell spheroids high-throughput generation and drug screening, ACS Applied Materials & Interfaces 2014, 6: 9488-95.

[54] Oliveira M. B. and Mano J. F., On-chip assessment of the protein-release profile from 3D hydrogel arrays, Analytical Chemistry 2013, 85:, 2391-6.

[55] Webster A., Greenman J., and Haswell S. J., Development of microfluidic devices for biomedical and clinical application, Journal of Chemical Technology and Biotechnology 2011, 86: 10–17.

[56] Gao D., Liu H., Jiang Y. and Lin J. -M., Recent developments in microfluidic devices for in vitro cell culture for cell-biology research, TrAC Trends in Analytical Chemistry 2012, 35: 150–64 .

[57] Lee W. G., Kim Y. –G., Chung B. G., Demirci U. and Khademhosseini A., Nano/Microfluidics for diagnosis of infectious diseases in developing countries, Advanced Drug Delivery Reviews 2010, 62: 449–57.

[58] Serra C. A. and Chang Z., Microfluidic-assisted synthesis of polymer particles, Chemical Engineering & Technology 2008, 31: 1099–115.

[59] Whitesides G. M., The origins and the future of microfluidics, Nature 2006, 442: 368–73.

[60] Choi C. –H. and Kim C. -J., Large slip of aqueous liquid flow over a nanoengineered superhydrophobic surface, Physical Reviews Letters 2006, 96: 066001.

[61] Lu C., Xie Y., Yang Y., Cheng M. M. C., Koh C. –G., Bai Y. and Lee L. J., New valve and bonding designs for microfluidic biochips containing proteins, Analytical Chemistry 2007, 79: 994–1001.

[62] Oliveira N. M., Neto A. I., Song W. and Mano J. F., Two-dimensional open microfluidic devices by tuning the wettability on patterned superhydrophobic polymeric surface, Applied Physics Express 2010, 3: 085205.

[63] Elsharkawy M., Schutzius T. M. and Megaridis C. M., Inkjet patterned superhydrophobic paper for open-air surface microfluidic devices, Lab Chip 2014, 14: 1168–75.

[64] Fang G., Li W., Wang X., Qiao G., Droplet motion on designed microtextured superhydrophobic surfaces with tunable wettability, Langmuir 2008, 24: 11651–60.

[65] Balu B., Berry A. D., Hess D. W., Breedveld V., Patterning of superhydrophobic paper to control the mobility of micro-liter drops for two-dimensional lab-on-paper applications, Lab Chip 2009, 9: 3066–75.

[66] Martinez A. W., Phillips S. T., Butte M. J. and Whitesides G. M., Patterned paper as a platform for inexpensive, low-volume, portable bioassays, Angewandte Chemie International Edition 2007, 46: 1318–20.

[67] Vella S. J., Beattie P., Cademartiri R., Laromaine A., Martinez A. W., Phillips S. T., Mirica K. A. and Whitesides G. M., Measuring markers of liver function using a micropatterned paper device designed for blood from a fingerstick, Analytical Chemistry 2012, 84: 2883–91.

[68] Sousa M. P. and Mano J. F., Patterned superhydrophobic paper for microfluidic devices obtained by writing and printing, Cellulose 2013, 20: 2185–2190.

[69] Obeso C. G., Sousa M. P., Song W., Rodriguez-Pérez M. A, Bushan B. and Mano J. F., Modification of paper using polyhydroxybutyrate to obtain biomimetic superhydrophobic substrates, Colloids and Surfaces A: Physicochemical and Engineering Aspects 2013, 416: 51-55.

[70] Sousa M. P. and Mano J. F., Superhydrophobic paper in the development of disposable labware and lab-on-paper devices, ACS Applied Materials & Interfaces 2013, 5: 3731–7.

[71] Draper M. C., Niu X., Cho S., James D. I. and Edel J. B., Compartmentalization of Electrophoretically Separated Analytes in a multiphase microfluidic platform, Analytical Chemistry 2012, 84: 5801-8.

[72] Piraino F., Camci-Unal G., Hancock M. J., Rasponi M. and Khademhosseini A., Multi-gradient hydrogels produced layer by layer with capillary flow and crosslinking in open microchannels, Lab Chip 2012, 12: 659–61.

[73] Oliveira N. M., Reis R. L. and Mano J. F., Superhydrophobic surfaces engineered using diatomaceous earth, ACS Applied Materials & Interfaces 2013, 5: 4202–8.

[74] Hancock M. J., He J., Mano J. F. and Khademhosseini A., Surface-tension-driven gradient generation in a fluid stripe for bench-top and microwell applications, Small 2011, 7: 892–901.

[75] Lee H. Y., Park H. K., Lee Y. M., Kim K. and Park S. B., A practical procedure for producing silver nanocoated fabric and its antibacterial evaluation for biomedical applications, Chemical Communications (Camb) 2007, 28: 2959–61.

[76] Dastjerdi R. and Montazer M., A review on the application of inorganic nano-structured materials in the modification of textiles: focus on anti-microbial properties, Colloids and Surfaces B: Biointerfaces 2010, 79: 5–18.

[77] Xue C. –H., Chen J., Yin W., Jia S. –T. and Ma J. -Z., Superhydrophobic conductive textiles with antibacterial property by coating fibers with silver nanoparticles, Applied Surfaces Science 2012, 258: 2468–2472.

[78] Shateri Khalil-Abad M. and Yazdanshenas M. E., Superhydrophobic antibacterial cotton textiles, Journal of Colloid and Interface Science 2010, 351: 293–8.

[79] Tomšič B., Simončič B., Orel B., Orel B., L. Černe, Tavčer P. F., Zorko M., Jerman I., Vilčnik A., Kovač J., Sol–gel coating of cellulose fibres with antimicrobial and repellent properties, Journal of Sol-Gel Science and Technology 2008, 47: 44–57 (2008).

[80] Vilcnik A., Jerman I., Surca Vuk A., Kozelj M., Orel B. Barbara Simončič B. and Kovač J., Structural properties and antibacterial effects of hydrophobic and oleophobic sol-gel coatings for cotton fabrics, Langmuir 2009, 25: 5869–80.

[81] Smith D. M., Snow D. E., Rees E., Zischkau A. M., Hanson J. D., Wolcott R. D., Sun Y., White J., Kumar S. and Dowd S. E., Evaluation of the bacterial diversity of pressure ulcers using bTEFAP pyrosequencing, BMC Medical Genomics 2010, 3: 41.

[82] Khorasani M. T. and Mirzadeh H, *In Vitro* blood compatibility of modified PDMS surfaces as superhydrophobic and superhydrophilic materials, Journal of Applied Polymer Science 2004, 9: 2042-47.

[83] Zhou M., Yang J. H., Ye X., Zheng A. R., Li G., Yang P. F., Zhu Y. and Cai L., Blood platelet's behavior on nanostructured superhydrophobic surface, Journal of Nano Research 2008, 2: 129–136.

[84] Sun T., Tan H., Han D., Fu Q. and Jiang L., No platelet can adhere-largely improved blood compatibility on nanostructured superhydrophobic surfaces, Small 2005, 1: 959–63.

[85] Hou X., Wang X., Zhu Q., Bao J., Mao C., Jian L. and Shen J., Preparation of polypropylene superhydrophobic surface and its blood compatibility, Colloids Surfaces B: Biointerfaces 2010, 80: 247–50.

[86] Deutsch M., Meinhart J., Fischlein T., Preiss P. and Zilla P., Clinical autologous in vitro endothelialization of infrainguinal ePTFE grafts in 100 patients: a 9-year experience, Surgery 1999, 126: 847-55.

[87] Esquivel C. O. and Blaisdell F. W., Why small caliber vascular grafts fail: a review of clinical and experimental experience and the significance of the interaction of blood at the interface, Journal of Surgical Research 1986, 41: 1–15.

[88] Herring M., Smith J., Dalsing M., Glover J., Compton R., Etchberger K. and Zollinger T., Endothelial seeding of polytetrafluoroethylene femoral popliteal bypasses: the failure of low density seeding to improve patency, Journal of Vascular Surgery 1994, 20: 650-5.

[89] Ariyoshi H., Okuyama M., Okahara K., Kawasaki T., Kambayashi J., Sakon M. and Monden M., Expanded polytetrafluoroethylene (ePTFE) vascular graft loses its thrombogenicity six months after implantation, Thrombrosis Research 1997, 88: 427–33.

[90] Busscher H. J., Stokroos I., Golverdingen J. G. and Schakenraad J. M., Adhesion and spreadng oh human fibroblasts on superhydrophobic FEP-Teflon, Cells & Materials 1991, 1: 243-9.

[91] Schakenraad J. M., Stokroos I., Bartels H., Busscher H. J., Patency of small caliber, superhydrophobic ePTFE vascular grafts, a pilot study in the rabbit carotid artery, Cells & Materials 1992, 2: 193-9.

[92] Toes G. J., van Muiswinkel K. W., van Oeveren W., Suurmeijer A. J., Timens W., Stokroos I. and van den Dungen J. J., Superhydrophobic modification fails to improve the performance of small diameter expanded polytetrafluoroethylene vascular grafts, Biomaterials 2002, 23: 255–62.

Chapter 3

Advances in Particulate Systems for Biomedical Applications: Non-Spherical and Compartmentalized Approaches

3.1. Abstract

The search for more efficient therapeutic strategies and diagnosis tools is a continuous challenge. The discovery of new active substances requires a significant adaptation of the existent formulations as well as the methodologies to produce carriers preserving drugs stability and bioactivity. Until few years ago the most relevant parameters in particles formulation were the chemistry and the size. Currently, it is known that other physical characteristics can remarkably affect the performance of particulate systems. Advances in understanding the biological mechanisms behind diseases and tissues regeneration have widened the field of applications of particulate systems. Particles are no more just protective systems for the encapsulated drugs, but they play an active role in the success of the therapy. Moreover, particles have been explored for innovative purposes as templates for cells growth and as diagnostic tools. Particles with non-conventional shapes exhibit advantages due to the increasing circulation time in blood stream, less clearance by the immune system and more efficient cell internalization and trafficking. Creation of compartments has been found useful to control drug release, to supply the target with more than one bioactive agent or even to act as theranostic systems. It is expected that such complex shaped and compartmentalized systems improve the therapeutic outcomes and also the patient's compliance, acting as devices that serve for simultaneous diagnosis and treatment of the disease, combining agents of very different features, at the same time. In this chapter, the most recent advances in particle shape and compartmentalization and applications of newly designed particulate systems on biomedical field are analyzed at the light of relevant examples.

This chapter is based on the following publication:
Lima A. C., Alvarez-Lorenzo C. and Mano J. F., Advances in particulate systems for biomedical applications: non-spherical and compartmentalized approaches, *Submitted*.

3.2. Drugs and Cells Encapsulation: Opportunities and Challenges

Particulate systems have been widely used as containers of drugs or cells with the purpose of releasing them in a certain site to prevent or treat a variety of diseases or trauma. Particles designed with adequate properties have also been used as diagnosis tools or even as bioreactors.

In the particular case of pharmaceutical applications, the discovery of new bioactive substances (*e.g.* peptides, proteins, and nucleic acids) brings new challenges related to the needs of overcoming the deficient solubility/stability of a large number of both synthetic and biotechnological-origin substances as well as of improving the efficiency and safety profiles of old drugs as a way to extend their therapeutic and commercial value [1,2]. Among other various approaches, encapsulation into optimized particles is opening new opportunities. In general terms, encapsulation is the process to confine bioactive agents into a matrix, generally in a particulate form, in order to confer protection, control the release and/or even target the molecules to the site of action. Prior to designing the carrier for a drug, several parameters that could affect the efficacy of the system must be considered – see Figure 3.1.

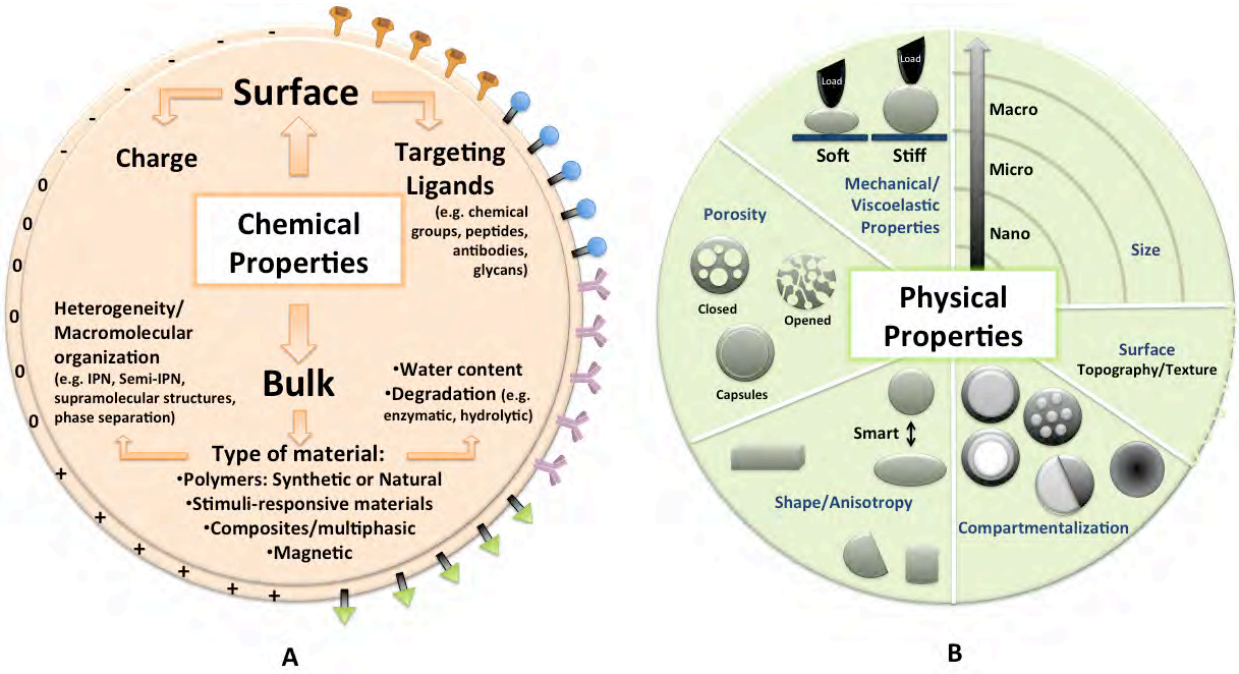

Figure 3.1. The chemistry at surface and bulk level as well as the physical features such as mechanical properties, size, porosity, surface topography/texture, shape and compartmentalization should be carefully considered during the design/engineering of particulate systems for biomedical applications.

Important challenges in the designing of drug delivery systems are efficient drug encapsulation and spatio-temporal control of the release. Particle features will define biodistribution, drug release profile, targeting and clearance of the encapsulated drugs [3]. The most used routes for drug administration are oral,

transdermal, intravenous, subcutaneous, *in situ* implanting and inhalation. In the last few years sophisticated advanced dosage forms have been presented to facilitate the administration and local or systemic release of the drugs, but also to sense the microenvironment along the pathway to achieve the target site circumventing certain barriers and responding to the therapeutic demands [4].

A huge challenge in particles engineering is the development of systems capable to mimic the natural phenomena of the human body´s. For example, particles have been proposed as artificial Antigen Presenting Cells (aAPCs), where the antigen may be encapsulated or disposed onto the particle surface, for vaccination, with the aim to protect or to treat diseases manipulating the immune responses. Vaccines could promote either immunity or tolerance and are responsible to generate antibodies and activate T or B cells in order to protect the body against future pathogens encounter as well as against the attack of diseased cells such as tumors. This is a complex process involving different cell types (*e.g.* dendritic cells, T and B cells) and signaling molecules such as inflammatory and suppressive cytokines [5].

Another example of the complexity of human body is occurred when a tissue is damaged. In such cases many natural biomolecules diffuse into the required sites to trigger the adequate cell response in an attempt to restore the tissue homeostasis. Growth factors and cytokines are very important biomolecules acting integrated with other biomolecules within a timing period and in a specific cell phenotype [6]. In general, orchestrated interactions are involved, determining a complex sequence of cell migration, proliferation, differentiation and protein synthesis. Skin wound healing [7], bone repair [8,9], reestablishment of vascularized networks [10] are examples of natural processes highly dependent on the coordinated activity of biomolecules release and different cell types activity. The administration of drug release systems capable to sustain the plasma concentration of natural bioactive agents or mimic the local signaling is a strategy explored in many therapeutic applications. Recombinant growth factors [6] or even cocktails of these kind of proteins obtained from the platelets existent in the blood plasma (platelet lysates) [11] have been used as bioactive agents for regeneration of several tissues. Vascular endothelial growth factor has been used to promote angiogenesis and for ischemia treatment [12,13]; bone morphogenic proteins for bone regeneration [14]; epidermal growth factor for treatment of skin lesions resultant from burns or chronic ulcers [15]; glial cell-line neurotrophic factor for spinal cord injuries or peripheral nerves regeneration [16]; and IL-10 for treatment of inflammatory bowel disease and to suppress inflammation [17–19]. Nevertheless, the main limitation of those systems relies on over simplification because typically only one bioactive agent is delivered with the risk of providing supraphysiological doses or even not triggers a complete and fast desired effect. Currently, it is known that in the natural *milieu* multiple signals act in a spatiotemporal controlled manner. Different cells could release the same biomolecule

simultaneously or at different time, and the same type of cells could release multiple biomolecules also simultaneously or following different patterns [20]. Thus, sophisticated drug carriers are required in order to mimic better the natural physiological processes.

Several strategies have been proposed to regulate the release of the bioactive agents (Figure 3.2) playing with the materials used to produce the particles as well as with the structural design of the system.

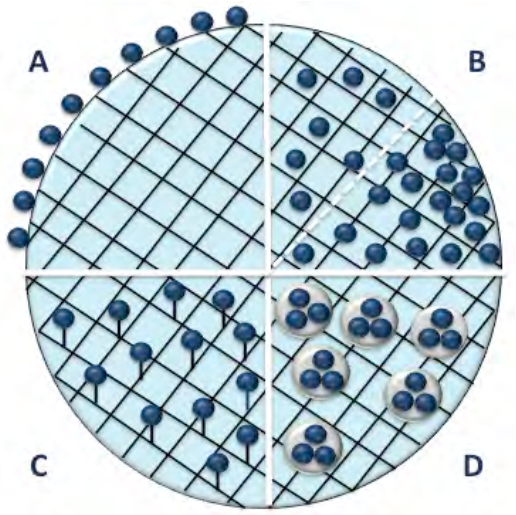

Figure 3.2. Strategies to encapsulate single bioactive agents in a matrix: A. adsorption/immobilization onto the surface of the particles; B. physical dispersion inside the matrix: homogeneous arrangement or exhibiting some special organization (e.g. gradients); C. establishment of links between the particle matrix and the bioactive agent (e.g. covalent bonds, electrostatic interactions, among others); D. encapsulation in a multiscale system where the bioactive agents are encapsulated into small matrices which in turn are encapsulated in higher scale structures (e.g. nanoparticles inside microparticles).

The simplest and more conventional strategies to encapsulate molecules are the surface adsorption/immobilization (Figure 3.2 A) and the physical dispersion of the drug inside a matrix (Figure 3.2 B). The dispersion into the matrix could be performed before the particles processing or by impregnation of the prepared ones. In this strategy, when more than one drug is encapsulated, the release of the substances will occur simultaneously; the differences in release rate may only depend on the molecular size and establishment of interactions of each molecule with the network (Figure 3.2 C). A more complex approach to control the release is to encapsulate the drugs into nano- or micro-particulate systems, which in turn will integrate bigger particles (Figure 3.2 D). Multicompartmentalization enables efficient protection of each substance when entrapped into individual compartments as well as a precise tailoring of its release pattern. The first steps in developing multicompartmentalized systems not only for drug release but also for cell encapsulation and diagnosis have already been done. However, the production of such sophisticated complex systems is quite far to be scaled up and commercialized.

Particulate systems have also demonstrated to be suitable for diagnosis. Combination of elements for diagnosis and therapeutics in the same particles has emerged due to the increased concern in development of noninvasive diagnostic and more efficient therapeutic tools. Theranostic systems have the ability to target and treat a specific disease while the particles localization is monitored by imaging tools. Depending on the contrast agent used, particles localization may be followed by optical and nuclear imaging, magnetic resonance imaging (MRI), computer tomography (CT) or ultrasound imaging (US) [21]. The design of such multiple functional particles should involve the definition of adequate materials to prepare the particles matrix and coatings, targeting, detection components, and the bioactive agents – Figure 3.3. The complexity of these systems, due to the wide range of characteristics, turns their production a challenging process.

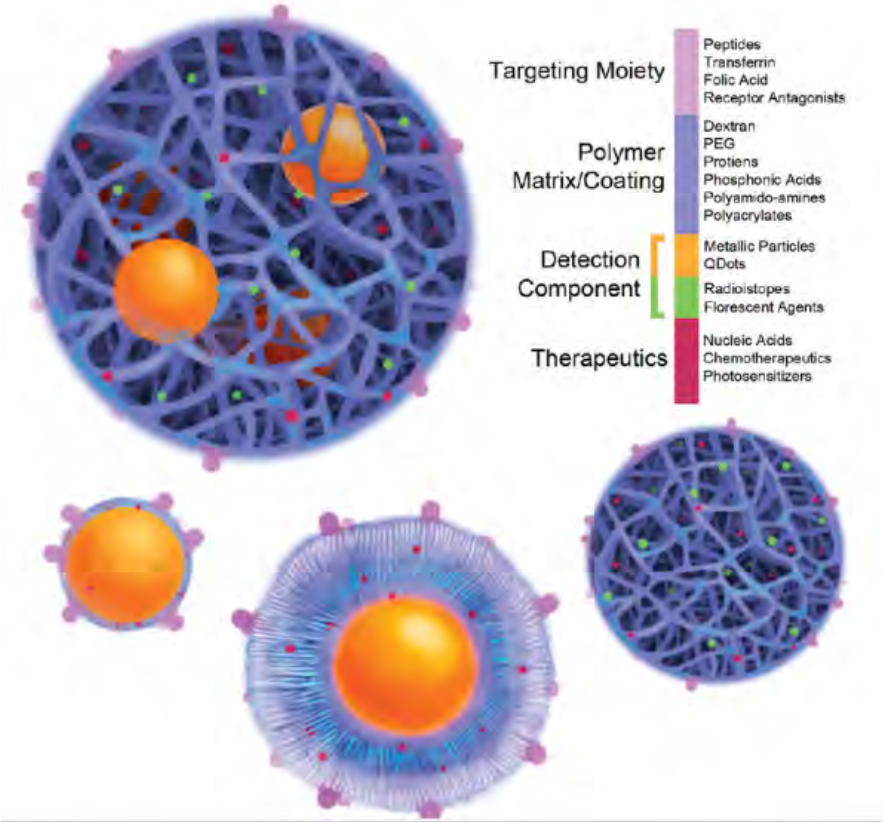

Figure 3.3. General architecture of theranostic particles and key components: targeting entities, therapeutic molecules, detection components and a coating or a polymeric matrix to support the previous enumerated entities. Image from the reference [21].

Although a strong evolution have been seen in the development of advanced particulate systems for drugs encapsulation and diagnosis, different strategies to treat the wide range of diseases that could affect the humans have been proposed as alternatives. The continuous development of innovative particulate

systems is a huge demand with the aim to achieve more efficient and faster treatments as well as to reduce the side effects of the existent treatments. In this context, the combination of cells with particulate systems has been emerged as new tools: particles may be capable to be internalized by the cells, may act as protection and support for cells encapsulated in the matrix of the particles or even act as cell support where cells may adhere onto the particle surface. In cell-based therapies, when the cells are administered without a biomaterial carriers occurs a fast loss of cells (>90%). A very small percentage of cells remain in the tissue site of interest [22–25]. In addition, many cell types require sites of adhesion in order to be alive and proliferate; the particles could then provide anchoring ligands or even an appropriate microenvironment to enhance the functions and integration of the transplanted cells [26–28]. Autologous or non-autologous cells could be isolated and immobilized in particulate systems capable to control the diffusion of molecules and the release of the cells – Figure 3.4. Adequate cell types should be selected and integrated in the particulate systems according to the needs of the patients. Primary cells [29], stem cells [30–32] and bioengineered cells [33,34] are considered a valuable strategy for treatment of disease or even for regeneration of tissues. The encapsulated cells could segregate biomolecules (e.g. growth factors) and the matrix could act simultaneously as a cell reservoir and a release system of bioactive agents. Cells could have a relevant role in therapies when are able to supply bioactive agents such as insulin in diabetes [35], erythropoietin in anemia [36] and factor VIII and IX in hemophilia [37]. Cells can be also manipulated to deliver non-autologous therapeutic agents for cancer therapy [38] and bone repair [39]. In xenotransplantation, the particles should also provide protection against the immune system through blocking antibodies and T cells [40].

Generally the cells are entrapped in homogeneous spherical matrices but the adequate structuring of particles may widen cell applications in therapeutics. For example, the encapsulation of more than one cell type, in individual compartments may be advantageous in complex therapies involving multiple cell types or signaling processes. The particles could help in reducing the necessity of immunosuppressant drugs and also fix protected cells in the place where they are necessary to promote the recreation and maintenance of functional tissues [41,42]. The cutting edge discoveries in the design of biomimetic and biodegradable microcarries with characteristics to be combined with different types of cells leads to a burgeoning number of possible therapeutic applications. An overview of microparticulate systems for cell encapsulation including the use of natural-based macromolecules and examples of application in biomedical field has been reported elsewhere [40,41].

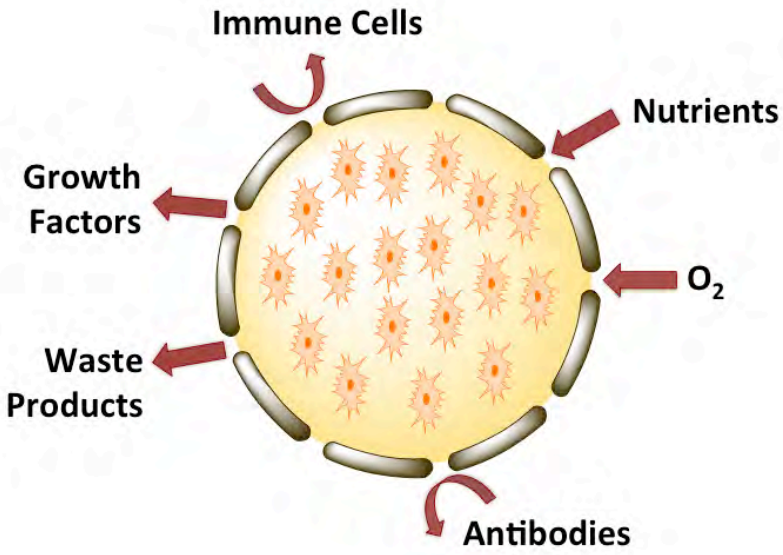

Figure 3.4. Main requirements of particles for cell encapsulation: protection against immune cells and antibodies, adequate diffusion properties to allow the entrance of nutrients and O_2, and the expelling of metabolites and growth factors.

It is important to notice that until now the most explored particles exhibit a spherical structure. This is the most stable shape resulting from the maximization of the volume/surface ratio. The surface tension tends to be minimized and the particles reach a spherical shape [43]. Spheres are obtained spontaneously in the most used methodologies to produce particles (e.g. emulsions and spraying) and for this reason it is the most studied type of architecture. However, particles with chemical and structural anisotropy have gained importance in the last few years due to the possibilities they offer for regulating several processes inside the human body. A huge variety of particles prepared from one or more materials, with varied chemical properties and architectures have been proposed for biomedical applications, namely therapies, diagnosis, vaccination and tissue regeneration. This chapter intends to provide an overview of the evolution of the particulate systems as drug and cell carriers in order to fulfill the complex demands of diagnosis and therapeutic strategies. An explanation of the main formulation and design parameters of the particles will be provided. In particular, our attention will be focused in the most sophisticated design of particulate systems, comprising the non-spherical shape and the compartmentalization. Non-conventional architectures are relatively recent emergent areas and for this reason a compilation of composition, preparation and biomedical applications of particles with those parameters will be extensively analyzed.

3.3. Design Criteria of Particulate Carriers

Strategies to improve the pharmacokinetics and biodistribution of the drugs in the organism have been developed mainly based on the use of polymeric particles, liposomes, dendrimers and micelles.

Depending on the application and administration route, several physicochemical parameters should be considered in the design formulation of such systems [44]. This is also valid for diagnosis particulate systems as well as for particles acting as cells carriers or cell support. In the case of particles combined with cells, the physical and chemical properties of the matrix should be capable to maintain the viability of the cells and to permit the integration of the system in the host to achieve the desired therapeutic effect. The main parameters to consider during the design of the particles will be discussed in the following subsections.

3.3.1. Surface and Bulk Characteristics

The properties of the biomaterials regulate their interaction with the biological *milieu*, thus dictating the success or the failure of the entire system. In the past, the development of biomaterials for drug delivery, tissue engineering and others biomedical purposes was greatly focused in controlling the chemical characteristics. Synthetic or natural-based polymers are the most used source of materials in particulate formulations for drug/cells encapsulation. Playing with their molecular weight, combination of different polymers (e.g. copolymers, interpenetrated networks, semi-interpenetrated networks) and with the nature of other excipients required for drugs stabilization, appropriated formulations can be designed to fulfill the required demands [45,46] (Figure 3.1 A). A lot of discussions have been centered in the use of either synthetic or natural polymers to meet on-going and evolving challenges in biomedical applications. Both types of polymers have advantages and disadvantages and for this reason great efforts have been done to formulate systems combining different polymers. Inorganic materials such as silica-based networks or metal oxides have also been proposed as components of drug delivery systems and diagnosis tools due to their biocompatible properties and their hydroxyl groups rich surface that prevents their clearance from the body [47]. Since the interaction of the particles with biological moieties occur firstly on the surface, great attention has been focused on the modification of the surface chemistry in order to minimize the recognition by the immune systems [48,49] or even to promote specific cell adhesion [50] (Figure 3.1 A). The spontaneous coating of particulate carriers upon administration, generally by albumin and antibodies, results in their quick immune clearance. The phagocytic cells are not capable to recognize particles without bound or adsorbed opsonins onto their surface. In the presence of opsonins there are different processes through which phagocytic cells can identify the particles: one of the processes is mediated by receptors of the phagocytic cells that recognize active proteins on the particle surface; the other is related to the non-specific adherence of the phagocytes to the particles exhibiting a hydrophobic surface due to the protein coating [51]. Opsonization was also shown to be dependent on the charge of the surfaces of

the particles [51]. Typically, due to the nature of the cellular phospholipid membrane, positively charged particles have high tendency to attach and being internalized, when compared with negative or neutral ones [52]. Thus, the main strategy used to minimize the recognition and the consequent early clearance of the particles is the coating of the surfaces with hydrophilic and non-ionic or negative-charged molecules. With a completely different objective, the surface of the particles could be modified with targeting ligands, which directly and indirectly control the biodistribution and clearance of the particles [53].

Similarly to the surface, the bulk of the particles also play a crucial role in the success of the systems. The materials used to obtain the bulk of the particles should degrade at adequate rates without releasing toxic degradation products.

In the case of drug release systems erosion and degradation (both at surface and bulk) affect directly the drug release rate [54]. In the case of drug carriers, the interaction of encapsulated drugs with the materials constituting the bulk of the particles is other strategy used to control release of the drug molecules. This involves the selection of materials able to establish physical or chemical linkages with drug molecules and, upon physiological environment, release them without loss of bioactivity [55,56]. The porosity and network density derived from the concentration or cross-linking of the material are also relevant parameters to have into account during the particles design, due to their influence on control of the bioactive agents release. In the case of cell encapsulation, a suitable matrix must biocompatible and support cell survival and prevent necrosis within the particles. Then, the matrix must be permeable to oxygen, to incoming nutrients and outgoing toxic metabolites [40]. In specific cases, when the entrapped cells are able to secret molecules of interest (*e.g.* growth factors), the matrix should also allow the diffusion out of those bioactive agents. Ideally, the bulk of the particles should also provide anchoring points for cell attachment and proliferation, which implies the selection of adequate materials [57] capable to mimic the extracellular matrix (ECM). The degradation kinetics of the bulk must also be considered. It should be adequate to application: it must be slow when the aim is protect the cells or more faster when the aim is to supply the damaged site with cells. Upon degradation, the entrapped cells may proliferate and fulfilling the damaged tissue and secreting their own ECM.

3.3.2. Size

Physical aspects of the particles, including size, shape, mechanical properties, surface texture and compartmentalization have gained increased attention of researchers due to the needs for improving the existent therapies or even to develop new strategies for diseases that currently do not have an effective therapy or an early diagnostic. Currently guidelines related with the most appropriated sizes are quite well

established according to the administration route as well as to obtain the therapeutic effect desired [58,59]. The size is one of the parameters that dictate the *in vivo* behavior of the particles, for example, circulation time, extravasation, targeting, immunological recognition, cellular internalization and trafficking, degradation and clearance [60]. Macro, micro and nano-scale systems have been produced using a variety of methodologies: emulsifying followed by cross-linking or solvent evaporation, self-assembly, microfabrication procedures, jet breaking, or superhydrophobic surface processing among many others methodologies [58,61]. Control of the particle size depends on the production method utilized, which in turn should be adequate to process the selected materials. Volumes of the precursor solutions dispensed by nozzles, micropipettes, spraying systems, or the mixing conditions (stirring, sonication, vortexing) control the size of the particles obtained.

In the case of intravenous applications, particle size has a significant impact on circulation time and in the hydrodynamics forces while flowing in the blood stream. Particles larger than 1.5 μm are not recommended due to the risk of obstruct the smallest capillaries and because they are rapidly cleared from the circulation. In general, particles smaller than 100 nm are capable to leave the blood stream through the fenestrations between the endothelial cells that composed the blood vessels [62]. This is the main driving force to develop passively target systems for tumor diagnosis and treatment, since such regions are highly and leaky vascularized [63].

Particles are susceptible to be cleared by spleen (>200 nm) and kidneys (<10 nm) [64], as well as to be captured by the Kupffer cells of the liver. Independently of the administration route, the size of the particles influences the cellular uptake, namely phagocytosis and endocytosis. Generally, smaller particles are internalized by endocytosis and larger ones (>500 nm) by phagocytosis, but the last pathway just occur in specialized cells, such as macrophages [43]. However, exceptions have been verified: for example endothelial cells have shown the capacity to internalize particles with 5 μm via endocytosis [65]. The intracellular transport to reach the targeted organelle is also dependent on the size of the particles. Non-phagocytic cells could internalize particles smaller than 1 μm through different pathways and smaller particles (<200 nm) reached faster the lysosomes than the larger ones. This information could be particularly important for drug and gene delivery because controlling the size of the particles, the residence time of the release systems inside the cells may be prolonged and a rapid lysosomal degradation may be avoided, improving the approximation of the particles to the nuclei of the cell [66]. Relevant sizes for *in vivo* performance are summarized in Table 3.1.

Table 3.1. Relevant sizes in biological systems. Adapted from [62].

Size	Statement
4.5 nm and 25 nm	Endothelium normal tissue has abundant small pores and a few large ones.
100 nm	Recurrent size of the drug-loaded polymeric micelles used in clinical trials.
150 nm	Adequate size for extravasation in liver. The fenestrations of blood vessels in the liver have 100-175 nm.
200 nm	Particles larger than 200 nm have short circulation because they are uptaken by the reticuloendothelial system.
380 nm	Appropriate size for application in tumor tissues. The cutoff of porous blood vessels in tumors is around 380-780 nm.
500 nm	Maximum size of particles aimed to penetrate through cell membrane.
1 μm	Particles below this size may enter in the lymphatic system and migrate to mesenteric lymph nodes.
5 μm	Maximal size for rigid particles to circulate within the smallest capillaries.
40 μm	Sizes higher than 40 μm are used in embolization therapies.

The size and density of the particles are also an important parameters of systems administered through the pulmonary route. The deposition of the particles occurs mainly at near airway bifurcations, where the velocity of airflow is high and where changes in the direction of bulk airflow occurs, generating inertial forces. Such inertial forces induce the impaction of large particles onto the airway surface. Gravitational sedimentation is responsible for the deposition of particles with sizes ranging from 0.5 to 5 μm in the small conducting airways, where the air velocity is low. Particles smaller than *ca.* 0.5 μm follow a Brownian motion and are mainly deposited in small airways and alveolar region, where the airflow is also low. Due to the Brownian movements, submicron particles require a long time to deposit, being exhaled in a very fast way after administration. In addition, particles with 5 μm or even more are highly susceptible to be cleared or even retained in the upper airways, being the combination of chemical and physical properties a strategy to circumvent such paradox [67]. In a general way, the particles for pulmonary administration are designed with geometrical sizes ranging from 1-5 μm with densities *ca.* 1 g/cm^3. Suitable particles for this application may also be designed with a non-standard density and geometrical size. Large porous particles, with a density of 0.1 g/cm^3 and diameter of *ca.* 7 μm, showed higher accumulation in the lungs than the non-porous counterparts (density *ca.* 0.94 g/cm^3) [68]. Porous particles with diameter >5 μm and non-porous particles with diameter <5 μm, derived from the same polymer and encapsulating insulin were compared [68]. Only porous particles were capable to maintain the high levels of insulin in the blood for more than 4 hours. The low clearance of the porous particles by phagocytic cells was also confirmed. After inhalation *ca.* 30% of phagocytic cells contained non porous particles and only *ca.* 8% contained porous particles [68]. Thus, the size is not the only parameter influencing the performance of the particles; such examples showed that the design of new carriers involves others particles characteristics, such as structure (density).

In the specific case of particles encapsulating cells, the size of such matrices should be adequate to ensure the adequate diffusion of nutrients and gases to all the cells entrapped in the network. This is particularly relevant when the particles have high diameters and, as a consequence, the cells in the core have restricted access to nutrients and O_2 and the metabolites do not diffuse out and accumulate around the cells causing viability loss.

3.3.3. Mechanical Properties

The capacity of the red blood cells to cross through the capillaries fenestrae even when the diameters are smaller than the own diameters of the erythrocytes, demonstrate that the mechanical properties of the carriers could be an important characteristic to achieve the target site. The potential of the rigid particles to clot the vessels turned the flexibility a relevant property of the particles. It has been demonstrated that flexible structures exhibit higher circulation times and suffered phagocytosis by macrophages in lower extension than rigid ones [69] for particles exhibiting similar chemistry and size; correlations between Young modulus of the particles and the uptake rate of internalization have been proposed [70]. Cells exhibit a different behavior when contact with materials having different mechanical properties [71,72]. In addition, it is important to note that the mechanical properties exert an effect on cell behavior in combination with other particles characteristics, namely material chemistry, size and shape [69,73]. The mechanical properties of the particles also influence the pathway followed in the endocytosis process [70]. For example, hydroxyethyl methacrylate (HEMA) particles were prepared with different crosslinking degrees to exhibit different mechanical properties [74]. Although the softer particles showed higher swelling when immersed in cell culture medium, the size of all the formulated particles was similar. Cells derived from a hepatocellular carcinoma (HepG2) internalized softer particles at a faster rate and larger amount than stiffer ones (Figure 3.5 I). The mechanical properties of the particles did not affect the cell viability. The cell adhesion was lower when the cells were cultured with stiffer particles. The organization of the cytoskeleton was also affected after internalization of both types of particles (Figure 3.5 II).

In the specific case of cell encapsulation for tissue engineering and regenerative medicine purposes, the mechanical properties of the matrices may greatly influence the differentiation of stem cells into certain phenotypes. One specific case is the differentiation of mesenchymal stem cells: on stiff substrates bone differentiation is promoted, but in soft matrices the differentiation into adipocytes is privileged [71]. When the cells are entrapped inside matrices they interact with the material, generally the first happening is cell adhesion. Regarding that the mechanical properties of materials surfaces exert an effect on cell differentiation, probably into 3D particles any effect could also occur. However, more studies are required

in order to deep the knowledge about the effect of mechanical properties of the matrices in the encapsulated cells.

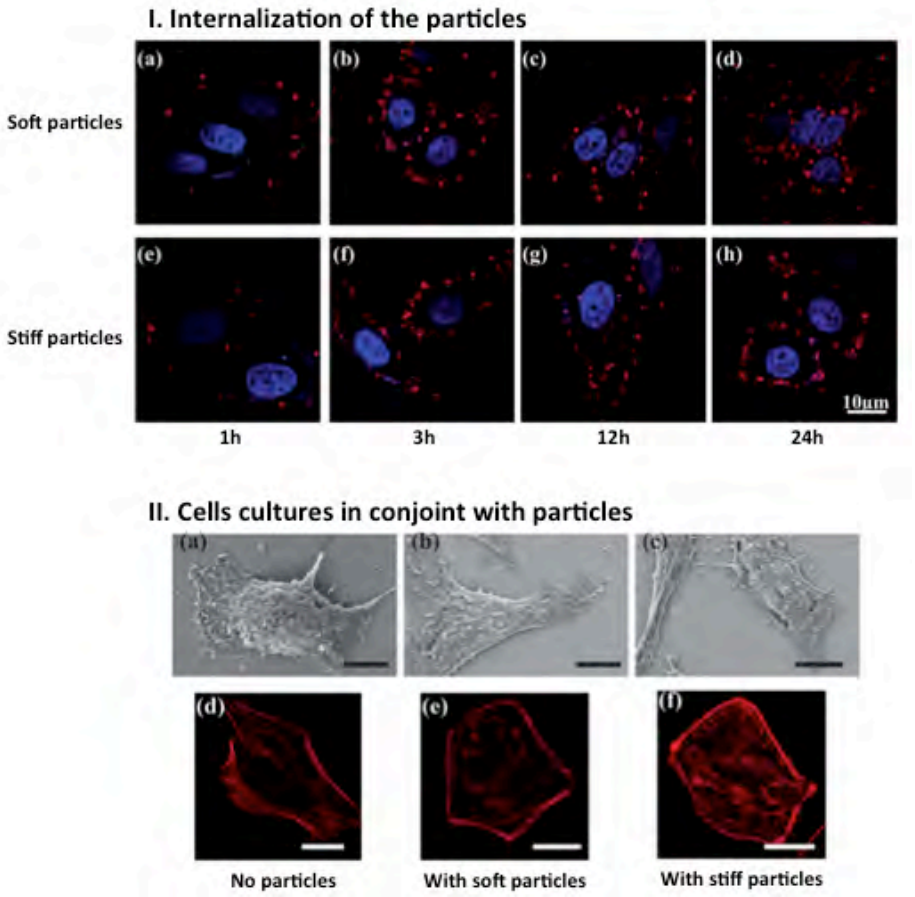

Figure 3.5. I. Internalization of HEMA particles exhibiting soft and stiff characteristics by HepG2 cells. The cells internalized higher amounts of soft particles. No particles (soft or stiff) were observed colonizing the cell nuclei. In both cases the particles were distributed in the cell cytoplasm (inside lysosomes) and no differences between both types of particles were observed. II. Effect of stiffness of the particles in cell cytoplasm after 24h. The F-actin organization changed after particles internalization. Independently of the mechanical properties of the particles a reduction of the oriented stress fibers was observed. Image adapted from [74].

3.3.4. Shape

Natural "particulate" systems are characterized by a huge variety of physical structures and shapes that facilitate their functioning. For example, bacteria are identified by their unique shapes, namely, rods, spirals and ellipsoids [75]. Even in the human body, very different shaped cells may be found: erythrocytes, platelets and endothelial cells have completely different shapes as well as mechanical properties, which are according to their different functions.

Currently, it is well known that shape, along size and chemistry, plays a crucial role in drug delivery [76]. Recent studies reporting the potential of anisotropic particles as drug carriers revealed, in most of cases, satisfactory results. The shape of the particles could be seen as an active parameter influencing directly and indirectly the performance of the systems. The anisotropic structure of the non-spherical particles confers unique degradation profiles to the particulate systems [76] and may greatly influence drug release kinetics. Several methodologies have been proposed to produce particles with complex shapes [77–79]. One versatile technique proposed by Mitragotri's group, permitted to obtain a wide range of particles shape comprising sizes between 60 nm and 30 μm is related with the stretching of spherical particles [79]. Films prepared from a suspension composed by spherical polymeric particles and polyvinyl alcohol were stretched enabling the production of particles with different shapes. Representative shapes of the obtained particles are depicted in Figure 3.6: rectangular disks, rods, worms, oblate ellipses, elliptical disks, UFO's, barrels, bullets, pills, pulleys, biconvex lenses, ribbons, bicones, diamond disks, emarginated disks, flat pills, elongated hexagonal disks, ravioli and tacos (Figure 3.6). The therapeutic benefits of non-spherical shaped particles when used mainly as drug carriers have been demonstrated in the last few years. The main differences in the interaction of spherical and non-spherical particles with biological entities will be described below.

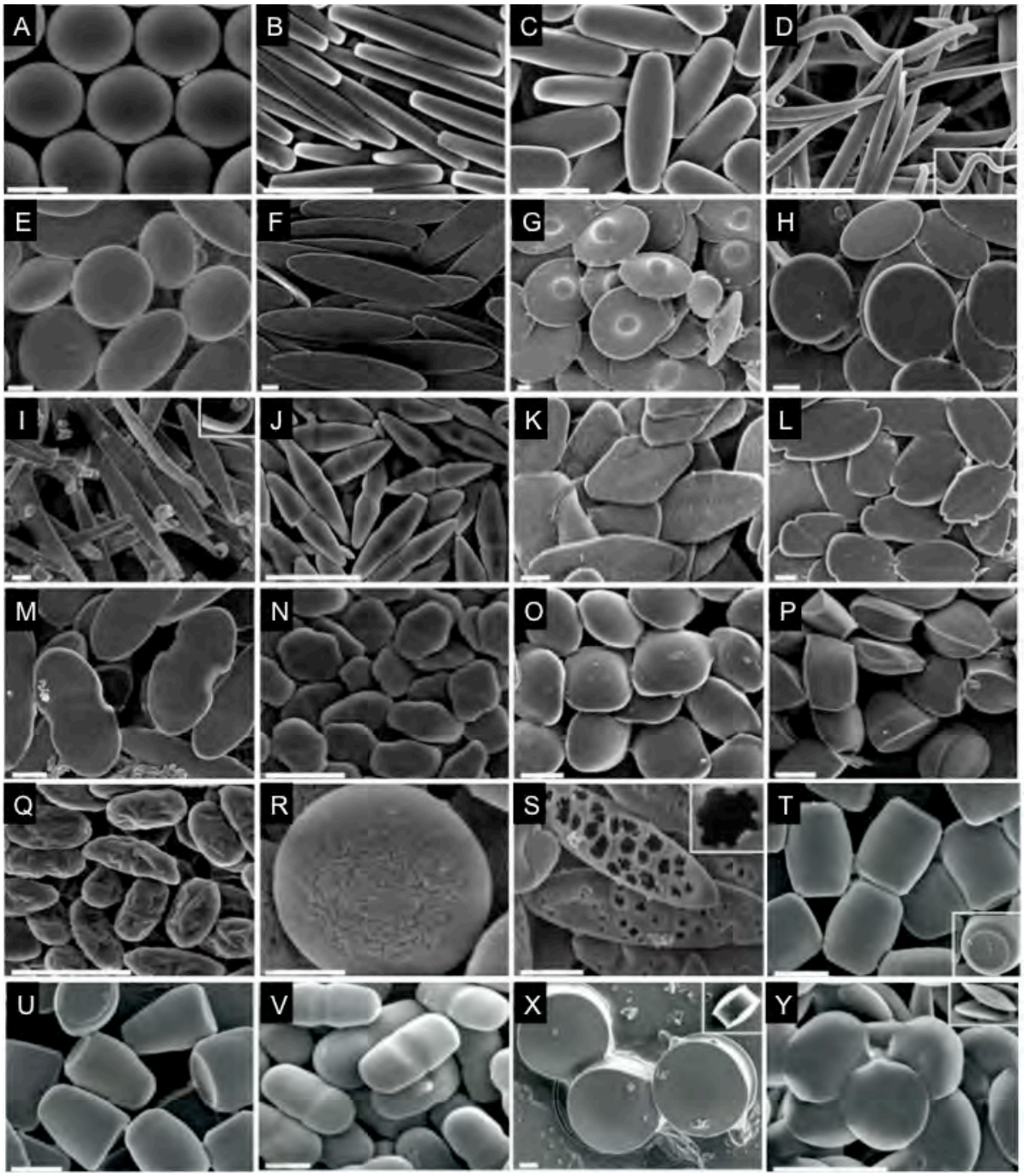

Figure 3.6. Variety particles shapes produced by heating and stretching polystyrene spheres in one and two dimensions: A) Spheres; B) Rectangular disks; C) Rods; D) Worms; E) Oblate ellipses; F) Elliptical disks; G) UFOs; H) Circular disks; I) Ribbons with curled ends; J) Bicones; K) Diamond disks; L) Emarginate disks; M) Flat pills; N) Elongated hexagonal disks; O) Ravioli; P) Tacos; Q) Wrinkled prolate ellipsoids; R) Wrinkled oblate ellipses; S) Porous elliptical disks; T) Barrels; U) Bullets; V) Pills; X) Pulleys; Y) Biconvex lenses. Adapted from [79].

3.3.4.1. Effect on Circulation and Biodistribution

Several *in vivo* studies demonstrated that particles with non-spherical shapes have different distribution/accumulation profiles in spleen, lungs, and tumor tissues, when compared with their spherical

counterparts [77]. The orientation of non-spherical particles when flowing in the blood stream is crucial for their clearance from circulation. In the case of spherical particles, circulation can be easily predicted due to their isotropy. However, the movements of non-spherical (anisotropic) particles are much more complex because such particles may align or tumble inside a fluidic stream [76]. For example, filamentous flexible micelles (filomicelles from di-block copolymers such as poly(ethylene glycol)-poly(caprolactone) (PEG-PCL) and poly(ethylene glycol)-poly(ethyl ethylene) (PEG-PEE)) were kept in the blood circulation for more time than spherical and shorter filomicelles due to their alignment with the blood flow [80]. Disk-shaped liposomes also demonstrated higher circulation time when compared with spherical counterparts [81].

Undesirable structures are filtered in the spleen and liver by passing through slits between the endothelial cells that compose the blood vessels. For example, spherical particles should have less than 200 nm in diameter to be eliminated in the spleen. Abnormal or worn-out red blood cells, which are disk-shaped structures with a diameter of *ca.* 10 μm, are normally eliminated in the spleen, liver and bone marrow, indicating that the shape and mechanical properties could be more relevant than the size itself. The flexibility of red blood cells allows their passage through very small fenestrations. The ability of the particles to cross the fenestrations of the blood vessels is extremely important in applications regarding tumor diagnosis and treatment. The effect of shape of silica particles on the accumulation in organs when injected intravenously was analyzed for spherical, hemispherical, discoidal and cylindrical particles comprising approximated volumes and sizes [82]. Organ accumulation varied significantly with the shape of the particles: in the lungs discoidal particles accumulated 4 times more than spheres and 8 times more than cylinders and hemispheres; in the liver cylinders accumulate 2 times more than spheres and hemispheres and 5 times more than discoidal particles, and no differences were visualized between spheres and hemispheres; in the heart discoidal particles accumulated in major level than the other three shapes; in the spleen no differences were obtained for discoidal and hemispherical particles, but both accumulate more than cylinders and spheres. The influence of the shape was not noticeable in tumorous tissues, brain and kidneys, probably due to the large size of the particles for being retained in these tissues. Although more studies are required to understand so different interactions, elongated particles, as the case of discoidal ones, seem to be more capable to escape to internalization by different cell types. Discoidal particles showed larger propensity to adhere to the vessel because they drifted laterally towards the walls when flowing in the blood stream, which justify their lower accumulation in the liver where the main sequestration mechanism is performed by Kupffer cells. In general, the cells easily internalized the other shapes, namely spherical, quase-hemispherical and cylindrical, which had an aspect ratio closer to the unit. The major conclusion from the studies described above is that geometry has a huge effect on

biodistribution and should be carefully considered during particles design depending on the final aim to be achieved both in therapeutic or imaging puroposes.

3.3.4.2. Effect on Internalization and Trafficking

The shape influences cell internalization as well as particle trafficking in the cell cytoplasm [43,83]. Cell attachment onto the particle surface is the first event in the internalization. Phagocytosis is an innate immune process related to the clearance of undesirable particles, such as rod-shaped and spiral-shaped bacteria, disc-shaped cells such as old erythrocytes and airbone particles such as pollen and dust. These examples present very peculiar non-spherical geometries [84]. In the case of more elongated particles, the region where the macrophages firstly adhere will dictate if the cells will be capable to internalize the particles or just spread onto their surface. Champion and Mitragotri [84] studied the effect of size and shape (spheres, oblate ellipsoids, prolate ellipsoids, elliptical disks, rectangular disks and particles with a shape similarly to UFO's) in phagocytosis, using polystyrene particles. The results confirmed a strong dependence on the shape, specifically on the point of the initial contact between particles and cells. For elliptical discs, if the contact occurs at the pointed end, the particles are internalized in a few minutes, but if the contact is done on the flat region, the macrophage is not able to internalize the particle (Figure 3.7 I). Similarly, UFO's-like particles were internalized when the contact between the macrophages and particle occurred either at the dome or the ring regions but not when it happened at the concave region (Figure 3.7 II). In a more detailed study, it was shown that the shape of the particles influences independently macrophages attachment and internalization. Attachment was higher for prolate and oblate ellipsoids than spheres, but for the same time period the most internalized particles were the oblate ellipsoids and the spheres. Phagocytosis is related with the remodeling of actin cytoskeleton and the shape determines the extent of this process, which in turn determines the velocity of the particle internalization. Probably, the lower aspect ratio of oblate ellipsoids is related with less actin rearrangement and a faster/more efficient internalization [85].

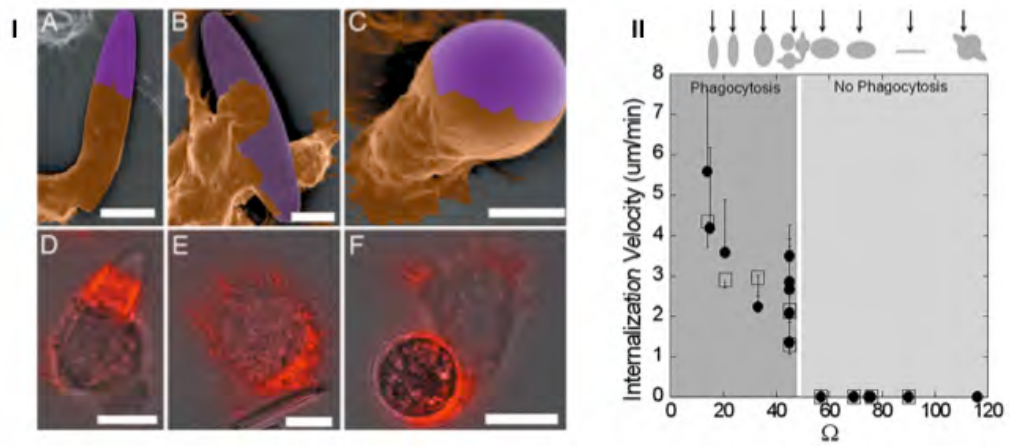

Figure 3.7. I. Interaction of macrophages with polystyrene particles with non-spherical (A, B D and E) and spherical (C and F) shapes. II. The plot indicates the first point of contact between the macrophages and the particles as well as the velocity of internalization. The images were adapted from [84].

The effect of the shape on endocytosis by HeLa cells (from cervical cancer) was studied using cubic and cylindrical-shaped PEG hydrogel particles obtained by particle replication in non-wetting templates [86]. Cubic particles with side lengths of 3 and 4 μm were not internalized whereas with 2 μm were internalized by most cells. Cylinders were internalized at higher percentage than cubes, but the kinetics of internalization varied with the aspect ratio: internalization was 4 times faster for cylindrical-shaped particles with high aspect ratio when compared with lower ones. Similar results were obtained in a study where larger amounts of higher aspect ratio rod-shaped mesoporous silica particles were internalized in a fast way by A375 human melanoma cells [87]. F-actin proteins of the cells that internalized the particles with high aspect ratio, appeared disrupted and disorganized. In addition, the F-actin network was anisotropic with poorly formed filament bundles accumulated in cell membrane and at the edges of the lamellopodium and filopodium. The adhesion of the cells was also influenced when cells and particles were cultured in conjoint. Higher cell adhesion onto the cell plates was found in cultures in the presence of particles with low aspect ratio. The cell migration was faster in the presence of particles, but the spherical ones had a stronger effect than the rod-shaped. All these findings indicate that cell functions were greatly influenced by the shape of the internalized particles. Asbestos particles exhibit a fiber shape and they are easily uptake by cells. Such particles are well know to affect cell signaling pathways, activation of transcription factors and gene expression implicated in the development of inflammation, fibroproliferative diseases, and cancers [88,89].

Kinetics of the intracellular trafficking was also demonstrated to be dependent on the particles shape. For example, spherical and elliptical-disk poly(lactic-co-glycolic acid) (PLGA) particles produced by emulsion

and film-stretching method, respectively, were internalized by Human Umbilical Vein Endothelial Cells (HUVECs) through an endocytosis process. The internalized spherical particles accumulated around the nuclei faster than the disks, meaning that the rate of internalization was higher for the spherical-shaped particles [90]– Figure 3.8. This information could be especially important for the design of DNA carriers that should deliver their content in the nuclei.

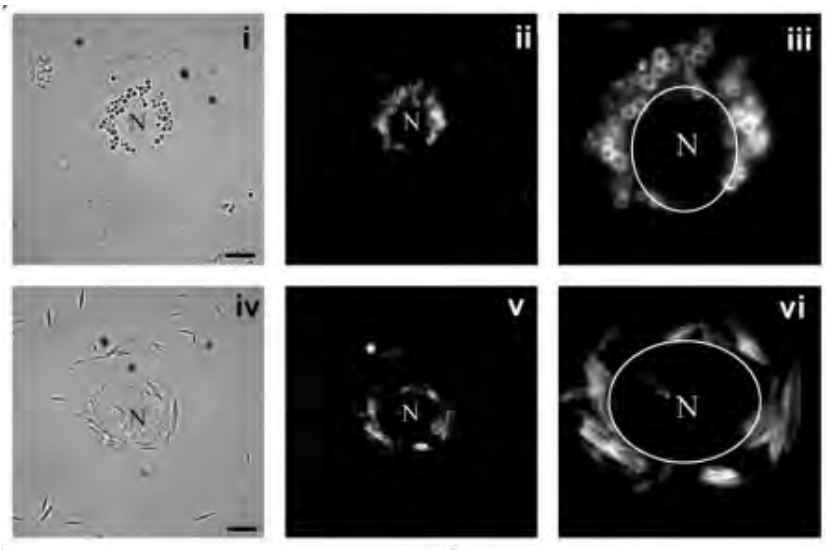

Figure 3.8. PLGA particles internalized by HUVECs by endocytosis accumuled around the cells nuclei. In images i, ii and iii it is possible visualize the spherical shaped particles and in images iv, v and vi the elliptical disks. Image adapted from [90].

3.3.4.3. Effect on Cytotoxicity

Particle shape can also determines cytotoxicity at sub-cellular scale [91]. Cytotoxicity and proinflammatory response against lung fibroblasts and alveolar macrophages, respectively, of poly(3,4-ethylenedioxythiophene) (PEDT) nanoparticles having three different shapes (obtained by chemical oxidation polymerization using sodium bis(2-ethylhexyl) sulfosuccinate micelles as the soft template) was systematically evaluated. The results demonstrated that not only the concentration and time affected the cell viability, but also the particles aspect ratio: when the aspect ratio increased, the apoptosis and necrosis decreased. It would be interesting verify cross-correlations with the total volume/size of the particles and to check if such behavior could be found in particles produced with other materials and surface chemistries. Different (opposite) results were obtained for rod-shaped mesoporous silica particles [87]: a slightly toxicity against A375 human melanoma cells was noticed for the particles with high aspect ratio. In addition, the cells that internalized this type of particles were more susceptible to apoptosis. For polystyrene particles obtained by a film stretching method, endothelial cells in contact with spheres and elliptical disks remained spread on the substrate and did not show morphological changes; as expected,

the particles were internalized by endocytosis and accumulated around the nucleus [92]. Differently, when cultured in conjoint with needle particles, the endothelial cells changed significantly the morphology and lower extent of internalization was observed. In this case, part of the cells contracted and others lifted off from the culture substrate. Despite of the cytoskeleton changes, these cells showed higher mobility than those cultured with spherical or disk-shaped particles allowing to conclude that the contraction of the cells was not permanent. The results also demonstrated that needles caused higher membrane disruption than spheres, but no significant differences were noticed in the metabolic activity of the cells, meaning that the particles were non-toxic. Such polymeric particles could be an innovative strategy for intentional transient disruption of cell membranes allowing the entrance of bioactive agents inside the cells and used as alternative to conventional methods such as electroporation, ultrasound or chemical penetration enhancers. However, very few studies are reported in literature relating the particles shape with the viability of the cells. More efforts in this area are required in order to establish the adequate characteristics that particles should have for specific applications.

3.3.5. Compartmentalization

Compartmentalization of particles could be regarded as a biomimetic strategy – Figure 3.9. The interior of the eukaryotic cells is divided in compartments (organelles) with a range of sizes varying from 10-25 nm to 100-500 nm [93]. The proper functioning of the cell depends on a variety of processes involving each one of the existent compartments. Although each cell compartment has a specific function, they work in cooperation to maintain the functionality of the cell. Even regarding to human body as an entire system, it has a very complex architecture divided into compartments (organs) that have specific functions and in conjoint have the aim to maintain the system alive.

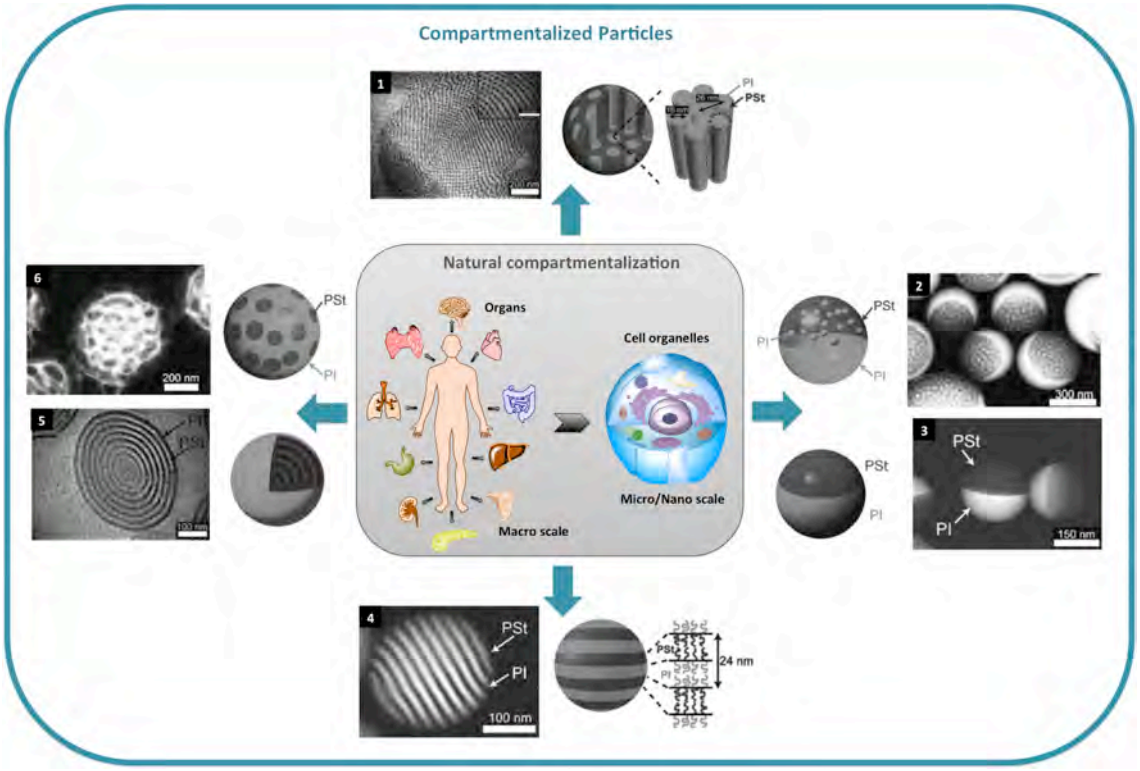

Figure 3.9. Based on the organized structure of the human body which is composed by macro scaled compartments (organs) as well as on the micro/submicro arrangement of the organelles inside the cells, compartmentalized particles with a wide range of structures have been developed to be applied in the biomedical field with the aim to simulate some complex natural biological processes. Images obtained from [94].

Multicompartmentalized particles have emerged as possible multicontainers to improve the efficiency of the particles in certain complex biological applications. In a general way, compartmentalization provide several advantages: (i) the possibility to encapsulate more than one drug, cell types or even combine drugs and cells in independent regions of the particles; (ii) controlled anisotropy and (iii) hierarchical compositions. A wide range of spherical and non-spherical compartmentalized particles with new architectures and varying the chemical properties of the compartments has been designed for application in the biomedical field. Although the evaluation of the effectiveness of those advanced systems is at an early stage, a more detailed discussion on the potential of the use of multicompartmentalized particles in multiple biomedical applications is provided in section 3.5 of this chapter.

3.4. Applications of Non-Spherical Particles

As described in the previous section, shape design may offer interesting possibilities for regulating particle interactions with biological entities: internalization, cell trafficking, clearance, circulation in blood stream, or toxicity. The control of the biological response through variation in the particles geometry is an

interesting point to be explored since the biological responses are, generally, strongly dependent on the chemical nature of the biomaterials. The use of systems with non-conventional shape and by playing with the aspect ratio of the particles may improve the performance of the system for given biomedical applications, as discussed in next subsections.

3.4.1. Elongated Particles

Non-spherical PLGA particles with an elongated shape were successfully prepared via emulsion/solvent evaporation and were loaded with a variety of bioactive agents: a hydrophobic drug (paclitaxel), a hydrophilic protein (bovine serum albumin,-), and nanoparticles (cadmium sulfide). PLGA particles deformation, size and encapsulation efficiency were tuned by controlling several parameters during the production, namely the pH of the aqueous phase, the volume of the oil phase, and the concentration of both surfactant and surface-active agents. Such particles were proposed as alternatives to spherical ones, with the aim to avoid their clearance during the circulation in the blood stream and also to improve their extravasation [95].

The effect of particle geometry on the interactions with the immunological system was investigated for vaccines and anticancer strategies using particles as artificial antigen presenting cells – Figure 3.10. T-cells are known to provide protective immunity to pathogens. In addition, it has been explored that T cells specific for antigens expressed on tumor cells could be an interesting strategy to treat cancer. Two main approaches have been used to amplify the T-cell response: *in vitro* isolation, expansion and administration of tumor-reactive T-cells and immunization of the patient (through administration of natural or artificial antigen presenting cells) to induce expansion of the tumor-specific T-cells *in vivo* [96]. PLGA particles coated with anti-CD28 antibody and MHC-IgG dimer were produced in spherical and ellipsoid-shape varying long axis lengths, and consequently the aspect ratio to be used as aAPCs [97]. The ellipsoidal particles increased the number of CD8+T cells in *ca.* 3-fold, after 7 days, when compared with spherical-shaped counterparts. In addition, cell expansion increased with increasing particles aspect ratio. The efficacy in activating T-cells *in vitro* was then analyzed. The formation of conjugates was 2.5-fold higher between T-cells and ellipsoids than spheres, which suggested the preference of T-cells for the flat parts of the particles. *In vivo* experiments also confirmed the importance of the shape in cancer treatment. Animals injected with ellipsoidal particles showed a delay in tumor growth and higher survival rate over the experimental period than animals treated with spherical counterparts.

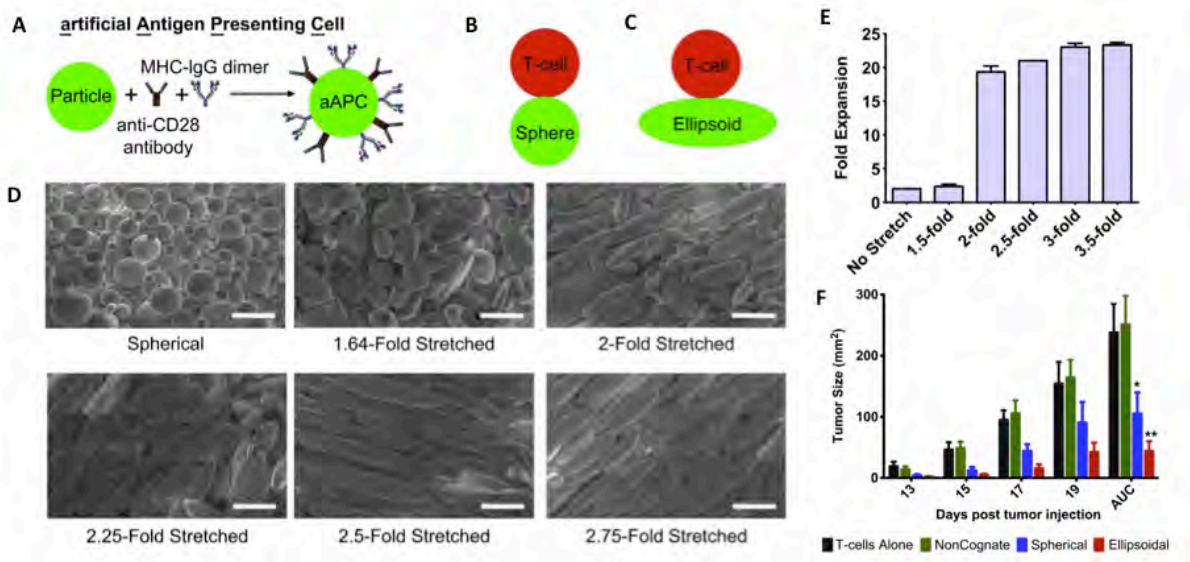

Figure 3.10. General formulation of aAPC: an antibody (anti-CD28) and a dimer (MHC-IgG) were immobilized on the surface of PLGA particles (A). The T-cells will recognize such molecules on the particle surface and will interact with particles (B and C). The particles with different aspect ratios (D) induced different cell proliferation (E). Higher aspect ratio seemed to increase significantly the T-cell expansion. When T-Cells were administered with ellipsoidal aAPCs the increase of the tumor size was lower than in the same conditions with spherical aAPCs (F), showing the potential of elongated particles in those types of treatments. Adapted from [97].

3.4.2. Erythrocyte-Shaped Particles

The ability of erythrocytes to circulate for long time periods, to repeatedly deform and pass through narrow capillaries and to act as delivery vehicles, has inspired the development of new advanced drug delivery systems. There are two main ways to obtain such biomimetic systems: (i) load natural erythrocytes without compromise their structure (cargo-erythrocytes or ghost-erythrocytes) or attach physical or covalently therapeutic molecules to their external surface; (ii) engineering artificial carriers (generally polymeric) mimicking the biological and physicochemical properties of erythrocytes [98]. Erythrocite-like carriers have been mainly tested for cancer and enzyme deficiencies treatment due to the capacity to efficiently transport proteins, nucleic acids and small-molecule drugs along the bloodstream until reach the targeted tissue [99,100].

Natural erythrocytes can be loaded with therapeutic agents after being soaked in hypotonic solution, which caused the formation of pores (10-500 nm) in the cell membrane. Through those pores, the cell will release their natural intracellular content while the therapeutic agents will passively diffuse into the cells. The pores have the capacity to reseal and the erythrocytes maintain their biophysical and immunological properties [101]. Alternative methodologies do not require the reversal lesion of the natural membranes of the erythrocytes. Such strategies consist in conjugation of the drugs to receptors on the cell membrane, or

preparing hierarchical carries using drug-loaded artificial lipid vesicles that can diffuse directly into the erythrocytes [102].

Completely artificial erythrocytes-like structures may be produced due to the advances in micro/nanotechnology as well as in materials science. Elliptical polystyrene disks were stretched in a plasticized film of poly(vinyl alcohol) and glycerol in order to obtain the discoid shape of the erythrocytes [65]. The obtained particles were coated with an anti-intercellular adhesion molecule (ICAM-1, a transmembrane glycoprotein used to target intra-endothelial drug delivery systems) and once injected in mice showed longer circulation time and lower retention in pulmonary blood vessels compared to spherical particles. This could be particularly useful when the accumulation in organs is not desired; poor biodistribution for one targeting strategy may be the ideal result for another.

Erythrocyte-shape soft-hydrogels, composed by PEG, were obtained by stop-flow lithography, in which monomers mixed with photoinitiators flowed in microfluidic channels and were crosslinked applying UV light irradiation [103]. Such particles were highly deformable and able to pass through very small microchannels simulating the small natural capillaries. Ring shaped particles were also produced using the same methodology and in comparison with erythrocyte-shaped hydrogels they demonstrated less resistance during the passage through the simulated capillaries. The lower cross-sectional area of the rings enables their bending with lower energy and an easier passage. This study demonstrated that the shape of the particles influence their behavior upon simulated physiological conditions, meaning that depending on the function of the carriers, the most appropriate shape should be selected.

Other strategy used to obtain this kind of shapes was based on particle replication in non-wetting templates (PRINT), allowing a precise control of distinct parameters (Figure 3.11) [104]. The obtained particles showed that increasing their deformability the circulation time also increased. Higher circulation times are interesting properties for drug delivery applications. In addition, the flexibility of the erythrocyte-like particles also influenced their biodistribution. Organ accumulation was dependent on the flexibility of the particles through controlling the crosslinking degree. As represented in Figure 3.11 D in some organs were accumulated higher amount of stiffer particles (*e.g.* in lungs and heart) and in other organs were accumulated more the flexible ones (*e.g.* spleen and blood). These results showed that such erythrocyte-like particles might be interesting systems for medical imaging where varied biodistributions are often desirable characteristics.

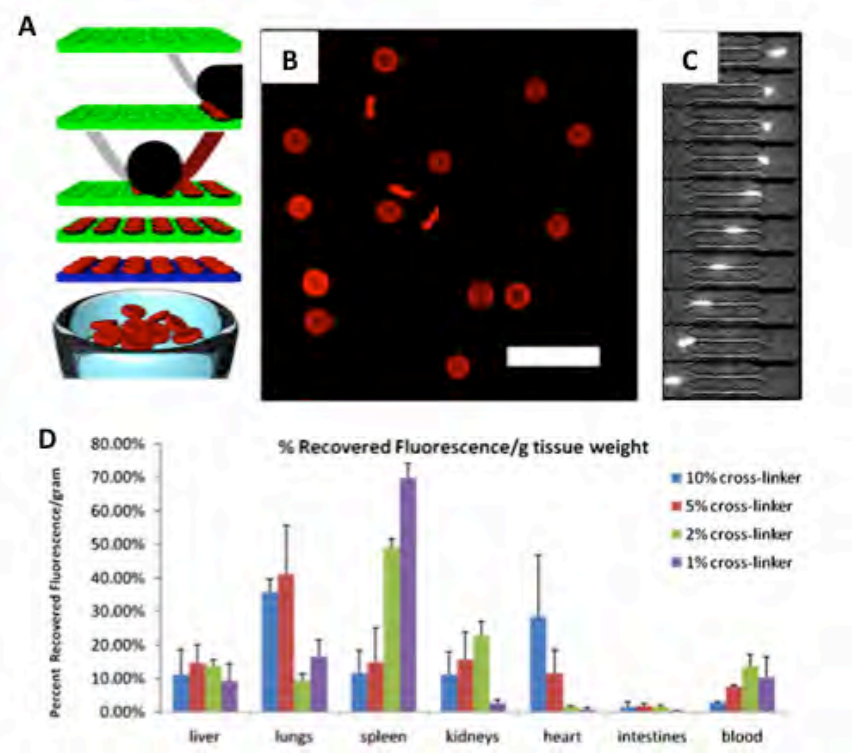

Figure 3.11. Using a PRINT technique (A), HEA hydrogel particles were obtained with erythrocyte-like structure (B). Such particles were capable to pass through very small fenestrations simulating blood capillaries (C). The accumulation of the particles in different tissues 2h after administration in mice demonstrated that those particles could accumulate in certain organs and such accumulation depended on the particles rigidity (D). Scale bar 20 μm. Image adapted from [104].

Biomimetic hydrogel particles of 2-hydroxyethyl acrylate (HEA) cross-linked with PEG diacrylate (PEGDA) with a negative surface charge and adequate elastic modulus exhibited mechanical properties similar to those of erythrocytes [104]. As observed for superhydrophobic technology used to produce spherical particles encapsulating drugs or cells [42,105–111], the incorporation of drugs (for example) inside such artificial erythrocyte-like particles should be relatively simple: just mix the bioactive compounds with the material before printing/crosslinking.

The formation of polyurethane (PU) erythrocyte-shaped particles starting from spherical ones obtained by electrohydrodynamic jetting, was analyzed in detail [112]. The concentration of the PU, the temperature and consequently the rate of solvent evaporation were crucial parameters to obtain particles with the above-mentioned non-spherical shape. In addition, using a co-jetting system, core-shell erythrocytes-like particles were obtained (described in detail in section 3.5). Although the main focus of this review is to analyze the shape of the particles, the chemistry is other important parameter in the design erythrocyte-

shaped artificial particles. Such property could be tailored and a compilation with the last advances in this area is reported elsewhere [98].

3.4.3. Non-Spherical Micelles

Amphiphilic molecules such block copolymers [44] are capable to assemble and form non-spherical shaped micelles. Similarly to the examples of particles above described, non-spherical micelles could have advantages when applied in the biomedical field either as drug carriers or as diagnosis systems.

Block copolymers composed by hydrophilic and hydrophobic blocks, namely PEG-PEE or PEG-PCL, have shown to form biocompatible filomicelles (worm-like micelles) that remain in circulation ten times longer than the spherical counterparts [80] – Figure 3.12. Once loaded with the same dose of paclitaxel, filomicelle carries (8 μm) were shown able to cause more cell apoptosis, and consequently be more efficient in the *in vivo* reduction of tumor size after 1 week, than non-encapsulated drug and smaller elongated micelles (1 μm). Moreover, compared to animals treated with spherical micelles, those treated with poly(ethylene oxide)-block-poly(ε-caprolactone) (PEO-b-PCL) filomicelles showed better tolerance to the treatment and greater and more sustained tumor shrinkage and tumor cell apoptosis [113]. Since flexibility is an important parameter to achieve the target tissues, the performance of PEO-PEE and PEO-poly(lactic acid) (PEO-PLA) spherical and worm-like micelles was studied through permeation in agarose gels as a strategy to mimic porous tissues [114]. Using gels with a pore size of 100 nm, it was verified that spherical vesicles stuck at the entrance of the gel whereas the worm-like micelles were capable to permeate through the gel due to their shape and flexibility. Paclitaxel-loaded PEO-b-PCL elongated micelles can be stored at low temperatures and neutral pH for months, without degradation [115]. In the tumor environment, the increase of temperature or environmental acidification triggers a transition from elongated to spherical shape, by a degradation process, and accelerates drug release. Such worm-like micelles may thus improve the efficiency/safety ratio of the treatment compared to micelles made of conventional surfactants.

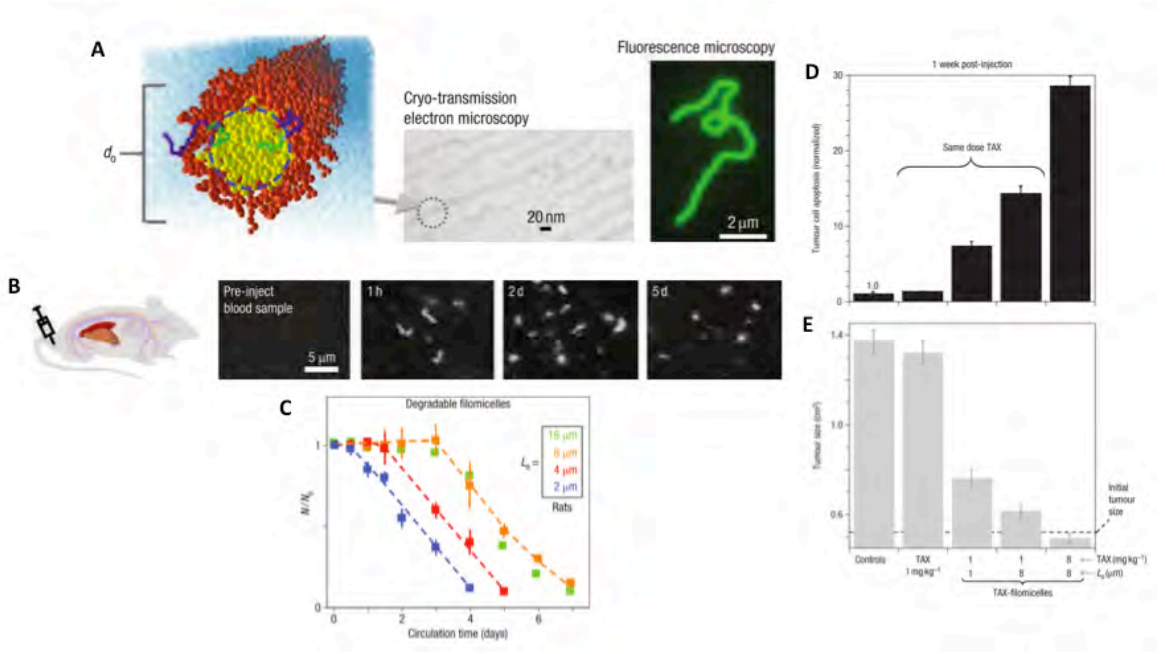

Figure 3.12. A. Filomicelles, in the nanometer scale, resulted from the self-assembly of amphiphilic di-block copolymers. B. Fluorescent filomicelles injected *in vivo* remained in the blood circulation up to one week. C. Longer degradable filomicelles circulate longer up to a limiting length. D. Filomicelles with two different lengths and loaded with paclitaxel were administered in mice. The filomicelles caused higher tumor cell apoptosis one week after when compared with free drug administration. Larger micelles were more effective E. The decrease of the tumor size was more visible in the mice treated with longest filomicelles and high drug dose. Adapted from with [80].

Non-spherical micelles also were effective in tumor diagnosis. PEO-PHB-PEO and Pluronic® 127 were combined to encapsulate a near-infrared fluorophore into elongated micelles. Such elongated shape prevents the clearance of the particles by the first mechanism that acts against particles systemically injected (*i.e.* reticuloendothelial system) through reducing the macrophages uptake. This increased the blood circulation time of the particles and their accumulation in tumor region and in liver 24 h post administration. Low levels of fluorescence were visualized in other organs, namely, spleen, heart, lung and kidney showing promising properties for tumor-targeted imaging and drug delivery [116].

3.4.4. Shape-Switching Particles

The dynamic modification of particles key properties has gained attention in view to precisely control the particle interactions with biological *milieu*. Stimuli-responsive materials may be used to prepare the systems for biomedical applications. These materials may be stable at may be stable along wide ranges of some external variable (*e.g.* pH, temperature, ionic strength) but undergo drastic conformational changes upon narrow modification of this variables around a given critical point [117]. Temperature and pH stimulus have been exploited and the obtained devices may be capable to display wettability changes in

the surface, switch their swelling capability, exhibit sol-gel transition, alter the permeability to molecules, exchange their aggregation status (colloidal systems) [117].

The optimization of particle geometry, parameter known to have a pivotal role in determining the biological applications [118], has been studied in detail. Shape-switching particles have been proposed with the aim to surpass the requirement of different shapes to achieve the optimum performance of a drug delivery system. From the information compiled above none specific shape has been identified as the best one to enable the particulate system to accomplish all the desired functions; this means that spherical shape may be advantageous for a given application but for others non-conventional shapes could improve the performance of the carrier. In many cases the conditions/stimuli that induce shape transitions are quite distant from the physiological conditions, limiting their applicability in the biomedical fields. In addition, if the shape switching is irreversible, their applicability could also be restricted. Having this into account shape-memory systems have been studied [119–121]. These systems can be deformed by application of an external stress and fixed in a second shape. This is the temporary shape, which in turn will be retained until the shaped body, is exposed to an appropriate stimulus. This stimulus will induce the recovery of the original shape.

Elliptical-shaped PLGA particles showed to switch in real time their shape in response to high temperatures (*ca.* 40 °C) and low pH (*e.g.* 5). The ellipsoids were obtained by a stretching a film containing spherical PLGA particles. Two competing forces (interfacial tension and polymer viscosity) modulate the shape of the particles: the interfacial tension between PLGA and surrounding liquid induces the change to an energetically favorable shape (spherical, in this case). The elliptical-sphere transition could be induced under physiological conditions (*e.g.* temperature increased by application of ultrasounds or phototermal activation and through the acidic pH of tumoral tissues) over periods ranging from minutes to hours or days, being this time controlled by appropriate selection of polymer molecular weight, particle size and strength of the stimulus. The increase of the temperature affects the viscosity of the polymer and the acidic pH influences the interfacial tension creating favorable characteristics to occur the shape switching. Shape change allowed the control of the interaction of the particles with macrophages, and this system was hypothesized being useful for preventing premature clearance in the blood stream, and being more efficiently used as drug delivery system. Switching of the shape modulates the interactions with the cells. The particles with higher aspect ratio (in this case ellipsoid disks) were able to mitigate the phagocytosis, increasing their blood circulation time and accumulation in target tissues. This type of particles may be useful for tumor therapy: elongated particles can accumulate in tumors via passive or active targeting but slow internalization by the target cells. Then, upon accumulation in the desired site,

the spherical shape will be advantageous to for faster cell internalization. The shape change of PLGA particles is not reversible. An higher level of control on the biological interaction could be possible with the use of more sophisticated systems enabling controlled reversible changes of particles shape under physiological conditions.

Six-arm PEG-PCL particles showed reversible shape switching. Such biocompatible and biodegradable particles changed their shape from spherical to elliptical either extracellularly or intracellularly with the cyclic heating and cooling between 43 °C and 0 °C under a stress-free condition. Similarly, with PLGA particles described above, the shape of PEG-PCL controlled the uptake of the particles by macrophages: spherical shaped were uptake whereas ellipsoidal with high aspect ratio avoid this interaction [121].

Spherical micelles composed by DNA-brush copolymers are transformed to cylinders in the presence of DNAzyme due to the rearrangement of the copolymer [122] – Figure 3.13. Shape transition was verified to be reversible: the cylinders recover the spherical after an input of DNA sequence in the micelles. Once again, cylindrical micelles showed prolonged blood circulation times [80], while the possibility to control in a reversible manner the shape of those particles was valuable for tailor the interaction with cells.

Another approach consists in playing with the degradation of the particles in order to modify the shape of the particles over time. For example, photo-curable hydrogels of PEG and PLA copolymers exhibit different degradation pattern depending on the UV exposure during the fabrication. The rupture of degradable bridges between non-degradable blocks allowed the division of the particles into smaller structures with distinct shapes [123].

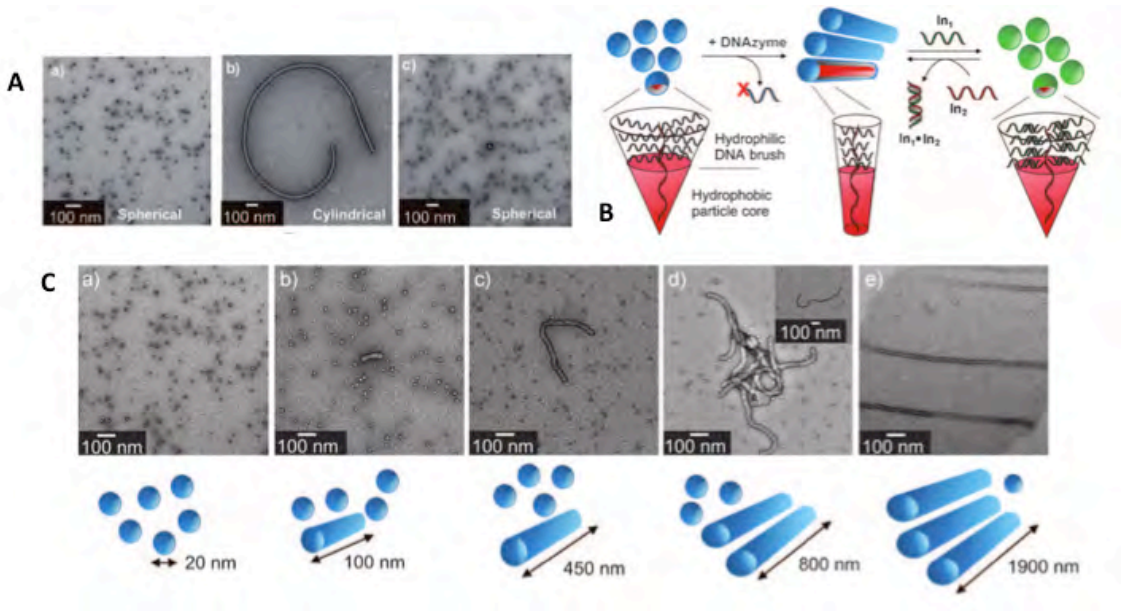

Figure 3.13. Micelles containing a DNA in the hydrophilic part of the polymer that compose the structure formed a spherical shape. In the presence of a DNAzyme the particles switch to an elongated shape due to the absence of DNA in the polymer

structure. The particles have the capacity to recover the spherical shape upon adding a DNA sequence. TEM images of the particles are represented in A and the explanation scheme in B. C represents the evolution of the particles length after adding DNAzyme: a) 0 min, b) 2 min, c) 2 h, d) 1 day and e) 2 days. Adapted from [122].

Particles prepared from other types of materials (not polymeric) such as gold or silver, also showed shape-switching capability. Gold nanoparticles have been explored in biomedical field for tumor therapeutics/diagnosis. They demonstrated capacity to switch their shape when irradiated with an intense pulsed laser radiation [124]. When exposed to radiation, nanorods melt and acquired a spherical shape. Similarly, prismatic silver nanoparticles may switch, in a reversible process, into disks when maintained in the dark [125]. Although this type of particles have been quite studied for applications in tumor therapies and diagnosis or even antimicrobial strategies, the influence of their shape in their performance for these specific application still remains to be elucidated.

3.4.5. Self-Folding Containers

Besides changes in the aspect ratio of the particles it would be interesting to envisage more general changes in the shape of polymer-based systems. For example, a very recent type of containers are based on self-folding structures: through self-assembly, thin films with a certain geometry spontaneously curve, roll-up or fold into particular three-dimensional structures such as cylindrical tubes, spirals, corrugated sheets or polyhedral [126]. The folding could occur in response to stimulus [127], such as electrical signals, pH, temperature, magnetic field or chemicals. 2D films may also fold immediately after removal from the substrate used as support for the 2D structures production. The application of self-folding systems in the biomedical field is currently in an immature stage, since there is still a paucity of information about shape stability under physiological conditions. Nevertheless, the possibility to control the shape of the 3D final system as well as wall chemistry, thickness and porosity, prompted the in vitro evaluation of those systems in encapsulation of drugs and cells [128,129]. A bilayer self-folding device composed by a pH-sensitive hydrogel (poly(methyacrylic acid) (PMAA) capable to swell when in contact with biological fluids (intestine), and a non-swelling layer of poly(hydroxyethyl methacrylate) (PHEMA) was proposed as drug carrier for prolonged release at the intestine site (where drugs are generally absorved) – Figure 3.14. A drug-containing layer, with adhesive characteristics, was deposited on the polymeric substrate. When adhered to the mucosa, the system curls due to the difference in swelling of both polymers. The mucoadhesion was improved and at the same time the drug was protected against leakage [130]. The system could be integrated in a capsule in order to reach the intestine and avoid the adherence of the device in other parts of gastrointestinal tract (*e.g.* stomach).

A self-folding porous microwell container was designed to allow the interaction of the encapsulated cells with the surrounding environment in all dimensions [131]. Conventional cell culture plates the cells are adhered onto a flat substrate, which do not accurately mimic the natural *milieu* due to the lack of 3D cues from the external media. The building of the 3D polyhedral microwell was obtained by the spontaneously fold of a 2D template caused by a surface-driven process due to the melting of the hinges between the adjacent faces. Such 3D microwells had porous faces to allow the entrance/exit of cell culture medium and other relevant molecules such as, nutrients and metabolites. Fibroblasts and pancreatic beta cells were successfully encapsulated in the polyhedral containers, with different shapes and sizes, composed by an epoxy negative photoresist (SU-8) and biodegradable PCL [132] .

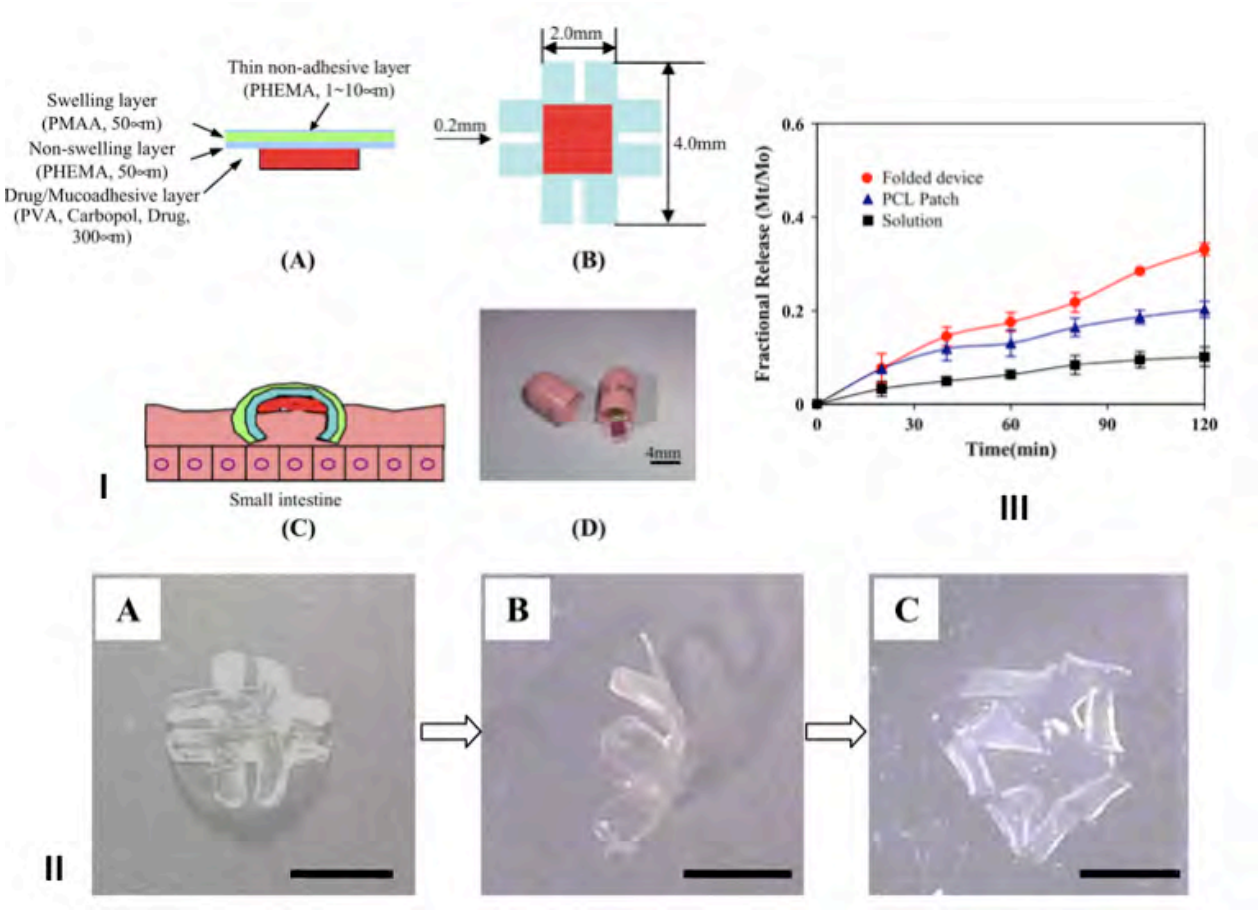

Figure 3.14. Multilayer system capable to fold preferentially in the small intestine (due to their pH-sensitive composition) protecting and controlling the release of a drug in this site. I. Schematic representation of the self-folding system. II. Optical images of the system before (a) and after folding (C) when immersed in a buffer solution simulating the conditions in the small intestine. III. Comparison of the performance of the self-folding device with other administration strategies, namely a patch and a solution. Adapted from [130].

3.5. Applications of Compartmentalized Particles

Particles with one compartment are the most studied for biomedical applications. Solid matrices, unilamellar liposomes, micelles and a variety of hollow particles, generally with a spherical shape, are recurrent systems used in drug delivery and cell encapsulation. Such architectures sometimes do not exert the optimal function due to their extreme simplicity. Using the Nature as inspiration source, sophisticated particulate systems with exotic geometries and multi-domains structures have been strongly hypothesized to have improved performances when applied in the biomedical field.

Several approaches have been proposed to develop systems capable to release more than one drug with appropriate kinetic profiles for the envisaged application. One possibility to encapsulate multiple molecules in different regions of the particles is playing with chemistry of system. A very interesting example is that of micelles composed by the biodegradable triblock copolymer poly(ethylene glycol)-b-poly(ε-caprolactone)-b-poly(2-aminoethyl ethylene phosphate) (PEG-b-PCL-b-PPEEA), which exhibit capacity to co-deliver siRNA and paclitaxel. *In vitro* and *in vivo* studies showed the synergistic effects that these particles might provide for tumor treatment. Paclitaxel is entrapped in the micelle core via hydrophobic interactions with PCL, while siRNA is adsorbed onto the micelle surface through ionic interaction with the PPEEA block. Although these micelles just have one compartment, by playing with the interactions between materials and bioactive agents it was possible to obtain a co-delivery system where the therapeutics are immobilized in distinct sites of the particles [133].

The aim of this particular section is to offer an overview of unconventional multicompartmentalized architectures. In the following subsections the most representative systems are described focusing on their advantages when applied as therapeutic, diagnosis or theranostic tools.

3.5.1. Core/Shell and Multilayered Particles

Core-shell particles are the simplest compartmentalized systems and have been widely used as drug carriers. This kind of particles could comprise a solid or a liquid or an empty (air) core surrounded by a solid shell. In addition, depending on the technique and materials used, multiple layers may be created in order to obtain multilayered particles.

Inspired by the water repellent behavior of the lotus leaf, artificial superhydrophobic surfaces have been explored as suitable platforms to obtain in an easy and fast way natural-based multilayered hydrogel particles – Figure 3.15. Those multicompartmentalized onion-like structures were obtained by dispensing a polymeric solution and subsequent crosslinking to form the core. Through a sequence of dispensing solutions to coat the previous solidified particle and crosslinking, the desired number of layers could be

produced [134]. This technique allowed the preparation of core/shell dextran/alginate particles where the core was designed to be a reservoir for bioactive agents and cells were encapsulated in the shell. As the cells were placed in the periphery of the particles, the design of such cell carriers avoided the problem of the access of nutrients and oxygen to the cells. Multiple dextran-layered particles were also produced and model drugs were encapsulated individually in each layer. Depending on their relative position, the release profile was different. This technique was also used to produce chitosan microgels coated with pectin for oral controlled release of a chemotherapeutical agent (5-fluorouracil) [109].

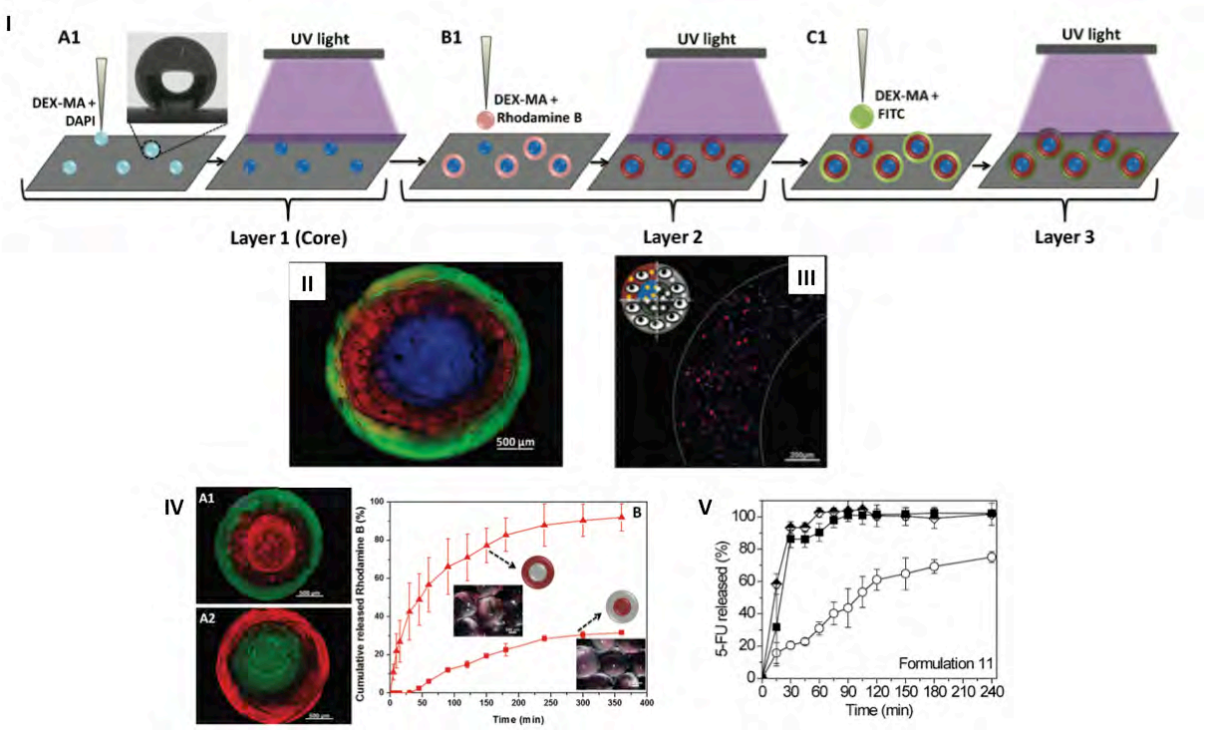

Figure 3.15. Compartmentalized particles were obtained using a biomimetic methodology that involved successive steps of dispensing liquid polymeric solutions and crosslinking strategies (I). Concentric multilayer (II) or core/shell (III) particles were prepared encapsulating model drugs or cells in individual compartments. Depending on the layer where the drug is immobilized, the release kinetic could be controlled (IV). A specific application was studied with 5-fluoraracil encapsulated in a chitosan core coated with one pectin layer. In acidic conditions the pectin layers led to remarkable lower drug release, meaning that depending on the pH, a controlled release of such chemotherapeutic agent was achieved (V). Images adapted from [108,109].

Onion-like structured hydrogels were also obtained by using a multi-step interrupted gelation process under controlled physico-chemical conditions [135]. Physical hydrogels composed by natural polymers, namely chitosan, were obtained without the need to recur to an external crosslinking process. The proportion of acetylated and deacetylated chitosan groups plays an important role in the balance between

hydrophilic and hydrophobic interactions. Upon a sequence of neutralization steps, membranes were formed due to the disappearance of ionic repulsions between polymer chains and subsequent establishment of hydrogen bonding, hydrophobic interactions and crystallite formation. Between each layer pair, intermembranar spaces were formed where cells (chondrocytes from rabbits) were injected with a syringe. The cells proliferated over 45 days secreting ECM that fulfilled the intermembranar space of the hydrogel. Alginate-based spherical hydrogels were also proposed as onion-like multilayered systems for biomedical applications. Particles were obtained through a dynamic self-assembly process based on the interaction of sodium alginate with calcium ions. In this processing technique cells or drugs could be encapsulated in the different layers during the particles preparation and the existence of intermembranar spaces may be tailored. The performance of the system as drug carriers was evaluated *in vitro* and showed a pulse-like drug release profile [136]. These technologies cannot present the advantages of the one involving the superhydrophobic supports that permit the sequential bottom-up deposition of individual layers in mild conditions and virtually with 100% of encapsulation efficiency.

Compartmentalized particles can also be integrated in other structures to improve the general performance of the system. In this context, core/shell PLGA particles were used as structural elements of a fibrous scaffold with the aim to control the release of proteins, avoiding the initial burst release (Figure 3.16). The particles were obtained by immiscible coaxial electrospraying and then incorporated into the fibers of the scaffold via electrohydrodynamic jetting. Control of protein release was dependent on the uniformity of the PLGA shell and on the adjuvant polymers incorporated in the core, which in turn had different interactions with the studied protein [137]. Since lysozyme is a positive charged protein, it was not able to establish electrostatic interactions with chitosan and the release was fast. However, when it was used Pluronic F68/poly(acrylic acid) (PAA), a polyelectrolyte complexation occurred between PAA and the protein and the release was much more slower.

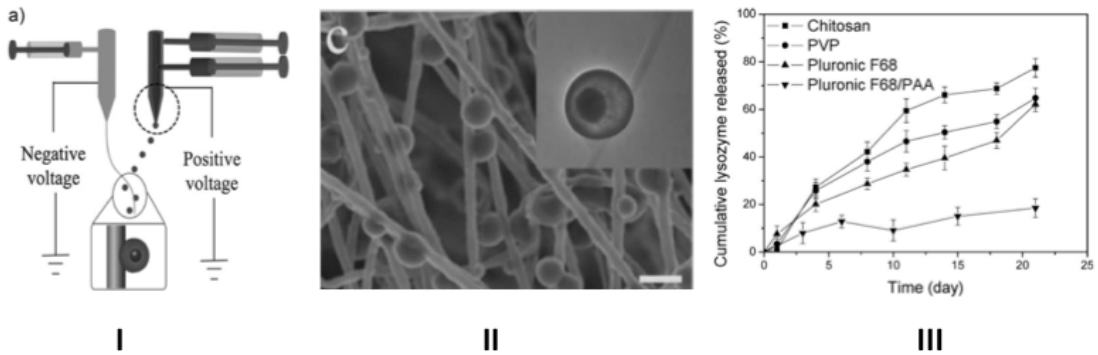

Figure 3.16. Core/Shell particles encapsulating lysozyme were obtained as structural elements of a fibrous scaffold (I and II). The particles allowed the control of lysozyme release, avoiding the typical initial burst (III). Image adapted [137].

Multicompartmentalization may be also achieved combining polymeric materials with inorganic entities. Hybrid core/shell particles were prepared with a gold core (*ca.* 60 nm) that was coated with a biocompatible hydrogel (NIPAAm and acrylic acid) shell with thickness varying between 20 to 90 nm. These particles demonstrated pH and temperature-responsiveness being adequate for drug delivery. The shell showed temperature-responsiveness when the cores were activated under light exposition [138]. Another hybrid core/shell system was produced by copolymerization of PNIPAAm with acrylamide surrounding multiple gold nanoparticles through an emulsion process combined with photopolimerization. The response kinetics of PNIPAAm to temperature, microwaves and light was accelerated due to the presence of the gold nanoparticles. The increased sensitivity allowed faster particle response and such behavior could be interesting for drug release applications that require very fast transitions [139]. More complex structures, namely core/double-shell microgels were prepared using PNIPAAm as the template (core) in the synthesis of two layers: N,N'-(1,2-dihydroxyethylene)bisacrylamide and poly(N-isopropylacrylamide-co-acrylic acid). The erosion of the inner shell transforms the particles in core/shell multiresponsive systems in which the core (temperature responsive) and the outer layer (pH and temperature responsive) behave as independent structures separated by the space correspondent to the dissolved shell. Such multicompartmentalized particles were suggested to be useful for co-encapsulation and release because the shell remains unperturbed by the properties, contents or responsiveness of the core [140].

Multicompartmentalized particles described above exhibited the most conventional particle shape: spherical. Advances in methodologies of particles preparation have allowed the development of procedures that combine multicompartmentalization with non-conventional shapes. Starting with a core/shell immiscible liquid system, composed by a photopolymerizable PEG in the shell and dextran in the core, a concave architecture was obtained [141]. Upon a selective polymerization, the dextran core remained liquid and migrated from the inner to the periphery yielding dextran-PEGDA particles with two compartments and an anisotropic structure [141].

Although in the most of the cases the particles produced were envisaged to be applied as drug delivery systems, studies to support this application still missing. A few *in vitro* results [109,134–136] demonstrated that core/shell and multilayered particles showed promising characteristics to be used as drug release systems and cell encapsulation.

3.5.1.1. Layer-by-Layer Coated Particles and Capsules

Layer-by-layer (LbL) technology has been used in a variety of biomedical applications [142]. Compartmentalized systems may also be obtained by LbL assembly through alternate deposition of oppositely charged materials onto a solid core. Besides electrostatic forces, other kinds of interactions can be used in this assembly process [143]. The core may remain solid or be liquefied (sacrificial structure) after the deposition of the layers. Depending on the materials used for the core, this procedure can avoid the use of organic solvents, which is important to encapsulate cells or labile molecules such as proteins or nucleic acids. Three main strategies are currently used to encapsulate drugs in those kind of systems: (I) using the bioactive agents as multilayer constituents; (II) preloading the core template and (III) post-loading by modifying the permeability of the multilayered structure – Figure 3.17. Low encapsulation efficiency is the main limitation of LbL particles [144], while their main advantage is a great flexibility that enables a successful internalization by the cells.

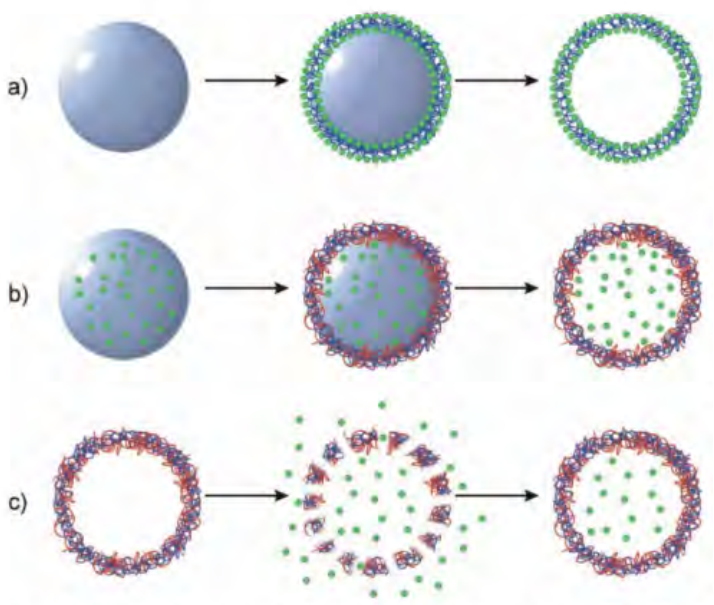

Figure 3.17. Schematic representation of the main strategies to encapsulate bioactive agents into LbL multilayered particles: a) use the bioactive agent to construct the multilayer shell; b) load the template with bioactive agent that will be retained inside the multilayer shell after core removal and c) bioactive agents entrapment through altering the permeability of the multilayered shell. Image obtained from [144].

A wide range of spherical LbL systems have been developed and loaded with bioactive agents (acting as drug carriers [142,144] or even cells (acting as cell supports in possible injectable systems [145–147] – Table 3.2.

Table 3.2. Examples of spherical LbL systems with adequate characteristics to be applied in biomedical field.

Core template	Layers	Type of particle	Drug	Characteristics	Applications	Ref.
Sulfonated polystyrene beads or carboxylated quantum dots	PLL modified with iminobiotin, followed by the linker protein (neutravidin) and biotin end-functionalized PEG	Solid	-	PEG was used to avoid rapid particles clearance; In acidic conditions (tumor regions) the particles gradually lose their PEG shells, allowing the exposed PLL layer to facilitate cellular uptake.	Drug delivery Cancer therapies	[148]
Silica core with a mesoporous shell	Poly(L-glutamic acid) (PGA) conjugated with doxorubicin cross-linked using 2,2′-diaminodiethyl disulfide dihydrochloride (cystamine) in the presence of 1-ethyl-3-(3-dimethylaminopropyl) carbodiimide hydrochloride	Solid and hollow	Doxorubicin	The particles were stable at neutral pH and in absence of hydrolases. In acidic conditions and presence of carboxypeptidase the amide bonds in PGA-Dox were cleaved and Dox was released; Less Dox was released from solid particles when compared with capsules due to the limit access of the enzyme to the polymer; Both types of particles were internalized by LIM1215 human colorectal tumor cells: within the cells, the liposomal hydrolases and the reducing environment caused the release of Dox and consequently, the tumor cells dead.	Drug delivery Cancer therapies	[149]
Calcium carbonate particles	Poly-L-arginine and dextran sulfate	Hollow	Antigens and immunomodulators	The immunostimulation of the capsules was achieved by using a lipid coating; The particles containing lipids were more effective in dendritic cells activation; Activation of dendritic cells could be modulated by deposition of different lipids.	Antigen carriers Vaccination	[150]
Silica	Poly(vinyl pyrrolidone) and poly(methacrylic acid)	Hollow	Rifampicin (Low water solubility drug)	Very fast release (90% of the encapsulated drug was released after 20min); The empty capsules were cytocompatible; The loaded particles demonstrated a similar effect of free drug due the fast release.	Drug release system Tuberculosis	[151]
Carboxylmethyl cellulose (CMC)– doped $CaCO_3$ particles	Chitosan, alginate Crosslinking: glutaraldehyde	Hollow	Doxorubicin	High loading capacity; Diffusion-controlled release; The system induced the apoptosis of HepG2 tumor cells; Encapsulated doxorubicin had better efficacy than when administered in the free form.	Drug delivery Cancer therapeuties	[152]
Artemisinin crystals	Chitosan, gelatin, and alginate	Solid	Artemisinin (low solubility)	Sustained release of artemisinin; The hydrophilicity of the drug was improved.	Drug release Cancer therapies	[153]
Magnetic alginate microspheres	sodium poly(styrene sulfonate) and poly(allylamine hydro- chloride)	Hollow	Doxorubicin	Noncontact high-frequency magnetic field application heated the system and increased the drug release; The doxorrubicin released from the capsules presented similar toxicity to free drugs; For high drug concentrations the loaded particles showed lower cytotoxicity.	Magnetic targeted drug delivery	[154]
Commercial microparticles (MF, from Microparticules GmbH)	Poly(allylamine hydrochloride) and poly(sodium-4-styrenesulfonate)	hollow	Photoacid generators and FITC-dextrans (drug models)	The photoacid generators were integrated in the shell multilayers; UV exposure caused the activation of the photoacides that released protons and induced particle swelling; Prolonged exposure led to a breakage of the capsules, which promoted a rapid release of the entrapped substances.	Controlled release	[155]
Amino-functionalized silica particles	Chitosan and dextran sulfate	Hollow	Bovine serum albumin	The burst release was controlled by its reduction in 10%; Good cytocompability.	Controlled drug release	[156]

$CaCO_3$ particles	Poly(allylamine hydrochloride), poly(sodium-4-styrenesulfonate), dextran sulfate sodium salt and poly-L-arginine hydrochloride	Hollow	Nonactive prodrug: a self-quenched fluorescence-labeled ovalbumine	Biodegradable particles; Upon internalization the shell of the particles were degraded by intracellular proteases; The enzymatic degradation converted the nonactive prodrug (non-fluorescent) into an active state (fluorescent).	Drug release Conversion of the nonactive prodrugs into active drugs inside the cells	[157]
Mesoporous silica particles	Chitosan and dextran sulfate	Hollow	FITC-albumin (protein drug model)	Biodegradable capsules; Enzymatic degradation; The control of the release was obtained by altering the surface charge of the particles, which had a large effect on the adsorption of enzymes; The larger amounts of chitosanase adhered onto anionic than onto the cationic surface.	Controlled drug release	[158]
Commercial microparticles (MF, from Microparticules GmbH)	Poly(ferrocenylsilane) (PFS)	Hollow	TRITC-dextran (drug model)	Redox change responsive particles; PFS polyelectrolytes feature redox-active ferrocene units in the main chain; Chemical oxidation caused the fast expansion of the particles and consequently an increase in the permeability; Additional external layers of poly(styrene sulfonate) (PSS−) and poly(allylamine hydrochloride) (PAH+) allowed the control of the swelling.	Controlled drug delivery	[159]
Amine-functionalized silica particles	Thiolated poly(methacrylic acid) (PMASH) and poly(vinylpyrrolidone) (PVPON)	Hollow	Oligopeptide antigens	Oligopeptide sequences were covalently linked to a negatively charged carrier polymer via biodegradable linkages; The resultant polymer+oligopeptide was adsorbed onto silica particles templates and then covered by the LbL shell; In the presence of a natural reducing agent, glutathione, cleavage of the disulfide bonds causes release of the peptide from the capsules; The peptide-loaded capsules were successfully used to deliver their cargo to APCs and activate CD8 T lymphocytes.	Drug delivery Vaccination	[160, 161]
$CaCO_3$ particles	Chitosan and a biomimetic elastinlike recombinamer (ELR)	Hollow	BSA (drug model)	Temperature-responsive system; The release of BSA was dependent on the number of layers; The relase was sustained over 14 days; Capsules cultured with L929 cells did not affect the cell viability.	Controlled drug release	[162]
$CaCO_3$ particles encapsulating micelles of polystyrene-b-poly(acrylic acid)	Poly(allylamine hydrochloride) and poly(sodium-4-styrenesulfonate)	Hollow	Rhodamine B and lysozyme	The negatively charged micelle remained in the inner of the capsules after core removal; The system selectively entrapped positively charged water soluble molecules; The content was released in a sustained manner.	Drug Release	[163]
Liposomes	Chitosan and dextran sulfate or DNA	Hollow	Glucose, Alendronate and 1-hydroxy pyrene-3,6,8-trisulfonic acid	The release was suppressed by the polymeric capsule; The release was triggered by DNA denaturation, which in turn improve the permeability of the shell.	Controlled drug release	[164]

Liposome	Alginate and chitosan	Hollow	osteogenic protein-1	No toxic effects were observed against MC3T3-E1.4 mouse preosteoblasts; The in vivo studies showed no significant toxicity, immune responses and/or change in organ functions; This hybrid core–shell nanoparticulate delivery system localizes the effect of the released bioactive load within the site of injection in muscle with no significant tissue distress.	Drug delivery Tissue Engineering	[165]
Nanocolloids of insoluble drugs	Poly(allylamine hydrochloride), poly(dimethyldiallylamide ammonium chloride) and sodium poly (styrene sulphonate)	Solid	Tamoxifen and paclitaxel	The release of the drugs was controlled s according to the composition, density and thickness of the shell; The particles were targeted by attaching specific ligands to the external polymer layer; The targeted particles showed higher toxicity against cancer cells than the non-targeted counterparts.	Controlled drug delivery Cancer therapies	[166]
Drug crystals	Poly(dimethyldiallyl ammonium chloride), sodium poly(styrenesulfonate) and gelatin A/B	Solid	Dexamethasone	The release could be controlled by the shell; however the release was very fast.	Drug release Systems for eye administration	[167]
Drug crystals	Poly(allylamine hydrochloride), protamine sulfate and BSA	Solid	Curcumin	LbL assembly with biocompatible polyelectrolytes was used to provide a particle coating with a high surface potential and stabilization of drug nanocolloids; Polyelectrolyte LbL encapsulation allowed sustained low water soluble drug over the range of 10-20 h	Release systems Cancer therapeutics	[168]
PS and silica	Poly-L-glutamic acid poly-L-lysine	Solid and hollow	BMP2 and TGFβ1	The GFs were embedded in the multilayer shell; Embryoid bodies (EBs) cultured in contact with capsules differentiated into mineralized structures which did not occur when both GFs were dispersed in culture medium; The multilayers protected the GFs from degradation and the capsules acted as reservoirs of bioactive agents; The subcutaneous implanting of capsules and EB embedded in an alginate matrix showed the appearance of bone forming cells and vascularization surrounding the implant.	Drug delivery Tissue Engineering	[169]
$MnCO_3$ particles	BSA deposition followed by glutaraldehyde crosslinking	Hollow	TRICT-dextran (macromolecule model)	Biocompatible and biodegradable of natural-based particles; Reversible pH-responsiveness; The capsules were permeable for macromolecules at pH below 4 or above 10, while were impermeable in other pHs; Macromolecules were loaded and sealed for at least for 2 weeks.	Drug release	[170]
Alginate	Chitosan and alginate	Hollow	Human osteoblast-like cells (SaOs-2)	The cell viability was not compromised in capsules with eight layers.	Mini-rectors or scaffolds or cell carriers for cell therapies	[145]
$CaCO_3$ particles	Chitosan and a biomimetic elastin-like recombinamer with bioactive RGD and scrambled non-functional RDG	Hollow	DQ-ovalbumin (drug model)	Cell viability was not affected even in the presence of high concentration of capsules: cells cultured in the presence of particles with functional RGD exhibited high viability; The capsules were successfully internalized by the cells; Surface functionalization did not influence capsules internalization by hMSCs	Drug delivery Intracellular release	[171]

The systems described in the Table 3.2 are suitable for being engineered and functionalized in order to have a good performance when administered *in vivo*. Regarding the shape of this type of particles, the majority of the capsules produced by LbL are spherical-shaped structures. The increasing attention on non-spherical shaped particles also pushed the development of more geometrically complex LbL systems, being currently in a very early stage. The size and shape of LbL particles could be tailored according to the template used to support the multilayers. For example, using a biconcave template and LbL technique, soft particles with erythrocyte-shape were prepared [59,172]. The elastic modulus of the studied particles was of the same order of magnitude as the natural erythrocytes and the artificial particles were capable to stretch to pass through small diameter capillaries and to recover the discoidal shape [59,172]. Rod-shape particles have been prepared using polystyrene microspheres as templates [173]. After assembly of poly(L-lysine) (PLL) and BSA, the particles maintained the spherical shape. The rod-shape was just obtained when the template was removed. The presence of the BSA was crucial to obtain such non-spherical shape. The mechanism proposed is related to the collapse of the LbL shell upon adding the THF. A gel-like interconnected structure was formed after the swelling and the release of polystyrene under sonication. The particles solidified upon water adding exhibiting a rod-shape [173].

Conventional LbL capsules are, generally, composed by two distinct phases; namely, a LbL shell with an air or a liquid core. However, more complex architectures are also possible. A three-phase system with a LbL shell surrounding a hydrogel bead where the space between the hydrogel bead and the LbL shell is fulfilled with liquid. Although no application was explored for this complex system, the authors hypothesized its potential in the biomedical field [174]. Other examples of complex systems are beads with self-exploding polyelectrolyte shells (dextran-hydroxyethyl methacrylate/dimethyl aminoethyl methacrylate (Dex-HEMA/DMAEMA) core surrounded by dextran sulfate/poly-L-arginine layers) [175]. These particles are capable to release micrometer-sized capsules (also composed by dextran sulfate/poly-L-arginine) at the time of explosion. Such hierarchical compartmentalized system was composed by beads with *ca.* 150 μm loaded with 3 μm LbL microcapsules. The rupture of the LbL shell could be triggered by the dex-HEMA degradation, which in turn increases the pressure inside the big capsule and favors the release of the small capsules. The release may be tuned by controlling the crosslinking density of the gel network. An interesting application for this self-exploding system could in vaccination field. An ideal vaccination system should allow the administration of the prime and booster doses (for generation of immunity) in a single injection and co-delivery of the adjuvant and the antigen to enhance the immune response.

A compartmentalized hierarchical system composed by capsules inside capsules was inspired by the cells structure [176] – Figure 3.18. Iron oxide magnetic nanoparticles and a drug model were encapsulated in LbL microcapsules protected by a temperature-responsive chitosan/elastin-like recombinamer (ELR) multilayer shell. Then, such loaded microcapsules were encapsulated in macro-capsules together with other small molecule, using an alginate bead as sacrificial template. The shell of the macro capsule was a multilayer of chitosan and alginate. A decrease in the release kinetics of a model drug was achieved changing the temperature from 25 to 37 °C, due to the presence of the temperature-sensitive ELR in the shell. The presence of the magnetic nanoparticles turns the system responsive to external magnetic fields. Playing with the shells (number and materials) the permeability may be tuned and other stimuli responsive strategies may be integrated, which makes these systems very versatile.

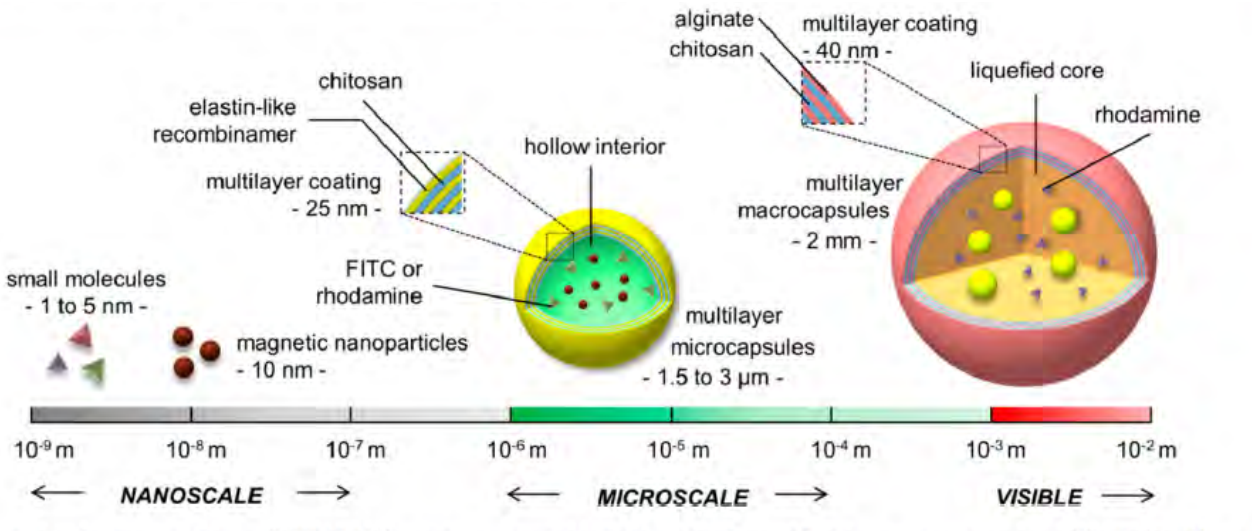

Figure 3.18. Schematic representation of hierarchical systems composed by nanoparticles and/or drugs inside LbL microcapsules, which in turn were encapsulated inside macro-scale LbL capsules. Image from [176].

Following the concept of hierarchical systems, poly(L-lactic acid) (PLLA) microparticles with cells adhered on their surfaces were encapsulated in macro capsules in which the shell was a multilayer assembly of PLL, alginate, and chitosan [146]. PLLA microparticles acted as adhesion points for anchorage-dependent cells, and the LbL shell in combination with the liquefied environment enhanced the diffusion of the molecules for cell survival [146,147] - Figure 3.19. These systems may also be customized to host different cell types and microparticles. In addition the solid microparticles may act as reservoirs of molecules of interest (*e.g.* growth factors). This hierarchical system may be useful as cell carriers or small bioreactors for cell expansion and micro-tissues formation or for models for drug screening.

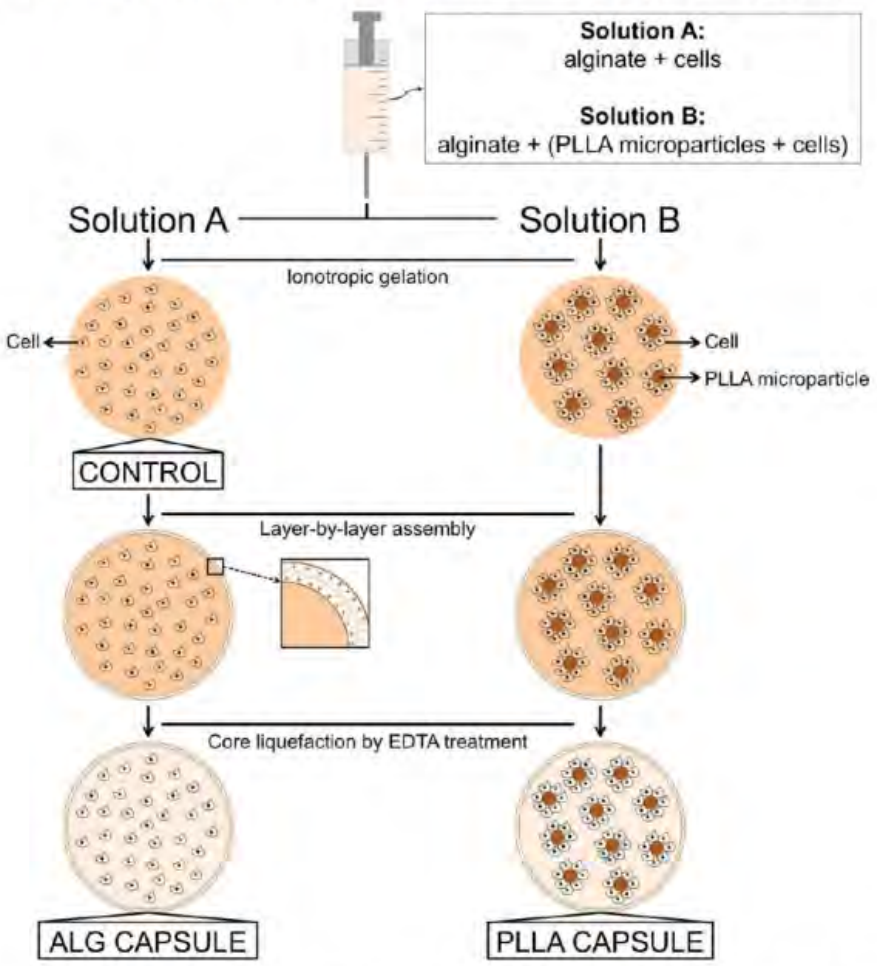

Figure 3.19. Hierarchical system composed by LbL capsules where PLLA microparticles were encapsulated and acted as supports for adherent cells expansion. Capsules without (A) and containing (B) solid PLLA microparticles inside the liquid liquefied core. Image from [146].

3.5.1.2. Mesoporous Particles

Mesoporous particles are particularly interesting for cancer diagnosis, anticancer drugs delivery, and targeted therapies due to their high surface area, easy and versatile surface modification, tunable pore size, particle size and shape and general good biocompatibility (*e.g.* silica) [177,178]. The simplest structures are hollow mesoporous particles combining a large void space in the core and the mesoporous network in the shell (one compartment) – Figure 3.20. The presence of a hollow, confer low density and the extensive presence of mesoporous channels on the shell turns those systems highly permeable.

The hollow could be used as a reservoir for drug storage and delivery. The shell of the particles could have a well-tuned thickness within the nanometer scale range being the structure responsible for the control of the mass transport during the release of the bioactive agents. The mesoporous particles may be loaded during their processing by using a template where the drug is encapsulated. The template may be

removed after the mesoporous shell growth onto its surface [179]. When this strategy is not suitable, the particles may be loaded after being processed. In this later case, the porous shells play an important role in allowing the entrance of the bioactive agents.

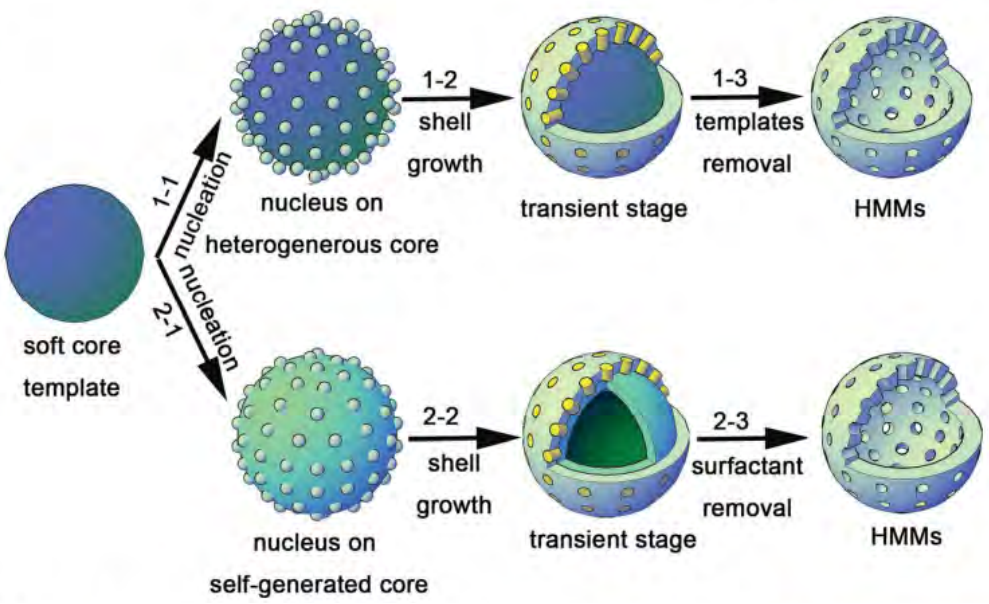

Figure 3.20. Representative scheme of preparation of hollow mesoporous particles. Using a soft-template, two routes may be followed: 1) heterogenerous and 2) self-generated. In the first case nucleation of the precursor/surfactant mixture occurs at the interface between the core and the liquid medium containing surfactants and precursor molecules. Then, the shell grows due to the precursor hydrolysis around the core template and the self-assembly of the surfactants. In the second process the precursor is integrated in the core. The core template is gradually consumed and the shell is formed by self-assembly of surfactants present in the liquid medium. In both strategies the final stem is the core and mesoporous templates removal. Image from [177].

The shells of these kinds of particles may be made from materials such as carbonates, metals and metals oxides [180–182]. Several morphologies of hollow mesoporous materials were then proposed: spheres [183], vesicles [184,185], helicoids [186]. Methodologies and different of types of mesoporous hollow structures developed up to now have been reviewed elsewhere [177]. Observing the general structure of those particles, they are simple core/shell systems in which the core is air and one bioactive agent is encapsulated; see some examples in Table 3.3. However, the advances in the design of mesoporous particles allowed the development of more complex systems, enabling the encapsulation of more than one entity or even more structures with higher complexity.

Table 3.3. Examples of hollow mesoporous particles with one compartment and used for drug release.

Hollow Mesoporous nanoparticles	Drug	Advantages	Ref.
Aluminosilicate treated with 3-aminopropyltriethoxysilane	Ibuprofen	Improved capacity to storage the drug.	[187]
Carbon spheres treated with tetraethoxysilane (TEOS) and n-octadecyltrimethoxysilane (C18TMS) and then PEGylated	Doxorrubicin	High stability and dispersity; Lower *in vitro* cytoxicity when compered with non loaded and non PEGylates counterparts; Higher *in vitro* cytoxicity against Hela and NIH3T3 cells for PEGylated loaded particles.	[188]
Hollow mesoporous silica nanoparticles with three pore sizes	Doxorubicin	Doxorubicin release dependent on the pore size; Negligible cytotoxicity and efficient cellular uptake; Higher pore sizes, more efficient cellular uptake of drug and faster intracellular release.	[189]
]mesoporous zirconia nanocapsules	Doxorubicin	Highly compatible; High loading capacity; pH dependent release; High drug released in cancer cells due to the acidic environment inside cells (more cytotoxicity in tumor than in normal cells).	[190]
Rattle-type Fe_3O_4@SiO_2 hollow mesoporous	Doxorubicin	Fast cell uptake; Sustained release; Doxorubicin-loaded spheres exhibited greater cytotoxicity than free drug.	[191]
Hollow silica nanocapsules	siRNA and Fe_3O_4 nanoparticles	Controlled porous size; Excellent loading capability; Successful intracellular transfection *in vitro*.	[192]

Hollow mesoporous silica nanoparticles are the most studied for biomedical applications. Such particles are ideal drug vehicles due to their high biocompatibility, biodegradability and high drug loading capacity as well as capacity to control the release of molecules. Such type of particles could be engineered in order to accomplish specific functions. Examples are molecularly/magnetically target drug delivery, simultaneous multi-modality bioimaging and therapeutic capability, *in vivo* stimuli responsive drug release and multiple bioactive agents release. One example of a hierarchical system involving porous core/shell particles is the entrapment of small-sized superparamagnetic Fe_3O_4 nanoparticles into a hollow silica mesoporous particle [192]. Fe_3O_4 nanoparticles entered inside the particle through the pores of the silica shell. The obtained system was multifunctional, being successful in siRNA transfection through internalization as well as acting as agent contrast for MRI. Other examples are double-shelled mesoporous silica particles developed for the encapsulation of multiple bioactive agents [193]. This system had a mesoporous silica shell (nanosphere or nanolayer) coated by other mesoporous silica shell. Both layers formed a hierarchical arrangement of the pores onto the particles capable to control and sustain the release of two anticancer drugs. Irinotecan and docetaxel were encapsulated in the particles to show the versatility of the particles in acting as carriers for hydrophilic and hydrophobic drugs, respectively. A sustained release of the hydrophilic drug was achieved due to the difficult diffusion through the two layers instead of one. Docetaxel was accommodated in the hollow core of the particles being diffused out slowly

due to its hydrophobic characteristic. The particles were successfully uptaken by the cells showing potential for intracellular delivery. The results demonstrated an enhanced anticancer effect when compared with drugs administered in a free way: the intracellular release is more effective than the diffusion of free drugs into the cells. Advances in procedures to prepare mesoporous particles have allowed the development of other complex architectures (e.g. combination of hierarchical and multilayered systems) with spherical and non-spherical shapes: (I) spherical hollow silica particles with double mesoporous shell; (II) spherical mesoporous silica particles coated by a double mesoporous shell; (III) ellipsoidal hollow particles with double mesoporous shell; (IV) ellipsoidal Fe_3O_4 particles encapsulated in silica mesoporous particles (1 layer) and then surrounded by the double mesoporous shell and (IV) ellipsoidal Fe_3O_4 particles inside the cavity of ellipsoidal double mesoporous shell – see Figure 3.21. Although not studied before, we hypothesized that non-spherical double mesoporous silica particles with a Fe_3O_4 core would be interesting systems for cancer theragnosis: the elongated shape would increase the circulation time of the particles and the cell uptake, the presence of Fe_3O_4 nanoparticles could act as contrast agent for MRI, and the double shells improve the control of the release of encapsulated drugs. Another way to obtain multilayered structures is combining mesoporous particles templates with LbL deposition [149]. Wang *et al.* [194] coated mesoporous silica nanoparticles previously loaded with a hydrophobic drug (*e.g.* thiocoraline or paclitaxel). The mesoporous particles were immersed in an organic-based drug solution allowing the diffusion of drug molecules into the particles. Then, a multilayer shell was build depositing poly(N-vinylpyrrolidone) and thiolated poly(methacrylic acid). After the core removal, were obtained the capsules loading a hydrophobic drug, which is quite difficult using conventional templates (e.g. $CaCO_3$, alginate). The examples described above show that hollow mesoporous particles could integrate multiple functions. Although the most studied application is related with intracellular delivery of bioactive agents, these particles could also be interesting systems for diagnosis. A few examples of mesoporous particles encapsulation functional inorganic nanostructures for theranostic purposes are reported in Table 3.4.

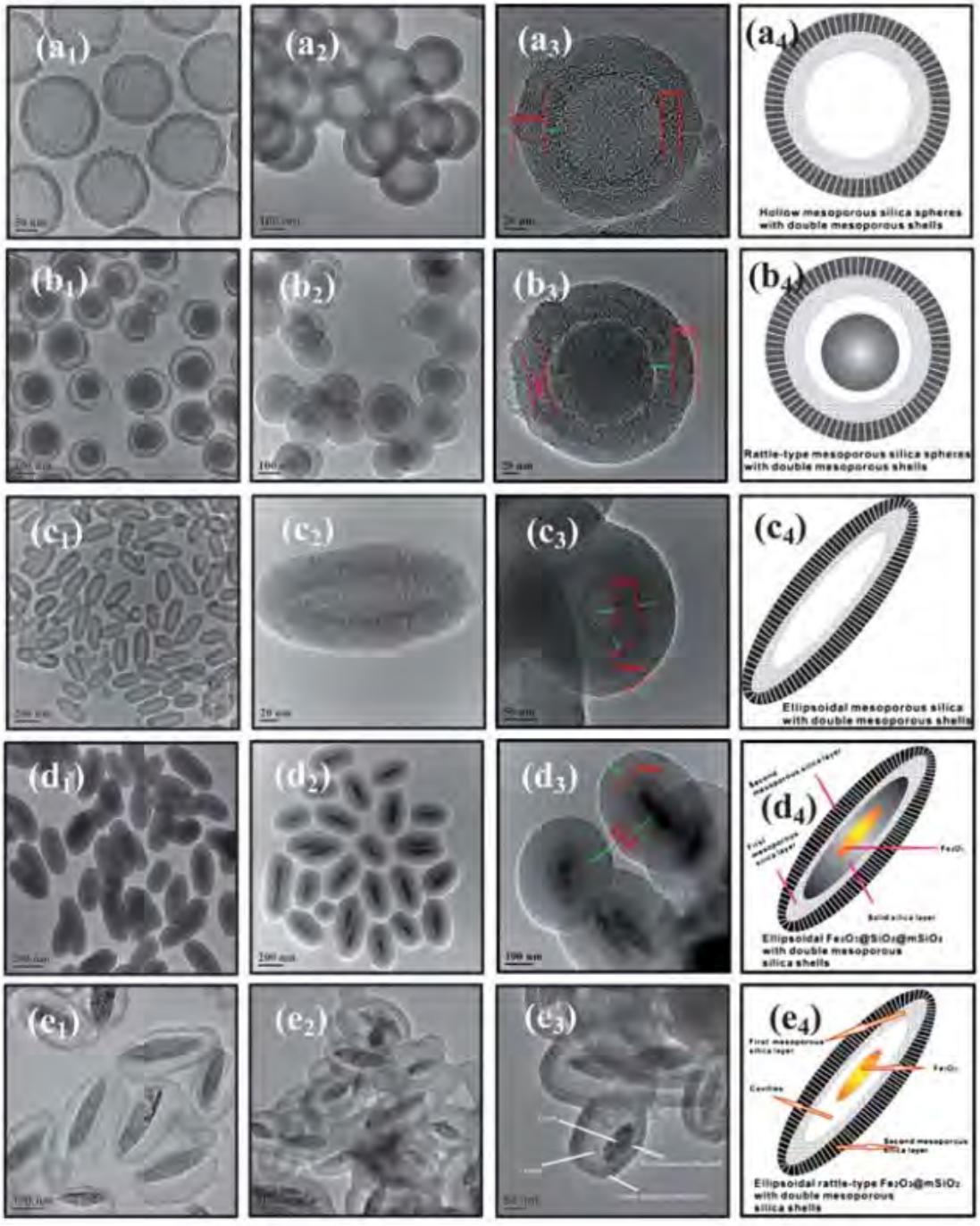

Figure 3.21. Architectures of the hollow mesoporous silica spheres with single (a1) and double (a2 and a3) mesoporous shells. Rattle-type mesoporous silica particles having a single (b1) and double (b2 and b3) mesoporous shells. Non-spherical hollow mesoporous silica (ellipsoids) with single (c1 and c2) and double (c3) mesoporous shells. Fe_2O_3 ellipsoidal particles (d1) coated with a single (d2) and double (d3) mesoporous shells. Finally, rattle-type Fe_2O_3 rattle-type particles exhibiting a single (e1) and double (e2 and e3) mesoporous shells. The set of images with number 4 are the schematic representations of the double-shelled structures. Image from [193].

Table 3.4. Examples of mesoporous particles for diagnosis and theranostic purposes.

Particles	Content	Properties	Ref.
Multi-shelled mesoporous silica nanospheres (double- and triple-walled) – rattle-type or hollow structures	Doxorubicin and fluorescein FITC	Inclusion of functional species into shell-to-shell cavities; Dual-modality for imaging and drug co-delivery vectors through the appropriate selection of pH-dependent molecules; Doxorubicin (DOX), loaded in the outer periphery space, was successfully carried and released in the cell cytoplasm; The fluorophore was effectively encapsulated in inner of the spheres; The particles showed capability to be used as tracking tools both *in vitro* and *in vivo*.	[195]
Hollow silica mesoporous nanocapsules composed by an inorganic core	Doxorubicin and Fe_3O_4 or Au nanoparticles	Anticancer drug delivery and MRI cell imaging applications; Very low cytotoxicity against various cell lines, low hemolyticity against human blood red cells and no significant coagulation effect against blood plasma.	[196]
Ellipsoidal multifunctional mesoporous nanostructures coated by positively charged polyelectrolyte (PAH) and negatively charged fluorescent quantum dots (QDs)	Doxorubicin and Fe_3O_4 elliptic core	High biocompatibility; Dose-dependent cell uptake; The nanoparticles accumulated mostly in the cytoplasm; Excellent capability of the nanocarriers as contrast agents in MRI.	[197]
Hollow mesoporous silica (HMS) nanocages composed by a hollow cubic core and a mesoporous shell The particles were PEGylated.	Doxorubicin and rhodamine B isothiocyanate	Cubic cores allowed much higher storage capacity than spherical counterparts; Sustained release of the drug; Good cell uptake and efficient cell death *in vitro*; Higher suppress of tumor growth when compared to free doxorubicin *in vivo;* Fluorescent candidates for optical imaging.	[198]
Hollow mesoporous silica nanocages	Doxorubicin and molecules labeled with dyes	Good biocompatibility; Molecules labeled with dyes were used as traceable detectors by fluorescence imaging; Chemotherapeutic sustained release.	[199]
Hollow magnetic mesoporous double-shell nanostructures with a nanorod-shaped core	Docetaxel or camptothecin and rhodamine B isothiocyanate and PEG	Excellent blood compatibility, very low cytotoxicity towards HeLa and MCF-7 cells; Particles could be taken up by cancer cells effectively in a dose-dependent manner; Potential application as MRI contrast agents and chemotherapeutic agent.	[200]
Mesoporous silica nanocapsules	Temperature-sensitive and biocompatible perfluorohexane (bubble generator)	Inorganic enhancement agent for high intensity focused ultrasound (HIFU) imaging; Excellent biocompatibility/degradability and uptake by tumor cells; Perfluorohexane bubbles were released, in a sustained way, through the particles mesopore channels when the local temperature rise due to the HIFU application; The rise of temperature caused tumor tissue destruction: pronounced coagulative necrosis effect on bovine liver tissues at low power, when compared with mesoporous particles without perfluorohexane.	[201]
Multifunctional mesoporous nanocapsules decorated with manganese	Perfluorohexane	MRI guided due to the manganese oxide presence; Good tumor location; Enhanced therapeutic effect; The application of HIFU allowed the release of perfluorohexane and consequently the destruction of tumor cells.	[202]
Multifunctional rattle-structured: porous silica shell doped with gadolinium	Cisplatin anticancer drug and radiosensitizer and gadolinium	Synergetic chemo-/radiotherapy and magnetic/luminescent dual-mode imaging; Loaded particles were more efficient than free cisplatin *in vitro*.	[203]
Mesoporous silica-coated hollow manganese oxide (HMnO@ $mSiO_2$) nanoparticles	No drug Magnetic resonance imaging (MRI) contrast agent	Adipose-derived mesenchymal stem cells (MSCs) were efficiently labeled using electroporation; The mesoporous shell and the large surface area-to-volume ratio resulted in an enhanced water accessibility to the core and consequently in the improvement of the signal.	[204]

3.5.2. Compartmentalized Vesicles and Micelles

Vesicles composed by lipids (liposomes) or by amphiphilic block-copolymers (polymersomes) with compartmentalized architectures have been also proposed for biomedical applications. For example, liposomes containing inside a hyaluronic acid microgel (one microgel or multiple microgels per liposome) were proposed by An *et al.* [205] to mimic the corneocyte cell structures. Mature corneocytes are dead cells, covered by a protein or lipid shell in which the matrix of such natural capsules is filled by keratin fibrillae, having a special role in skin homeostasis. Such particles may be ideal vehicles to be employed in cosmetics, dermatology and in the pharmaceutical field.

Multicompartmentalized spherical liposomes were also proposed for a few biomedical applications, namely salmon calcitonin administration by a oral route for osteoporosis treatment [206] and cisplatin release inside tumoral cells for cancer therapy [207].

Multivesicular liposomes showed to be capable to sustain the release of morphine in Beagle dogs for more than 12 days, upon administration in the epidural space [208]. The release of ciprofloxacin from normal liposomes revealed a lower performance when compared with hierarchical liposomes composed by small liposomes encapsulated into bigger ones. After 30 min the total content of the normal liposomes was released, whereas just 50% of the hierarchical liposomes content was released after 6h [209].

Polymersomes have also been developed with complex architectures. Multicompartmentalized poly(dimethylsiloxane)-graft-poly(ethylene oxide) (PDMS-g-PEO) and poly(butadiene)-block-poly(ethylene oxide) (PBut-b-PEO) polymersomes were developed using multiple emulsion into a microfluidic device [210]. Besides being multicompartmentedb (small polymersomes inside a big polymersome), non-spherical polymersomes with regular polyhedral shapes were also produced by double emulsions (aggregation of polymersomes). In addition, polymersomes-in-polymersomes, composed by one or multiple bilayers of PEG-b-PLA diblock-copolymers, were developed also using emulsions in microfluidic devices [211]. Two architectures were developed: (i) polymersomes containing a single inner polymersome and (ii) polymersomes containing several inner polymersomes. The existence of multiple reservoirs was demonstrated to be suitable to encapsulate different bioactive agents and for releasing molecules in a programmed fashion due to the sequential dissociation of the membranes [211].

Nanosized poly(trimethylene carbonate)-b-poly(l-glutamic acid) polymersomes were encapsulated in larger ones PBut-b-PEO creating independent compartments in each particle [212]. The lumen of the nanosized vesicle is one compartment and the cavity of the giant polymersome is other compartment. Doxorrobicin was then encapsulated in the nanosized polymersomes during the vesicles formation leadind to a subsequent controlled and sustained release of the drug. In this case the diffusion of the molecules was

hampered by the existence of more than one membrane. Although just one drug was encapsulated, such system could be explored for multidrug release due to the existence of multiple individual compartments. Compartmentalized micelles were also obtained from the combination of water-soluble PEO with two hydrophobic, but immiscible components (a polymeric hydrocarbon and a perfluorinated polyether). Playing with the proportions between the polymers, the shape of such compartmentalized particles was also controlled [213]. A few examples of multicompartmentalized micelles derived from the conjugation of PEE, PEO and poly(γ-methyl-ε-caprolactone) are depicted in Figure 3.22.

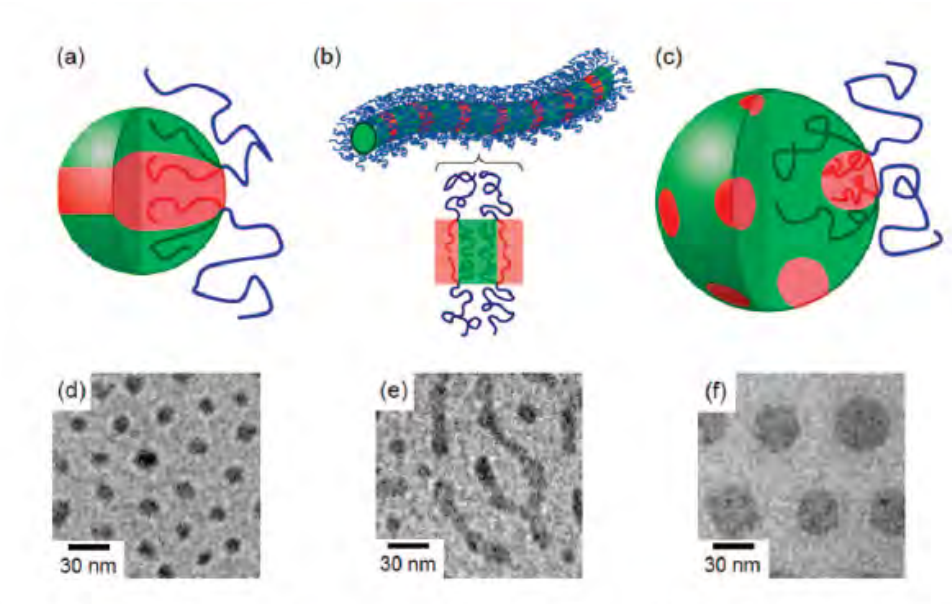

Figure 3.22. Self-assembled compartmentalized structures with stratified spherical (a); segmented worm-like (b) and raspberry-like spherical (c) architectures. The correspondent cryo-TEM images are labelled with d, e, and f, respectively. Image adapted from [213].

The ability of micelles to be loaded with two different molecules was proved by multicompartmented structures formed by self-assembly of mikto-arm star block copolymers. Such copolymers were composed by PEO which confers water dispersibility, PEE and polyperfluoropropylene oxide (PFPO) both segregate within the micelle cores. The obtained compartmentalized micelles were immersed in an aqueous solution where two poor water-soluble molecules were dispersed and used as model drugs. Then, pyrene was selectively uptake and entrapped in PEE domains whereas 1-naphthyl perfluoroheptanyl ketone was entangled in the PFPO chains [214].

3.5.3. Janus Particles

Very peculiar compartmentalized particulate systems are the Janus structures, characterized by possessing non-centrosymmetric architectures and the hemistructures may comprise different compositions and functionalities [215,216]. Such particles may have controlled size and shape as well as unique surface characteristics in which the compartmentalization transform such structures in multifunctional entities. Depending on the envisaged application, hard (inorganic), soft (polymeric) or hybrid soft/hard anisotropic functional and structural structures may be designed with morphologies comprising spherical-, dumbbell-, rod-, disk-, sheet-like, among other structures – Figure 3.23. Several methodologies can be used to produce those kind of structures [215]: self-assembly, emulsions/phase separation, microfluidics, biphasic electrified jetting, protonation-deprotonation cycling, among others [215–218].

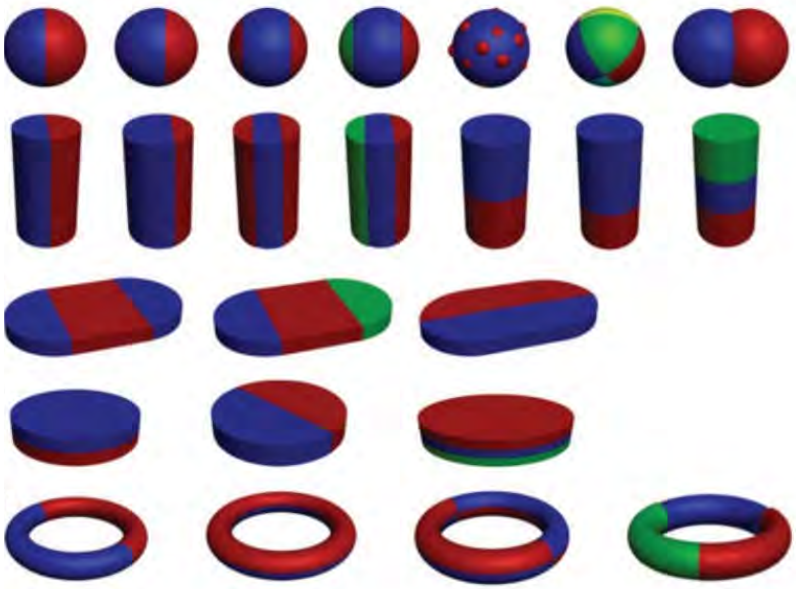

Figure 3.23. Schematic representation of possible Janus structures. Image from [219].

Soft Janus particles have gained particular attention for applications as drug vehicles due to the possibility to encapsulate independently more than one bioactive agent and release them in a controlled manner. A recurrent strategy to produce Janus polymeric particles is the phase separation method because it is considered a simple method and allows the production of many biphasic soft particles with a vast range of morphologies and sizes. The limitations of this procedure are related to the difficulty in the control of the size of the particles and in some cases (self-assembly of block copolymers) the yield is very low [215]. Microfluidic devices are alternative strategies to produce this kind of particles. The monomers solutions flow in Y-shaped channels to form the two-phase stream with a planar sheath-flow geometry. The final

structures may be obtained by crosslinking through light exposure, for example [215]. A wide range of Janus structures with different morphologies have been produced by electrodynamic cojetting methodology. Briefly, two immiscible polymers are dispensed using needles, controlling their diffusion rate [217]. Afterwards, the solidification is also controlled through the rate of evaporation of the solvent. This technique was improved and such kind of particulate systems were also produced using aqueous-based solutions. With electrohydrodynamic cojetting two very similar polymers solutions could be used [220]. However, this technique is confined to a certain types of materials: for example just conductive polymers may be employed.

Other techniques such as lithography, templating and surfaces-controlled nucleation have been used to produce such particular compartmentalized particles. However, these techniques present several limitations namely the requirement of complex apparatus, difficulties in preparation of nano-scaled particles, uncontrollable sizes and structures, and limitations in the type of materials used [215].

Hard Janus particles could be obtained by the follow mechanisms: direct heterogeneous nucleation, non-epitaxial deposition followed by coalescence/crystallization, reaction at liquid/liquid interfaces and self-regulated homogeneous or heterogeneous nucleation [221]. Such particles are composed by at least two different inorganic materials with magnetic, electric, semiconducting, optical, among others properties.

The combination of polymeric materials with inorganic entities forms the hybrid soft/hard particles. Such particles aimed to combine properties of the both groups. The most used techniques to obtain hybrid Janus are phase separation [222,223], controlled surface nucleation of polymeric particles onto inorganic structures [216,224] and self-organized precipitation [225,226].

Table 3.5 lists several examples of soft, hard and hybrid Janus particles being highlighted their shape and properties.

Table 3.5. Representative examples of soft, hybrid and hard Janus particles.

	Type of Janus particles	Materials	Preparation Method	Properties/Applications	Ref.
Soft Particles	Dumbbell	Polystyrene, poly(butylmethacrylate) and poly(methyl methacrylate)	Phase separation (seeded polymerization technique)	Particles with controlled shape and surface chemistry; Amphiphilic particles; No application	[227]
	Dumbbell	Amphoteric polystyrene	Phase separation (seeded polymerization technique)	Particles with chemical anisotropy; pH-sensitive anisotropy due to the different surface coatings; No application.	[228, 229]
	Spherical	Poly(9,9-bis(2-ethylhexyl)fluorine-2,7-diyl) Poly(para-phenylene)	Miniemulsion	Multicomponent spherical particles; No application.	[230]
	Snowman-like	Polystyrene and poly(methyl-methacrylate)	Phase separation (different homopolymers in the polymer blend)	The morphology could be tuned by changing the molecular weight of the polymers; Broad size distribution and the use of surfactant could limit certain biomedical applications. No specific application	[231]
	Multiple structures	Polystyrene, polyisoprene and their block-copolymers	Self organized precipitation	Depending on the copolymerization ratios, different structures were obtained; Different polymer ratio: one-dimensionally stacked lamellar structures, onion-like concentric-layered lamellar structures, and hexagonally arranged dots and aligned striations inside the particles; Polymer ratio 1:1: hemispherical shaped particles where the variation of the concentration caused different proportions between both hemispheres; No application.	[232]
	Spherical and cylindrical micelles	Polystyrene-*block*-polybutadiene-*block*-poly(methyl methacrylate) (SBM) triblock terpolymer having symmetric end blocks and a very small fraction of polybutadiene	Crosslinking the lamella-sphere Morphology of the SBM triblock terpolymer in the bulk state *via* cold vulcanization with sulphur monochloride (S_2Cl_2)	These Janus particles consist of a tightly crosslinked polybutadiene nanoparticle core with *ca.*13 chains each of PMMA and PS protruding out of it, in separated hemispheres; No application.	[233–235]
	Spherical	Polystyrene Poly(propylene carbonate) Poly(9,9-dioctyl- fluorene-2,7-diyl-co-bis-N,N-fluorene-2,7-diyl-co-bis-N,N- phenyl-1,4-phenylenediamine) (PFB) Poly(9,9- dioctylfluorene-2,7-diyl-co-benzothiadiazole) (F8BT)	Miniemulsion, phase separation	No application	[236]
	Spherical micelles	Polybutadiene Poly(methacrylic acid) Polystyrene Triblock copolymer	Cross-linking the middle block of a microphase separated triblock copolymer followed by alkaline hydrolysis of the poly(methyl methacrylate) (PMMA) ester groups	Amphiphilic Janus micelles with a hydrophobic polystyrene hemicorona and a hydrophilic poly(methacrylic acid) hemicorona, both surrounding a cross-linked polybutadiene core; No application.	[237]
	Cylinders, sheets, and ribbons	Poly(tert-butoxystyrene)-b-poly(butadiene)-b-poly(tert-butyl methacrylate)	Self-assembly via film casting followed by crosslinking (photo or with sulfur monochloride)	The shape of the final system was defined by the selected solvent and crosslinking conditions; No application.	[238]

	Spherical micelles	Poly(2-vinylpyridine)-b-poly(methyl methacrylate)-b-Poly(acrylic acid) (P2VP-PMMA-PAA)	Phase separation (self –assembly of block copolymers in aqueous solvent)	No organic solvents were required; The middle block of the polymer was hydrophobic and the other blocks were amphoteric and hydrophilic; Two-compartment shells (Janus micelles with segregated arms) were obtained at pH 1-2; No application.	[239]
	Janus micelle with a prolate ellipsoidal (cigar-like) overall shape and an oblate ellipsoidal (disc-like) core	poly(N-methyl-2-vinyl pyridinium iodide) (P2MVP) and Poly(acrylic acid) (PAA), poly(ethylene oxide) (PEO) or Poly(acryl amide) PAAm.	Phase-separation (co-assembly of two fully water-soluble block copolymers, which one composed by polyelectrolyte block and a neutral block)	One-step procedure was used; Janus particles formed spontaneously in a reversible process, controlling the polymer mixing fraction, solution pH, and ionic strength; The polymers aimed to constitute the core (PAA and P2MVP) were intrinsically mixed while the corona segments (PEO and PAAm) repelled each other as much as possible. No application.	[240]
	Disk-like micelles	Poly(2-methylvinylpyridinium iodide)-b-poly(ethylene oxide) Poly(acrylic acid)-b-poly(acryl amide)	Phase-separation (co-assembly of two fully water-soluble block copolymers)	No application.	[241]
	Spherical micelles	P2VP-b-PEO and P2VP-b-PNIPAAm	Phase separation (self –assembly of block copolymers followed by crosslinking of the core)	pH-responsive core composed of P4VP and a mixed shell composed of thermosensitive PNIPAM and hydrophilic PEG; Temperatures above LCST of PNIPPAm caused a phase separation of the mixed PNIPAM/PEG shell resulted in core–shell–corona micelles; In acidic conditions the core is unstable, and the high level of swelling of P4VP caused micelles disintegration; No application.	[242]
	Patchy spherical micelles	Poly(ethylene oxide)-b-poly(3-caprolactone)-b-poly(2-aminoethyl methacrylate) (PEO-b-PCL-b-PAMA)	Phase separation (self –assembly of block copolymers in aqueous solvents)	The core of the micelles was formed by PCL. The PEO and PAMA chains formed the phase-segregated patchy; The formation of the Janus structure was achieved by adding tetramethyl orthosilicate: the deposition of the silica was catalized by the cationic polymer present in the system (PAMA block); No application.	[243]
	Spherical	Isobornyl acrylate	Microfluidic (co-flow device)	Magnetic anisotropic particles were obtained by dispensing magnetite (Fe_3O_4) crystals in one hemisphere; No application.	[244]
	Two and three-phase spherical particles	Methacryloxypropyl dimethylsiloxane and a mixture of PEG diacrylate, pentaerythritol triacrylate and acrylic acid	Microfluidic (co-flow device)	Amphiphilic particles with selective functionalization; Epoxy groups were integrated in the hydrophilic compartment of the particle, turning this part of the system preferred for protein attachment; No specific application.	[245]
	Rectangles	PEG diacrylate (PEGDA)	Photolithographic –based microfluidic	PEGDA particles with different chemistries in the same particle; No application.	[246]
	Unimolecular particles	Polystyrene-b-poly(2-vinylpyridine)-b-poly(ethylene oxide) (PS-b-P2VP-b-PEO or SVEO) triblock copolymer	Chemical crosslinking induced micellization	Intramolecular crosslinking of the middle P2VP block using 1,4- dibromobutane (DBB); Increasing the solution concentration allowed the self-assembly of the unimolecular polymeric Janus nanoparticles into supermicelles; No application.	[247]

Hybrid Soft/hard particles	Spherical	Poly(MMA co -HEMA)/CdS QD–polymer hybrids and nanoparticles with poly(MMA- co -HEMA)/Cd(AA)$_2$ ionomers mixed with modified ferroferric oxide (Fe_3O_4)	Microfluidic (co-flow device)	Magnetic and fluorescent particles; No application.	[248]
	Spherical	Poly(acrylamide-co-acrylic acid) and Au nanoparticles	Electrohydrodinamic cojetting followed by thermal crosslinking	Bicompartmented system with a hierarchical structured hemisphere composed by the Au nanoparticles; No application.	[220]
	Dumbbell or snowman	Polystyrene/SiO_2	Seeded emulsion polymerization process: the styrene monomer was polymerized onto the silica surfaces in the presence of hydrophilic macromonomers.	The silica was able to be functionalized with methacrylate groups but other groups may be added; No application.	[224]
	Dumbbell	Polystyrene/SiO_2 Texto	Miniemulsion polymerization of nanodroplets of styrene, inorganic tetraethoxysilane, and silane coupling agent (3-aminopropyl)trimethoxysilane; The high temperature caused the elastic stress driven by the entropy change in the swollen networks resulting in a phase separation.	Magnetite nanoparticles were encapsulated in the polystyrene hemisphere – magnetic responsive particles; No application.	[222]
	Spherical	Negatively charged poly(acrylic acid) (PAA)-coated Fe_3O_4 nanoparticles partially functionalized by polystyrene sodium sulfonate (PSSNa) or polydimethylamino ethylmethacrylate (PDMAEMA)	Masking technique was used to prepare stable dispersions of Janus nanoparticles in water.	The particles were capable to form small clusters with controlled size by lowering the pH; pH below the pKa of PAA rendering that the part of the particle coated with PAA was hydrophobic while the part functionalized with PSSNa or PDMAEMA remained hydrophilic; When the two polymers bear opposite charges aggregation occurs, being this process reversible. No application.	[249]
	Spherical	Polystyrene/γ-Fe_2O_3 and polyisoprene	Self-organized precipitation.	The magnetic nanoparticles were firstly encapsulated in amphiphilic block-copolymer inverse micelles; Magnetic particles were composed by a polyisoprene and a polysyrene hemisphere being the magnetic micelles accumulated in the second compartment. No application.	[250]
Hard particles	Dumbbell	Au and Fe_3O_4	Epitaxial growth of Fe_3O_4 particles on the surface of Au particles by decomposition of iron pentacarbonyl, $Fe(CO)_5$.	The particles exhibited surface plasmon absorption (Au) and magnetic properties (Fe_3O_4); Particles suitable for tracking drug delivery, however the application was not studied in detail.	[251]
	Dumbbell	Fe_3O_4- Ag FePt - Ag Au - Ag	Fe_3O_4 or Au or FePt nanoparticles were dissolved in a proper organic solvent and mixed with an aqueous solution of silver nitrate and then the emulsion was stabilized by ultrasounds.	The nanoparticles self-assemble in the liquid-liquid interface of the emulsion and just part of the nanoparticles was exposed to to contact with Ag; For this reason, the particles formed are anisotropic with dumbblell architecture; The size of the Ag compartment could be controlled by the reaction time; Each compartment could be specifically functionalized via ligand exchange; Magnetic responsive particles with hydrophilic and fluorescent properties were obtained; No specific application.	[252]
	Spherical	γ-Fe_2O_3/SiO_2	Flame synthesis technique where both precursors suffered combusting; The high temperatures melt the SiO_2 and the γ-Fe_2O_3, and consequently occurred a phase separation process.	Amphiphilic particles were obtained by functionalization of SiO_2 hemisphere with oleylamine, being capable to form magnetic capsules; Application: partially sacrificial templates for hollow magnetic capsules. γ-Fe_2O_3/SiO_2 were coated with PVP and Au nanoparticles and then the SiO_2 removed. The magnetic core remained inside the PVP/AU capsules. No application for biomedical field.	[253]

In the last years several types of Janus particles have been produced but the study of their specific application in the biomedical field is quite scarce. Examples of systems used for sensing, diagnosis, therapeutics, theranosis and tissue engineering applications that were reported in literature will be described in this subsection [254]. The tunable and controllable architecture of the Janus particles provide spatially controlled functionalities in a wide range of sizes, which could be useful for biomedical applications. For example, disk-shaped Janus particles composed by a fluorescent graphically encoded region and a probe-loaded region were used to detect DNA oligomers [255]. The particles were designed to detect DNA sequences specifically. The systems could also be used in high throughput analyses.

The same concept was used to multiplex detection of proteins. PEG-based microparticles were obtained having a distinctive graphical code (unpolymerized holes in the wafer structure of the microparticles). This code is used to identify the antibody probe covalently incorporated in an individual compartment of the particle. The particles may be suspended in the sample of the medium that is desired to test providing an enhanced binding capacity when compared with 2D surface techniques (*e.g.* ELISA). Those particles may be used in a microfluidic system, where combining different particles, different proteins may be quantified in a single assay [256]. Magnetic particles integrating a color-barcode were also designed for multiplex detection of DNA. Due to the magnetic properties, the particles could be actively positioned for code readouts and be stirred for improvement of the reaction kinetic in microscale environments [257].

In gene delivery, the enhancement of both drug bioavailability and targeting are very important characteristics in carriers design. The most usual approach to obtain a targeted drug delivery system is the use of conjugated ligands on the surface of the particles. In some cases it could be advantageous to decoupling the target function from the therapeutic functions in the same particle. In this context, biosegmented metallic nanorods were used to deliver exogenous genes, in which one compartment of the particle was used to immobilize the targeting molecule and the other acted as the reservoir for the nucleic acid [258]. This strategy allowed to control the ligand density and the type of ligand could be changed according to the target. This system owns toxicity issues inherent to the use of metals. We believe that, whenever possible, biocompatible polymers should be used as they offer a large spectrum of chemistry possibilities and high control of the degradation kinetics and water uptake.

PLGA Janus solid matrices were also proposed as multicompartmented structures for delivery of multiple payloads [259]. A hydrophilic (doxorubicin hydrochloride) and a hydrophobic (paclitaxel) drug were encapsulated in the individual compartments of the Janus nanoparticles, showing the versatility of such structures in encapsulating drugs with different properties. Two different drugs (benzyl alcohol (BA) and 3-phenylpropionic acid (PPA)) linked onto different parts of the Janus PEG-based dendrimers showed a

sequential release profile. The BA showed a faster release and PPA a slower release kinetics [260]. The obtained Janus dendrimers were not cytotoxic against red blood cells and human umbilical vein endothelial cells, demonstrating potential to be used as drug delivery systems for combinatorial therapies. Multicompartmentalized Janus structured liposomes composed by two different types of vesicles connected through a tight bilayer interface (like two vesicles connected), were proposed for the combinatory release of chemotherapeutics [261]. However the optimization of the methodology to obtain nanosized systems and the study of the kinetic releases and biodistribution upon administration are still required.

Theranostic approaches constitute another biomedical application for Janus particles. The combination of therapeutic agents and imaging modalities into a single particulate system could maximize the final effect. Janus spherical systems composed by two hemispheres, in which one was polystyrene able to be functionalized with ligands for targeting and the other hemisphere was coated with a gold film are one example [262]. The gold could be used for sensing or imaging via surface-enhanced Raman scattering being possible to follow the interaction of the particles with the target cells.

The advances in the techniques to produce those compartmentalized particles lead to use of a microfluidic platform to produce hydrogels with magnetic anisotropy where cells and magnetic nano or submicron beads were encapsulated in individual compartments of alginate, with the aim to reduce the contact between the two moieties. The particles presented good cytocompatibility and super-paramagnetic properties [263]. The combination of polymeric biomaterials and magnetic nanoparticles may be useful in Tissue Engineering strategies [264,265]. Recently, an interesting system for vascular tissue engineering was developed based on the concept of Janus architecture combined with magnetic response [266]. 3D cell aggregates (spheroids) were build up and combined with magnetic nanoparticles being the cells and the magnetic nanoparticles confined in independent compartments (Figure 3.24). The main advantage of this strategy was to avoid the uptake of the magnetic particles by the cells, thus decreasing adverse effects related with the internalization of nanoparticles. Using a Janus structure, the cell viability, activity and phenotype were not significantly affected. In addition, the possibility to control the spatial distribution of the magnetic spheroids in combination with their easy capacity to fuse with each others, allowed obtaining a vascular construct with 5 mm in diameter using magnetic force assembly. This work demonstrated the importance of the development of advanced engineered structures in order to achieve a structured tissue, without significant cell loss and modification.

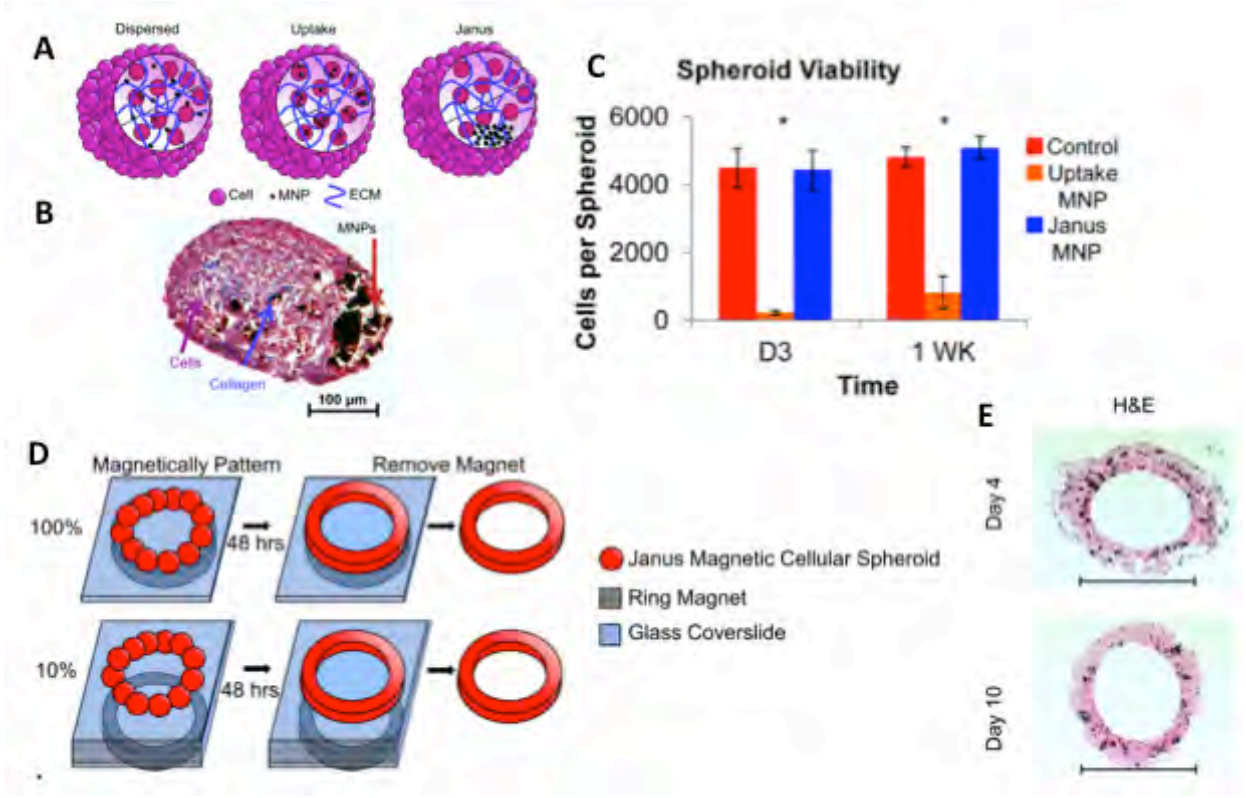

Figure 3.24. When magnetic nanoparticles are in embedded the ECM and mixed with the cells of a spheroid (A), the particles are internalized by the cells causing a significant decrease in the viability (C). Janus spheroids, where the particles are separated from the cells (A and B), seemed to be advantageous, not affecting the cell viability (C). Applying a magnetic force it was possible to control the position of the Janus spheroids (D). After a certain time, the spheroids found and formed continuous tissues (E). Image from [266].

Even more complex Janus structures could be obtained; such as Janus particles with more than two compartments. For example, highly organized complex particles were obtained using electrohydrodynamic co-jetting methodology in combination with synthetic polymer chemistry. Each obtained particle had three compartments (created by dispensing three polymeric solutions in parallel) displaying orthogonal anchoring groups on distinct surfaces of the compartments. Such PLGA disk-shaped compartmentalized particles had 10-15 µm in diameter and an average aspect ratio of 1:2 (height:diameter) and were chemically functionalized with different PLA derivatives. This showed that each compartment was susceptible to be specifically modified. Such multifunctional particles could be interesting systems for cancer therapies because beyond having compartments for compounds encapsulation, the entire surface could be modified using different ligands [267].

3.6. Conclusions and Future Perspectives

We overviewed the importance of several characteristics of the particulate systems for applications in therapies and diagnosis. Both chemical and physical properties influence the performance of the particles. The materials used to prepare the particulate systems define the bulk and surface chemistry. The chemical properties will play an important role the interaction of the particles with biological *milieu* and entrapped moieties. When administered in the human body, the first contact between the particles and the biological occurs at the surface of the particles being the charge, the hydrophilicity/hydrophobicity nature and targeting elements important properties to have into account in particles formulation and design. The surface characteristics dictate the initial biological reaction, this means if the particles are cleared or maintained in circulation as well as the internalization kinetics by the target cells. In the case of physical properties, an emerging attention has been focused on shape and compartmentalization. Non-spherical shapes could be useful to control the particle circulation time, extravasation and internalization by the different types of cells. Compartmented particles are quite complex systems but with several advantages, namely the possibility to encapsulate different bioactive agents, cells or even other particles, turning the therapy or diagnosis more efficient. Although it is known that mechanical properties have also influence in particles internalization and cell attachment, deep studies are required in order to understand in a detailed way the effect of such characteristic. It is predictable a continuous development of sophisticated architectures executing more and precise functions is order to fulfill all the demands of the complexity of human disorders.

3.7. References

[1] Peppas N. A., Historical perspective on advanced drug delivery : How engineering design and mathematical modeling helped the field mature, Advanced Drug Delivery Reviews 2013, 65: 5-9.

[2] De Koker S., De Cock L. J., Rivera-Gil P., Parak W. J., Auzély Velty R., Vervaet C., Remon J. P., Grooten J., De Geest B.G., Polymeric multilayer capsules delivering biotherapeutics, Advanced Drug Delivery Reviews 2011, 63: 748-761.

[3] Nguyen N., Ali S., Shaegh M., Kashaninejad N. and Phan D., Design, fabrication and characterization of drug delivery systems based on lab-on-a-chip technology, Advanced Drug Delivery Reviews. 2013, 65: 1403-1419.

[4] Alvarez-lorenzo C. and Concheiro A., Bioinspired drug delivery systems, Current Opinion in Biotechnology 2013, 24: 1167-1173.

[5] Irvine D. J., Swartz M. A. and Szeto G. L., Engineering synthetic vaccines using cues from natural immunity, Nature Materials 2013, 12: 978-990.

[6] Lee K., Silva E. A. and Mooney D. J., Growth factor delivery-based tissue engineering : general approaches and a review of recent developments, Journal of Royal Society Interface 2011, 8: 153-70.

[7] Velnar T., Bailey T. and Smrkolj V., The wound healing process : an overview of the cellular and molecular mechanisms, The Journal of International Medical Research 2009, 37: 1528-42.

[8] Santo V. E., Gomes M. E., Mano J. F. and Reis R. L., Controlled release strategies for bone, cartilage, and osteochondral engineering — part I: recapitulation of native tissue healing and variables for the design of delivery systems, Tissue Engineering Part B Reviews 2013, 19: 308-26.

[9] Santo V. E., Gomes M. E., Mano J. F. and Reis R. L., Controlled Release Strategies for Bone, Cartilage, and Osteochondral Engineering — Part II : Challenges on the Evolution from Single to Multiple Bioactive Factor Delivery, Tissue Engineering Part B Reviews 2013, 19: 327-52.

[10] Risau W., Mechanisms of angiogenesis, Nature 1997, 386: 671-4.

[11] Radtke S., Giebel B., Wagner W. and Horn P. A., Platelet lysates and their role in cell therapy, ISBT Science Series 2014, 9: 193-7.

[12] Sun Q., Chen R. R., Shen Y., Mooney D. J., Rajagopalan S. and Grossman P. M., Sustained vascular endothelial growth factor delivery enhances angiogenesis and perfusion in ischemic hind limb, Pharmaceutical Research 2005, 22: 1110-6.

[13] Formiga F. R., Pelacho B., Garbayo E., Abizanda G., Gavira J. J., Simon-Yarza T., Mazo M., Tamayo E., Jauquicoa C., Ortiz-de-Solorzano C., Prósper F. and Blanco-Prieto M. J., Sustained release of VEGF through PLGA microparticles improves vasculogenesis and tissue remodeling in an acute myocardial ischemia – reperfusion model, Journal of Controlled Release 2010, 147: 30-37.

[14] Bessa P. C., Casal M. and Reis R. L. Bone morphogenetic proteins in tissue engineering : the road from laboratory to clinic, part II (BMP delivery), Journal of Tissue Engineering and Regenerative Medicine 2008, 2: 81-96.

[15] Kyu J., Jang J., Jang W.H., Kim J., Bae I. H., Bae J., Park Y. H., Kim B. J., Lim K. M. and Park J. W., Biomaterials The effect of epidermal growth factor (EGF) conjugated with low-molecular- weight protamine (LMWP) on wound healing of the skin, Biomaterials 2012,33: 8579-90.

[16] Terenghi G., Peripheral nerve regeneration and neurotrophic factors, Journal of Anatomy 1999, 194: 1-14.

[17] Herfarth H. and Schölmerich J., IL-10 therapy in Crohn's disease: at the crossroads, Gut 2002, 50: 146-7.

[18] Marlow G. J., Van Gent D. and Ferguson L. R., Why interleukin-10 supplementation does not work in Crohn's disease patients, World Journal of Gastroenterology 2013, 19: 3931-41.

[19] Asadullah K., Sterry W. and Volk H. D., Interleukin-10 therapy — review of a new approach, Pharmacological Reviews 2003, 55: 241-69.

[20] Balmert S. C. and Little S. R., Biomimetic Delivery with micro- and nanoparticles, Advanced Materials 2012, 23: 3757-78.

[21] Caldorera-moore M. E., Liechty W. B. and Peppas N. A., Responsive theranostic systems: integration of diagnostic imaging agents and responsive controlled release drug delivery carriers, Accounts of Chemical Research 2011, 44: 1061-70.

[22] Mooney D. J. and Vandenburgh H., Review cell delivery mechanisms for tissue repair, Cell Stem Cell 2008, 2: 205-13.

[23] Hofmann M., Wollert K. C., Meyer G. P., Menke A., Arseniev L., Hertenstein B., Ganser A., Knapp W. H. and Drexler H., Monitoring of bone marrow cell homing into the infarcted human myocardium, Circulation 2005, 111: 2198-202.

[24] Toma C., Pittenger M. F., Cahill K. S., Byrne B. J., Kessler P. D., Human mesenchymal stem cells differentiate to a cardiomyocyte phenotype in the adult murine heart, Circulation 2002, 105: 93-8

[25] Fisher R. A. and Strom S. C., Human hepatocyte transplantation: worldwide results, Transplantation 2006, 82: 441-9.

[26] Malafaya P. B., Silva G. A. and Reis R. L., Natural-origin polymers as carriers and scaffolds for biomolecules and cell delivery in tissue engineering applications, Advanced Drug Delivery Reviews 2007, 59: 207-33.

[27] Sittinger M., Hutmacher D. W. and Risbud M. V., Current strategies for cell delivery in cartilage and bone regeneration, Current Opinion on Biotechnology 2004, 15: 411-8.

[28] Kim B. S., Baez C. E. and Atala A., Biomaterials for tissue engineering, World Journal of Urology 2000, 18: 2-9.

[29] Kulig K. M. and Vacanti J. P., Hepatic tissue engineering, Transplant Immunology 2004,12: 303-10.

[30] Simon Lunn J., Sakowski S. A. And Feldman E. L., Concise Review: Stem Cell Therapies for Amyotrophic Lateral Sclerosis: Recent Advances and Prospects for the Future, Stem Cells 2014, 32: 1099-109.

[31] Fan X., Sun D., Tang X., Cai Y., Yin Z. Q. and Xu H., Stem-cell challenges in the treatment of alzheimer's disease : a long way from bench to bedside, Medicinal Reseach Reviews 2014, 34: 957-78.

[32] Cook G., Williams C., Brown J. M., Cairns D. A., Cavenagh J., Snowden J. A., Ashcroft A. J., Fletcher M., Parrish C., Yong K., Cavet J., Hunter H., Bird J. M., Chalmers A., O'Connor S., Drayson M. T. and Morris T. C., High-dose chemotherapy plus autologous stem-cell transplantation as consolidation therapy in patients with relapsed multiple myeloma after previous autologous stem-cell transplantation (NCRI Myeloma X Relapse [Intensive trial]): a randomised, open-label, phase 3 trial, The Lancet Oncology. 2014,15: 874-85. -1.

[33] Lathuilière A., Bohrmann B., Kopetzki E., Schweitzer C., Jacobsen H., Moniatte M., Aebischer P., Schneider B. L., Genetic engineering of cell lines using lentiviral vectors to achieve antibody secretion following encapsulated implantation, Biomaterials 2014, 35: 792-802.

[34] Wang D., Zhang B., Gao H, Ding G., Wu Q., Zhang J., Li Liao L. and Chen H., Clinical research of genetically modified dendritic cells in combination with cytokine-induced killer cell treatment in advanced renal câncer, BMC cancer. 2014;14:251.

[35] Efrat S., Beta-cell replacement for insulin-dependent diabetes mellitus, Advanced Drug Delivery Reviews 2008,60: 114-23.

[36] Orive G., De Castro M., Ponce S., Hernández R. M., Gascón A. R., Bosch M., Alberch J., Pedraz J. L., Long-term expression of erythropoietin from myoblasts immobilized in biocompatible and neovascularized microcapsules, Molecular Therapy 2005, 12: 283-9.

[37] Liras A., Segovia C. and Gabán A. S., Advanced therapies for the treatment of hemophilia: future perspectives, Orphanet Journal of Rare Diseases 2012, 7: 97.

[38] Cirone P., Bourgeois J. M., Austin R. C., Chang P. L., A novel approach to tumor suppression with microencapsulated recombinant cells, Human Gene Therapy 2002, 13: 1157-1166.

[39] Zilberman Y., Turgeman G., Pelled G, Xu N., Moutsatsos I. K., Hortelano G. and Gazit D., Polymer-encapsulated engineered adult mesenchymal stem cells secrete exogenously regulated rhbmp-2, and induce osteogenic and angiogenic tissue formation, Polymers for Advanced Technologies 2003, 13: 863-70.

[40] Gasperini L., Mano J. F. and Reis R. L., Natural polymers for the microencapsulation of cells, Journal of Royal Society Interface 2014, 11: 20140817.

[41] Hernández R. M., Orive G., Murua A. and Pedraz J. L., Microcapsules and microcarriers for in situ cell delivery, Advanced Drug Delivery Reviews 2010, 62: 711-30.

[42] Lima A. C., Batista P., Valente T. A. M., Silva A. S., Correia I. J. and Mano J. F., Novel methodology based on biomimetic superhydrophobic substrates to immobilize cells and proteins in hydrogel spheres for applications in bone regeneration, Tissue Engineering Part A 2013, 19: 1175-87.

[43] Daum N., Tscheka C., Neumeyer A. and Schneider M., Novel approaches for drug delivery systems in nanomedicine: effects of particle design and shape. Wiley Interdisciplinary Reviews Nanomedicine and Nanobiotechnology 2012, 4: 52-65.

[44] Simões S. M., Figueiras A. R., Veiga F., Concheiro A. and Alvarez-Lorenzo C., Polymeric micelles for oral drug administration enabling locoregional and systemic treatments, Expert Opinion on Drug Delivery 2014, 17: 1-22.

[45] Matricardi P., Di C., Coviello T., Hennink W. E. and Alhaique F., Interpenetrating Polymer Networks polysaccharide hydrogels for drug delivery and tissue engineering, Advanced Drug Delivery Reviews 2013, 65: 1172-1187.

[46] Zhang Y., Chan H. F. and Leong K. W., Advanced materials and processing for drug delivery: the past and the future, Advanced drug delivery reviews 2013, 65: 104-20.

[47] Barbé B. C., Bartlett J., Kong L-, Finnie K., Lin H. Q., Larkin M., Calleja S., Bush A. and Calleja J., Silica particles : a novel drug-delivery system, Advanced Materials 2004, 16: 1959-1966.

[48] Storm G., Belliot S., Daemen T. and Lasic D. D., Surface modification of nanoparticles to oppose uptake by the mononuclear phagocyte system, Advanced Drug Delivery Reviews 1995, 17: 31-48.

[49] Rodriguez P. L., Harada T., Christian D. A., Pantano D. A., Tsai R. K. And Discher D. E., Minimal "self" peptides that inhibit phagocytic clearance and enhance delivery of nanoparticles, Science 2013, 339: 971-5.

[50] Custódio C. A., Santo V. E., Oliveira M. B., Gomes M. E., Reis R. L. and Mano J. F., Functionalized microparticles producing scaffolds in combination with cells, Advanced Functional Materials 2014, 24: 1391- 400.

[51] Owens III D. E. and Peppas N. A., Opsonization, biodistribution, and pharmacokinetics of polymeric nanoparticles, International Journal of Pharmaceutics 2006, 307: 93-102.

[52] Yoo J., Doshi N. and Mitragotri S., Adaptive micro and nanoparticles : Temporal control over carrier properties to facilitate drug delivery, Advanced Drug Delivery Reviews 2011, 63:1247-1256.

[53] Longmire M. R., Ogawa M., Choyke P. L. and Kobayashi H., Biologically optimized nanosized molecules and particles : more than just size, Bioconjugate Chemistry 2011, 22: 993-1000.

[54] Lisa L., Peppas N. A., Yin F., Boey C. and Venkatraman S. S., Modeling of drug release from bulk-degrading polymers, International Journal of Pharmaceutics 2011, 418: 28-41.

[55] Yang C., Ebrahim A. B., Tan J. P. K., Ke X., Gao S., Hedrick J. L. and Yang Y. Y., The role of non-covalent interactions in anticancer drug loading and kinetic stability of polymeric micelles, Biomaterials 2012, 33: 2971-9.

[56] Chan A., Orme R. P., Fricker R. A. and Roach P., Remote and local control of stimuli responsive materials for therapeutic applications, Advanced drug delivery reviews 2013, 65: 497-514.

[57] Bajaj P., Schweller R. M., Khademhosseini A., West J. L. and Bashir R., 3D Biofabrication strategies for tissue engineering and regenerative medicine, Annual Reviews of Biomedical Engineering 2014, 16: 247-76.

[58] Oliveira M. B. and Mano J. F., Polymer-based microparticles in tissue engineering and regenerative medicine, Biotechnology Progress 2011, 27: 897-912.

[59] Doshi N., Zahr A. S., Bhaskar S., Lahann J., Mitragotri S., Red blood cell-mimicking synthetic biomaterial particles, Proceedings of the National Academy of Sciences of the United States of America 2009, 106: 21495-9.

[60] Gaumet M., Vargas A., Gurny R. and Delie F., Nanoparticles for drug delivery : The need for precision in reporting particle size parameters, European Journal of Pharmaceutics and Biopharmaceutics 2008, 69: 1-9.

[61] Lima A. C., Sher P. and Mano J. F., Production methodologies of polymeric and hydrogel particles for drug delivery applications, Expert Opinion on Drug Delivery 2012, 9: 231-48.

[62] Han Y. and Park K., Targeted drug delivery to tumors: Myths, reality and possibility, Journal of Controlled Release 2011, 153: 198-205.

[63] Jain R. K. and Stylianopoulos T., Delivering nanomedicine to solid tumors, Nature Reviews Clinical Oncology 2010, 7: 653-664.

[64] Longmire M., Choyke P. L. and Kobayashi H., Clearance properties of nano-sized particles and molecules as imaging agents: considerations and caveats, Nanomedicine (Lond.) 2008, 3: 703-17.

[65] Muro S., Garnacho C., Champion J. A., Leferovich J., Gajewski C., Schuchman E. H., Mitragotri S. and Muzykantov V. R., Control of Endothelial Targeting and Intracellular Delivery of Therapeutic Enzymes by Modulating the Size and Shape of ICAM-1-targeted Carriers, Molecular Therapy 2008,16: 1450-8.

[66] Rejman J., Oberle V., Zuhorn I. S. and Hoekstra D., Size-dependent internalization of particles via the pathways of clathrin- and caveolae-mediated endocytosis, Biochemical Journal 2004,169: 159169.

[67] Pilcer G., and Amighi K., Formulation strategy and use of excipients in pulmonary drug delivery, International Journal of Pharmaceutics 2010, 392: 1-19.

[68] Edwards D. A., Hanes J., Caponetti G., Hrkach J., Ben-Jebria A., Eskew M. L., Mintzes J., Deaver D., Lotan N. and Langer R., Large porous particles for pulmonary drug delivery, Science 1997, 276: 1868-71.

[69] Beningo K. A., Wang Y., Fc-receptor-mediated phagocytosis is regulated by mechanical properties of the target, Journal of Cell Science 2002, 115: 849-56.

[70] Banquy X., Suarez F., Argaw A, Rabanel J, Grutter P, Couchar J. F., Hildgen P. and Giasson S., Effect of mechanical properties of hydrogel nanoparticles on macrophage cell uptake, Soft Matter 2009, 5: 3984-91.

[71] Engler A. J., Sen S., Sweeney H. L. and Discher D. E., Matrix elasticity directs stem cell lineage specification, Cell 2006, 126: 677-89.

[72] Watt F. M. and Huck W. T. S., Role of the extracellular matrix in regulating stem cell fate, Nature Reviews Molecular Cell Biology 2013, 14: 467-73

[73] Rehfeldt F., Engler A. J., Eckhardt A., Ahmed F. and Discher D. E. Cell responses to the mechanochemical microenvironment — Implications for regenerative medicine and drug delivery, Advanced Drug Delivery Reviews 2007, 59: 1329-39.

[74] Liu W., Zhou X., Mao Z., Yu D., Wang B. and Gao C., Uptake of hydrogel particles with different stiffness and its influence on HepG2 cell functions, Soft Matter 2012, 8: 9235-45.

[75] Young K. D., The selective value of bacterial shape, Microbiology and Molecular Biology Reviews 2006, 70: 660-703.

[76] Champion J. A., Katare Y. K. and Mitragotri S., Particle shape: a new design parameter for micro- and nanoscale drug delivery carriers, Journal of Controlled Release 2007,121: 3-9.

[77] Venkataraman S., Hedrick J. L., Ong Z. Y., Yang C., Rachel P. L., Hammond P. T. and Yang Y. Y., The effects of polymeric nanostructure shape on drug delivery, Advanced Drug Delivery Reviews 2011, 63: 1228-46.

[78] Wang J. –T., Wang J. and Han J. -J., Fabrication of advanced particles and particle-based materials assisted by droplet-based microfluidics, Small 2011, 7: 1728-54.

[79] Champion J. A., Katare Y. K., Mitragotri S. Making polymeric micro- and nanoparticles of complex shapes, Proceedings of the National Academy of Sciences of the United States of America 2007,104: 11901-4.

[80] Geng Y. A. N., Dalhaimer P., Cai S., Tsai R., Tewari M., Minko T. and Discher D. E., Shape effects of filaments versus spherical particles in flow and drug delivery, Nature Nanotechnology 2007, 2: 249-55.

[81] Li S., Nickels J. and Palmer A. F., Liposome-encapsulated actin–hemoglobin (LEAcHb) artificial blood substitutes, Biomaterials 2005, 26: 3759-69.

[82] Decuzzi P., Godin B., Tanaka T., Lee S. Y., Chiappini C., Liu X., Ferrari M., Size and shape effects in the biodistribution of intravascularly injected particles, Journal of Controlled Release 2010,141: 320-7.

[83] Mitragotri S., In drug delivery, shape does matter, Pharmaceutical Research 2009, 26: 232-4.

[84] Champion J. A. and Mitragotri S., Role of target geometry in phagocytosis, Proceedings of the National Academy of Sciences of the United States of America 2006, 103: 4930-4.

[85] Sharma G., Valenta D. T., Altman Y., Harvey S., Xie H., Mitragotri S. and Smith J.W., Polymer particle shape independently influences binding and internalization by macrophages, Journal of Controlled Release 2010, 147: 408-412.

[86] Gratton S. E. A., Ropp P. A., Pohlhaus P. D., Luft J. C., Madden V. J., Napier M. E. and DeSimone J. M., The effect of particle design on cellular internalization pathways, Proceedings of the National Academy of Sciences of the United States of America 2008, 105: 11613-8.

[87] Huang X., Teng X., Chen D., Tang F. and He J., The effect of the shape of mesoporous silica nanoparticles on cellular uptake and cell function, Biomaterials 2010, 31: 438-48.

[88] Manning C. B., Vallyathan V. and Mossman B. T., Diseases caused by asbestos: mechanisms of injury and disease development, International Immunopharmacology 2002, 2: 191-200.

[89] Nagai H. and Toyokuni S., Differences and similarities between carbon nanotubes and asbestos fibers during mesothelial carcinogenesis: shedding light on fiber entry mechanism, Cancer Science 2012, 103: 1378-90.

[90] Yoo J., Doshi N. and Mitragotri S., Endocytosis and intracellular distribution of plga particles in endothelial cells : effect of particle geometry, Macromolecular Rapid Communications 2010, 31: 142-8.

[91] Oh W., Kim S., Yoon H. and Jang J., Shape-dependent cytotoxicity and proinflammatory response of poly(3,4-ethylenedioxythiophene) nanomaterials, Small 2010, 6: 872-9.

[92] Doshi N. and Mitragotri S., Needle-shaped polymeric particles induce transient disruption of cell membranes, Journal of the Royal Society Interface 2010, 7: S403-10.

[93] Hosta-Rigau L., Shimoni O., Städler B. and Caruso F., Advanced subcompartmentalized microreactors : polymer hydrogel carriers encapsulating polymer capsules and liposomes, Small 2013, 9: 3573-83.

[94] Higuchi T., Tajima A. and Shimomura M. Spontaneous formation of polymer nanoparticles with inner micro-phase separation structures, Soft Matter 2008, 4:1302-5.

[95] Heslinga M. J., Willis G. M., Sobczynski D. J., Thompson A. J. and Eniola-Adefeso O., One-step fabrication of agent-loaded biodegradable microspheroids for drug delivery and imaging applications, Colloids and Surfaces B: Biointerfaces 2014, 116: 55-62.

[96] Turtle C. J. and Riddell S. R., Artificial antigen-presenting cells for use in adoptive immunotherapy, Cancer Journal 2011, 16: 374-81.

[97] Sunshine J. C., Perica K., Schneck J. P., Green J. J., Particle shape dependence of CD8+ T cell activation by artificial antigen presenting cells, Biomaterials 2014, 35: 269-77.

[98] Hu C. -M. J., Fang R. H. and Zhang L., Erythrocyte-inspired delivery systems, Advanced Healthcare Materials 2012, 1: 537-47.

[99] Godfrin Y., Horand F., Franco R., Dufour E., Kosenko E., Bax B. E., Banz A., Skorokhod O. A., Lanao J. M., Vitvitsky V., Sinauridze E., Bourgeaux V. and Gunter K.C., International seminar on the red blood cells as vehicles for drugs, Expert Opinion on Biological Therapy 2012, 12: 127-33.

[100] Magnani M., Erythrocytes as carriers for drugs: the transition from the laboratory to the clinic is approaching, Expert Opinion on Biological Therapy 2012, 12: 137-8.

[101] Hemmingsen B.B., Steinberg N. A. and Hemmingsent E. A. Intracellular gas supersaturation tolerances of erythrocytes and resealed ghosts, Biophysical Journal, 1985, 47: 491-496.

[102] Nicolau C. and Gersonde K. Incorporation of inositol hexaphosphate into intact red blood cells, Naturwissenschaften 1979, 566: 563-6.

[103] Haghgooie R., Toner M. and Doyle P. S., Squishy non-spherical hydrogel microparticles, Macromolecular Rapid Communications 2010, 31: 128-34.

[104] Merkel T. J., Jones S. W., Herlihy K. P., Kersey F. R., Shields A. R., Napier M., Luft J. C., Wug H., Zaboni W. C., Wang A. Z., Bear J. E. and DeSimone J. M., Using mechanobiological mimicry of red blood cells to extend circulation times of hydrogel microparticles, Proceedings of the National Academy of Sciences of the United States of America 2011, 108: 586-91.

[105] Song W., Lima A. C. and Mano J. F., Bioinspired methodology to fabricate hydrogel spheres for multi-applications using superhydrophobic substrates, Soft Matter 2010, 6: 5868.

[106] Lima A. C., Song W., Blanco-Fernandez B., Alvarez-Lorenzo C. and Mano J. F., Synthesis of temperature-responsive dextran-MA/PNIPAAm particles for controlled drug delivery using superhydrophobic surfaces, Pharmaceutical Research 2011, 28: 1294-305.

[107] Lima A. C., Correia C. R., Oliveira M. B. and Mano J. F., Sequential ionic and thermogelation of chitosan spherical hydrogels prepared using superhydrophobic surfaces to immobilize cells and drugs, Journal of Bioactive and Compatible Polymers 2013, 29: 50-65.

[108] Lima A. C., Custódio C. A., Alvarez-Lorenzo C. and Mano J. F., Biomimetic methodology to produce polymeric multilayered particles for biotechnological and biomedical applications, Small 2013, 9: 2487-92.

[109] Puga A. M., Lima A. C., Mano J. F., Concheiro A. and Alvarez-Lorenzo C., Pectin-coated chitosan microgels crosslinked on superhydrophobic surfaces for 5-fluorouracil encapsulation, Carbohydrate Polymers 2013, 98: 331-40.

[110] Lima A. C., Puga A. M., Mano J. F., Concheiro A. and Alvarez-lorenzo C. Free and copolymerized γ-cyclodextrins regulate the performance of dexamethasone-loaded dextran microspheres for bone regeneration, Journal of Materials Chemistry B 2014, 2: 4943-56.

[111] Lima A. C., Mano J. F., Concheiro A. and Alvarez-lorenzo C., Fast and mild strategy, using superhydrophobic surfaces, to produce collagen/platelet lysate gel beads for skin regeneration, Stem Cells Reviews and Reports 2014. doi:10.1007/s12015-014-9548-6 (In Press).

[112] Ho C., Chung N. and Lee J., Monodisperse red blood cell-like particles via consolidation of charged droplets, Journal of Colloid and Interface Science 2011, 361: 423-8.

[113] Christian D. A., Cai S., Garbuzenko O. B., Harada T., Zajac A. L., Minko T. and Disher D. E., Flexible filaments for in vivo imaging and delivery : persistent circulation of filomicelles opens the dosage window for sustained tumor shrinkage, Molecular Pharmaceutics 2009, 6: 1343-52.

[114] Kim Y., Dalhaimer P., Christian D. A. and Discher D.E., Polymeric worm micelles as nano-carriers for drug delivery, Nanotechnology 2005, 16: 484-91.

[115] Geng Y. and Discher D.E., Visualization of degradable worm micelle breakdown in relation to drug release, Polymer 2006, 47: 2519-25.

[116] Kim T. H., Mount C. W., Dulken B. W., Ramos J., Fu C. J., Khant H. A., Chiu W., Gombotz W. R. and Pun S. H., Filamentous, Mixed micelles of triblock copolymers enhance tumor localization of indocyanine green in a murine xenograft model, Molecular Pharmaceutics 2012, 9: 135-43.

[117] Mano J. F., Stimuli-responsive polymeric systems for biomedical applications, Advanced Engineering Materials 2008, 10: 515-27.

[118] Yoo J, -W. and Mitragotri S., Polymer particles that switch shape in response to a stimulus, Proceedings of the National Academy of Sciences of the United States of America 2010, 107: 11205-10.

[119] Correia C. O., Caridade S. G. and Mano J.F., Chitosan membranes exhibiting shape memory capability by the action of controlled hydration, Polymers 2014, 6: 1178-86.

[120] Correia C. O. and Mano J. F., Chitosan scaffolds with a shape memory effect induced by hydration, Journal of Materials Chemistry B 2014, 2: 3315-23.

[121] Gong T., Zhao K., Wang W., Chen H., Wang L. and Zhou S., Thermally activated reversible shape switch of polymer particles, Journal of Materials Chemistry B 2014, 2: 6855-66.

[122] Chien M. P., Rush A. M.,Thompson M. P. and Gianneschi N. C., Programmable shape-shifting micelles, Angewandte Chemie International Edition 2010, 49: 5076-80.

[123] Hwang D. K., Oakey J., Toner M., Arthur J. A., Anseth K. S., Lee S., Zeiger A., Van Vliet K. J., Doyle P. S., Stop-flow lithography for the production of shape-evolving degradable microgel particles, Journal of the American Chemical Society 2009, 131: 4499-504.

[124] Link S, Burda C, Nikoobakht B., El-Sayed M. A., Laser-induced shape changes of colloidal gold nanorods using femtosecond and nanosecond laser pulses, The Journal of Physical Chemistry B 2000, 104: 6152-63.

[125] Lee G. P., Minett A. I., Innis P. C. and Wallace G. G., A new twist : controlled shape-shifting of silver nanoparticles from prisms to discs, Journal of Materials Chemistry 2009, 19: 8294-8.

[126] Fernandes R. and Gracias D. H., Self-folding polymeric containers for encapsulation and delivery of drugs, Advanced Drug Delivery Reviews 2012, 64: 1579-89.

[127] Leong T. G., Zarafshar A. M. and Gracias D. H., Three-dimensional fabrication at small size scales, Small 2010, 6: 792-806.

[128] Kalinin Y. V., Randhawa J. S. and Gracias D. H., Three-dimensional chemical patterns for cellular self-organization, Angewandte Chemie International Edition 2011, 50: 2549-53.

[129] Randall C. L., Gultepe E. and Gracias D.H., Self-folding devices and materials for biomedical applications, Trends in Biotechnology 2012, 30: 138-46.

[130] He H., Guan J. and Lee J. L., An oral delivery device based on self-folding hydrogels, Journal of Controlled Release 2006, 110: 339-46.

[131] Randall C. L., Kalinin Y. V., Jamal M., Manohar T. and Gracias D. H., Three-dimensional microwell arrays for cell culture, Lab on a Chip 2011, 11: 127-31.

[132] Azam A., Laflin K. E., Jamal M., Fernandes R. and Gracias D. H., Self-folding micropatterned polymeric containers, Biomedical Microdevices 2011, 13: 51-58.

[133] Sun T. M., Du J. Z., Yao Y. D., Mao C. Q., Dou S., Huang S. Y., Zhang P. Z., Leong K. W., Song E. W. and Wang J., Simultaneous delivery of siRNA and paclitaxel via a "two-in-one" micelleplex promotes synergistic tumor suppression, ACS Nano 2011, 5: 1483-94.

[134] Lima A. C., Custódio C. A., Alvarez-Lorenzo C. and Mano J. F. Biomimetic methodology to produce polymeric multilayered particles for biotechnological and biomedical applications, Small 2013, 9: 2487-92.

[135] Ladet S., David L., Domard A.. Multi-membrane hydrogels, Nature 2008, 452: 76-9.

[136] Dai H., Li X., Long Y, Wu J., Liang S., Zhang X., Zhao N. and Xu J., Multi-membrane hydrogel fabricated by facile dynamic self-assembly, Soft Matter 2009, 5: 1987-9.

[137] Park C. H. and Lee J., One-step immobilization of protein-encapsulated core/shell particles onto nanofibers, Macromolecular Materials and Engineering. 2010, 295: 544-50.

[138] Kim J. and Lee T. R., Thermo- and ph-responsive hydrogel-coated gold nanoparticles, Chemical Materials 2004, 16: 3647-51.

[139] Budhlall B. M., Marquez M. and Velev O. D., Microwave, photo- and thermally responsive pnipam-gold nanoparticle microgels, Langmuir 2008, 24: 11959-66.

[140] Hu X., Tong Z. and Lyon L. A, Multicompartment core/shell microgels, Journal of the Americal Chemical Society 2010, 132: 11470-2.

[141] Ma S., Thiele J., Liu X., Bai Y., Abell C. and Huck W. T. S., Fabrication of microgel particles with complex shape via selective polymerization of aqueous two-phase systems, Small 2012, 8: 2356-60.

[142] Costa R. R. and Mano J. F., Polyelectrolyte multilayered assemblies in biomedical technologies, Chemical Society Reviews 2014, 43: 3453-79.

[143] Borges J. and Mano J. F., Molecular interactions driving the layer-by-layer assembly of multilayers, Chemical Reviews 2014, 114: 8883-8942.

[144] Becker A. L., Johnston A. P. R. and Caruso F., Layer-by-layer-assembled capsules and films for therapeutic delivery, Small 2010, 6:1836-52.

[145] Costa N. L., Sher P. and Mano J. F., Liquefied capsules coated with multilayered polyelectrolyte films for cell immobilization, Advanced Engineering Materials 2011, 13: B218-24.

[146] Correia C. R., Reis R. L. and Mano J. F., Multilayered hierarchical capsules providing cell adhesion sites, Biomacromolecules 2013, 14: 743-51.

[147] Correia C. R., Sher P., Reis R. L. and Mano J. F., Liquified chitosan–alginate multilayer capsules incorporating poly(l-lactic acid) microparticles as cell carriers, Soft Matter 2013, 9: 2125-30.

[148] Poon Z., Chang D., Zhao X. and Hammond P.T., Layer-by-Layer Nanoparticles with a pH Sheddable Layer for In Vivo Targeting of Tumor Hypoxia, ACS Nano 2011, 5: 4284–92.

[149] Wang Y., Bansal V., Zelikin A. N. and Caruso F., Templated synthesis of single-component polymer capsules and their application in drug delivery, Nano Letters 2008, 8: 1741-5

[150] De Temmerman M. -L., Rejman J., Lucas B., Vandenbroucke R.E., Libert C., Demeester J. and De Smedt S. C., Modulation of dendritic cells by lipid grafted polyelectrolyte microcapsules, Advanced Functional Materials 2012, 22: 4236-43.

[151] Kumar K. N. A., Ray S. B., Nagaraja V. and Raichur A. M., Encapsulation and release of rifampicin using poly(vinyl pyrrolidone)-poly(methacrylic acid) polyelectrolyte capsules, Materials Science and Engineering: C 2009, 29: 2508-13.

[152] Zhao Q., Han B., Wang Z., Gao C., Peng C. and Shen J., Hollow chitosan-alginate multilayer microcapsules as drug delivery vehicle: doxorubicin loading and in vitro and in vivo studies, Nanomedicine 2007, 3: 63-74.

[153] Chen Y., Lin X., Park H. and Greever R., Study of artemisinin nanocapsules as anticancer drug delivery systems, Nanomedicine 2009, 5: 316-22.

[154] Liu J., Zhang Y., Wang C., Xu R., Chen Z. and Gu N., Magnetically sensitive alginate-templated polyelectrolyte multilayer microcapsules for controlled release of doxorubicin, The Journal of Physical Chemistry C 2010, 114: 7673-9.

[155] Koo H. Y., Lee H.-J., Kim J. K. and Choi W. S., UV-triggered encapsulation and release from polyelectrolyte microcapsules decorated with photoacid generators, Journal of Materials Chemistry 2010, 20: 3932-7.

[156] Shu S., Sun C., Zhang X., Wu Z., Wang Z. and Li C., Hollow and degradable polyelectrolyte nanocapsules for protein drug delivery, Acta Biomaterialia 2010, 6: 210-7.

[157] Rivera-Gil P., De Koker S., De Geest B. G. and Parak W. J., Intracellular processing of proteins mediated by biodegradable polyelectrolyte capsules, Nano letters 2009, 9: 4398-402.

[158] Itoh Y., Matsusaki M., Kida T. and Akashi M., Enzyme-responsive release of encapsulated proteins from biodegradable hollow capsules, Biomacromolecules 2006, 7: 2715-8.

[159] Ma Y., Dong W. –F., Hempenius M. A., Möhwald H. and Vancso G. J., Redox-controlled molecular permeability of composite-wall microcapsules, Nature Materials 2006, 5: 724-9.

[160] Becker A. L., Zelikin A. N., Johnston A. P. R. and Caruso F., Tuning the formation and degradation of layer-by-layer assembled polymer hydrogel microcapsules. Langmuir : the ACS journal of surfaces and colloids, Langmuir 2009, 25: 14079-85.

[161] Chong S. –F., Sexton A., De Rose R., Kent S. J., Zelikin A. N. and Caruso F., A paradigm for peptide vaccine delivery using viral epitopes encapsulated in degradable polymer hydrogel capsules, Biomaterials 2009, 30: 5178-86.

[162] Costa R. R., Custódio C. A., Arias F. J., Rodríguez-Cabello J. C. and Mano J. F., Nanostructured and thermoresponsive recombinant biopolymer-based microcapsules for the delivery of active molecules, Nanomedicine 2013, 9: 895-902.

[163] Li X., Lu T., Zhang J, Xu J., Hu Q., Zhao S. and Shen J., A study of properties of "micelle-enhanced" polyelectrolyte capsules: structure, encapsulation and in vitro release, Acta biomaterialia 2009, 5: 2122-31.

[164] Fukui Y. and Fujimoto K., The preparation of sugar polymer-coated nanocapsules by the layer-by-layer deposition on the liposome, Langmuir 2009, 25: 10020-5.

[165] Haidar Z. S., Hamdy R. C. and Tabrizian M., Biocompatibility and safety of a hybrid core-shell nanoparticulate OP-1 delivery system intramuscularly administered in rats, Biomaterials 2010, 31: 2746-54.

[166] Agarwal A., Lvov Y., Sawant R. and Torchilin V., Stable nanocolloids of poorly soluble drugs with high drug content prepared using the combination of sonication and layer-by-layer technology, Journal of Controlled Release 2008, 128: 255-60.

[167] Pargaonkar N., Lvov Y. M., Li N., Steenekamp J. H., and De Villiers M. M., Controlled release of dexamethasone from microcapsules produced by polyelectrolyte layer-by-layer nanoassembly, Pharmaceutical Research 2005, 22: 826-35.

[168] Zheng Z., Zhang X., Carbo D., Clark C., Nathan C. –A. and Lvov Y., Sonication-assisted synthesis of polyelectrolyte-coated curcumin nanoparticles, Langmuir 2010, 26: 7679-81.

[169] Facca S., Cortez C., Mendoza-Palomares C., Messadeq N., Dierich A., Johnston A. P. R., Mainard D., Voegel J. –C., Caruso F. and Benjirane-Jessel N., Active multilayered capsules for in vivo bone formation, Proceedings of the National Academy of Sciences of the United States of America 2010, 107: 3406-11.

[170] Tong W., Gao C. and Möhwald H., pH-responsive protein microcapsules fabricated via glutaraldehyde mediated covalent layer-by-layer assembly, Colloid and Polymer Science 2008, 286: 1103-9.

[171] Costa R. R., Girotti A., Santos M., Arias F. J. and Mano J. F. and Rodríguez-cabello J. C., Cellular uptake of multilayered capsules produced with natural and genetically engineered biomimetic macromolecules, Acta Biomaterialia 2014, 10: 2653-62.

[172] Luo R., Mutukumaraswamy S., Venkatraman S. S. and Neu B., Engineering of erythrocyte-based drug carriers : control of protein release and bioactivity, Journal of Materials Science: Materials in Medicina 2012, 23: 63-71.

[173] Zhou Z., Anselmo A. C. and Mitragotri S., Synthesis of protein-based, rod-shaped particles from spherical templates using layer-by-layer assembly, Advanced Materials 2013, 25, 2723-7.

[174] Bai J., Beyer S., Mak W. C. and Trau D., Fabrication of inflated LbL microcapsules with a “bead-in-a-capsule” morphology, Soft Matter 2009, 5: 4152-60.

[175] De Geest B. B. G., De Koker S., Immesoete K., Demeester J., De Smedt S. C. and Hennink W. E., Self-exploding beads releasing microcarriers, Advanced Materials 2008, 20: 3687-91.

[176] Costa R. R., Castro E., Javier Arias., Rodrígues-Cabello J. C. and Mano J. F., Multifunctional compartmentalized capsules with a hierarchical organization from the nano to the macro scales, Biomacromolecules 2013, 14: 2403-10.

[177] Li Y. and Shi J., Hollow-structured mesoporous materials : chemical synthesis , functionalization and applications, Advanced Materials 2014, 26:3176-205.

[178] Wang T., Zhang L., Su Z., Wang C., Liao Y. and Fu Q., Multifunctional hollow mesoporous silica nanocages for cancer cell detection and the combined chemotherapy and photodynamic therapy, ACS Applied Materials and Interfaces 2011, 2: 2479-86.

[179] Zhao B. Y., Lin L., Lu Y., Chen S., Dong L. and Yu S., Templating synthesis of preloaded doxorubicin in hollow mesoporous silica nanospheres for biomedical applications, Advanced Materials 2010, 22: 5255-5259.

[180] Wang Z., Wu L., Chen M. and Zhou S., Facile synthesis of superparamagnetic fluorescent FE_3O_4/ZnS hollow, Journal of the American Chemical Society 2009, 131: 11276-7.

[181] Caruso F., Caruso R. A. and Mohwald H., Nanoengineering of inorganic and hybrid hollow spheres by colloidal templating, Science 1998, 282: 1111-4.

[182] Chen Y., Chen H., Zeng D., Tian Y., Chen F., Feng J. and Shi J., Core/shell structured hollow mesoporous nanocapsules : a potential platform for simultaneous cell imaging and anticancer drug delivery, ACS Nano 2010, 4: 6001-13.

[183] Fowler C. E., Khushalani D., Mann S., Interfacial synthesis of hollow microspheres of mesostructured silica, Chemical Communications 2001, 2028-2029.

[184] Fornasieri G., Badaire S., Backov R., Mondain-Monval O., Zakri C. and Poulin P., Mesoporous and homothetic silica capsules in reverse-emulsion microreactors, Advanced Materials 2004, 16: 1094-7.

[185] Gu D., Bongard H., Deng Y., Feng D., Wu Z., Fang Y., Mao J., Tu B., Schuth F. and Zhao D., An aqueous emulsion route to synthesize mesoporous carbon vesicles and their nanocomposites, Advanced Materials 2010, 22: 833-37.

[186] Yang S. M., Sokolov I., Coombs N., Kresge C. T. and Ozin G. A. Formation of Hollow Helicoids in Mesoporous Silica: Supramolecular Origami, Advanced Materials 1999, 11: 1427-31.

[187] Zhu Y., Shi J., Li Y., Chen H., Shen W. and Dong X., Storage and release of ibuprofen drug molecules in hollow mesoporous silica spheres with modified pore surface, Microporous and Mesoporous Materials 2005, 85: 75-81.

[188] Zhu Y., Fang Y., Borchardt L. and Kaskel S. PEGylated hollow mesoporous silica nanoparticles as potential drug delivery vehicles, Microporous and Mesoporous Materials 2011, 141: 199-206.

[189] Gao Y., Chen Y., Ji X., He X., Yin Q., Zhang Z., Shi J. and Li Y., Controlled intracellular release of doxorubicin in multidrug-resistant cancer cells by tuning the shell-pore sizes of mesoporous silica nanoparticles, ACS -Nano 2011, 5: 9788-98.

[190] Tang S., Huang X., Chen X. and Zheng N., Hollow Mesoporous zirconia nanocapsules for drug delivery, Advanced Functional Materials 2010, 20: 2442-7.

[191] Zhu Y., Ikoma T., Hanagata N. and Kaskel S., Rattle-type Fe_3O_4@SiO_2 hollow mesoporous spheres as carriers for drug delivery, Small 2010, 6: 471-8.

[192] Chen Y., Chu C., Zhou Y., Ru Y., Chen H. Chen F., He Q., Zhang Y., Zhang L. Shi J., Reversible pore-structure evolution in hollow silica nanocapsules: large pores for siRNA delivery and nanoparticle collecting, Small 2011, 7: 2935-44.

[193] Chen Y., Chen H., Ma M., Chen F., Guo L., Zhang L. and Shi J., Double mesoporous silica shelled spherical/ellipsoidal nanostructures : synthesis and hydrophilic/hydrophobic anticancer drug delivery, Journal of Materials Chemistry 2011, 21:5290-8.

[194] Wang Y., Yan Y., Cui J., Hosta-Rigau L., Heath J. K., Nice E. C. and Caruso F., Encapsulation of water-insoluble drugs in polymer capsules prepared using mesoporous silica templates for intracellular drug delivery, Advanced Materials 2010, 22: 4293-7.

[195] Huang C. –C., Huang W. and Yeh C. -S., Shell-by-shell synthesis of multi-shelled mesoporous silica nanospheres for optical imaging and drug delivery, Biomaterials 2011, 32: 556-64.

[196] Chen Y., Chen H., Zeng D., Tian Y., Chen F., Feng J. and Shi J., Core/shell structured hollow mesoporous nanocapsules: a potential platform for simultaneous cell imaging and anticancer drug delivery, ACS nano 2010, 4: 6001-13.

[197] Chen Y., Chen H., Zhang S., Chen F., Zhang L., Zhang J., Zhu M., Wu H., Guo L., Feng J. and Shi J., Multifunctional mesoporous nanoellipsoids for biological bimodal imaging and magnetically targeted delivery of anticancer drugs, Advanced Functional Materials 2011, 21: 270-8.

[198] Wang T., Chai F., Fu Q., Zhang L., Liu H., Li L., Liao Y., Su Z., Wang C., Duan B. and Ren D., Uniform hollow mesoporous silica nanocages for drug delivery in vitro and in vivo for liver cancer therapy, Journal of Materials Chemistry 2011, 21: 5299-306.

[199] Wang T., Zhang L., Su Z., Wang C., Liao Y. and Fu Q., Multifunctional hollow mesoporous silica nanocages for cancer cell detection and the combined chemotherapy and photodynamic therapy, ACS Applied Materials & Interfaces 2011, 3: 2479-86.

[200] Wu H., Zhang S., Zhang J., Liu G., Shi J., Zhang L., Cui X., Ruan M., He Q. and Bu W., A hollow-core, magnetic, and mesoporous double-shell nanostructure: in situ decomposition/reduction synthesis, bioimaging, and drug-delivery properties, Advanced Functional Materials 2011, 21: 1850-62.

[201] Wang X., Chen H., Chen Y., Ma M., Zhang K., Li F., Zheng Y., Zeng D., Wang Q. and Shi J., Perfluorohexane-encapsulated mesoporous silica nanocapsules as enhancement agents for highly efficient high intensity focused ultrasound (HIFU), Advanced Materials 2012, 24: 785-91.

[202] Chen Y., Chen H., Sun Y., Zheng Y., Zeng D., Li F., Zhang S., Wang X., Zhang K., Ma M., He Q., Zhang L., Shi J., Multifunctional mesoporous composite nanocapsules for highly efficient MRI-guided high-intensity focused ultrasound cancer surgery, Angewandte Chemie International Edition 2011, 50: 12505-9.

[203] Fan W., Shen B., Bu W., Chen F., Zhao K., Zhang S., Zhou L., Peng W., Xiao Q., Xing H., Liu J., Ni D., He Q. and Shi J., Rattle-structured multifunctional nanotheranostics for synergetic chemo-/radiotherapy and simultaneous magnetic/luminescent dual-mode imaging, Journal of the American Chemical Society 2013, 135: 6494-503.

[204] Kim T., Momin E., Choi J., Yuan K., Zaidi H., Kim J., Park M., Lee N., McMahon M. T., Quinones-Hinojosa A., Bulte J. W., Hyeon T., Gilad A. A. Mesoporous silica-coated hollow manganese oxide nanoparticles as positive T1 contrast agents for labeling and MRI tracking of adipose-derived mesenchymal stem cells, Journal of the American Chemical Society 2011, 133: 2955-61.

[205] An E., Jeong C. B., Cha C., Kim D. H., Lee H., Kong H., Kim J. and Kim J. W., Fabrication of Microgel-in-Liposome Particles with Improved Water Retention, Langmuir 2012, 28, 4095-101.

[206] Yamabe K., Kato Y., Onishi H. and Machida Y., Potentiality of double liposomes containing salmon calcitonin as an oral dosage form, Journal of Controlled Release 2003, 89: 429-436.

[207] Xiao C., Qi X., Maitani Y. and Nagai T., Sustained release of cisplatin from multivesicular liposomes : potentiation of antitumor efficacy against S180 murine carcinoma, Journal of Pharmaceutical Sciences 2004, 93: 1718-24.

[208] Mantripragada S., A lipid based depot (DepoFoam technology) for sustained release drug delivery, Progress in Lipid Research 2002, 41: 392–406

[209] Wong B., Boyer C, Steinbeck C, Peters D., Schmidt J., van Zanten R., Chmelka B. and Zasadzinski J. A., Design and In Situ Characterization of Lipid Containers with Enhanced Drug Retention, Advanced Materials 2011, 23, 2320-5.

[210] Perro A., Nicolet C., Angly J., Lecommandoux S., Le Meins J. F. and Colin A., Mastering a double emulsion in a simple co-flow microfluidic to generate complex polymersomes, Langmuir 2011, 27: 9034-42.

[211] Kim S., Shum H. C., Kim J. W., Cho J and Weitz D. A., Multiple Polymersomes for Programmed Release of Multiple Components, Journal of the American Chemical Society 2011, 133: 15165-71.

[212] Marguet M., Edembe L. and Lecommandoux S., Polymersomes in Polymersomes : Multiple Loading and Permeability Control, Angewandte Chemie International Edition 2012, 51: 1173-6.

[213] Saito N,. Liu C., Lodge T. P. and Hillmyer M. A, Multicompartment Micelles from Polyester-Containing ABC Miktoarm Star Terpolymers, Macromolecules 2008, 41: 8815-22.

[214] Lodge T. P., Rasdal A., Li Z. and Hillmyer M. A., Simultaneous, segregated storage of two agents in a multicompartment micelle, Journal of the Americal Chemical Society 2005, 127: 17608-9.

[215] Pang X., Wan C., Wang M. and Lin Z., Strictly biphasic soft and hard Janus structures : synthesis, properties, and applications, Angewandte Chemie International Edition 2014, 53: 5524-38.

[216] Perro A-, Reculusa S., Ravaine S., Bourgeat-Lami E. and Duguet E., Design and synthesis of Janus micro- and nanoparticles, Journal of Materials Chemistry 2005, 15: 3745-60.

[217] Roh K., Martin D. C., Lahann J., Biphasic Janus particles with nanoscale anisotropy, Nature Materials 2005, 4: 759-63.

[218] Lattuada M. and Hatton T. A., Synthesis, properties and applications of Janus nanoparticles, Nano Today 2011, 6: 286-308.

[219] Yang S., Guo F., Kiraly B., Mao X., Lu M., Leong K. W., and Huang T. J., Microfluidic synthesis of multifunctional Janus particles for biomedical applications, Lab on a Chip 2012, 12: 2097-102.

[220] Lim D. W., Hwang S., Uzun O., Stellacci F. and Lahann J., Compartmentalization of gold nanocrystals in polymer microparticles using electrohydrodynamic co-jetting, Macromolecular Rapid Communications 2010, 321: 176-182.

[221] Carbone L. and Cozzoli P. D., Colloidal heterostructured nanocrystals : Synthesis and growth mechanisms, Nano Today 2010, 5: 449-93.

[222] Teo B. M., Suh S. K., Hatton T. A., Ashokkumar M. and Grieser F., Sonochemical Synthesis of Magnetic Janus Nanoparticles, Langmuir 2011, 27: 30-33.

[223] Rahman M., Montagne F., Fessi H. and Elaissari A., Anisotropic magnetic microparticles from ferrofluid emulsion, Soft Matter 2011, 7: 1483-90.

[224] Reculusa S., Poncet-Legrand C., Perro A,. Duguet E., Bourgeat-Lami E. Mingotaud C., and Ravaine S., Hybrid Dissymmetrical Colloidal Particles, Chemistry of Materials 2005, 17: 3338-44.

[225] Yabu H., Higuchi T., Ijiro K. and Shimomura M., Spontaneous formation of polymer nanoparticles by good-solvent evaporation as a nonequilibrium process, Chaos 2005, 15: 047505.

[226] Yabu H., Kanahara M., Shimomura M., Arita T., Harano K., Nakamura E., Higuchi T. and Jinnai H., Polymer janus particles containing block-copolymer stabilized magnetic nanoparticles, ACS Applied Materials & Interface 2013, 5: 3262-6.

[227] Kim J., Larsen R. J. and Weitz D. A., Synthesis of nonspherical colloidal particles with anisotropic properties, Journal of the American Chemical Society 2006, 128: 14374-7.

[228] Mock E. B. and Zukoski C. F. Emulsion polymerization routes to chemically anisotropic particles, Langmuir 2010, 26: 13747-50.

[229] Mock E. B., De Bruyn H., Hawkett B. S., Gilbert R. G., Zukoski C. F., Synthesis of anisotropic nanoparticles by seeded emulsion polymerization, Langmuir 2006, 22: 4037-43.

[230] Kietzke T., Neher D., Landfester K., Montenegro R., Güntner R., Scherf U., Novel approaches to polymer blends based on polymer nanoparticles, Nature Materials 2003, 2: 408-12.

[231] Tanaka T., Nakatsuru R., Kagari Y., Saito N. and Okubo M., Effect of molecular weight on the morphology of polystyrene/poly(methyl methacrylate) composite particles prepared by the solvent evaporation method, Langmuir 2008, 24: 12267-71.

[232] Higuchi T., Tajima A., Yabu H. and Shimomura M., Spontaneous formation of polymer nanoparticles with inner micro-phase separation structures, Soft Matter 2008, 4: 1302-5.

[233] Erhardt R., Bo A., Zettl H., Kaya H., Pyckhout-Hintzen H., Krausch G., Abetz V. and Müller A. H. E., Janus micelles, Macromolecules 2001, 34: 1069-75.

[234] Liu Y., Abetz V. and Müller A. H. E., Janus cylinders, Macromolecules 2003, 36: 7894-8.

[235] Walther A., Drechsler M., Rosenfeldt S., Harnau L., Ballauff M., Abbetz V., and Müller A. H. E., Self-Assembly of Janus Cylinders into Hierarchical Superstructures, Journal od the American Chemical Society 2009, 131: 4720-8.

[236] Kietzke T., Neher D., Kumke M., Ghazy O., Ziener U. and Landfester K., Phase separation of binary blends in polymer nanoparticles, Small 2007, 3: 1041-8.

[237] Erhardt R., Zhang M., Boker A., Zettl H., Abetz C., Frederik P., Krouch G., Abetz V. and Müller A. H. E., Amphiphilic janus micelles with polystyrene and poly(methacrylic acid) hemispheres, Journal of the American Chemical Society 2003, 125: 3260-7.

[238] Wolf A., Walther A. and Müller A. H. E., Janus triad: three types of nonspherical, nanoscale janus particles from one single triblock terpolymer, Macromolecules 2011, 44: 9221-9.

[239] Sfika V., Tsitsilianis C., Kiriy A., Gorodyska G. and Stamm M., pH Responsive heteroarm starlike micelles from double hydrophilic ABC terpolymer with ampholitic A and C blocks, Macromolecules 2004, 37: 9551-60.

[240] Voets I. K., Fokkink R., Hellweg T, King S. M., De Waard P., De Keizer A. and Stuart M. A. C., Spontaneous symmetry breaking: formation of Janus micelles, Soft Matter 2009, 5: 999-1005

[241] Voets I. K., De Keizer A., De Waard P, Fredrik P. M., Bomans P. H. H., Schmalz H., Walther A., King S. M., Leermakers F. A. M. And Stuart M. A. C., Double-faced micelles from water-soluble polymers, Angewandte Chemie International Edition 2006, 45: 6673-6.

[242] Ma R., Wang B., Xu Y., An Y., Zhang W., Li G., and Shi L., Surface phase separation and morphology of stimuli responsive complex micelles, Macromolecular Rapid Communications 2007, 28: 1062-9.

[243] Du J. and Armes S.P., Patchy multi-compartment micelles are formed by direct dissolution of an ABC triblock copolymer in water, Soft Matter 2010, 6: 4851.

[244] Nisisako T., Torii T., Takahashi T. and Takizawa Y., Synthesis of monodisperse bicolored Janus particles with electrical anisotropy using a microfluidic co-flow system, Advanced Materials 2006,18: 1152-6.

[245] Nie Z., Li W., Seo M., Xu S. and Kumacheva E., Janus and ternary particles generated by microfluidic synthesis: design, synthesis, and self-assembly, Journal of the American Chemical Society 2006, 128: 9408-12.

[246] Dendukuri D., Pregibon D. C., Collins J., Hatton T. A. and Doyle P. S., Continuous-flow lithography for high-throughput microparticle synthesis, Nature Materials 2006, 5: 365-9.

[247] Cheng L., Hou G., Miao J., Chen D., Jiang M. and Zhu L., Efficient synthesis of unimolecular polymeric janus nanoparticles and their unique self-assembly behavior in a common solvent, Macromolecules 2008, 41: 8159-66.

[248] Yin S. –N., Wang C. –F., Yu Z. –Y., Wang J., Liu S. –S. and Chen S., Versatile bifunctional magnetic-fluorescent responsive Janus supraballs towards the flexible bead display, Advanced Materials 2011, 23: 2915-9.

[249] Lattuada M. and Hatton T. A., Preparation and controlled self-assembly of Janus magnetic nanoparticles, Journal of the American Chemical Society 2007, 129: 12878-89.

[250] Yabu H., Kanahara M., Shimomura M., Arita T., Harano K., Nakamura E., Higuchi T. and Jinnai H., Polymer Janus particles containing block-copolymer stabilized magnetic nanoparticles, ACS Applied Materials & Interfaces 2013, 5: 3262-6.

[251] Yu H., Chen M., Rice P. M., Wang S. X., White R. L and Sun S., Dumbbell-like bifunctional Au–Fe3O4 nanoparticles, Nano Letters 2005, 5: 379-82.

[252] Gu H., Yang Z., Gao J., Chang C. K. and Xu B., Heterodimers of nanoparticles: formation at a liquid-liquid interface and particle-specific surface modification by functional molecules, Jounal of the American Chemical Society 2005, 127: 34–5.

[253] Zhao N. and Gao M., Magnetic janus particles prepared by a flame synthetic approach: synthesis, characterizations and properties, Advanced Materials 2009, 21: 184-7.

[254] Tran L. T., Lesieur S. and Faivre V., Janus nanoparticles: materials, preparation and recent advances in drug delivery, Expert Opinion on Drug Delivery 2014, 11: 1061-74.

[255] Pregibon D. C., Toner M. and Doyle P. S., Multifunctional encoded particles for high-throughput biomolecule analysis, Science 2007, 315: 1393-6.

[256] Appleyard D. C., Chapin S. C., Srinivas R. L. and Doyle P. S., Bar-coded hydrogel microparticles for protein detection: synthesis, assay and scanning, Nature Protocols 2011, 6: 1761-74.

[257] Lee H., Kim J., Kim H., Kim J. and Kwon S., Colour-barcoded magnetic microparticles for multiplexed bioassays, Nature Materials 2010, 9: 745-9.

[258] Salem A. K., Searson P. C. and Leong K. W., Multifunctional nanorods for gene delivery, Nature Materials 2003, 2: 668-71.

[259] Xie H., She Z. -G., Wang S., Sharma G. and Smith J. W., One-step fabrication of polymeric Janus nanoparticles for drug delivery, Langmuir 2012, 28: 4459-63.

[260] Acton A. L., Fante C., Flatley B., Burattini S., Hamley I. W., Wang Z., Greco F. and Hayes W., Janus PEG-based dendrimers for use in combination therapy: controlled multi-drug loading and sequential release, Biomacromolecules 2013, 14: 564-74.

[261] Al-jamal W. T. and Kostarelos K., Construction of nanoscale multicompartment liposomes for combinatory drug delivery, International Journal of Pharmaceutics 2007, 331: 182-5.

[262] Wu L. Y., Ross B. M., Hong S. and Lee L. P., Bioinspired nanocorals with decoupled cellular targeting and sensing functionality, Small 2010, 6: 503-7.

[263] Zhao L. B., Pan L., Zhang K, Guo S. S., Liu W., Wang Y., Chen Y., Zhao X. Z., Chan H. L., Generation of Janus alginate hydrogel particles with magnetic anisotropy for cell encapsulation, Lab on a Chip 2009, 9: 2981-6.

[264] Gil S. and Mano J. F., Magnetic composite biomaterials for tissue engineering, Biomaterials Science 2014, 2: 812-8.

[265] Castro E. and Mano J. F., Magnetic force-based tissue engineering and regenerative medicine, Journal of Biomedical Nanotechnology 2013, 9: 1129-36.

[266] Mattix B. M., Olsen T. R., Casco M., Reese L., Poole J. T., Zhang J., Visconti R. P., Simionescu A., Simionescu D. T. and Alexis F., Janus magnetic cellular spheroids for vascular tissue engineering, Biomaterials 2014, 35: 949-60.

[267] Rahmani S., Saha S., Durmaz H., Donini A., Misra A. C., Yoon J. and Lahann J., Chemically orthogonal three-patch microparticles, Angewandte Chemie 2014, 126: 2364-70.

Section II

Materials and Methods

Chapter 4

Detailed Description of Experimental Testing and Materials

The aim of this chapter is to present detailed information about the materials and techniques used under the scope of this thesis. Although the experimental procedure is described in the experimental section of each corresponding chapter of the section III, herein the objective is to give some general theoretical concepts and justify the selection of the materials and methods employed to develop the systems proposed. The information described here will complement those given in each chapter. It is important to highlight that information related with reagents suppliers and specification of general equipment's are described in each chapter of section III and will not be mentioned here.

4.1. Superhydrophobic Surfaces Methodology

In all the chapters of the experimental work described in this thesis (see section III) the superhydrophobic methodology was used to obtain the proposed particulate systems. In 2010, Song *et al.* [1] suggested the use of biomimetic superhydrophobic surfaces as platforms to produce hydrogel particles. This methodology was inspired in the water repellent properties of the lotus leaves. As described in the chapter 1 and 2, the water droplets acquire an almost spherical shape when are on the top of those natural surfaces due to the combination of micro/nano topographical features and low surface energy. Thus, Song *et al.* [1] hypothesized that dispensing a polymeric precursor solution on the top of substrates exhibiting water repellency similar to lotus leaves, followed by a crosslinking step, it would be possible to obtain almost spherical particles. On the scope of this thesis, different polymeric hydrogel systems were developed demonstrating the versatility of the superhydrophobic surfaces methodology in encapsulation of drugs and cells as well as in preparation of complex architectures. All the characteristics and advantages of this technique in preparation of spherical particulate systems have already been described in the chapter 2.

Two different materials were modified in order to obtain biomimetic superhydrophobic surfaces. Their properties and the procedure to obtain superhydrophobic characteristics will be described in the follow subsections.

4.1.1. Superhydrophobic Surfaces Preparation

4.1.1.1. Polystyrene

Polystyrene (PS) superhydrophobic surfaces were used in chapters 5, 6, 7 and 8. Such surfaces were obtained by a phase separation method, which is a simple, fast and inexpensive method. In addition, PS is a recurrent material used in the labs namely in cell culture tissue plates, as well as main compound of particles for biomedical applications [2]. PS superhydrophobic surfaces could even be implanted *in vivo* causing minimal inflammatory responses [3], this means that it should not release toxic or undesirable species that could contaminate the particles during the solidification process. As referred above, to prepare PS superhydrophobic surfaces a phase separation method was employed [4]. Briefly, a PS solution in tetrahydrofuran (THF) was prepared with a concentration of 70 mg/mL and then mixed with ethanol in the proportion 2:1.3 (v:v). Ethanol is a nonsolvent of PS and acts as a precipitator. This was the reason that led to the appearance of some aggregates when the ethanol was mixed with the PS solution. However, after several minutes, the aggregates dissolved in the mixture. Then, the solution was dispensed on the top of smooth PS substrates (obtained from commercial petri dishes) previously cleaned with ethanol. The reaction occurred during approximately 1 min and then, the substrates were immersed in ethanol for at least 1 min – Figure 4.1 I. Two macroscopic phases were formed: one polymer rich phase and one polymer poor phase. The precipitated polymer acted as a nuclei and the polymer rich phase preferred to aggregate around the nuclei in order to decrease the surface tension, which explain the almost spherical structures aggregated onto the PS formed film (Figure 4.1 II). In addition, the mixture of THF and ethanol is less volatile than THF solely, causing an increase of reaction time and a more uniform formation of the micro/nano spheres [5,6].

Figure 4.1. I. Schematic representation of the procedure to obtain PS superhydrophobic surfaces. II. Smooth PS exhibiting a contact angle (CA) of *ca.* 77° (before modification) and the topographical structures of the superhydrophobic PS surface (after modification). The water CA achieved was higher than 150° and the surfaces exhibited aggregates of nanostructures onto microstructures recreating the hierarchical structure of the natural water repellent systems. Images adapted from [7].

In order to improve the hydrophobicity of the obtained surfaces a chemical surface treatment was also performed. A self-assembly monolayer of perfluorodecyltriethoxysilanes (1% (v/v) PFDTS in ethanol) coated the micro/nano topographical features of the PS modified substrates, after being activated by an argon plasma treatment (40 s, 30 W, Plasma Prep5; Gala Instruments). This treatment activated the surfaces generating hydroxyl groups, which are reactive groups that interacted with fluorinated hydrocarbons existing in the PDFTS. Having into account that hydroxyl groups are water adsorption sites, this treatment eliminated possible water anchor sites [8].

4.1.1.2. Copper

In chapter 9, it was used copper (Cu) superhydrophobic surfaces obtained by a chemical-base deposition method where a micro/nanostructured film was spontaneously deposited onto such substrates [9]. In comparison with PS surfaces, slightly higher water repellency and resistance to UV light exposure were achieved [7]. However, the fragility of the film can limit the application on those surfaces.

The process of the preparation of Cu superhydrophobic surfaces was the following (Figure 4.2 I): the Cu substrates were immersed in ammonium hydroxide solution (0.03 M, pH 9-10), for 5 days at 4 °C, that caused the formation of a uniform blue film coating. The Cu surfaces had to be very well cleaned with solutions of HCl (1 M), otherwise the film was not deposited or was heterogeneous. The film was composed by a large number of $Cu(OH)_2$ needles that growth through a crystallization process (Figure 4.2

II). The Cu platform was further modified by a deposition of a self assembly monolayer of PFDTS (1% (v/v) in ethanol) in order to improve the water repellency properties [9].

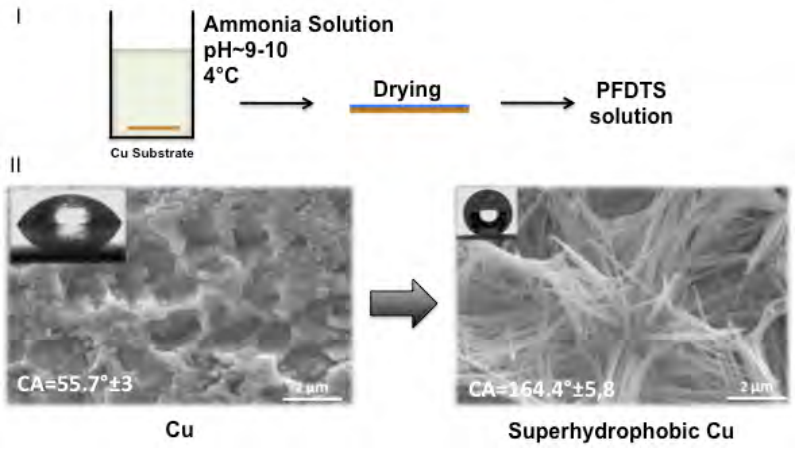

Figure 4.2. I. Schematic representation of the procedure to obtain Cu superhydrophobic surfaces. II. Cu substrate before film deposition, exhibiting CA around 56° and after immersion in ammonia and PFDTS solution. On the surface of the Cu grew up micro and nano structures of $Cu(OH)_2$ which combined with a PFDTS increased the water contact angle to *ca.* 164°. Image adapted from [7].

4.1.2. Materials, Bioactive Agents and Cells Used in the Preparation of the Particulate Systems

4.1.2.1. Natural-Based Hydrogels

Hydrogels are three-dimensional structures obtained through crosslinking of water-soluble polymers creating a water insoluble network. A variety of formulations at chemical and physical level may be obtained. Particles, films, coatings, scaffolds are examples of hydrogel structures widely used in biomedical applications, namely tissue engineering and regenerative medicine [10,11], drug release systems [12,13], diagnostics [14], cell immobilization [15-17], separation of biomolecules or cells [18,19], and as materials to regulate biological adhesions [20].

Hydrogels are highly porous networks and their structure may be tuned by controlling the density of the crosslinking. With this, their swollen rate when immersed in aqueous environments is also controlled. The porosity of the hydrogels is the main responsible for the loading and release of molecules when used as drug carriers. Small or even macromolecules may diffuse in and out of the hydrogel network at a rate dependent on the diffusion coefficient. The high water content within the hydrogel structure turns those materials typically highly biocompatible. In addition, hydrogels exhibit physicochemical similarities with native extracellular matrix (ECM) due to the composition (particularly in the case of carbohydrate-based hydrogels) and mechanical properties [15]. In most of the cases, the hydrogels are quite deformable

which could be an advantage to adapt their shape to the site where they are applied, as for example when implanted in injured tissues or even to be administered through injectable procedures. On the other side, hydrogels also have a few limitations mainly as the result of their low tensile strength, being not the most appropriated materials for applications where strong mechanical properties are required. When used as drug carriers, hydrogels have two main restraints derived from their high affinity to aqueous environments and from their porous structure: (I) the limited capacity to be loaded with hydrophobic drugs and (II) the rapid release of the content. In addition, some hydrogels do not allow cell attachment and proliferation being problematic when it is desired to use them as cell carriers or scaffolds. In such cases, the recurrent strategy is to modify the polymer backbone with adhesive peptides, such as RGD [21].

Hydrogel crosslinked networks may be obtained through the establishment of physical or chemical interactions between the polymer chains. Physical crosslinked gels are, generally, obtained through simple and fast procedures. Examples are ionic interactions, crystallization, hydrogen bonds, protein interactions, among others. Chemical crosslinking may be achieved by radical polymerization, chemical reaction of complementary groups (crosslinker agents), high-energy irradiation and using enzymes [22].

Natural-based materials were selected to develop the different systems proposed in this thesis. They have the advantage of showing low/non toxicity, low immunogenicity and general good biocompatibility. In addition, natural-based polymers could be processed in mild conditions [23]. The most relevant properties of such polymers will be described in detail in the next subsections.

I. Dextran

Dextran is a polysaccharide obtained from bacteria cultures of *Leuconostoc mesenteroides*. It shows a linear polymer backbone composed mainly by D-glucopyranose residues connected by 1,6- and some 1,3-glycosidic linkages (Figure 4.3) [24].

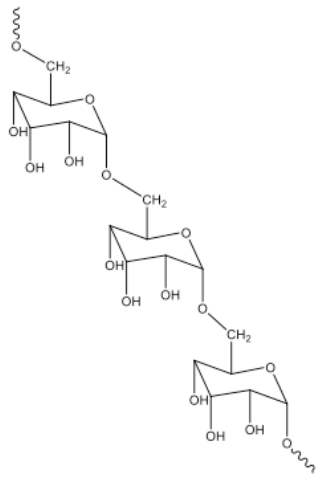

Figure 4.3. Structure of Dextran.

Moulds, bacteria and also mammalian cells may degrade such glycosidic linkages [25]. Bacteroides are anaerobic gram-negative intestinal bacteria present in the colon, exhibiting dextranase activity meaning that are capable to hydrolyze the glycosidic linkages. Various drug-dextran prodrugs have been proposed [26] because the drug-dextran conjugation remains intact and unabsorbed from the stomach to the small intestine, but in the colon the dextranases cleave the dextran chain randomly at the terminal linkages, and release the drug [24]. Dextran have also been used to produce particles for colon-specific drug delivery [24, 27] and used in tissue engineering [28-30].

Dextran hydrogels can be created by either physical or chemical crosslinking. Physical crosslinking was obtained by self-assembling of enantiomeric lactic acid oligomers (stereocomplex formation) grafted onto dextran backbone [31]. Chemical crosslinking was already achieved by using quite aggressive molecules such as isocyanates and glutaraldehyde [27,32]. Owing to its chemically reactive hydroxyl groups (3 groups per glucopyranose unit), dextran can be modified with functional groups (*e.g.* methacrylate) to form 3D network structures by UV light exposure. The main advantage of using a photo crosslinkable polymer and superhydrophobic surfaces is that just is necessary to dispense one solution onto the surface, unlike in the ionic crosslinking that it is necessary dispense the polymeric solution and then the crosslinking agent. Furthermore, in chapters 5 and 9, dextran-methacrylate (dextran-MA, Figure 4.4) allowed to produce the particles just using aqueous soluble molecules, avoiding the use of organic solvents. The polymer was modified following a protocol described in literature [33]. Approximately 25 g of dextran were dissolved in 225 mL of dimethyl sulfoxide (DMSO) under a nitrogen atmosphere. Then, 5 g of 4-(N,N-dimethylamido)pyridine (DMAP) were added and after being completely dissolved, 20.5 mL of glycidyl methacrylate (GMA) were incorporated. The solution was stirred at room temperature for 48 h. The reaction was stopped by adding 3.3 mL of HCl (37%), which induced the neutralization of the DMAP. The solution was then dialyzed against water for 1 month using membranes with a MWCO of 12 400 Da, and finally frozen and lyophilized.

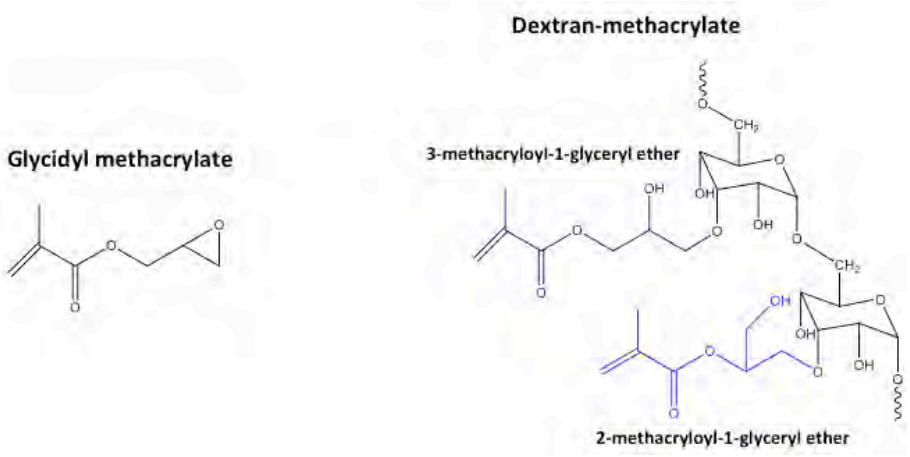

Figure 4.4. Structure of the glycidyl methacrylate used to modify the dextran. After the reaction, two isomers may be obtained: 3-methacryloyl-1-glyceryl ether or 2-methacryloyl-1-glyceryl ether.

II. Chitosan

Chitosan is a derivate of chitin, the most abundant natural polysaccharide after cellulose. Chitin is the main component of the exoskeleton of crustaceans, insects, spiders and cells walls of algae, fungi and yeast. When the chitin is deacetylated, it becomes soluble in acidic conditions and it is denominated chitosan.

Chitosan is a linear polysaccharide composed by randomly distributed β-(1-4)-linked D-glucosamine (deacetylated unit) and N-acetyl-D-glucosamine (acetylated unit) (Figure 4.5). The protonation of the $-NH_2$ on the C-2 position of the D-glucosamine unit, is the responsible for its solubilization. In addition, chitosan solubility is limited to acidic environments (pH < 6.5) and neutralization is required prior to biological applications.

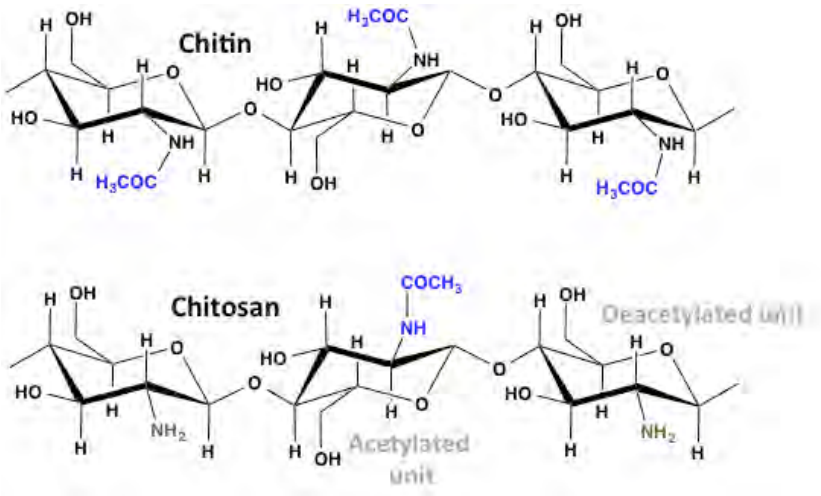

Figure 4.5. Chemical structure of chitin and chitosan.

Chitosan 3D structures are commonly obtained by crosslinking the chitosan acidic solution using dialdehydes (glutaraldehyde, formaldehyde, PEG dialdehyde diethyl acetal) and other molecules such as genipin. Most of the crosslinkers used to perform covalent crosslinking may induce toxicity both in the encapsulated cells as well as in the body if found free traces when the gel is administered or implanted. Ionic crosslinking provides mild conditions because non-toxic agents are required. It is known that chitosan is a polycationic polymer capable to interact with negatively charged components, either ions or molecules, forming a network through establishment of ion bridges [34]. As said before, the neutralization of the chitosan is a requirement for biomedical applications. The acidic solution of chitosan may be easily neutralized with a polyol counterionic dibase salt such as β-glycerophosphate (β-GP). This is achieved just mixing the acidic solution of chitosan with a β-GP solution. The obtained mixture is thermosensitive and it is suitable to gelify at physiological temperatures. This system showed promising characteristics to be used injectable system for biomedical applications [35,36]. Playing with neutralization and ionic crosslinking, in chapter 6, chitosan hydrogels were prepared using mild conditions for cell encapsulation.

Purification of chitosan

The chitosan used in chapter 6 was previously purified through dissolution in an acetic acid solution followed by precipitation. The purification was carried out in order to eliminate some impurities or even insoluble fractions (*e.g.* chitin) that could remain in the commercial chitosan. Around 10 g of commercial powder of chitosan were slowly dissolved in 1 L of an aqueous acetic acid solution (2% v/v) at room temperature. The obtained solution was filtered twice using a nylon filter and a Millipore membrane (5 μm). The pH of the chitosan solution was adjusted to 8 by adding NaOH 2M. The increase of the pH caused the precipitation of the chitosan. Afterwards, the chitosan precipitate was collected by filtration and washed with water until reach the pH 7. Upon complete neutralization, the chitosan precipitate was dehydrated in ethanol-water solutions, frozen at -80 °C and finally dried by lyophilization.

III. Collagen

Collagen is the major insoluble fibrous protein in the ECM and in the connective tissue, being the most abundant protein in the animal kingdom. Although there are around 16 types of collagen, the most common in the human body are type I, II and III. Despite having different structures all types of collagen have a common role: imparts strength, support and elasticity of the tissues. Fibroblasts and epithelial cells secrete the different types of collagen.

In chapter 7, this protein was used to prepare gels in a fast way for applications in skin regeneration. Models of bioengineered skin capable to mimic the anatomy, physiology, biological stability and aesthetic nature are difficult to achieve. Tissue engineering strategies for skin should have some essential characteristics, such as, being easy-to-handle to apply in the wound site, provide a functional barrier with appropriate water and oxygen flux, be adherent, have adequate mechanical properties, undergo controlled degradation, and avoid toxic and inflammatory responses [37]. In this way, type I collagen could be particularly important in scenarios such as chronic wounds, where the healing process is extremely difficult. In these cases, the dermis and epidermis layers are disrupted due to an inflammatory process where an abnormal presence of proteinases cause the destruction of the ECM and consequently the dead of the cells [38]. Type I collagen was selected because it is highly present in the skin (around 70-80% of the dry weight of the skin is type I collagen) [39] and it has been demonstrating potential to be used as a scaffold [40].

Collagen shows a fibrillar structure because the molecules pack together to form long thin fibrils with similar structure – Figure 4.6. Type I collagen was the first type to be characterized. Its abundance in tendon tissue and in rat tails made it easy to isolate. It is composed by long (100-200 nm) and thin (1.5 nm in diameter) fundamental structural units. These units consist in three coiled subunits: two $\alpha 1$ chains and one $\alpha 2$. Each chain contains precisely 1050 amino acids wound around one another in a characteristic right-hand triple-helix (Figure 4.6). The most abundant amino acids in collagen structure are glycine (Gly), proline (Pro) and hydroxyproline being, in general, in the follow sequence: Gly-Pro-X, where X can be any amino acid. Each amino acid has a precise function to maintain the three-stranded collagen helix in a stable state [41].

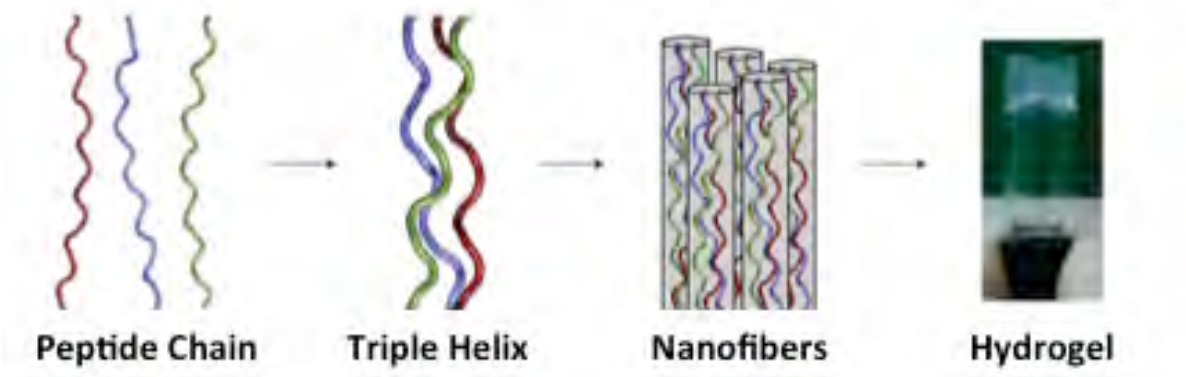

Figure 4.6. Assembly of collagen type I. The peptide chains form triple helices with approximately 100-200 nm in length and then are assembled via the staggered lateral packing into nanofibers which form a hydrogel. Image adapted from [42].

Collagen type I is soluble in acidic conditions, but changes in pH, ionic strength and temperature trigger the self-assembly process described in Figure 4.6, where hydrogels are formed in a very fast way. The conditions to obtain those gels are very mild for encapsulation of cells and labile molecules, leading to develop strategies for tissue engineering applications.

IV. Alginate

Alginate is an anionic polysaccharide extracted from brown algae or produced by some bacteria. It is a linear unbranched copolymer composed by blocks of β-D-mannuronic acid (M) and α-L-guluronic acid (G) residues linked by 1,4-glycosidic bonds. Both residues are covalently linked in different sequences, namely, rearranged in homopolymeric (GG blocks and MM blocks) or heteropolymeric block structures (GM blocks). Alginate-based gels have been widely explored and used in biomedical applications due to their minimal toxicity, low cost and easy processing. Alginate-based hydrogels could be formed in a fast way via ionic interactions between carboxylic acids and divalent cations such as Ca^{2+}, Mg^{2+} and Ba^{2+} - Figure 4.7. The crosslinking of the alginate via ionic interactions have been demonstrated to be mild for cell encapsulation, unlike other covalent crosslinking strategies. The main disadvantage of alginate for cell encapsulation is related with the absence of anchorage points for adhesive cells. For these purposes the functionalization of the alginate with RGD domains [43] has been proposed or the re-formulation of the system adding specific molecules capable to promote cell adhesion.

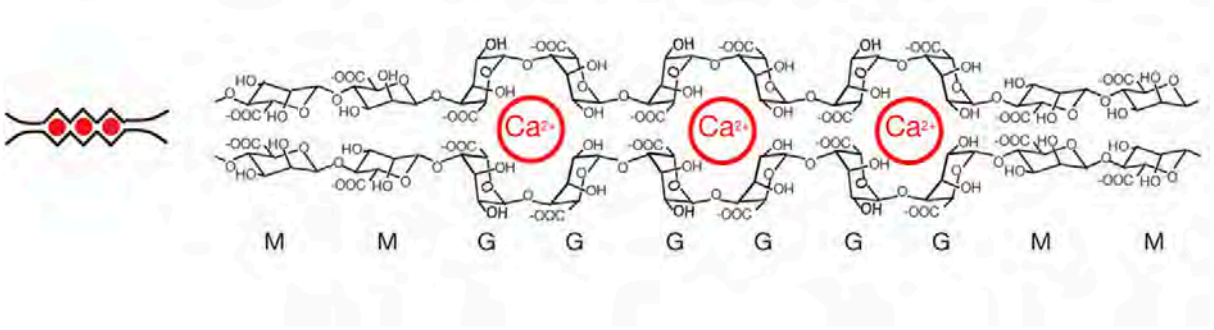

Figure 4.7. Alginate-based hydrogels could be prepared by ionic crosslinking following an egg-box model. The Ca^{2+} ions are placed in the interstices of guluronate blocks of one polymer chain and junctions with the guluronate blocks of adjacent polymer chains are formed. Image adapted from [44].

Alginate has been the most explored polymer for cell encapsulation purposes due to its abundance, water solubility, mild gelling properties and biocompatibility [45-47]. In addition, it is being used in proof of concepts or as controls to other polymers in cell encapsulation purposes [48]. Due to the resemblance to the natural ECM [21], alginate systems have been successful in encapsulation of transplanted cells,

providing immunoisolation for the cells and avoiding the need of immunosuppression additional treatments [49, 50].

Alginate spherical gels obtained by ionic crosslinking with Ca^{2+} ions and encapsulating different types of cells were prepared in various chapters of this thesis. Differently from the conventional procedures to prepare alginate particles, here the use of superhydrophobic surfaces methodology avoided the use of coagulation baths. In the chapter 6, alginate particles containing L929 cells were used as controls in order to evaluate the efficiency of the strategy used to encapsulate cells in chitosan gels. In chapter 8, alginate particles were prepared encapsulating a protein (fibronectin, FN) and cells (mesenchymal stem cells, MSCs), and subsequently studied as a suitable system for bone regeneration. In chapter 9, cells (L929 cells) were encapsulated into alginate layers with the aim to proof the concept that superydrophobic surfaces methodology is a suitable procedure to prepare compartmented particles, namely core/shell.

4.1.2.2. Cyclodextrins: γ-cyclodextrins

Cyclodextrins (CDs) are a family of cyclic oligosaccharides composed by glucopyranose units linked by α-(1,4) bonds. There are three main types of CDs (α, β and γ, Table 4.1) which are composed by 6, 7 or 8 α-(1,4)-linked glycosyl units, respectively [51]. CDs are obtained as a result of intramolecular transglycosylation reaction from degradation of starch by cyclodextrin glucanotransferase enzyme. The most important characteristic of the CDs is the ability to form inclusion complexes, *i.e.* host-guest complexes with hydrophobic solid, liquid and gaseous compounds. Molecular complexation occurs inside the hydrophobic cavity of the CDs and no covalent bonds are formed. The complexation occurs through the release of water molecules from the cavity. This displacement is caused by the hydrophobic guest molecules to attain an apolar-apolar association, decreasing the CD ring strain and achieving a more stable energy state. This is a dynamic equilibrium [51].

Table 4.1. Properties of the most common CDs. Table adapted from [51].

Property	α-Cyclodextrin	β-Cyclodextrin	γ-Cyclodextrin
Number of glucopyranose units	6	7	8
Molecular weight (g/mol)	972	1135	1297
Solubility in water at 25 °C (%, w/v)	14.5	1.85	23.2
Outer diameter (Å)	14.6	15.4	17.5
Cavity diameter (Å)	4.7–5.3	6.0–6.5	7.5–8.3
Height of torus (Å)	7.9	7.9	7.9
Cavity volume ($Å^3$)	174	262	427

CDs have been widely used in pharmaceutics approaches due to their capacity to form inclusion complexes with hydrophobic bioactive agents. Currently, it is well known that poor water-soluble drugs

prevent the achievement of therapeutic concentrations in physiological fluids, being required innovative strategies to circumvent these limitations. CDs may be used as building blocks in drug delivery systems because their capacity to host bioactive agents is enhanced when they self-assemble to form aggregates, crosslink together or copolymerize with other compounds. Consequently, each obtained carrier has a particular drug release kinetic [52]. In addition, all types of CDs are non-toxic when administered orally due to lack of absorption from the gastrointestinal tract. Through parenteral administration, γ-CD, 2-hydroxypropyl-β-CD, sulphobutylether β-CD, sulphated β-CD and maltosyl β-CD appeared to be safe. Since the γ-CDs (Figure 4.8) are the less studied and having into account that such molecules have also interesting properties for medical applications when compared with α- and β-CDs (insignificant irritation, rapid and complete degradation into glucose units by intestinal enzymes and less toxicity than the other types), we select them to be used in the work presented in chapter 5. It was hypothesized that the performance of dextran-MA particles in loading and releasing a hydrophobic drug (dexamethasone) could be improved if CDs were incorporated in the network. Two formulations were prepared and studied: dextran-MA particles containing free γ-CDs and Dex-MA particles containing γ-CDs as structural monomers.

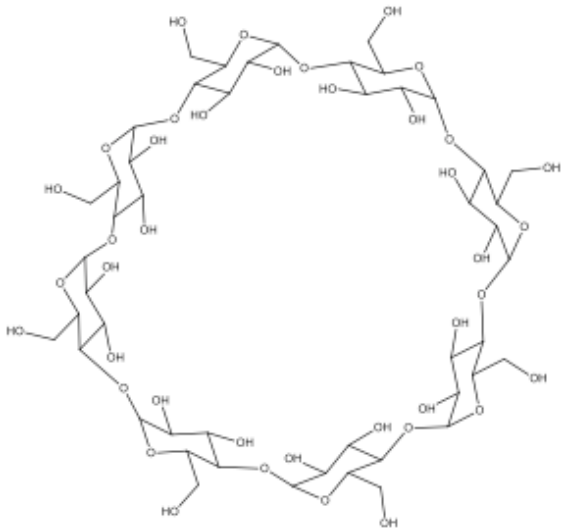

Figure 4.8. Structure of the γ-CD.

To obtain the monomers of CDs, these molecules were modified by functionalizing their structure with methyl groups [53] capable to establish covalent linkages with Dex-MA or between γ-CD monomers. Acrylamidomethyl-γ-CDs (γ-CD-NMA) (Figure 4.9) were synthesized mixing 17.12 g of γ-CD and 13.36 g of (hydroxymethyl)acrylamide (NMA) in 50 mL of HCl solution (1% v/v). The solution was stirred and kept at

80 °C for 30 min. The precipitation of the γ-CD-NMA was induced by adding 300 mL of acetone. The suspension containing the γ-CD-NMA was stored overnight at 4 °C and after filtered and washed with acetone (2-3 cycles). The collected product was dried under vacuum for 2 days at room temperature and stored at 4 °C.

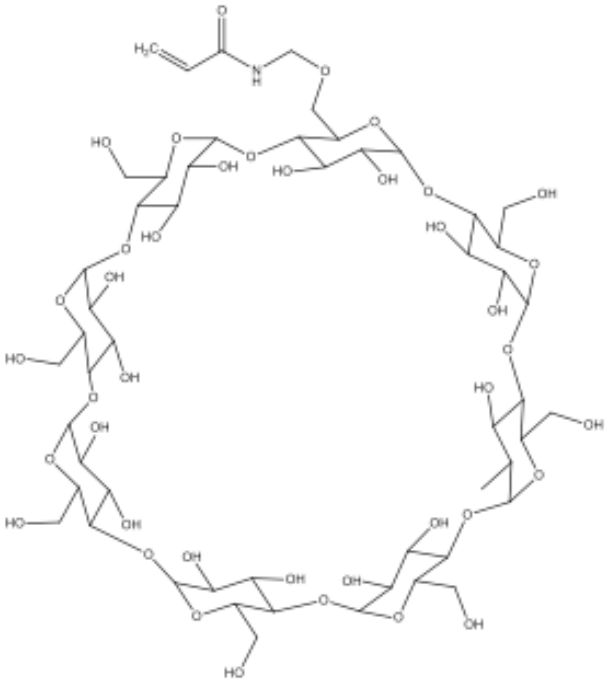

Figure 4.9. Structure of the γ-CD-NMA.

4.1.2.3. Bioactive Agents

I. Dexamethasone

Dexamethasone is a small drug (MW 392.46) that acts as anti-inflammatory and immunosuppressant, and it is also known to stimulate the up-regulation of same major bone-related genes during osteogenesis [54]. When used as stimulus for cell osteo differentiation, it causes variations in cell proliferation, up regulation of alkaline phosphatase (ALP) and increases the mineral deposition. This synthetic glucocorticoid was employed in chapter 5 and 6. Such type of drugs has appeared as alternatives to growth factors (GFs) in musculoskeletal regeneration. The small size of those drugs does not trigger immune responses. In addition, the bioactivity of the small molecules does not require structural integrity and are, in comparison with recombinant proteins, inexpensive compounds. Small drugs are capable to diffuse across the cell membrane to reach the target acting as signaling molecules. The optimal concentration to achieve the osteogenic differentiation is between 10 and 100 nM; concentrations above 1000 nM trigger side effects

and prolonged exposures cause osteoporosis. Then, the encapsulation and controlled release is an interesting strategy to overcome those problems.

Dexamethasone is a hydrophobic bioactive agent, being difficult to encapsulate high quantities of this drug inside hydrophilic matrices. A recurrent strategy is to dissolve it in an organic solvent (e.g. ethanol, chloroform, DMSO, among others) and then dilute the concentrated solution in aqueous buffers (strategy used in chapter 6). However, traces of such aggressive solvents may remain in the developed formulations, turning the systems not appropriate for certain applications. A different approach to load hydrophilic matrices with dexamethasone was evaluated in chapter 5. The loading capacity of Dex-MA hydrogels as well as the release profile of dexamethasone were studied in detail when γ-CDs were included in the particle network. No organic solvents were required to load the particles with this hydrophobic drug.

II. Platelet Lysates

Platelet cells are key components in homeostasis, in stimulation of connective tissue and revascularization. These small cells, with a regular shape and 2-3 μm in diameter, have a lifespan of 5-9 days. The physiological range of platelets in humans varied from 150 to 400 x 10^9 cells/L, circulating normally in the blood. The blood is composed by 93% erythrocytes, 6% platelets and 1% white blood cells. In the body, the platelets are activated when contact with von Willebrand factor, collagen and by thrombin action. Upon activation they secrete the content of their alpha (responsible for the platelet adherence to the endothelium) and dense granules (responsible for the activation of the intrinsic coagulation pathway). In addition, the GFs released by the platelets have a role in the healing, namely in inflammation, proliferation and remodeling processes [55].

Human platelet lysates (PLs) have been successfully used as substitute of fetal bovine serum (FBS) in cell cultures avoiding the risk of xenogeneic immune reactions or transmission of bovine pathogens [56].

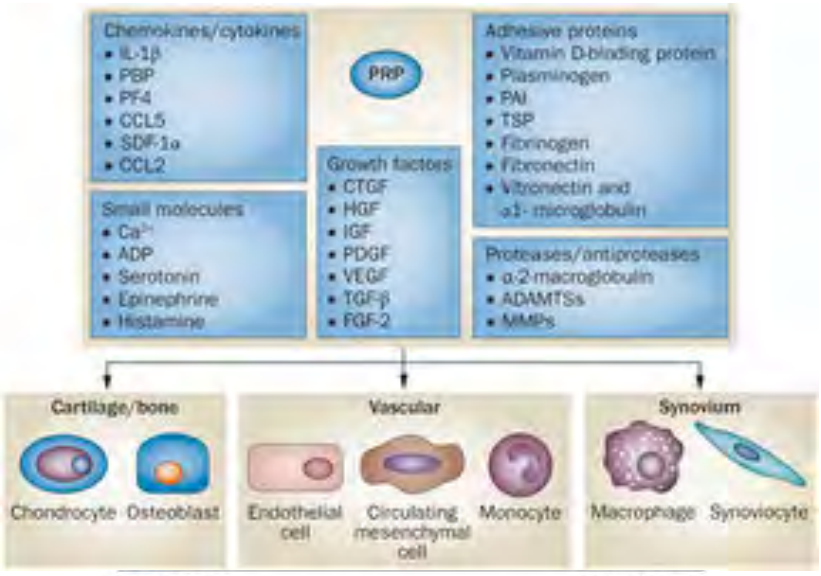

Growth factor	Content (ng/mL)
Platelet-derived growth factor (PDGF)-AB	~50–300
PDGF-BB	~10–30
PDGF-AA	~1–10
Tumor growth factor (TGF)-β1	~50–300
TGF-β2	~0.5
Brain-derived neurotrophic factor (BDNF)	~10–50
Vascular endothelial growth factor (VEGF)	~5–20
Endothelial growth factor (EGF)	~0.5–20
Insulin-like growth factor (IGF)-1	~50–200

Figure 4.10. – Molecules secreted by platelets: signaling proteins (growth factors, chemokines and other cytokines), adhesive proteins and proteases, and small molecules. The table describes the approximate contents of GFs in human PL. Image adapted from [55] and table from [57].

PLs are obtained from the blood, which in turn is centrifuged to separate the platelets from the other cell types. Upon activation, platelets release a pool of biologically active proteins and other substances (Figure 4.10) constituting an appealing autologous source of GFs for biomedical applications. There are several methods to induce the release of the GFs from the platelets: adding bovine thrombin, calcium chloride, collagen type I and by mechanical disruption through freeze-thaw cycles. In chapter 7, PLs from different apheresis collections were processed by freeze-thaw methodology, which is a simple, fast and cheap method, and it was demonstrated to be more efficient in platelets activation than other techniques [58,59]. The blood samples used to prepare the PL were obtained at Galicia Blood Transfusion Center (Spain) from three different donors. The samples were centrifuged at 1400 rpm, at 25 °C, during 15 min. The plasma was collected carefully in order to not mix with the red blood cells deposited at the bottom of the centrifuge tubes. Then, three cycles of frozen at -80 °C and heating at 37 °C were performed to the collected plasma in order to cause the disruption of the platelet membranes to release their content. After

this step, the samples were again centrifuge at 4 °C, 12000 rpm for 12 min with the aim to remove remaining platelets and potential antigens. The supernatant was carefully collected and stored at -80 °C. The concentrated PLs were obtained by PL lyophilization in aliquots of 1 mL followed by their reconstruction in adequate volumes of PBS pH 7.4 to obtain the desired concentrations: 500 µl or 333.33 µl to obtain the PL concentrated 2x and 3x, respectively.

III. Fibronectin

Fibronectin (FN) was entrapped in alginate particles in chapter 8. This is a large multifunctional glycoprotein (≈450 KDa), present in ECM, and involved in numerous physiological processes: cell adhesion, spreading, migration, differentiation and survival as well as wound healing [60-62]. It is composed by homologous repeating structural motifs designed type I, II and III modules. Those motifs are grouped together into functional domains with specific biological activities. This protein has protein-protein interaction sites distributed along the FN structure and cell binding sites localized in FNIII: RGD28 on FnIII10 and the synergy site PHSRN on FnIII9 [63,64] – Figure 4.11. Due to the well-known effect on cell behavior, FN was selected to integrate in the alginate mesh in order to provide adhesion sites for the cells as well as to improve the general performance of the system.

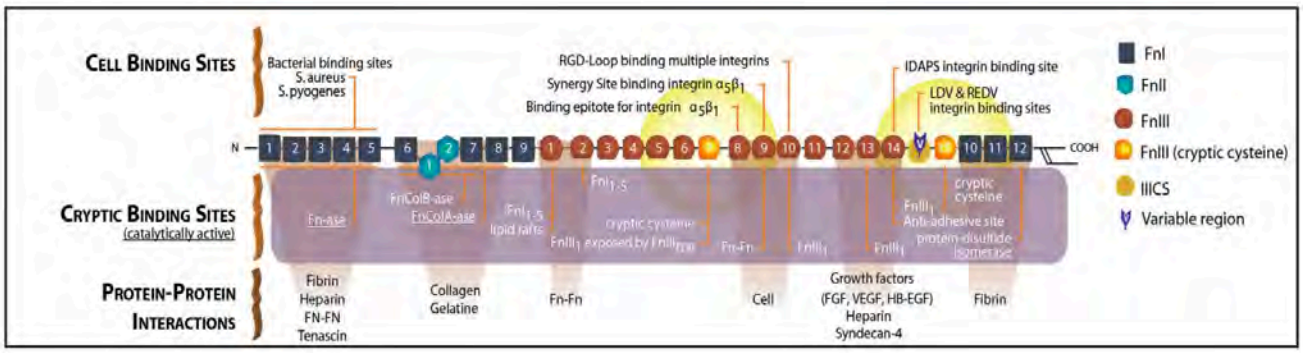

Figure 4.11. Fibronectin structure with its binding sites. FN contains cell binding sites (RGD28 on FNIII10 and the synergy site PHSRN on FNIII9) and protein-protein interaction sites. Image from [64].

Adsorbed FN onto scaffolds [65], as a coating layer, was a strategy employed to promote cell adhesion onto the PCL fibers as well as in chitosan/alginate scaffolds [66]. In other strategy, hydrogels matrices where FN was immobilized in a hyaluronic acid network also demonstrated to be effective in enhancement of cell adhesion [67]. In addition, the inclusion of FN in an alginate hydrogel matrix contributed to improve the regeneration of nerves [68]. In chapter 8, FN was mixed with alginate where mesenchymal stem cells were entrapped. The effect of the FN on cell viability was studied.

4.1.2.4. Cells Immobilized in the Hydrogel Particles

I. Cell Lines

Cell lines have the particularity to proliferate indefinitely, this means that they have unlimited cell division and an infinite lifespan, being also named immortalized cells. Such modification in cell growth control is generally induced by viral or tumorigenic transformations. In addition, cell lines are not susceptible to being differentiated. Cell lines are suitable to study a number of biological responses *in vitro*, offering the advantage of being more homogeneous and standardized than primary cells. In chapters 6 and 9 L929 cells were encapsulated into the hydrogel spherical gels. L929 cells (purchased from European Collection of Cells Cultures - NCTC clone 929 ATCC®CCL-1™) are fibroblasts isolated from *Mus Musculus* mice. These adherent cells are suitable for toxicity testing. L929 cells were expanded at pH 7.4 in low-glucose DMEM supplemented with 3.7 g/L sodium bicarbonate, 10% (v/v) FBS and 1% (v/v) penicillin-streptomycin. The cells were incubated at 37 °C in humidified air atmosphere of 5% CO_2 in 75 cm^2 flasks. At approximately 90% of confluence the cells were washed with PBS, and collected by adding 0.05% trypsin-EDTA for 5 min at 37 °C. Tripsyn-EDTA is a mixture of proteases derived from porcine pancreas and due to its digestive strength; it is widely used for cell dissociation, routine cell culture passaging and primary tissue dissociation. After the detachment of the cells, the trypsin was inactivated by adding fresh cell culture medium. The cell suspension obtained was then centrifuged at 300 *g* at 25 °C. The supernatant was discarded and the cell pellet was suspended in a neutralized chitosan (chapter 6) or sodium alginate (chapter 6 and 9) solution in order to be encapsulated.

II. Primary cells

Primary cells are cells obtained directly from the subject and maintained for growth *in vitro*. The main advantage of primary cell cultures is that they mimic more closely the physiological state of cells *in vivo*, generating more relevant data. When compared with cells containing mutations and chromosomal abnormalities (*e.g.* cell lines), which provides poor indicators of normal cell phenotype and progression of early-stage diseases, primary cells are considered the best representatives of the main functional component of the tissue *in vivo* from which they are derived. Primary cells undergo a limited, predetermined number of cell divisions before entering senescence. In addition, such cells are quite fastidious. They require optimized growth conditions, where tissue specific cytokines and GFs are necessary for their propagation in serum-free or low-serum growth media. The cell types most frequently found in primary cell culture are epithelial cells, fibroblasts, keratinocytes, melanocytes, endothelial cells, muscle cells, hematopoietic and mesenchymal stem cells. In this thesis, two primary cell types were used.

In chapter 7, human adipose derived stem cells (hASCs) (StemPRO® purchased from Gibco®) isolated from human lipoaspirate tissue were expanded to 5-8 passages and encapsulated in hydrogel particles. The characterization of these cells by the supplier demonstrated very similar phenotypic and functional characteristics to bone-marrow-derived mesenchymal stem cells, being capable to differentiate into multiple mature cell phenotypes *in vitro:* adipocytes, osteoblasts, and chondrocytes. These cells also could be differentiated into non-mesenchymal cell types: neuronal and glial progenitors, hepatocytes and vascular endothelial progenitors, cardiomyocytic, pancreatic and epithelial phenotypes. Another particularity of those hASCs is their capacity to secrete pro-angiogenic, immunomodulatory and anti-apoptotic factors [69-76]. hASCs are interesting cells for studies of cell differentiation and tissue engineering strategies with potential to be used in clinical applications. hASCs were expanded in appropriate media supplied by Gibco®: MesenPro® supplemented with 2% (v/v) growth supplement (FBS), 1% (v/v) L-glutamine and 1% (v/v) penicillin/streptomycin. The cells were maintained in humid conditions at 37°C and 5% CO_2. Upon confluence, the cells were tripsinised and the obtained cell suspension was centrifuged. The pellet of the cells was then suspended in a polymeric solution to prepare the hydrogel spherical systems.

In chapter 8, it was used mesenchymal stem cells isolated from Wistar rats femoral bone marrow (rMSCs), using protocols reported in literature [77,78]. The isolation and characterization of the obtained cells was performed by the group that collaborates in the experimental activities under the scope of this work (CICS, University of Beira Interior). Autologous MSCs were selected according to the aim of the work, this means capacity to regenerate bone. It is known that rMSCs could be differentiated into mesodermal lineage cells including osteoblasts, chondrocytes, muscle cells, adipocytes and tenocytes when properly stimulated [79]. rMSCs were expanded in DMEM-F12 supplemented with 10% (v/v) FBS, penicillin (100 U/cm^3), streptomycin (100 μg/cm^3), and amphotericin (0.25 μg/cm^3) at 37 °C and 5% CO_2 humidified atmosphere. After reached the confluence, the cells were collected using 0.18% trypsin in 5mM EDTA for 3-5 min at 37 °C, posteriorly neutralized with fresh cell culture medium. The cell suspension was centrifuge and the cells were used to encapsulate in hydrogel beads.

4.2. Characterization of the Modified Materials

4.2.1. Fourier Transform InfraRed

Fourier transform infrared (FTIR) is a spectroscopy technique where the IR radiation passes through the sample and part of the radiation is absorbed by the sample and the other part is transmitted. The obtained spectrum represents the molecular absorption/transmission and results from transitions

between vibrational energy states, ranging from simple coupled motion of two atoms in a diatomic molecule to a more complex motion in large polyfunctional molecules. Each spectrum is unique, and it is possible to detect specific functional groups and identify compounds [80]. FTIR is a very fast technique and requires very small amounts of samples. The samples should be as dried as possible in order to avoid the interferences of water molecules.

In chapter 5, FTIR was used to verify if the γ-CD were modified as expected. This was achieved by detecting the group added onto the γ-CD by measuring characteristic absorption and comparing it with the spectra of the unmodified γ-CD. The samples in a powder form were mixed with KBr in order to form a pellet to be analyzed. KBr is a commonly used material because it has good transmission properties, not exhibiting peaks and thus not interfering with the spectrum of the added substance. The IR spectrum was recorded over the range 400-4000 cm^{-1} (Bruker IFS 66V FT-IT).

4.2.2. Proton Nuclear Magnetic Resonance

Nuclear magnetic resonance (NMR) is a recurrent technique to determine the structure of organic molecules as well as interaction of various molecules and the composition of mixtures of biological or synthetic solutions or composites. The principle of NMR is that the nuclei of elemental isotopes have a characteristic spin. When subjected to a strong magnetic field, the nuclei resonate at a characteristic frequency in the radio frequency range of the electromagnetic spectrum. This means that when an external magnetic field is applied could occur an energy transfer between the base energy to a higher energy level. Such energy transfer happens at a certain wavelength that corresponds to radio frequencies, and when the spin returns to its base level energy is emitted at the same frequency. Then, this signal is detected and processed [81]. Pronton NMR (^{1}H NMR) was performed in chapter 5 to characterize the modified dextran and γ-CDs. Using this technique, the number of protons in a molecule, the groups attached and the number of "neighbor" hydrogen atoms were detected. The ^{1}H NMR spectra were recorded (Mercury 300, 300MHz) dissolving 0.3 g of modified and non-modified dextran in 0.7 mL of deutered water and 30 mg of γ-CD and γ-CD-NMA in 1 mL of deutered water. The degree of substitution was determined using the integral of key protons existent in the groups added to the dextran and γ-CD. The description of the peaks and equations used are described in detail in chapter 5.

4.3. Preparation of Spherical Hydrogel Particles Using Biomimetic Superhydrophobic Surfaces

In this thesis, two main types of particles were produced using the PS or Cu biomimetic superhydrophobic surfaces: simple particles composed by homogeneous matrices and multicompartmented core/shell and multilayered particles. According to the material used, adequate procedures to harden the particles were used. A detailed description of the procedure used to obtain each system developed under the scope of this thesis, will be present in the follow subsections.

4.3.1. Simple Homogeneous Matrices

Homogeneous matrices were obtained by dispensing a solution containing the polymer or the precursors monomers as well as the bioactive agents or cells that were desired to encapsulate, onto the superhydrophobic surface. Micropipettes were used as dispensing systems and the volumes dispensed could be controlled adjusting the volumes of these devices. However, using this kind of dispensing systems volumes lower than 2 µL were not possible to be dispensed, preventing the preparation of smaller particles. The hardening of the particles was achieved by adequate procedures selected according with the polymers used. In the Figure 4.12 are summarized the systems proposed:

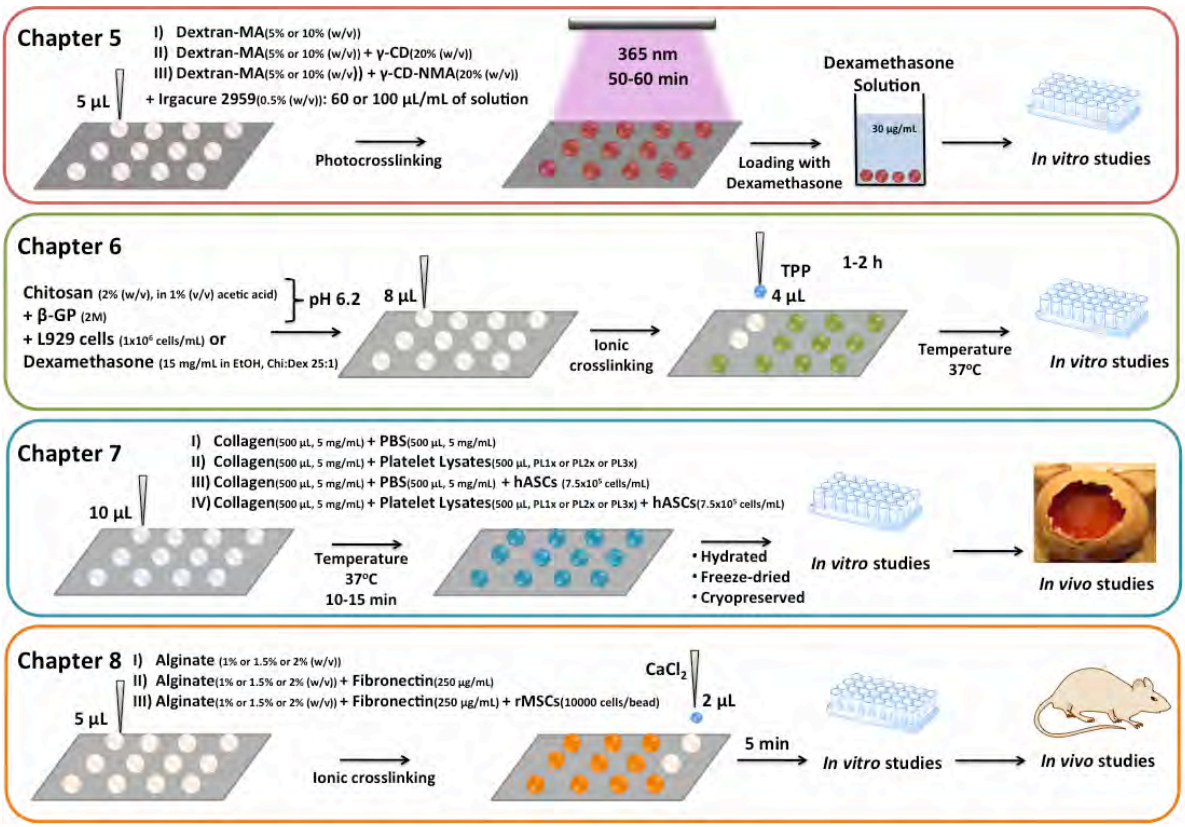

Figure 4.12. Schematic representation of the procedures to prepare the different homogeneous matrices proposed in this thesis.

4.3.2. Core/Shell and Multilayered Particles

Particles with more complex structures were also prepared using the superhydrophobic surfaces methodology. Core/shell and multilayered particles were prepared and are described in chapter 9. Both types of particles were obtained by subsequent deposition of liquid droplets onto the superhydrophobic surfaces followed by a crosslinking to obtain the core structure. The core/shell particles were finalized by dispensing another amount of a liquid precursor solution onto the hardened cores. The liquid coated the solid core, and upon hardening it formed a shell layer. The multilayered particles were obtained in the same way, but repeating the process until reach the desired number of layers – Figure 4.13. It was observed that the number of layers was limited by the effect of the gravity, which caused the deformation of the spheres. Different applications were proposed to use the core/shell and multilayered particles; the details are extensively described in the chapter 9.

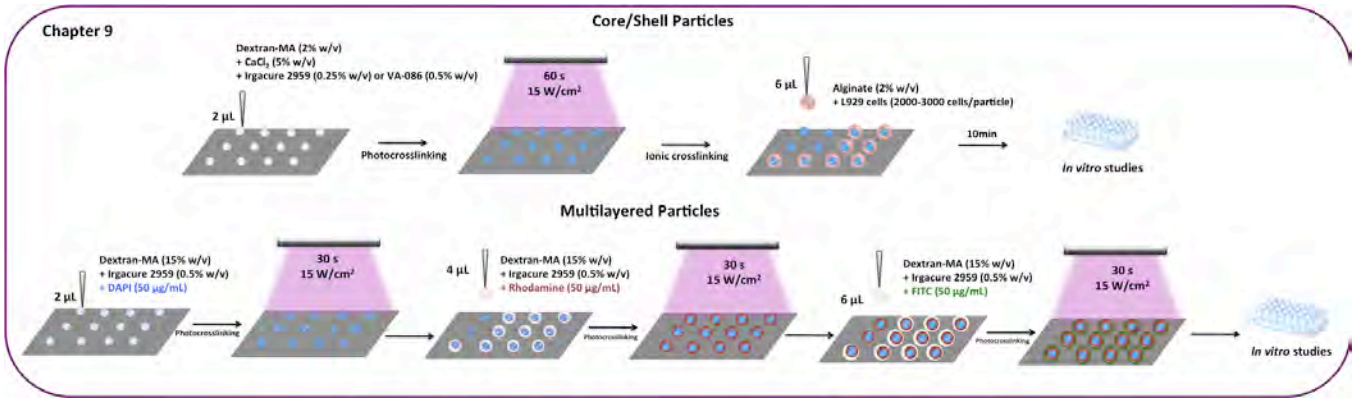

Figure 4.13. Schematic representation of the procedure to prepare multicompartmentalized spherical particles (core/shell and multilayered) using the superhydrophobic surfaces methodology.

4.4. Characterization of the Particulate Systems

4.4.1. Particle Size

The size of the systems developed under the scope of this thesis was accurately measured. The particles were examined using a stereomicroscope and images obtained using a camera coupled to the stereomicroscope. Then, using an image treatment software such as ImageJ and Soft Imaging System®, the diameter of the particles was measured.

4.4.2. Degree of Swelling

An intrinsic property of the hydrogel networks is related to the capacity to retain high amounts of water in their structure. The evaluation of degree of swelling of each hydrogel is an important parameter to characterize these systems. The extension of the swelling in the presence of a liquid (generally, water) is

dependent on the several factors such as the nature of the polymer that compose the mesh and the degree of the crosslinking. The degree of swelling of the systems proposed in chapter 5 and 6 was measured based on the follow equation (eq.):

$$\%\text{Swelling} = \frac{m_i - m_0}{m_0} \times 100 \quad \text{Eq. 1}$$

where m_i and m_0 are the weights of the swollen and dry beads, respectively.

A certain number of particles were immersed in a medium (selected according to the applications and characteristics of the system) and at pre-defined time points, the particles were collected. The excess of the medium was removed with a filter paper and the samples were immediately weighted. The details related with number of particles used in the experiment and the medium content are described in each corresponding chapter.

4.4.3. Morphological Characterization

Scanning electron microscopy (SEM) is a commonly used technique to analyze the topography of the solid materials and structures. This procedure consists in the use of a focused beam of high-energy electrons capable to generate signals at the surface of the solid sample. The accelerated electrons carry significant amounts of kinetic energy and when interact with the surface of the material they are decelerated and part of the energy is dissipated. Consequently, a variety of signals are generated. The electron-sample interactions (secondary electrons) are collected from a selected area and the information related with external morphology (texture) is translated in a 2D image. The main advantage of SEM relies on the examination of the topographical features at high magnifications, allowing the observation of the morphology at sub-micron scales.

In this thesis, SEM was employed in chapters 5, 7 and 8 for the assessment of surface of the particles as well as the inner morphology when the particles were previously sectioned. Prior to analysis, all the samples were coated with a conductive material (gold) by sputtering, with the aim to increase the degree of magnification avoiding the damage of the samples by the high-energy electron beam. Freeze-dried or air-dried particles were immediately coated with gold and visualized. Particles in a hydrogel state were firstly fixed in 0.25-2.5% (v/v) glutaraldehyde, overnight, at 4 °C. Then, the particles were dehydrated in ethanol solutions (70%, 80%, 90% and 100%) for at least 10 min each and finally coated with gold and observed.

4.4.4. Mechanical Properties

The mechanical properties of the hydrogels proposed in chapter 6 were evaluated by dynamic mechanical analysis (DMA). The test consists in applying an oscillatory force to the sample followed by the analysis of the sample response to that force. This technique allows obtaining information about the mechanical properties of materials as a function of time, temperature and frequency. The properties may be expressed in terms of elastic modulus, viscous modulus and damping capability. The samples need to have specific geometries such as cylinders or cubes in order to have a uniform distribution of the applied load during the compression experiments. In the analysis of spherical samples, the load is applied on the top of the sphere and non-accurate results could be obtained. Having this in consideration, gels were prepared in 96-well plates exhibiting a cylindrical shape following the same procedure and the same proportions of materials as described for the fabrication of spherical systems onto the superhydrophobic surfaces. Data was collected using a range of frequencies between 0.1 and 15 Hz, under physiologic simulated conditions, this means immersed in PBS pH 7.4. The strain amplitude was constant and was approximately 1% of the original height of the sample. Before initialization of the test, a small preload was applied to ensure the contact between the sample and the compression plates. The effect of temperature on the mechanical properties of the gels was evaluated by collecting data at two temperatures: 20 °C and 37 °C.

4.4.5. Double Bond Detection

The presence of double bonds (C=C) in the particles formulated in the chapter 5 was evaluated by using the bromine test. The presence of double bonds means that the particle was not completely crosslinked, being C=C bonds available to establish linkages. Bromine test is a simple qualitative assay to detect the presence of carbon to carbon double and triple bonds and also phenols. The bromine solution has a characteristic yellow-orange color and reacts with sites of unsaturation through an addition reaction. The reaction is represented in Figure 4.14.

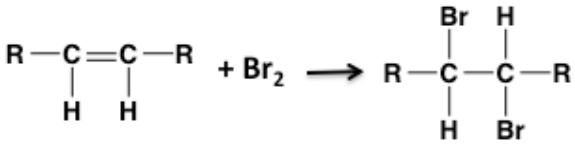

Figure 4.14. Reaction of bromine with unsatured compounds.

This test was performed to ascertain whether all the double bonds were consumed. Particles (8 spherical gels) of each formulation were immersed in 200 μL of bromine solution. The bromine aqueous solution was composed by 32 mL of water, 7.6 mL of NaClO (33 mg/mL) and 10.7 mL of NaBr solution (1.1 g of NaBr in HCL (1M)). The color of the solutions, after 5 minutes, was compared with equivalent amounts of precursor liquid solutions and the original bromine solution.

4.4.6. Quantification of Unreacted Photoinitiator

The quantification of the exceeding photoinitiator in the formulations described in chapter 5 was determined by high-performance liquid chromatography (HPLC). HPLC is a method that allows the separation of the components, their identification and quantification. This method is particularly useful when the sample is a mixture of molecules and when the compound that is desired to quantify is present in small amounts. The technique consists in the passage of the sample mixture through a column filled with a solid adsorbent material. In the column, the compounds of the sample are separated due to differences in interaction with the adsorbent material (physical interactions), which cause different flow rates. The compounds that are more strongly attracted to the adsorbent material slowed down, while the other compounds move faster. The sample is injected in the column (stationary phase) mixed with a pressurized solvent that is referred as the mobile phase. Both composition of the mobile phase and temperature influence the interactions on the sample with the adsorbent material in the column and consequently the separation of the products. After the compounds of the sample being separated, a signal correlated to the amount of each one is generated by a detector (e.g. UV/VIS or mass spectrometry).

The unreacted photoinitiator (Irgacure 2959) released from the photocrosslinked particles was quantified after particles immersion in acetonitrile to release all traces of unconsumed molecule. Three particles of each formulation were immersed in 1 mL of acetonitrile and kept under stirring for at least 6 h. The mobile phase used was composed by acetonitrile:water (90:10) and the sample was injected in the column (Accucore C18, 3 mm x 150 mm, particle size 2.6 μm) with a flow rate of 0.5 mL min^{-1}. The column was kept at 37 °C and the Irgacure 2959 was sensed by a UV-VIS detector (SpectraSystem UV8000).

4.4.7. Drug Loading

In chapter 5, the particles prepared were loaded with a hydrophobic drug (dexamethasone) after being crosslinked. The different formulated particles were immersed in an aqueous solution of dexamethasone (30 μg/mL, 10 particles in 10 mL of drug solution). The total amount of dexamethasone loaded in each

formulation was determined by UV-VIS spectrophotometry (described in detail in the subsection 4.4.10.1 of this chapter). Part of the dexamethasone loading was due to the swelling capacity of the formulations, this means the dexamethasone dissolved in the amount of water uptake by the particles. The other part is due to the improved affinity of the system caused by the presence of CDs. Then, the amount of drug loaded via equilibrium due to the water uptake capacity of the particles was estimated following the eq. 2 [82]

$$\text{Loading (aqueous phase)} = \left(\frac{V_s}{W_p}\right) \times C_0 \quad \text{Eq. 2}$$

where V_s is the volume of water sorbed by each particle, W_p is the weight of the particle in a dry state and C_0 is the concentration of drug in the loading solution.

Dextran particles combined with CDs were designed to have a special affinity to uptake hydrophobic drugs. Then, the partition coefficient $K_{N/W}$ between the particles and the loading solution was determined from the equation:

$$\text{Loading (total)} = \frac{(V_s + K_{N/W} \times V_p) \times C_0}{W_p} \quad \text{Eq. 3}$$

where V_p is the volume of the dried particles, and the other parameters are the same of Eq. 2. This parameter was important to determine the differences in drug loading capacity between systems without CDs, with free CDs and copolymerized CDs.

4.4.8. Distribution of Molecules Inside the Particles

The spatial distribution of bioactive agents inside the particles was visualized using widefield fluorescent microscopy. In this technique, the labeling of the bioactive agents, materials and even cells with a fluorophore is required. The samples are excited and then emitted light in a certain wavelength allowing the visualization of the sample. Each fluorophore has a specific excitation and emission wavelength. The labeled samples were maintained in the dark in order to prevent the rapid loss of fluorescence.

In chapter 8, the distribution of the FN was observed by modification of the protein with Alexa fluor 555 dye. A solution of FN (1 mg/mL) was modified. Briefly, 50 µL of sodium bicarbonate solution (1 M) were mixed with FN solution in order to increase the pH of the solution because the succinimidyl esters involved in the reaction between Alexa fluor 555 and FN react efficiently at pH 7.5-8.5. This solution was mixed with Alexa fluor 555 under magnetic stirring for 1 h. Finally, the labeled protein was purified using a

column with Bio-Rad BioGel P-30 Fine size exclusion purification resin. The particles encapsulating the labeled protein were prepared following the same procedure as described in the subsection 4.3.1 of this chapter. The particles were then visualized using a widefield fluorescent microscope (Stemi 1000 PG-HITEC Zeiss) applying appropriate filter for excitation (555 nm) and emission (565 nm).

In chapter 9, three fluorophores were encapsulated in the particles as models of drugs: 4′,6-diamidino-2-phenylindole (DAPI), Rhodamine B and fluorescein-5(6)-isothiocyanate (FITC). They were encapsulated in the different layers of the particles, just by mixing 50 μg of their powder with 1 mL of dextran-MA (15% (w/v)) solution. Then the particles were sectioned, using a bisturi, and visualized using widefield fluorescent microscope (Stemi 1000 PG-HITEC Zeiss) in order to observe the distribution of the different molecules in the particles.

4.4.9. Enzymatic Degradation Assay

The degradation of biomaterials is an important characteristic of implantable systems in the human body. In the case of drug release systems this is particularly relevant because it will also influence the release kinetic of the molecules. The effect of the presence of PLs in the degradation of Coll particles was performed in an extremely harsh environment (chapter 7). Considering that one possible application of this system is the treatment of skin ulcers, where a significant amount of enzymes capable to degrade the proteins of the ECM are concentrated, it is important to know the resistance of the systems under these conditions.

In chapter 7, the degradation of the particles was followed during 24h. Particles of each formulation (collagen solely and collagen combined with PL) were immersed in an enzymatic solution (collagenase 50 μg/mL in tricine buffer pH 7.5) at 37 °C. Images of the particles were collected using a camera connected to a stereomicroscope.

4.4.10. Drug Release Studies and Quantification Techniques

The release kinetics of the bioactive agents entrapped in the developed systems was studied *in vitro*. Drug release studies allowed having an insight about the potential of the system under controlled conditions, being particularly useful to redesign the systems when the release profile achieved does not follow the desired kinetics. To monitor the amount of the drugs released by the particulate systems, a defined number of particles was immersed in a release medium, pre-established according to the experimental design. Then, pre-defined volumes of release medium were collected and the amount of bioactive agent determined according to different procedures. The following subsections will describe the techniques used

in the quantification of the different released molecules. The experimental details, such as number of particles, volume of the release medium, volume of the release medium collected (sample) as well as the pre-defined times at which samples were collected are described in detail in the corresponding chapters of section III.

4.4.10.1. Ultraviolet–Visible Spectrophotometry

In chapters 5 and 6, the release of dexamethasone was followed by UV-VIS spectrophotometry. This technique is commonly used in analytical chemistry for quantification of substances, using light in the visible and ultraviolet ranges. This technique assumes that the absorbance characteristics of the liquid samples follow the Beer-Lambert law. According to this law, the absorbance is directly proportional to the path length and to the concentration of the specie in the solution. This means that, the absorbance of a solution increased when the attenuation of the light beam that cross the sample also increase. Different molecules absorb radiation in different wavelengths. The record of the release of a molecule through UV-Vis spectrophotometry requires a previous scan of the molecule absorbance spectrum in order to detect a defined peak suitable to be correlated with known concentrations. For example, the absorbance peak of dexamethasone was found at 241-242 nm. The following step was the construction of a calibration curve where the absorption values of solutions with well-known concentrations were correlated with the concentration values. The establishment of such correlations, usually based on a straight line function, permit to determine unknown concentrations using the absorbance measurements.

I. Bicinchoninic Acid Method

The total protein released from the particles of collagen+PL described in chapter 7 was determined by UV-VIS method. Firstly, a colorimetric assay based on bicinchoninic acid (BCA) method was performed. It was employed because it was not possible to have a defined absorbance peak of the samples and correlate it with known protein concentrations. The BCA method is based on reduction of Cu^{2+} to Cu^{1+} by the proteins in an alkaline medium (the buriet reaction). The Cu^{1+} cations are detected with high sensitivity using the reagent containing BCA. The chelation of two molecules of BCA with one cuprous ion formed a water-soluble purple-colored reaction product with a strong absorbance at 562 nm. The color formation depends on the macromolecular structure of the proteins, the number of peptide bonds and on the presence of four particular amino acids: cysteine, cysteine, tryptophan and tyrosine. Then, protein concentrations are determined with reference to standards, used to obtain a calibration curve. Generally bovine serum albumin (BSA) is the protein used to perform the standard solutions. However the standard selected

should exhibit structure as close as possible to the protein under study. This test is not specific; this means that all the proteins in the solution having the properties above mentioned are quantified.

II. Enzyme-Linked Immunosorbant Assay

The quantification of the released GFs, namely VEGF and PDGF-BB, as well as their content in the platelet lysates were determined by enzyme-linked immunosorbant assay (ELISA), in chapter 7. This method allows the quantification of small amounts of a specific protein when mixed in a cocktail of molecules. The principle of the method (Figure 4.15) consisted in the using of a 96-well plate coated with specific capture antibodies, where the target protein in the sample could bind. After, the biotin-labeled detection antibody could attach to the immobilized conjugate previously formed. Finally, HRP-conjugated streptavidin is added and then the colorimetric substrate solution. The intensity of the color developed is proportional to the amount of target protein bound. The absorbance of the samples was measured by UV-VIS spectrophotometry at 440 nm and then correlated with a calibration curve.

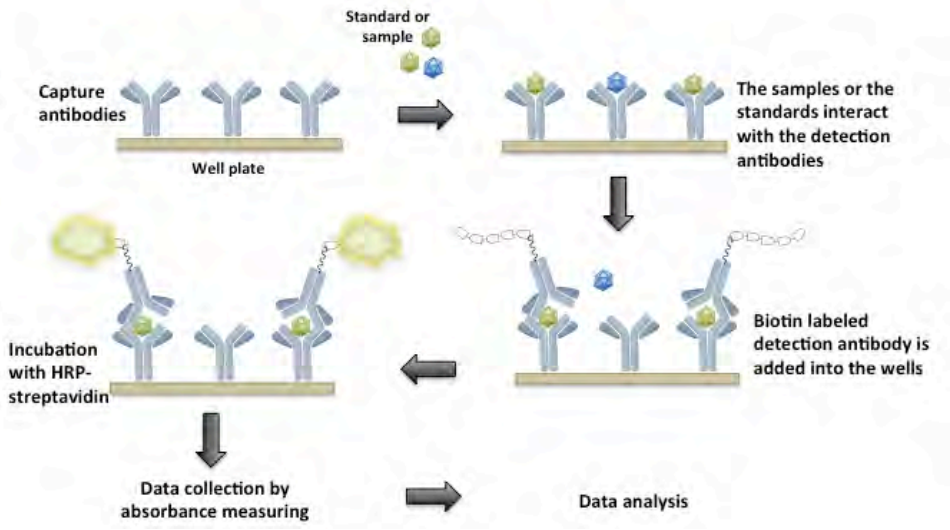

Figure 4.15. Schematic representation of the ELISA method.

4.2.10.2. Inductive Coupled Plasma Spectroscopy

This technique determines chemical elements in the samples. In chapter 8, inductive coupled plasma (ICP) allowed to quantify the Ca^{2+} released from the alginate beads to have an insight about the stability of the particles when immersed in cell culture medium. The samples collected were injected in the ICP equipment and the argon plasma excited the ions present in the samples. Then, the electrons emitted energy at a characteristic wavelength when they return to ground state. The light emitted was measured by an optical spectrometer, yielding an intensity measurement that was converted to concentrations by

comparison with calibration standards. In order to avoid the obstruction of the small pipes of the equipment, the collected samples were diluted in a HNO_3 solution (1% v/v) to guaranty the dissolution/digestion of any solid trace that could remain.

4.4.11. Mathematical Models

The study of the release kinetics provides important information about the function of systems. Drug release is the process in which drugs migrate from the initial position in the polymeric network to the outside of the system and then to the release medium. This process is affected by multiple complex factors: physicochemical properties of the drugs, structural characteristics of the particles, release environment and possible interactions between these factors. It is critical to correlate the macroscopic data and the transport behavior at molecular level to elucidate the release mechanism of the system. The diffusion properties, swelling capability and material degradation are the main factors that influence the performance of a release system and define the release kinetics [83]. Mathematical modeling provides insights into the release mechanisms of a specific system simplifying the complex release processes [84]. In this way, each mathematical model is focused in one or two factors that influence the release kinetics, which cause some inaccuracy between theoretical and experimental obtained data.

In chapters 6 and 9, the application of the several mathematical models was useful to have an insight about the type of drug release mechanism occurred in the developed systems. The equations used were the following:

Chapter 6:

Zero order: $\mathrm{M_t = M_0 + k_0 t} \quad \mathrm{Eq.\,4}$

First order: $\mathrm{\log M_t = \log M_0 + \frac{k_1}{2.303} t} \quad \mathrm{Eq.\,5}$

Higuchi: $\mathrm{M_t = M_0 + k_H t^{1/2}} \quad \mathrm{Eq.\,6}$

Korsmeyer-Peppas: $\mathrm{M_t = k_{KP} t^n} \quad \mathrm{Eq.\,7}$

Chapter 9:

Considering the lag time: $\mathrm{M_t/M_\infty = k(t - t_{lag})^{0.5}} \quad \mathrm{Eq.\,8}$

Where M_0 was the initial amount of drug, M_t was the cumulative amount released at time t, t_{lag} was the lag time between the start of the experiment and the detection of the drug, and k, k_0, k_1, k_H, and k_{KP} were specific constants of each model.

Zero-order release kinetics is related to systems capable to release the drug with a constant rate over a period of time. The first order model, the release of the drug is dependent on the drug concentration. The Higuchi model is related with the release of water soluble and low soluble drugs incorporated into semi-

solid or solid matrices by diffusion processes. In the Korsmayer-Peppas equation, *n* characterizes the release mechanism. The release of the drug follows an anomalous mode when 0.43<n<0.85, meaning that the release is controlled by diffusion and by swelling. Using the software OriginPro8 the experimental data, in the 10-60% amount released interval, was treated and the best fit was selected based on the highest correlation coefficient (R^2).

4.5. Biological Studies

4.5.1. *In vitro* Tests

In vitro tests, to evaluate the status of the cells, were performed in all the chapters of this thesis. In some cases were evaluated the viability, proliferation and differentiation of the cells entrapped in the spherical gels (3D cell cultures), and in other cases it was evaluated the effect of a bioactive agent released by the particles in a monolayer of cells (2D cell cultures). *In vitro* tests are essential to obtain the first screening about the performance of the proposed system under conditions mimicking the *in vivo* environment.

4.5.1.1. Cell Cultures

I. 2D Cell Cultures

2D cell cultures were performed in some chapters of this thesis in order to evaluate the toxicity of the Dex-MA+CDs particles or the effect of the release bioactive agents from collagen+PLs spherical gels in the cell proliferation/migration.

In chapter 5, SaOs-2 cell line (HTB-85™ from ATCC®) was used to evaluate the effect of the formulations composed by Dex-MA solely or combined with γ-CDs or γ-CD-NMA on cell viability. Those cells were collected from human osteosarcoma and are widely used to study for bone applications due to their osteoblastic features. SaOs-2 cells were expanded in DMEM-F12 supplemented with 10% (v/v) FBS and 1% (v/v) penicillin/streptomycin at 37 °C in humidified incubator with 5% CO_2. Cells were then tripsinized and seeded onto 48-well plates with a density of 50 000 cells/well in 1 mL of cell culture medium. After cell adhesion, 2 particles of each formulation were added into the wells. After 24h and 48h, the cell viability was evaluated by LDH assay (described in detail in subsection 4.1.3). The same formulations but loaded with dexamethasone were cultured in contact with a monolayer of hASCs in order to evaluate the potential of the system in inducing the osteogenic differentiation. The characteristics of hASCs were already described in the section 2.4.2 of this chapter. In this assay, the hASCs were seeded in 6 well plates with a density of 25 000 cells/well with 5 mL of culture medium which was slightly modified in

order to provide the phosphates and the ascorbic acid required in osteogenic differentiation. In addition, multiple controls were performed to evaluate the effect of dexamethasone in a precise way.

I) Culture medium of the experiment: MesenPro® supplemented with 2% (v/v) growth supplement (FBS), 1% (v/v) L-glutamine and 1%(v/v) penicillin/streptomycin, **10 mM β-GP, 50 μM ascorbic acid;**

II) Negative control 1: MesenPro® supplemented with 2% (v/v) growth supplement (FBS), 1% (v/v) L-glutamine and 1%(v/v) penicillin/streptomycin.

III) Positive control 1: MesenPro® supplemented with 2% (v/v) growth supplement (FBS), 1% (v/v) L-glutamine and 1%(v/v) penicillin/streptomycin, **10 mM β-GP, 50 μM ascorbic acid and 100 nM dextamethasone.**

IV) Negative control 2: MesenPro® supplemented with 2% (v/v) growth supplement (FBS), 1% (v/v) L-glutamine and 1%(v/v) penicillin/streptomycin, **10 mM β-GP, 50 μM ascorbic acid.**

V) Positive Control 2: MesenPro® supplemented with 2% (v/v) growth supplement (FBS), 1% (v/v) L-glutamine and 1%(v/v) penicillin/streptomycin, **10 mM β-GP, 50 μM ascorbic acid and 400 ng/mL of dextamethasone.**

In chapter 7, the particles composed by collagen+PL were cultured in contact with a monolayer of hASCs. To evaluate the cell proliferation due to the released bioactive agents contained in the PLs, hASCs were seeded onto 48 well plates in a density of 7 500 cells/well in 100 μL of the same medium used for cell expansion, described in the subsection 4.1.2.4 of this chapter. After 24h (to allow the adhesion of the cells) the medium was replaced by 200 μL of culture medium without FBS, in order to avoid the stimulus of the FBS in cell proliferation, and then evaluate precisely the effect of the PL. Two particles of each formulation were immersed in each well, contacting directly with the cell monolayer. The plates were incubated in the standard conditions: 37 °C and humidified atmosphere with 5% CO_2. The medium was replaced every 3 days. The cell proliferation was evaluated at pre-established time points using the CCK-8 kit, described in detail in de subsection 4.5.1.5 The effect of the PL in the filling of a cell gap was also performed, by performing a scratch in a monolayer culture. A detailed description of this test will be provided in the subsection 4.5.1.2.

II. 3D Cell Cultures

In chapters 6, 7, 8, and 9, different cell types were encapsulated in the different spherical hydrogel systems. The characteristics of the cells used were already described in the subsection 4.1.2.4 of this chapter. After being encapsulated following the procedures described in the section 4.3 of this chapter,

the particles were collected from the superhydrophobic surface and immersed in appropriate cell culture medium.

The Chi (chapter 6) and the core/shell dextran-MA/alginate (chapter 9) particles encapsulating L929 cells were cultured in the same medium as described for the expansion of this type of the cells. In both cases, the cell viability was evaluated by live/dead assay, following the procedure described in the subsection 4.5.1.4.

The collagen and collagen+PLs beads (chapter 7) encapsulating hASCs were cultured in a slightly modified medium. Since the aim of the work was to evaluate the effect of the PLs, the medium used was free of FBS in order to not stimulate the cells with the GFs or other cytokines that compose the FBS. The hardened gels were then collected and cultured in 200 μL of culture medium, 2 particles/well in 96 well plates. At 1, 3 and 7 days the cell proliferation was evaluated using the live/dead assay and the CCK-8 kit, that are described in detail in the subections 4.5.1.4 and 4.5.1.5.

The alginate formulations described in chapter 8 were cultured in the same medium used for rMSCs expansion. The cell viability was then evaluated by live/dead fluorescent assay as well as using the LDH and MTS kits – see section 4.5.1.4. The same formulations were also cultured in osteogenic medium. This medium was composed the same type used in the previous experiments but supplemented with the standard molecules used in induction of osteogenic differentiation: 0.1 mM L-ascorbic acid 2-phosphate, 10 mM β-GP and 100 nM dexamethasone.

4.5.1.2. Scratch Wound Assay

The scratch wound assay was performed in chapter 7 using commercial silicon inserts purchased from Ibidi®, which allowed the formation of a defined cell-free gap – Figure 4.16. hASCs were seeded in each compartment of the insert. After reach confluence, the cell culture medium and the inserts were removed from the petri dish carefully in order to prevent the detachment of the cell monolayer. The cells were washed with PBS and 1 mL of fresh culture medium was added. The particles described in the chapter 7 (collagen or collagen+PL beads) were placed in direct contact with a cell monolayer in a density of 10 particles/mL of culture medium. Since the aim of the work was to evaluate the effect of the PL in cell proliferation/migration the cell culture medium used was FBS-free. Optical microscope images of the gap between both cell groups were collected starting from the moment that the particles were added: 0, 2, 4, 8, 12, 24 and 48h.

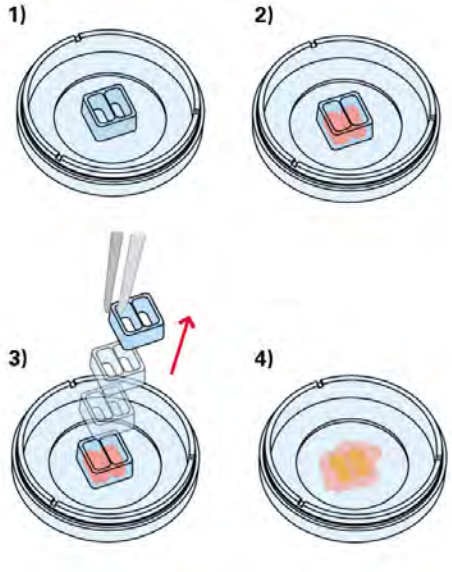

Figure 4.16. 1) Silicon inserts and micro-dishes used in the scratch wound assay; 2) the cells were seeded in each compartment of the silicon insert; 3) the inserts were removed when the cells reach confluence; 4) cell culture medium was added to the micro-dish and then the particles were immersed in the culture medium. Image adapted from [85].

4.5.1.3. Cell Distribution and Morphology Inside the Particles

I. Optical Microcopy

Optical microscopy was used routinely in chapters 7 and 8 to observe the cells inside the particles, their migration from the particles to the bottom of the well plates as well as to discard contaminations during the culture period that was quite long. The observation of the cells inside the particles was possible because the produced gels were transparent. Images were collected at pre-established time periods, using cameras coupled to the used microscopes.

II. Confocal Microscopy: Phalloidin/DAPI

Confocal microscopy was used to have an insight of the cell distribution inside the spherical hydrogels. In chapters 7, 8 and 9, the cells were labeled with Phalloidin and DAPI fluorophores and after were observed at confocal microscope allowing the acquisition of images. Unlike other kinds of microscopy (e.g. widefield microscopy), confocal allows to collect information selectively along thick samples, being a valuable tool to analyze 3D structures. This is possible because the depth of field is controlled and a serial of optical sections are collected throughout of Z-axis of the sample.

Phalloidin belongs to a group of bicyclic heptapeptides, denominated by phallotoxins, and it is obtained from poisonous mushrooms. Labelled phallotoxins binds to actin allowing its identification and quantification in cell cultures. In general, phallotoxins have similar affinity for large and small filaments

and the binding is established in a stoichiometric ratio of 1 phallotoxin molecule per actin subunit. The contrast between stained and unstained areas is extremely large. Phallotoxins are capable to stabilize F-actin, inhibiting depolymerization by cytoshalasins, potassium iodide and elevated temperatures. Fluorescent phalloidins only binds to the native quaternary structure of F-actin and generally do not permeate the cell membrane. For these reason correct fixation procedures should be used to retain the quaternary structure of the protein and to permeabilize the cells [86].

DAPI is a blue fluorescent stain with specificity to stain the double-stranded DNA (dsDNA) inside the cell nuclei. DAPI attaches to adenine-thymine clusters in the DNA minor groove in the follow proportion: one molecule of stain per 3 base-pairs. The fluorescence is directly proportional to the amount of DNA [87].

In all cases the particles with the cells were fixed using 4% (v/v) paraformaldehyde and then incubated in Phalloidin solution for 45 min and then in DAPI solution for 3-10 min. This was performed always in the dark in order to avoid the loss of fluorescence of these molecules. Between each immersion/incubation, the particles were washed several times with appropriate solutions (*e.g.* PBS pH 7.4 or 0.15 M of NaCl supplemented with 10 mM $CaCl_2$) to remove all the traces of the fluorophores. The concentrations used in each system are described in the respective chapter in the section III of this thesis.

4.5.1.4. Cell Viability

In this subsection will be described the mechanism of each used technique to evaluate the viability of the cells both in 2D and 3D cultures. The experimental procedure, namely reagent volumes, concentrations, incubation times and temperatures as well as other measurement details are extensively described in each respective chapter of section III. These details varied slightly according to the brand of the kit used and they were always adapted and optimized for each system.

I. Live/Dead Assay

Live/dead assay is a simple, fast and accurate tool for screening cell viability by fluorescence detection. Calcein AM was used to identify the live cells. Despite not being fluorescent, this hydrophobic molecule easily permeates intact live cells. Upon hydrolysis by intracellular esterases, the Calcein AM is converted into Calcein, which is a hydrophilic fluorescent dye. The Calcein retained in the cell cytoplasm allowed the visualization of the live cells through adequate methods (fluorescent/confocal microscopy, excitation ≈ 495 nm and emission ≈ 515 nm). The dead cells were labeled by propidium iodide (PI), which is not permeant in live cells. PI binds to DNA by intercalating between the bases, with little or no sequence preference. The stoichiometry is one dye molecule per 4-5 base pairs of DNA [88]. Upon binding the

fluorescence of the PI is enhanced 20-30 fold (excitation ≈495nm and emission ≈ 635 nm). The cells with not damaged membrane will exclude the PI. Calcein-AM/PI was performed in chapters 6, 7, 8 and 9.

II. Lactate Dehydrogenase Detection

Lactate dehydrogenase (LDH) is an oxidoreductase enzyme that catalyzes the interconversion of pyruvate and lactate. Having into account that LDH is a fairly stable enzyme and that dead cells release it, LDH detection/quantification has been used to evaluate the tissues and cells status. The LDH reduces NAD to NADH, which is specifically detected by colorimetric assay (UV-VIS spectrophotometry). In chapter 5 and 8 a LDH kit was used to quantify the percentage of the viable cells existent at pre-established periods of time.

III. MTS

In chapter 8 was used the (3-(4,5-dimethylthiazol-2-yl)-5-(3-carboxymethoxyphenyl)-2-(4-sulfophenyl)-2H-tetrazolium) (MTS) assay to evaluate the viability of the cells. The cells are capable to produce reducing agents, namely NADH or NADPH, that pass their electrons to an intermediate transfer reagent which in turn can reduce the tetrazolium into formazan. The formazan product is soluble in aqueous medium and is proportional to the number of viable cells in culture, being detected by UV-VIS spectrophotometry. Upon death, the cells lose the ability to reduce the tetrazolium products [89].

4.5.1.5. Cell Proliferation

I. MTT

In chapter 5 was used (3-[4,5-dimethylthiazol-2-yl]-2,5-diphenyltetrazolium bromid) (MTT) assay. This method is based on the cleavage of the yellow tetrazolium salt MTT to purple formazan crystals by metabolic active cells [90]. Similarly with MTS, the pyridine nucleotide cofactors NADH and NADPH are the main responsible for this cellular reduction. The formazan crystals formed were solubilized resulting in a colored solution that was evaluated by UV-VIS spectrophotometry. The correlation with the cell number was established using a calibration curve obtained by testing a series of sample with known numbers of cells.

II. CCK-8

This assay, utilized in chapter 7, use the highly water soluble tetrazolium salt WST-8 [2-(2-methoxy-4-nitrophenyl)-3-(4-nitrophenyl)-5-(2,4-disulfophenyl)-2H-tetrazolium, monosodium salt] to produce water-

soluble formazan dye upon a reduction process, similarly with MTS and MTT. The dehydrogenases in the cells reduce the WST-8 into a yellow colored formazan, which is soluble in tissue culture medium. The amount of formazan formed is proportional to the number of living cells. The sensitivity of CCK-8 is higher than MTT and MTS.

4.5.1.6. Differentiation Studies

In the chapter 5 and 8 was studied the osteogenic differentiation of the cells both in 2D and 3D. To evaluate the effectiveness of the applied stimulus, the follow techniques were performed.

I. Alkaline Phosphatase Activity Quantification

ALP is an important cell surface metalloenzyme with a role in hard tissue formation. It is highly expressed in mineralized tissue cells. Although the mechanism of this enzyme in not completely understood, it appears to act both to increase the local concentration of inorganic phosphatase, a mineralization promoter, and to decrease the concentration of extracellular pyrophosphate, an inhibitor of mineral formation. In this way, the high level of activity provides information related to hard tissue formation. In addition, it is known that ALP is one of the first functional genes expressed in the calcification process, indicating that acts in an early stage. This means that ALP is one of the first key players to be recognized in the process of osteogenesis [91]. The activity of ALP is commonly evaluated using a p-nitrophenol assay. At pH 10.5 and 37 °C the ALP is capable to hydrolyze the paranitrophenyl phosphate into free paranitrophenol causing a color transition from colorless to yellow. The expression of ALP, both in a membrane form or in a secretory form, is a characteristic of osteoblasts, being a strong indicator of these type of cells [92].

To quantify the ALP activity, in chapter 5, the hASCs were lysed after being cultured for 3, 7 and 12 days. In each well it was added 300 μL of 10 mM Tris–HCl buffer (pH 7.5) with 0.1% Triton X-100. The cell lysate was collected and exposed to freezing-thawing cycles: at least 45 min at -80 °C and then at room temperature during the time necessary to thawing. This step was to ensure that all the cells were lysed. The follow step was the centrifugation of the lysates (14 000 rpm, 15 min at 4 °C) in order to separate pieces of cell membranes that could remain in the suspension. 50 μL of the supernatant was collected carefully and incubated with ALP substrate for 30 min at 37 °C. During the incubation the absorbance at 405 nm was read at 5, 10, 15, 20 and 30 min. The final calculations were performed using a calibration curve prepared using solutions with known concentrations of p-nitrophenyl phospate. In addition, the results were presented normalized by the protein concentration, which was measured by the BCA method

already described. This allowed expressing the activity of the ALP as amount of ALP per time per amount of total protein.

II. Alkaline Phosphatase Staining

ALP staining was performed in chapter 5 to complement the results of the ALP quantification. After 12 days in culture, the culture medium in the wells was removed and the cells were fixed with 4% (v/v) paraformaldehyde in PBS for 5 min at room temperature. The cells were, then, washed with PBS and finally stained for 10 minutes, at room temperature, and in the dark using the follow mixture: 0.2% naphthol AS-BI phosphate in 112 mM 2-amino-2-mathylpropanediol and 0.2% fast red violet in a 1:1 (v:v) proportion. Images were immediately taken using an inverted light microscope coupled to a camera.

III. Alizarin Red Staining

Calcium and inorganic phosphates are accumulated, serving as nucleating agents for the formation of the main inorganic component of bone: hydroxyapatite ($Ca_{10}(PO_4)_6(OH_2)_2$). Some cells, when cultured *ex vivo* could form minerals if stimulated appropriately. The mineralization may be accessed by the follow procedures: fluorescent calcein binding, Von Kossa staining and Alizarin red staining. Alizarin red staining allows observing the mineral distribution, namely the calcium deposits and could be used to stain *in vitro* cell cultures as well as histological samples [93].

Alizarin red is a fast and cheap method and for this reason was used in chapter 8 to visualize the mineral deposition by the cells encapsulated in alginate particles when cultured in osteogenic medium. The cell-laden particles were fixed overnight in an aqueous solution of glutaraldehyde (2.5% v/v) at 4 °C. Then the particles were dehydrated in solutions of ethanol and finally embedded in paraffin. Using a microtome, slices with 4-5 μm thick were obtained and then stained by immersion in an alizarin red aqueous solution (40 mM, pH 4.3). This procedure was advantageous to study the inner of the particles and not only the surface.

4.5.1.7. Cryopreservation of Cell-Laden Particles

The storage of materials containing cells for later application is a critical step in the development of tissue engineering strategies involving cells. The most simple preservation technique is refrigeration, however the limited shelf life and risks of contamination are problematic. The cryopreservation of the materials with cells has been studied as possible method to circumvent the obstacle related to preserving and storing of "living" biomaterials [94], although very few studies have focused this problem. The principle of this

approach is that chemical, biological and physical processes are "suspended" at cryogenic temperatures. In chapter 7, cell-laden particles were cryopreserved in order to investigate the effect of the standard cryopreservation procedure in the hASCs entrapped in collagen+PLs particles. Cell-laden particles were suspended in a cryopreservative solution composed by FBS:DMSO (90:10 v/v). Then the suspension of particles was kept at -20 °C for 24h and then stored at -80 °C. DMSO is a cryoprotectant required to protect the cells against freeze injuries, namely in avoiding the formation of ice crystals. Studies have been proved that DMSO has toxic side effects to human body [95]. After 1 month, the cryopreserved particles were thawed at 37 °C, the mixture of FBS:DMSO was discarded quickly and the particles were washed with cell culture medium at 37 °C several times to remove all traces of DMSO. Afterwards, the cells were cultured normally and the viability of the cells was study using the Live/Dead essay (already described in this chapter) after 7days.

4.5.2. *In Vivo T*ests

Studies using animal models are, generally, considered reliable and appropriate analogues to specific clinical conditions. Adequate models are selected according to the application aimed for the developed system. *In vivo* studies are mainly used to evaluate the preclinical status of translational technologies [96], where are included the performance of materials or systems as the hydrogels spherical systems proposed in this thesis.

4.5.2.1. Chorioallantoic Membrane Model

The chicken embryo chorioallantoic membrane (CAM) is a recurrent test for neovascularization analysis. The complete development of the embryo lasts 21 days before hatching. During the embryo development three membranes are formed aiming the embryo protection and nourishing: the yolk sac membrane, the amnion and the CAM. CAM is responsible by mediate the gas and nutrient exchanges until hatching. This membrane has a very dense network composed by arteries, veins, and an intricate capillary plexus (Figure 4.17). The vascular system of the chick embryo attains its final arrangement on day 18, just before hatching. The current legislation about the animal experimentation in the European Union allows experimentation with chick embryos without authorization from animal experimentation committees. However, the experiments should begin and end before hatching.

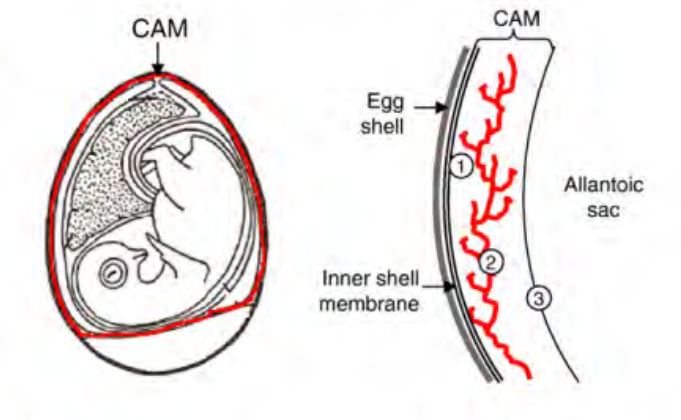

Figure 4.17. Localization of the CAM inside the egg and the detailed description of the CAM. 1: chorionic epithelium; 2: mesoderm with blood vessels depicted in red; 3: allantoic epithelium. Image adapted from [97].

This assay consists in implanting the material on the chick embryo chorioallantoinc membrane through a hole cut in the eggshell. The number of blood vessels formed can be quantified via image analysis. Technically, CAM is a quick, simple and inexpensive test when compared with mammalian models, and have been demonstrated suitable to give strong and accurate indications about the angiogenic performance of the systems under study [98,99]. This *in ovo* test was performed in chapter 7 to evaluate the angiogenesis potential of theagen and collagen+PL systems. Firstly, the fertilized eggs were incubated horizontally at 37 °C and 60% humidity. At day 3, around 2 mL of albumin was removed by punctured the egg with a needle. A circular window was performed in the eggshell and the eggs returned to the incubator for 4 days more. The opened window was very well covered with parafilm in order to avoid contaminations or the drying of the exposed membrane. At day 7, two beads of each formulation were placed in contact with the CAM and controls were also performed by dispensing equivalent amounts of PL without being encapsulated in collagen beads. Images of the membrane were collected 3 days after the beads being implanted using a camera coupled to a stereomicroscope. The membranes were fixed with 10% (v/v) formaldehyde for at least 10 min at room temperature. Then, using a bisturi, the membranes were cut and disposed carefully in a glass slide. The images collected were used to count manually the blood vessels growth.

4.5.2.2. Cranial Defect Model

Calvarial defect is a versatile model that allows the evaluation of biomaterials and bone tissue engineering approaches within a reproducible, nonload-bearing orthotopic site. Wistar rats were used to examine the healing of cranial bone defects filled with alginate-based particulate systems (chapter 8). All procedures involving use of the animals were conducted in accordance with the guidelines of the National Institutes of

Health Guide for the care and use of laboratory animals. The surgery consisted on drilling circular defects with approximately 5 mm in diameter in the parietal bones of the skull. Extremely care was taken to not damage the dura matter beneath the bone as well as the sagittal suture line. The rats were anesthetized with ketamine (40 mg/kg) and xylazine (5 mg/kg) administered by an intraperitonial injection. Twelve rats were used (three groups of four rats each):

(I) controls: empty defects

(II) alginate beads with FN (4 beads/defect)

(III) alginate beads with FN and rMSCs (4 beads/defect).

After the surgery the rats were maintained in individual cages with free access to water and food. Four weeks post-surgery, animals were euthanized with an overdose of anesthetic and the crania were removed and fixed immediately in formaldehyde for further analysis. During this procedure other organs were also collected and fixed: brain, heart, lungs, liver, spleen and kidneys, in order to check the existence of pathological abnormalities.

I. MicroComputed Tomography

Microcomputed tomography (μCT) uses an X-ray source to obtain cross-sectional images of 3D objects without damage the samples. Then, the images obtained may be combined to reconstruct a 3D model [100]. In chapter 8, μCT technique enabled the collection of data from the cranial bone of the rats to evaluate the formation of new tissue in the damaged sites. Images of the rats skulls were acquired using a Skyscan 1072 scanner. Scans were performed using a X-ray with 51 kV of energy, 195 μA of current and an exposure time of 1.7 seconds using a pixel size of 14.7 μm. The raw data was transformed into binary using a dynamic threshold of 42-255 (SkyScan CT Analyzer v1.5.1.5 software). Then a 3D virtual model of calvaria bones was created using the SkyScan ANT 3D creator v2.4 software.

II. Histology: Hematoxylin and Eosin Staining

Hystological sections of the bone collected from the calvaria of the rats could show the formation of new bone in the defect site as well as the status of the tissues surrounded the damaged area, *e.g.* the presence of inflammatory cells. The collected calvaria bones were processed, starting with decalcification in hydrochloric acid. Then, the decalcified samples were dehydrated in a series of ethanol concentrations followed by xylene solution to remove the water from the tissues. After this, the samples were embedded in paraffin blocks, which were sectioned using a microtome to obtain 4-5 μm thick sections. Using a glass slides as supports for the sections containing the sample, the tissue was depparaffined by a quick

immersion in xylene and stained using Hematoxylin and Eosin (H&E). H&E staining is a standard protocol to identify microscopically the morphology of the cells and tissues. Hematoxylin stains the nucleus with a dark blue color, whereas the eosin stains the cell cytoplasm with a pink color. Finally, the samples were visualized using optical microscopy.

4.6. Statistical Analysis

All the experiments were performed with at least three replicates. The results were expressed by mean ± standard deviation. The data collected was treated with the GraphPad Prism statistic software. Firstly, the Shapiro-Wilk test was used to ascertain about the normality distribution of the population. The null hypothesis assumed was that the means of each set were equal. The hypothesis was evaluated with 95% confidence level (α=0.05). Then, the groups were compared performing analysis of variance (one-way ANOVA) followed by Tukey's multiple comparison test and the significant differences between groups were determined.

4.7. References

[1] Song W., Lima A. C. and Mano J. F., Bioinspired methodology to fabricate hydrogel spheres for multi-applications using superhydrophobic substrates, Soft Matter 2010, 6: 5868.

[2] Holzapfel V., Musyanovych A., Landfester K., Lorenz M. R. and Mailänder V., Preparation of fluorescent carboxyl and amino functionalized polystyrene particles by miniemulsion polymerization as markers for cells, Macromolecular Chemistry and Physics 2005, 206: 2440–9.

[3] Oliveira M. B., Ribeiro M. P., Miguel S. P., Neto A. I., Coutinho P., Correia I. J. and Mano J. F., In Vivo high-content evaluation of three-dimensional scaffolds biocompatibility, Tissue Engineering Part C Methods 2014, 31;1–53.

[4] Erbil H. Y., Demirel A. L., Avci Y. and Mert O., Transformation of a simple plastic into a superhydrophobic surfasse, Science 2003, 299: 1377–80.

[5] Yuan Z., Chen H., Tang J., Chen X., Zhao D. and Wang Z. Facile method to fabricate stable superhydrophobic polystyrene surface by adding etanol, Surface and Coatings Technology 2007, 201: 7138–42.

[6] Zhao N., Xu J., Xie Q., Weng L., Guo X., Zhang X. and Shi L., Fabrication of Biomimetic Superhydrophobic Coating with a Micro-Nano-Binary Structure, Macromolecular Rapid Communications 2005, 26: 1075–80.

[7] Lima A. C., Song W., Blanco-Fernandez B., Alvarez-Lorenzo C. and Mano J. F., Synthesis of temperature-responsive dextran-MA/PNIPAAm particles for controlled drug delivery using superhydrophobic surfaces, Pharmaceutical Research 2011, 28: 1294–305.

[8] De Givenchy E. T., Amigoni S., Martin C., Andrada G., Caillier L., Géribaldi S. and Guittard F., Fabrication of superhydrophobic PDMS surfaces by combining acidic treatment and perfluorinated monolayers, Langmuir 2009, 25: 6448–53.

[9] Yao X., Chen Q., Xu L., Li Q., Song Y, Gao X., et al. Bioinspired Ribbed Nanoneedles with Robust Superhydrophobicity, Advanced Functional Materials 2010, 20: 656–62.

[10] Lee K. Y. and Mooney D. J., Hydrogels for Tissue Engineering, Chemical Reviews 2001, 101: 1869-79.

[11] Khademhosseini A. and Langer R., Microengineered hydrogels for tissue engineering, Biomaterials 2007, 28: 5087–92.

[12] Qiu Y. and Park K., Environment-sensitive hydrogels for drug delivery, Advanced Drug Delivery Reviews 2001, 53: 321–39.

[13] Hamidi M., Azadi A., Rafiei P., Hydrogel nanoparticles in drug delivery, Advanced Drug Delivery Reviews 2008, 60: 1638–49.

[14] Luchini A., Geho D. H., Bishop B., Tran D., Xia C., Dufour R. L., Jones C. D., Espina V.,Patanarut A. Zhou W., Rosa M. M., Tessitore A., Petricoun E. F. and Liotta L. A. ,Smart Hydrogel Particles : Biomarker Harvesting : One-Step Affinity Purification, Size Exclusion, and Protection against Degradation, Nano Letters 2008, 8: 350-61.

[15] Geckil H., Zhang X., Moon S., and Demirci U., Engineering hydrogels as extracellular matrix mimics, Nanomedicine (Lond) 2010,5: 469–84.

[16] Nicodemus G. D. and Bryant S. J., Cell encapsulation in biodegradable hydrogels for tissue engineering applications, Tissue Engineering Part B Reviews 2008, 14:149–65.

[17] Jen A .C., Wake M. C and Mikos A. G., Review : Hydrogels for Cell Immobilization, Biotechnology and Bioengineering 1996, 50: 357–64.

[18] Tokarev I. and Minko S. Stimuli-responsive porous hydrogels at interfaces for molecular filtration, separation, controlled release, and gating in capsules and membranes, Advanced Materials 2010, 22: 3446–62.

[19] Arai F., Ng C., Maruyama H., Ichikawa A., El-Shimy H. and Fukuda T., On chip single-cell separation and immobilization using optical tweezers and thermosensitive hydrogel, Lab Chip 2005, 5:1399–403.

[20] Custódio C. A., Reis R. L. and Mano J. F., Engineering Biomolecular Microenvironments for Cell Instructive Biomaterials, Advanced Healthcare Materials 2014, 3: 797–810.

[21] Rowley J .A., Madlambayan G. and Mooney D. J., Alginate hydrogels as synthetic extracellular matrix materials, Biomaterials 1999, 20: 45–53.

[22] Hennink W. E. and van Nostrum C. F., Novel crosslinking methods to design hydrogels, Advanced Drug Delivery Reviews 2012, 64: 223–36.

[23] Wang W., Liu X., Xie Y., Zhang H., Yu W., Xiong Y., Xie W. and Ma X., Microencapsulation using natural polysaccharides for drug delivery and cell implantation, Journal of Materials Chemistry 2006, 16: 3252-67.

[24] Sinha V. R. and Kumria R., Polysaccharides in colon-specific drug delivery, International Journal of Pharmaceutics 2001, 224: 19–38.

[25] Kalia S. and Averous L., Biopolymers: Biomedical and Environmental Applications, John Wiley & Sons 2011, DOI: 10.1002/9781118164792

[26] Larsen C., Dextran prodrugs — structure and stability in relation to therapeutic activity, Advanced Drug Delivery Reviews 1989, 3: 103-154.

[27] Brøndsted H., Andersen C., Hovgaard L, Crosslinked dextran — a new capsule material for colon targeting of drugs, Journal of Controlled Release 1998, 53: 7–13.

[28] Ferreira L. S., Gerecht S., Fuller J., Shieh H. F., Vunjak-Novakovic G. and Langer R., Bioactive hydrogel scaffolds for controllable vascular differentiation of human embryonic stem cells, Biomaterials 2007, 28: 2706–17

[29] Liu Y. and Chan-Park M. B., Hydrogel based on interpenetrating polymer networks of dextran and gelatin for vascular tissue engineering. Biomaterials 2009, 30: 196–207.

[30] Lévesque S. G., Lim R. M. and Shoichet M. S., Macroporous interconnected dextran scaffolds of controlled porosity for tissue-engineering applications, Biomaterials 2005, 26: 7436–46.

[31] De Jong S. J, De Smedt S. C., Wahls M. W. C., Demeester J., Kettenes-van den Bosch J. J. and Hennink W. E., Novel self-assembled hydrogels by stereocomplex formation in aqueous solution of enantiomeric lactic acid oligomers grafted to dextran, Macromolecules 2000, 33: 3680–6.

[32] Hovgaard L. and Brndsted H., Controlled release Dextran hydrogels for colon-specific drug delivery, Journal of Controlled Release 1995, 36: 159–66.

[33] van Dijk-Wolthius V. N. E., Franssen O., Talsma H., van Steenbergen M. J., Kettenes-van den Bosch J. J. and Henninkt W. E., Synthesis, characterization, and polymerization of glycidyl methacrylate derivatized dextran, Macromolecules 1995, 28: 6317–6322.

[34] Berger J., Reist M., Mayer J. M., Felt O., Peppas N. and Gurny R., Structure and interactions in covalently and ionically crosslinked chitosan hydrogels for biomedical applications, European Journal of Pharmaceutics and Biopharmaceutics 2004, 57: 19–34.

[35] Ruel-Gariépy E., Shive M., Bichara A., Berrada M., Le Garrec D., Chenite A. and Leroux J. –C., A thermosensitive chitosan-based hydrogel for the local delivery of paclitaxel, European Journal of Pharmaceuticals and Biopharmaceuticals 2004, 57: 53–63.

[36] Couto D. S., Hong Z. and Mano J. F., Development of bioactive and biodegradable chitosan-based injectable systems containing bioactive glass nanoparticles, Acta Biomaterialia 2009, 5: 115–23.

[37] Metcalfe A. D. and Ferguson M. W. J., Tissue engineering of replacement skin: the crossroads of biomaterials, wound healing, embryonic development, stem cells and regeneration, Journal of the Royal Society Interface 2007, 4: 413–37.

[38] Helary C., Zarka M. and Giraud-Guille M. M., Fibroblasts within concentrated collagen hydrogels favour chronic skin wound healing, Journa of Tissue Engineering and Regenerative Medicine 2012, 6: 225–37.

[39] Waller J. M. and Maibach H. I., Age and skin structure and function, a quantitative approach (II): protein, glycosaminoglycan, water, and lipid content and structure, Skin Research and Technology 2006, 12: 145–54.

[40] Glowacki J. and Mizuno S., Collagen scaffolds for tissue engineering, Biopolymers 2008, 89: 338–44.

[41] Lodish H., Berk A., Zipursky S. L., *et al.* Molecular Cell Biology. 4th edition. New York: W. H. Freeman; 2000. Section 22.3, Collagen: The Fibrous Proteins of the Matrix, Available from: http://www.ncbi.nlm.nih.gov/books/NBK21582/

[42] O'Leary L. E. R., Fallas J. A., Bakota E. L., Kang M. K. and Hartgerink J. D., Multi-hierarchical self-assembly of a collagen mimetic peptide from triple helix to nanofibre and hydrogel, Nature Chemistry 2011, 3: 821–8.

[43] Bidarra S. J., Barrias C. C., Fonseca K. B., Barbosa M. A., Soares R. A. and Granja P. L., Injectable in situ crosslinkable RGD-modified alginate matrix for endothelial cells delivery, Biomaterials 2011, 32: 7897–904.

[44] Sun J. –Y., Zhao X., Illeperuma W. R. K., Chaudhuri O., Oh K. H., Mooney D. J., Vlassak J. J. and Suo Z., Highly stretchable and tough hydrogels, Nature 2012, 489: 133–6.

[45] Hernández R. M., Orive G., Murua A. and Pedraz J. L., Microcapsules and microcarriers for in situ cell delivery, Advanced Drug Delivery Reviews 2010, 62: 711–30.

[46] Tan W. -H., Takeuchi S., Monodisperse Alginate Hydrogel Microbeads for Cell Encapsulation, Advanced Materials 2007, 19: 2696–701.

[47] Brun-Graeppi A. K. A. S., Richard C., Bessodes M., Scherman D. and Merten O. -W., Cell microcarriers and microcapsules of stimuli-responsive polymers, Journal of Controlled Release 2011, 149: 209–24.

[48] Correia C. R., Reis R. L. and Mano J. F., Multilayered Hierarchical Capsules Providing Cell Adhesion Sites, Biomacromolecules 2013, 14: 743-51

[49] Li R., Materials for immunoisolated cell transplantation, Advanced Drug Delivery Reviews 1998, 33: 87–109.

[50] Yu J., Du K. T., Fang Q., Gu Y., Mihardja S. S., Sievers R. E., Wu J. C. and Lee R. J., The use of human mesenchymal stem cells encapsulated in RGD modified alginate microspheres in the repair of myocardial infarction in the rat, Biomaterials 2010, 3: 7012–20.

[51] Del Valle E. M. M., Cyclodextrins and their uses: a review, Process Biochemistry 2004, 39: 1033–46.

[52] Moya-Ortega M. D., Alvarez-Lorenzo C., Concheiro A. and Loftsson T., Cyclodextrin-based nanogels for pharmaceutical and biomedical applications, International Journal of Pharmaceutics 2012 428: 152–63.

[53] Siemoneit U., Schmitt C., Alvarez-Lorenzo C., Luzardo A., Otero-Espinar F., Concheiro A. and Blanco-Méndez J., Acrylic/cyclodextrin hydrogels with enhanced drug loading and sustained release capability, International Journal of Pharmeceutics 2006, 312: 66–74.

[54] Langenbach F. and Handschel J., Effects of dexamethasone, ascorbic acid and β-glycerophosphate on the osteogenic differentiation of stem cells in vitro, Stem Cell Research & Therapy 2013, 4: 117.

[55] Andia I. and Maffulli N., Platelet-rich plasma for managing pain and inflammation in osteoarthritis, Nature Reviews Rheumatology 2013, 9: 721–30.

[56] Walenda G., Hemeda H., Schneider R. K., Merkel R., Hoffmann B. and Wagner W., Human platelet lysate gel provides a novel three dimensional-matrix for enhanced culture expansion of mesenchymal stromal cells, Tissue Engineering Part C Methods 2012, 18: 924-34.

[57] Shih D. T. –B. and Burnouf T., Preparation, quality criteria, and properties of human blood platelet lysate supplements for ex vivo stem cell expansion, New Biotechnology 2014, DOI: 10.1016/j.nbt.2014.06.001 (in press).

[58] Sell S. A., Ericksen J. J., Reis T. W., Droste L. R., Bhuiyan M. B. and Gater D. R., A case report on the use of sustained release platelet-rich plasma for the treatment of chronic pressure ulcers, Journal of Spinal Cord Medicine 2011, 34: 122–7.

[59] Matsui M. and Tabata Y., Enhanced angiogenesis by multiple release of platelet-rich plasma contents and basic fibroblast growth factor from gelatin hydrogels, Acta Biomaterialia 2012, 8: 1792–801.

[60] Ruoslahti E., Fibronectin in cell adhesion and invasion, Cancer Metastasis Reviews 1984, 3: 43–51.

[61] Miyamoto S., Katz B. –Z., Lafrenie R. M. and Yamada K. M., Fibronectin and Integrins in Cell Adhesion, Signaling, and Morphogenesis, Annals of the New York Academy of Sciences 1998, 857: 119-29.

[62] Risau W. and Lemmon V., Changes in the vascular extracellular matrix during embryonic vasculogenesis and angiogenesis, Developmental Biology 1988, 125: 441-50

[63] Custódio C. A., Alves C. M., Reis R. L. and Mano J. F., Immobilization of fibronectin in chitosan substrates improves cell adhesion and proliferation, Journal of Tissue Engineering and Regenerative Medicin2 2010, 4: 316–23.

[64] Li B., Moshfegh C., Lin Z., Albuschies J. and Vogel V., Mesenchymal stem cells exploit extracellular matrix as mechanotransducer, Scientific Reports 2013, 3: 2425.

[65] Regis S., Youssefian S., Jassal M., Phaneuf M. D., Rahbar N. and Bhowmick S., Fibronectin adsorption on functionalized electrospun polycaprolactone scaffolds: experimental and molecular dynamics studies, Journal of Biomedical Materials Research A 2014, 102: 1697–706.

[66] Oliveira M. B., Salgado C. L., Song W. and Mano J. F., Combinatorial on-chip study of miniaturized 3D porous scaffolds using a patterned superhydrophobic platfor, Small 2013, 9: 768–78

[67] Seidlits S. K., Drinnan C. T., Petersen R. R., Shear J. B., Suggs L. J. and Schmidt C. E., Fibronectin-hyaluronic acid composite hydrogels for three-dimensional endothelial cell culture. Acta Biomaterialia 2011, 7: 2401–9.

[68] Mosahebi A., Wiberg M. and Terenghi G., Addition of fibronectin to alginate matrix improves peripheral nerve regeneration in tissue engineered conduits, Tissue Engineering 2003, 9: 209-18.

[69] Schäffler A. and Büchler C., Concise review: adipose tissue-derived stromal cells-basic and clinical implications for novel cell-based therapies, Stem Cells 2007, 25: 818–27.

[70] Strem B. M., Hicok K. C., Zhu M., Wulur I., Alfonso Z., Schreiber R. E., Fraser J. K. and Hedrick M. H., Multipotential differentiation of adipose tissue-derived stem cells, The Keio Journal of Medicine 2005, 54: 132-141.

[71] Fraser J. K., Wulur I., Alfonso Z. and Hedrick M. H., Fat tissue: an underappreciated source of stem cells for biotechnology, Trends Biotechnology 2006, 24: 150–4.

[72] Fraser J. K., Schreiber R., Strem B., Zhu M., Alfonso Z, Wulur I. and Hedrick M. H., Plasticity of human adipose stem cells toward endothelial cells and cardiomyocytes. Nature Clinical Practice Cardiovascular Medicine 2006, 3: S33–7.

[73] Safford K. M. and Rice H. E., Stem cell therapy for neurologic disorders: therapeutic potential of adipose-derived stem cells, Current Drug Targets 2005, 6: 57–62.

[74] Rehman J., Traktuev D., Li J., Merfeld-Clauss S., Temm-Grove C. J., Bovenkerk J. E., Pell C. L., Johnstone B. H. Considine R. V. and March K. L., Secretion of angiogenic and antiapoptotic factors by human adipose stromal cells, Circulation 2004, 109:1292–8.

[75] Puissant B., Barreau C., Bourin P., Clavel C., Corre J., Bousquet C., Taureau C., Cousin B., Abbal M., Laharrague P., Penicaud L., Casteilla L. and Blancher A., Immunomodulatory effect of human adipose tissue-derived adult stem cells: comparison with bone marrow mesenchymal stem cells, British Journal of Haematology 2005,129: 118–29.

[76] Yañez R., Lamana M. L., García-Castro J., Colmenero I., Ramírez M. and Bueren J. A., Adipose tissue-derived mesenchymal stem cells have in vivo immunosuppressive properties applicable for the control of the graft-versus-host disease, Stem Cells 2006, 24: 2582–91.

[77] Schoubben A., Blasi P., Giovagnoli S., Rossi C. and Ricci M., Development of a scalable procedure for fine calcium alginate particle preparation, Chemical Engineering Journal 2010, 160: 363–9.

[78] Rouillard A. D., Berglund C. M., Lee J. Y., Polacheck W. J., Tsui Y., Bonassar L. J. and Kirby B. J., Methods for photocrosslinking alginate hydrogel scaffolds with high cell viability. Tissue Engineering Part C: Methods 2011, 17: 173-9.

[79] Karaoz E., Aksoy A., Ayhan S., Sariboyaci A. E., Kaymaz F. and Kasap M., Characterization of mesenchymal stem cells from rat bone marrow: ultrastructural properties, differentiation potential and immunophenotypic markers, Histochemistry and Cell Biology 2009, 132: 533–46.

[80] Griffiths P. R., Fourier Transform Infrared Spectrometry, United States of America: John Wiley and Sons, 2007.

[81] Jacobsen N. E., NMR Spectroscopy explained: simplified theory, applications and examples for organic chemistry and structural biology, John Wiley & Sons 2007.

[82] Kin S. W., Bae Y. H. and Okano T., Hydrogels: swelling, drug loading and release, Pharmaceutical Research 1992, 9: 283-90.

[83] Fu Y. and Kao W. J., Drug release kinetics and transport mechanisms of non-degradable and degradable polymeric delivery systems, Expert Opinion on Drug Delivery 2010, 7: 429–444.

[84] Arifin D. Y., Lee L. Y. and Wang C.-H., Mathematical modeling and simulation of drug release from microspheres: Implications to drug delivery systems, Advanced Drug Delivery Reviews 2006, 58: 1274–325.

[85] Culture Inserts Instructions provided by Ibidi®, Version 2014-08-08.

[86] Cooper J. A., Effects of Cytochalasin and Phalloidin on Actin, The Journal of Cell Biology 1987, 105:1473–8.

[87] Szer W., Interactions of 4', 6-diamidine-2-phenylindole with synthetic polynucleotides, Nucleic Acids Research 1979, 6: 3519–34.

[88] Waring M. J., Complex formation between ethidium bromide and nucleic acids, Journal of Molecular Biology 1965, 13: 269-82.

[89] Berridge M. V., Herst P. M. and Tan A. S., Tetrazolium dyes as tools in cell biology: new insights into their cellular reduction, Biotechnology Annual Reviews 2005, 11: 127–52.

[90] Vistica D.T., Skehan P., Scudiero D., Monks A., Pittman A. and Boyd M. R., Tetrazolium-based assays for cellular viability : a critical examination of selected parameters affecting formazan production, Cancer Research 1991, 51: 2515–20.

[91] Whyte M.P., Hypophosphatasia and the role of alkaline phosphatase in skeletal mineralization, Endocrine Reviews 1994; 15: 439–461.

[92] Magnusson P. E. R., Larsson L., Magnusson M., Davie M. W. J. and Sharp C. A., Isoforms of bone alkaline phosphatase : characterization and origin in human trabecular and cortical boné, Journal of Bone and Mineral Research 1999, 14: 1926–33.

[93] Gregory C. A., Gunn W. G., Peister A., Prockop D. J., An Alizarin red-based assay of mineralization by adherent cells in culture: comparison with cetylpyridinium chloride extraction, Analytical Biochemistry 2004, 329: 77–84.

[94] Costa P. F., Dias A. F., Reis R. L. and Gomes M. E., Cryopreservation of cell/scaffold tissue-engineered constructs, Tissue Engineering Part C Methods 2012, 18: 852-8.

[95] Galvao J., Davis B., Tilley M., Normando E., Duchen M. R. and Cordeiro M. F., Unexpected low-dose toxicity of the universal solvent DMSO, The FASEB Journal 2014, 28: 1317-30.

[96] Spicer P. P., Kretlow J. D., Young S., Jansen J. A., Kurtis F. and Mikos A. G. Evaluation of Bone Regeneration Using the Rat Critical Size Calvarial Defect, Nature Protocols 2012, 7: 1918-29.

[97] Samkoe K. S. and Cramb D. T. Application of an ex ovo chicken chorioallantoic membrane model for two-photon excitation photodynamic therapy of age-related macular degeneration, Journal of Biomedical Optics 2003, 8: 410-17.

[98] Vargas A., Zeisser-Labouèbe M., Lange N., Gurny R. and Delie F., The chick embryo and its chorioallantoic membrane (CAM) for thein vivo evaluation of drug delivery systems, Advanced Drug Delivery Reviews 2007, 59: 1162–1176.

[99] Auerbach R., Lewis R., Shinners B., Kubai L. and Akhtar N., Angiogenesis assays : a critical overview, Clinical Chemistry 2003, 49: 32–40.

[100] Ho S. T., Hutmacher D. W., A comparison of micro CT with other techniques used in the characterization of scaffolds, Biomaterials 2006, 27: 1362–76.

Section III

Natural-Based Spherical Systems, Prepared on Superhydrophobic Surfaces, for Applications in the Biomedical Field

Chapter 5

Free and Copolymerized γ-Cyclodextrins Regulate the Performance of Dexamethasone-Loaded Dextran Microspheres for Bone Regeneration

5.1. Abstract

Polymeric particles acting as sources of biological cues to promote tissue regeneration are currently an interesting topic in bone tissue engineering research. In this study, microspheres of dextran-methacrylate (dextran-MA) and γ-cyclodextrins (γ-CD) for the delivery of osteogenic agents were prepared by means of photopolymerization on biomimetic superhydrophobic surfaces. The effects of the incorporation of the γ-CD units as free entities or as structural monomers (acrylamidomethyl-γ-cyclodextrin, γ-CD–NMA) on dexamethasone loading and release performance were evaluated in detail in order to achieve osteogenic differentiation of human stem cells. The copolymerization of dextran-MA with γ-CD–NMA improved the loading capacity of the particles and also provided a sustained release of dexamethasone for several days. The biological studies revealed that such microspheres were cytocompatible and capable of inducing the differentiation of human adipose-derived stem cells (hASCs) to osteoblasts, as determined from an increase of alkaline phosphatase (ALP) activity between days 3 and 7. Such results were also confirmed using ALP staining. Therefore, immobilization of γ-CDs onto the dextran-MA network may be particularly useful for the development of cytocompatible implantable spherical biomaterials for bone tissue engineering purposes.

This chapter is based on the following publication:
Lima A.C., Puga A. M., Mano J. F., Concheiro A. and Alvarez-Lorenzo C., Free and copolymerized γ-cyclodextrins regulate the performance of dexamethasone-loaded dextran microspheres for bone regeneration, Journal of Materials Chemistry B 2014, 2: 4943-56.

5.2. Introduction

Cyclodextrins (CDs) are appealing biocompatible tools for the design of drug delivery systems based on hydrophilic hydrogels [1]. The capability of CDs to form inclusion complexes with a variety of active substances usually does not diminish, but enhances even when the CDs are trapped in a polymer network [2,3]. Thus, poorly soluble drugs can be homogeneously loaded up to a great extent in hydrophilic networks forming complexes with CDs [4-6]. Regarding control of the release kinetics, the inclusion complex capability of CDs can be exploited in two different ways: (a) as free entities, i.e., not chemically bound to the network, CDs can accelerate or retard drug diffusion through the network depending on drug solubility and interactions with the polymer component of the hydrogel; and (b) as chemically bound moieties, CDs act as binding points for the drug, regulating the release by an affinity-dependent mechanism [1]. Different from other additives, such as micelle-forming surfactants or liposome-forming lipids that require self-assembly for hosting drugs and regulating the diffusion from polymer networks [7,8], CDs offer relevant advantages as highly stable unimolecular guest agents. Several approaches can be followed to immobilize CDs in polymer networks through covalent bonds under mild conditions [1,9,10]. Recently, γ-CD nanogels obtained via direct crosslinking in an emulsified system were shown to be able to load dexamethasone for application as eye drops, being highly biocompatible in in vivo studies performed in rabbits [11].

The aim of this work was to use the superhydrophobic surface technology [12] to produce spherically shaped microgels combining dextran-MA and γ-CD that can deliver dexamethasone and induce the differentiation of stem cells into osteoblasts, for tissue engineering or regenerative medicine purposes. The influence of free γ-CDs and copolymerized γ-CD–NMA on the capability of hydrogel particles to load and to control the release of the poorly water soluble corticoid drug was evaluated in detail. Dextran is a highly hydrophilic and biocompatible natural polysaccharide consisting mainly of linear chains of α-1,6-linked glucopyranose monomers, widely used as carriers for hydrophilic bioactive agents and as components of scaffolds [13,14]. On the other hand, γ-CDs are highly soluble in water (18.5–39 g per 100 mL at 20–35 °C) allowing the production of hydrogels with high content in freely dispersed γ-CDs [9]. Moreover, monomers of γ-CD have been previously shown to be useful to enhance the uptake of hydrophobic drugs by acrylic networks [15]. Despite the potential advantages of combining dextran and CDs, very few binary systems have been reported yet. Fernández et al. [16] synthesized a copolymer of dextran and amino derivatives of β-CD to be applied as a thermoprotectant of trypsin. Later, Ramirez et al. [17] reported covalently bonded β-CD-dextran as a macromolecular carrier for naproxen, a poorly soluble non-steroidal anti-inflammatory drug. Using click chemistry, Nielsen and co-workers [18] synthesized an open-chain

polymer resultant of the combination of alkyne-modified dextran and β-CDs functionalized with azide groups. Using two formulations proposed in such work, Fülöp et al. [19] studied their complex forming properties with a model drug and their aggregation ability. Stable nanoassemblies spontaneously formed by mixing dextran-β-CD polymers and dextran-adamantyl have been explored for drug delivery due to their low toxicity [20]. However, to the best of our knowledge, dextran–CD networks have not been explored yet for sustained release in tissue engineering applications. In this context, particulate drug delivery systems are especially attractive due to its potential to be implanted via minimal invasive maneuvers [21-24].

Under osteogenic stimuli, some stem cells have the ability to differentiate into osteoblasts, expressing characteristic markers such as bone-specific ALP [25]. This ability of the stem cells can be favorable in the development of bone tissue engineering strategies. For example, human adipose-derived stem cells (hASCs) have been shown to exhibit potential to differentiate into mesodermal phenotypes including osteoblasts, chondrocytes, adipocytes, endothelial, neural and muscle cells [26,27]. An advantage of adipose tissue as a source of stem cells is its abundance and easy accessibility. The osteogenic differentiation of hASCs in vitro has been reported by supplementing the cell culture medium with ascorbic acid, β-glycerophosphate (β-GP) and a glucocorticoid such as dexamethasone [28,29]. The osteogenic differentiation varies with the dexamethasone dose; the optimal concentration being between 10 and 100 nM. Toxic effects have been found at 1000 nM dexamethasone [30]. In fact, the prolonged duration of exposure in vivo may cause severe osteoporosis [31,32].

To prepare the proposed spherical microgels (dextran + CDs) a technique consisting of the photopolymerization of aqueous dispersion droplets onto superhydrophobic surfaces was implemented. Compared to other techniques, this bioinspired methodology is simpler, cheaper and faster, does not require the use of organic solvents or a complex apparatus and allows obtaining particles with narrow size distribution and 100% encapsulation yield of freely diffusible species [33]. This technology permits also the production of multilayered particles [34] for protein or cell encapsulation under mild conditions [35]. The loading capability, the ability to sustain the release of dexamethasone, the cytocompatibility of the final formulated systems and their potential to be applied in bone regeneration were evaluated in detail.

5.3. Experimental Section

5.3.1. Materials

PS sheets from square Petri dishes (Bdbioscience, Enzifarma, Portugal) and polystyrene granules from a grade for injection molding (Styrolution PS 158k; UL Ides, Portugal) were used in the preparation of the superhydrophobic substrates. Tetrahydrofuran (THF, 99.9%) was from Riedel de Haen (Germany).

1H,1H,2H,2H-Perfluorodecyltriethoxysilane (PFDTS, 97%), dextran from Leuconostoc mesenteroids (MW 100–200 kDa), 4-(N,N-dimethylamido)pyridine (DMAP, 99%), hydrochloric acid (HCl, 37%), acetone, dexamethasone for cell culture, penicillin/streptomycin solution, L-glutamine, β-glycerophosphate disodium salt hydrate (β-GP), ascorbic acid, ALP substrate, p-nitrophenyl phosphate liquid substrate, naphthol AS-BI phosphate disodium salt, fast red violet, 2-amino-2- methyl-1,3-propanediol, and Dulbecco's Modified Eagle medium (DMEM) nutrient mixture F-12 Ham were obtained from Sigma-Aldrich (USA). The BCA kit was purchased from Pierce (USA), the cell proliferation kit (MTT) and the cytotoxicity detection kit (LDH) were supplied by Roche (Switzerland). Paraformaldehyde tablets were obtained from Panreac (Spain). Mesenchymal stem cells, StemPRO® human adipose-derived stem cells (hASCs), MesenPro RS basal medium and MesenPro RS growth supplement were from Gibco (Invitrogen, USA). Phosphate buffer solution 10x and dimethyl sulfoxide (DMSO) were from Fisher Chemicals (UK). Glycidyl methacrylate (GMA) was from Fluka (Sigma-Aldrich, USA), Irgacure 2959 from Ciba (BASF, Germany) and dexamethasone was from Fagron (Spain). γ-Cyclodextrin (γ-CD) Cavamax W8 was from ISP and N-(hydroxymethyl)acrylamide (NMA) from Merck (Germany). Purified water (resistivity >18MU cm; MilliQ®, Millipore, Spain) was obtained by means of reverse osmosis. All the other chemicals were used as received.

5.3.2. Polystyrene Superhydrophobic Surfaces

Polystyrene (PS) superhydrophobic surfaces were prepared using a phase separation method as described elsewhere [36]. Briefly, a PS solution (70 mg/mL) in THF was mixed with ethanol (2:1.3 v/v). The mixture was dispensed onto smooth PS commercial substrates which were then immersed in ethanol for 1 min and dried under nitrogen flow. In order to increase the superhydrophobicity of obtained surfaces, the rough PS surfaces were modified with PFDTS (1% v/v in ethanol) after argon plasma treatment for 40 s at 30 W (Plasma Prep5, Gala Instruments, Germany).

5.3.3. Synthesis of Dextran-Methacrylate

Dextran-MA was synthesized as previously described [37]. Briefly, dextran (25 g) was dissolved in DMSO (225 mL) under a nitrogen atmosphere. Then, 4-(N,N-dimethylamino)pyridine (5 g) was added and, when the dissolution was complete, glycidyl methacrylate (20.5 mL) was incorporated. The solution was stirred at room temperature for 48 h, and then the reaction was stopped by adding an equimolar amount of concentrated HCl solution (3.3 mL of HCl, 37%) to neutralize 4-(N,N-dimethylamino)pyridine. The reaction mixture was transferred to a dialysis tube (MWCO 12400 Da) and dialyzed during 1 month against

demineralised water. Finally, dextran-MA was lyophilized (Manifold freeze-drier, Telstar cryodos, Spain). 1 H NMR spectra of unmodified and modified dextrans (0.3 g in 0.7 mL of deutered water) were recorded (Mercury 300, 300 MHz, Varian, Australia) and then analyzed using MestReNova software (MestreLab, Spain).

5.3.4. Synthesis of Acrylamidomethyl-γ-Cyclodextrins

γ-CD (17.12 g) and NMA (13.36 g) (NMA–γ-CD 10:1 molar ratio) were added to 50 mL of HCl solution (1% v/v). The solution was heated at 80 °C and stirred continuously for 30 min. Then, 300 mL of acetone were added to precipitate γ-CD–NMA. The flask was kept at 4 °C overnight. The precipitate was filtered (Albet® 145, Spain), repeatedly washed with acetone (200 mL) and filtered again (2–3 cycles). Finally, the product was dried under vacuum for 2 days at room temperature and stored at 4 °C. The IR spectrum of the γ-CD–NMA monomer was recorded over the range 400–4000 cm^{-1} (Bruker IFS 66V FT-IR, Germany) using the potassium bromide (KBr) pellet technique, and 1H NMR spectra of unmodified and modified γ-CD (30 mg/mL in deutered water) were recorded (Mercury 300, 300 MHz, Varian, Australia) and then analyzed using MestReNova software (MestreLab, Spain).

5.3.5. Microgels Preparation

Dextran-MA solutions (5% or 10% w/v; 1 mL) were prepared in water or in an aqueous medium containing 200 mg of γ-CD or γ-CD–NMA. Irgacure 2959 (60 mL or 100 mL of 0.5% w/v in water) was added to the solutions (Table 5.1). 5 mL of each solution were dispensed onto the PS superhydrophobic surfaces, and crosslinked under UV light (365 nm; Camag, Switzerland) for 50–60 min. The solid particles were dried in air overnight, washed with water for 48 h and dried again in air at room temperature.

Table 5.1. Composition of the dispersions used to prepare the microgel particles. Amounts refer to 1 mL of water

Code	Dextran-MA	g-CD	g-CD–NMA	Irgacure
5% Dextran-MA	50 mg	–	–	60 µL
5% Dextran-MA+20% γ-CD	50 mg	200 mg	–	60 µL
5% Dextran-MA+20% γ -CD–NMA	50 mg	–	200 mg	60 µL
10% Dextran-MA	100 mg	–	–	100 µL
10% Dextran-MA+20% γ -CD	100 mg	200 mg	–	100 µL
10% Dextran-MA+20% γ -CD–NMA	100 mg	–	200 mg	100 µL

5.3.6. Microgels Characterization

5.3.6.1. Quantification of Unreacted Photoinitiator

Three particles of each formulation were immersed in 1 mL of acetonitrile and kept under magnetic stirring for at least 6 h at room temperature. The amount of Irgacure 2959 released was quantified by HPLC using an Accucore C18 (3 mm x 150 mm, 2.6 mm) column kept at 37 °C, a UV-Vis detector (275 nm, SpectraSystem UV8000 – Thermo Scientific) and acetonitrile:water (90:10, 0.5 mL/min flow) as the isocratic mobile phase.

5.3.6.2. Double Bond (C=C) Detection (Bromine Test)

5% (w/v) dextran-MA, 10% (w/v) dextran-MA, 20% (w/v) γ-CD and 20% (w/v) γ-CD–NMA precursor solutions (40 µL , equivalent volume to prepare 8 particles) and the different formulated cross-linked particles (8 units) were placed in contact with 200 mL of bromine in water at room temperature. After 5 min, the color of the solutions was observed and compared with the original bromine in water solution. The bromine in water was prepared mixing 32 mL of water, 7.6 mL of NaClO solution (33 mg/mL) and 10.7 mL of a solution of NaBr (1.1 g) in 1 M HCl.

5.3.6.3. Degree of Swelling

The degree of swelling was evaluated in sextuplicate as the difference between the weight of 10 particles swollen in water for 6 days (m_i) and the initial weight of the dried particles (m_0) as follows:

$$\%\ \text{Swelling} = \frac{m_i - m_0}{m_0} \times 100 \quad \text{Eq. 1}$$

5.3.6.4. Particle Size

The sizes of dried and swollen particles were evaluated using an Olympus SZ-CTV optical stereomicroscope (Tokyo, Japan) connected to a JCV TK-S350 video camera (Tokyo, Japan). Eight particles of each formulation were sized using image analysis software (Soft Imaging System®, Mu¨nster, Germany).

5.3.6.5. Scanning Electron Microscopy

The particles were allowed to swell in water at room temperature. Then, some were collected and allowed to dry in air, and the others were immediately frozen in liquid nitrogen and freeze-dried. The images of the particles, after gold coating, were obtained using an EVOLS15 microscope (Zeiss, Oberkochen, Germany).

5.3.6.6. Dexamethasone Solubilization

A large excess of dexamethasone (8 mg) was dispersed into 50 mL of water and maintained under magnetic stirring during 48 h. Then, the dispersions were filtered through a 0.22 μm nylon membrane to remove the non-dissolved drug. The concentration of the dissolved dexamethasone was spectrophotometrically measured at 241 nm (Agilent 8453, Waldbornn, Germany).

5.3.6.7. Dexamethasone Loading

Ten particles of each formulation were dried in air overnight and then immersed in 10 mL of aqueous solution of dexamethasone (30 μg /mL) for 6 days at room temperature. The absorbance of each solution was measured at 241 nm over time. The experiments were repeated six times for each formulation. The amount of drug loaded *via* equilibrium between the aqueous phase of the microgels and the loading solution was estimated as follows [37]:

$$\text{Loading (aqueous phase)} = \frac{V_s}{W_p} \times C_0 \quad \text{Eq. 2}$$

where V_s is the volume of water sorbed by each particle, W_p is the dried weight of the particles, and C_0 is the concentration of drug in the loading solution.

5.3.6.8. Dexamethasone Release

Dexamethasone-loaded particles (10 units) were dried overnight and then immersed directly in 2 mL of water and placed in an incubating mini shaker (VWR) at 37 °C and 200 rpm. At 24, 120, 264, 336 and 432 h, 1 mL of water was added to the initial release medium. Samples of the release medium were taken periodically and returned to the container after measuring the absorbance at 241 nm. The experiments were repeated four times for each formulation.

5.3.6.9. Cytocompatibility Studies

Two particles of each formulation (4 replicates) were placed in 48 well plates containing SaOs-2 cells (ATCC HTB-85; 50 000 cells per well, 1 mL) in DMEM-F12 with 10% FBS and 1% penicillin/streptomycin, and kept in a humidified incubator at 5% CO_2 and 37 °C. After 24 h and 72 h of incubation, aliquots of 100 μL of the culture medium were taken and mixed with 10 μL of the reaction medium contained in the Cytoxicity Detection kit (LDH). Blank (100 μL of the cell culture medium), negative (an aliquot collected from a well containing just cells) and positive (an aliquot collected from a well to which 20 μL lysis factor

was added) controls were also performed. The plates were incubated for 10 min at room temperature protected from light. 50 μL of stop solution was added to each well and the absorbance was measured at 490 nm using a microplate reader (BIORAD Model 680 Microplate Reader). The cytotoxicity was estimated as follows:

$$\%\text{Cytotoxicity} = \frac{\text{abs}_{\text{experiment}} - \text{abs}_{\text{negative control}}}{\text{abs}_{\text{positive control}} - \text{abs}_{\text{negative control}}} \times 100 \quad \text{Eq. 3}$$

5.3.6.10. Osteogenic Differentiation

hASCs were cultured in MesenPro® RS medium supplemented with 2% (v/v) growth supplement (FBS), 1% (v/v) L-glutamine (200 mM) and 1% (v/v) penicillin/streptomycin (Medium 1). Then, they were seeded (passage 5, 25000 cells per well, 1 mL) in 6 well plates and after 24 h the medium was replaced by 5 mL of fresh medium. Three particles of each formulation (placebo or loaded with dexamethasone) were placed in direct contact with the cells and the Medium 1 was supplemented with 10 mM β-glycerophosphate and 50 mM ascorbic acid. Four controls were carried out in this experiment:

i) negative control 1: cells cultured in MesenPro® supplemented with 2% (v/v) growth supplement, 1% (v/v) L-glutamine (200 mM) and 1% (v/v) penicillin/streptomycin (Medium 1);

ii) positive control 1: cells cultured in standard osteogenic differentiation medium, i.e., Medium 1 supplemented with 10 mM β-GP, 100 nM dexamethasone for cell culture and 50 mM ascorbic acid (Medium 2);

iii) negative control 2: cells cultured in Medium 1 supplemented with 10 mM β-GP and 50 mM ascorbic acid (Medium 3);

iv) positive control 2: cells cultured in Medium 1 supplemented with 10 mM β-GP, 50 mM ascorbic acid and 400 ng mL^{-1} of dexamethasone were used to load the formulations under study (Medium 4).

The plates were incubated at 37 °C in a humidified atmosphere with 5% CO_2 and 2 mL of medium were replaced twice a week. The cells were routinely observed using inverted microscopy (x10) in order to discard any contamination. Experiments were carried out in triplicate. Cell proliferation was evaluated using the MTT assay. At 3, 7 and 12 days of incubation 4 mL of culture medium were withdrawn and 100 μL of MTT solution (5 mg/mL in PBS) were added to each well. These plates were incubated at 37 °C for

4 h and then 1 mL of MTT solvent (10% SDS in 0.01 M HCl) was added to each well and the plates were incubated again at 37 °C overnight. Aliquots of 200 μL were transferred to 96 well plates and the absorbance was read at 550 nm (BIORAD Model 680 Microplate Reader). The respective calibration curve was constructed using cultures with a known number of cells in order to estimate the cell number in the experiment. For ALP quantification, the cells were lysed at 3, 7 and 12 days by addition of 300 μL 10 mM Tris–HCl buffer (pH 7.5) with 0.1% Triton X-100. Samples were exposed to three freezing (-80 °C for 45 min)/thawing cycles. Lysates were centrifuged at 14000 rpm for 15 min at 4 °C. 50 μL of the supernatant were incubated with 150 μL of the ALP substrate in 96 well plates at 37 °C for 30 min. The absorbance at 405 nm was read at 5, 10, 15, 20 and 30 min using an ELISA plate reader (BIORAD Model 680 Microplate Reader). The ALP activity was quantified using a calibration curve prepared with p-nitrophenylphosphate solutions. The obtained values were normalized by the protein concentration measured using a BCA protein detection kit in order to express the results as nmoles of ALP per min per mg of protein.

ALP staining was carried out as follows. After each culture period, the medium was removed, and the cells were fixed with 4% paraformaldehyde in PBS for 5 min at room temperature and then washed twice with PBS. The cells were then soaked in a staining solution prepared by mixing 0.2% naphthol AS-BI phosphate in 112 mM 2-amino-2-methylpropanediol (AMPD) and 0.2% fast red violet in a 1:1 (v:v) proportion, incubated in darkness for 10 min at room temperature and visualized through an inverted light microscope.

5.3.6.11. Statistical Analysis

All data are presented as mean ± s.d. for at least three independent measurements. Groups were compared using one-way ANOVA (Tukey's multiple comparison test), with $p < 0.05$ indicating statistical significance.

5.4. Results and Discussion

5.4.1. Synthesis of Dextran-MA and γ-CD–NMA

Dextran functionalized with methacrylate groups (dextran-MA) was obtained by reaction of dextran with glycidyl methacrylate (GMA) in DMSO in the presence of a base (DMAP) as a catalyst [37]. After 48 h of reaction at room temperature, DMAP was neutralized with hydrochloric acid in order to avoid alkaline hydrolysis of the methacrylic ester, and finally dextran-MA was purified by dialysis. The hydroxyl groups of dextran were ionized at alkaline pH and reacted with methylene carbon of the epoxy group of GMA to form

the 3-methacryloyl-1-glyceryl ether of dextran or the respective isomer 2-methacryloyl-1-glyceryl, as shown in Scheme 5.1.

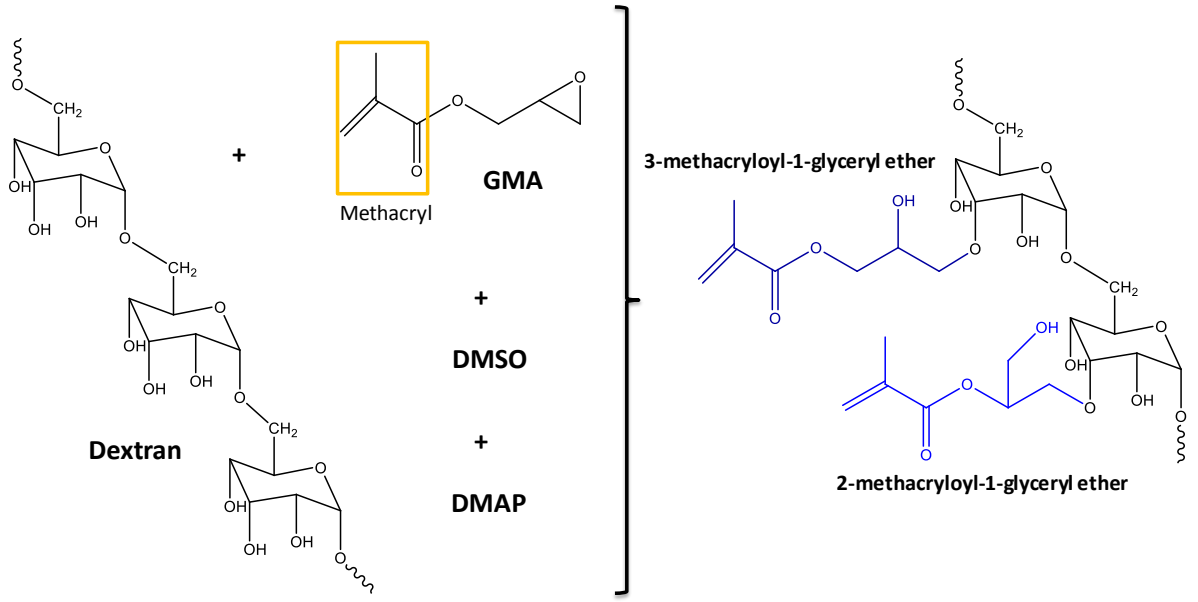

Scheme 5.1. Reaction of dextran with GMA in the presence of DMSO and DMAP. The glycidyl group may interact with any of the hydroxyl groups present in the dextran structure, and two region isomers could be created: 2-methacryloyl-1-glyceryl ether and 3-methacryloyl-1-glyceryl ether.

In the reaction mixture, the molar ratio of GMA to glucopyranose units was approximately 1. Based on ^{1}H NMR spectra (Figure 5.1) and taking into account that each glucopyranose unit has 3 hydroxyl groups that could react with GMA, the degree of substitution (DS) was determined as (100X/Y)/3; X being the average integral of the protons in the double bond present in the added groups (5.75 and 6.2 ppm), and Y the integral of the peak at 4.95–5.1 ppm corresponding to the anomeric proton [37]. The DS obtained was *ca.* 32%, which indicated that, on average, 1 hydroxyl group per glucopyranose unit was substituted [55]. These results were in agreement with the high yield of reaction previously reported in the literature, which indicated that more than 90% of the added GMA was incorporated into the polysaccharide [37].

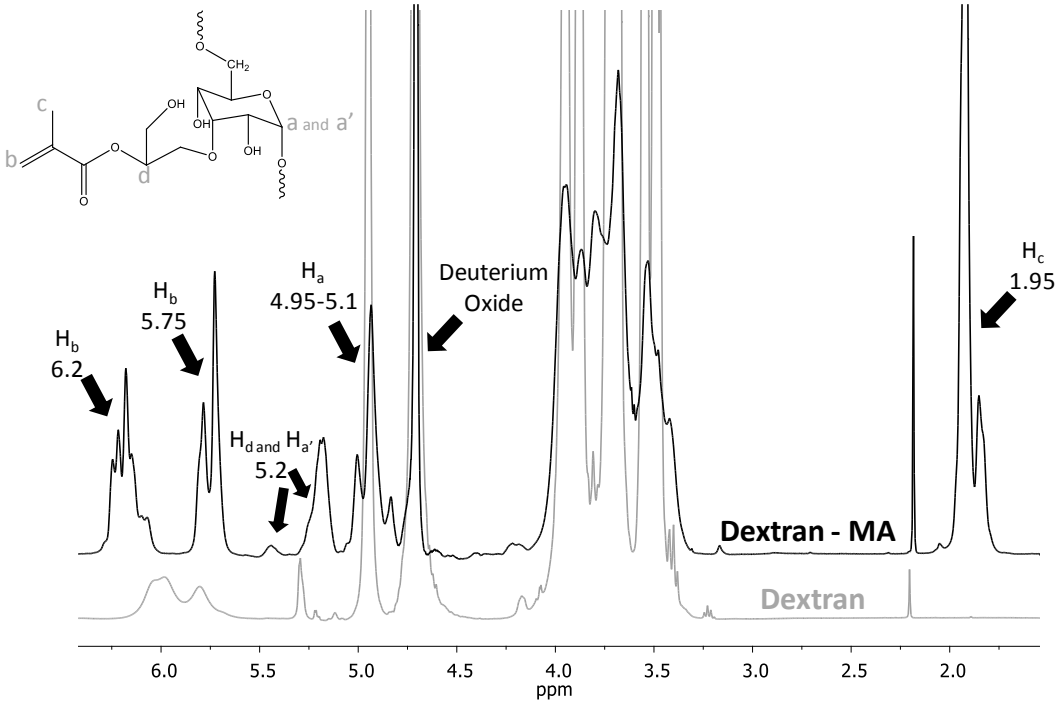

Figure 5.1. ^{1}H NMR spectra of dextran as supplied (gray line) and after reaction with GMA (black line) dissolved in deutered water.

The γ-CD–NMA monomer was prepared according to a previously established protocol that renders one CH2=CH– group per γ-CD, as confirmed from the 1H NMR spectrum (Figure 5.2 B). The DS was estimated from [100X/(Y/8)]/3, where X was the average integral of the protons in the vinyl groups (6.2 and 5.8 ppm), and Y the integral of the peak (5.0 ppm) corresponding to 8 protons of the γ-CD (1 proton per glucopyranose unit). The obtained result indicates that *ca.* 12% of the glucopyranose units were modified, meaning that on average each γ-CD had one NMA group. Thus the MW of γ-CD–NMA can be estimated to be 1378.24 g mol^{-1} [15] (Scheme 5.2). FTIR analysis of γ-CD–NMA clearly showed the bands of carboxylic (C=O) and amide II (NH) groups at approximately 1700 cm^{-1} and 1540 cm^{-1}, respectively, and a small peak due to C=C vinyl groups at 1665 cm^{-1} (Figure 5.2 A) in agreement with previous reports [15,39].

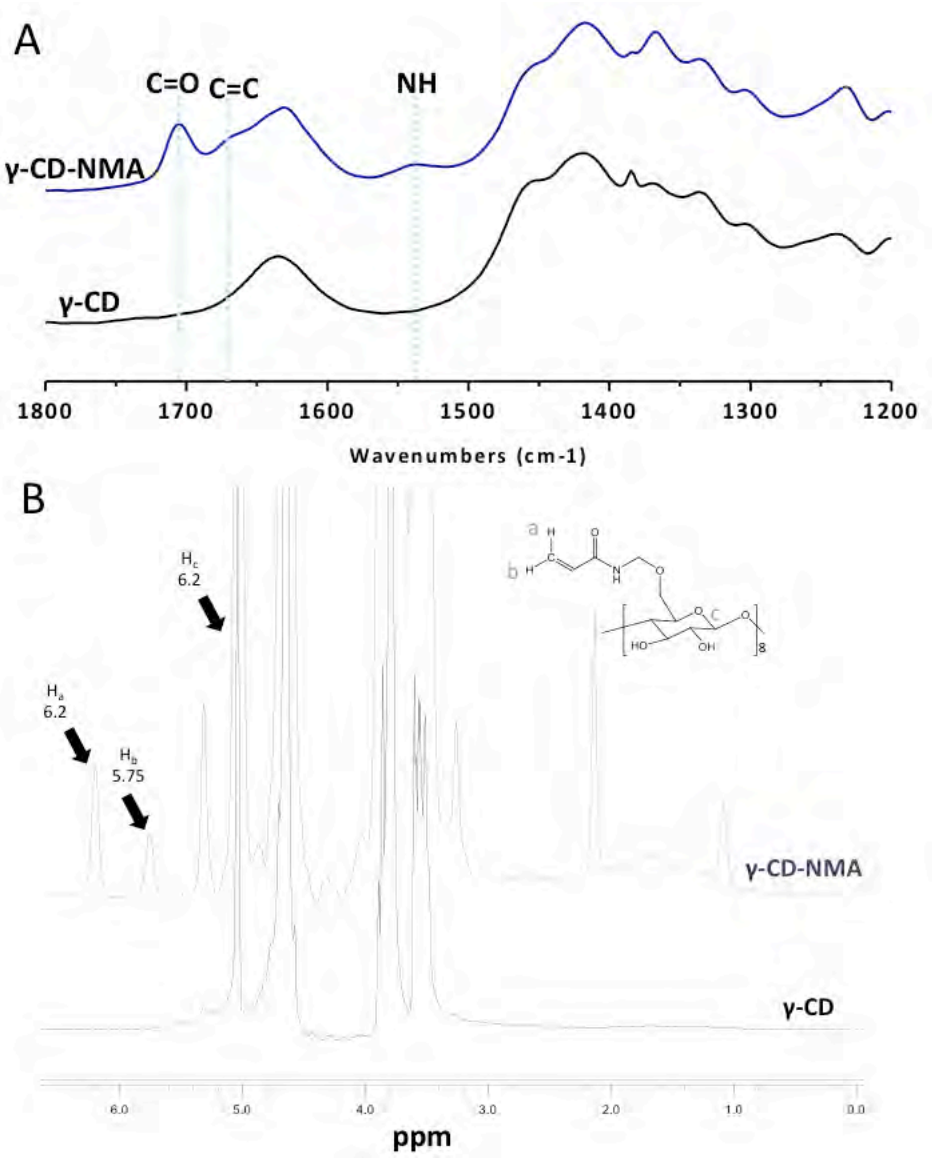

Figure 5.2. (A) FTIR and (B) ^{1}H NMR spectra of γ-CD (black lines) and γ-CD–NMA (blue lines).

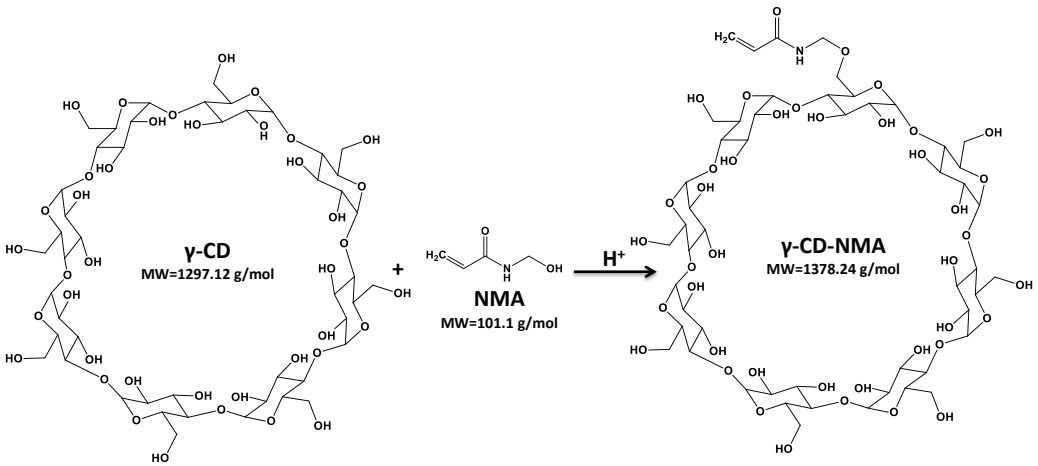

Scheme 5.2. Scheme of the γ-CD monomer (γ-CD–NMA) after reaction with one N-(hydroxymethyl)acrylamide (NMA). The molecular weight of the monomer was estimated assuming that each γ-CD has one NMA group.

5.4.2. Hydrogel Particles Production and Characterization

The spherical particulate hydrogels were obtained under mild conditions on superhydrophobic surfaces [12]. Fixed volumes of dextran-MA solutions containing γ-CD or γ-CD–NMA (Table 5.1) were dispensed onto the PS superhydrophobic platform and cross-linked under UV light using Irgacure 2959 as the photoinitiator. The particle size ranged from 681 to 915 μm (Table 5.2). Three different network types were prepared using two dextran-MA concentrations (5% and 10% (w/v)): (i) particles formed by a dextran-MA solely network; (ii) particles that consist of a dextran-MA network with free γ-CDs; and (iii) particles formed by copolymer networks of dextran-MA and γ-CD–NMA.

Table 5.2. Size and swelling degree of particles prepared with different combinations of dextran-MA and γ-CDs, and the amount of unreacted Irgacure 2959 remnant in each particle formulation after UV photocrosslinking.

Code	Particle size (mean ± SD) (μm)		Swelling degree (mean ± SD) (%)	Irgacure 2959 unreacted (% of the initial amount added)
	Dried particles	Swollen particles		
5% Dextran-MA	681±36	1008±55	223±11	0.48
5% Dextran-MA + 20% γ-CD	683±36	1041±75	248±33	8.12
5% Dextran-MA+ 20% γ-CD-NMA	790±37	1197±78	253±15	1.06
10% Dextran-MA	862±27	1377±81	338±18	0.99
10% Dextran-MA + 20% γ-CD	873±36	1477±70	329±15	2.40
10% Dextran-MA + 20% γ-CD-NMA	915±37	1536±82	242±13	0.87

The inter- and intra-chain bonds that may occur in such formulations are depicted in Scheme 5.3. Hardening of the precursor spherical droplets under UV radiation was affected by the presence of γ-CD units. Droplets without γ-CD showed faster and more successful cross-linking by just adding half of the volume of Irgacure 2959 (0.5% w/v) indicated in Table 5.1. It has been previously reported that CDs interact selectively with alkyl side chains [40]. Both dextran-MA and Irgacure 2959 have alkyl groups, namely methyl groups (–CH_3), that may form inclusion complexes with γ-CDs in the precursor solution, which in turn may limit the interaction of the photochemically generated free radicals with the monomers and consequently decrease the polymerization efficiency [41]. To overcome this problem, the amount of Irgacure 2959 was increased (Table 5.1). The unreacted photoinitiator was quantified in freshly prepared (unwashed) particles. Significant amounts were found in microgels prepared with free γ-CD (Table 5.2). In contrast, almost all the photoinitiator was consumed during preparation of the formulations composed of dextran-MA solely and dextran-MA + 20% γ-CD–NMA. In the absence of CDs, all Irgacure 2959 molecules and methacrylate groups of dextran-MA are available for reaction. In the dextran-MA and γ-CD–NMA

mixtures, the presence of more reactive double bonds caused greater consumption of the photoinitiator. Nevertheless, even under the most unfavorable conditions, more than 90% of the photoinitiator was consumed in the crosslinking. To gain further insight into the polymerization yield, double bonds remaining after cross-linking were quantified by means of a bromine test. Bromine reacts very rapidly with alkenes leading to attenuation of the characteristic yellow-orange color of the bromine solution.

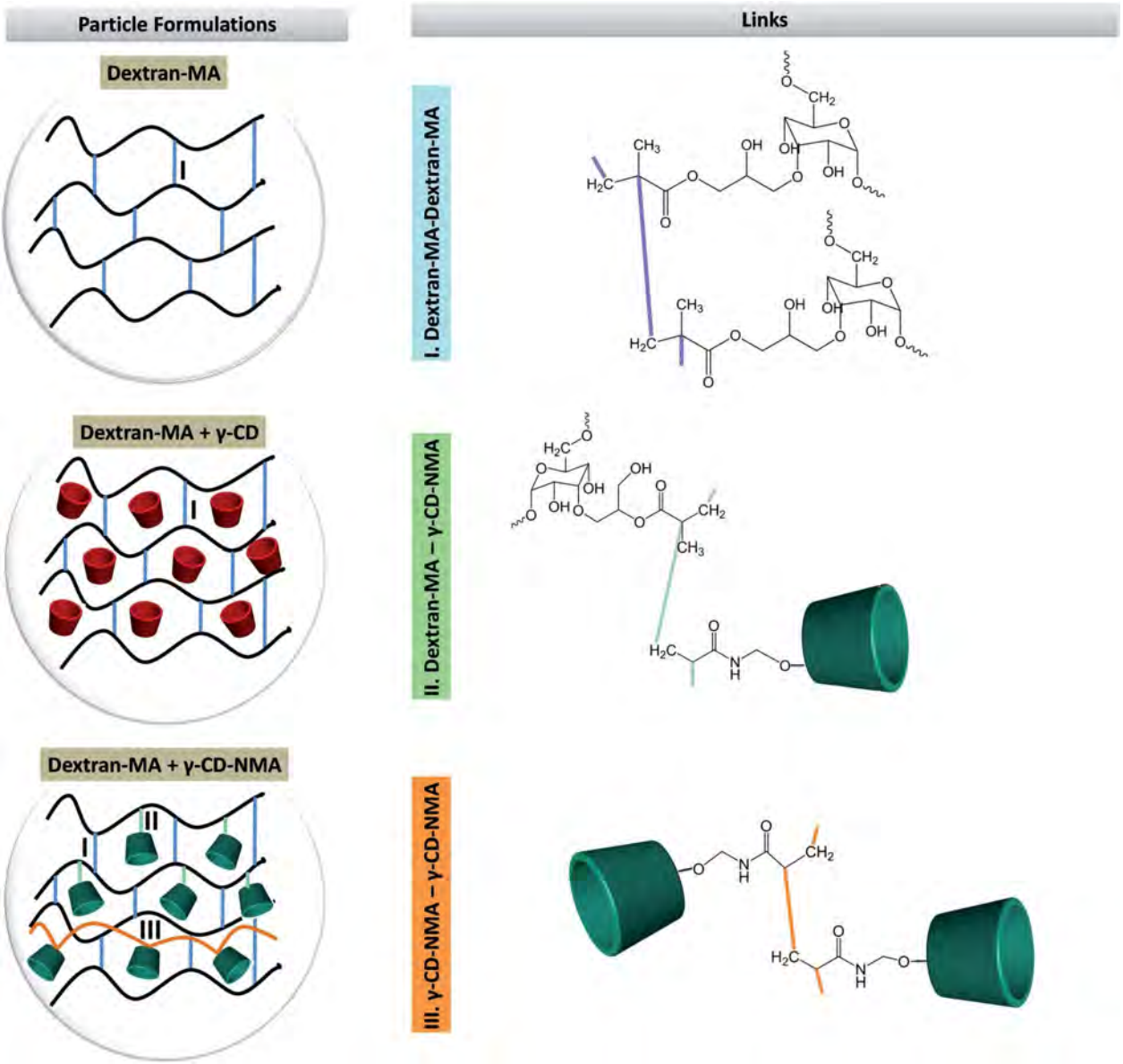

Scheme 5.3. Photocrosslinking of the dextran-MA solution drops may result in three distinct covalent bonds: (A) dextran-MA–dextran-MA; (B) dextran-MA–γ-CD–NMA; (C) g-CD–NMA–γ-CD–NMA.

As expected, dextran-MA solutions (precursor solutions used to prepare the particles) dramatically altered the color of the bromine solution (Figure 5.3 A and E); the attenuation being more accentuated for higher polymer concentration solutions. The γ-CD–NMA solution also showed a slight lightening of the original

color (Figure 5.3 K), which was not induced by γ-CD solution (Figure 5.3 J). Such color modifications confirmed the presence of C=C double bonds in dextran-MA and γ-CD–NMA through the methacrylic and acrylic added groups, respectively. By contrast, the particles did not cause modifications in the color of bromine solution (Figure 5.3 B–D and F–H) meaning that the UV cross-linking was efficient and almost all C=C bonds disappeared. Therefore, the process implemented to prepare dextran-MA particles enables the obtaining of spherical microparticles with nearly 100% crosslinking yield, with minor amounts of the residual photoinitiator. For subsequent experiments, the particles were washed to remove the traces of the unreacted photoinitiator.

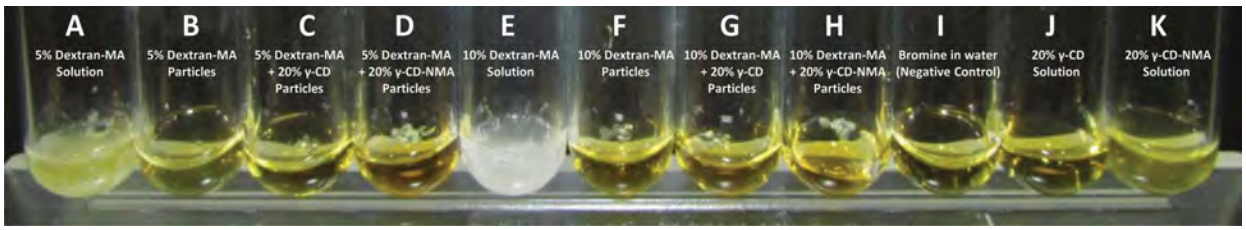

Figure 5.3. Color of bromine aqueous solutions 5 min after pouring 40 μL of precursor solutions used for particle production or 8 particles of each formulation.

Stereomicroscope images of the particles after being dried are shown in Figure 5.4. The particles made from 5% dextran-MA solutions were ca. 200 μm smaller than those prepared with the 10% polymer (Table 5.2) due to the lower polymer density. For the same content in dextran-MA, copolymerization with γ-CD–NMA increased the particle size, probably due to the considerable volume occupied by the γ-CD units in the copolymer mesh. In contrast, free γ-CDs did not significantly modify the size of dextran-MA solely networks. The low standard deviations obtained in size measurements clearly indicate that the accurate volume of precursor solution dispensed on the superhydrophobic surfaces allows the production of particles with a narrow particle size distribution. After swelling, the increase in the particle diameter (300–400 μm and 600–700 μm for 5% and 10% dextran-MA formulations, respectively) confirmed their high ability for water uptake. In the 5% dextran-MA particles, γ-CD or γ-CD–NMA did not affect the swelling (225–250% for the three studied formulations) (Table 5.2). The swelling degree of 10% dextran-MA particles without and with free γ-CD was around 338 ± 18% and 329 ± 15%, respectively. However, the dextran-MA + γ-CD–NMA copolymer particles exhibited a lower swelling degree, approximately 242 ± 13%, which is in agreement with the denser interconnected network that can be created due to the additional covalent linkages that γ-CD–NMA molecules can establish among themselves and with dextran-MA (Scheme 5.3).

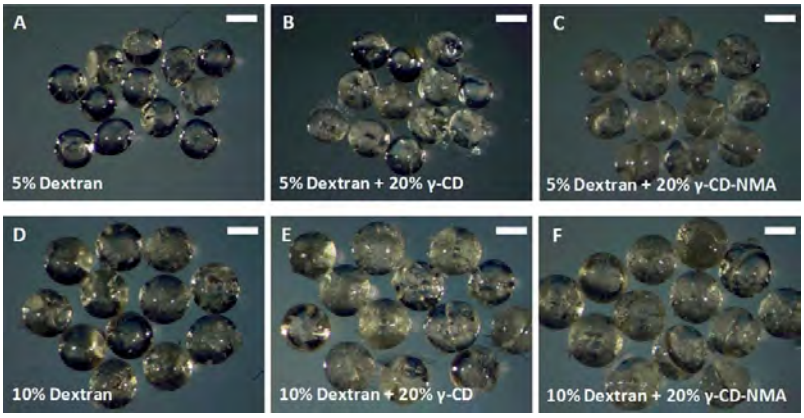

Figure 5.4. Stereomicroscope images of the dried particles. The scale bar is 500 μm.

The digital (Figure 5.4) and SEM (Figure 5.5 and 5.6) micrographs confirmed the spherical shape of the formulated gels. Regarding the structure of the particles, the SEM micrographs of the freeze-dried particles (Figure 5.5) revealed a porous surface due to the dry process used; conversely, the air-dried particles (Figure 5.6) showed a smooth surface. It is also noticeable that all particles exhibited a heterogeneous internal structure, as visualized in freeze-dried and in air-dried particles. The particles seemed to have a coating layer that probably resulted from the non-homogeneous cross-linking due to a more intense UV photocrosslinking efficiency on the surface than in the inner part of the spherically shaped gels.

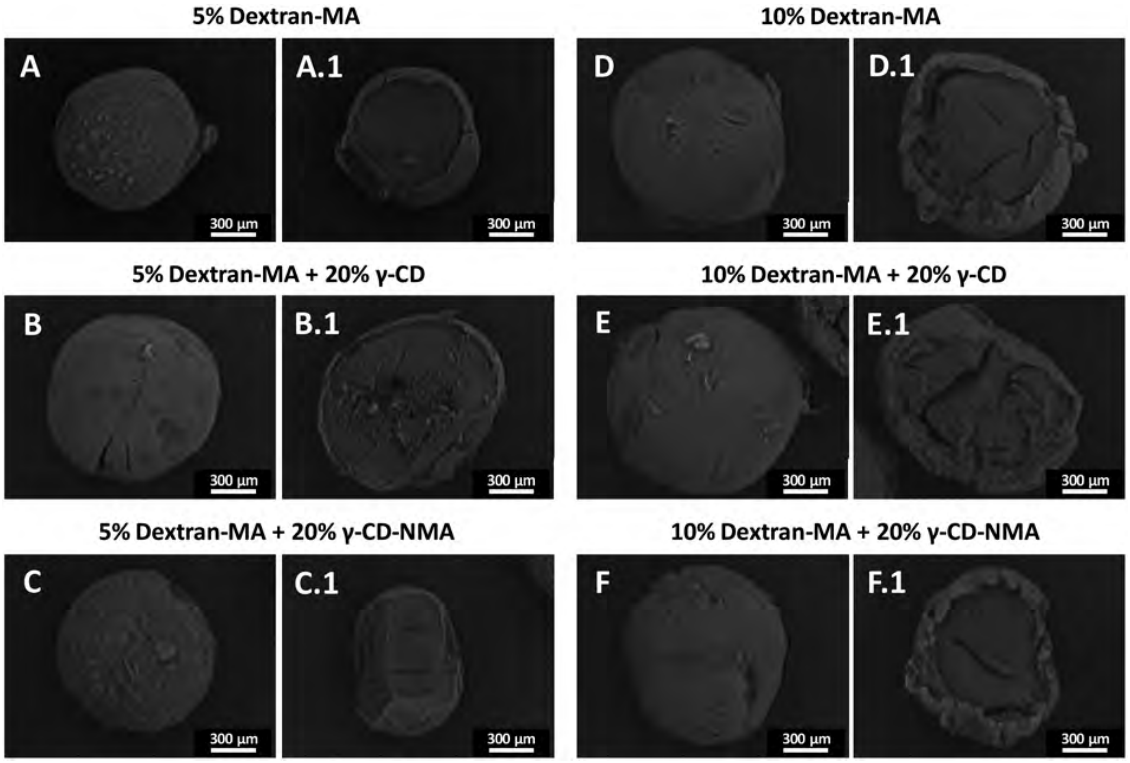

Figure 5.5. SEM micrographs of swollen freeze-dried particles and their respective cross-sections.

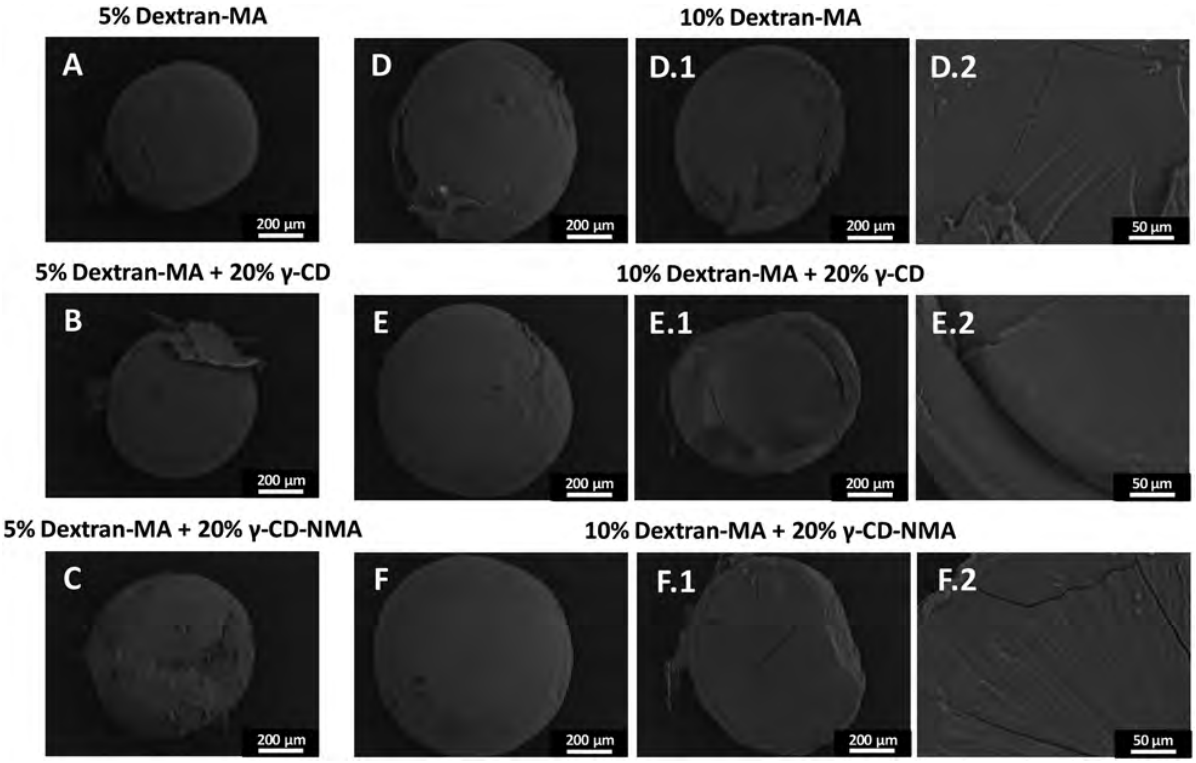

Figure 5.6. SEM micrographs of the air-dried particles, cross-sections and respective magnifications.

5.4.3. Dexamethasone Loading and Release

The loading of a drug in a hydrogel depends on: (i) the easiness of the drug molecules to diffuse into the hydrogel mesh (which is determined by the cross-linking degree and the affinity of water for the network), (ii) the drug concentration in the loading solution and (iii) the affinity of the drug for the network [9,38,42]. The maximum solubility of dexamethasone was experimentally determined to be 64.2±1.95 µg/mL. The loading of the particles was carried out by soaking in a 30 µg/mL drug solution to avoid the precipitation risk. As explained before, all dextran microgel particles presented high affinity to water (Table 5.2). The swelling values observed suggest that the mesh sizes of the swollen hydrogels are enough for the free entrance of dexamethasone molecules. Nevertheless, the capability of dextran-MA solely particles to uptake the drug was quite limited (Figure 5.7). The main aim of this work was to engineer a system with enhanced drug–network interactions by means of the incorporation of free γ-CD or the copolymerization with γ-CD–NMA. The polarity and size of dexamethasone make it suitable to form inclusion complexes with γ-CDs [11,9]. Thus, a greater uptake by the formulations that contained CDs (free or attached to the dextran backbone) was hypothesized. In fact, the particles containing γ-CD–NMA were the most effective: 5% dextran-MA+ 20% γ-CD–NMA particles captured *ca.* 15.24 µg/mg and 10% dextran-MA + 20% γ-CD–NMA *ca.* 8.69 µg/mg (Table 5.3).

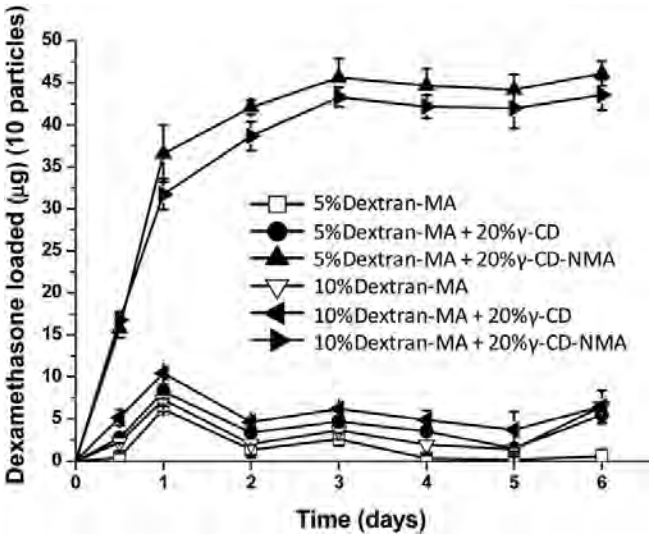

Figure 5.7. Dexamethasone loaded by 10 particles of dextran-MA particles immersed in 30 μg/mL drug solution at room temperature.

Microgels with free γ-CD showed an intermediate behavior, probably because free γ-CDs were partially removed during the washing step but also due to the absence of the cooperative contributions that can take place when the CDs form part of the polymer network. The amount of dexamethasone loaded by simple equilibrium between the aqueous phase of the network and the loading solution, which leads the drug concentration within the particles to be approximately equal to that of the loading solution, and can be estimated to be close to 0.067 μg/mg for 5% dextran-MA microgels and 0.101 μg/mg for 10% dextran-MA microgels (Table 5.3).

Table 5.3. Dexamethasone loaded by the microgels and network/water partition coefficient ($K_{N/W}$). Mean values and, in parenthesis, standard deviation.

Formulation	Total amount of drug loaded (μg/mg)	Drug loaded in aqueous phase (μg/mg)	$K_{N/W}$
5% Dextran-MA	0.28 (0.37)	0.067	7.3 (12.2)
5% Dextran-MA + 20% γ-CD	2.54 (0.50)	0.070	82.4 (16.8)
5% Dextran-MA + 20% γ-CD-NMA	15.24 (0.50)	0.075	505.5 (16.7)
10% Dextran-MA	1.08 (0.47)	0.101	32.8 (15.7)
10% Dextran-MA + 20% γ-CD	1.47 (0.42)	0.098	45.8 (14.0)
10% Dextran-MA + 20% γ-CD-NMA	8.69 (0.31)	0.073	287.2 (10.5)

Experimental loading data were slightly greater than these amounts for dextran-MA microgels prepared in the absence of γ-CDs (Table 5.3), which means that unspecific hydrophobic interactions of dexamethasone with dextran weakly contribute to the loading. To gain an insight into the role of the CDs units in the loading process, the partition coefficient, $K_{N/W}$, between the microgel particles and the drug loading solution was estimated from the following expression [38]:

$$\text{Loading(total)} = \frac{(V_s + K_{N/W}V_P)\times C_0}{W_P} \qquad \text{Eq. 4}$$

where V_p is the volume of the dried polymer and the other symbols maintain the same meaning as in Eq. (2). The values of $K_{N/W}$ for 5% dextran-MA + 20% γ-CD–NMA particles and 10% dextran-MA + 20% γ-CD–NMA particles were as high as 505 and 287, respectively, while the respective formulations prepared with free γ-CD had $K_{N/W}$ values of 82 and 46, respectively (Table 5.3). These findings clearly prove the advantage of the immobilization of γ-CDs by means of copolymerization, and also that the greater the relative content in γ-CD (either free or copolymerized), the higher the increase in affinity of the network for dexamethasone. Compared to a previously reported macrogel of crosslinked γ-CD units that exhibited $K_{N/W}$ values in the 60–180 range [9], the microgels prepared by copolymerization of dextran-MA with γ-CD–NMA are clearly advantageous. This finding may be related to the higher degree of swelling that dextran chains communicate to the networks, which should facilitate the access of dexamethasone to the γ-CDs. Tuning the time of immersion in the loading solution and the amount of particles, it is possible to regulate the amount of dexamethasone loaded in order to attain concentrations which are able to induce osteogenic differentiation (40–400 ng/mL [30] with a low mass of particles. Regarding dexamethasone release (Figure 5.8), if the drug only interacts with dextran-MA, the release rate should be practically independent of the γ-CD proportion in the hydrogel, except if the mesh size becomes altered [43]. Conversely, if drug–γ-CD complexation occurs, the release rate would be controlled not only by the diffusion of the free drug (hosted in the aqueous phase) but also by the stability constant of the complexes. In such a case, the greater the content in γ-CDs, the slower is the release [43]. Dexamethasone release from air-dried microgel particles is depicted in Figure 5.8. Copolymerization of dextran-MA with γ-CD–NMA was advantageous in terms of the amount of dexamethasone loaded and ability to sustain the release for a long period of time. Disregarding the dextran-MA proportion, the particles exhibited a rapid release in the first 24 h (45–47% release) followed by a more sustained release for at least 10 days. Moreover, the release of dexamethasone from copolymerized dextran-MA and γ-CD–NMA particles became much slower when a certain drug concentration in the medium was reached, even under sink conditions, as observed previously by Rosa dos Santos et al. [44] for soft contact lenses with b-CD pendant groups. This finding indicates that the equilibrium between drug release and drug reabsorption by the microgel particles is attained. To trigger the release of the drug, at certain time points (24, 120, 264, 336 and 432 h), 1 mL of fresh medium was added to the initial volume of release medium (2 mL) in order to disturb the equilibrium. 5% dextran-MA + 20% γ-CD–NMA and 10% dextran-MA + 20% γ-

CD–NMA particles released 71% and 77% dexamethasone in 11 days. Differently, particles containing free γ-CDs exhibited a faster delivery (*ca.* 60%) in the first 24 h, reaching 90% release after 11 days. The amount of dexamethasone released from dextran-MA solely was too low for precise quantification (in agreement with the previous low loading).

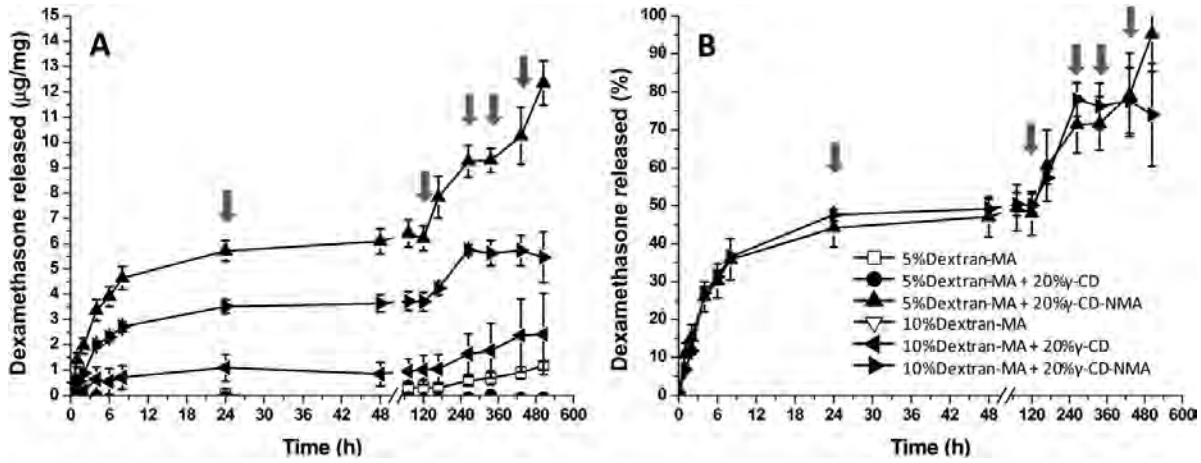

Figure 5.8. Dexamethasone release profiles in water referred to the particle mass (A) and to the total amount of dexamethasone loaded (B). Arrows indicate the moment at which an additional volume (1 mL) of release medium was added.

In sum, γ-CD covalently integrated in the hydrogel network provided a unique way to control the loading and the release of dexamethasone, which may be useful for the design of osteogenic systems. Comparing the three studied formulations, the copolymerization of γ-CD–NMA with dextran allows the increase in the amount and the period of time during which dexamethasone is released. The drug:CD decomplexation that rapidly occurs when free complexes enter into contact with physiologic fluids [45] is slowed down due to the anchorage of γ-CD–NMA onto the dextran-MA chains (Scheme B. Dextran-MA–γ-CD–NMA links) and due to the entanglement of dextran-MA and γ-CD–NMA networks (Scheme 5.3 A. Dextran-MA–dextran-MA + B. γ-CD–NMA–γ-CD–NMA).

5.4.4. Cytotoxicity of the Hydrogel Particles

A preliminary screening of the cytocompatibility of dexamethasone-loaded and non-loaded particle formulations was carried out against a human cell line of osteoblasts. The formulations were placed in direct contact with cells previously adhered to the bottom of the wells. The LDH released was evaluated and correlated with the percentage of live/dead cells (Figure 5.9). At 24 h, dexamethasone-loaded dextran-MA particles exhibited lower cell compatibility (one-way ANOVA, Tukey's multiple comparison test, $p < 0.05$) when compared with the same non-loaded formulations. However, such differences were not observed for the other formulations at this time point. At 72 h cell viability was close to 100% for all

formulations, which indicates that the materials and the drug released do not cause relevant cytotoxic effects. These findings are in agreement with the well-known biocompatibility of the starting materials (dextran and γ-CD), and also confirm that there is no leakage of unreacted monomers that could trigger unfavorable cell reactions.

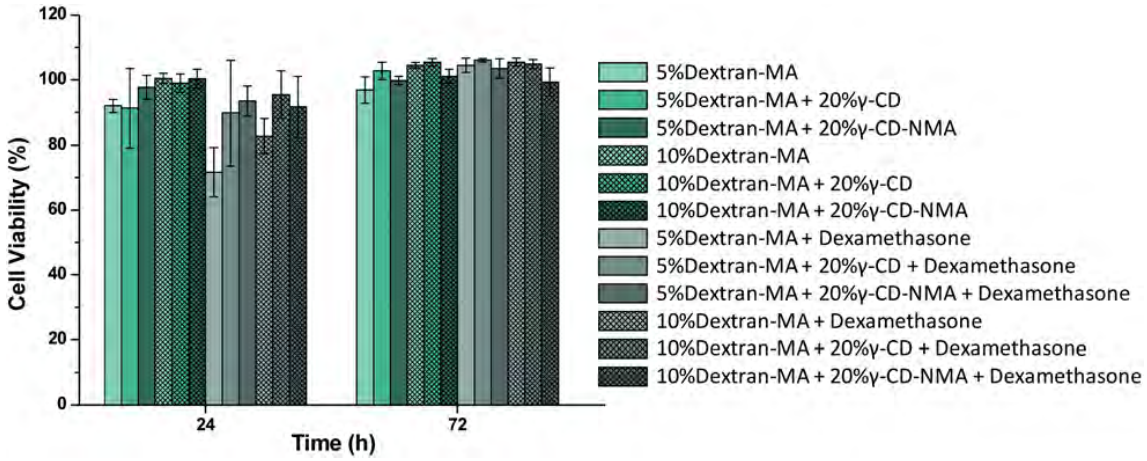

Figure 5.9. Viability of SaOs-2 cells after being in direct contact with dexamethasone loaded and non-loaded particles for 24 and 72 h (n=4, error bars represent standard deviations).

5.4.5. Effect of Hydrogel Particles on hASCs

5.4.5.1. *In vitro* Proliferation

The hASCs were seeded on the well bottom and allowed to proliferate for 12 days under direct contact with particles loaded or not with dexamethasone (Figure 5.10). The proliferation was on average higher in the presence of dexamethasone, the differences being more accentuated at day 7 ($p < 0.05$). Previous studies demonstrated that dexamethasone either alone or in combination with β-GP + ascorbic acid stimulates the human bone marrow mesenchymal stem cell proliferation [46]. Such evidence can be correlated with the ability of glucocorticoids, at low concentrations, to stimulate the proliferation and/or differentiation of osteoprogenitor cells [46,31]. Moreover, ascorbic acid solely also demonstrated capability of stimulating the proliferation of mesenchymal stem cells and their derived cell types, namely osteoblasts, adipocytes, chondrocytes, etc., [47] while β-GP solely exerted the opposite effect [46]. The similar cell proliferation observed in the negative controls 1 and 2 revealed that the combination of β-GP and ascorbic acid does not alter cell proliferation (no significant statistic differences), probably due to their antagonic effect. On the other hand, the greater cell number recorded in positive control 2 compared to that obtained in negative control 2 ($p < 0.05$) at days 7 and 12 indicates that the presence of dexamethasone has a stimulating effect on hASC proliferation.

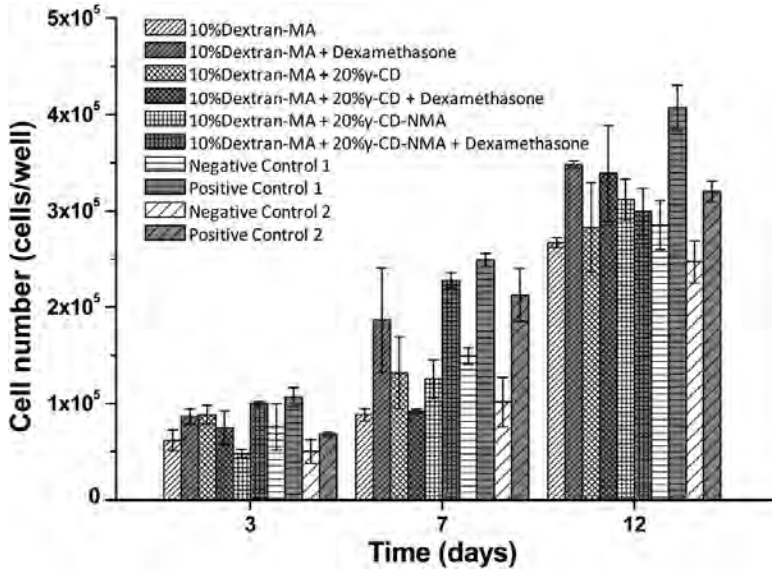

Figure 5.10. Proliferation of hASCs cultured in direct contact with dexamethasone loaded and non-loaded particles and in the respective controls up to day 12. Cell number per well was calculated using a calibration curve of known cell numbers (n=3, bars represent standard deviations).

5.4.5.2. *In Vitro* Osteogenic Differentiation

The osteoinductive potential of the particles was evaluated by recording ALP activity. ALP is an enzyme present in the osteoblast membrane (early osteogenic marker) involved in ion phosphate hydrolysis stimulating the mineralization through the formation of hydroxyapatite crystals. As can be observed in Figure 5.11, the ALP activity increased over time. At day 3 the levels were similar for all formulations. At day 7 the dexamethasone-loaded formulations showed an early ALP activity peak with statistically significant differences ($p < 0.05$) when compared with the respective non-loaded formulations or the negative controls. For dexamethasone-loaded 10% dextran- MA and 10% dextran-MA + 20% γ-CD the results were similar to those obtained with the positive control (1 and 2). By contrast, the presence of γ-CD–NMA in the particles induced a higher ALP activity (statistically different to positive control 1; $p < 0.05$) probably due to the increased capacity of the particles to load dexamethasone and release it in a sustained way during the period required to induce the cell differentiation. During the experiment, part of the cell culture medium was replaced with a fresh one in order to guarantee the feeding of the cells and the clearance of waste products. Such medium renovation may be advantageous because it should trigger the release of more drug from the particles in order to maintain a constant level of dexamethasone in the medium, as observed in the in vitro release studies. In all studied time points, the non-loaded particles presented an ALP activity similar to that of negative controls (undifferentiated cells), which means that the materials per se did not have osteoinductive properties. Moreover, the incorporation of β-GP + ascorbic acid to the culture medium without dexamethasone did not cause any effect on ALP activity (negative

control 2). Therefore, dexamethasone plays a key-role in osteogenesis induction being at the maximum between days 3 and 7. Previous studies demonstrated that hASCs stimulated by medium supplement with β-GP, ascorbic acid and 10 or 100 nM of dexamethasone also showed an ALP peak after 7 days in culture [27].

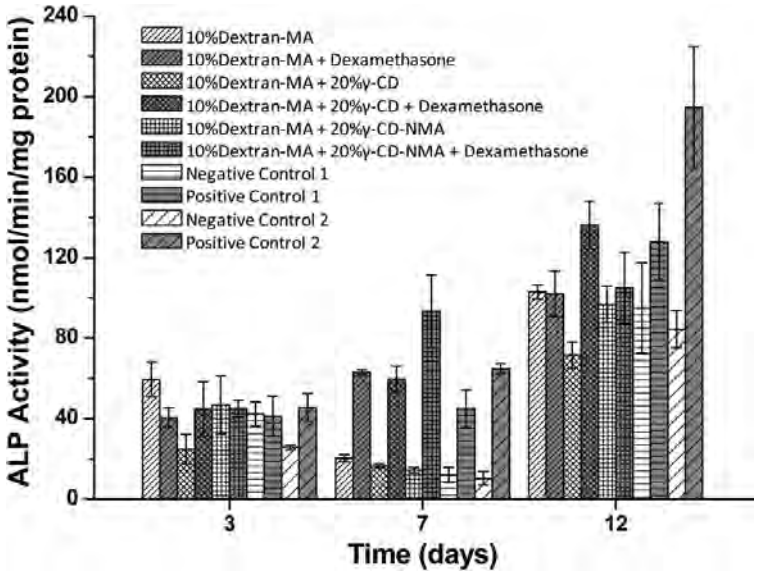

Figure 5.11. ALP activity in hASCs induced by dexamethasone loaded and non-loaded particles and the respective positive and negative controls after 3, 7 and 12 days in culture. The results are expressed in mean±standard deviation within n=3 for each bar.

The quantitative results about differentiation of the hASCs to osteoblasts were also visualized by means of ALP staining after 12 days of cell culture (Figure 5.12). Cells in contact with dexamethasone-loaded particles exhibited a more intense red color. Again, the drug-loaded 10% dextran-MA + 20% γ-CD–NMA particles caused the highest red staining (similar to those cells in positive control 2, which were supplemented with the maximum amount of dexamethasone that particles can release). This is explained by the increased capacity of such particles to load dexamethasone. The non-loaded formulations and the negative controls did not induce significant increase in ALP activity. Distinct polymeric systems encapsulating dexamethasone have been successfully reported for osteogenic differentiation, namely PLGA scaffolds [48,49], microparticles [23] and nanoparticles [50], carboxymethylchitosan/poly(amidoamine) dendrimer nanoparticles [25,51,52], polycaprolactone [53] and poly-(L-lactide-co-caprolactone)/collagen fibers [54]; however none studied the combination of polymers with cyclodextrins and their respective roles in loading and release of such a corticoid drug and the effect on osteogenic cell differentiation. The particles developed in this work demonstrate high potential to be

applied in in situ bone regeneration avoiding the use of unstable proteins (*e.g.* growth factors) or even genetic manipulation of cells, and using a simple and cost effective method.

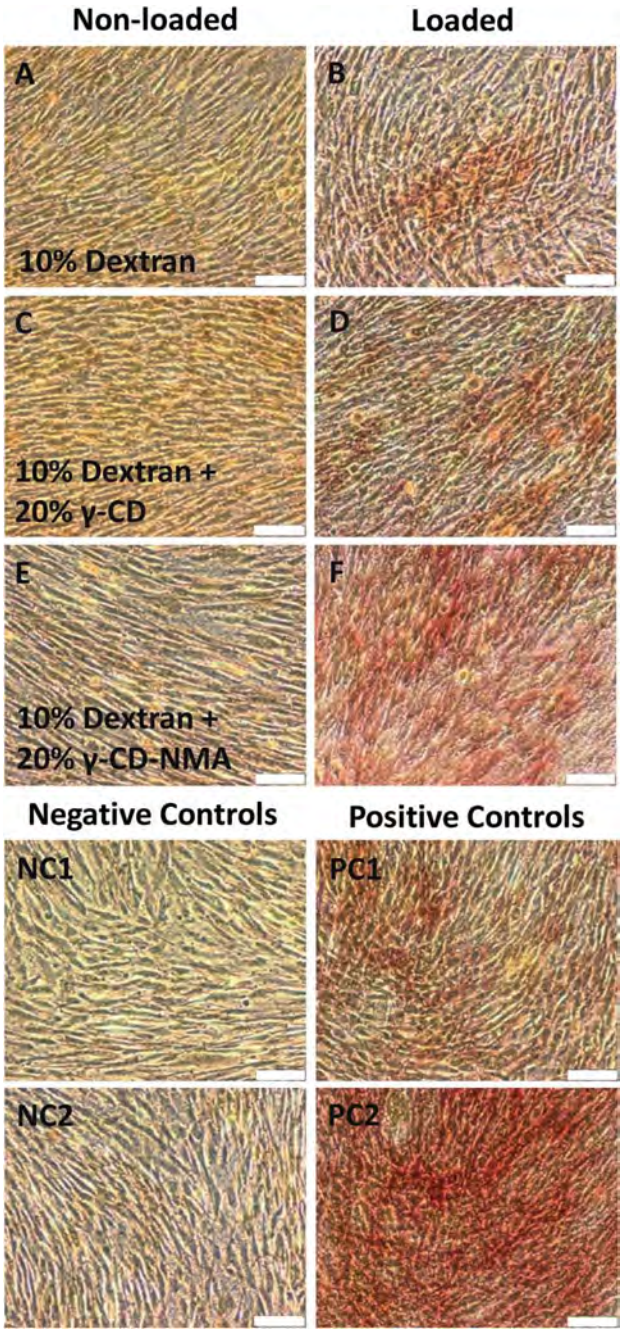

Figure 5.12. ALP staining of hASCs in direct contact with non-loaded and loaded particles, and their respective controls at 12 days. The scale bar is 100 μm.

5.5. Conclusions

Dextran-MA photocrosslinked spherical particles can be obtained using the superhydrophobic surface methodology and their performance to load hydrophobic drugs is improved via copolymerization with γ-CDs. Copolymer networks of γ-CDs (γ-CD–NMA) and 10% dextran-MA are *ca.* 7 times more effective in

loading dexamethasone than the formulations with free γ-CDs and dextran-MA solely, meaning that the anchorage of CDs is advantageous. The in vitro release of dexamethasone from dextran-MA + 20% γ-CD–NMA particles can be sustained for at least 10 days due to the hindered drug:CD decomplexation inside the network. These particles show an excellent cytocompatibility and are able to induce the osteogenic differentiation of hASCs after 3–7 days in culture. To summarize, the improved characteristics of the developed system could be useful for applications in bone regeneration.

5.6. Acknowledgments

A.C. Lima acknowledges the Portuguese Foundation for Science and Technology (FCT) for the PhD grant SFRH/BD/71395/2010 and A.M. Puga thanks Ministerio de Economia y Competividad (MINECO) for an FPI fellowship (BES2009-024735). The research leading to these results has received funding from the European Union's Seventh Framework Programme (FP7/2007-2013) under grant agreement no. REGPOT-CT2012-316331-POLARIS, FEDER through the Competitive Factors Operation Program –COMPETE, National funds through FCT (PTDC/FIS/115048/2009 and PTDC/CTM-BIO/1814/2012), MINECO (SAF2011-22771) and Luso-Spanish Integrated Actions (ref. E122/12; PRI-AIBPT-2011-1211), and Operational Human Potential Program (POPH) developed under the scope of the National Strategic Reference Framework (QREN) from the European Social Fund (FSE). The authors would like to thank Prof. Asuncion Lage for the quantification of Irgacure 2959 released from the particles, and the Instituto de Ortopedia y Banco de Tejidos Musculoesqueléticos (Universidad de Santiago de Compostela, Spain) for help with cell cultures.

5.7. References

[1] Concheiro A. and Alvarez-Lorenzo C., Chemically cross-linked and grafted cyclodextrin hydrogels: From nanostructures to drug-eluting medical devices, Advanced Drug Delivery Reviews 2013, 65: 1188–1203.

[2] Hishiya T., Asanuma H. and Komiyama M., Spectroscopic Anatomy of Molecular-Imprinting of Cyclodextrin. Evidence for Preferential Formation of Ordered Cyclodextrin Assemblies, Journal of the American Chemical Society 2002, 124: 570–575.

[3] García-Zubiri I. X., González-Gaitano G. and Isasi J. R., Sorption models in cyclodextrin polymers: Langmuir, Freundlich, and a dual-mode approach, Journal of Colloid and Interface Science 2009, 337: 11–18.

[4] Salmaso S., Semenzato A., Bersani S., Matricardi P., Rossi F. and Caliceti P., Cyclodextrin/PEG based

hydrogels for multi-drug delivery, International Journal of Pharmaceutics 2007, 345: 42–50.

[5] Rodriguez-Tenreiro C., Alvarez-Lorenzo C., Rodriguez-Perez A., Concheiro A. and Torres-Labandeira J. J., Estradiol sustained release from high affinity cyclodextrin hydrogels, European Journal of Pharmaceutics and Biopharmaceutics 2007, 66: 55–62.

[6] Moya-Ortega M. D., Alvarez-Lorenzo C., Concheiro S. and Loftsson T., Cyclodextrin-based nanogels for pharmaceutical and biomedical applications, International Journal of Pharmaceutics 2012, 428: 152–163.

[7] Allen T. M. and Cullis P. R., Liposomal drug delivery systems: From concept to clinical applications, Advanced Drug Delivery Reviews 2013, 65: 36–48.

[8] Barreiro-Iglesias R., Alvarez-Lorenzo C. and Concheiro A., Incorporation of small quantities of surfactants as a way to improve the rheological and diffusional behavior of carbopol gels, Journal of Controlled Release 2001, 77: 59–75.

[9] Moya-Ortega M. D., Alvarez-Lorenzo C., Sigurdsson H. H., Concheiro A. and Loftsson T., γ-Cyclodextrin hydrogels and semi-interpenetrating networks for sustained delivery of dexamethasone, Carbohydate Polymers 2010, 80: 900–907.

[10] Ma D., Zhang L- M., Yang C. and Yan L., UV photopolymerized hydrogels with β-cyclodextrin moieties, Journal of Polymer Research 2008, 15: 301–307.

[11] Moya-Ortega M. D., Alves T. G. F., Alvarez-Lorenzo C., Concheiro A., Stefansson E., Thorsteinsdóttir M. and Loftsson T., Dexamethasone eye drops containing γ-cyclodextrin-based nanogelsm International, Journal of Pharmaceutics 2013, 441: 507–515.

[12] Song W., Lima A. C. and Mano J. F., Bioinspired methodology to fabricate hydrogel spheres for multi-applications using superhydrophobic substrates, Soft Matter 2010, 6: 5868–5871.

[13] Peng K., Tomatsu I., Korobko A. V. and Kros A., Cyclodextrin–dextran based in situ hydrogel formation: a carrier for hydrophobic drugs, Soft Matter, 2010, 6, 85–87.

[14] Lima A. C., Song W., Blanco-Fernandez B., Alvarez-Lorenzo C. and Mano J. F., Synthesis of temperature-responsive dextran-MA/PNIPAAm particles for controlled drug delivery using superhydrophobic surfaces, Pharmaceutical Research 2011, 28:1294–1305.

[15] Siemoneit U., Schmitt C., Alvarez-Lorenzo C., Luzardo A., Otero-Espinar F., Concheiro A. and Blanco-Méndez J., Acrylic/cyclodextrin hydrogels with enhanced drug loading and sustained release capability, International Journal of Pharmaceutics 2006, 312: 66–74.

[16] Fernández M., Villalonga M. L., Caballero J., Fragoso A., Cao R. and Villalonga R., Effects of β-

cyclodextrin–dextran polymer on stability properties of trypsin, Biotechnology and Bioengineering 2003, 83: 743– 747.

[17] Ramirez H. L., Valdivia A., Cao R., Fragoso A., Torres Labandeira J. J., Banõs M. and Villalonga R., Preparation of β-Cyclodextrin-Dextran Polymers and their Use as Supramolecular Carrier Systems for Naproxen, Polymer Bulletin 2007, 59: 597–605.

[18] Nielsen T. T., Wintgens V., Amiel C.,Wimmer R. and Larsen K.L., Facile Synthesis of β-Cyclodextrin-Dextran Polymers by "Click" Chemistry, Biomacromolecules 2010, 11: 1710–1715.

[19] Fulop Z., Nielsen T. T., Larsen F. L. and Loftsson T., Dextran-based cyclodextrin polymers: Their solubilizing effect and self-association, Carbohydrate Polymers 2013, 97: 635–642.

[20] Wintgens V., Nielsen T. T., Larsen K. L. and Amiel C., Size-Controlled Nanoassemblies Based on Cyclodextrin-Modified Dextrans, Macromolecular Biosciemce 2011, 11: 1254–1263.

[21] Liang C. Z., Li H., Tao Y. Q., Zhou X. P., Yang Z. R., Xiao Y. X., Li F. C., Han B. and Chen Q. X., Dual delivery for stem cell differentiation using dexamethasone and bFGF in/on polymeric microspheres as a cell carrier for nucleus pulposus regeneration, Journal of Materials Science: Matererials in Medicine 2012, 23: 1097–1107.

[22] Hickey T., Kreutzer D., Burgess D. J. and Moussy F., Dexamethasone/PLGA microspheres for continuous delivery of an anti-inflammatory drug for implantable medical devices, Biomaterials 2002, 23: 1649–1656.

[23] Dawes G. J. S., Fratila-Apachitei L. E., Necula B. S., Apachitei I., van Leeuwen J. P. T. M., Duszczyk J. and Eijken M., Effects of dexamethasone-loaded PLGA microspheres on human fetal osteoblasts, Journal of Biomaterials Applications 2012, 27: 477–483.

[24] Santo V. E., Gomes M. E., Mano J. F. and Reis R. L., Chitosan–chondroitin sulphate nanoparticles for controlled delivery of platelet lysates in bone regenerative medicine, Journal of Tissue Engineering and Regenerative Medicine, 2012, 6: s47–s59.

[25] Oliveira J. M., Kotobuki N., Marques A. P., Pirraco R. P., Benesch J., Hirose M., Costa S. A., Mano J. F., Ohgushi H. and Reis R. L., Surface Engineered Carboxymethylchitosan/Poly(amidoamine) Dendrimer Nanoparticles for Intracellular Targeting, Advanced Functional Matererials 2008, 18: 1840–1853.

[26] Zuk P. A., Zhu M., Ashjian P., De Ugarte D. A., Huang J. I., Mizuno H., Alfonso Z. C., Fraser J. K., Benhaim P.and Hedrick M. H., Human Adipose Tissue Is a Source of Multipotent Stem Cells, Molecular Biology of the Cell, 2002, 13: 4279–4295.

[27] De Girolamo L., Sartori M. F., Albisetti W. and Brini A. T., Osteogenic differentiation of human adipose-derived stem cells: comparison of two different inductive media, Journal of Tissue Engineering and Regenerative Medicine 2007, 1: 154–157.

[28] Rada T., Santos T. C., Marques A. P., Correlo V. M., Frias A. M., Castro A. G., Neves N. M., Gomes M. E. and Reis R. L., Osteogenic differentiation of two distinct subpopulations of human adipose-derived stem cells: an in vitro and in vivo study, Journal of Tissue Engineering Regenerative Medicine 2012, 6: 1–11.

[29] Santo V. E., Duarte A. R. C., Popa E. G., Gomes M. E., Mano J. F. and Reis R. L., Enhancement of osteogenic differentiation of human adipose derived stem cells by the controlled release of platelet lysates from hybrid scaffolds produced by supercritical fluid foaming, Journal of Controlled Release 2012, 162: 19–27.

[30] Jaiswal N., Haynesworth S. E., Caplan A. I. and Bruder S. P., Osteogenic differentiation of purified, culture-expanded human mesenchymal stem cells in vitro, Journal Cellular Biochemistry 1997, 64: 295–312.

[31] Walsh S., Jordan G. R., Jefferiss C., Stewart K. and Beresford J. N., High concentrations of dexamethasone suppress the proliferation but not the differentiation or further maturation of human osteoblast precursors in vitro: relevance to glucocorticoid-induced osteoporosis, Rheumatology 2001, 40: 74–83.

[32] Shi X., Wang Y., Varshney R. R., Ren L., Gong Y. and Wang D. A., Microsphere-based drug releasing scaffolds for inducing osteogenesis of human mesenchymal stem cells in vitro, European Journal of Pharmaceutical Science 2010, 39: 59–67.

[33] Lima A. C., Sher P. and Mano J. F., Production methodologies of polymeric and hydrogel particles for drug delivery applications, Expert Opinion on Drug Delivery 2012, 9: 231–248.

[34] Lima A. C., Custódio C. A, Alvarez-Lorenzo C. and Mano J. F., Biomimetic Methodology to Produce Polymeric Multilayered Particles for Biotechnological and Biomedical Applications, Small 2013, 9: 2487–2492.

[35] Lima A. C., Batista P., Valente T. A. M., Silva A. S., Correia I. J. and Mano J. F., Novel Methodology Based on Biomimetic Superhydrophobic Substrates to Immobilize Cells and Proteins in Hydrogel Spheres for Applications in Bone Regeneration, Tissue Engineering Part A 2013, 19: 1175–1187.

[36] Oliveira N. M., Neto A. I., Song W. and Mano J. F., Two-dimensional open microfluidic devices

by tuning the wettability on patterned superhydrophobic polymeric surface, Applied Physics Express 2010, 3: 085205.

[37] van Dijk-Wolthius V. N. E., Franssen O., Talsma H., van Steenbergen M. J., Kettenes-van den Bosch J. J. and Henninkt W. E., Synthesis, Characterization, and Polymerization of Glycidyl Methacrylate Derivatized Dextran, Macromolecules 1995, 28: 6317–22.

[38] Kim S. W., Bae Y. H. and Okano T., Hydrogels: Swelling, Drug Loading, and Release, Pharmaceutical Research 1992, 9: 283– 290.

[39] Lee M. H. A. K., Yoon K. E. E. J. and Ko S., Synthesis of a vinyl monomer containing β-cyclodextrin and grafting onto cotton fiber, Journal of Applied Polymer Science 2001, 80: 438–446.

[40] Kawaguchi Y. and Kamachi M., Recognition of Alkyl Groups on a Polymer Chain by Cyclodextrins, Macromolecules 1997, 30: 5181–5182.

[41] Balta D. K., Bagdatli E., Arsu N., Ocal N. and Yagci Y., Chemical incorporation of thioxanthone into β-cyclodextrin and its use in aqueous photopolymerization of methyl methacrylate, Journal of Photochemistry andPhotobiology A 2008, 196: 33–37.

[42] Rodriguez-Tenreiro C., Alvarez-Lorenzo C., Rodriguez- Perez A., Concheiro A. and Torres-Labandeira J. J., New Cyclodextrin Hydrogels Cross-Linked with Diglycidylethers with a High Drug Loading and Controlled Release Ability, Pharmaceutical Research 2006, 23: 121–130.

[43] Rosa dos Santos J. F., Couceiro R., Concheiro A, Torres-Labandeira J. J. and Alvarez-Lorenzo C., Poly(hydroxyethyl methacrylate-co-methacrylated-β-cyclodextrin) hydrogels: Synthesis, cytocompatibility, mechanical properties and drug loading/release properties, Acta Biomaterialia 2008, 4: 745–755.

[44] Rosa dos Santos J. F., Alvarez-Lorenzo C., Silva M., Balsa L., Couceiro J., Torres-Labandeira J. J. and Concheiro A., Soft contact lenses functionalized with pendant cyclodextrins for controlled drug delivery, Biomaterials 2009, 30: 1348–1355.

[45] Liu Y. Y. and Fan X. D., Synthesis, properties and controlled release behaviors of hydrogel networks using cyclodextrin as pendant groups, Biomaterials, 2005, 26, 6367–6374.

[46] Coelho M. J. and Fernandes M. H., Human bone cell cultures in biocompatibility testing. Part II: effect of ascorbic acid, β-glycerophosphate and dexamethasone on osteoblastic differentiation, Biomaterials 2000, 2:1095–1102.

[47] Choi K. M., Seo Y. K., Yoon H. H., Song K. Y., Kwon S. Y., Lee H. S. and Park J. K., Effect of ascorbic acid on bone marrow-derived mesenchymal stem cell proliferation and differentiation, Journal of Bioscience and Bioengineering 2008, 105: 586–594.

[48] Kim H., Kim H. W. and Suh H., Sustained release of ascorbate-2-phosphate and dexamethasone from porous PLGA scaffolds for bone tissue engineering using mesenchymal stem cells, Biomaterials 2003, 24: 4671–4679.

[49] Kim H., Suh H., Jo S. A., Kim H. W., Lee J. M., Kim E. H., Reinwald Y., Park S. H., Min B. H. and Jo I., In vivo bone formation by human marrow stromal cells in biodegradable scaffolds that release dexamethasone and ascorbate-2-phosphate, Biochemical and Biophysical Research Communications 2005, 332: 1053–1060.

[50] Wang Q., Wang J., Lu Q., Detamore M. S. and Berkland C., Injectable PLGA based colloidal gels for zero-order dexamethasone release in cranial defects, Biomaterials 2010, 31: 4980–4986.

[51] Oliveira J. M., Sousa R. A., Kotobuki N., Tadokoro M., Hirose M., Mano J. F., Reis R. L. and Ohgushi H., The osteogenic differentiation of rat bone marrow stromal cells cultured with dexamethasone-loaded carboxymethylchitosan/poly(amidoamine) dendrimer nanoparticles, Biomaterials 2009, 30: 804–813.

[52] Oliveira J. M., Kotobuki N., Tadokoro M., Hirose M., Mano J. F., Reis R. L. and Ohgushi H., Ex vivo culturing of stromal cells with dexamethasone-loaded carboxymethylchitosan/poly(amidoamine) dendrimer nanoparticles promotes ectopic bone formation, Bone 2010, 46: 1424–1435.

[53] Martins A., Duarte A. R. C., Faria S., Marques A. P., Reis R. L. and Neves N. M., Osteogenic induction of hBMSCs by electrospun scaffolds with dexamethasone release functionality, Biomaterials 2010, 31: 5875–5885.

[54] Su Y., Su Q., Liu W., Lim M., Venugopal J. R., Mo X., Ramakrishna S., Al-Deyab S. S. and El-Newehy M., Controlled release of bone morphogenetic protein 2 and dexamethasone loaded in core–shell PLLACL–collagen fibers for use in bone tissue engineering, Acta Biomaterialia 2012, 8: 763–771.

[55] Ho F. F. L., Kohler R. R. and Ward G. A., Determination of molar substitution and degree of substitution of hydroxypropyl cellulose by nuclear magnetic resonance spectrometry, Analytical Chemistry 1972, 44: 178–181.

Chapter 6

Sequential Ionic and Thermogelation of Chitosan Spherical Hydrogels Prepared Using Superhydrophobic Surfaces to Immobilize Cells and Drugs

6.1. Abstract

Chitosan (CHI) is soluble in acidic media, which makes it incompatible for the encapsulation of cells and pH-sensitive molecules. In this work, a mild chitosan-based system with two sequential gelation steps is proposed, where the model drug dexamethasone and L929 cells are immobilized inside hydrogel beads. Superhydrophobic surfaces were used to produce the spherical hydrogel particles that provided favorable conditions to encapsulate cells or bioactive agents. First, the chitosan acidic solution was neutralized with β-glycerophosphate (β-GP) at room temperature to pH 6.2. Suspended cells (or dexamethasone) in the formulation were dispensed in controlled volumes onto biomimetic polystyrene superhydrophobic surfaces, to form spherical shapes. The addition of sodium tripolyphosphate (TPP) on the top of each sphere induced an ionic gelation process of the chitosan through electrostatic interactions. At 37 °C, the hydrophobicity of the chitosan-based formulations increased and a second gelation step occurred, which increased the elastic modulus. In addition, the pH-responsive behavior characteristic of chitosan was maintained. The softness and flexibility of the system can potentially be utilized to implant cells and therapeutic molecules using less invasive procedures.

This chapter is based on the following publication:
Lima A.C., Correia C. R., Oliveira M. B. and Mano J. F., Sequential ionic and thermogelation of chitosan spherical hydrogels prepared using superhydrophobic surfaces to imobilize cells and drugs, Journal of Bioactive and Compatible Polymers 2013, 29: 50-65.

6.2. Introduction

CHI is a linear cationic polysaccharide derived by partial depolymerization and dea- cetylation of chitin extracted from the exoskeleton of crustaceans [1,2]. CHI has been used in preparation of hydrogels using the free amino groups as crosslinking sites. Due to its strong intermolecular hydrogen bonds, CHI can primarily be dissolved in acidic conditions, making the system aggressive to cells [3] and even to molecules that could lose their biological activity under such harsh environment. Few studies reported cell encapsulation utilizing water-soluble CHI [4-6]. A strategy to overcome this drawback was to add β-GP to the acidic CHI solution [7], which can also make the CHI system thermoresponsive, forming gel at physiological temperatures [8-12]. Unlike materials such as gelatin, which are liquid at high temperatures and turn into a gel upon cooling, CHI/β-GP constitutes a reverse thermo-sensitive system for injectable applications due to a shift in attractive versus repulsive interchain forces during gelation [9,13]. Three mechanisms may be involved in this gelation process: (I) electrostatic attraction between CHI amino groups and the phosphate groups of β-GP (ionic crosslinking), (II) establishment of hydrogen bonds between CHI chains after reduction of electrostatic repulsive forces due to the CHI neutralization, and (III) CHI–CHI hydrophobic interactions. Later studies found that ionic crosslinking cannot be responsible for CHI/β-GP gelation and that the hydrophobic interactions caused the gelation at high temperatures [8]. More recently, Lavertu *et al*. [11] suggested that the gelation of CHI in the presence of β-GP occurred due to a proton transfer from the CHI to the phosphate moiety of β-GP upon heating. The precipitation of the CHI takes place when the amount of phosphates was sufficient to accept the released protons. There was no ionic crosslinking between the phosphates and the CHI chains, meaning that the phosphate salt was free to diffuse out of the gel.

Due to the mild sol–gel transition at body temperature, CHI/β-GP has been explored to immobilize and retain in a specific site distinct types of cells, with potential use in tissue engineering, including mesenchymal stem cells [14], intervertebral disk cells [7], and chondrocytes [15]. However, the mechanical properties of the resulting gels may not be sufficient for several applications. Therefore, it would be desirable to combine the thermogelation ability of CHI/β-GP with other crosslinking processes to enhance the mechanical performance of the final biomaterial.

The covalent crosslinkers commonly used to form CHI three-dimensional (3D) stable structures are formaldehyde [16] and glutaraldehyde [17-19], which present higher levels of toxicity [2,20] (especially if the unreacted molecules are not completely removed) when compared with ionic crosslinkers such as sodium sulfate [21] and sodium TPP [22,23]. We hypothesize that CHI/β-GP thermogelation could take place even if the CHI was previously crosslinked using non-toxic ions. Taking this into account, the

purpose of this study is to investigate whether CHI/β-GP hydrogels can be processed with a defined and manageable spherical shape, through a previous crosslinking step with TPP, in order to confer mild conditions to enable effective encapsulation of cells and therapeutic molecules. The methodology selected to produce spherical particles was the superhydrophobic surface technology due to its advantages to other conventional techniques [24]. This method is based on the rolling of water droplets onto natural superhydrophobic surfaces, as it is the case with lotus leaf [25], allowing the production of individual particles without contact with other liquid media and with a narrow particle size distribution. No organic solvents, mechanical forces, and extreme temperatures or pressures are required. This method was used to produce CHI microgels crosslinked within a glutaraldehyde atmosphere for oral and topical chemotherapy applications [26]. Mesenchymal stem cells and fibronectin were also immobilized in alginate (ALG) spheres using polystyrene (PS) superhydrophobic surfaces [27], and this technique provides adequate conditions to retain the viability of the cells during processing the particles. To the best of our knowledge, the proposed polymeric system (CHI/β-GP:TPP) combined with this production methodology has not been reported for applications in drug delivery [24] and tissue engineering [28].

6.3. Experimental Section

6.3.1. Materials

PS, an injection molding grade (Styrolution PS 158k), was purchased from UL IDES (USA), and used in a granular shape for the preparation of the superhydrophobic substrates. Tetrahydrofuran (THF; 99.9%) was purchased from Riedel de-Haen (Germany). 1H,1H,2H,2H-perfluorodecyltriethoxysilane (PFDTS; 97%), phosphate-buffered saline (PBS), sodium ALG, dexamethasone (98%), CHI (medium molecular weight), sodium TPP, β-GP disodium salt, low-glucose Dulbecco's modified Eagle's medium (DMEM), and sodium bicarbonate were purchased from Sigma–Aldrich (USA). Fetal bovine serum (FBS), penicillin–streptomycin, and trypsin-ethylenediaminetetraacetic acid (EDTA) solution were purchased from Invitrogen (USA). Ethanol was purchased from Aga (Portugal). Calcium chloride ($CaCl_2$) was purchased from Merck (Germany). Sodium hydroxide (NaOH) was obtained from JMGS (Portugal), and acetic acid was purchased from Pronalab (Spain). The immortalized mouse lung fibroblast cell line (L929) was purchased from the European Collection of Cell Cultures. Calcein-acetomethoxy (AM) and propidium iodide (PI) dyes were purchased from Molecular Probes (USA)—Invitrogen. CHI was purified using a reprecipitation method described elsewhere [29]. All the other chemicals were used as received.

6.3.2. Polystyrene Superhydrophobic Surfaces Preparation

PS superhydrophobic surfaces were prepared using a phase separation method as described before [25,30]. Briefly, a PS solution in THF (70 mg/mL) was prepared and mixed with ethanol (2:1.3 v/v). The mixture was dispensed onto smooth PS commercial substrates, which were then immersed in ethanol for 1 min and dried under nitrogen flow. In order to increase the superhydrophobicity, the rough PS surfaces were modified with PFDTS (1% v/v in ethanol) after argon plasma treatment for 40 s at 30 W (Plasma Prep5; Gala Instruments, Germany).

6.3.3. CHI/β-GP:TPP Particles

A 2% (w/v) CHI solution was prepared by solubilizing CHI in 1% (v/v) acetic acid overnight. The CHI/β-GP solution was prepared by adding the 2 M β-GP (in water) drop-wise into the stirring CHI solution until pH 6.2 was reached. L929 cells (1×10^6 cells/mL) or dexamethasone (15 mg/mL in ethanol, CHI:dexamethasone 25:1) were added to the neutralized CHI solution to produce the different formulations containing cells or the drug model, respectively. The spherical beads were produced by dispensing 4 μL of 4% (w/v) TPP solution on the top of 8 μL CHI/β-GP solution previously dispensed on the surface of the PS superhydrohobic platforms. The ionic crosslinking was allowed to occur during approximately 1–2 h at room temperature. Finally, the hydrogel beads were collected from the PS superhydrophobic surfaces.

6.3.4. Mechanical Characterization: Dynamic Mechanical Analysis

The viscoelastic properties of the CHI gels neutralized with β-GP and crosslinked with TPP were studied using a TRITEC8000B dynamic mechanical analysis (DMA) from Triton Technology (UK), equipped with the compressive mode. The gels used for this study were prepared using the same proportions of CHI/β-GP:TPP as described for the fabrication of the particles. However, in order to have a well-known geometry compatible with mechanical testing, hydrogels were produced in 96-well plates to obtain cylindrical specimens. The DMA spectra were obtained during a frequency scan between 0.1 and 15 Hz, with the materials immersed in a PBS bath, either at 20°C or 37°C, in order to mimic both pre- and post-implantation situations, respectively. The experiments were performed under constant strain amplitude, corresponding to approximately 1% of the original height of the sample. A small preload was applied to each sample to ensure that the entire scaffold surface was in contact with the compression plates before testing. At least three samples were used for each condition.

6.3.5. Swelling Studies

Non-loaded beads (five units), *i.e.*, without cells or dexamethasone, were collected from the superhydrophobic surface, weighted, and immersed at 37 °C in: (I) water supplemented with 1 M HCl solution to reach pH 2, (II) phosphate buffer saline (pH 7.4), and (III) water supplemented with 1 M NaOH solution to reach pH 9. Beads were collected at given periods of time. After removing the excess of medium with a filter paper, samples were immediately weighted. The experiment was carried out in triplicate.

The swelling degree was estimated as follows:

$$\%\text{Swelling} = \frac{m_i - m_0}{m_0} \times 100 \qquad \text{Eq. 1}$$

Where m_i and m_0 are the weights of the swollen and dry beads, respective.

6.3.6. Particle Size

The samples used for swelling studies were photographed using a stereo microscope (Zeiss–Stemi 1000 PG-HITEC, Germany) at different time points. The diameters of the beads were measured using the ImageJ software (NIH, USA).

6.3.7. *In vitro* Drug Release

CHI/β-GP:TPP + dexamethasone beads (10 units) were placed in 4 mL (n=9) of distinct pH-dependent media: (I) water supplemented with 1 M HCl solution to reach pH 2, (II) phosphate buffer saline (pH 7.4), and (III) water supplemented with 1 M NaOH solution to reach pH 9. The vials containing the particles were kept under agitation (*ca.* 60 rpm) at 37 °C. At pre-established periods of time, aliquots of 1 mL of the supernatant were taken out and replaced with equal volume of fresh medium to maintain the volume constant during the release study. The amount of dexamethasone was spectrophotometrically quantified, by measuring the UV absorbance at 242 nm (Synergie HT; Bio-Tek, USA). A calibration curve of dexamethasone solutions with pre-defined concentrations was constructed.

6.3.8. Release Kinetic Models

In order to investigate the mechanism of dexamethasone release from CHI/β-GP:TPP particles at different pHs, the release data obtained were analyzed with different models including: zero-order (Eq.2), first-order (Eq.3), Higuchi (Eq.4), and Korsmeyer–Peppas (Eq.5) [31,32].

$$M_t = M_0 + k_0 t \qquad \text{Eq. 2}$$

$$l\text{og}M_t = \log M_0 + \frac{k_1}{2.303} t \qquad \text{Eq. 3}$$

$$M_t = M_0 + k_H t^{1/2} \qquad \text{Eq. 4}$$

$$M_t = k_{KP} t^n \qquad \text{Eq. 5}$$

where M_0 is the initial amount of drug, M_t is the cumulative amount of drug release at time t, k_0 is the zero-order release constant, k_1 is the first-order release constant, k_H is the Higuchi constant, k_{KP} is the Korsmeyer–Peppas constant, and n is an exponent characterizing the release mechanism. The model that best fits the experimental data was selected based on the highest correlation coefficient (R^2) values. OriginPro8 was used to perform the data treatment.

6.3.10. Cell Viability: Live/Dead Assay

L929 cells were routinely cultured with low-glucose DMEM supplemented with 3.7 g/L sodium bicarbonate, 10% FBS, and 1% penicillin–streptomycin at pH 7.4. Cells were grown in 75 cm^2 tissue culture flasks and incubated at 37 °C in a humidified air atmosphere of 5% CO_2. At 90% of confluence, the cells were washed with PBS and detached by a chemical procedure using 0.05% trypsin–EDTA solution for 5 min at 37 °C in a humidified atmosphere of 5% CO_2. After this period, cell culture medium was added to inactivate the trypsin effect. The obtained cell suspension was centrifuged at 300 g and 25 °C. After discarding the supernatant, cells were suspended in CHI/β-GP or 1.5% (w/v) ALG (control) at cell density of 1×10^6 cells/mL. The resultant suspensions were used to produce particles onto PS superhydrophobic as previously described. The obtained particles were then maintained in culture similar to L929 cells before being encapsulated. Calcein-AM and PI dyes (1 mg/mL) were used to evaluate the viability of the immobilized L929 cells inside CHI/β-GP:TPP and ALG particles. After 1, 3, and 7 days of culture, the cell culture medium was removed and 1 mL of PBS containing 2 µL of calcein-AM and 1 µL of PI was added to each well (n=3). The particles were then incubated at 37 °C for 10 min protected from light. After this period, samples were washed several

times with PBS to remove all traces of excessive dyes. Samples were immediately visualized in the dark by fluorescence microscopy (Axioimage RZ1M; Zeiss, Germany).

6.4. Results and Discussion

6.4.1. Superhydrophobic Surfaces Methodology

The modification performed onto the PS smooth substrates, as described previously [30], created an ordered roughness composed of micro- and nanotopographic features. In addition, to improve the repellent properties of the PS, the roughness was conjugated with a chemical treatment. The obtained superhydrophobic surfaces presented an apparent water contact angle of 165° ± 4.9°. Aqueous-based solutions, when dispensed onto the superhydrophobic surfaces, assumed an almost spherical shape (Figure 6.1 (a)). The volume can control the sphere diameter [25]. A dispensing system, a superhydrophobic surface, and the precursor solutions are required to prepare particles, making this technique very cost-effective. Moreover, the use of significant amounts of solvents was avoided and no waste was produced. Unlike conventional techniques for particles production [24], this method allowed the individual solidification of the spherical hydrogels in a dry environment at room temperature. Such conditions were advantageous because the efficiency of the encapsulation process was very high as entrapped molecules had no possibility of being lost through migration to a surrounding medium. Moreover, the system was suitable for cell culture since encapsulated cells could maintain their viability (results discussed later).

The CHI/β-GP:TPP particles are assumed to be produced from liquid precursors containing dexamethasone (Figure 6.1 (b)) or L929 cells (Figure 6.1 (c)) as generally shown in Figure 6.1. The superhydrophobic surfaces methodology allowed producing almost spherical hydrogel particles without mechanical stress, agitation, use of organic solvents, high temperatures, or pressures (Figure 6.1 (d)). Unlike other techniques/systems [33], CHI/β-GP:TPP hydrogels prepared on PS superhydrophobic surfaces do not require to be washed.

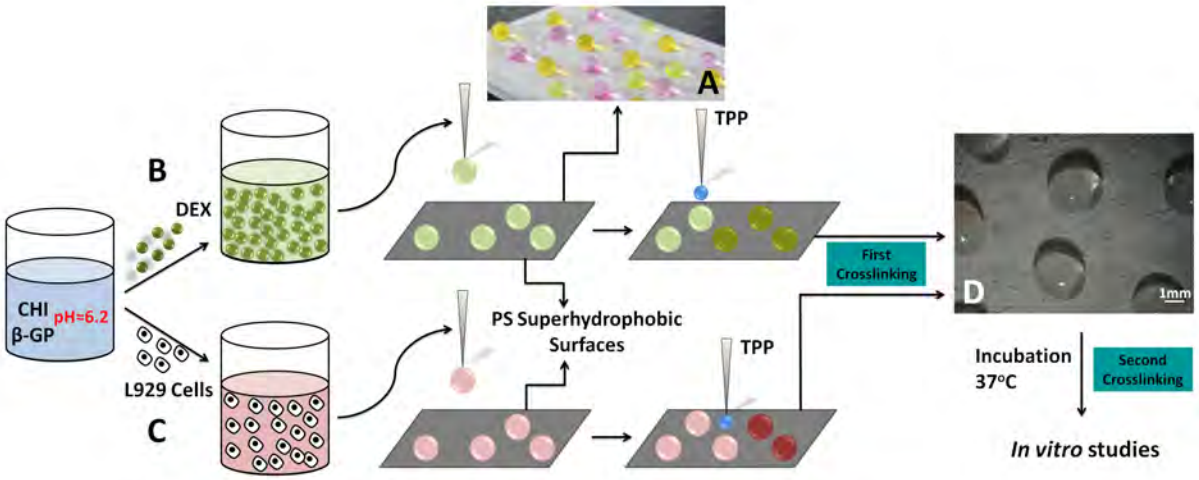

Figure 6.1. PS superhydrophobic surfaces were used as platforms to support aqueous-based droplets (A) for the preparation of CHI/β-GP:TPP spherical particles immobilizing (B) dexamethasone or (C) L929 cells. In any case, stable hydrogel beads were obtained upon ionic (D) crosslinking.

6.4.2. CHI/β-GP:TPP Particles

In the first step, the CHI/β-GP precursor solution was dispensed onto the PS superhydrophobic surfaces and the drops acquired a stable spherical shape. It is described in literature that β-GP neutralizes CHI allowing the incorporation of cells [7,34,35] as well as CHI gelation at physiological temperatures [9,10,36,37]. However, the CHI/β-GP gels obtained upon heating did not have a firm structure, and it was difficult to mold them in defined shapes such as spheres. In this context, an earlier crosslinking process of the CHI/β-GP solution may be an interesting strategy to obtain soft but manageable structures. A non-toxic polyanion crosslinker (TPP) was dispensed on the top of CHI/β-GP liquid droplets previously deposited on the PS superhydrophobic surfaces (first crosslinking mechanism in Figure 6.2).

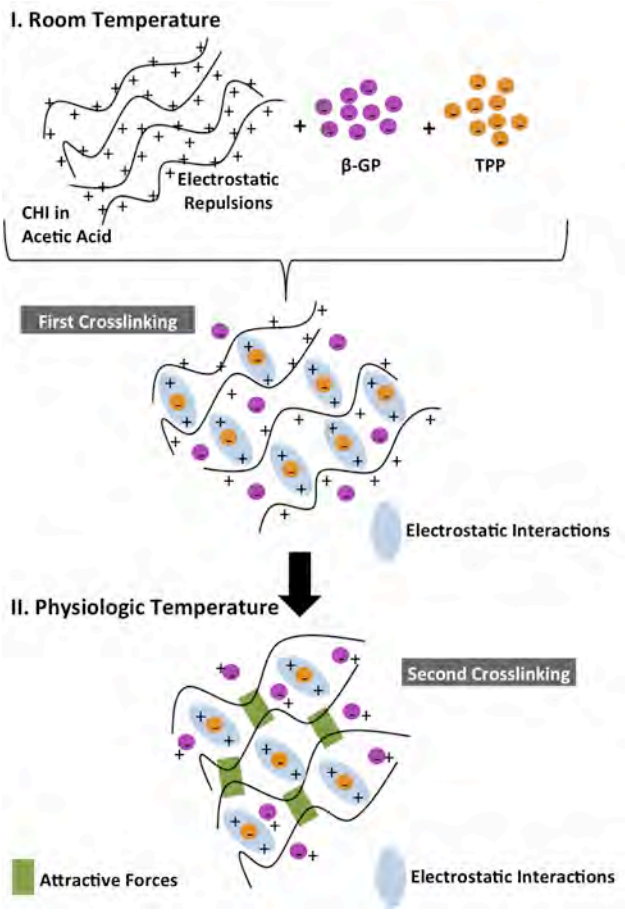

Figure 6.2. Schematic representation of CHI/β-GP:TPP hydrogel networks derived from physical associations formed by ionic interactions (first crosslinking) and other attractive forces (second crosslinking).

In the presence of water or acidic solutions, sodium TPP dissociates into OH^- and $P_3O_{10}^{5-}$ ions that interact with $-NH_3^+$ groups of CHI by deprotonation or ionic crosslinking [38]. The process of crosslinking started immediately after dispensing TPP. The diffusion of TPP through the CHI/β-GP droplets was very efficient as the ionic crosslinking occurred in less than 2 h. At physiological temperature, the presence of β-GP allowed the release of protons from the remaining CHI protonated amino group [11] and the subsequent appearance of attractive CHI–CHI forces that induced the reinforcement of the hydrogel physical structure (second crosslinking step in Figure 6.2). The proton receptor (β-GP) and the temperature increase turned the system kinetically unstable. Consequently, the reduction of the CHI charge decreased the repulsive chain–chain interactions and allowed the attractive forces (van der Walls, hydrogen bonding, and hydrophobic interactions) to predominate [11]. To determine whether any hardening effect had occurred after the thermogelation, DMA was performed on the CHI/β-GP:TPP hydrogels immersed in PBS at 20 °C and 37 °C. Both storage (elastic) modulus and loss (viscous) modulus are shown in Figure 6.3 (a) and (b), respectively.

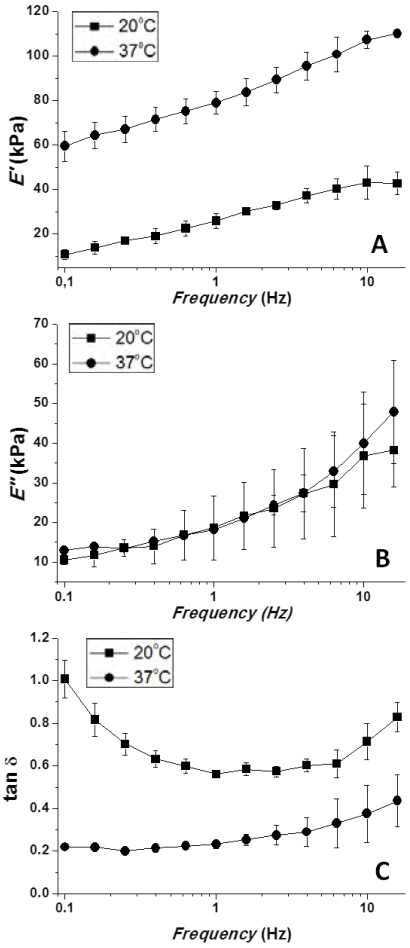

Figure 6.3. (a) Storage modulus (*E'*), (b) loss modulus (*E''*), and (c) loss factor (tan δ) of CHI/β-GP:TPP gels at 20 °C and 37 °C, within the frequency range of 0.1–15 Hz.

The storage modulus, *E'*, is a measurement of the sample stiffness, and the loss modulus, *E''*, indicates the amount of mechanical energy lost during a cycle. At both temperatures, *E'* increased with increasing frequency. For the same frequency, *E'* was significantly higher at 37 °C as a result of the thermogelation effect. For example, at f =1 Hz, the storage modulus at 20 °C was 25.9 ± 3.4 kPa, which was significantly lower than the storage modulus of 78.9 ± 5.1 kPa at 37 °C. These results demonstrated that the stiffness of the formulated gels was increased when placed at simulated physiological conditions, meaning that the system could be hardened in situ upon implantation. The values of *E'* in such conditions are within the range of values reported for hydrogels applied in cartilage regeneration strategies [39,40].

Regarding the *E''* values, the results were similar at both temperatures, which indicated that temperature does not affect the viscous component of the dynamic modulus. The damping capability of the gels can be evaluated by analyzing the tan δ (Figure 6.3 (c)), corresponding to *E''*/*E'* ratio. At 20

°C, the tan δ varied between 1 and 0.6. However, at 37 °C, it was significantly lower, varied between 0.2 and 0.4. This means that the formulation under study exhibited a significant viscous component at 20 °C, but displayed a much higher elastic nature at physiological temperature. Even in these conditions, the CHI/β-GP:TPP gels exhibited damping properties, showing the ability to partially dissipate the inputted mechanical energy, which might be advantageous in some biomedical applications.

For the volume of the liquid precursor used, the diameter of the obtained particles was about 2.70±0.29 mm. The low standard deviation value indicates that the superhydrophobic methodology allows producing particles with a narrow size distribution. However, such size can be easily manipulated by decreasing or increasing the volume of the dispensed solutions [25]. The size and water uptake of the particles should be dependent on the pH of the surrounding media. The pH sensitivity of the CHI/β-GP:TPP particles was verified through swelling studies under different pH conditions. The CHI network contains pH-ionizable groups that when immersed in acidic, neutral, or basic environments lead to distinct network electrical states, causing the structure to swell or shrink [41]. After preparation, CHI/β-GP:TPP particles were immediately soaked in phosphate buffer saline at pH 7.4, water supplemented with HCl at pH 2, or water supplemented with NaOH at pH 9 (at 37 °C). The swelling degree of the particles immersed in different solutions is shown in Figure 6.4.

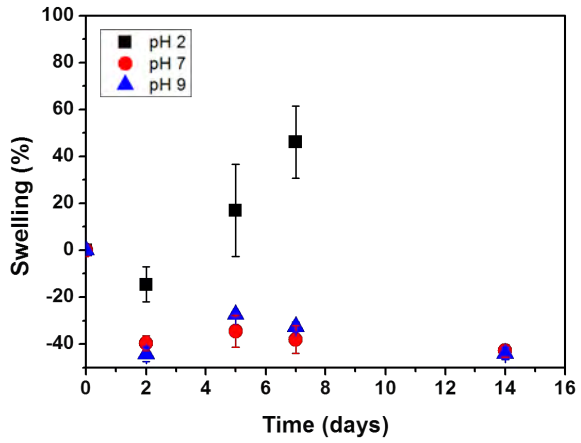

Figure 6.4. Swelling of the CHI/β-GP:TPP particles after 2, 5, 7, and 14 days of immersion in pH 2, 7.4, and 9 media at 37 °C.

For 2 days, the particles shrunk in all three media. Probably, the increased attraction of CHI chains due to thermogelation caused by β-GP induced the release of water molecules that were in excess in the initially prepared particles (shrinking of the hydrogel structure). Comparing the swelling degree at this

time point, the particles at low pH shrunk less than those immersed in neutral or basic medium. After this period, the CHI/β-GP:TPP particles immersed in pH 2 medium started to swell. After day 7, the structure was completely disintegrated, impairing further characterization. We can conclude that the system was not stable in acidic conditions. Similar results were obtained for CHI particles crosslinked with TPP using a spray-drying procedure [42]. However, a completely different effect occurred in the particles immersed in basic or neutral pH. From day 2 to day 5, the particles swollen slightly and started to shrink after 5 days. The protonation of amino groups in acidic conditions increased the electrical density and consequently increased the repulsive forces between the CHI crosslinked network [18]. This promoted the swelling of the CHI/β-GP:TPP structure until complete disintegration of the network. In neutral and basic medium, the protonation did not occur, and the particles kept their integrity for at least 14 days. The conservation of the 3D structure of particles during this time period indicated that the developed system remained stable. Shown in Figure 6.5 are aspects of the particles upon immersion in the solutions at different pH values. Essentially, the particles remained spherical.

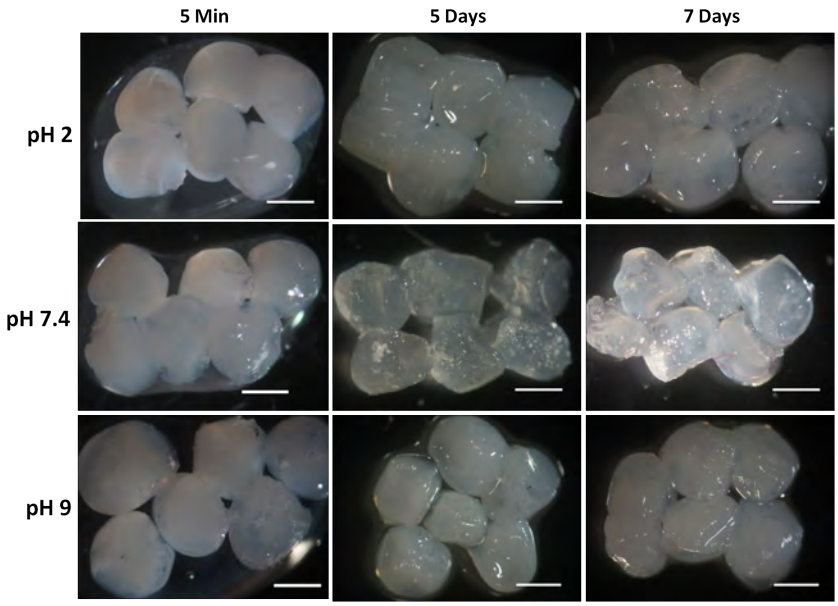

Figure 6.5. Stereomicroscope images of CHI/β-GP:TPP particles immediately after preparation (5 min) and after immersion in pH 2, 7.4, and 9 media for 5 and 7 days at 37 °C (scale bar: 1 mm).

6.4.3. Drug Release

To investigate the ability of the designed system to act as drug reservoirs, CHI/β-GP:TPP particles were loaded with dexamethasone, a synthetic glucocorticoid with efficient anti-inflammatory properties [43]. Dexamethasone has also been used combined with β-GP and ascorbic acid to support the osteogenic differentiation of mesenchymal stem cells [44]. During the preparation of the particles, the droplets

were surrounded by air. Since the encapsulating molecules are not volatile, an encapsulation efficiency of virtually 100% could be expected. The amount of dexamethasone released was assessed by UV spectrophotometry. The respective release profiles for 5 h at different pH values are shown in Figure 6.6.

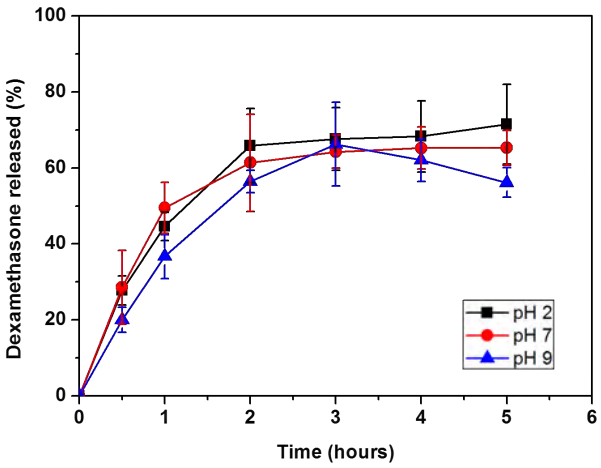

Figure 6.6. Dexamethasone release profiles from CHI/β-GP:TPP particles immersed in media with pH 2, 7.4, and 9 at 37 °C.

The profiles presented a relatively fast drug release, where almost 60%–70% of the encapsulated dexamethasone was released after 3 h. Despite their limited lifetime in physiological media, physical crosslinked systems have great advantages for short-term drug release applications [20]. The dexamethasone release profile observed at pH 2 was similar to the one at pH 7.4. However, at pH 9, the amount of dexamethasone released in each time point was slightly lower compared to the other cases. This may be due to the electrostatic attractive interactions between anions and CHI at basic pH [21], which may hinder the diffusion of dexamethasone to the release medium. The drug release kinetics was characterized by fitting the experimental data with the standard release equations (2)–(5). According to the R^2 values in Table 6.1, the best fit was with the Higuchi model. This indicated that the release rate was significantly dependent on the rate of dexamethasone diffusion (Fickian diffusion) through the crosslinked CHI/β-GP:TPP networks. However, a good fitting was also observed in the Korsmeyer–Peppas model, which was applied as the mechanism of drug release and is used when more than one type of mechanism is involved. Based on the Korsmeyer–Peppas kinetic model, the dexamethasone release from CHI/β-GP followed an anomalous mode ($0.43 < n < 0.85$) [31]. This indicated that the release was controlled by diffusion as well as by the changes in the water uptake of the particles.

Table 6.1. Mathematical models and respective parameters obtained from the fitting of the experimental data corresponding to a dexamethasone release from CHI/β-GP:TPP particles at different pH values. The interval from 10% to 60% of the amount of dexamethasone release was used in all fittings.

Mathematical models	Zero-order		First-order		Higuchi		Korsmeyer-Peppas		
pH	R^2 (±SD)	K_0 (±SD) ($\mu g h^{-1}$)	R^2 (±SD)	K_1 (±SD) (h^{-1})	R^2 (±SD)	K_H (±SD) ($h^{0.5}$)	R^2 (±SD)	K_{KP} (±SD)	n (±SD)
2	0.947 (±0.0833)	9.43 (±2.71)	0.857 (±0.109)	0.548 (±0.130)	0.978 (±0.0504)	20.414 (±5.795)	0.976 (±0.0477)	16.41 (±1.439)	0.621 (±0.148)
7.4	0.813 (±0.129)	7.76 (±2.62)	0.720 (±0.147)	0.486 (±0.146)	0.869 (±0.118)	17.157 (±5.453)	0.856 (±0.152)	16.61 (±3.258)	0.578 (±0.185)
9	0.931 (±0.0895)	8.98 (±1,00)	0.808± (0.113)	0.661 (±0.103)	0.967 (±0.0508)	19.471 (±2.008)	0.963 (±0.0482)	13.12 (±1.491)	0.751 (±0.106)

To tailor the release profiles to an appropriate efficiency for certain applications, it would be necessary to change the formulation of the liquid precursor (*e.g.* concentration of CHI or TPP) to modify the structure of the particles. As reported before [45], superhydrophobic surfaces' technology can control drug release by increasing the structural complexity of the particles, namely, by the production of multilayer spherical systems where non-loaded layers may act as barriers to control the release of drugs immobilized in the inner layers.

6.4.4. Cells Immobilization

The cytocompatibility of the proposed system is an important property, especially due to its potential to immobilize cells inside the particles. The materials used should be noncytotoxic, and cell viability must be maintained during processing. Droplet deposition onto PS superhydrophobic surfaces has been validated as a mild technology to immobilize cells [25]. In this context, the viability and cell distribution inside CHI/β-GP:TPP particles were analyzed by Live/Dead staining. L929 cells were immobilized inside the spherical gels and then cultured under appropriated conditions for 7 days. Based on the fluorescent microscopy images in Figure 6.7, the cells were homogeneously distributed and viable (green spots) after 7 days. ALG (1.5% w/v) crosslinked with $CaCl_2$ was used as control; such system could maintain viability of the mesenchymal stem cells for 21 days [27]. Compared with control (cells encapsulated in ALG using the same processing technique), the results were similar, and hence, the CHI/β-GP:TPP particles could provide a suitable system to encapsulate living cells without significant loss of viability.

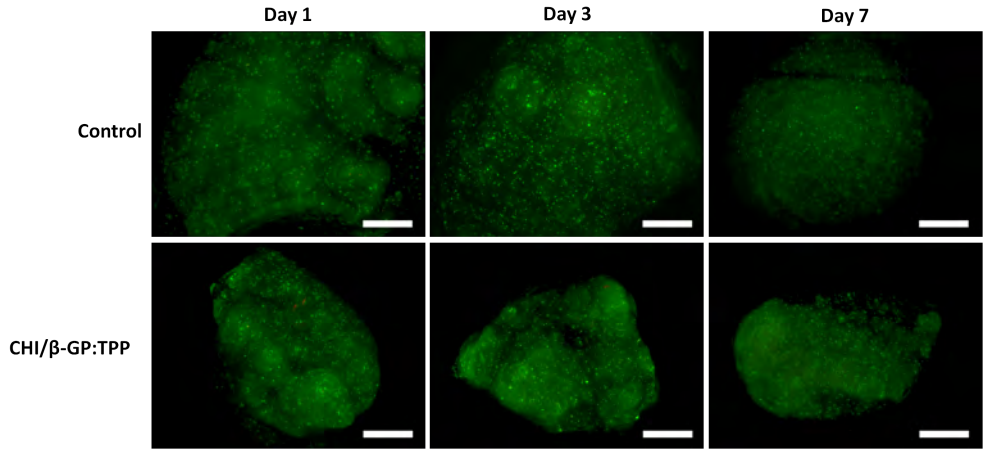

Figure 6.7. Fluorescent microscopy images of Live/Dead assay at 1, 3, and 7 days of culture. ALG particles (control) and CHI/β-GP:TPP particles were analyzed. Living cells were stained in green by calcein-AM, and dead cells were stained in red by propidium iodide (scale bar: 500 μm).

6.5. Conclusions

Solid particles were prepared by crosslinking neutralized CHI/β-GP solutions with TPP. The use of biomimetic superhydrophobic surfaces as particle production methodology is advantageous since the particles are obtained in mild conditions conserving the viability of the encapsulated cells, with a narrow particle size distribution and without aggregation. Due to the particle–air interface, no dexamethasone was lost in our study; during the solidification of the drops, the encapsulation efficiency of the system was very high. The spherical systems were pH sensitive and transitioned from soft viscoelastic to a more elastic and stiff nature after being exposed to physiological conditions. The system maintains cells well distributed and viable up to 7 days. Dexamethasone was also encapsulated in the particles that sustained its release for 2–3 h. The fabrication and the particle features of the CHI/β-GP:TPP system have interesting properties that should be explored for more specific biomedical applications.

6.6. Acknowledgments

The authors of this work received PhD grants from the Portuguese Foundation for Science and Technology (FCT): SFRH/BD/71395/2010, SFRH/BD/69529/2010, and SFRH/BD/71396/2010. The research leading to these results has received funding from the European Union's Seventh Framework Programme (FP7/2007-2013) under grant agreement no. REGPOT-CT2012-316331-POLARIS. The research was also funded by FEDER through the Competitive Factors Operation Program—COMPETE and by National Funds through FCT in the scope of the project PTDC/CTM-

BIO/1814/2012. This work was also cofinanced by the Operational Human Potential Program (POPH), developed under the scope of the National Strategic Reference Framework (QREN) from the European Social Fund (FSE).

6.7. References

[1] Peniche C., Argüelles-Monal W., Peniche H. and Acosta N., Chitosan: an attractive biocompatible polymer for microencapsulation, Macromolecular Bioscience 2003, 3: 511–520.

[2] Denkbas E.B. and Ottenbrite R.M., Perspectives on: chitosan drug delivery systems based on their geometries, Journal of Bioactive and Compatible Polymers 2006, 21: 351–368.

[3] Kubota N., Tatsumoto N., Sano T. and Toya K., A simple preparation of half N-acetylated chitosan highly soluble in water and aqueous organic solvents, Carbohydrate Research 2000, 324: 268–274.

[4] Zhu J. H., Wang X. W., Ng S., Quek C. H., Ho H. T., Lao X. J. and Yu H., Encapsulating live cells with water-soluble chitosan in physiological conditions. Journal of Biotechnology 2005, 117: 355–365.

[5] Correia C. R., Reis R. L. and Mano J. F., Multilayered hierarchical capsules providing cell adhesion sites, Biomacromolecules 2013, 14: 743–751.

[6] Costa N. L., Sher P. and Mano J. F., Liquefied capsules coated with multilayered polyelectrolyte films for cell immobilization, Advanced Engineering Materials 2011, 13: B218–B224.

[7] Roughley P., Hoemann C., DesRosiers E., Mwale F., Antoniou J. and Alini M., The potential of chitosan-based gels containing intervertebral disc cells for nucleus pulposus supplementation, Biomaterials 2006, 27: 388–396.

[8] Cho J., Heuzey M. C., Bégin A. and Carreau P. J., Physical gelation of chitosan in the presence of beta-glycerophosphate: the effect of temperature, Biomacromolecules 2005, 6: 3267–3275.

[9] Chenite A., Buschmann M., Wang D., Chaput C. and Kandani N., Rheological characterisation of thermogelling chitosan/glycerol-phosphate solutions, Carbohydrate Polymers 2001, 46: 39–47.

[10] Ruel-Gariépy E., Chenite A., Chaput C., Guirguis S. and Leroux J., Characterization of thermosensitive chitosan gels for the sustained delivery of drugs, International Journal of Pharmaceutics 2000, 203: 89–98.

[11] Lavertu M., Filion D. and Buschmann M. D., Heat-induced transfer of protons from chitosan to glycerol phosphate produces chitosan precipitation and gelation, Biomacromolecules 2008; 9: 640–650.

[12] Couto D. S., Hong Z. and Mano J. F., Development of bioactive and biodegradable chitosan-based injectable systems containing bioactive glass nanoparticles, Acta Biomaterialia 2009, 5: 115–123.

[13] Chenite A., Chaput C., Wang D., Combes C., Buschmann M. D., Hoemann C. D., Leroux J. C., Atkinson B. L., Binette F. and Selmani A., Novel injectable neutral solutions of chitosan form biodegradable gels in situ, Biomaterials 2000, 21: 2155–2161.

[14] Richardson S. M., Hughes N., Hunt J. A., Freemont A. J. and Hoyland J. A., Human mesenchymal stem cell differentiation to NP-like cells in chitosan-glycerophosphate hydrogels, Biomaterials 2008, 29: 85–93.

[15] Ngoenkam J., Faikrua A., Yasothornsrikul S. and Viyoch J., Potential of an injectable chitosan/starch/beta-glycerol phosphate hydrogel for sustaining normal chondrocyte function, International Journal of Pharmaceutics 2010, 391: 115–124.

[16] Ganza-González A., Anguiano-Igea S., Otero-Espinar F. J. and Blanco Méndez J., Chitosan and chondroitin microspheres for oral-administration controlled release of metoclopramide, European Journal of Pharmaceutics and Biopharmaceutics 1999, 48: 149–155.

[17] Kildeeva N. R., Perminov P. A., Vladimirov L. V., Novikov V. V. and Mikhailov S. N., About mechanism of chitosan cross-linking with glutaraldehyde, Russian Journal of Bioorganic Chemistry 2009, 35: 360–369.

[18] Malafaya P. B., Pedro A. J., Peterbauer A., Gabriel C., Redl H., Reis R. L., Chitosan particles agglomerated scaffolds for cartilage and osteochondral tissue engineering approaches with adipose tissue derived stem cells, Journal of Material Science: Materials in Medicine 2005; 16: 1077–1085.

[19] Grech J. M. R., Mano J. F. and Reis R. L., Chitosan beads as templates for layer-by-layer assembly and their application in the sustained release of bioactive agents, Journal of Bioactive and Compatible Polymers 2008, 23: 367–380.

[20] Bhattarai N., Gunn J. and Zhang M., Chitosan-based hydrogels for controlled, localized drug delivery, Advanced Drug Deliver Reviews 2010, 62: 83–99.

[21] Shu X. Z. and Zhu K. J., Controlled drug release properties of ionically cross-linked chitosan beads: the influence of anion structure, International Journal of Pharmaceutics 2002, 233: 217–225.

[22] Jătariu Cadinoiu A. N., Popa M., Curteanu S. and Peptu C. A., Covalent and ionic co-cross-linking - an original way to prepare chitosan-gelatin hydrogels for biomedical applications, Journal of Biomedical Materials Research Part A 2011, 98: 342–350.

[23] Hosseinzadeh H., Atyabi F., Dinarvand R. and Ostad S. N., Chitosan-Pluronic nanoparticles as oral delivery of anticancer gemcitabine: preparation and in vitro study, International Journal of Nanomedicine 2012, 7: 1851– 1863.

[24] Lima A.C., Sher P. and Mano J. F., Production methodologies of polymeric and hydrogel particles for drug delivery applications, Expert Opinion on Drug Delivery 2012, 9: 231–248.

[25] Song W., Lima A. C. and Mano J. F., Bioinspired methodology to fabricate hydrogel spheres for multi-applications using superhydrophobic substrates, Soft Matter 2010, 6: 5868–5871.

[26] Puga A. M., Lima A. C., Mano J. F., Concheiro A. and Alvarez-Lorenzo C., Pectin-coated chitosan microgels crosslinked on superhydrophobic surfaces for 5-fluorouracil encapsulation, Carbohydrate Polymers 2013, 98: 331– 340.

[27] Lima A. C., Batista P., Valente T. A. M., Silva A. S., Correia I. J. and Mano J. F., Novel methodology based on biomimetic superhydrophobic substrates to immobilize cells and proteins in hydrogel spheres for applications in bone regeneration, Tissue Engineering Part A 2013, 19: 1175–1187.

[28] Oliveira M. B. and Mano J. F., Polymer-based microparticles in tissue engineering and regenerative medicine, Biotechnology Progress 2011, 27: 897–912.

[29] Mano J. F., Viscoelastic properties of chitosan with different hydration degrees as studied by dynamic mechanical analysis, Macromolecular Bioscience 2008, 8: 69–76.

[30] 20. Lima A. C., Song W., Blanco-Fernandez B., Alvarez-Lorenzo C. and Mano J.F., Synthesis of temperature-responsive dextran-MA/PNIPAAm particles for controlled drug delivery using superhydrophobic surfaces, Pharmeceutical Research 2011, 28: 1294–1305.

[31] Siepmann J. and Göpferich A., Mathematical modeling of bioerodible, polymeric drug delivery systems, Advanced Drug Delivery Reviews 2001, 48: 229–247.

[32] Aydin R. S. T. and Pulat M., 5-fluorouracil encapsulated chitosan nanoparticles for pH-stimulated drug delivery: evaluation of controlled release kinetics, Journal of Nanomaterials 2012, 313961 (10 pp.).

[33] Peptu C. A., Buhus G., Popa M., Perichaud A. and Costin D., Double cross-linked chitosan-gelatin particulate systems for ophthalmic applications, Journal of Bioactive and Compatible Polymers 2010, 25: 98–116.

[34] Chen H. and Fan M., Novel thermally sensitive pH-dependent chitosan/carboxymethyl cellulosehydrogels, Journal of Bioactive and Compatible Polymers 2008, 23: 38–48.

[35] Sun B., Ma W., Su F., Wang Y., Liu J., Wang D. and Liu H., The osteogenic differentiation of dog bone marrow mesenchymal stem cells in a thermo-sensitive injectable chitosan/collagen/β-glycerophosphate hydrogel: in vitro and in vivo, Journal of Materials Science: Materials in Medicine 2011, 22: 2111–8.

[36] Ruel-Gariépy E. and Leroux J.C., In situ-forming hydrogels—review of temperature-sensitive systems, European Journal of Pharmaceutics and Biopharmaceutics 2004, 58: 409–26.

[37] Ta H. T., Dass C. R. and Dunstan D. E., Injectable chitosan hydrogels for localised cancer therapy, Journol of Controlled Release 2008, 126: 205–16.

[38] Mi F. L., Shyu S. S., Wong T. B., Jang S.-F., Lee S.-T. and Lu K.-T., Chitosan-polyelectrolyte complexation for the preparation of gel beads and controlled release of anticancer drug. II. Effect of pH-dependent ionic crosslinking or interpolymer complex using tripolyphosphate or polyphosphate as reagente, Journal of Applied Polymer Science 1999, 74: 1093–107.

[39] Oliveira J. T., Santos T. C., Martins L., Picciochi R., Marques A. P., Castro A. G., Neves N. M., Mano J. F. and Reis R. L., Gellan gum injectable hydrogels for cartilage tissue engineering applications: in vitro studies and preliminary in vivo evaluation, Tissue Engineering Part A 2010, 16: 343–53.

[40] Nettles D. L., Vail T. P., Morgan M. T., Grinstaff M. W. and Setton L. A., Photocrosslinkable hyaluronan as a scaffold for articular cartilage repair, Annals of Biomedical Engineering 2004, 32: 391–7.

[41] Mano J. F., Stimuli-responsive polymeric systems for biomedical applications, Advanced Engineering Materials 2008, 10: 515–27.

[42] Desai K. G. H. and Park H. J., Preparation and characterization of drug-loaded chitosan-tripolyphosphate microspheres by spray drying, Drug Development Research 2005, 64: 114–28.

[43] Gómez-Gaete C., Fattal E., Silva L., Besnard M., and Tsapis N., Dexamethasone acetate encapsulation into Trojan particles, Journal of Controlled Release 2008; 128: 41–9.

[44] Su Y., Su Q., Liu W., Venugopal J. R., Mo X., Ramakrishna S., Al-Deyab S. S., and El-Newehy M., Controlled release of bone morphogenetic protein 2 and dexamethasone loaded in core-shell PLLACL-collagen fibers for use in bone tissue engineering, Acta Biomaterialia 2012, 8: 763–71.

[45] Lima A. C., Custódio C. A., Alvarez-Lorenzo C. and Mano J. F., Biomimetic methodology to produce polymeric multilayered particles for biotechnological and biomedical applications, Small 2013, 9: 2487–92.

Chapter 7

Fast and Mild Strategy, Using Superhydrophobic Surfaces, to Produce Collagen/Platelet Lysate Gel Beads for Skin Regeneration

7.1. Abstract

Platelet lysates (PL) were encapsulated in collagen (Coll) millimetric gel beads, on biomimetic superhydrophobic surfaces, under mild conditions, with the aim of obtaining easy-to-handle formulations able to provide sustained release of multiple growth factors (GFs) for skin ulcers treatment. The gel particles were prepared with various concentrations of PL incorporating or not stem cells, and tested as freshly prepared or after being freeze-dried or cryopreserved. Coll+PL particles were evaluated regarding degradation in collagenase-rich environment (simulating the aggressive environment of the chronic ulcers), sustained release of total protein, PDGF-BB and VEGF, cell proliferation (using particles as the only source of growth factors), scratch wound recovery and angiogenic capability. Compared to Coll solely particles, incorporation of PL notably enhanced cell proliferation (inside and outside gels) and favored scratch wound recovery and angiogenesis. Moreover, cell-laden gel particles containing PL notably improved cell proliferation and even migration of cells from one particle towards a neighbor one, which led to cell- cell contacts and the spontaneous formation of tissue layers in which the spherical gels were interconnected by the stem cells.

This chapter is based on the following publication:
Lima A.C., Mano J. F., Concheiro A. and Alvarez-Lorenzo C., Fast and mild strategy, using superhydrophobic surfaces, to produce collagen/platelet lysate gel beads for skin regeneration, Stem Cells Reviews and Reports 2014, DOI 10.1007/s12015-014-9548-6 (*in press*).

7.2. Introduction

Skin ulcers caused by diabetes, peripheral vascular diseases, and disorders that hinder patient mobility can easily lead to severe states that are very difficult to treat [1]. Despite enormous efforts carried out to find efficient, standardized therapeutic strategies, until now this aim was not achieved. Moreover, the socio-economic costs associated to the treatments of chronic non-healing ulcers are still very relevant [1].

Normal wound healing process occurs sequentially and does not require any significant intervention. Platelets circulating in the blood stream reach the injured skin site and secrete growth factors (GFs). Macrophages recruitment and GFs release attract endothelial cells to migrate and proliferate in the wound site [2]. Angiogenesis and synthesis of Coll are also stimulated until skin reaches the anatomic and functional integrity [3]. Despite the different etiologies, chronic skin ulcers are characterized by failure in the healing process, requiring always intervention. A severe inflammatory process is triggered where large amounts of proteinases, such as plasmin and matrix metalloproteinases, and also reactive oxygen species are produced. Due to the presence of abnormal amount of proteinases, an excessive destruction of the extra-cellular matrix occurs, and the epidermis layer is disrupted causing cell dead [4]. Moreover, poor blood vessels formation is characteristic of chronic skin ulcers, meaning that therapeutic strategies are required to re-establish the normal vascular network. Three distinct mechanisms are involved in neovascularization process: the sprouting of preexisting resident endothelial cells, maturation and enlargement of the preexisting small vessels, and recruitment of bone marrow-derived endothelial progenitor cells [5]. Topical application of GFs that stimulate the formation of a neovascularized network constitutes an alternative, but human-recombinant GFs are expensive, have short shelf life, and repeated doses may be required to achieve therapeutic effects [5]. Strategies to avoid invasive procedures (such as skin grafts) while supplying efficiently the wound site with GFs and cells have been also a target of research [6].

Platelet derived products have been evaluated for regeneration of soft and hard tissues including ligament [7], bone [8], cartilage [9], skin wounds [10], and cornea [11]. In a safe and cost-effective manner, autologous platelets and fibrinogen are collected from blood and concentrated. After activation with thrombin, calcium, collagen or via mechanical destruction (freeze-thaw cycles), platelet cells release a large number of biologically active substances allowing obtaining a cocktail of GFs and cytokines that stimulate cell recruitment (chemotaxis), proliferation and differentiation [12], and also anti- inflammatory mediators such as lipoxins [13]. Platelet derived products are known as platelet lysates (PL), platelet-rich plasma (PRP), platelet-rich plasma releasates (PRPr) or plasma rich in growth factors (PRGF) [14]. Such products are topically applied or locally administered via injection in the damaged tissue. The main

drawbacks of this approach are the low retention in the injury site or the rapid access of the GFs to the blood stream, which in turn leads to a fast degradation of GFs and cytokines and failure of the therapy [5, 15]. Therefore, easy-to-handle systems able to control the delivery of GFs and cytokines, and that also could eventually encapsulate stem cells, would be advantageous.

Some natural-based hydrogels have been reported as candidates to release platelet-derived products [16]. Alginate beads loaded with PL have been shown to increase cell proliferation in vitro and to accelerate the healing of skin pressure ulcers in hospitalized patients [13]. Encapsulation of PL and vancomycin hydrochloride into alginate led to particles able to absorb wound exudates and to increase the cell number in proliferation phase [17]. Co-encapsulation of PL and adipose-derived stem cells into alginate microspheres revealed osteogenic and angiogenic potential [18]. Similarly, gelatin hydrogels encapsulating PL and bFGF behaved as multiple GFs release systems with angiogenic capability [19].

Alternatively to above described materials, Coll could constitute an interesting option to produce carriers of cells and bioactive agents for chronic ulcers treatment. Coll is the most abundant extracellular protein in tissues such as cartilage, ligaments, tendons, bone and skin. Its main function is to stabilize tissues and to maintain their structural integrity. In the case of skin, collagen is the base of dermal layer and it is secreted during the wound healing process [4, 20].

The purpose of this study was to develop millimetric gel particles composed by Coll and PL, using a fast and mild process, for application in chronic ulcers for skin regeneration. Employing superhydrophobic surface methodology [21], here is not waste of materials (100 % encapsulation efficiency) and cells may be even immobilized inside the gels without significant cell viability loss. Performance of the produced Coll+PL gel particles regarding cell proliferation was elucidated both as freshly prepared (in hydrated form) and after being freeze-dried, in order to identify adequate strategies for implantation and use of the obtained particles. To carry out the work, gel particles prepared with Coll and PL (as obtained or concentrated 2 and 3×) and exposed to cell medium without FBS, were compared with Coll solely particles cultured in medium with and without FBS. Encapsulation of human adipose-derived stem cells (hASCs) was also investigated to determine whether these gels could act as cell carriers to the ulcer sites and trigger the formation of tissue layers. Performance of cell-laden gel particles was evaluated before and after cryopreservation with the aim of elucidating the feasibility of preserve the obtained systems.

7.3. Experimental Section

7.3.1. Materials

Polystyrene sheets (square Petri dishes, Bdbioscience, Enzifarma, Portugal) and polystyrene granules

(injection molding grade, Styrolution 158 k, UL Ides, Portugal) were used in the preparation of the superhydrophobic substrates. Tetrahydrofuran (THF, 99.9 %) was from Riedel de-Haen (Germany). 1H,1H,2H,2H-perfluorodecyltriethoxysilane (PFDTS, 97 %), penicillin-streptomycin solution (10,000 units of penicillin and 10 mg streptomycin/mL), L-glutamine, trypsin-EDTA, cell counting kit-8 (CCK-8), calcein-AM (17783), propidium iodide (PI, P4170), 4′,6-diamidino-2-phenylindole dihydrochloride (DAPI, 32670) and phosphate buffer saline (PBS, 10×) were from Sigma-Aldrich (St. Louis, MO, USA). Rat tail collagen type I high concentration was from BD Biosciences (USA). Paraformaldehyde tablets were from Panreac (Spain). Ethanol was purchased from Merck (Germany). Triton X-100 was from Analema (Spain). Glutaraldehyde was from Scharlau (Spain). Mesenchymal stem cells StemPRO® human adipose-derived stem cells (hASCs), MesenPro RS basal Medium and MesenPro RS Growth sup- plement (fetal bovine serum, FBS) were from Gibco® (Life Technologies; USA). Bodipy 650/665 Phalloidin was from Invitrogen™ Molecular Probes® (Life Technologies; USA). Dimethyl sulfoxide (DMSO) was from Fisher Chemicals (UK). PierceTM BCA Protein Assay Kit was from Thermo Scientific (USA). Human VEGF and human PDGF-BB ELISA kits were from RayBiotech (USA). Purified water (resistivity >18 MΩ cm; MilliQ®, Millipore, Spain) was obtained by means of reverse osmosis. All the other chemicals were used as received.

7.3.2. Polystyrene Superhydrophobic Surfaces

A phase separation method was applied to make PS surface superhydrophobic [21, 22]. Briefly, a PS solution (70 mg/mL) in THF was prepared and then mixed with ethanol (2:1.3 v/v). The mixture was dispensed onto smooth PS commercial substrates, which were then immersed in ethanol for 1 min and dried under nitrogen flow. The rough PS surfaces were treated with PFDTS (1 % v/v in ethanol) after argon plasma exposure for 40 s at 30 W (Plasma Prep5, Gala Instruments, Germany).

7.3.3. Platelet Lysates Preparation

Platelet lysates were obtained from three different blood collections performed at Galicia Blood Transfusion Center (Spain). Blood samples were centrifuged at 1400 rpm, 25 °C for 15 min. The plasma was isolated and subjected to three repeated temperature cycles (frozen at −80 °C and heated at 37 °C). Remaining platelets and potential antigens were removed by means of centrifugation at 4 °C, 12000 rpm during 12 min. PL was frozen at −80 °C until use. Concentrated PL was prepared from liquid PL, which was divided in aliquots of 1 mL, frozen at −80 °C and then freeze-dried for 36 h. The mass of solids per volume unit of liquid PL was determined. After that, the freeze-dried PL was reconstituted in 500 μL or 333.33 μL of PBS pH 7.4 to obtain PL concentrated 2 and 3×.

7.3.4. Gel Beads of Collagen Combined with Platelet Lysates

Gel particles of Coll solely or combined with PL (Coll+PL) were prepared using the superhydrophobic surface methodology [21, 23–26]. Solutions of Coll and Coll+PL were placed on ice to prevent premature gelation. Coll solely formulation was prepared from a stock solution (5 mg/mL, neutralized according to the supplier instructions) that was diluted with PBS up of 2.5 mg/mL. Coll+PL was obtained mixing collagen stock solution and PL at 50:50 (v/v), as indicated in Table 7.1.

Table 7.1. Composition of the solutions used to prepare the gel particles.

Formulation	Collagen neutralized (5 mg/mL)	PL	PBS
Coll	500 μL		500 μL
Coll+PL1x	500 μL	500 μL (PL1x)	
Coll+PL2x	500 μL	500 μL (PL2x)	
Coll+PL3x	500 μL	500 μL (PL3x)	

Hydrated gels were used or characterized immediately after hardening on the superhydrophobic surfaces (incubation at 37 °C for 10–15 min) or after being freeze-dried and re-hydrated into PBS pH 7.4. Freeze-dried particles were obtained after fast frozen in liquid nitrogen of gels previously immersed in water (5 gels/100 μL of water) to prevent the adhesion of gel beads to the walls of the containers.

The size of hydrated, freeze-dried and re-hydrated gel particles was evaluated using an optical stereomicroscope (Olympus SZ-CTV; Tokyo, Japan) connected to a video camera (JCV TK-S350; Tokyo, Japan). Five particles of each formulation were sized using an analysis image software analysis (Image J, NIH, USA). The structure of the particles was visualized using Scanning Electron Microscopy (SEM). Immediately after hardening, some particles were collected, and fixed in glutaraldehyde (0.25 % v/v aqueous solution) overnight at 4 °C. The particles were then dehydrated in ethanol aqueous solutions of increasing concentration. Images of freeze-dried and dehydrated formulations were obtained using a Zeiss FESEM ULTRA Plus microscope (Zeiss, Oberkochen, Germany) after gold coating.

7.3.5. Total Protein and Growth Factors Release

In vitro release studies were performed in triplicate incubating 15 Coll+PL particles (Coll+PL2× in hydrated state) in 1 mL of PBS pH 7.4 at 37 °C inside Eppendorf LoBind tubes. At various time intervals, aliquots of 0.4 mL were withdrawn and replaced with the same volume of fresh PBS. Total protein released was quantified using a BCA protein detection kit (absorbance read at 595 nm), while PDGF-BB and VEGF released were quantified using specific ELISA kits (absorbance read at 440 nm; FLUOstar Optima microplate reader, BMG Labtech, Ortenberg, Germany).

7.3.6. Gel Beads of Collagen Combined with Platelet Lysates Encapsulating hASCs

hASCs were cultured in MesenPro® RS medium supplemented with 2 % (v/v) growth supplement (FBS), 1 % (v/v) L-glutamine solution (200 mM) and 1 % (v/v) penicillin/streptomycin in humid conditions at 37 °C with 5 % CO_2. Then, cells were trypsinised and resuspended in Coll or Coll+PL solutions (formulations described in Table 7.1) with a density of 7.5×10^5 cells/mL. The cell suspensions were dispensed through pipetting on the superhydrohobic surfaces in volumes of 10 μL and incubated inside sterile Petri dishes at 37 °C during 10–15 min for the gelling process.

7.3.7. hASCs Viability, Proliferation and Morphology Inside Gel Beads

Hardened gel particles were collected and cultured in 96 well plates for 1, 3 and 7 days (2 particles/well, 200 μL of cell culture medium). Coll gels cultured in medium with or without FBS were used as controls. All the formulations containing PL were cultured in medium without FBS. The cells were routinely observed using inverted microscopy (x10) (Nikon Eclipse TS100, Nikon Corporation, Tokyo, Japan) in order to discard any contamination. hASCs proliferation was determined by quantification of metabolic activity following the CCK-8 kit supplier protocol. Briefly, part of the medium in each well was removed, and particles immersed in 100 μL of cell culture medium were incubated with 10 μL of CCK-8 solution at 37 °C for 3 hours. Aliquots of the medium (80 μL) were transferred to 96 well plates and their absorbance measured at 450 nm using a microplate reader (BIORAD, Model 680, USA). Blank (100 μL of cell culture medium) and controls (gel particles without cells) were similarly processed. hASCs proliferation was determined from the measured absorbance values using a calibration curve prepared with known amount of cells seeded into the wells. In parallel, cell viability was assessed by means of live/dead test using Calcein-AM and propidium iodide staining. Briefly, at each time point, gel particles were washed with PBS and incubated at 37 °C for 10 min immersed in a PBS: Calcein-AM (1 mg/mL):propidium iodide (1 mg/mL) 98.5:1:0.5 v/v/v solution. Afterwards the particles were washed with PBS to remove all traces of the dyes and then fixed with 4 % paraformaldehyde in PBS for 20 min at room temperature. Finally, the particles were again washed with PBS and visualized using confocal microscopy (LEICA TCS-SP2, Leica Microsystems GMbH, Mannheim, Germany). hASCs morphology inside Coll or Coll+PL gels was visualized using DAPI to stain cell nuclei (stock solution 1 mg/ml in H_2O) and Phalloidin to stain the F-actin filaments in the cytoskeleton (stock solution 5 mg/1.5 mL in methanol). In brief, the cell-laden gels at 1, 3 and 7 days of incubation in culture medium were immersed in 4 % paraformaldehyde in PBS for 20 min at room temperature to fix the cells. Then, the cells were permeabilized with 0.1 % Triton X-100 for 2 min at room temperature and subsequently washed with PBS several times. Afterwards, the cells were stained with

Phalloidin (3 μL of stock solution per 100 μL of PBS) for 45 min at room temperature. Then, they were washed with PBS and stained with DAPI (2.5 μL of stock solution per 1 mL of PBS) for 10 min also at room temperature protected from the light. After being washed again with PBS to remove all traces of the dyes, the particles were visualized using confocal microscopy (Leica Microsystems GMbH, Mannheim, Germany).

7.3.8. Cryopreservation and Subsequent Viability and Proliferation Capacity

After 24 h of culture, some cell-laden gel particles were cryopreserved. To do that, 10 particles of each type were suspended in 1 mL of FBS:DMSO 90:10 v/v. The particles were kept at −20 °C for 24 h and then stored at −80 °C. After 1 month of cryopreservation, the particles were removed from the −80 °C container and partially thawed at 37 °C. The medium was removed and the particles were washed several times with cell culture medium in order to remove traces of DMSO. The particles were cultured for 7 days (2 gels/well, 200 μL of cell culture medium) and then cell viability assessed using live/dead assay following the procedure described above.

7.3.9. Gel Beads of Collagen Combined with Platelet Lysates as Growth Factors Release Systems

Beads prepared as described above (without encapsulating cells) were also studied as possible reservoirs to release GFs in skin injuries. The tests performed are described below.

7.3.10. *In Vitro* Degradation Assay

Hydrated Coll and Coll+PL gels (5 particles per formulation) were incubated in 1 mL of collagenase solution (50 μg/mL) in tricine buffer pH 7.5 and incubated at 37 °C. Images of the gel particles were recorded at 30, 90, 150, 210, 270 min and 24 hours using an optical stereomicroscope (Olympus SZ-CTV; Tokyo, Japan) connected to a video camera (JCV TK- S350; Tokyo, Japan).

7.3.11. Effect of the Released GFs on hASCs Proliferation

hASCs were seeded (passage 7, 7500 cells/well, 100 μL of cell culture medium) in 48 well plates, and after 24 h the culture medium was replaced by 200 μL of fresh medium without FBS. Two particles of each formulation (hydrated or freeze-dried) were placed into direct contact with the cells. The plates were incubated at 37 °C in a humidified atmosphere with 5 % CO_2 and the medium was replaced every 3 days. The cells were routinely observed using inverted microscopy (x10) (Nikon Eclipse TS100, Nikon

Corporation, Tokyo, Japan) in order to discard any contamination. Experiments were carried out in triplicate. Cell proliferation was evaluated using CCK-8 as described above.

7.3.12. Scratch Wound Assay

The scratch assay was performed as previously described [27, 28]. hASCs were seeded into cell culture dishes with culture inserts (μ-dishes 35 mm, Ibidi, Martinsried, Germany) and allowed to proliferate at 37 °C, 5 % CO_2 and humidified atmosphere until reach confluence. Such inserts were composed by two cell culture reservoirs which were separated by a 500 μm thick wall. The culture insert and the culture medium were then removed, and the cells were rinsed with phosphate buffer saline (PBS) and incubated with 1 mL of culture medium without FBS. 10 particles/mL where placed in direct contact with the cells. After 0, 2, 4, 8, 12, 24 and 48 h of incubation, pictures of the gap were taken using an inverted microscope (Nikon Eclipse TS100, Nikon Corporation, Tokyo, Japan). The percentage of the gap filled by hASCs was determined with respect to the initial cell-free gap, and used as an index of wound healing.

7.3.13. Angiogenic Potential of the Gel Beads: Chick Chorioallantoic Membrane Test

Fertilized eggs purchased from a local farm were placed horizontally in an incubator at 37 °C with 60 % humidity. After 3 days, the eggs were punctured and 2 mL of albumin was removed. A circular window was performed in the eggshell and covered with tape, and the eggs were returned to the incubator. On day 7, two beads of Coll+PL (1 and 2×, in a hydrated state) were placed in contact with the Chorioallantoic Membrame (CAM) of each egg. Two controls were also performed with eggs to which Coll solely (2 hydrated beads) or non-encapsulated PL (10 μL of PL1 and 10 μL of PL2×; equivalent to the same amount of PL encapsulated in the Coll+PL formulations) was directly dispensed on the CAM surface. All tests were carried out in triplicate. Three days after placing the gels in contact with CAM, images were collected to analyze vasculature development. To do that, the membranes were fixed with 10 % formaldehyde for at least 10 min at room temperature. The membranes were cut, disposed carefully on a glass slide, and visualized in a stereomicroscope (Olympus SZ-CTV, Tokyo, Japan). Images were captured using a connected JVC TK-S350 video camera (Tokyo, Japan) and used to quantify the blood vessels growth.

7.3.14. Statistical Analysis

All the experiments were performed with at least three replicates. Results are expressed as mean±standard deviation. Differences between experimental results were analyzed using one-way ANOVA

(Tukey's multiple comparison test), with the limit for statistical significance being defined as $p < 0.05$.

7.4. Results

7.4.1. Preparation and Crosslinking of Gel Beads

Superhydrophobic surface methodology allowed the production of almost spherical gels of Coll and PL with the optional simultaneous encapsulation of cells. Coll concentration was fixed to 2.5 mg/mL, according to previous studies [29]. PL concentration was varied in order to investigate its effect on cell proliferation inside and outside the gels, wound healing capacity and angiogenesis potential. The hardening of the gel beads was achieved by incubation of liquid droplets dispensed onto PS superhydrophobic surfaces at 37 °C during 10–15 min (Figure 7.1 A and B). The presence of hASCs did not affect the self-assembly hardening of collagen.

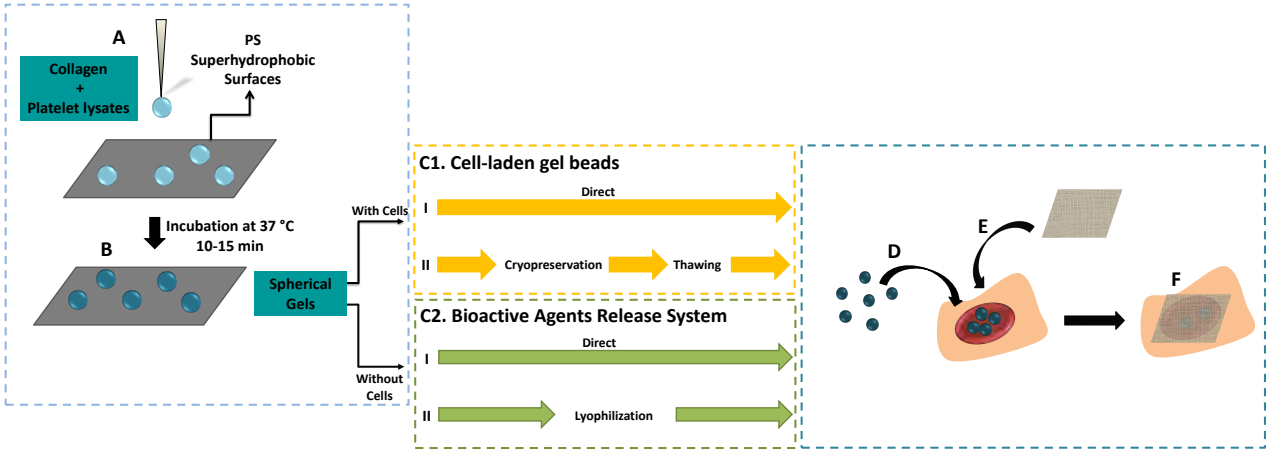

Figure 7.1. Flow chart of the preparation and evaluation of Coll+PL gel particles. (A) A mixture of Coll and PL was dispensed onto PS superhydrophobic surfaces, as droplets of controlled volume. (B) The platform with liquid droplets was incubated at 37 °C for 10–15 minutes and almost spherical gels in a hydrated state were obtained. Two main strategies were hypothesized in this work: (C.1) spherical particles encapsulating hASCs to be directly applied (I) or stored by cryopreservation and later thawing and use (II), (C.2) gels without cells which could act as bioactive agents release systems, also applied immediately after production (hydrated form) (I) or later, after being freeze-dried and stored (II). Each formulation could be then ingraft in a skin lesion (*e.g.* ulcer) (D) which in turn could be coated or not by a dressing (E and F).

The obtained particles (1.5–2.5 mm in diameter) had gel appearance (Figure 7.2 A, D, G and J) with some sticky properties; the particles that contained PL were easier to handle (probably due to the formation of a fibrin mesh) than the ones made of collagen solely. Fibrillar Coll beads (hardened via the self- assembly process) contained large amounts of fluid in their matrix and thus showed soft consistency. Coll+PL spherical-shaped gels without cells had greater consistency and could be easily collected and

freeze-dried for storage (Figure 7.2 B, E, H and K). The dried beads recovered their gel appearance after immersion into PBS pH 7.4 (Figure 7.2 C, F, I and L), but were more fragile when compared with particles immersed into PBS immediately after production. SEM images confirmed the fibrillar structures characteristic of Coll (Figure 7.2 III). Significant differences were visualized between freeze-dried particles and the fixed ones. As expected, the freeze-dried particles were much more porous. In the freeze-dried Coll formulation a dense random mesh of nanofibers (<300 nm) was observed. Formulations with PL showed fibers with greater diameters. Fixed and dehydrated gel beads had a compact fibrillar nanostructure, without pores.

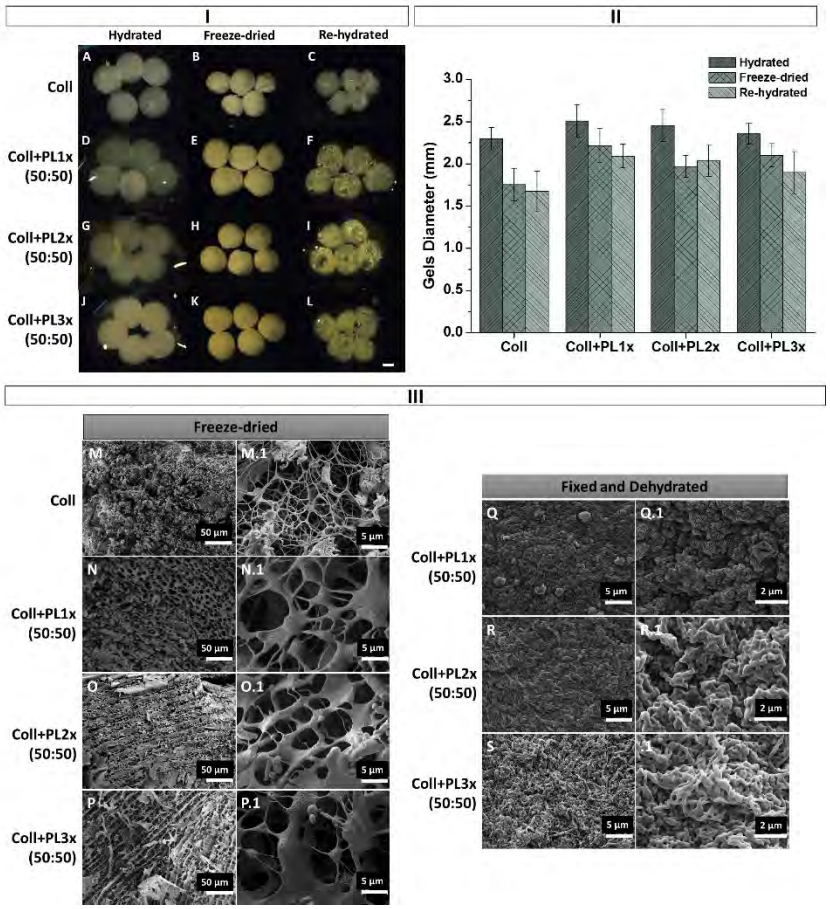

Figure 7.2. I) Stereomicroscope images of Coll and Coll+PL (1, 2, and 3×) spherical gels prepared dispensing 10 µL of precursor solutions onto PS superhydrophobic surfaces and hardening at 37 °C for 10–15 min. Particles without cells were evaluated as hydrated gels obtained immediately after incubation (A, D, G and J), as freeze-dried particles (B, E, H and K) and as re-hydrated gels obtained after hydration of freeze-dried particles through immersion in PBS at pH 7.4 (C, F, I and L). Scale bar represents 1 mm. II) Diameter of hydrated, freeze-dried and re-hydrated gel beads (n=5). III) SEM images of the surface of freeze-dried spherical particles (M, N, O, P) and of the surface of the gels with PL without cells, fixed and dehydrated (Q, R, S). Two images with different magnifications of each gel formulation are shown.

The PL used was characterized in terms of mass of solids, total protein content and amount of VEGF and PDGF-BB before and after freeze-drying (Table 7.2). VEGF is known to be an angiogenic molecule [30], while PDGF promotes cell mitogenesis and migration of fibroblasts, smooth muscle cells and capillary endothelial cells [31]. Recombinant human PDGF-BB also shows beneficial effects when applied topically in skin wounds [32, 33]. Freeze drying of PL does not affect the cytokines role in wound healing [34, 35]. We observed that freeze-drying did not modify the contents in VEGF and PDGF-BB (Table 7.2).

Table 7.2. Characterization of the PL before and after freeze-drying.

PL	Mass of solids	Total protein content	VEGF	PDGF-BB
Before freeze-drying (PL1x)	-	56.61±1.24 mg/mL	1.01±0.15 ng/mL Or 17.9±2.6 pg/mg of total protein	15.8±3.1 ng/mL Or 462.4±54.0 pg/mg of total protein
After freeze-drying (resuspended in PBS)	79.03±5.54 mg/mL	57.62±1.62 mg/mL Or 0.73±0.02 mg/mg of freeze-dried PL	0.96±0.19 ng/mL Or 16.6±3.2 pg/mg of total protein	22.1±2.5 ng/mL Or 383.2±43.0 pg/mg of total protein

PL has a complex composition, and firstly total protein released from the beads was quantified. Beads evaluated were prepared with PL concentrated 2× (Coll+PL2×). Each particle released 0.40–0.45 mg of protein within 8 h (nearly 90 % total protein) which indicated that the release was independent of the degradation of the bead structure (Figure 7.3 A). As expected, both VEGF and PDGF-BB were released in a sustained way for a relatively short time period (Figure 7.3 B).

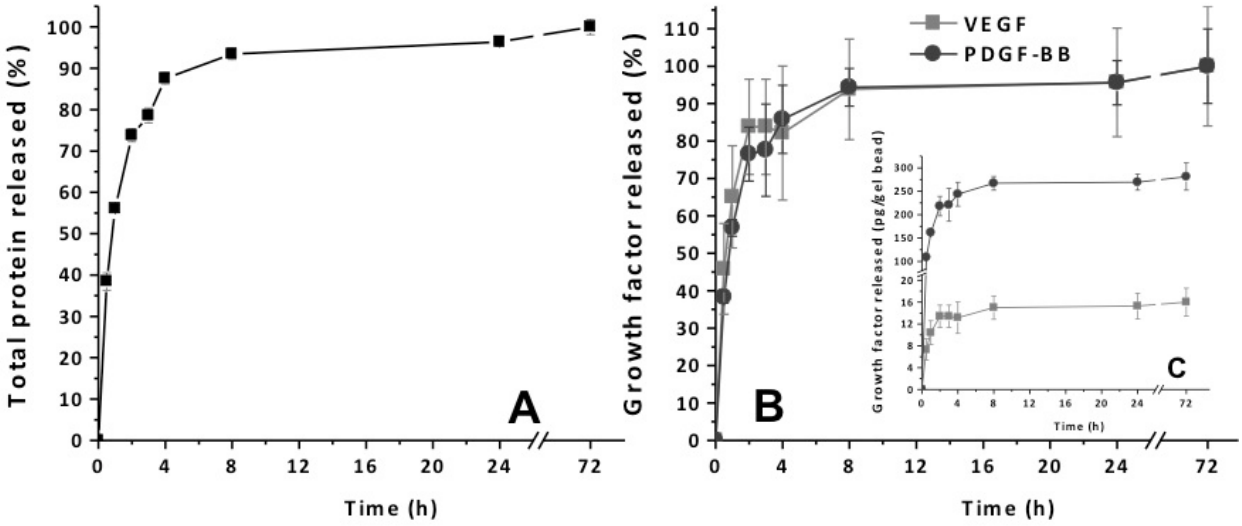

Figure 7.3. Total protein (A), VEGF and PDGF (B, C) released from Coll+PL2× particles over 72 h. Data are shown as percentage (A, B) and as amount released per bead (C).

7.4.2. Gel Beads of Collagen Combined with Platelet Lysates Encapsulating hASCs

As described in the Figure 7.1 (C.1), gel beads with hASCS were obtained in a rapid and simple way after hardening onto the superhydrophobic surfaces under mild temperature. Firstly, the number of cells encapsulated inside the gels over 7 days in culture without FBS was assessed for three different Coll+PL formulations, varying the amount of PL (Figure 7.4). The comparison was performed against cells encapsulated in beads of Coll solely and cultured into a standard medium with FBS (Coll with FBS) and without FBS (Coll without FBS). Cell proliferation pattern was similar for Coll beads cultured in the presence or absence of FBS, but higher number of hASCS was found in the first case. Particles with PL behaved quite differently; for Coll+PL1 and Coll+PL2× the cell number increased from day 1 to day 7. The cells encapsulated in Coll+PL3× beads rapidly proliferated in the first day, but the number of cells was slightly lower than for Coll+PL1 and Coll+PL2× at days 3 and 7.

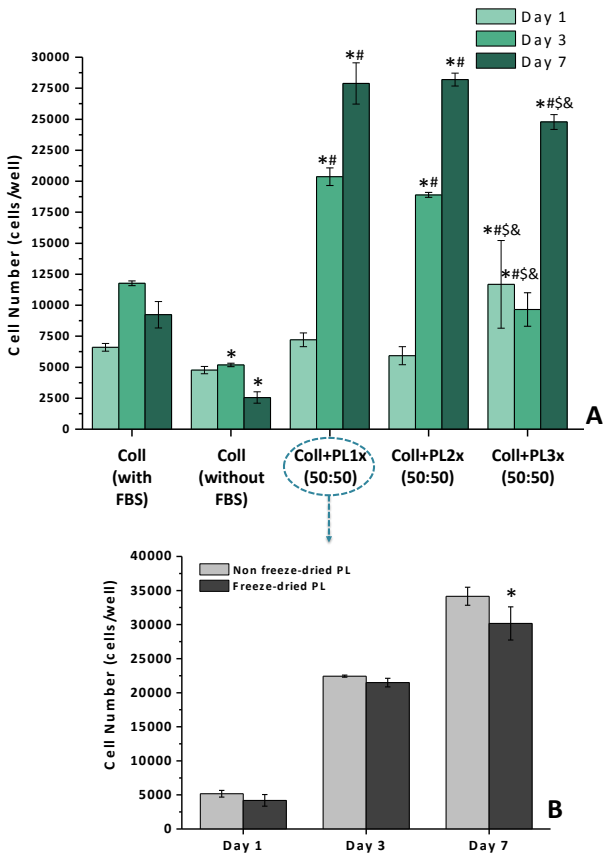

Figure 7.4. A) hASCs growth within Coll and Coll+PL gel beads for 7 days. Gels without PL cultured in medium with and without FBS were used as controls. The effect of PL concentration on hASCs proliferation capability was evaluated.*$p<0.05$, significantly different from Coll with FBS. #$p<0.05$, significantly different from Coll without FBS. $$$p<0.05$, significantly different from Coll+PL1×. &$p<0.05$, significantly different from Coll+PL2×. The comparisons were performed between data collected in the same time point. B) hASCS proliferation within Coll+PL1× prepared using freeze-dried or non freeze-dried (fresh) PL. The

influence of freeze drying process on effect of PL was evaluated. *p < 0.05, significantly different from Coll+PL1× when non freeze-dried PL was used, at day 7.

In order to verify if freeze-drying may compromise the positive effect of PL on hASCs proliferation, a comparative study of the performance of Coll+PL1× formulations prepared using either liquid PL or freeze dried PL resuspended in PBS pH 7.4 was carried out. The results (Figure 7.4 B) did not show statistically significant differences in the first 3 days, and only a minor decrease in proliferation at day 7 was observed for freeze-dried PL.

Fluorescence images of the live/dead assay confirmed the good cytocompatibility of the formulations studied. After 24 h, almost all encapsulated hASCs were alive, proving the mild conditions of the superhydrophobic surface methodology for cell encapsulation. Dead hASCs were not found in Coll gels cultured in medium with FBS after 3 (Figure 7.5 A.D3) and 7 (Figure 7.5 A.D7) days, but when the same beads were incubated in medium without FBS an important percentage of cells died (Figure 7.5 B.D3 and B.D7). Coll+PL beads were able to supply the needed GFs to the cells and most cells were alive after 7 days of incubation. PL concentration (1, 2 and 3×) seemed not have significant effect on cell viability (Figure 7.5 C, D and E).

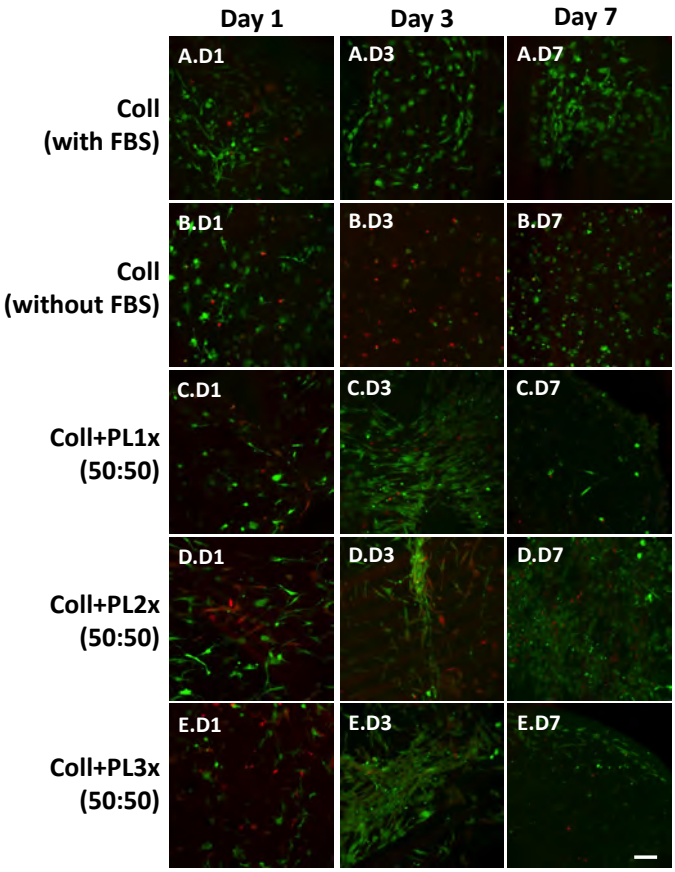

Figure 7.5. Live/dead fluorescent assay at 1, 3 and 7 days of culture. Coll (cultured in medium with or without FBS, controls)

and Coll+PL particles with three different PL concentrations were tested. Living cells were stained green (calcein-AM) and dead cells were stained red (propidium iodide). Scale bar represents 100 μm.

Although collagen has RGD domains that induce the cell spreading, after 24 h the actin cytoskeleton reorganization was much more visible in Coll+PL beads (Figure 7.6 C.D1, D.D1 and E.D1 versus A.D1 and B.D1). hASCs were protected by a dense meshwork of collagen fibrils and PL that allowed cell-matrix interactions and cell migration. Phalloidin/DAPI staining revealed a rapid hASCs migration from the Coll+PL gels (visible in Figure 7.6 C.D1), facilitating cell-cell direct contact among hASCs from different particles.

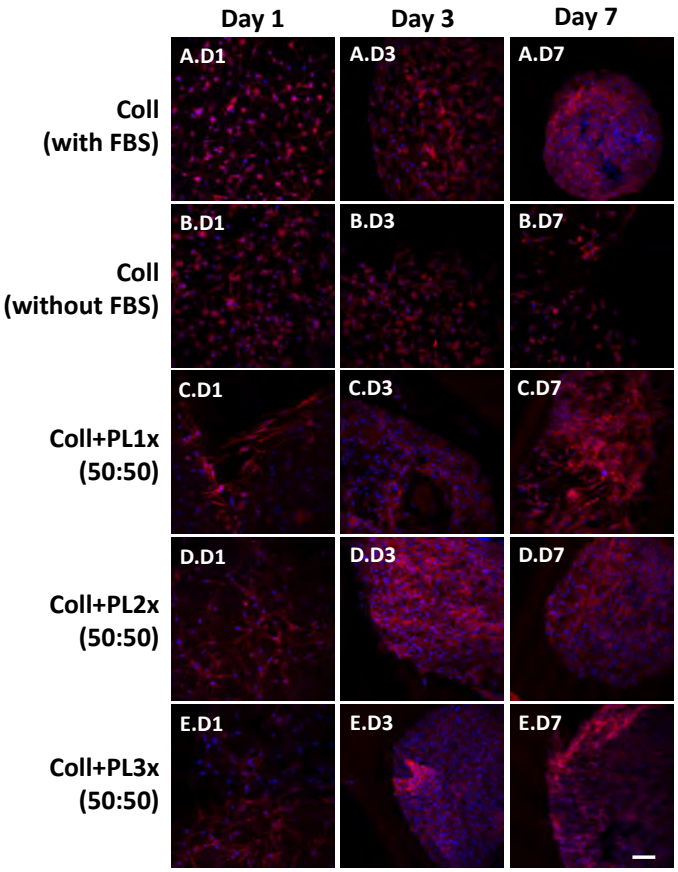

Figure 7.6. Phalloidin/DAPI fluorescence assay at 1, 3 and 7 days of culture. Coll (cultured in medium with or without FBS, controls) and Coll+PL particles with three different PL concentrations were tested. Cells F-actin filaments in cytoplasm were stained red by Phalloidin, and nuclei were stained in blue by DAPI. Scale bar represents 100 μm.

The images of optical microscopy (Figure 7.7) also evidenced the ability of hASCs to migrate out the particles, grow up at the bottom of the well plate and also act as bridges between gel beads. The release of PL components, such as fibrinogen which created a fibrin mesh, led to the formation of an organized membrane in which the spherical gels were interconnected by hASCs (Figure 7.7 V). The schematic representation of the successive events occurred in Coll+PL formulations is depicted in Figure 7.7 I-IV.

Interestingly, very few cells migrated from Coll particles cultured with and without FBS even after 3 and 7 days in culture (Figure 7.7 A.D3, A.D7, B.D3, and B.D7). In agreement with previous works [4, 29], the Coll gels that encapsulated hASCs shrank over time, as revealed by the reduction of the volume of the particles (Figure 7.7 A.D3 and A.D7). Such shrinking was attenuated in the presence of PL.

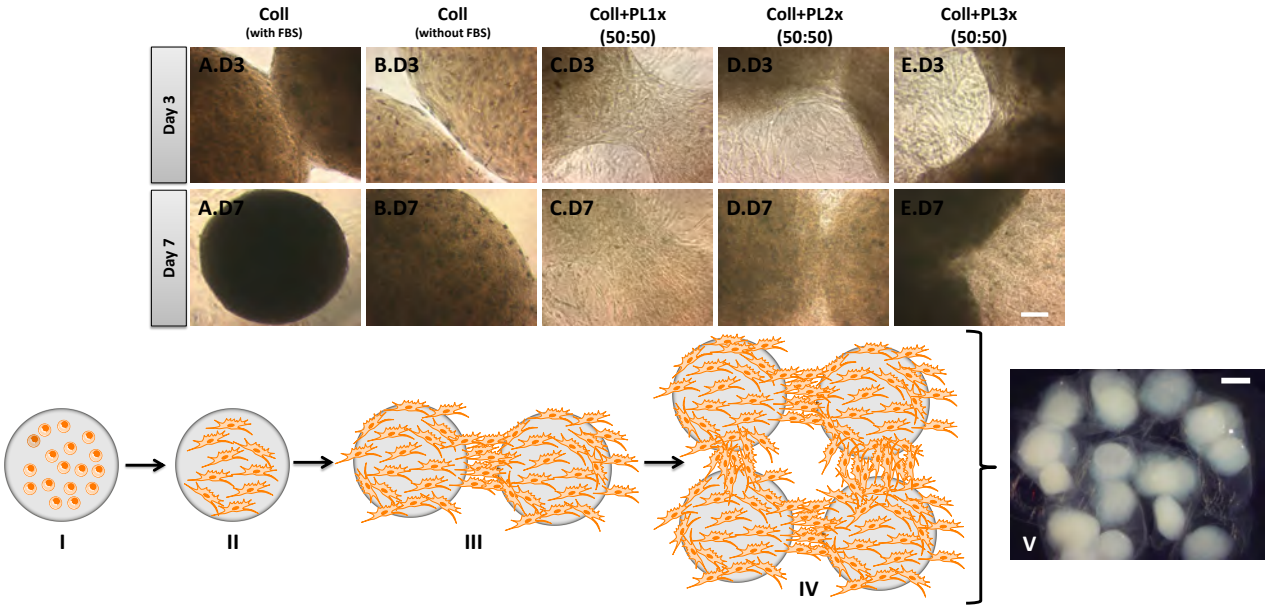

Figure 7.7. Optical microscope images of gel beads encapsulating hASCs and cultured for 3 and 7 days and the respective scheme representing the state of the cells when encapsulated in Coll+PL gels. Immediately after gels hardening, cells exhibited a round shape typical of non-adhered cells (I), over time, the cells started to extend their cytoplasmatic elongations (II), proliferated and established connections between adjacent particles (III). Finally, a membrane composed by gels unified by hASCs and gelified released PL was obtained (IV). Image V is the stereomicroscope image of a membrane composed by Coll+PL2× encapsulating hASCs and cultured for 7 days in a 12-well cell culture plate. Scale bar represents 1 mm. Coll formulations did not exhibit a significant hASCs proliferation neither cell established connections between adjacent particles after 3 (A.D3 and B.D3) and 7 (A.D7 and B.D7) days. Only in the formulations where PL was present the bond of adjacent particles was observed after 3 (C.D3, D.D3 and E.D3) and 7 days (C.D7, D.D7 and E.D7). Scale bar represents 100 μm.

Beads containing hASCs were cryopreserved during 1 month and evaluated again as described above. Three days after thawing part of the cells remained viable (Figure 7.8). However, their capability to elongate inside Coll and Coll+PL gel beads was affected as well as their migration and proliferation. Even after 7 days, no cell migration or proliferation outside the gels was visible in the optical microscope observations. This means that although the cells withstood the freeze-thawing cycle, their normal performance was seriously affected.

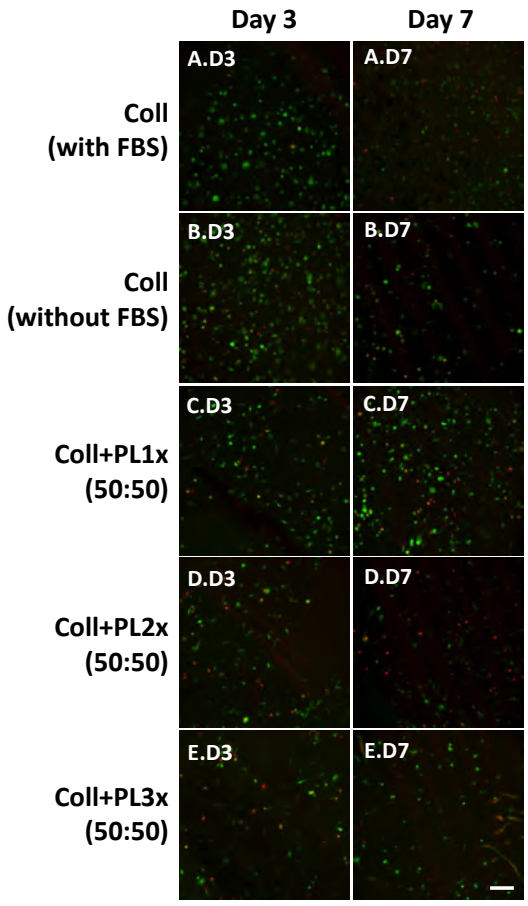

Figure 7.8. Live/dead assay of the gels in culture for 3 and 7 days after being cryopreserved for 1 month. Sale bar represents 100 μm.

7.4.3. Gel Beads of Collagen Combined with Platelet Lysates as Growth Factors Release Systems

In a second step, Coll+PL gels without encapsulating cells were evaluated (as freshly prepared and after freeze-drying) as GFs reservoirs able to promote cell proliferation and wound healing (Figure 7.1 C.2). Stability of the beads was tested in media of different composition. In tricine buffer pH 7.5 without collagenase no significant degradation was observed after 24 h. In PBS pH 7.4, without enzymes, Coll and Coll+PL beads maintained their integrity for more than 1 month (data not shown). Oppositely, in the presence of collagenase (50 μg/mL) beads degraded faster (Figure 7.9). Coll beads exhibited significant signals of erosion in collagenase medium after 30 min, and only small residues remained in the wells after 90 min. Incorporation of PL increased resistance of the gel beads to collagenase degradation. Even after 150 min some frag- ments of Coll+PL1 and Coll+PL2× beads were still visible.

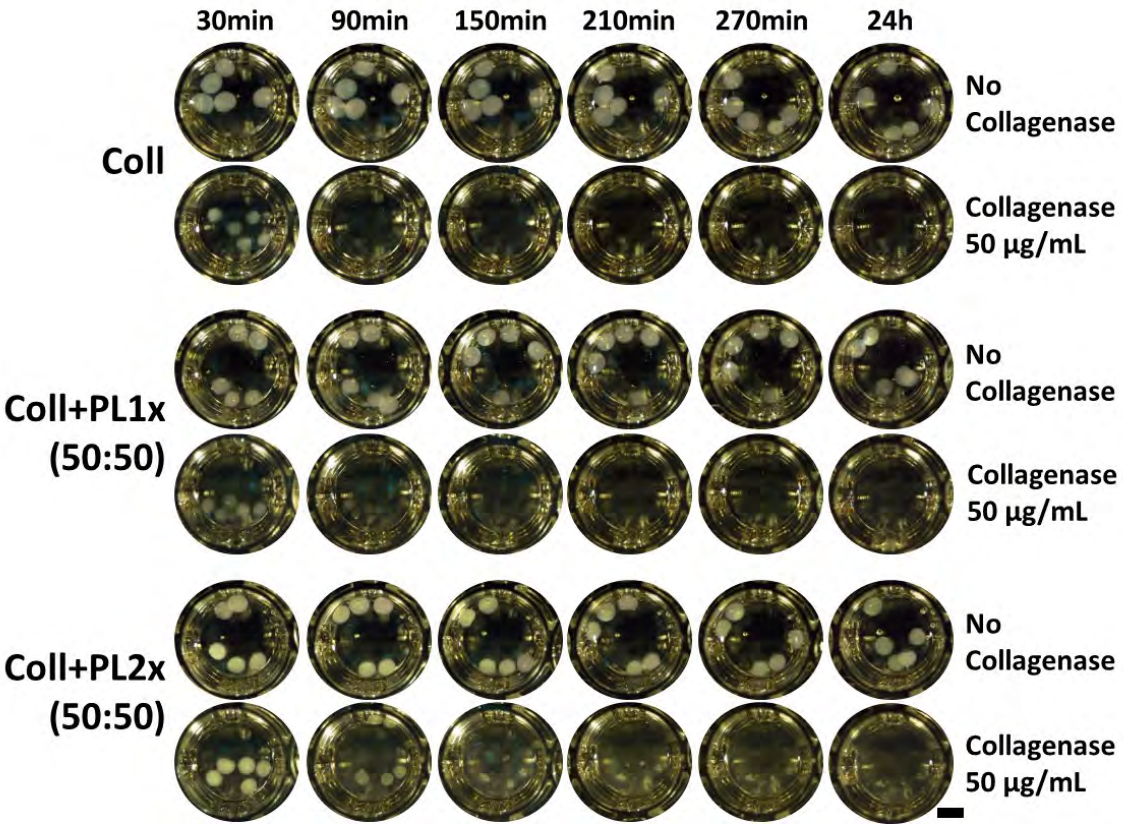

Figure 7.9. Stereomicroscopeimages monitoring the enzymatic degradation of Coll and Coll+PL gel beads over time. High collagenase concentration (50 µg/mL, in tricine buffer pH 7.5) was used in order to mimic exudates of untreatable skin ulcers. Particles immersed in tricine buffer pH 7.5 were used as controls. Scale bar represents 3 mm.

The effect of Coll+PL beads on hASCs proliferation was also evaluated using both hydrated and re-hydrated freeze- dried particles. hASCs in contact with Coll solely (hydrated or re-hydrated) particles and cultured in cell culture medium without FBS did not proliferate over the 5 days of the study. PL was shown again essential for cell proliferation (Figure 7.10 A). hASCs proliferated well using either hydrated or re-hydrated Coll+PL1× particles as the only source of GFs, as much as those incubated with culture medium to which non-capsulated PL was directly added (control tests). Comparing hydrated and re-hydrated beads, freeze-dried Coll+PL2 and Coll+PL3× beads led to lower number of cells at day 3, but the differences attenuated at day 7. No significant changes in cell proliferation were observed when particles prepared with fresh PL were replaced with the ones prepared with freeze- dried PL (Fig. 7.10 B), which means that using fresh (liquid) or freeze-dried (powder) PL in the preparation of the Coll+PL1× particles did not alter the bioactivity of the growth factors.

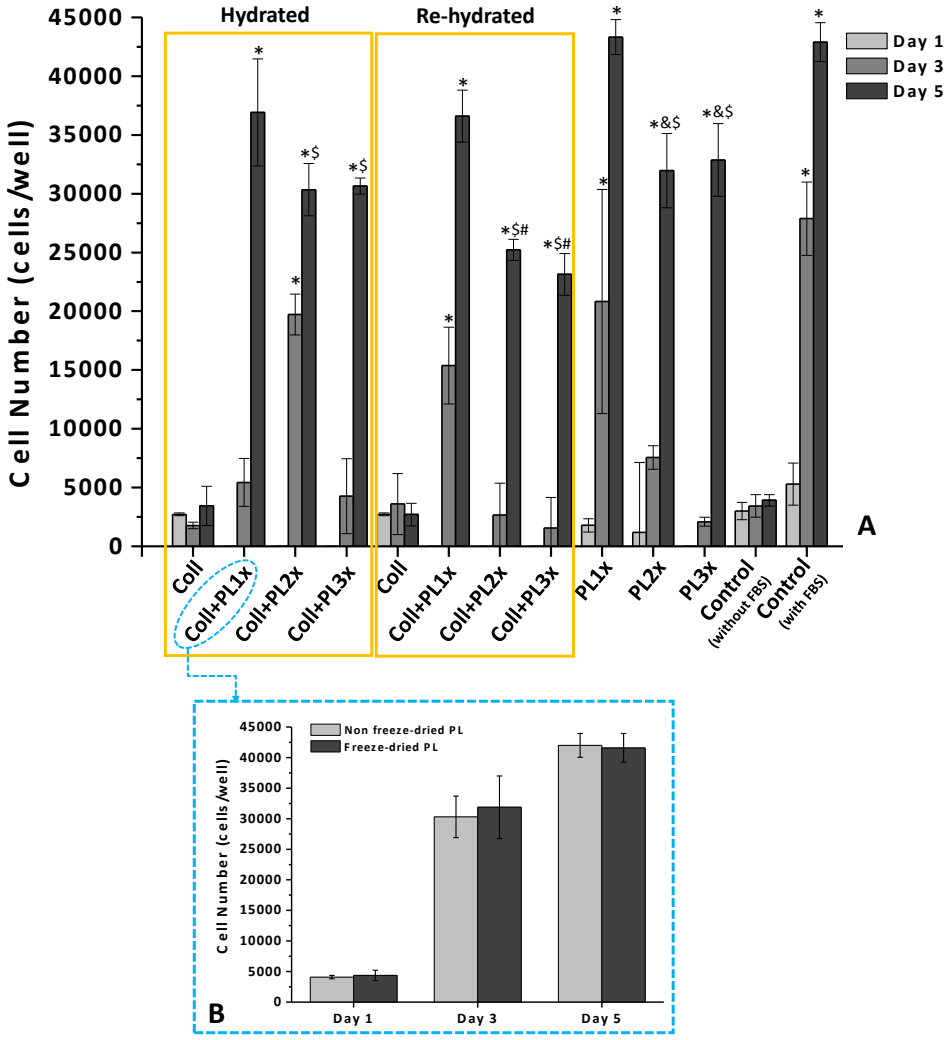

Figure 7.10. A) Effect of released PL from hydrated and re-hydrated particles on hASCs proliferation. hASCs cultured in the presence of PL without being encapsulated (PL1, PL2 and PL3×) and in medium with or without FBS were used as controls. *p<0.05, significantly different from Coll hydrated, re-hydrated and control (without FBS) at day 1, 3 and 5. #p<0.05, significantly different from Coll+PL1× re-hydrated (day 5). &p<0.05, significantly different from PL1× (day 5). $p<0.05, significantly different from control with FBS (day 5). B) Effect of PL released from Coll+PL1× hydrated particles prepared with freeze-dried or non freeze- dried (fresh) PL on hASCs proliferation.

Scratch wound assay results are shown in Figure 7.11. After 48 h, hASCs cultured in medium without FBS and in direct contact with Coll gels were not able to migrate or proliferate to fill the gap between both cell groups. Beads with PL significantly accelerated the filling of the scratch and after 12 h, the gap was completely filled by cells. In addition, interaction of the cells with Coll+PL beads was observed. A number of hASCs were capable to migrate from the bottom of the cell culture plate and adhere onto the surface of the beads, as shown in detail in Figure 7.12. The cells formed long filopodia trying to connect adjacent

particles, also helped by a fibrin mesh formed outside the gels. This behavior was not observed in the absence of PL (Figure 7.12 A and E).

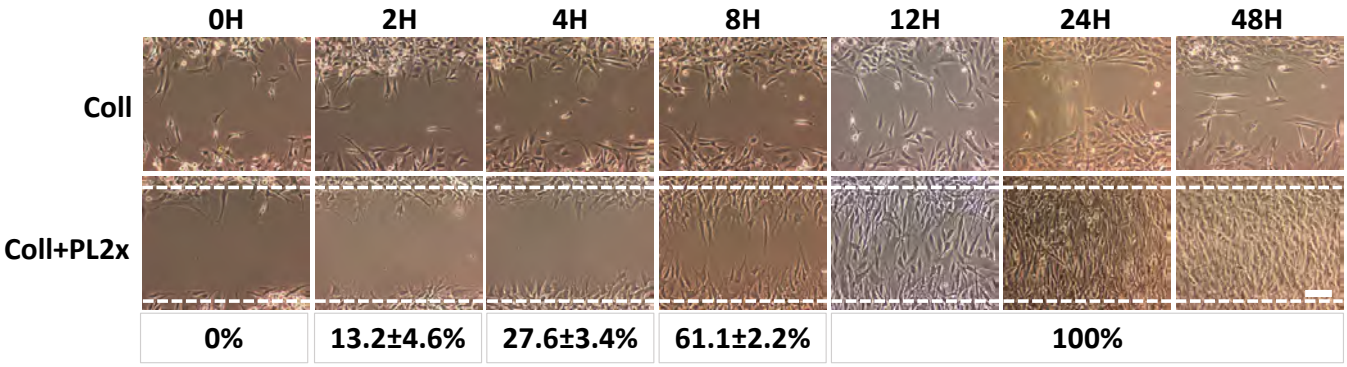

Figure 7.11. Scratch test: hASCs were cultured physically separated by a distance of 500 µm. The presence of PL significantly accelerated cell migration and the filling of the scratch area. Scale bar represents 100 µm.

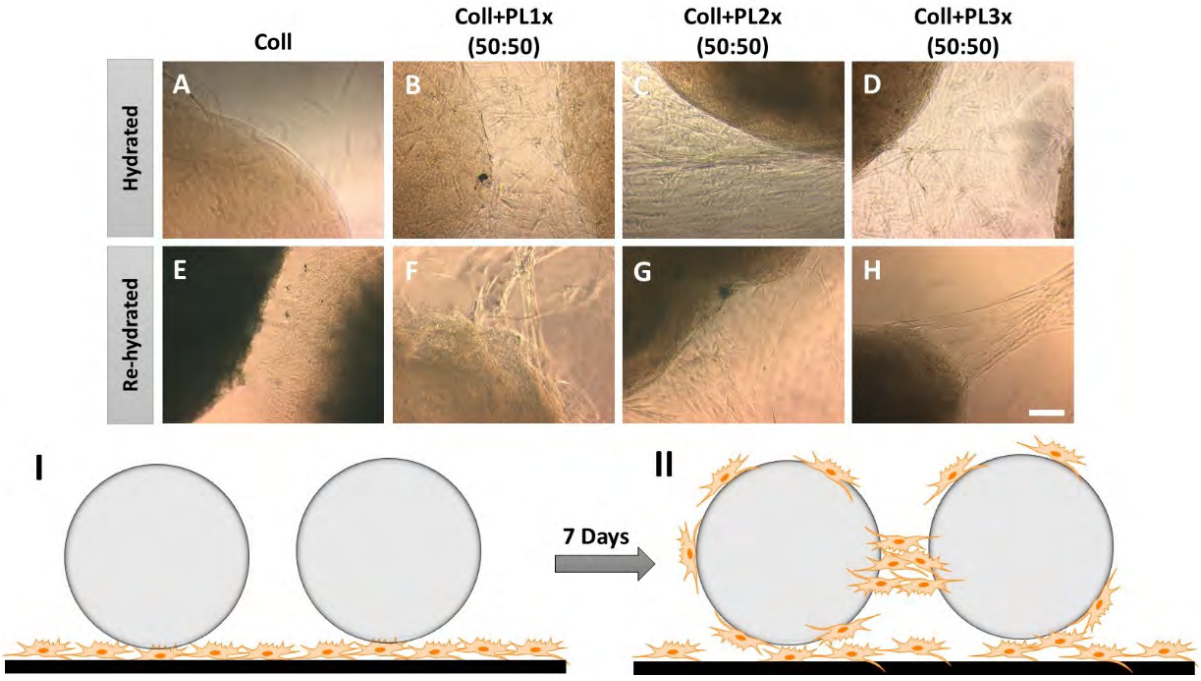

Figure 7.12. Interaction of hydrated and re-hydrated gels with a monolayer of hASCs (cells adhered onto the bottom of cell culture plates). The particles were cultured in direct contact with a cell monolayer (I). After some days in culture, hASCs migrate to the particles surface (II). In the case of Coll gels (A, E), cells were not found on the gels surface, neither extending elongations to connect adjacent gels. Oppositely, hASCs adhered to the surface of Coll+PL gels (B-D and F-H) and tried to establish connections between the gel particles after 7 days in culture. Scale bar represents 100 µm.

To gain a further insight into the benefits of encapsulating PL, the angiogenic potential of the beads was studied using the chick CAM model. The effect of Coll and Coll+PL spherical-shaped gels on direct blood

vessel growth was quantified by counting the total number of blood vessels that grew radially from the particles. No direct blood vessels growth was observed towards Coll gels. Oppositely, vascularization was clearly observed for Coll+PL1 and Coll+PL2× gel beads, with *ca.* 16 and 33 vessels respectively protruding from the area where the beads were implanted (Figure 7.13). Moreover, 3 days post-implantation Coll+PL gels were integrated in the CAM of the chicks, while Coll gels did not exhibit any signal of interaction. Similar experiments were carried out using non- encapsulating PL1 and PL2× fluid samples (positive controls), which coagulated immediately after being dispensed on the top of CAM. As occurred for Coll+PL gels, coagulated PL1 and PL2× were integrated by the membrane. No significant differences were observed between encapsulated and non-encapsulated PL, which confirm the release of active GFs from the beads.

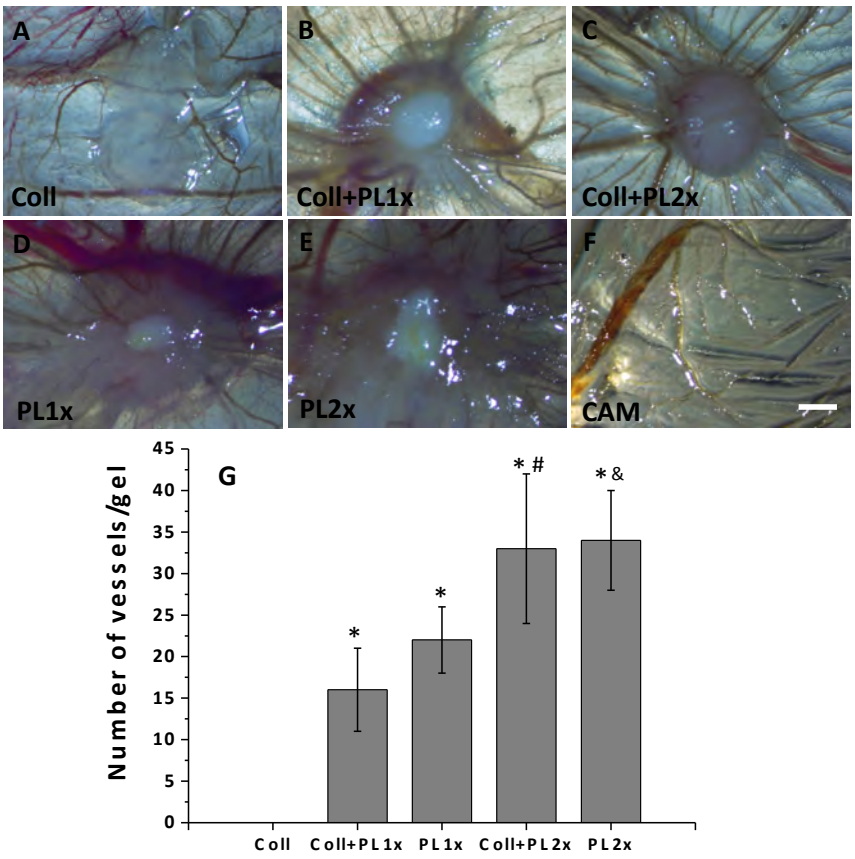

Figure 7.13. Representative stereomicroscope images of the excised chick CAMs after implantation of 2 particles of Coll (A), Coll+PL1x (B), Coll+PL2x (C), 10 µL of PL1x (D) and 10 µL of PL2× (E). (F) is a representative image of a normal CAM. Direct blood vessels growth was observed towards the Coll+PL formulations 3 days post-implantation, but no direct blood vessels growth was observed towards Coll solely. The Coll+PL beads were integrated in the chick CAM. Scale bar represents 1 mm. (G) Number of converging vessels at 3 days post- implantation. *$p<0.05$, significantly different from the Coll. #$p<0.05$, significantly different from Coll+PL1×. &$p<0.05$, significantly different from PL1×.

7.5. Discussion

7.5.1. Preparation and Crosslinking of Gel Beads

To the best of our knowledge, handleable spheres combining both fibrillar type I Coll and PL for cell encapsulation or bioactive agents release have not been previously reported. The sol–gel transition of Coll is a multi-hierarchical self-assembly process starting from a helical structure which winds around other and forms a super helical trimer (Coll triple helix). Then, the triple helix continues to pack forming nano fibrous structures (Coll fibrils), which in turn follow a self-assembly process forming an interconnected random hydrogel network [36]. Overall it is an entropy-driven process favored by the displacement of water from Coll molecules [37, 38]. Hydrophobic interactions between non-polar groups, hydrogen bonding be- tween polar residues and salt bridges (electrostatic interactions) are the main phenomena that cause the gelification of Coll type I under appropriate conditions [39]. The acidic Coll extraction process (applied to obtain the Coll used in this work) does not cleave the Coll terminal telopeptides, which are responsible for crosslinks formation between triple helices and then improvement of Coll stabilization [40]. Temperature, pH, collagen con- centration and ionic strength are the main factors that influence the formation of Coll fibers. Native type Coll fibrils are formed at pH range of 5.0–8.5, ionic strength between 0.1 and 0.8 and temperatures varying from 15 to 37 °C [39]. In our case these variables were fixed at 37 °C, pH 7.4 and collagen concentration of 2.5 mg/mL. The in vitro formed fibrils are expected to have similar morphologies to those found *in vivo* [40]. Compared to commercially available skin substitutes that use collagen solely at 0.66 mg/mL, an increase in Coll concentration may improve the mechanical properties, cell viability and biological stability and also increase the resistance to proteinases degradation [4].

Superhydrophobic surfaces methodology allowed the encapsulation of high amounts of bioactive molecules (PL) or mammalian cells without appreciable losses, because the particles hardened at the solid-air interface, in the absence of a surrounding liquid medium to which molecules/cells could escape via diffusion or migration (Figure 7.1) [21, 24]. Thus, the content can be known a priori and is only limited by the capacity of collagen to crosslink in the presence of the bioactive agents. In this work, we observed that the use of PL concentrated more than 3× did not allow collagen crosslinking.

Platelets are generally activated by calcium, thrombin, collagen or freeze-thawing cycles, resulting in a cocktail of proteins, glycoproteins and other platelets cytoskeletal components; *e.g.* GFs, albumin, immunoglobulins, fibrinogen and transferrin. Activation of the platelets triggers clot formation *in vivo*. During this process, the fibrinogen existent in PL is transformed in a fibrin mesh causing the gelation of PL. However, this mechanism is usually not sufficient to obtain handleable spherical gels. For this reason,

Coll was used as a biomimetic support. Coll provides a stronger structure and also plays a role in stabilization of the clots against excessive retraction [41]. In the present work, PL was obtained via the activation of the platelets through freeze-thaw cycles, which was demonstrated to be more efficient than activation by thrombin and/or $CaCl_2$ [13, 19]. This explains that the concentrations of both VEGF and PDGF-BB (Table 7.2) were higher than those reported in literature [35, 42].

Although superhydrophobic surfaces methodology allow to obtain particles sizes from micro [43, 44] to macro-scale [21, 24–26], in this work particles of 1.5–2.5 mm (10 μL) (Figure 7.2 II) were produced in order to facilitate their manage- ability during both the *in vitro* assays and also for *in vivo* applications (Figure 7.1 D). In skin ulcers such particle size may be easily applied as freshly prepared gel particles or as a dry powder for direct delivery of GFs or cells in the damaged region (Figure 7.1 C.1 and C.2 strategies). After hardening, the gel beads can be used as wet, swollen particles or can be dried applying conventional methods for a more convenient storage. The dried beads were shown to swell again when enter into contact with aqueous medium (Figure 7.2).

Sustained release of GFs from gel beads for several hours (Figure 7.3) is advantageous in comparison with direct PL application, which leads to a rapid clearance of GFs from the application site. Coll+PL2× particles could be used as ingraft release systems that remain in the application site and release GFs in a controlled way.

7.5.2. Gel Beads of Collagen Combined with Platelet Lysates Encapsulating hASCs

Direct injection of cells into skin ulcers may lead to loss of cells due to the blood-flow [29, 45] and dead of remaining ones due to the absence of a structured matrix where cells could adhere and proliferate, caused by the activity of the proteinases present in wound exudates. Injectable polymeric systems, which harden after being applied in the injured site, have been reported as cell supports conferring protection; however in most of the cases the polymer dispersions do not have sufficient viscosity and stiffness to retain the cells [46]. Moreover, the shear stress and turbulences generated during the injection may cause cell viability loss [29]. Having into account all these issues, the encapsulation of cells inside spherical particles may offer protection against aggressive environment while provide support for adhesion and proliferation. So far, alginate-based materials with immobilized cells have been explored for cell-based therapies applications [24], but alginate does not have anchorage points for adherent cells, requiring the incorporation of certain proteins or even the modification of the polymer backbone with RGD domains [47]. As a natural extracellular matrix, Coll provides anchorage points and acts as an excellent support for cell encapsulation due to the enhancement of adhesion and proliferation [29]. Although Coll is also an

interesting skin substitute for regeneration of dermis [48], its poor mechanical properties, weak shape stability and incompatibility with conventional encapsulation techniques [49] have so far prevented their use in cell- based strategies. In this work, hardening of Coll was carried out according to a previously developed method [29] with some improvements: cells were suspended in previously neutralized collagen solution and then incubated at 37 °C. The main innovations refer to the incorporation of PL as an additional source of GFs and the use of non-adhesive superhydrophobic surfaces to obtain almost perfect spherical gel particles.

Our first strategy focused on hASCs encapsulation in Coll+PL gel beads to act as GFs and cell suppliers for skin ulcers treatment (Figure 7.1 C.1). Several studies have previously shown that hASCs exert beneficial effects on skin ulcer treatments [11, 50]. Adipose tissue is abundant in human body and can be easily accessed using low-invasive procedures. hASCs have extensive proliferation capacity and secret soluble factors that promote human dermal fibroblast proliferation and migration even when both cell types are physically separated, being such effect dose-dependent [51]. Mixtures of hACS and collagen have previously demonstrated synergic effects on wound healing rate [51]. As described in the Figure 7.1 (C.1) we hypothesized that gel beads with hASCS could be obtained in a fast way and applied immediately in the injured site or cryopreserved and stored to be used later or for subsequent applications to the patient. In a very simple way, particles hardened onto the superhydrophobic surfaces can be collected and applied directly in the injury site or previously adhered into a dressing which could be used to cover the ulcer. In this context, the application of spherical particles instead of continuous membranes could be advantageous since the interstitial spaces between the spheres may act as pores that allow O_2 access, which also contributes to the healing process [52].

Encapsulated hASCs proliferated more in Coll+PL beads than in Coll solely gels (Figure 7.4). The presence of PL was advantageous in all cases and the cells number was significantly higher after 3 and 7 days incubation, disregarding the used PL had been freshly prepared or stored as a freeze-dried product before incorporation to the beads. Nevertheless, proliferation in the presence of PL1 or PL2× was more intense than with PL3×, which is in agreement with previous studies that have shown that very high concentrations of PL exert an inhibitory effect on proliferation and viability of several cell types [34, 53, 54]. A healing retarded effect was observed in keratinocyte-based tissues when PL concentration higher than 2.5 times the physiological levels was used [55].

Importantly, Coll+PL beads were able to supply the needed GFs to the cells when incubated in medium without any other source of growth supplements, and most cells were alive after 7 days of incubation. Moreover, the bead network of collagen and PL created a physiologically relevant environment, which

allowed cell-matrix interactions, cell migration and formation of cell layers interconnecting the cell-laden beads (as observed in Figures 7.6 and 7.7). These phenomena were not observed for Coll solely beads, demonstrating the role of PL in cell proliferation and tissue formation. Additionally, cell-laden Coll+PL beads did not shrink over time, which could be advantageous in the process of skin regeneration as a way to minimize the contraction of the new tissue. Studies performed in adult pig skin wounds demonstrated a direct correlation between tissue regeneration and delay of wound contraction [56, 57]. Therefore, Coll+PL beads provide an environment that may benefit integration in the host at cellular and molecular levels.

Cryopreservation of cell-laden Coll+PL beads negatively affected the ability of hASCs to migrate and proliferate. Probably, the diffusion of the cryoprotectant into the gel particles was not completely achieved, and the cells were not efficiently protected. In addition, after thawing traces of DMSO may remain inside the Coll mesh creating a non-pleasant environment for the encapsulated cells.

7.5.3. Gel Beads of Collagen Combined with Platelet Lysates as Growth Factors Release Systems

The second strategy focused on the potential of the Coll+PL gels to act as reservoirs for sustained release of GFs able to promote efficient skin wound healing without encapsulating cells (Figure 7.1 C.2). Gel particles were tested both as freshly prepared and after freeze-drying. In a medium that mimicked the proteinase-rich environment in non-treatable skin ulcers (50 μg collagenase/mL) [58], Coll+PL beads maintained their integrity for more time than Coll solely beads (Figure 7.9). This finding can be explained by the presence of a fibrin mesh reinforced Coll structure, which in turn made the particles more biologically stable. Regarding hASCs proliferation, Coll+PL beads were shown able to provide the growth supplements required for proliferation. In fact, Coll+PL beads were as efficient as free PL as substitute of cell culture supplements (*e.g.* FBS) [59, 60]. Compared to freshly prepared beads, the slower cell proliferation observed when rehydrated freeze-dried beads were used (Figure 7.10) can be attributed to a certain slowdown of GFs release, as the drying procedure may favor hydrogen bonding of bioactive substances and collagen. In addition, the cells proliferated more in contact with Coll+PL1× than in the presence of PL2 and PL3×, which can be correlated to References supra-physiological GFs concentrations for the used cell-number. The beneficial effect of PL was confirmed in a scratch wound healing assay (Figure 7.11). The advantageous performance of Coll+PL beads indicates that the early controlled release of GFs (Figure 7.3 B) plays a very important role in cell migration for wound healing. In addition, cells favorably interacted with Coll+PL beads acting as bridges among adjacent particles (Figure 7.12). Overall, these findings suggest that acellular Coll+PL beads could also be easily integrated in the tissues by local

cells. Finally, one of the major problems of the skin substitutes is the failure in the vascularization process [61]. While Coll beads did not induce angiogenesis, Coll+PL1 and Coll+PL2× gel beads notably promoted vascularization (Figure 7.13). These results corroborate the crucial role of PL in bio integration and vascularization features of the Coll+PL beads.

7.6. Conclusions

Superhydrophobic surface methodology allows the preparation of handleable spherical-shaped Coll+PL gels in a fast way and under mild conditions that enable cell encapsulation. The developed gel beads act as scaffold suitable for cell adhesion and proliferation. hASCs can migrate from the particles and promote the connection between adjacent particles forming a membrane which can be easily handled to place in the target site. However, more efficient procedures to cryopreserve 3D cell-laden systems are required. Thus, so far the acellular approach seems to be more reliable. As an in situ release system, Coll+PL beads can act as depots of GFs that induce cell migration, proliferation and angiogenesis. The freeze-drying process of Coll+PL beads did not affect the bioactivity of the encapsulated PL. The developed Coll+PL beads open the possibility of using an efficient autologous product, instead of expensive recombinant GFs, in an easy-to-handle way.

7.7. Acknowledgments

A.C. Lima acknowledges to the Portuguese Foundation for Science and Technology (FCT) for the PhD grant SFRH/BD/71395/2010. Work supported by the European Union's Seventh Framework Programme (FP7/2007-2013) under grant agreement n°REGPOT-CT2012-316331-POLARIS, FEDER through the Competitive Factors Operation Program–COMPETE, Portugal national funds through FCT (PTDC/CTM-BIO/1814/2012), Operational Human Potential Program (POPH) developed under the scope of the National Strategic Reference Framework (QREN) from the European Social Fund (FSE), and Spain MICINN (SAF2011- 22771). The authors thank Ibidi for culture inserts samples, Luis Diaz-Gomez and Patricia Días Rodríguez for the help with PL preparation and CAM assay, and Instituto de Ortopedia y Banco de Tejidos Musculoesqueléticos (Universidad de Santiago de Compostela, Spain) for the help with cell cultures.

7.8. References

[1] Sen C. K., Gordillo G. M., Roy S., Kirsner R., Lambert L., Hunt T. K., Gottrup F., Gurtner G. C. and Longaker M.T., Human skin wounds: a major and snowballing threat to public health and economy, Wound Repair and Regeneration 2010, 17: 763–771.

[2] Nathan C. F., Secretory products of macrophages, Journal of Clinical Investigation 1987, 79: 319–326.

[3] Tonnesen M. G., Feng X. and Clark R. A. F., Angiogenesis in wound healing, Journal of Investigative Dermatology Symposium Proceedings 2000, 5: 40–46.

[4] Helary C., Zarka M. and Giraud-Guille M. M., Fibroblasts within concentrated collagen hydrogels favour chronic skin wound healing, Journal of Tissue Engineering and Regenerative Medicine 2012, 6: 225–237.

[5] Bir S. C., Esaki J., Marui A., Sakaguchi H., Kevil C. G., Ikeda T., Komeda M., Tabata Y. and Sakata R., Therapeutic treatment with sustained-release platelet-rich plasma restores blood perfusion by augmenting ischemia-induced angiogenesis and arteriogenesis in diabetic mice, Journal of Vascular Research 2011, 48: 195–205.

[6] Brem H., Balledux J., Bloom T., Kerstein M. D. and Hollier L., Healing of diabetic foot ulcers and pressure ulcers with human skin equivalent, Archives of Surgery 2000, 135: 627–634.

[7] Murray M. M., Spindler K. P., Abreu E., Muller J. A., Nedder A., Kelly M., Frino J., Zurakowski D., Valenza M., Snyder B. D. and Connolly S. A., Collagen-platelet rich plasma hydrogel enhances primary repair of the porcine anterior cruciate ligament, Journal of Orthopaedic Research 2007, 25: 81– 91.

[8] Hokugo A., Ozeki M., Kawakami O., Sugimoto K., Mushimoto K., Morita S. and Tabata Y., Augmented bone regeneration activity of platelet-rich plasma by biodegradable gelatin hydrogel, Tissue Engineering 2005, 11: 1224–1233.

[9] Moreira Teixeira L. S., Leijten J. C. H., Wennink J. W. H., Chatterjea A. G., Feijen J., van Blitterswijk C. A., Dijkstra P. J. and Karperien M., The effect of platelet lysate supplementation of a dextran- based hydrogel on cartilage formation, Biomaterials 2012, 33: 3651–3661.

[10] Bhang S. H., Park J., Yang H. S., Shin J., and Kim B. S., Platelet-rich plasma enhances the dermal regeneration efficacy of human adipose-derived stromal cells administered to skin wounds, Cell Transplantation 2013, 22: 437–445.

[11] Anitua E., Muruzabal F., Alcalde I., Merayo-Lloves J. and Orive G., Plasma rich in growth factors (PRGF-Endoret) stimulates corneal wound healing and reduces haze formation after PRK surgery, Experimental Eye Research 2013, 115: 153–61.

[12] Albanese A., Licata M. E. Polizzi B. and Campisi G., Platelet-rich plasma (PRP) in dental and oral surgery: from the wound healing to bone regeneration, Immunity & Ageing 2013, 10: 23–33.

[13] Sell S. A., Ericksen J. J., Reis T. W., Droste L. R., Bhuiyan M. B. A. and Gater D. R., A case report

on the use of sustained release platelet-rich plasma for the treatment of chronic pressure ulcers, Journal of Spinal Cord Medicine 2011, 34: 122–127.

[14] Hildner F., Albrecht C., Gabriel C., Redl H. and van Griensven M., State of the art and future perspectives of articular cartilage regeneration: a focus on adipose-derived stem cells and platelet-derived products, Journal of Tissue Engineering and Regenerative Medicine 2011, 5: e36–e51.

[15] Foster T. E., Puskas B. L., Mandelbaum B. R., Gerhardt M. B. and Rodeo S. A., Platelet-rich plasma: from basic science to clinical applications, American Journal of Sports Medicine 2009, 37: 2259–2272.

[16] Lu H. H., Vo J. M., Chin H. S., Lin J., Cozin M., Tsay R., Eisig S. and Landesberg R., Controlled delivery of platelet-rich plasma-derived growth factors for bone formation, Journal of Biomedical Materials Research Part A 2008, 86: 1128–1136.

[17] Mori M., Rossi S., Bonferoni M. C., Ferrari F., Sandri G., Riva F., Del Fante C., Perotti C.and Caramella C., Calcium alginate particles for the combined delivery of platelet lysate and vancomycin hydrochloride in chronic skin ulcers, International Journal of Pharmaceutics 2014, 461: 505–513.

[18] Man Y., Wang P., Guo Y., Xiang L., Yang Y., Qu Y., Gong P. and Deng L., Angiogenic and osteogenic potential of platelet-rich plasma and adipose-derived stem cell laden alginate microspheres, Biomaterials 2012, 33: 8802–8811.

[19] Matsui M. and Tabata Y., Enhanced angiogenesis by multiple release of platelet-rich plasma contents and basic fibroblast growth factor from gelatin hydrogels, Acta Biomaterialia 2012, 8: 1792–1801.

[20] Walter M. N. M., Wright K. T., Fuller H. R., MacNeil S. and Johnson W. E. B., Mesenchymal stem cell-conditioned me- dium accelerates skin wound healing: an in vitro study of fibroblast and keratinocyte scratch assays, Experimental Cell Research 2010, 316: 1271–1281.

[21] Song W., Lima A. C. and Mano J. F., Bioinspired methodol- ogy to fabricate hydrogel spheres for multi-applications using superhydrophobic substrates, Soft Matter 2010, 6: 5868–5871.

[22] Oliveira N. M., Neto A. I., Song W. and Mano J. F., Two-dimensional open microfluidic devices by tuning the wettability on patterned superhydrophobic polymeric surface, Applied Physics Express 2010, 3, 085205.

[23] Lima A. C., Song W., Blanco-Fernandez B., Alvarez-Lorenzo C. and Mano J. F., Synthesis of temperature-responsive dextran- MA/PNIPAAm particles for controlled drug delivery using superhydrophobic surfaces, Pharmaceutical Research 2011, 28: 1294– 1305.

[24] Lima A. C., Batista P., Valente T. A. M., Silva A. S., Correia I. J. and Mano J. F., Novel methodology based on biomimetic superhydrophobic substrates to immobilize cells and proteins in hydrogel spheres for applications in bone regeneration, Tissue Engineering Part A 2013, 19: 1175–1187.

[25] Lima A. C., Custódio C. A., Alvarez-Lorenzo C. and Mano J. F., Biomimetic methodology to produce polymeric multilayered particles for biotechnological and biomedical applications, Small 2013, 9: 2487–2492.

[26] Lima A. C., Correia C. R., Oliveira M. B. and Mano J. F. Sequential ionic and thermogelation of chitosan spherical hydrogels prepared using superhydrophobic surfaces to immobilize cells and drugs, Journal of Bioactive and Compatible Polymers 2013, 29: 50–65.

[27] Liang C. C., Park A. Y. and Guan J. L., In vitro scratch assay: a convenient and inexpensive method for analysis of cell migration in vitro, Nature Protocols 2007, 2: 329–333.

[28] Ghazi K., Deng-Pichon U., Warnet J. M. and Rat P., Hyaluronan fragments improve wound healing on in vitro cutaneous model through P2X7 purinoreceptor basal activation: role of molecular weight, PloS One 2013, 7: e48351.

[29] Chan B. P., Hui T. Y., Yeung C. W., Li J., Mo I. and Chan G. C. F., Self-assembled collagen-human mesenchymal stem cell microspheres for regenerative medicine, Biomaterials 2007, 28: 4652–4666.

[30] Bao P., Kodra A., Tomic-Canic M., Golinko M. S., Ehrlich H. P. and Brem H., The role of vascular endothelial growth factor in wound healing, Journal of Surgical Research 2009, 153: 347–358.

[31] Agren M. S., Steenfos H. H., Dabelsteen S., Hansen J. B. and Dabelsteen E., Proliferation and mitogenic response to PDGF-BB of fibroblasts isolated from chronic venous leg ulcers is ulcer-age dependent, Journal of Investigative Dermatology 1999, 112: 463–9.

[32] Steed D. L., Clinical evaluation of recombinant human platelet-derived growth factor for the treatment of lower extremity diabetic ulcers, Journal of Vascular Surgery 1995, 21: 71–80.

[33] Smiell J. M., Wirman T. J., Steed D. L., Perry B. H., Sampson A. R. and Schwab B. H., Efficacy and safety of becaplermin (recombinant human platelet-derived growth factor-BB) in patients with nonhealing, lower extremity diabetic ulcers: a combined analysis of four randomized studies, Wound Repair and Regeneration 1999, 7: 335–46.

[34] Ito R., Morimoto N., Pham L. H., Taira T., Kaway K. and Suzuki S., Efficacy of the controlled release of concentrated platelet lysate from a collagen/gelatin scaffold for dermis-like tissue regeneration, Tissue Engineering Part A 2013, 19: 1398–1405.

[35] Pietramaggiori G., Kaipainen A., Czeczuga J. M., Wagner C. T. and Orgill D. P., Freeze-dried

platelet-rich plasma shows beneficial healing properties in chronic wounds, Wound Repair and Regeneration 2006, 14: 573–580.

[36] O'Leary L. E. R., Fallas J. A., Bakota E. L., Kang M. K. and Hartgerink J. D., Multi-hierarchical self-assembly of a collagen mimetic peptide from triple helix to nanofibre and hydrogel, Nature Chemistry 2011, 3: 821–828.

[37] Kadler K. E., Holmes D. F., Trotter J. A. and Chapman J. A., Collagen fibril formation, Biochemistry Journal 1996, 316: 1–11.

[38] George A. and Veis A., FTIRS in H2O demonstrates that collagen monomers undergo a conformational transition prior to thermal self-assembly in vitro, Biochemistry 1991, 30: 2372–2377.

[39] Li Y., Asadi A., Monroe M. R. and Douglas E. P., pH effects on collagen fibrillogenesis in vitro: electrostatic interactions and phosphate binding, Materials Science and Engineering C 2009, 29: 1643–1649.

[40] Abou Neel E. A., Bozec L., Knowles J. C., Syed O., Mudera V., Day R., Hyun J. K., Collagen-emerging collagen based therapies hit the patient, Advanced Drug Delivery Reviews 2013, 65: 429–456.

[41] Fufa D., Shealy B., Jacobson M., Kevy S. and Murray M. M., Activation of platelet-rich plasma using soluble type I collagen, Journal of Oral and Maxillofacial Surgery 2008, 66, 684–690.

[42] Alsousou J., Thompson M., Hulley P., Noble A. and Willett K., The biology of platelet-rich plasma and its application in trauma and orthopaedic surgery: a review of the literature, Journal of Bone and Joint Surgery (British) 2009, 91: 987–996.

[43] Puga A. M., Lima A. C., Mano J. F., Concheiro A., and Alvarez- Lorenzo C., Pectin-coated chitosan microgels crosslinked on superhydrophobic surfaces for 5-fluorouracil encapsulation, Carbohydrate Polymers 2013, 98: 331–340.

[44] Costa A. M. S., Alatorre-Meda M., Oliveira N. M. and Mano J. F., Biocompatible polymeric microparticles produced by a sim- ple biomimetic approach, Langmuir 2014, 30: 4535–4539.

[45] Crevensten G., Walsh, A. J. L., Ananthakrishnan D., Page P., Wahba G. M., Lotz J. C. and Berven S., Intervertebral disc cell therapy for regeneration: mesenchymal stem cell implantation in rat intervertebral discs, Annals of Biomedical Engineering 2004, 32: 430–434.

[46] Humes H. D., Stem cells: the next therapeutic frontier, Transactions of the American Clinical and Climatological Association 2005, 116: 167–184

[47] Yu J., Du K. T., Fang Q., Gu Y., Mihardja S. S., Sievers R. E., Wu J. C. and Lee R. J., The use of human mesenchymal stem cells encapsulated in RGD modified alginate microspheres in the repair of

myocardial infarction in the rat, Biomaterials 2010, 31, 7012–7020.

[48] Ruszczak Z., Effect of collagen matrices on dermal wound healing, Advanced Drug Delivery Reviews 2003, 55: 1595–1611.

[49] Lima A. C., Sher P. and Mano J. F., Production methodologies of polymeric and hydrogel particles for drug delivery applications, Expert Opinion on Drug Delivery 2012, 9: 231–248.

[50] Ebrahimian T. G., Pouzoulet F., Squiban C., Buard V., André M., Cousin B., Gourmelon P., Benderitter M., Casteilla L. and Tamarat R., Cell therapy based on adipose tissue-derived stromal cells promotes physiological and pathological wound healing, Arteriosclerosis, Thrombosis, and Vascular Biology 2009, 29: 503–510.

[51] Kim W. S., Park B. S., Sung J. H., Yang J. M., Park S. B., Kwak S. J., Park J. S., Wound healing effect of adipose-derived stem cells: a critical role of secretory factors on human dermal fibroblasts, Journal of Dermatological Science, 2007, 48: 15–24.

[52] Sen, C. K., Wound healing essentials: let there be oxygen, Wound Repair and Regeneration 2009, 17: 1–18.

[53] Bertrand-Duchesne M. P., Grenier D. and Gagnon G., Epidermal growth factor released from platelet-rich plasma promotes endothelial cell proliferation in vitro, Journal of Periodontal Research 2010, 45: 87–93.

[54] Hsu C. W., Yuan K. and Tseng C. C., The negative effect of platelet-rich plasma on the growth of human cells is associated with secreted thrombospondin-1, Oral Surgery, Oral Medicine, Oral Pathology, Oral Radiology, and Endodontics 2009, 107: 185–192.

[55] Backly R. E., Ulivi V., Tonachini L., Cancedda R., Descalzi F. and Mastrogiacomo M., Platelet lysate induces in vitro wound healing of human keratinocytes associated with a strong proinflammatory response, Tissue Engineering Part A 2011, 17: 1787– 1800.

[56] Yannas I. V., Lee E., Orgill D. P., Skrabut E. M. and Murphy G. F., Synthesis and characterization of a model extracellular matrix that induces partial regeneration of adult mammalian skin, Proceedings of the National Academy of Sciences of the United States of America 1989, 86: 933–937.

[57] Soller E. C., Tzeranis D. S., Miu K., So P. T. C. and Yannas I. V., Common features of optimal collagen scaffolds that disrupt wound contraction and enhance regeneration both in peripheral nerves and in skin, Biomaterials 2012, 33: 4783–4791.

[58] Moor A. N., Vachon D. J. and Gould L. J., Proteolytic activity in wound fluids and tissues derived from chronic venous leg ulcers, Wound Repair and Regeneration 2009, 17: 832–839.

[59] Marx R. E., Carlson E. R., Eichstaedt R. M., Schimmele S. R., Strauss J. E. and Georgeff K. -R.,

Platelet-rich plasma: growth factor enhancement for bone grafts, Oral Surgery, Oral Medicine, Oral Pathology, Oral Radiology, and Endodontics 1998, 85: 638–646.

[60] Hokugo A., Sawada Y., Hokugo R., Iwamura H., Kobuchi M., Kambara T., Morita S. and Tabata Y., Controlled release of platelet growth factors enhances bone regeneration at rabbit calvaria, Oral Surgery, Oral Medicine, Oral Pathology, Oral Radiology, and Endodontics 2007, 104: 44–48.

[61] Metcalfe A. D. and Ferguson M. W. J., Tissue engineering of replacement skin: the crossroads of biomaterials, wound healing, embryonic development, stem cells and regeneration, Journal of the Royal Society Interface 2007, 4: 413–437.

Chapter 8

Novel Methodology Based on Biomimetic Superhydrophobic Substrates to Immobilize Cells and Proteins in Hydrogel Spheres for Applications in Bone Regeneration

8.1. Abstract

Cell-based therapies for regenerative medicine have been characterized by the low retention and integration of injected cells into host structures. Cell immobilization in hydrogels for target cell delivery has been developed to circumvent this issue. In this work mesenchymal stem cells isolated from Wistar rats bone marrow (rMSCs) were immobilized in alginate (ALG) beads fabricated using an innovative approach involving the gelification of the liquid precursor droplets onto biomimetic superhydrophobic surfaces without the need of any precipitation bath. The process occurred in mild conditions preventing the loss of cell viability. Furthermore, fibronectin (FN) was also immobilized inside alginate beads with high efficiency in order to mimic the composition of the extracellular matrix. This process occurred in a very fast way (around 5 min), at room temperature, without aggressive mechanical strengths or particle aggregation. The methodology employed allowed the production of alginate beads exhibiting a homogenous rMSCs and FN distribution. Encapsulated rMSCs remained viable and were released from the alginate for more than 20 days. *In vivo* assays were also performed, by implanting these particles in a calvarial bone defect to evaluate their potential for bone tissue regeneration. Microcomputed tomography and histological analysis results showed that this hybrid system accelerated bone regeneration process. The methodology employed had a dual role by preventing cell and FN loss and avoiding any contamination of the beads or exchange of molecules with the surrounding environment. In principle, the method used for cell encapsulation could be extended to other systems aimed to be used in tissue regeneration strategies.

This chapter is based on the following publication:
Lima A.C., Batista P., Valente T. A. M., Silva A. S., Correia I. J. and Mano J. F., Novel methodology based on biomimetic superhydrophobic substrates to immobilize cells and proteins in hydrogel spheres for applications in bone regeneration, Tissue Engineering Part A 2013, 19: 1175-87.

8.2. Introduction

Mesenchymal stem cells (MSCs) due to their multipotent properties and high rate of proliferation have been studied for regenerative medicine strategies [1,2]. When cultured under specific environments and appropriated supplemented culture media, MSCs can differentiate into lineages of mesenchymal tissues such as bone, cartilage, fat, muscle, tendon, and marrow stroma [3]. Hydrogels have been used as carrier's materials to specifically deliver cells directly into damaged tissues, thus avoiding cell loss through the blood stream [1,4–6] The highly hydrated microenvironment and similar structure to the extracellular matrix (ECM) of these carriers provide good permeability for low molecular weight solutes, such as metabolites, nutrients, or other bioactive molecules that can present biochemical, cellular, and physical stimuli for cell differentiation, proliferation, and migration [7]. The cells immobilized inside hydrogels are physically isolated and consequently protected from the deleterious outside environment [8–11]. Although other shapes can be employed, spheres have been the most explored due to their large surface area, the ability to immobilize greater amount of biologically active molecules, or cells per unit volume [12] and due to the possibility of application in most complex systems such as cell-induced aggregates, cell carriers for cell expansion, and organ printing [13]. Several polysaccharides have been proposed as biomaterials for tissue engineering and regenerative medicine [14]. The vast majority of them, such as alginate, are currently used in the form of hydrogels to create structures with size features ranging between 0.1 and 10 mm [15]. MSCs encapsulated in alginate hydrogels have been reported in the literature for different applications, such as bone [15] and cartilage regeneration [16], angiogenesis [17], and tumor treatment [18]. The easy gelling and biocompatible properties of alginate hydrogels, obtained by ionic crosslinking, have led to their study as cell transplantation vehicles for tissue regeneration [19]. However, since alginate based hydrogels poorly bind serum proteins, different ECM compounds such as fibronectin (FN) [20], collagen [16,21], or RGD sequences [22,23] have been added to these polysaccharides in order to offer adhesion sites to mammalian cells. So far, the techniques used for cell immobilization inside hydrogels required the mixing of gelling precursor with cells, followed by gelation through a physical, chemical, or ionic crosslinking. Several technologies have been proposed for cell immobilization in hydrogel particles, and some of them adopted from methodologies used in the pharmaceutical industry [24,25]: emulsification, photolithography, microfluidics, or coagulation baths using special dispensing systems of cell suspension in polymeric solutions. However, a significant part of these methodologies imply the contact of the gelling phase containing the cells or bioactive molecules with another liquid phase, which may be responsible for cells or molecules loss, due to their diffusion from the gel to the supporting liquid. The uncontrolled entrance of solvents may also lead to the contamination of the forming hydrogels, which

may compromise the viability of the cells entrapped inside the matrix. In this work an innovative methodology involving the use of superhydrophobic substrates [26] was employed to produce spherical hydrogels able to immobilize cells and bioactive compounds with high efficiency. The major advantages of this procedure include the use of mild processing conditions, high encapsulation loading, lower production costs, control of the particle size, and absence of mechanical forces during particles formation. This methodology has already been validated for production of controlled drug delivery systems [27]. We hypothesize that the method could be adapted to be used to encapsulate MSCs in hydrogel spheres containing bioactive molecules for posterior use in bone tissue engineering strategies. *In vitro* studies were performed to analyze the effect of the immobilization method on cell viability and also to evaluate cell differentiation over time. After that, *in vivo* studies were also performed to characterize the applicability of this system for bone tissue regeneration.

8.3. Experimental Section

8.3.1. Materials

Polystyrene (PS) from a grade for injection molding was used in a granular shape for the preparation of the superhydrophobic substrates. Tetrahydrofuran (THF, 99.9%) was purchased from Riedel de-Haen. 1H,1H,2H,2Hperfluorodecyltriethoxysilane (PFDTS, 97%), low-viscosity sodium alginate (ALG), FN from human plasma, Dulbecco's modified Eagle's medium (DMEM-F12), trypsin, albumin bovine serum (BSA, 96%), 4,6-diamidino-2-phenyindole, dilactate (DAPI), tetramethylrhodamine B isothiocyanate (Phalloidin), and *in vitro* toxicology assay kit (lactate dehydrogenase [LDH] quantification) were purchased from Sigma-Aldrich. Ethanol was purchased from Panreac. Calcium chloride ($CaCl_2$) was purchased from Merck. Fetal bovine serum (FBS) was purchased from Biochrom AG. 3-[4,5-dimethylthiazol-2-yl]-5-(3-carboxy-methoxyphenyl)-2-(4-sulfophenyl)-2H-tetrazolium, inner salt (MTS) and electron coupling reagent (phenazine methosulfate; PMS) were purchased from Promega. FN was labeled using Molecular Probes' Alexa Fluor 555 Protein Labeling kit and cells were labeled with Hoechst 33342 and calcein acetoxymethyl ester (calcein-AM) purchased from Invitrogen. Propidium iodide (PI) was purchased from VWR. Hydrochloric acid solution was purchased from Surgipath. All chemicals were used as received.

8.3.2. Polystyrene Superhydrophobic Surfaces

PS superhydrophobic surfaces were prepared using a phase separation method as described elsewhere [26,27]. Briefly, a PS solution (70 mg/mL) in THF was prepared and then mixed with ethanol (2:1.3 v/v). The mixture was dispensed onto smooth PS commercial substrate, which was then immersed in ethanol

for 1 min and dried with nitrogen flow. In order to increase the superhydrophobicity of obtained surfaces, the rough PS surfaces were modified with PFDTS (1% v/v in ethanol) after argon plasma treatment for 40 s at 30 W (Plasma Prep5; Gala Instruments).

8.3.3. Preparation of the Hydrogel Particles

The beads were produced using different ALG concentrations: 1%, 1.5%, and 2% (w/v). Five microliters of ALG solution were dispensed on the PS superhydrophobic surface. The alginate hydrogel beads were obtained on the surface after addition of 2 mL of 5% (w/v) $CaCl_2$ solution on the top of each liquid sphere.

8.3.4. Stability of the Alginate Particles in Culture Medium

The stability of the produced beads was analyzed through quantification of calcium released from crosslinked alginate beads immersed in cell culture medium. Five alginate beads of each concentration were placed in 5 mL of cell culture medium (n = 3): DMEM-F12 supplemented with FBS (10%, v/v), penicillin G (100 U/cm^3), streptomycin (100 μg/cm^3), and amphotericin B (0.25 μg/cm^3). The vials containing the beads were kept at 37 °C. At pre-established periods of time, aliquots of 1 mL of the supernatant were taken out and replaced with equal volume of fresh cell culture medium to maintain the volume constant during the release study. The calcium concentration of the collected samples was measured using Coupled Plasma Spectrometry (ICP, JY 2000-2; Horiba Jobin Yvon), after diluted 10x in 1% HNO_3 (v/v) solution.

8.3.5. Cell Culture and Immobilization in Alginate Beads

MSCs from Wistar rats femoral bone marrow [28,29] were isolated as previously described [30]. Then, cells were seeded in T-flasks with DMEM-F12 supplemented with FBS (10% v/v), penicillin G (100 U/cm^3), streptomycin (100 μg/cm^3), and amphotericin B (0.25 μg/cm^3). rMSCs were kept in culture inside an incubator at 37 °C with a 5% CO_2 humidified atmosphere. After reached confluence, rMSCs were subcultivated by a 3–5 min incubation in 0.18% trypsin (1:250) and 5 mM ethylenediaminetetraacetic acid. Subsequently, the rMSCs were centrifuged, resuspended in culture medium, and then encapsulated in alginate beads. Cells were added to 1, 1.5, and 2 wt% alginate solutions in order to obtain ≈10,000 cells/bead. Some studies were carried out in the presence of FN. In those cases, FN with a concentration of 250 μg/mL [31] was added to alginate cell suspension. Five microliters of cell suspension with or without FN was dispensed on the PS superhydrophobic surface (Figure 8.1 A). The alginate hydrogel beads were obtained on the surface after addition of 2 μL of 5% (w/v) $CaCl_2$ solution on the top of each sphere

(Figure 8.1 B). After that, the spheres were kept in culture with 150 μL of cell culture medium (Figure 8.1 C). The distribution of FN in alginate beads was observed by fluorescent microscopy (Zeiss) using 250 μg/mL of FN labeled with Alexa Fluor 555 dye following the protocol of Molecular Probe's Alexa Fluor 555 Protein Labeling kit. Phalloidin and DAPI staining to visualize actin cytoskeleton and to label the DNA, respectively, were conducted as outlined by the supplier's protocol. Briefly, the particles were washed with 0.15 M of NaCl supplemented with 10 mM of $CaCl_2$, fixed in freshly prepared 4% (v/v) of formaldehyde in phosphate-buffered saline for 15 min at room temperature (RT), and washed extensively to remove all traces of the fixative. The cells were then stained with 50 μg/mL fluorescent phalloidin for 45 min at RT. DAPI labeling solution (0.5 μg/mL) was incubated for 3 min at RT. The particles were washed again to remove remaining staining solutions and visualized using a Zeiss LSM 710 confocal microscope equipped with a 10x/0.5 dry Fluor objective (Carl Zeiss SMT, Inc.). Beads distribution size was investigated using a stereo microscope (Stemi 1000 PG-HITECH; Zeiss). After being prepared, alginate beads were immersed in cell culture media and observed under stereomicroscope immediately. The mean particle size was calculated by analyzing the images using the ImageJ software.

8.3.6. *In Vitro* Live/Dead Assay

rMSCs immobilized in alginate beads were kept in culture, in a 96-well plate, with 150 μL of DMEM-F12 supplemented with FBS (10%, v/v), penicillin G (100 U/cm^3), streptomycin (100 μg/cm^3), and amphotericin B (0.25 μg/cm^3) and incubated at 37 °C, with a 5% CO_2 humidified atmosphere. After an incubation period of 24, 48, and 72 h, cells viability was assessed through the reduction of the MTS into a water-soluble formazan product [32]. Briefly, the medium of each well was removed and replaced with a mixture of 100 μL of fresh culture medium and 20 μL of MTS/PMS reagent solution. Then, the beads were incubated for 4 h at 37 °C. The absorbance was measured at 492 nm using a microplate reader (Sanofi; Diagnostics Pauster). Wells containing cells in the culture medium without being immobilized in alginate were used as negative controls (K^-). EtOH (96%) was added to wells with cells, to be used as a positive control (K^+) [32]. Moreover, the amount of dead cells was also quantified by the LDH assay, in 2% ALG+FN particles due to the higher beads stability. LDH is released to the medium through the damaged cell membrane and convert a yellow tetrazolium salt into a red formazan dye, which is quantified by reading its absorbance at 492 nm using a microplate reader. The optical density is proportional to the number of lysed cells [33]. After 24, 48, and 72 h the well plates containing the beads in culture were shaken briefly to homogenize the released LDH into the cell culture medium. Then, 50 μL of the cell culture medium was transferred into a fresh 96-well plate and 100 μL of LDH assay mixture was added to each well [34]. After

30–45 min the enzymatic activity was stopped by adding 7.5 μL of HCl and the absorbance was measured. Wells containing cells in the culture without being immobilized in alginate were used as negative control and lysis solution was added to wells containing cells as a positive control. The results obtained were expressed as the mean – the standard error of the mean for at least three independent experiments. Live/dead staining was also performed on 2% ALG+FN particles. The beads were incubated for 15 min at 37 °C and immersed in 0.15 M of NaCl complemented with 10 mM of $CaCl_2$ where 2 μL of Calcein AM (1 mg/mL) and 1 μL of PI (1 mg/mL) were added. After incubation, the Calcein AM/PI solution was removed and the beads were washed and finally visualized in a Zeiss LSM 710 confocal microscope with appropriated filters to detect green (live cells) and red (dead cells).

8.3.7. Cell Morphology: Optical Microscopy, Scanning Electron Microscopy, and Fluorescent Microscopy.

rMSC morphology, adhesion, and proliferation were firstly visualized using an Olympus CX41 inverted light microscope, equipped with an Olympus SP-500 UZ digital camera. Scanning electron microscopy (SEM) was also used to observe the morphology of the rMSCs immobilized in the alginate particles. To do so, samples were fixed overnight using 2.5% glutaraldehyde in water, at 4 °C. After that, they were rinsed with distilled water and dehydrated in graded ethanol of 70%, 80%, 90%, and 100% for 10 min each. Finally, the samples were mounted in supports using double-size adhesive tape and coated with gold by using Emitech K550 sputter coater. Samples were analyzed using a Hitachi S-2700 SEM. Moreover, to visualize the rMSCs immobilized in alginate, a Hoechst dye (H1399) was used to label cell nucleus. A trihydrochloride trihydrate solution (2 μg/mL) was added to a cell pellet obtained by centrifugation and then resuspended in culture media. After 30 min in contact with Hoechst solution, rMSCs were encapsulated in alginate in the same conditions as previously described. rMSCs were visualized after 0, 24, 48, and 72 h of incubation in a Zeiss AX10 microscope and analyzed with the Axio Vision Real 4.6 software (Carl Zeiss SMT, Inc.).

8.3.8. Osteogenic Induction

To induce osteogenic differentiation, rMSCs immobilized in alginate beads were cultured in osteogenic medium, which consisted on DMEM-F12 containing FBS (10%, v/v), penicillin G (100 U/cm^3), streptomycin (100 μg/cm^3), amphotericin B (0.25 μg/cm^3), and supplemented with 0.1 mM l-ascorbic acid 2-phosphate, 10 mM beta-glycerol phosphate (β-GP), and 100 nM dexamethasone [35]. At 1, 7, 14, and 21 days postinduction, alginate beadswere fixed overnight in 2.5% glutaraldehyde in water, at 4 °C,

dehydrated in graded ethanol solutions, and finally embedded in paraffin blocks. Sections of 4–5 μm were stained with alizarin red dye for the detection of calcium deposits. Microscope images were acquired with Zeiss Imager A.1.

8.3.9. *In Vivo* Assays

The *in vivo* experiments were performed using 12 Wistar rats with an average weight of 200 g. Such studies were done accordingly to the guidelines set forth in the National Institutes of Health Guide for the care and use of laboratory animals. Animals were anesthetized by intraperitoneal injection of ketamine (40 mg/kg) and xylazine (5 mg/kg). Bone defects with ≈5 mm diameter were made on calvarial bone and four beads with ≈10 000 rMSCs and FN (250 μg/mL) were implanted inside it. The alginate concentration with best results *in vitro* was selected to be tested in animals (2% ALG). For that, three groups (n = 4) were created: (1) controls with empty defects; (2) alginate beads just with FN were implanted; and (3) an experimental group where alginate beads with FN and immobilized rMSCs were implanted. After its implantation into bone defects, animals were maintained in individual cages with free access to commercial rat food and water ad libitum. Then, animals were euthanized after 4 weeks with an overdose of anesthetic.

8.2.10. MicroComputed Tomography

Cranial bone samples obtained at week 4 by necropsy were fixed in formaldehyde. After dehydration, the samples were analyzed using a high resolution microcomputed tomography (μCT) Skyscan 1072 scanner (Skyscan). Scannings were performed in high resolution mode using a pixel size of 14.7 μm and integration time of 1.7 s. The X-ray source was set at 51 kV of energy and 195 mA of current. For all samples, representative data sets were transformed into binary using a dynamic threshold of 42–255. This data was used for morphometric analysis (CT Analyzer v1.5.1.5; SkyScan). Three-dimensional (3D) virtual models of calvarial bones were created, visualized, and registered using the image-processing software (ANT 3D creator v2.4; SkyScan).

8.3.11. Histology

Cranial bones samples used for μCT analysis were then decalcified in a hydrochloric acid solution and embedded in paraffin blocks. Furthermore, sample organs (brain, heart, lung, liver, spleen, and kidney) were also collected, fixed in formaldehyde, and embedded in paraffin blocks for routine histological

processing in order to check for any morphological alteration. Sections of 4–5 μm were stained with hematoxylin and eosin and finally visualized using a light microscope (Zeiss Imager A.1).

8.3.12. Statistical Analysis

Statistical analysis (GraphPad Prism; GraphPad Software) concerning MTS and LDH assays was performed using one-way analysis of variance following the Tukey's post-hoc test with a significant set at $p < 0.05$. All the results are presented as the mean ± standard deviation.

8.4. Results and Discussion

8.4.1. rMSC and FN Immobilization in Alginate Beads

Cell encapsulation is an important strategy to prevent the escape and the elimination of the entrapped cells when implanted in damaged tissue sites [18]. The most important objective of this work was the evaluation of the applicability of superhydrophobic surfaces as a method to immobilize cells (rMSCs previously isolated from Wistar rats) and unstable molecules (as it is the case of proteins and glycoproteins, such as FN) inside spherical hydrogels to be used in tissue engineering purposes (see Figure 8.1).

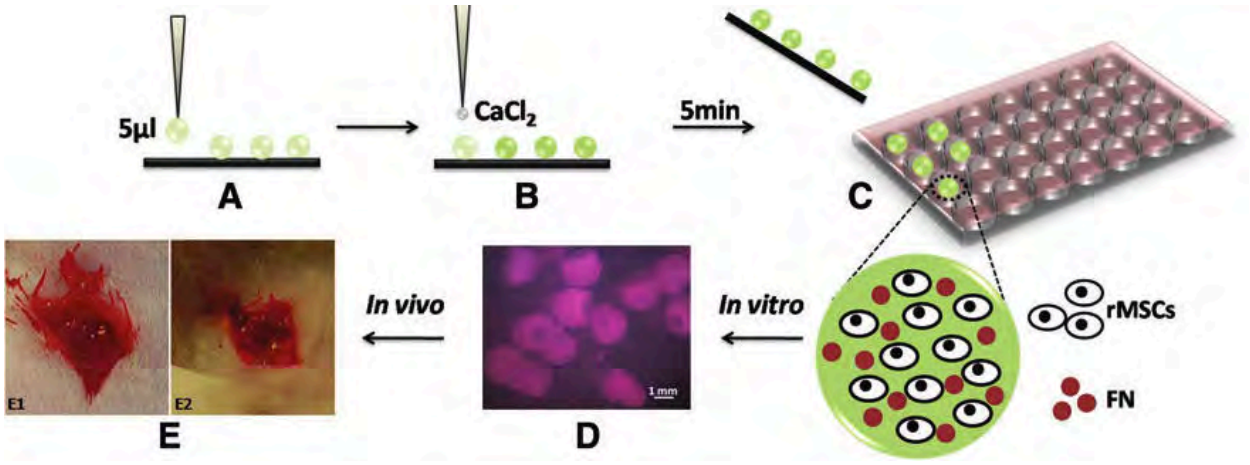

Figure 8.1. Schematic representation of cell and protein immobilization in alginate hydrogels using polystyrene (PS) superhydrophobic substrates: 5 μL drops of mesenchymal stem cells isolated from Wistar rats bone marrow (rMSCs) + fibronectin (FN) suspension in a sodium alginate (ALG) solution were dispensed on PS superhydrophobic substrates (A). After, 2 μL of $CaCl_2$ was dispensed on the top of each drop to crosslink alginate (B). After 5 min the spheres with rMSCs + FN immobilized were collected (C) and *in vitro* (D) and *in vivo* (E) tests were performed. A bone defect was created in calvarial bone (E1) and filled in with particles (E2) in order to evaluate the regeneration of the bone.

The water-repellent properties of PS superhydrophobic surfaces allowed the production of nearly spherical shape hydrophilic particles (Figure 8.1 D). Different concentrations of alginate in the liquid precursors were

used (1%, 1.5%, and 2% w/v). The final diameter of the obtained beads tended to increase with increasing alginate concentration, despite the same volume of the precursor solution was used (see Table 8.1).

Table 8.1. Mean size of the produced beads (n=6) obtained using different alginate concentrations.

Beads Formulation	Beads Size (μm)
1% ALG	1930 ±160
2% ALG	2030 ±190
3% ALG	2180 ±160

As an innovative methodology capable to immobilize mammalian cells and proteins, superhydrophobic surfaces show several advantages when compared with traditional techniques. For example, some of those methodologies to produce polymeric particles have a spread particle size distribution [36], which constitutes a problem when a narrow range of sizes is required. As it is possible to verify in the obtained results, the particles produced using superhydrophobic surfaces own a narrow size distribution, highly controlled by the volume of the liquid precursors dispensed over the substrates. This volume control could be interesting to produce particles with a specific required size. In addition, the small range of particle size obtained avoids additional steps for particle selection, saving production time and costs. The absence of mechanical forces that are sometimes responsible for cell damage and loss of biological activity of molecules constitutes another advantage of this methodology.

The dry environment where droplets harden into hydrogels avoids the particle aggregation and provide very high encapsulation efficiency (almost 100%) because cells or bioactive molecules are not in contact with surrounding fluid media and they cannot migrate or diffuse outside the volume of the spherical objects. This is particularly useful because FN molecules are water soluble [37], which is a bottleneck of the encapsulation procedures previously described in literature [24], since water-soluble molecules are easily lost to the wet media commonly used in those techniques. Moreover, this characteristic is particularly important when expensive molecules such as growth factors, or even genes, are desired to be encapsulated. Compared with other immobilization techniques, superhydrophobic surfaces allowed a very fast particle production because the particles became completely solid within the time of the cross-linking reaction, usually a fast chemical or physical process. The results obtained show (Figure 8.2 A, B) that FN molecules and cells were homogenously distributed on the beads, in agreement to our previous work, where BSA labeled with fluorescein isothiocyanate was encapsulated in dextran/poly(N-isopropylacrylomide (PNIPAAm) beads as a model drug [27]. The three studied formulations exhibited similar FN and rMSC distribution (data not showed). To our knowledge, the co-encapsulation of FN and rMSCs in alginate hydrogels for bone regeneration applications was never studied before.

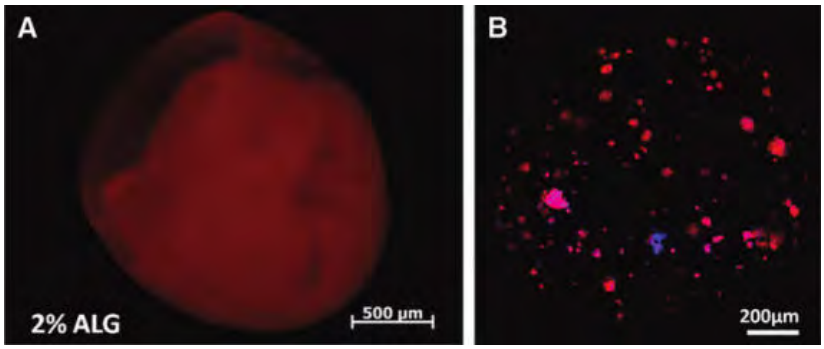

Figure 8.2. Fluorescent microscopy images of FN (250 µg/mL) labeled with Alexa Fluor 555 (A) and rMCSs labeled with Phalloidin/ DAPI (B) inside 2% ALG beads.

8.4.2. *In Vitro* Alginate Cytotoxicity and rMSC Morphology Studies

The synergistic effect of FN in cell viability was first explored quantitatively through cytotoxicity evaluation. Figure 8.3 shows MTS assay results and a significant difference between encapsulated cells and positive controls (dead cells), both in the presence and in the absence of FN, for 24, 48, and 72 h was observed. This means that the material is noncytotoxic and the rMSCs maintain their viability for at least 3 days. The general decrease in cell viability observed between 24 and 48 h for all alginate formulations may be explained by the need of an accommodation period by the rMSCs to adapt to new conditions. After this period the cell viability remains constant [38].

When compared the amount of viable cells immobilized in the presence or absence of FN, it is possible to observe that in the first 48 h of culture, there is a significant difference between both conditions. This difference was attenuated after 72 h, indicating that the effect of FN was more relevant in the initial anchorage of the cells in the hydrogel structure. The fraction of viable cells was higher in the presence of FN for all alginate formulations (1%, 1.5%, and 2% ALG) (Figure 8.3). It is well known that FN is an ECM constituent with a relevant role in regulation of cell adhesion, proliferation, and differentiation [39], which are very important factors for osteogenesis of human MSCs [21], as also that FN presence in the plasma modulates the response of the body against new implanted biomaterials constituting a good strategy to improve the performance of biomedical devices [40]. Having this into account, the entrapment of FN in alginate beads, beyond contributing to increase cell viability should also improve the acceptance of the studied system *in vivo*. To further characterize the carrier's biocompatibility and corroborate the MTS results, LDH assay was also performed in the particles with FN and the corresponding fraction of dead cells is shown in Figure 8.4. LDH is a stable cytoplasmatic enzyme that is released to the extracellular media when the cytoplasmatic membrane is damaged being directly proportional to the percentage of dead

cells [33]. Figure 8.4 shows that during at least 72 h the percentage of dead rMSCs encapsulated in alginate were maintained around 20%–25%, which is similar to the value obtained for the negative control (normal cell culture).

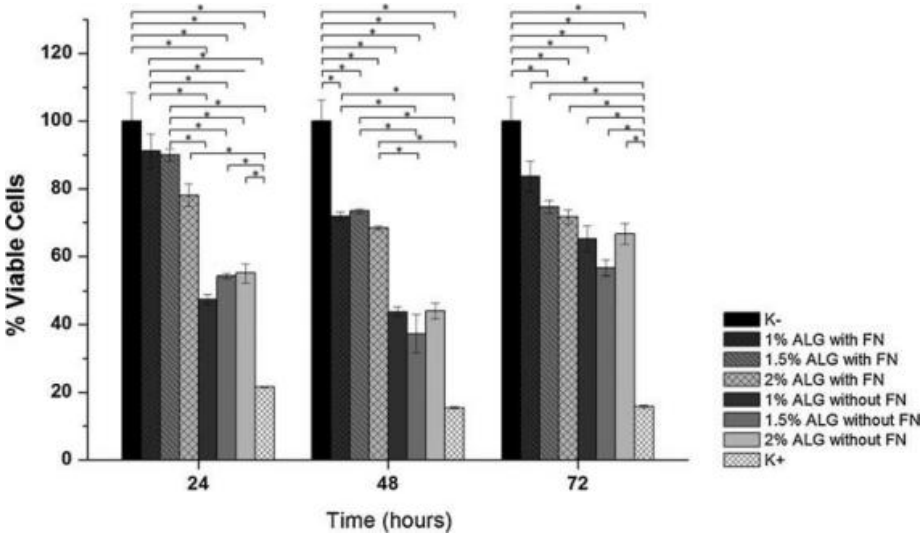

Figure 8.3. Cellular activity quantified by MTS assay: (K-), negative control where cells were cultivated in wells; (K+), positive control where the cells were dead and rMSCs immobilized in three different alginate concentrations with and without FN. Each result is the mean and respective standard error of at least three independent experiments.

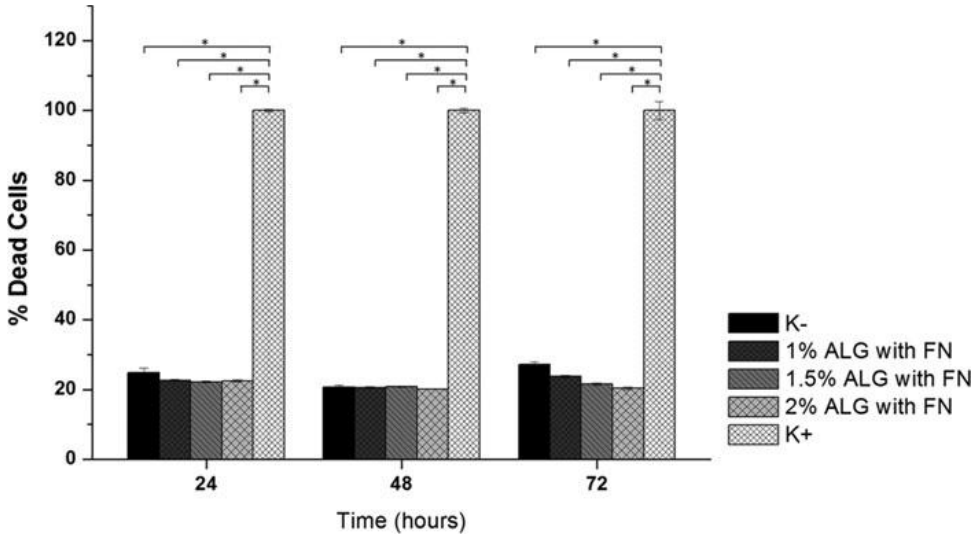

Figure 8.4. LDH quantification of rMSCs immobilized in alginate beads with FN in culture after 24, 48, and 72 h: (K) is the negative control where cells were cultivated in wells; (K+) is the positive control where the cells were dead.

Finally, the distribution of the live and dead rMSCs inside the 2% ALG+FN (the most stable formulation) particles was accessed by calcein-AM/PI staining for 21 days of culture. As it is possible observe in Figure 8.5, the majority of the cells were green which means that were live and significant differences were not

observed over time. The beads provided good conditions for rMCS survival and representative confocal microscopy images are observed in Figure 8.5.

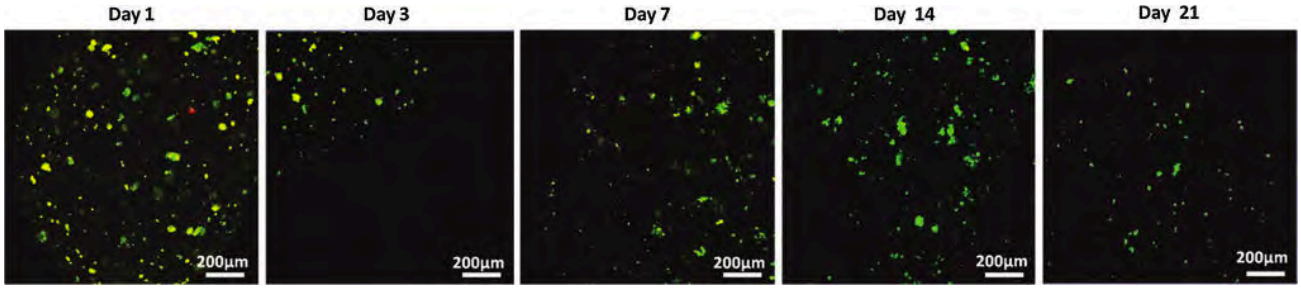

Figure 8.5. Live/dead staining of rMSCs immobilized into 2% ALG + FN beads over 21 days in culture.

Regarding the fraction of viable cells inside our alginate beads, similar results were previously obtained by Zhao *et al.* [41] for human umbilical cord stem cell encapsulated in alginate, where the percentage of viable cells ranged from ≈90% to 70%, after 7 days of culture. Figure 8.6 presents optical microscopy images of beads with different alginate concentrations in the presence and absence of FN after 72 h in culture. After 1 day the cells were seen well confined in the volume of the beads. Over 3 days in culture, rMSCs remained with their typically round shape and were homogeneously distributed inside the alginate beads. However, at this time point, it was possible to detect a slight particle disintegration and the consequently cell release (white arrows in Figure 8.6) principally in weaker beads corresponding to the ones prepared with lower alginate concentrations. The released rMSCs migrated from the particle core to the surface, adhered in the wells, and probably the proliferation started. The referred continuous cell release and proliferation was accessed and followed by optical microscopy for more 18 days in all alginate concentrations even after beads transferring to new well plates (see images in Figure 8.7). The 1% ALG beads released a higher number of rMSCs when compared to that of 1.5% and 2% ALG, for the same period. Such finding can be explained by the alginate particle disintegration, which occurred at higher rate for low concentration alginate beads. Similar results were earlier reported by Hunt *et al.* [42] They studied the degradation of 2% and 5% w/v alginate matrix with immobilized fibroblasts under normal cell culture conditions where it was shown that the alginate degradation process was not influenced by the presence of fibroblasts and that lowering the alginate concentration from 5% to 1% increased the rate of disintegration.

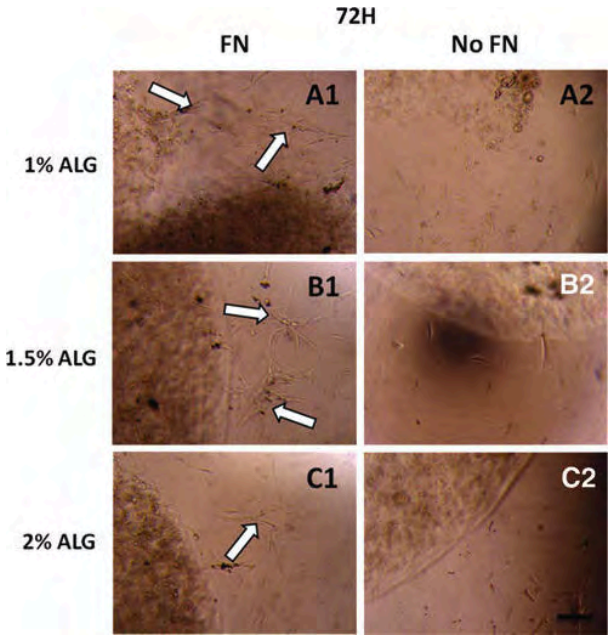

Figure 8.6. Optical microscopy images of alginate particles loaded with rMSCs. Group A were beads composed by 1% ALG after 72 h in culture in presence (A1) and absence (A2) of FN. The same order of images disposition was followed for the other alginate beads concentration: in group B was 1.5% ALG and group C 2% ALG. The white arrows show the cells released due to the slight particle disintegration.

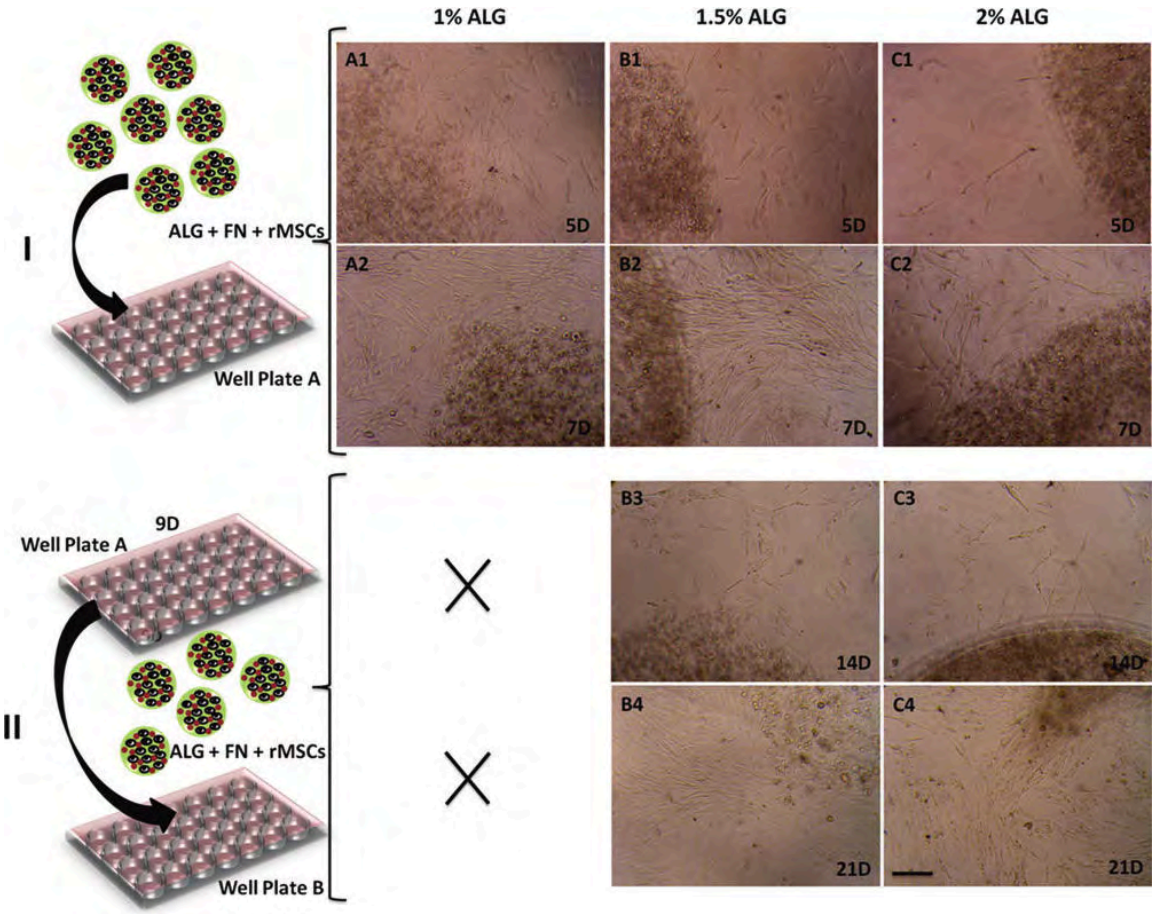

Figure 8.7. Part I. The alginate particles with rMSCs+FN were cultured in a well plate for 9 days and the rMSC morphology was accessed by optical microscopy: (A) correspond to 1% ALG, (B) to 1.5% ALG, and (C) to 2% ALG after 5 days (A1, B1, C1)

and 7 days (A2, B2, C2) in culture. Part II. When the released rMSCs reach the confluence in the surface of the well plate, the particles were transferred for a new plate. 1% ALG beads were not transferred because were completely disintegrated before day 9. The other alginate formulations were cultured for more days and the continuous rMSC release was observed at day 14 (B3, C3) and 21 (B4, C4). Scale bar 20 μm.

The degradation of the alginate beads structure could be explained by crosslinked chain disintegration caused by the replacement of calcium cations (responsible for the crosslinking) by monovalent cations such as sodium or potassium present in cell culture medium [43,44]. This was confirmed by the release calcium studies, in which calcium was released from alginate beads for 24 h (Figure 8.8). Moreover, it was hypothesized by Drury *et al.* [45] that ion exchange and the reordering of the alginate chain occur within the first 7 days and stabilize thereafter. In our study the 1% ALG beads disintegrates completely after 7 days in culture medium, while 1.5% and 2% ALG beads (or fragments) remained stable for more than 21 days. However, there was no significant effect on the concentration of alginate and the quantity of calcium ions released within this time period.

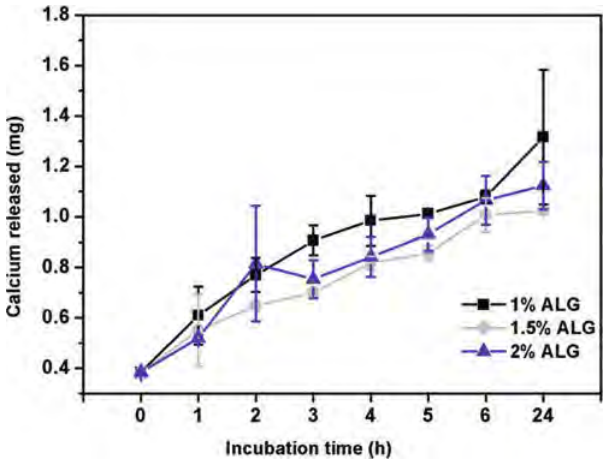

Figure 8.8. Cumulative release of calcium ions from alginate beads (1%, 1.5%, and 2% ALG) crosslinked with $CaCl_2$ after immersion in cell culture medium. The calcium at 0h corresponds to the amount content in cell culture medium.

Calcium is an essential element and plays a key role in skeletal mineralization. During the bone formation, osteoblasts capture calcium from bloodstream (that has been absorbed previously in the intestine or resulted from osteoclasts activity) and deposit it in an appropriate site in the form of calcium phosphate complexes [46]. Regarding this, it is possible that the in situ calcium delivered may help the mineralization process during bone defect regeneration. Another important parameter is the number of the cells immobilized inside the beads because studies reported that cell density must be sufficiently high to provide cell contact and consequently the proliferation [38]. Based on that, about 10 000 cells were encapsulated

in beads with ≈2 mm. Other studies reported the use of particles containing cells with similar dimensions. Alginate beads with 3.6, 2.2, and 1 mm were produced for cell encapsulation and used as components of calcium phosphate cements and polymer pastes [41]. The purpose of these beads is that they could quickly degrade and release the cells throughout the entire scaffolds. However, a considerable part of alginate beads produced so far did not present fast degradable properties and cell release was not observed. Zhou and Xu [47] reported that it is desirable to have beads with a fast degradation profile in order to promote a quick stem cells release, differentiation, and consequently enhance production of new tissue. Having this into account, it was expected that the fast release of the rMSCs over time and their adhesion into a defect site allowed a continuous and faster regeneration of the damaged tissue. Due to the higher stability of 2% ALG+FN beads, this formulation was selected to pursue the studies. The SEM analysis revealed that 2% ALG beads without cells (Figure 8.9 A) present a smooth surface structure. The alginate beads loaded with cells exhibit several protuberances with almost 10 µm diameter, which may be caused by the presence of rMSCs immobilized inside the hydrogel (Figure 8.9 B). To complement this assay, the rMSC nuclei were stained and the immobilized cells were observed through a fluorescent microscope (Figure 8.9 C). The images showed that cells were inside alginate hydrogels and even on surface having a typical round shape. These results corroborate those obtained by SEM analysis.

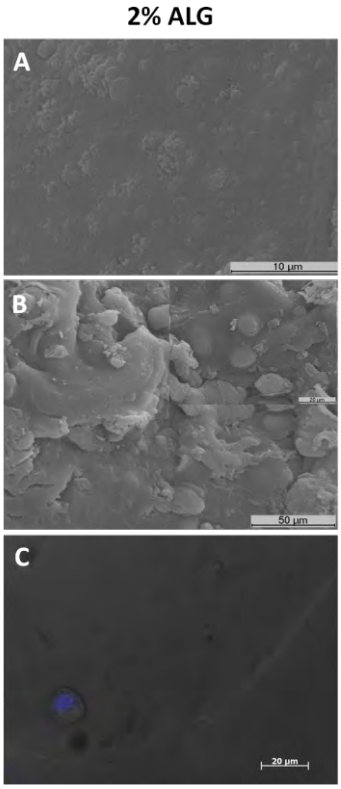

Figure 8.9. Scanning electron microscopy micrographs of 2% ALG+FN without rMSCs (A) and with rMSCs immobilized (B), after 48 h in culture. (C) Corresponds to fluorescent microscopy images of rMSCs stained with Hoechst 33342 immediately after immobilization in 2% ALG+FN.

8.4.3. Osteogenic Differentiation Assay

Bone regeneration is a complex physiologic process that includes cell recruitment and proliferation of progenitor cells followed by its differentiation along osteoblastic lineage, osteoid formation (deposition of ECM components), and finally mineralization [48]. The matrix mineralization consists in calcium deposits [49]. Alizarin red staining (Figure 8.10), which is a specific dye for calcium detection [50], showed a staining increase in 2% ALG+FN+rMSCs from day 1 to 14 (Figure 8.10 A2, C2) and especially between day 14 and 21 (Figure 8.10 C2, D2), when the beads were cultured under osteogenic conditions. The same beads formulation maintained under basal conditions did not show any difference in the color of the staining over time (Figure 8.10 A1, B1, C1, D1). The high permeability of alginate beads allowed the creation of an enabling *in vitro* environment for differentiation of encapsulated rMSCs. Similar results were previously obtained by Abbah *et al.* [51] using murine-derived adipose-tissue stromal cells encapsulated in alginate for 21 days. These results also demonstrate that the produced alginate beads had appropriated diffusion characteristics to allow the entrance of nutrients or other molecules that play an important role in rMSC viability and differentiation.

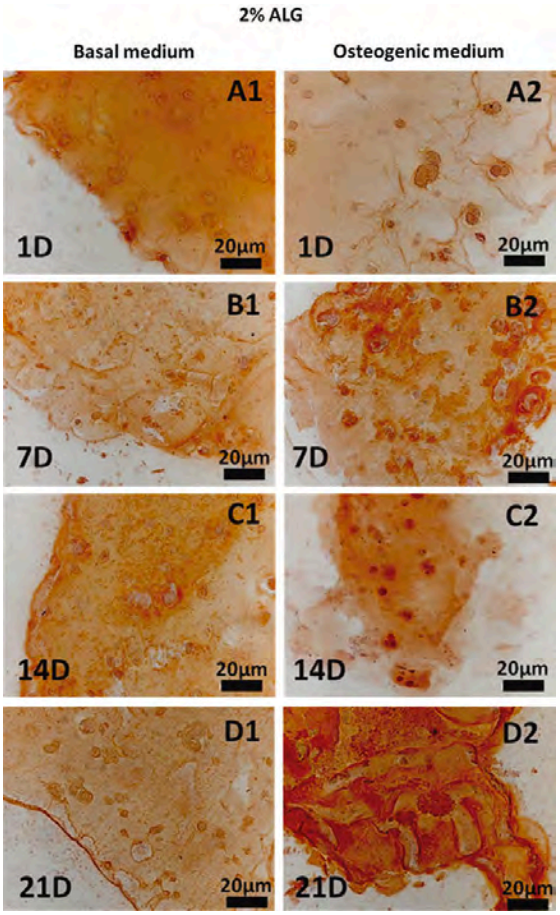

Figure 8.10. Alizarin red staining of 2% ALG+FN+rMSCs after 1 (A1, A2), 7 (B1, B2), 14 (C1, C2), and 21 days (D1, D2) in culture under basal and osteogenic conditions.

8.4.4. *In Vivo* Bone Regeneration

Wistar rats were used to perform the *in vivo* studies in order to evaluate the biocompatibility of the carriers with immobilized rMSCs and also their capability in stimulating the regeneration of a bone defect not affected by high mechanical stresses. In all studied groups, no specific inflammation or reactive granulomas were observed in tissues surrounded the site where alginate beads were implanted. Furthermore, no pathological abnormalities were observed in the brain, lung, liver, spleen, heart, and kidney samples. Representative μCT reconstructions of ex vivo bone explants around the defect regions are shown in Figure 8.11, 4 weeks postimplantation. In the defects of the control group, where no beads were implanted, is not observed bone tissue growth (see Figure 8.11 I). Otherwise, in the group II (Figure 8.11 II) where alginate beads loaded with FN were implanted, the 3D reconstructions show a lower level of bone infiltration compared with group III (Figure 8.11 III), where alginate beads loaded with FN and rMSCs were implanted.

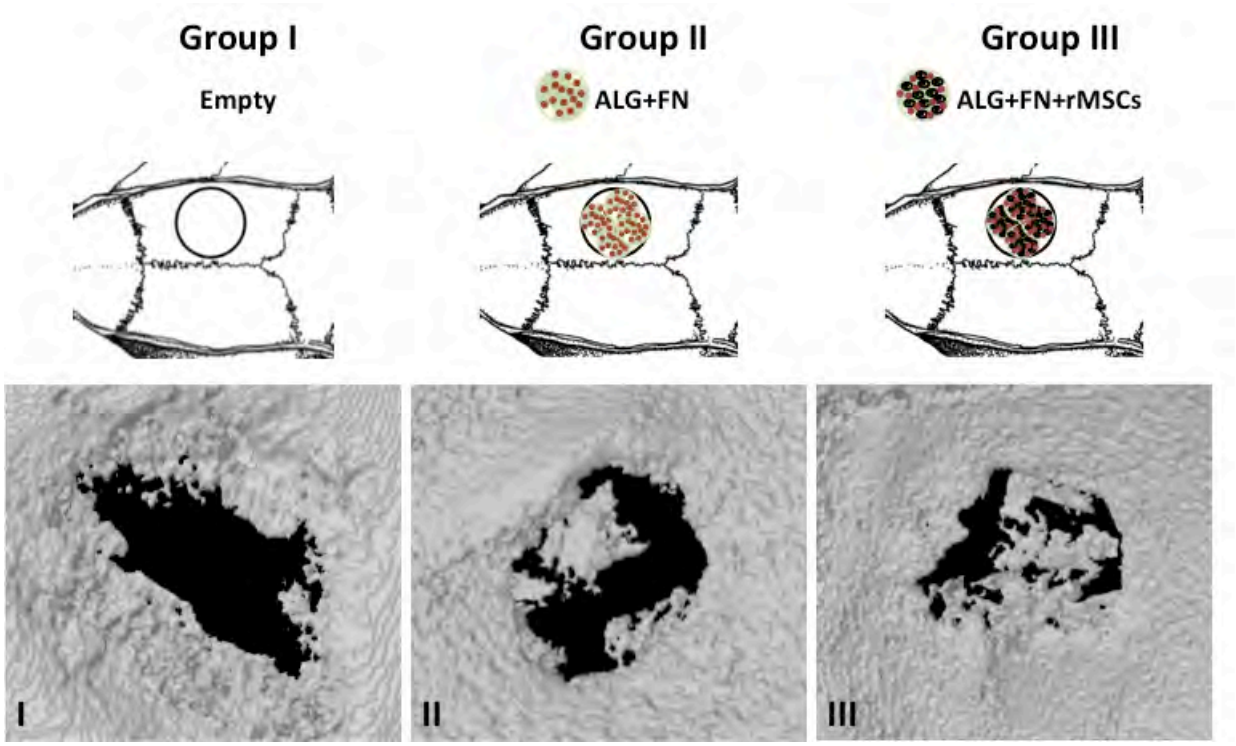

Figure 8.11. MicroComputed Tomography analysis of calvaria defects in Wistar rats. Images show the endpoint result after 4 weeks of bone regeneration of empty defects (I) and upon implantation of 2% ALG beads (II) loaded with FN and (III) loaded with FN and rMSCs.

Histological analysis was performed in order to confirm the previous described results and also to obtain complementary information related to host response and tissue/cellular organization (see Figure 8.12). The light microscopic examination of decalcified sections showed that in control (group I) and group II, new

bone tissue formation inside of the defect was not observed; only fragments of periosteum were present. However, neo bone tissue was formed circumferentially along the defects of group III and a significant amount of new bone tissue was visualized in the central areas. In addition, the histology results show an active periosteum and osteoblasts deposition which formed circular structures that give rise to circular pieces of bone tissue (black arrows in Figure 8.12 III) without connection to the border of the defect. The presence of osteoclastic-like cells was not visualized as also reactive or granulomatous inflammatory reactions in the surround tissue and fibrous connective tissue in the local where beads were implanted. This supports the local and systemic histocompatibility of these beads. These last results showed that the presence of cells induced the growth of higher amount of new bone tissue after 4 weeks. Furthermore, the visualized deposition of osteoblasts (black arrows in Figure 8.12 III) could be correlated with the release of rMSCs by alginate beads, which in turn had the appropriated diffusion properties to allow the differentiation of rMSCs under osteogenic conditions. On the other hand, the differentiated cells released or even the ones remained inside the particles could have delivered key proteins (*e.g.*, growth factors) [52,53] which recruited other cells to the damaged site and consequently accelerate the tissue regeneration. Lee *et al.* [54] demonstrated that calcium crosslinked alginate beads mineralized when injected subcutaneously or implanted intramuscularly after 1–6 months during which bone-like apatite deposits were found throughout the microparticles. This information reinforce that alginate is a very interesting material to induce biomineralization and also confirms its application for regeneration of bone damaged tissue. Taking into account these results, the immobilization of rMSCs with a component of ECM, namely FN, in alginate hydrogels using superhydrophobic surfaces constitute an interesting strategy to obtain particles for cell encapsulation and delivery and to improve tissue regeneration in a cheap, fast, and efficient way.

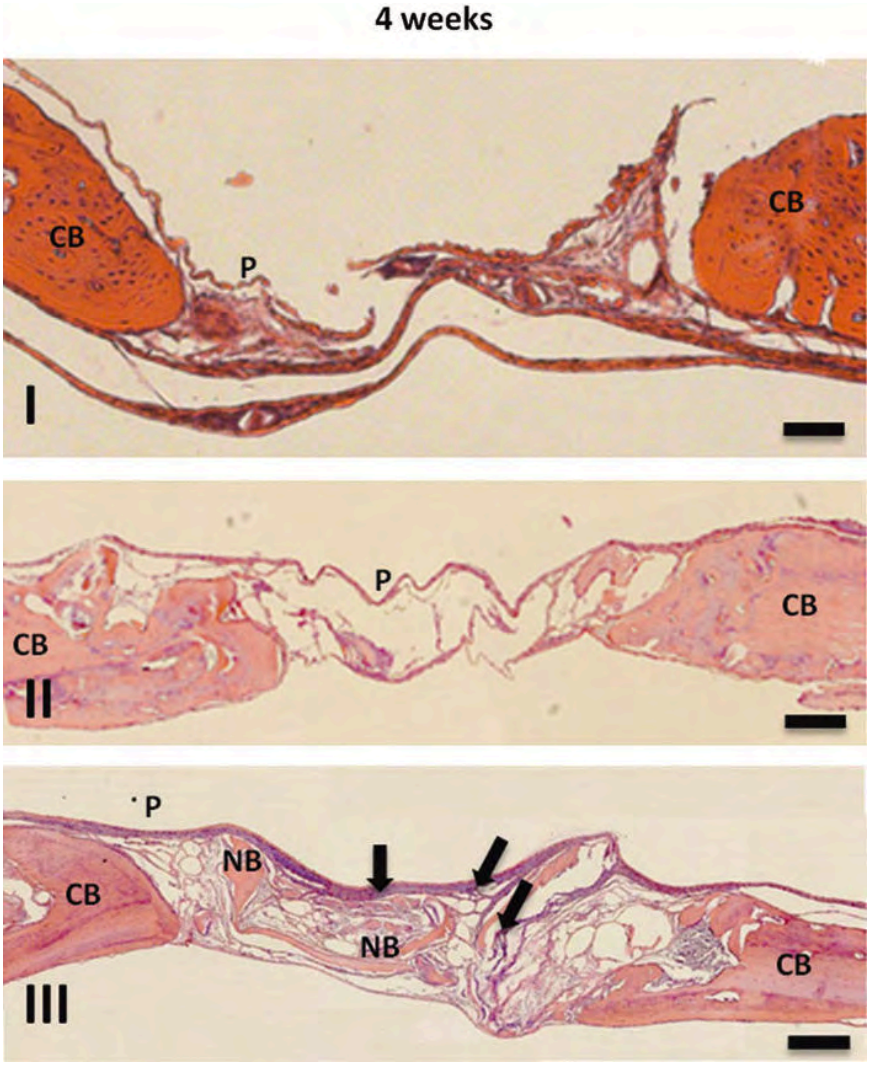

Figure 8.12. Hematoxylin and eosin stained histological images of calvaria defects at 4 weeks: empty control group (I), defects filled with beads loaded with FN (II), and beads loaded with FN and rMSCs (III). The black arrows represent the deposition of osteoblasts and formation of circular bone pieces. CB, compact bone; NB, new bone; P, periosteum. Scale bar 200 μm.

8.5. Conclusions

The present work evaluated the efficiency of an innovative methodology for the encapsulation of unstable bioactive molecules and cell immobilization in hydrogel spheres to be used in tissue engineering strategies. The use of superhydrophobic PS substrates allowed the production of biocompatible calcium crosslinked alginate beads with viable rMSCs entrapped. This methodology avoided important disadvantages exhibited by conventional encapsulation techniques, such as mechanical forces, particles aggregation, cell and bioactive molecules loss, and wet conditions. The application of the hybrid alginate beads for bone regeneration was evaluated under *in vitro* and *in vivo* conditions, and the results showed that the synergy effect between FN and rMSCs was crucial for bone regeneration. The ALG beads have good permeability for nutrients and O_2, which provides to the cells optimal conditions to survive for at least 21 days. In

addition, the encapsulation of the cells allowed their fixation in a proper site of the damaged tissue, avoiding the possibility of cells being removed by the blood stream. Moreover, the rMSCs were released at the same time of alginate degradation, constituting an advantage since it allowed the continuous bone regeneration without cell loss.

8.6. Acknowledgments

The authors acknowledge the financial support of the Portuguese Foundation for Science and Technology (PTDC/EME-TME/103375/2008 and PTDC/EBB-BIO/114320/2009) for the PhD fellowship to Ana Catarina Lima (SFRH/BD/71395/2010), A. Sofia Silva (SFRH/BD/51584/2011), and Patricia Batista (SFRH/BD/45511/2008).

8.7. References

[1] Ma H. -L., Hung S. -C., Lin S. -Y., Chen Y. -L., and Lo W. -H. Chondrogenesis of human mesenchymal stem cells encapsulated in alginate beads, Journal of Biomedical Matererials Research Part A 2003, 64A: 273-281.

[2] Steinert A., Weber M., Dimmler A., Julius C., Schütze N., Nöth U., Cramer H., Eulert J., Zimmermann U., and Hendrich C., Chondrogenic differentiation of mesenchymal progenitor cells encapsulated in ultrahigh-viscosity alginate, Journal of Orthopedic Research 2003, 21: 1090-1097.

[3] Pittenger M. F., Mackay A. M., Beck S. C., Jaiswal R. K., Douglas R., Mosca J. D., Moorman M. A., Simonetti D. W., Craig S., and Marshak D. R., Multilineage potential of adult human mesenchymal stem cells, Science 1999, 284: 143-7.

[4] Pereira D. R., Silva-Correia J., Caridade S. G., Oliveira J. T., Sousa R. A., Salgado A. J., Oliveira J. M., Mano J. F., Sousa N., and Reis R. L., Development of gellan gum-based microparticles/hydrogel matrices for application in the inter- vertebral disc regeneration, Tissue Engineering Part C Methods 2011, 17: 961-72.

[5] Costa N. L., Sher P., and Mano J. F., Liquefied capsules coated with multilayered polyelectrolyte films for cell immobilization, Advanced Engineering Materials 2011, 13: B218-24.

[6] Hu M., Kurisawa M., Deng R., Teo C. -M., Schumacher A., Thong Y. -X., Wang L., Schumacher K. M. and Ying J. Y., Cell immobilization in gelatin-hydroxyphenylpropionic acid hydrogel fibers, Biomaterials 2009, 30: 3523-31.

[7] Vermonden T., Fedorovich N. E., van Geemen D., Alblas J., van Nostrum C. F., Dhert W. J. A. and Hennink W. E., Photopolymerized thermosensitive hydrogels: synthesis, degradation, and cytocompatibility, Biomacromolecules 2008, 9: 919-26.

[8] Orive G., Hernandez R. M., Gascon A. R., Calafiore R., Chang T. M. S., Vos P. D., Hortelano G., Hunkeler D., Lacik I., Shapiro A. M. J. and Pedraz J. L., Cell encapsulation: promise and progress, Nature Medicine 2003, 9: 104-7.

[9] Hunt N. and Grover L., Cell encapsulation using biopolymer gels for regenerative medicine, Biotechnology Letters 2010, 32: 733-42.

[10] Joki, T., Machluf M., Atala A., Zhu J., Seyfried N. T., Dunn I. F., Abe T., Carroll R. S. and Black P. M., Continuous release of endostatin from microencapsulated engineered cells for tumor therapy, Nature Biotechnology 2001, 19: 35-9.

[11] Chang T. M. S., Therapeutic applications of polymeric artificial cells, Nature Reviews Drug Discovery 2005, 4: 221-35.

[12] Silva G. A., Ducheyne P. and Reis R. L., Materials in particulate form for tissue engineering. 1. Basic concepts, Journal of Tissue Engineering and Regenerative Medicine 2007, 1: 4-24.

[13] Oliveira M. B. and Mano J. F., Polymer-based microparticles in tissue engineering and regenerative medicine, Biotechnology Progress 2011, 27: 897-912.

[14] Mano J. F., Silva G. A., Azevedo H. S., Malafaya P. B., Sousa R. A., Silva S. S., Boesel L. F., Oliveira J. M., Santos T. C., Marques A. P., Neves N. M. and Reis R. L., Natural origin biodegradable systems in tissue engineering and regenerative medicine: present status and some moving trends, Journal of the Royal Society Interface 2007, 4; 999-1030.

[15] Grellier M., Granja P. L., Fricain J. -C., Bidarra S. J., Renard M., Bareille R., Bourget C., Amédée J. and Barbosa M. A., The effect of the co-immobilization of human osteoprogenitors and endothelial cells within alginate microspheres on mineralization in a bone defect, Biomaterials 2009, 30: 3271-8.

[16] Endres M., Wenda N., Woehlecke H., Neumann K., Ringe J., Erggelet C., Lerche D. and Kaps C. Microencapsulation and chondrogenic differentiation of human mesenchymal progenitor cells from subchondral bone marrow in Ca-alginate for cell injection, Acta Biomaterialia 2010, 6: 436-44.

[17] Bidarra S. J., Barrias C. C., Barbosa M. A., Soares R. and Granja P. L., Immobilization of human mesenchymal stem cells within RGD-grafted alginate microspheres and assessment of their angiogenic potential, Biomacromolecules 2010, 11: 1956-64.

[18] Goren A., Dahan N., Goren E., Baruch L. and Machluf M., Encapsulated human mesenchymal stem cells: a unique hypoimmunogenic platform for long-term cellular therapy, FASEB Journal 2010, 24: 22-31.

[19] Hernández R. M., Orive G., Murua A. and Pedraz J. L., Microcapsules and microcarriers for in situ cell delivery, Advanced Drug Delivery Reviews 2010, 62: 711-30.

[20] Mosahebi A., Wiberg M. and Terenghi G., Addition of fibronectin to alginate matrix improves peripheral nerve regeneration in tissue-engineered conduits, Tissue Engineering 2003, 9, 209-18.

[21] Tsai K. -S., Kao S. -Y., Wang C. -Y., Wang Y. -J., Wang J. -P. and Hung S. -C., Type I collagen promotes proliferation and osteogenesis of human mesenchymal stem cells via activation of ERK and Akt pathways, Journal of Biomedical Materials Research Part A 2010, 94A: 673-82.

[22] Alsberg E., Anderson K. W., Albeiruti A., Franceschi R. T. and Mooney D. J., Cell-interactive alginate hydrogels for bone tissue engineering, Journal of Dental Research 2001, 80: 2025-9.

[23] Augst A. D., Kong H. J. and Mooney, D. J., Alginate hydrogels as biomaterials, Macromolecular Bioscience 2006, 6: 623-33.

[24] Lima A. C., Sher P. and Mano J. F., Production methodologies of polymeric and hydrogel particles for drug delivery applications, Expert Opinion on Drug Delivery 2012, 9: 231-48.

[25] Khademhosseini A. and Langer R., Microengineered hydrogels for tissue engineering, Biomaterials 2007, 28: 5087-92.

[26] Song W., Lima A. C. and Mano J. F., Bioinspired methodology to fabricate hydrogel spheres for multi-applications using superhydrophobic substrates, Soft Matter 2010, 6: 5868-71.

[27] Lima A. C., Song W., Blanco-Fernandez B., Alvarez-Lorenzo C. and Mano J. F., Synthesis of temperature-responsive dextran-MA/PNIPAAm particles for controlled drug delivery using superhydrophobic surfaces, Pharmaceutical Research 2011, 28: 1294-305.

[28] Xu S., De Becker A., Van Camp B., Vanderkerken K. and Van Riet I., An improved harvest and in vitro expansion protocol for murine bone marrow-derived mesenchymal stem cells, Journal of Biomedicine and Biotechnolology 2010, 2010: 105940.

[29] Wang Y., Liu J., Xu C., Zhang W., Bai L., Li N., Liu Y., Wang Y., Su Y. and Hu D., Bone marrow transplantation combined with mesenchymal stem cells induces immune tolerance without cytotoxic conditioning, Journal of Surgical Research 2011, 171: e123-31.

[30] Soleimani M. and Nadri S., A protocol for isolation and culture of mesenchymal stem cells from mouse bone marrow, Nature Protocols 2009, 4: 102-6.

[31] Novikova L. N., Mosahebi A., Wiberg M., Terenghi G., Kellerth J. -O. and Novikov L. N., Alginate hydrogel and matrigel as potential cell carriers for neurotransplantation, Journal of Biomedical Materials Research Part A 2006, 77A: 242-52.

[32] Coimbra P., Alves P., Valente T. A. M., Santos R., Correia I. J. and Ferreira P. Sodium hyaluronate/chitosan polyelectrolyte complex scaffolds for dental pulp regeneration: synthesis and characterization, International Journal of Biological Macromolecules 2011, 49: 573-9.

[33] Fotakis G. and Timbrell J. A., In vitro cytotoxicity assays: comparison of LDH, neutral red, MTT and protein assay in hepatoma cell lines following exposure to cadmium chloride, Toxicology Letters 2006, 160: 171-7.

[34] Jin C., Kaewintajuk K., Jiang J., Jeong W., Kamata M., Kim H. -S., Wataya Y. and Park H., Toxoplasma gondii: a simple high-throughput assay for drug screening in vitro, Experimental Parasitology 2009, 121: 132-6.

[35] Vater C., Kasten P. and Stiehler M., Culture media for the differentiation of mesenchymal stromal cells, Acta Biomaterialia 2011, 7: 463-77.

[36] Franco C. L., Price J. and West J. L., Development and optimization of a dual-photoinitiator, emulsion-based technique for rapid generation of cell-laden hydrogel microspheres, Acta Biomaterialia 2011, 7: 3267-76.

[37] Tai B. C., Wan A. C. and Ying J. Y., Modified polyelectrolyte complex fibrous scaffold as a matrix for 3D cell culture. Biomaterials 2010, 31: 5927-35.

[38] Herrero E. P., Dell Valle E. M. and Galán M. A., Immobilization of mesenchymal stem cells and monocytes in biocompatible microcapsules to cell therapy, Biotechnology Progress 2007, 23: 940-5.

[39] Toworfe G. K., Bhattacharyya S., Composto R. J., Adams C. S., Shapiro I. M. and Ducheyne P., Effect of functional end groups of silane self-assembled monolayer surfaces on apatite formation, fibronectin adsorption and osteoblast cell function, Journal of Tissue Engineering and Regenerative Medicine 2009, 3: 26-36.

[40] Keselowsky B. G., Bridges A. W., Burns K. L., Tate C. C., Babensee J. E., LaPlaca M. C. and García A. J., Role of plasma fibronectin in the foreign body response to biomaterials, Biomaterials 2007, 28: 3626-31.

[41] Zhao L., Weir M. D. and Xu H. H., Human umbilical cord stem cell encapsulation in calcium phosphate scaffolds for bone engineering, Biomaterials 2010, 31: 3848-57.

[42] Hunt N. C., Shelton R. M. and Grover L., An alginate hydrogel matrix for the localised delivery of a fibroblast/keratinocyte co-culture, Biotechnology Journal 2009, 4: 730-7.

[43] Hunt N. C., Smith A. M., Gbureck U., Shelton R. M. and Grover L. M., Encapsulation of fibroblasts causes accelerated alginate hydrogel degradation, Acta Biomaterialia 2010, 6: 3649-56.

[44] Bajpai S. K. and Sharma S., Investigation of swelling/degradation behaviour of alginate beads crosslinked with Ca^{2+} and Ba^{2+} ions, Reactive and Functional Polymers 2004, 59: 129-40.

[45] Drury J. L., Dennis R. G. and Mooney D. J., The tensile properties of alginate hydrogels, Biomaterials 2004, 25: 3187-99.

[46] Peacock M., Calcium metabolism in health disease, Clinical Journal of the American Society of Nephrology 2010, 5: S23-30.

[47] Zhou H. and Xu H. H., The fast release of stem cells from alginate-fibrin microbeads in injectable scaffolds for bone tissue engineering, Biomaterials 2011, 32, 7503-13.

[48] Oreffo R. O. and Triffitt J. T., Future potentials for using osteogenic stem cells and biomaterials in orthopedics, Bone 1999, 25: 5S-9S.

[49] Martins A. M., Alves C. M., Reis R. L., Mikos A. G. and Kasper F. K., Toward osteogenic differentiation of marrow stromal cells and in vitro production of mineralized extracellular matrix onto natural scaffolds. Biological Interactions on Materials Surfaces. New York: Springer 2009, pp. 263–281.

[50] Evangelista M. B., Hsiong S. X., Fernandes R., Sampaio P., Kong H. -J., Barrias C. C., Salema R., Barbosa M. A., Mooney D. J. and Granja P. L., Upregulation of bone cell differentiation through immobilization within a synthetic extracellular matrix, Biomaterials 2007, 28, 3644-55.

[51] Abbah S. A., Lu W. W., Chan D., Cheung K. M., Liu W. G., Zhao F., Li Z. Y., Leong J. C. and Luk K. D., In vitro evaluation of alginate encapsulated adipose-tissue stromal cells for use as injectable bone graft substitute, Biochemical and Biophysical Research Community 2006, 347: 185-91.

[52] Keshaw H., Forbes A., and Day R. M., Release of angiogenic growth factors from cells encapsulated in alginate beads with bioactive glass, Biomaterials 2005, 26: 4171-9.

[53] Penolazzi L., Tavanti E., Vecchiatini R., Lambertini E., Vesce F., Gambari R., Mazzitelli S., Mancuso F., Luca G., Nastruzzi C. and Piva R., Encapsulation of mesenchymal stem cells from Wharton's jelly in alginate microbeads, Tissue Engineering Part C 2010, 16: 141-55.

[54] Lee C. S., Moyer H. R, Gittens R. A, Williams J. K., Boskey A. L., Boyan B. D. and Schwartz Z., Regulating in vivo calcification of alginate microbeads, Biomaterials 2010, 31: 4926-34.

Chapter 9

Biomimetic Methodology to Produce Polymeric Multilayered Particles for Biotechnological and Biomedical Applications

9.1. Introduction

Polymeric particles can serve as versatile carriers/containers of a variety of active substances and even cells for a wealth of applications, including drug therapy, tissue engineering and biotechnology [1-4]. Strategies to optimize their performance for a specific application are mostly based on adjusting the chemistry and the structural architecture by means of increasingly sophisticated designs, which in the particular case of drug release try to overcome the short diffusion path [5-7]. Multi-compartmentalized particles are envisioned to offer simultaneous release of various bioactive agents at different kinetics that can fulfill the therapeutic demands of multifactor diseases and regenerative processes [8-10]. Specifically, multilayered particles exhibiting predefined diameter and layers thickness may offer high drug loading, improved drug stability, and programmable drug release schedules, such as delayed or pulsate, avoiding burst phenomena [3,11]. They can also incorporate diverse bioactive agents isolated from each others in every single particle. However, most methodologies suitable to produce multilayered particles, namely emulsion solvent evaporation [8,12], dip coating (including capsules obtained by layer-by-layer technique) [5], spray-drying [13,14], coaxial ultrasonic atomization [15], multi-step interrupted gelation [16], and precision particle fabrication [6], involve the production/hardening of the particles in a liquid or aggressive environments, with the inherent risk of that a relevant fraction of the bioactive molecules to be loaded may be lost [1]. Moreover, these methods employ harsh conditions (organic solvents, extreme temperatures, mechanical stress, pressures) that prevent their use for the encapsulation of cells, proteins or other unstable molecules [13,17]. Even in the mentioned particle fabrication technologies, the production of triple or more layered systems is challenging and until now a very few applications of such complex particles were reported.

This chapter is based on the following publication:
Lima A.C., Custódio C. A., Alvarez-Lorenzo C. and Mano J. F., Biomimetic methodology to produce polymeric multilayered particles for biotechnological and applications, Small 2013, 9: 2487-92.

The absence of a simple methodology capable to produce multilayered particles under mild conditions, where cells and/or multiple molecules can be independently encapsulated with very high efficiency, was the main motivation of the present work.

9.2. Experimental Section

9.2.1. Materials

The copper (Cu) substrates were from a local hardware store; hydrochloric acid (HCl, 37%) was from Laborspirit; and ammonium hydroxide solution, 1H,1H,2H,2H-perfluorodecyltriethoxysilane (PFDTS), phosphate-buffered saline (PBS), dextran from *Leuconostoc mesenteroides* (MW 100–200 kDa), rhodamine B isothiocyanate (RhoB), fluorescein-5(6)-isothiocyanate (FITC), 4,6-diamidino-2-phenyindole dilactate (DAPI), Dulbecco's modified Eagle's medium (DMEM), sodium alginate were from Sigma- Aldrich Co. Calcein AM was from Invitrogen; propidium iodide (PI) from Alfagene; MTS and calcium chloride ($CaCl_2$) from VWR. All chemicals were used as received.

9.2.2. Fabrication of Copper Superhydrophobic Surfaces

Cu superhydrophobic surfaces were prepared by a chemical-base deposition method [18,19]. Briefly, Cu commercial substrates previously cleaned with 1 M HCl were immersed in ammonium hydroxide aqueous solution (0.03M, pH 9–10) at 4 °C. After 5 days the surfaces were collected, washed with water and completely dried in air. Finally, the Cu plates were immersed in a PFDTS solution (1% v/v) in ethanol during at least 24 h, and then dried in air.

9.2.3. Dextran Modification

Dextran (DEX) was modified as previously described [19]. Briefly, DEX (25 g) was dissolved in DMSO (225 mL) under nitrogen atmosphere to prevent oxidation. After dissolution of 4-(N,N-dimethylamino)pyridine (5 g), glycidyl methacrylate (20.5 mL) was added. The solution was stirred at room temperature for 48 h, and then the reaction was stopped by adding an equimolar amount of concentrated HCl (37% w/w) solution to neutralize 4-(*N,N*-dimethylamino)pyridine. The reaction mixture was transferred to a dialysis tube (MWCO 12400 Da) and dialyzed during 1 month against deionized water. Finally, DEX-MA was lyophilized (Manifold freeze-drier, Telstar cryodos, Spain).

9.2.4. Fabrication of Bi- and Tri-Layered Particles for Drug Release Applications

Particles were produced following the scheme shown in Figure 9.1 (A1, B1 and C1). 15% (w/v) DEX-MA was dissolved in distilled water containing 0.5% (w/v) of Irgacure 2959. For each layer a specific dye was added to the solution: DAPI, RhoB, and FITC (50 μg/mL). For the internal layer (core), 2 μL of DEX-MA+DAPI solution was dispensed onto the Cu superhydrophobic surface and irradiated with UV light (15 W/cm^2) for 30 s (Omnicure series 2000 EXFO S2000-XLA). After, 4 μL of DEX-MA+RhoB solution was dispensed in the top of each previously prepared sphere and again irradiated with UV light for 30 s under the conditions reported above. For the third layer, 6 μL of DEX-MA+FITC was dispensed and one more time the particles where irradiated with UV light. In each processing step, particles were visualized in fluorescent microscope (Stemi 1000 PG-HITEC Zeiss) with blue, green and red filters.

9.2.5. Drug Release Experiments

RhoB was used as a model of low molecular weight drug. Two groups of particles were prepared with: (i) RhoB immobilized in the most external layer of the particles and (ii) RhoB immobilized in the core of the particles. After being crosslinked, 4 particles were suspended in 1mL of PBS, pH 7.4, at 37 °C and the system kept under oscillatory stirring at 60 rpm for 6 h. Aliquots of 200 μL were collected at predetermined time intervals, and the same volume of fresh medium was added to the solution in order to maintain the initial volume. Three independent experiments were performed. The fluorescence of the samples was analyzed (λ_{exc} = 540 nm; λ_{em} = 573 nm) in a microplate reader (Bio-Tek, USA). Calculations of the amount of drug released took into account the replacement of aliquots with fresh medium. The release profiles were fitted to the square-root kinetics in the 10 to 60% amount released interval, taking into account the lag time [31]:

$$M_t/M_\infty = k(t - t_{lag})^{0.5} \quad \text{Eq.1}$$

where M_t and M_∞ represent the amount of RhoB released at time t and the initial content in the particles, and t_{lag} the lag time between the start of the experiment and the detection of drug released.

9.2.6. Fabrication of Bi-layered Particles for Cell Immobilization

Cores were prepared using a 2% (w/v) DEX-MA solution in water containing 5% (w/v) of $CaCl_2$ and 0.5% (w/v) of VA-086 or 0.25% (w/v) of Irgacure 2959. 2 μL of this solution was dispensed on Cu superhydrophobic surface and irradiated with UV light (15 W/cm^2) for 60 s. An immortalized mouse lung

fibroblast cell line (L929) purchased from European Collection of Cells Cultures (ECACC) was suspended in 2% (w/v) sodium alginate solution, and 6 μL of this suspension were dispensed on the top of DEX-MA cores in order to have a density of 2000–3000 cells/particle. The diffusion of $CaCl_2$ from the core of the particle allowed the gelation of the alginate external layer. After 10 min the particles were immersed in 1 mL of PBS for 10 min to remove the surplus of $CaCl_2$ and the free radicals resultant of the non reacted photoinitiator. Particles were incubated at 37 °C for 3 days in complete DMEM in a humidified atmosphere of 5% CO_2.

9.2.7. Alizarin Red Staining

The release of Ca^{2+} from DEX-MA particles crosslinked using VA-086 photoinitiator was analyzed in order to gain an insight into the crosslinking of the alginate external layer. Freshly prepared DEX-MA particles as well as washed (20 min in water) DEX-MA particles were stained with a 40 mM alizarin red solution at pH 4.3. The particles were then observed using a stereomicroscope (Stemi 1000 PG-HITECH, Zeiss).

9.2.8. Cell Viability, Morphology and Distribution

The viability of the cells encapsulated in cell-loaded bi-layered particles was evaluated at various times by means of the 3-(4,5-dimethylthiazol-2-yl)-5-(3-carboxymethoxy-phenyl)-2-(4-sulphophenyl)-2H-tetrazolium (MTS) assay. Briefly, after each time period, fresh culture media without phenol red was added to the particles with cells. MTS was used in a 5:1 ratio to the culture medium and incubated with the particles for 3 h (37 °C, 5% CO_2). After the incubation period, the optical density (OD) was read at 490 nm in a microplate reader (Bio-Tek, USA). Particles without cells were used as controls in order to verify that the materials do not react with MTS. Common 2D control (cells not exposed to particles) was not carried out since cells encapsulated in a 3D system are known to proliferate at different rate, leading to non comparable MTS results.

After each period of culturing in standard conditions, cell viability was also assessed by staining the cell-loaded bi-layered particles with Calcein AM/PI solution. Particles were incubated at 37 °C with 2 μL of Calcein AM (1 mg/mL) diluted in DMEM without phenol red. After 10 min, the Calcein AM solution was removed and the particles were washed with PBS. 1 μL of PI (1 mg/mL) diluted in PBS was added to the particles and incubated for 5 min at room temperature protected from the light. The particles were collected, washed with PBS and visualized in fluorescence microscope (Stemi 1000 PG-HITEC Zeiss) with appropriate filters to detect green (live) and red (dead) stained cells. Phalloidin and DAPI staining to visualize actin cytoskeleton and to label the DNA, respectively, were conducted as outlined by the supplier's protocol (Sigma, Germany). Briefly, the particles were washed with PBS, fixed in freshly pre- pared 4% (v/v) of formaldehyde

in PBS for 15 min at room temperature and washed extensively in PBS to remove traces of the fixative. The cells were then stained with 50 μg/mL fluorescent phalloidin-conjugate solution in PBS for 45 min at room temperature. DAPI labelling solution (0.5 μg/mL) was incubated for 3 min at room temperature. The particles were washed in PBS to remove remaining staining solutions, and imaged using Olympus FluoView FV 1000 confocal laser microscope in order to visualize cell morphology and distribution inside the particles outside layers.

9.2.9. Statistical Analysis

All data are presented as mean ± s.d. for at least three independent measurements. Assessment of normality distribution of the population was performed by Shapiro-Wilk test. Groups were compared using one-way ANOVA (Tukey's multiple comparison test), with $p < 0.05$ indicating statistical significance.

9.3. Results and Discussion

Here we report the development of a simple biomimetic strategy, inspired by the rolling of water droplets onto the superhydrophobic surfaces of some plant leaves, to prepare compartmentalized multilayered polymeric spherical particles. Mimicking the micro and nano hierarchical structure and the low surface free energy of Lotus leaf, superhydrophobic surfaces were obtained by a chemical-based deposition method using copper substrates [18]. These surfaces were already characterized in a previous work [19]. Droplets of aqueous solutions of polymeric precursors containing bioactive agents (drugs, enzymes, pesticides, flavors, odors, or other type of molecules) or cells (eukaryotic and prokaryotic) can be dispensed onto such superhydrophobic surfaces with well-defined volumes, maintaining a close spherical geometry and a negligible contact area with the substrate due to the surface roughness. The size of the particles can be finely tuned by the volume of polymeric precursor solution dispensed [20]. Crosslinking and/or solvent evaporation under mild conditions renders spherical particles. The use of a fast liquid dispensing system and well-known crosslinking routes should permit the scale-up production of particles. Subsequent deposition of liquid droplets onto the preformed spherical particles followed by crosslinking with a suitable agent renders the first coating layer. Repetition of this process (with the same/different volume/composition of the droplets) leads to multilayer structures. The number of layers is limited by the particle deformation when the size increases and the effect of the gravity is stronger than the superhydrophobic capacity of the surface [21]. A remarkable advantage of the proposed technique is that high encapsulation efficiencies (≈100%) of non-volatile molecules can be achieved under mild conditions because each particle layer solidifies surrounded by air (not by a liquid solvent), avoiding the possibility of

molecules migration from the inner of the particle to the surrounding environment. Moreover, these particles can be concomitantly loaded with a sequence of different cell types or molecules confined in individual layers that can be tailor-crosslinked in order to endow the resultant particles with a notable physical stability. For drug delivery applications, non-loaded polymeric layers may be added with the aim to act as a barrier to control the release of drugs immobilized in the previous layers.

Two main approaches were explored in this work: (i) the preparation of multilayered hydrogel particles (onion-like structure) for sequential release of multiple molecules, and (ii) the preparation of bilayered particles composed by different hydrogels to immobilize living animal cells in the outer layer and bioactive molecules in the core for possible applications in cell therapies. The resultant particles in the micro- to milli-meter range could be suitable for topical and oral drug delivery, wound healing and for a variety of other biomedical applications, including tissue engineering scaffolds, cell reservoirs to implant inside damaged tissues and organ printing [11,22-27].

For the proof-of-concept dextran-based multilayered particles were prepared containing three different fluorophores (DAPI, RhoB and FITC; simulating low molecular weight drugs) in the different concentric layers. Dextran was modified previously by adding methacrylic groups in the polymer structure (DEX-MA) to enable the crosslinking under UV exposure for the minimum time and the lowest power, in order to avoid the fluorophores photobleaching phenomena. Through the proposed bottom-up procedure, multilayered hydrophilic particles (with a narrow particle size distribution) were obtained (Figure 9.1 A1, B1 and C1). Fluorescent microscope images of mono- (Figure 9.1 A2), bi- (Figure 9.1 B2, B3 and B4) and tri-layered (Figure 9.1 C2) DEX-MA based particles evidenced the separate distribution of the different dyes. The simultaneous emission of fluorophores spectra confirmed the successful immobilization of up to 3 dyes in independent compartments in the same particle (Figure 9.1 C2). The thickness of one specific layer was finely tuned by controlling the volume of the polymeric solution dispensed (Figure 9.1 B2, B3 and B4). Depositing droplets of 2, 4 or 6 μL onto preformed cores (first layer of 2 μL rendered core diameter=1355±41 μm; n=3) resulted in particles of increasing sizes (Figure 9.1 B5). The layer thickness could be also kept almost constant by progressively increasing the volume of the deposited droplets, due to the crescent particle surface area. Measurements of the thickness of each layer in four distinct points rendered similar values (small standard deviation), which means that the distribution of the polymeric precursor solution around each previously crosslinked layer occurred homogeneously. In addition, the low standard deviation values corresponding to the core particle size indicates that this methodology is capable to produce particles with a narrow size distribution. Dual and triple-layered DEX-MA particles

showed high stability and did not evidence layer separation after 6 h in the release medium under oscillatory stirring.

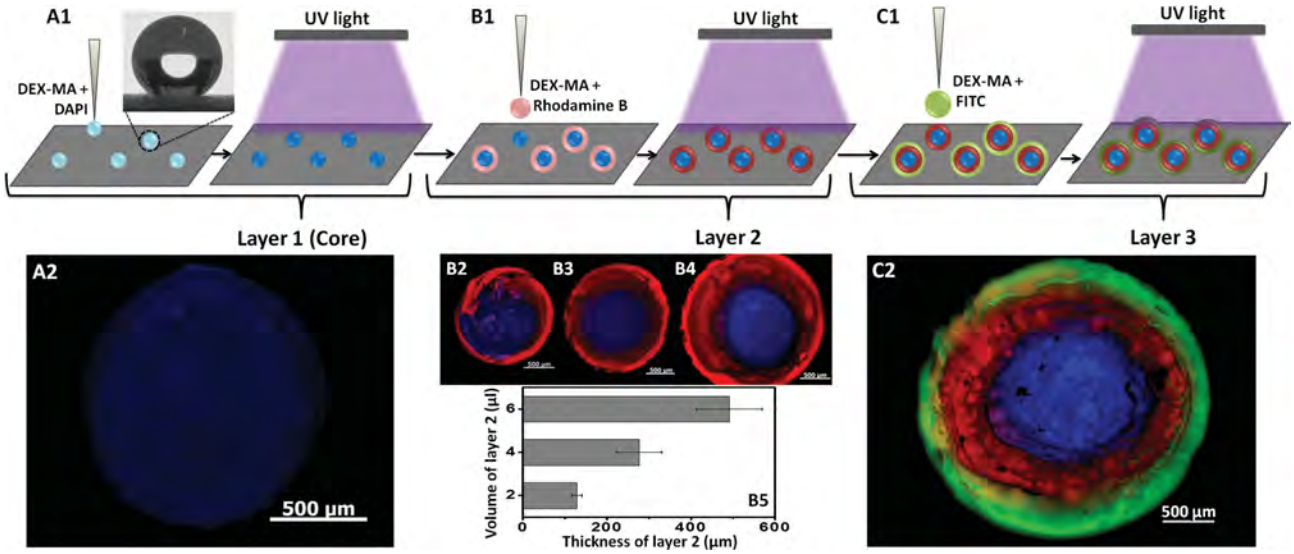

Figure 9.1. Biomimetic approach using copper superhydrophobic surfaces to produce multilayered particles: (A1) the core (Layer 1) is produced dispensing 2 µL of DEX-MA+DAPI solution onto the superhydrophobic surface and then crosslinking by UV light exposure; (B1) the follow layer (Layer 2) is obtained dispensing µL of DEX-MA+Rhodamine B solution around the previous obtained particle and again crosslinking by UV light exposure; and (C1) the third layer (Layer 3) is obtained following the same procedure but using 6 µL DEX-MA+FITC solution. Fluorescent microscopic images (A2, B2, B3, B4 and C2) of the particles obtained in each step of the procedure; and (B5) thickness of the particle layers that where obtained by dispensing different volumes of polymeric precursor solutions in the second layer: 2 µL (B2), 4 µL (B3) and 6 µL (B4).

The loading efficiency of those particles is limited by the solubility of the bioactive agents in the polymer aqueous solution as also by the thickness of each layer. During the preparation process of polymeric particles using superhydrophobic surfaces, the loss of molecules that are desired encapsulate is not significant, as verified in a previous work [20] and we may say that this process have an encapsulation efficiency of 100%. The versatility of the process to permute the order of layers containing different molecules is shown in Figure 9.2 A. This could allow for a distinct release profile of the two sub- stances with an expectable delay of the one located in the inner side. This last statement was confirmed by combining non-loaded and RhoB-loaded layers in a single particle and monitoring the release for 6 h: Figure 9.2 B. This experimental design avoided the interferences that came up when simultaneous monitoring of the release of several fluorescent molecules was tried. The release of RhoB molecules was controlled varying the relative location of the layers; namely RhoB encapsulated in the outside layer of DEX-MA particles exhibited a relatively rapid release ($k=7.6\ min^{-0.5}$; s.d. 1.2, n=3), while the molecules

encapsulated in the core of the particles showed a lag time of 45 min and were released at much slower rate (k=2.1 $min^{-0.5}$; s.d. 0.1, n=3). Thus, the outside layer acts as a barrier allowing the control of the molecules release. In addition, these release profiles show that it is possible to encapsulate molecules in different particle compartments and their delivery may be time-programmed.

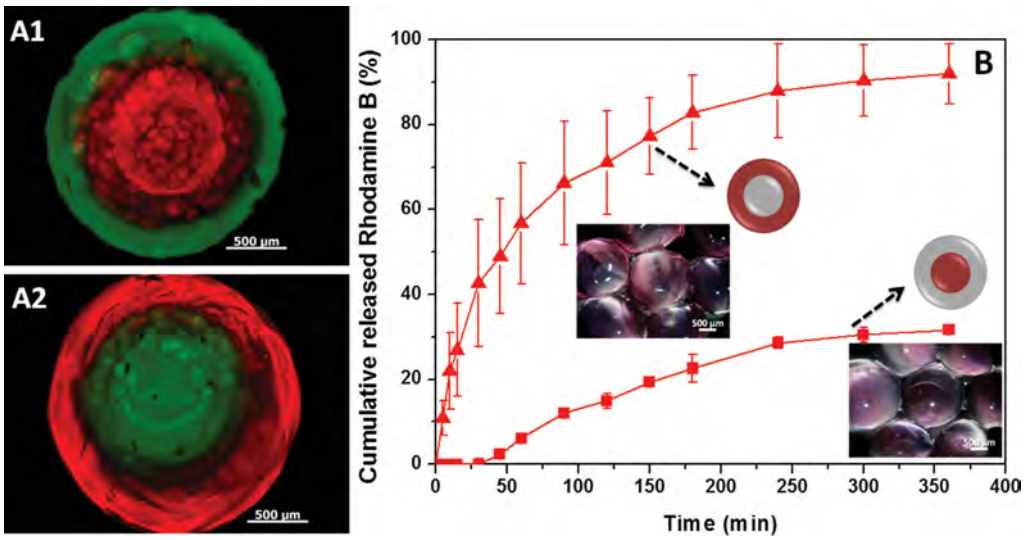

Figure 9.2. (A1 and A2) Bi-layered DEX-MA particles with red and green dyes immobilized in opposite positions; (B) *In vitro* release of Rhodamine B from 15% (w/v) bi-layered DEX-MA particles, where Rhodamine B was encapsulated on the external layer (triangles) and in the internal layer/core (squares).

The second approach explored dealt with the ability of these concentric multilayered systems to immobilize living animal cells in the external layers for possible applications in biomedical field, namely cell therapies through implantation. Such configuration may be useful in devices where the inner regions of the particles could act as reservoirs for bioactive or therapeutic substances that, after being released, could influence the behavior of the cells in the periphery or even of those in the surrounded tissues. In addition, the presence of the cells in the external layer of the particle facilitates the access to nutrients and O_2 and the clearance of cell metabolites. To demonstrate the potential of these particles, a bi-layered system was designed in which the core regions delivered calcium ions that crosslinked the outer alginate-based layer containing cells. In conventional processing methodologies, alginate beads may be obtained by external gelation (dipping of sodium alginate drops in $CaCl_2$ solution), internal gelation (water-insoluble calcium salt dispersed in the sodium alginate solution is triggered to act as crosslinker when the pH drops) or their combination [28]. These procedures are quite aggressive for cell encapsulation and could cause the loss of cell viability. Moreover, if drugs or proteins have to be concomitantly encapsulated, the wet environment may not ensure high encapsulation efficiency. Then, starting the polymer crosslinking

from the center of the particle to the surface, not requiring the acidification of the environment where the particles are being produced, represents an innovative engineered strategy to crosslink an alginate layer. $CaCl_2$ was encapsulated in DEX-MA cores and when a L929 cell suspension in sodium alginate was dispensed on the cores, the alginate solidified immediately creating the second layer: see Figure 8.3 (scheme A1 and A2). The surface of the DEX-MA core became hydrated due to the sodium alginate solution and the Ca^{2+} ions diffused immediately from the core to the layer 2 allowing the alginate crosslinking. As observed in Figure 8.3, our strategy is a mild procedure that allows the cell immobilization in alginate in an air environment and in a very fast way. The cell viability assays (Figures 8.3 B and C) showed that the cells remained viable for 3 days and were homogenously distributed on the external layer of the particle (Figure 8.3 D). To complete this study, two different photoinitiators were used to produce the solid DEX-MA core particles and their effect on cell viability was evaluated. As reported in the literature, chemical photoinitiators may be cytotoxic both in precursor and radical forms, and organic solvents maybe required to dissolve them in the polymer precursor solution [29]. In this work Irgacure 2959 (a well-known cytocompatible initiator) [29] and VA-086 were tested avoiding the use of organic solvents. Although Irgacure 2959 is described as a non water soluble photoinitiator, it could be dissolved up to 5 mg/mL (under stirring at 37 °C during 24 h). The minimal concentrations able to crosslink DEX-MA were used to prepare the core particles. MTS assays showed that the cells inside the particles produced using VA-086 had higher viability after 72 h in culture than those encapsulated over core particles crosslinked using Irgacure 2959. This means that for the same UV light exposure conditions, Irgacure 2959 probably generates more photodissociated radical species that diffused from the core of the particles to the shell where the cells were immobilized [29]. Moreover, in both conditions, cell viability decayed between 4 h and 24 h, probably, due to the cells needing a period of accommodation for new conditions within the hydrogel shell. After that time, their metabolic activity backs to normal [30].

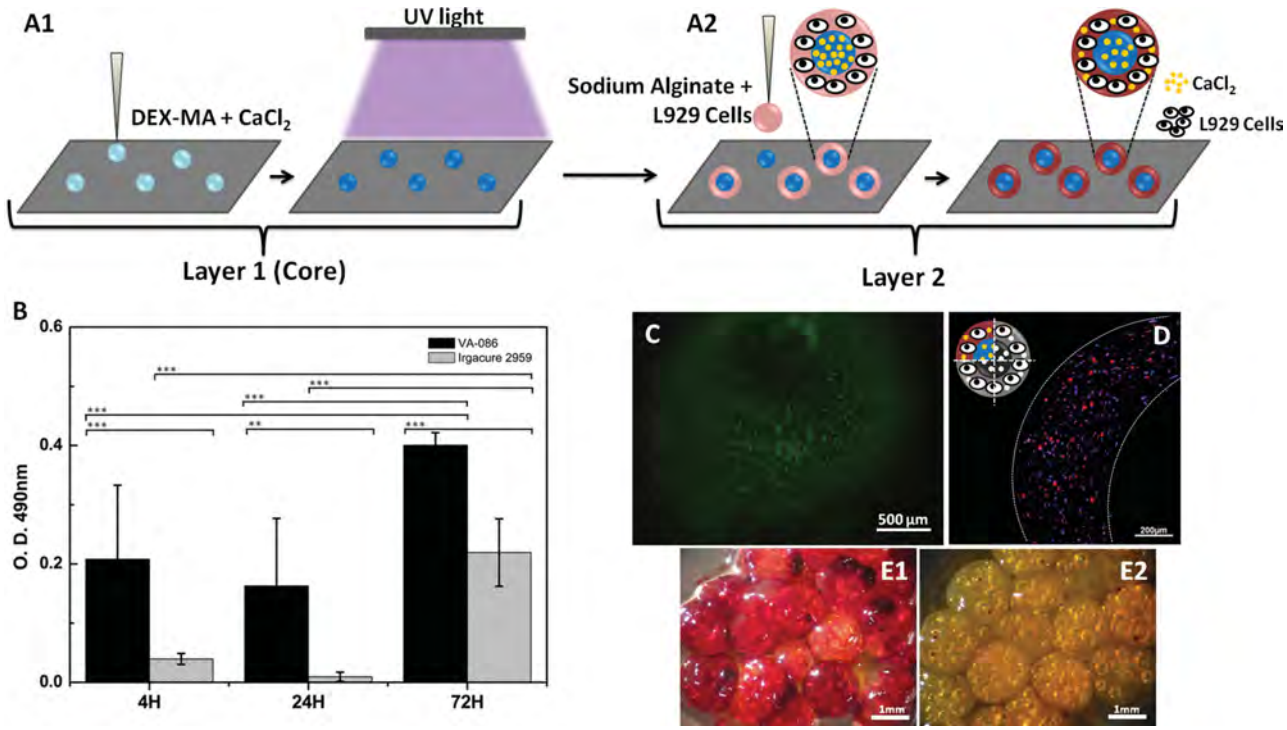

Figure 9.3. Bi-layered particles where cells were immobilized in the external layer: (A1) 2 µL of DEX-MA solution containing a photoinitiator and $CaCl_2$ was dispensed onto the superhydrophobic surface and then crosslinked under UV light; (A2) the external layer was obtained dispensing a L929 cell suspension in sodium alginate over the previously obtained particles. The release of the calcium immobilized in the cores allowed the crosslinking of the alginate layer; (B) MTS viability assay of bi-layered particles where the core was crosslinked with two different photoinitiators (Irgacure 2959 and VA-086) after 4 h, 24 h and 72 h of cell culture (mean values with standard deviations, n = 3; *** indicate significant differences between testing conditions as a function of time); (C) Fluorescent microscopy image of loaded particles where cells were stained with Calcein-AM and propidium iodide and cultured for 4 h; (D) confocal microscopy image of a quarter-circle of a bi-layered particles where cells were stained with DAPI (nucleus) and phalloidin (cytoskeletons) cultured for 4 h; (E1) and (E2) stereo microscope images of core particles stained with Alizarin red immediately after being produced and after being immersed in water for 20 min, respectively.

In order to confirm the release of $CaCl_2$ from the DEX-MA particles, alizarin red staining - a well-established test to identify calcium deposits - was applied to the core particles immediately after being produced and after immersion in water for 20 min (Figure 8.3 E1 and E2). The red color characteristic of calcium deposits was not observed in the particles after being immersed in water, meaning that calcium ions were rapidly released under wet conditions. This fast diffusion of calcium allowed the crosslinking of alginate. Minimal quantities of $CaCl_2$ were used and their release did not affect the cell viability after 72 h in culture. In principle, the developed methodology would allow the encapsulation of bioactive molecules, with important roles in cell behavior, to be released when implanted, avoiding the additional supplying of bioactive agents. This compartmentalized particle design allows the immobilization of different cell types

(co-cultures) or bioactive factors in distinct layers which may be particularly useful for complex tissues regeneration.

9.4. Conclusions

In sum, this work proposes a new methodology based on the use of superhydrophobic surfaces and the dispensing of controlled volumes of polymeric solutions to produce, under mild conditions, micro- to millimeter multilayered particles that could incorporate molecules or living cells with high efficiency, and with the potential to be used in a wide range of applications including cosmetics, pharmacy, agriculture, food technology and biomedicine. This simple procedure permits to obtain multilayered particles with controlled size and layer thicknesses of distinct materials which allow tailoring molecules release profiles and gathers appropriate conditions to support viable cells. If a particular application would require smaller particles, these hierarchical structures could be pre- pared using a dosing system to deliver smaller droplets.

9.5. Acknowledgements

The authors acknowledge the financial support from Fundação para a Ciência Tecnologia (FCT) through the PhD grants SFRH/BD/71395/2010 and SFRH/BD/61390/2009, Fundo Social Europeu (FSE) and Programa Operacional Potencial Humano (POPH) Portugal, and MICINN (SAF2011-22771 and PRI-AIBPT-2011-1211) Spain.

9.6. References

[1] Lima A. C., Sher P. and Mano J. F., Production methodologies of polymeric and hydrogel particles for drug delivery applications, Expert Opinion on Drug Delivery 2012, 9, 231-48.

[2] Oliveira M. B., Mano J. F., Polymer-based microparticles in tissue engineering and regenerative medicine, Biotechnology Progress 2011, 27: 897-912.

[3] Lee W. L., Yu P., Hong M., Widjaja E., Loo S. C. J., Designing multilayered particulate systems for tunable drug release profiles, Acta Biomaterialia 2012, 8: 2271-8.

[4] Tong W. and Gao C., Multilayer microcapsules with tailored structures for bio-related applications, Journal of Matererials Chemistry 2008, 18: 3799-812.

[5] De Cock L. J., De Koker S., De Geest B. G., Grooten J., Vervaet C., Remon J. P., Sukhorukov G. B., Antipina M. N., Polymeric multilayer capsules in drug delivery, Angewandte Chemie International Edition 2010, 49: 6954-73.

[6] Berkland C., Pollauf E., Pack D. W. and Kim K., Uniform double-walled polymer microspheres of controllable shell thickness, Journal of Controlled Release 2004, 96: 101-11.

[7] Jagur-Grodzinski J., Polymeric gels and hydrogels for biomedical and pharmaceutical applications, Polymers for Advanced Technologies 2010, 21: 27-47.

[8] Lee W. L., Widjaja E. and Loo S. C. J., One-step fabrication of triple-layered polymeric microparticles with layer localization of drugs as a novel drug-delivery system, Small 2010, 6, 1003-11.

[9] Delcea M., Yashchenok A., Videnova K., Kreft O., Möhwald H., Skirtach A. G., Multicompartmental Micro- and Nanocapsules: Hierarchy and Applications in Biosciences, Macromolecular Bioscience 2010, 10: 465-74.

[10] Zou Y., Brooks J. L., Talwalkar V., Milbrant T. A. and Puleo D. A., Development of an injectable two-phase drug delivery system for sequential release of antiresorptive and osteogenic drugs, Journal of Biomedical Materials Research Part B 2012, 100B: 155-62.

[11] Degim Z., Use of microparticulate systems to accelerate skin wound healing, Journal of Drug Targeting 2008, 16: 437-48.

[12] Koppolu B., Rahimi M., Nattama S., Wadajkar A. and Nguyen K. T., Development of multiple-layer polymeric particles for targeted and controlled drug delivery, Nanomedicine: Nanotechnology. Biology and Medicine 2010, 6: 355-61.

[13] Lee H. K., Park J. H. and Kwon K. C., Double-walled microparticles for single shot vaccine, Journal of Controlled Release 1997, 44: 283-93.

[14] Liu W., Wu W. D., Selomulya C. and Chen X. D., Facile Spray-Drying Assembly of Uniform Microencapsulates with Tunable Core–Shell Structures and Controlled Release Properties, Langmuir 2011, 27: 12910-5.

[15] Dalmoro A., Barba A. A., Lamberti G., d'Amore M., Intensifying the microencapsulation process: Ultrasonic atomization as an innovative approach, European Journal of Pharmaceutics and Biopharmaceutics 2012, 80: 471-7.

[16] Ladet S., David L. and Domard A., Multi-membrane hydrogels, Nature 2008, 452, 76-9.

[17] Akagi T., Baba M. and Akashi M., Biodegradable Nanoparticles as Vaccine Adjuvants and Delivery Systems: Regulation of Immune Responses by Nanoparticle-Based Vaccine, Advances in Polymer Science 2012, 247, 31-64.

[18] Yao X., Chen Q., Xu L., Li Q., Song Y., Gao X., Quéré D., Jiang L., Bioinspired Ribbed Nanoneedles with Robust Superhydrophobicity, Advanced Functional Materials 2010, 20, 656-62.

[19] Lima A. C., Song W., Blanco-Fernandez B., Alvarez-Lorenzo C. and Mano J. F., Synthesis of temperature-responsive dextran-ma/pnipaam particles for controlled drug delivery using superhydrophobic surfaces, Pharmaceutical Research 2011, 28, 1294-305.

[20] Song W., Lima A. C. and Mano J. F., Bioinspired methodology to fabricate hydrogel spheres for multi-applications using superhydrophobic substrates, Soft Matter 2010, 6: 5868-71.

[21] Extrand C. W. and Moon S. I., Contact angles of liquid drops on super hydrophobic surfaces: understanding the role of flattening of drops by gravity, Langmuir 2010, 26, 17090-9.

[22] Malafaya P. B., Pedro A. J., Peterbauer A., Gabriel C., Redl H. and Reis R. L., Chitosan particles agglomerated scaffolds for cartilage and osteochondral tissue engineering approaches with adipose tissue derived stem cells, Journal of Materials Science: Materials for Medicine 2005, 16: 1077.

[23] Malafaya P. B., Oliveira J. T. and Reis R. L., The effect of insulin-loaded chitosan particle-aggregated scaffolds in chondrogenic differentiation, Tissue Engineering Part A 2010, 16: 735-47.

[24] Miranda E. S., Silva T. H., Reis R. L. and Mano J. F., Nanostructured natural-based polyelectrolyte multilayers to agglomerate chitosan particles into scaffolds for tissue engineering, Tissue Engineering Part A 2011, 17, 2663-74.

[25] Sher P., Custódio C. A. and Mano J. F., Layer-By-Layer Technique for Producing Porous Nanostructured 3D Constructs Using Moldable Freeform Assembly of Spherical Templates, Small 2010, 6: 2644-8.

[26] Costa N. L. Sher P. and Mano J. F., Liquefied Capsules Coated with Multilayered Polyelectrolyte Films for Cell Immobilization, Advances Engineering Materials 2011, 13: B218-24.

[27] Mironov V., Visconti R. P., Kasyanov V., Forgacs G., Drake C. J., Markwald R. R., Organ printing: tissue spheroids as building blocks, Biomaterials 2009, 30: 2164-74.

[28] Schoubben A., Blasi P., Giovagnoli S., Rossi C. and Ricci M., Development of a scalable procedure for fine calcium alginate particle preparation, Chemical Engineering Journal 2010, 160, 363-9.

[29] Rouillard A. D., Berglund C. M., Lee J. Y., Polacheck W. J., Tsui Y., Bonassar L. J., Kirby B. J., Methods for photocrosslinking alginate hydrogel scaffolds with high cell viability, Tissue Eng. Part C-Methods 2011, 17: 173-9.

[30] Herrero E. P., Del Valle E. M. M., Galán M. A., Immobilization of mesenchymal stem cells and monocytes in biocompatible microcapsules to cell therapy, Biotechnology Progress 2007, 23, 940-5.

[31] Ford J. L., Mitchell K., Rowe P., Armstrong D. J., Elliott P. N. C., Rostron C., Hogan J., Mathematical modelling of drug release from hydroxypropylmethylcellulose matrices: Effect of temperature, International Journal of Pharmaceutics 1991, 71: 95-104.

Section IV

Concluding Remarks

Chapter 10

Conclusions and Future Perspectives

Biomimetic superhydrophobic surfaces inspired in the behavior and properties of lotus leaf demonstrated to be an adequate methodology to produce a variety of spherical-based hydrogel particles for biomedical applications. Simple homogeneous matrices and compartmentalized spherical systems were obtained in a fast way. This versatile technique allowed the production of particles with different diameters ranging from *ca.* 700 μm to *ca.* 3 mm. The volume dispensed on the top of the surfaces defined the size of the particles. Four different natural-based polymers crosslinked through adequate mild procures were used in the production of manageable particles. In each proposed system we were able to encapsulate cells, bioactive agents or a combination of both. The efficiency of encapsulation was very high (except in the chapter 5 where the particles were loaded after being produced) because the particles hardened in dry environments, avoiding the diffusion of the bioactive agents from the particles to the surrounded medium. The conditions to produce the particles were mild and did not compromise the viability of the cells and the activity of labile bioactive agents. In addition, the particles were obtained individually, no aggregation occurred during the processing and no mechanical forces (*e.g.* stirring) were applied to the particles. All the obtained systems under the scope of this thesis exhibited an almost spherical shape.

The first system proposed was successfully obtained by UV light exposure of a surface containing liquid droplets of a modified dextran and CDs. It was observed that the use of monomers of CDs (γ-CD-NMA) improved the general performance of the system, when compared with dextran solely particles and systems where the γ-CDs were free inside the dextran gels. The copolymerization of γ-CD-NMA increased the loading capacity of the particles in approximately 7 folds to a hydrophobic drug (dexamethasone), and sustained its release for at least 10 days. This strategy demonstrates that the difficulties associated to hydrophilic systems, as the case of hydrogel-based particles, in encapsulation of hydrophobic drugs may be overcome by integrating anchored CDs in the polymer network. This particulate system showed good

cytocompatibility and was effective in inducing the osteogenic differentiation of hASCs after 3-7 days, demonstrating potential to be used in bone regeneration strategies.

Another proposed system was based on chitosan. The mild conditions were obtained increasing the pH of the chitosan acidic solution by adding β-GP. The particles were successfully hardened following two steps: ionic crosslinking and temperature exposure. The obtained particles were pH sensitive and easy-to-handle after ionic crosslinking. In addition, under physiological temperatures the structure of the network was reinforced at mechanical level due to the attractive forces between chitosan chains caused by β-GP. Entrapped L929 cells in this hydrogel remained viable for 7 days. The dexamethasone-loaded particles released almost 70% of the total content into 2-3 h. For effective biomedical applications several improvements would be required, namely, a better control of the drugs release as well as the inclusion of anchorage sites in the hydrogel network for adherent cells. In this context, a third system was developed in this thesis by combining collagen as a structural support, PLs as a GFs source and hASCs. The application envisaged for this system was skin regeneration because in the particular case of ulcers, the new collagen formed during the healing process is immediately destroyed due to the high concentration of proteases, the cells died due to the absence of a support to adhere and proliferate, and angiogenesis is an issue due to a fast degradation of GFs. The presence of PLs in the proposed particulate system was crucial for the biological performance of the system in both explored cellular and acellular strategies. The particles obtained provided mild conditions for cell encapsulation and stimulated the hASCs adhesion and proliferation. A very interesting event occurred in the cell-laden gels: the cells were capable to migrate and establish cell-cell communications; consequently, a membrane composed by particles connected by cells was formed. Such membranes were easy-to-handle and could be straightforwardly implanted in the skin damaged sites. In the case of particles without cells the system was tested as *in situ* GFs release demonstrating great capacity to stimulate the hASCs proliferation and migration, and to induce the angiogenesis. The use of superhydrophobic surfaces and physiological temperatures to produce those particles constituted a very fast and mild strategy to obtain multifunctional systems without compromise the viability of the cells and the bioactivity of GFs, as well as without risk of lose GFs due to the dry environment where the particles hardened.

The last monocompartmentalized spherical system proposed was obtained by encapsulating a cell adhesive protein (FN) and MSCs. Alginate particles were prepared by ionic gelation, under a gaseous environment; both *in vitro* and *in vivo* tests were performed, namely the implantation in a bone defect created in the calvaria of rats. The FN entrapped into the particles increased the percentage of viable cells inside the particles. In addition, the results obtained, when the particles were implanted *in vivo,*

demonstrated that the presence of the cells was crucial for a more efficient regeneration of bone tissue. Similarly to the Coll+PL gels, alginate particles were hardened into 10-15 min, in mild conditions for cells and for the protein.

The versatility of the superhydrophobic surfaces methodology was extended to produce multicompartmentalized particles, through a bottom-up approach. Core/shell and multilayered particles were successfully obtained using photocrosslinkable dextran and alginate. Cells and bioactive agents were encapsulated into individual compartments in different proposed strategies. It was showed that such complex architectures were suitable for control temporally the release of a model drugs. The cells encapsulated in the external layer were maintained viable for at least 3 days.

The work developed herein showed that multiple systems, ranging from homogeneous monocompartmented matrices to multicompartmented architectures, might be produced using the superhydrophobic surfaces methodology. In addition, different materials to obtain the solid particles (dextran, chitosan, collagen, alginate) were used as well as different hardening processes (UV light irradiation, ionic crosslinking and temperature exposure). Regarding the content of the particles, also a variability of bioactive agents (small synthetic drugs, proteins and GFS) and cell types (cell lines and primary cells) were successfully entrapped in the hydrogel spherical matrices.

Although superhydrophobic surfaces had several abovementioned advantages when compared with conventional methodologies, this procedure also has some limitations that in the future have to be surpassed. The most obvious is the limitation to repeal just aqueous solutions; superhydrophobic surfaces are not capable to repeal organic solvents preventing the production of synthetic-based particles. The use of superamphiphobic surfaces instead of superhydrophobic may be a reasonable alternative. Other limitation refers to the minimal volume dispensed to produce the particles. Using a micropipette, volumes lower than 2 μL are not possible to be dispensed. In this sense, accurate and automatic systems to dispense droplets to prepare particles in the micro scale range are required and should be accompanied with the engineering of surfaces with lower-scale roughness. This technology demonstrate potential to be scaled up by a continuous mass production, for example by developing an automatic system capable dispense the liquid particles precursors in a belt conveyor with repellent properties on the surface. Then, the droplets could harden into solid particles along of the route of the belt conveyor and be collected in the end.

In the future, it is expected the preparation of more sophisticated and complex systems in order to mimic closely the complex biological events occurred during the regeneration of damaged tissues, as well as to produce systems for other biomedical and biotechnological applications.